THE EFFECTS OF BUFFETING AND OTHER TRANSONIC PHENOMENA ON MANEUVERING COMBAT AIRCRAFT

Advisory Group for Aerospace Research and Development

Prepared for:

North Atlantic Treaty Organization

July 1975

AGARD-AR-82

AGARDograph

COLOR ILLUSTRATIONS REPRODUCED
IN BLACK AND WHITE

AGARD ADVISORY REPORT No. 82

on

The Effects of Buffeting and other Transonic Phenomena on Maneuvering Combat Aircraft

REPORT DOCUMENTATION PAGE

1. Recipient's Reference	2. Originator's Reference	3. Further Reference	4. Security Classification of Document
	AGARD-AR-82		UNCLASSIFIED

5. Originator Advisory Group for Aerospace Research and Development
North Atlantic Treaty Organization
7 rue Ancelle, 92200 Neuilly sur Seine, France

6. Title
The Effects of Buffeting and Other Transonic Phenomena on Maneuvering Combat Aircraft

7. Presented at

8. Author(s)	9. Date
Various	July 1975
10. Author's Address	**11. Pages**
Various	276

12. Distribution Statement This document is distributed in accordance with AGARD policies and regulations, which are outlined on the Outside Back Covers of all AGARD publications.

13. Keywords/Descriptors			14. UDC
Aerodynamic stability	Buffeting	Human factors engineering	533.652.5:533.6.011.35
Flight characteristics	Control		
Transonic flight	Environment		
Pilot (personnel)	Design		
	Fighter aircraft		

15. Abstract

This report concerns buffeting and stability and control problems experienced by combat aircraft in transonic maneuvering flight. It addresses the problems from the operational pilot's viewpoint and discusses human physiological aspects, man's performance in the environment, basic aerodynamic phenomena, aerodynamic-structural coupling dynamics, stability and control, aircraft design considerations, and engineering analysis and test techniques. Recommendations for future combat aircraft design improvements and technology efforts are included.

This report was prepared by a Working Group sponsored by the Flight Mechanics Panel of AGARD with contributions from the Aerospace Medical, Fluid Dynamics, and Structures and Materials Panels.

COLOR ILLUSTRATIONS REPRODUCED IN BLACK AND WHITE

NORTH ATLANTIC TREATY ORGANIZATION

ADVISORY GROUP FOR AEROSPACE RESEARCH AND DEVELOPMENT

(ORGANISATION DU TRAITE DE L'ATLANTIQUE NORD)

AGARD Advisory Report No.82

THE EFFECTS OF BUFFETING AND OTHER TRANSONIC PHENOMENA ON MANEUVERING COMBAT AIRCRAFT

This report was prepared by a Working Group sponsored by the Flight Mechanics Panel of AGARD with contributions from the Aerospace Medical Panel, Fluid Dynamics Panel and Structures and Materials Panel.

THE MISSION OF AGARD

The mission of AGARD is to bring together the leading personalities of the NATO nations in the fields of science and technology relating to aerospace for the following purposes:

- Exchanging of scientific and technical information;
- Continuously stimulating advances in the aerospace sciences relevant to strengthening the common defence posture;
- Improving the co-operation among member nations in aerospace research and development;
- Providing scientific and technical advice and assistance to the North Atlantic Military Committee in the field of aerospace research and development;
- Rendering scientific and technical assistance, as requested, to other NATO bodies and to member nations in connection with research and development problems in the aerospace field;
- Providing assistance to member nations for the purpose of increasing their scientific and technical potential;
- Recommending effective ways for the member nations to use their research and development capabilities for the common benefit of the NATO community.

The highest authority within AGARD is the National Delegates Board consisting of officially appointed senior representatives from each member nation. The mission of AGARD is carried out through the Panels which are composed of experts appointed by the National Delegates, the Consultant and Exchange Program and the Aerospace Applications Studies Program. The results of AGARD work are reported to the member nations and the NATO Authorities through the AGARD series of publications of which this is one.

Participation in AGARD activities is by invitation only and is normally limited to citizens of the NATO nations.

Published July 1975

533.652.5:533.6.011.35

Set and printed by Technical Editing and Reproduction Ltd
Harford House, 7–9 Charlotte St, London, W1P 1HD

PREFACE

In the Fall 1972 the North Atlantic Military Committee requested AGARD to perform a technology study assessing the effects of buffeting on the aerial combat capability of combat aircraft. The need for this study stemmed from the growing importance of improving transonic maneuvering capabilities and the lack of reliable criteria by which buffeting and its effects on military requirements could be considered during the design stage of combat aircraft. The AGARD Steering Committee approved the study and assigned the responsibility for its implementation to the Flight Mechanics Panel.

A Working Group was formally established by the Flight Mechanics Panel in October 1972. The Panel recommended that the Working Group expand the scope of the study to include consideration of other transonic phenomena, primarily stability and control problems, which impact on combat capability. The panel also solicited representation on the Working Group from the AGARD Aerospace Medical, Fluid Dynamics and Structures and Materials Panels. Prior to the first meeting of the Working Group, an extensive documentation search was performed by the AGARD Technical Information Panel and an additional literature survey in the USA was made by the Working Group Chairman.

The Working Group members were:

Mr W.E.Lamar (Chairman and Flight Mechanics Panel Member)
Air Force Flight Dynamics Laboratory
Wright-Patterson Air Force Base, Ohio 45433
USA

Dr Ing. G.Bucciantini
Aeritalia
10146 Torino
Italy

Lt Col. P.J.Butkewicz, USAF
Aeronautical Systems Division
Wright-Patterson Air Force Base, Ohio 45433
USA

Squadron Leader B.I.L.Hamilton, RAF (Flight Mechanics Panel Member)
Royal Aircraft Establishment
Bedford MK41 6AE, Bedfordshire
United Kingdom

Dr-Ing. B.Laschka (Structures and Materials Panel Member)
Messerschmitt-Bölkow-Blohm GmbH
8 München 80
Federal Republic of Germany

Dr R.Mautino (Flight Mechanics Panel Member)
Aeritalia
10146 Torino
Italy

Dipl-Ing. H.Max (Flight Mechanics Panel Member)
Dornier GmbH
7990 Friedrichshafen/Bodensee
Federal Republic of Germany

M.B.Monnerie (Fluid Dynamics Panel Representative)
ONERA
92320 Châtillon sous Bagneux
France

Lt Col. R.N.Slarve, USAF, MC (Aerospace Medical Panel Representative)
6570th Aerospace Medical Research Laboratory
Wright-Patterson Air Force Base, Ohio 45433
USA

In the period from May 1973 to July 1974 the Working Group held four meetings and received considerable assistance from advisors and observers who attended one or more of these meetings. Notable in their participation were Mr W.P. de Boer of the National Aerospace Laboratory (NLR), Amsterdam, Netherlands and Dr-Ing. H.John, Messerschmitt-Bölkow-Blohm GmbH, München, Federal Republic of Germany.

This final report was prepared by the Working Group members and the following collaborating authors whose efforts were coordinated by the Group:

Dipl.-Ing. J.Becker
Messerschmitt-Bölkow-Blohm GmbH
8 München 80
Federal Republic of Germany

Mr P.W.Hanson
NASA Langley Research Center
Hampton, Virginia 23665
USA

Dr C.Hwang
Northrop Corporation
Hawthorne, California 90274
USA

Mr J.L.Lockenour
Air Force Flight Dynamics Laboratory
Wright-Patterson Air Force Base, Ohio 45433
USA

Mr D.G.Mabey
Royal Aircraft Establishment
Bedford MK41 6AE, Bedfordshire
United Kingdom

Mr W.G.Williams
Air Force Flight Dynamics Laboratory
Wright-Patterson Air Force Base, Ohio 45433
USA

Mr R.J.Zwaan
National Aerospace Laboratory (NLR)
Amsterdam 1017
Netherlands

In the report, principal authorship is indicated for chapters or major sections, and recognition of additional assistance is contained in footnoted acknowledgements. The appreciation of the Working Group is extended to those who generated the basic information referenced in this report as well as to those who contributed the knowledge which is now simply identified as the "state-of-the-art".

All portions of this report were reviewed in detail by the Working Group members and they concurred in the principal findings. Final editing and the preparation of the report for printing was performed by Mr R.J.Wasicko, Flight Mechanics Panel Executive.

It is believed that this report provides a unique perspective of the buffeting and stability and control problems experienced in transonic maneuvering flight. The report addresses the problems from the operational pilot's viewpoint and discusses human physiological aspects, man's performance in the environment, basic aerodynamic phenomena, aerodynamic-structural coupling dynamics, stability and control, aircraft design considerations, and engineering analysis and test techniques. In addition, recommendations for future design improvements and technology efforts are included to highlight the many gaps that exist in current knowledge and the need for continuing research and development.

W.E.LAMAR
Working Group Chairman

CONTENTS

INTRODUCTION

by

W.E.Lamar

Superior transonic maneuverability is a prime requisite for a modern fighter aircraft. The high turn rates and accelerated flight conditions necessary for maneuverability result in flight at high angles of attack which normally involve aerodynamic flow separations on the wing. These flow separations lead to increased drag, buffet, and stability and control problems which degrade combat capabilities. The buffeting involves vibration throughout the aircraft structure which results in multi-axis vibrations at the pilot's seat. The stability and control problems may evolve gradually or involve sudden roll, yaw, or pitch rates or large oscillations that are difficult for the pilot to control.

An adequate understanding of these problems is important for the improvement of existing aircraft as well as the design of new aircraft. Recent developments of high thrust-to-weight ratio fighter aircraft with capabilities for sustained high turn rates and extensive vertical climbs and maneuvers have expanded the flight envelope and further increased the importance of developing satisfactory high angle-of-attack transonic flight characteristics.

Buffeting and its effect on fighter aircraft design and combat capability are the principal subjects of this report. However, attention is also given to stability and control because of its importance to maneuvering and combat capabilities. The need to do this became clear early during the study of the factors limiting transonic maneuvering and gunsight aiming accuracy. While drag, performance, armament systems, and many other parameters also exert a marked affect on fighter design and combat capability, their consideration is beyond the scope of this report. The overall fighter combat problem, human tolerance and capabilities, basic transonic aerodynamic flow field factors, and structural response analysis methods are reviewed to provide perspective for more detailed discussions of buffeting and stability and control. Detailed coverage is given to buffeting in the areas of analysis, design, wind tunnel test, flight test, and solution of problems.

How really important is transonic high angle-of-attack buffeting compared to other stability and control problems? Is it the limiting factor in maneuvering or in gunsight aiming accuracy? Pilot opinion available to the study group clearly indicated that buffet onset and increases in buffeting intensity did not normally deter a pilot in combat from attempting to attain a "firing position" by increasing the maneuvering angle of attack. Rather, the real maneuver limit is generally reached when the aircraft encounters a significant stability and control problem, such as a severe wing rock, or imminent stall departure. A clear appreciation of operational experiences and factors involved can be gained from Chapter 1. Opinion on factors limiting sighting accuracy is not as clear. Buffet may severely degrade sighting accuracy on some aircraft, but may have relatively little impact on others. Severe stability and control problems can be expected to affect sighting as limits are approached. Clear resolution of these problems is hampered by significant differences in effects among different designs and the lack of data from systematic testing to quantitatively assess and correlate gunsighting capability with angle of attack information, buffet levels at the wing or tail, and vibrations at the pilot's station.

Correction of any potential problems is important during aircraft design before the costs for such corrections escalate. Thus, design modifications are often made during the design and wind tunnel test development stage, with the goal of attaining the required maneuver capability free from buffet. In the flight test or operational phase, correction of flow separation problems to eliminate unacceptable maneuvering performance or stability and control deficiencies is sometimes necessary to assure a satisfactory aircraft. While such changes may also alleviate buffet, they are usually not made just because of the onset of buffet during maneuvering flight. However, occurrence of buffet within the normal cruise flight regime, or tail buffet, will excessively limit flight operations and usually requires correction.

While delay of flow separation and buffeting is desirable, the onset of buffeting during transonic maneuvering provides a useful indication to the pilot of the beginning of flow separation which, as the angle of attack or transonic Mach number is further increased, will lead to more extensive stability and control problems. The rate of buffet intensity growth in some aircraft provides a useful means of assessing the maneuvering margins available after occurrence of buffet onset. These cues are also useful to the designer. Thus, means of predicting or testing for buffet onset and intensity growth as a function of design parameters is of considerable interest in the design process.

A more complete understanding of the phenomena and the development of effective analysis, design and test methods for delaying buffeting and preventing flight control problems is important for a number of reasons:

(1) Occurrence of tnese problems is detrimental to pilot control and gunsight aiming accuracy.

(2) Full use of the maneuvering potential of the aircraft is inhibited or prevented.

(3) Inadvertent stall departure is a possible consequence which not only impairs combat effectiveness, but has caused loss of numerous aircraft.

(4) Correction of deficiencies discovered during flight test or operational usage is normally very costly and far exceeds the cost of doing the job correctly during the design phase.

(5) Increased drag reduces combat effectiveness.

Buffet may be defined as a repeated tapping, hitting, or pounding. As far back as 1903, Wilbur Wright observed peculiar tapping sounds from the structure of his aircraft as it approached stall. According to Fung, the term buffeting was originated by British investigators of the crash of a Junkers F-13 in England on 21 July 1930, and applied to describe irregular oscillations of the tail due to its emergence in the turbulent separated flow wake of the wing. Usage of the term expanded and for many years buffeting has been associated with the vibration of structural components due to flow separation from the wing or the impingement of separated flows or wakes on other portions of the structure, especially the tail.

As noted, some types of buffeting are considered very helpful. For years, pilots have relied on a mild but increasing degree of buffeting to warn of an approaching stall condition as the aircraft approaches maximum lift. Aircraft that had such characteristics were good aircraft; those that did not were considered dangerous. In many modern aircraft, it has been found necessary to add devices such as horns, stick shakers, or even stick pushers to provide the pilot with adequate stall warning.

Other types of buffeting can be very detrimental. While buffet can occur as a result of many types of flow separation or impact of turbulent wakes, the transonic high angle-of-attack buffeting resulting from separated flows induced by shock wave – boundary layer interactions is of special interest in the design of highly maneuvering fighter aircraft. Buffet loads generally increase in severity as Mach number and angle of attack increase. Shock waves become stronger and the boundary layer is separated over larger areas of the wing, with more intense pressure fluctuations in the area of separated flow. Separated flows extending into the wake produce pressure divergence at the trailing edge which causes fluctuations in circulation and wing lift. The combination of these unsteady pressure fluctuations, or buffet loads, cause a dynamic response or buffeting of the structure which interacts with the natural structural modes and is transmitted throughout the aircraft. Vibration levels at the pilot's seat are, therefore affected by the strength of the fluctuating buffet loads, the response of the structure, and the location of the pilot's seat in relation to the natural structural nodes. In addition to their effect on the elastic structure of the aircraft, the buffet forces can also cause rigid body motions of the aircraft and induce stability and control problems. These may be coupled with the structural vibrations or with control system induced oscillations.

The detailed review of flow fields and separated boundary layers in Chapter 3 and the extensive coverage of wing and tail buffet in Chapter 7 will provide a more complete insight into the causes and nature of buffet. Since weapon bays on some aircraft designs must be open during transonic flight, a review of weapon bay buffeting is also covered in Chapter 7.

Buffet is perceived by the pilot when its intensity at his cockpit station reaches ±.035 to 0.1 g_z (head to toe), depending on the sensitivity of the pilot and the degree to which he is absorbed by other tasks. In Chapter 1 buffeting of ±0.1 to 0.2 g_z is termed definitely perceptible, from ±0.2 to 0.6 g_z is termed annoying, and from ±0.6 to 1.0 g_z is termed intolerable for more than a few seconds. As expected, these definitions are not standardized and vary in the literature. For example, ±0.05 g_z is frequently used as an indication of buffet onset. Buffeting frequencies in the 4–10 Hertz range appear to have the most adverse effect on pilot tracking performance. While considerable data is available on both pilot tolerance and performance in a buffeting environment, much of this data is limited to 1 "G" flight. It is well known that an acceleration environment degrades pilot tolerance and tracking performance. While meager data is available on the combined effects, Chapter 2 presents limited data which shows that the combined effects of sustained "G" and vibration in the "z" and "y" (lateral) direction were only slightly worse than the effects of "G" alone. Quantitative data in the real maneuvering flight environment under combined "G" and buffeting conditions during tracking tasks is very limited and a clear candidate for more research.

Since buffeting and many of the stability and control problems which affect maneuverability can be traced to aerodynamic flow separations which also affect drag and, thus, performance, extensive interest has existed for some time in the basic phenomena as well as in the specific problems. This has led to much emphasis on the development of basic aerodynamic flow theories and methods of analyzing and testing flows and boundary layer separations which induce buffeting and stability and control problems. The type and extent of flow separation depend on many factors such as airfoil shape, wing planform, related aircraft configuration details, angle of attack, Reynolds number, and Mach number.

The underlying reasons for the phenomena are generally understood, but complete quantitative methods for their analysis in aircraft design are either inadequate or lacking. The mixture of subsonic and supersonic flows, vortices, spanwise flows, boundary layer – shock interactions, boundary layer separations and reattachments which occur at transonic speeds on the low aspect ratio, highly swept, three-dimensional wings of modern fighters presents a highly complex flow situation that is not yet amenable to full understanding or quantitative analysis. Typically, a combination of theoretical techniques, empirical data, and wind tunnel tests are used to estimate the onset and subsequent development of buffet and flight control problems. Although wind tunnel testing is the primary means of obtaining detailed data on buffet onset, degree of flow separation, and buffeting intensity during aircraft design,

factors such as modeling limitations, tunnel turbulence, and scaling problems lead to many uncertainties in the results. In this report discussions of the basic flow fields are presented in Chapter 3, and buffet analysis, wind tunnel test and flight test methods are discussed in Chapters 8 and 9. Comparisons of ground-to-flight methods are made in Chapter 10, configuration effects described in Chapter 11, and means of improving buffet characteristics are presented in Chapter 12.

The need to predict the structural response due to flight in turbulence, as well as buffeting, has led to the development of useful analysis techniques capable of predicting responses throughout the aircraft to known forcing functions. The dynamic response of the aircraft structure, factors involved, and the basic methods of analyzing structural response due to random fluctuating modes are detailed in some depth in Chapter 4.

The stability and control problems limiting maneuvering transonic flight include those caused by wing rock, Dutch roll, wing drop, nose slice, nose wander, pitch up or down, stall departure, and others which are defined and discussed in both Chapters 1 and 5. Other parameters such as short period damping, control harmonization, stick force per "G" and the control laws of the augmentation systems can also significantly affect tracking capability, and are discussed in Chapters 5 and 6.

Stability and control problems resulting from the rigid body response to flow separations and the buffeting modes, the use of augmentation systems, and the development of design features and innovative techniques which will alleviate and extend the boundaries of satisfactory controlled flight and improved tracking performance, are discussed in Chapters 5 and 6. Since variations in handling qualities can produce statistically significant differences in weapon release parameters and impact dispersions, these chapters cover other stability and control problems which affect aircraft maneuverability and precise tracking capabilities. In order to provide a perspective on the overall problem, Chapter 6 summarizes the interrelationship of flight control systems and configuration innovations being considered for advanced aircraft. Means of improving capabilities are also covered in Chapter 12.

The study of the literature conducted in preparation for this report indicates that considerable attention has been given to research and development related to the basic problems of highly maneuvering flight. Steady progress is being made in analyzing flow fields. Numerous efforts to develop practical analysis and test methods to predict buffet onset and intensity have led to some limited but useful techniques. Flight test data and correlations with theory and ground test results are available for a number of aircraft, and progress is continuing. Structural response analysis methods now permit calculation of the buffeting environment at the pilot's seat. However, data on the effect of buffeting environments, coupled with maneuvering "G" loads, on pilot gunsight aiming accuracy is sparse. Considerable research has led to the development of stability and control augmentation systems which can significantly improve the ability to maneuver and effectively track a target. Configuration aerodynamics has led to effective use of vortex flows to delay separation and numerous innovations and techniques to improve aerodynamic flows and to extend angle of attack capabilities.

However, despite the progress to date, the study shows many gaps. More effective analysis, test, and design methods are needed to avoid problems and assure maximum combat potential for new aircraft during the preliminary design process. Proper design and prevention of problems during this stage of development will do much to reduce development costs and assure superior combat aircraft.

CHAPTER 1

THE OPERATIONAL PROBLEMS ENCOUNTERED DURING PRECISE MANOEUVRING AND TRACKING

by

B.I.L.Hamilton

1.0 INTRODUCTION

Manoeuvring air combat is an immensely complex subject that embraces all the topics relating to aircraft design as well as weapon systems, combat tactics, physiological factors, countermeasures, and the nature of the adversary. To provide the basis for a full appreciation of the report, this chapter provides a summary of the main events that occur in air combat, describing the manoeuvre and handling limitations. In this treatment of the subject it is not possible to deal with specific aircraft weapons, fire control systems, or tactics; in addition, although dealt with briefly, multi-aircraft combat is not discussed in depth as the 'section tactics' employed are so various as to be a subject in themselves.

The problems that will be described are those which have been experienced on the current range of fighters and on those that have recently been withdrawn from front line service. Many of the references in this report relate to work carried out on non-combat aircraft – often they are pure research aircraft. However this in no way affects the relevance of the references as, in each case, the subject under consideration is a basic aerodynamic principle; indeed, often the test vehicle in question has been the forerunner of an operational type.

1.1 AIR TO AIR COMBAT

When the fighter pilot is asked to state the essential criteria that his aircraft must meet, he invariably gives as his first requirement 'the aircraft must turn – controllably'. In this he means that the aircraft must turn only when he wants it to and in the direction and at the rate that he wants it to. This report is all about turning in the context of air combat where, for the majority of the time, the pilot is demanding the maximum turning performance that his aircraft can give. At the same time he requires the necessary level of control to manoeuvre his aircraft tactically and to meet the tracking requirements of his weapon system. There are a number of handling qualities degradations that will influence his effectiveness.

1.1.1 The Air Combat Arena

Figure 1-1 from Reference 1-1 is an illustration of the ranges of speeds and heights to be expected when contemporary fighter aircraft are engaged in air combat. The determining factors that result in this pattern are: the aircraft specific excess power (SEP) characteristics, the basic aircraft envelope limits, the Mach/altitude combination giving the maximum sustained turn capability, and the pilot's 'g' tolerance. In particular, because of the pilot's 'g' tolerance, when altitude is reduced in combat the maximum speeds which are used generally decrease.

Figure 1-2 from Reference 1-2 shows how the air combat arena varied between the offensive and defensive aircraft when air combat, between various fighter configurations, was computer simulated.

When two modern aircraft maintain aggressive tactics in hard manoeuvring combat the heights and speeds always decrease. When one aircraft attempts evasion or breakout from the fight, excursions to the higher speeds occur. Figure 1-3 illustrates the percentage of time spent within various speed and height bands throughout a number of engagements in a flight trial.

1.1.2 Air Combat Manoeuvring

A primary relationship in the study of a particular aircraft's manoeuvring capability is that between longitudinal and normal acceleration when turning at maximum rated engine thrust. This is illustrated in Figure 1-4 which shows that at a given speed and altitude, two aircraft may each have advantages over the other depending on the manoeuvres in progress. The SEP ratio at zero turn rate illustrates the potential for one aircraft to gain an energy advantage over the other; on the other hand the turn rate difference at zero SEP shows the potential angular rate advantage available

to the attacking aircraft in a maximum sustained turn situation. Also shown is the difference between the maximum instantaneous turn capabilities. This is achieved by trading energy (speed or height) for turn rate up to the maximum limit dictated by structural constraints or by handling limitations imposed by the maximum usable lift coefficient C_L.

Considerable deceleration or height loss may occur at the negative SEP levels achieved at the maximum instantaneous turn rate. The fighter with an initial energy advantage can afford to turn at a greater negative SEP level than his adversary, exchanging his energy advantage for turn rate advantage.

Some of the handling deficiencies which result from high C_L stability and control degradations are illustrated in Figures 1-5 and 1-6. Not all of these phenomena would occur on any given aircraft, nor would they necessarily occur in the order shown. Figure 1-6 does demonstrate, however, that the 'defacto' turn limit may be well below the maximum trimmed lift.

1.2 PHASES OF AIR COMBAT

Air combat can be broken down into many different sequences. The following is convenient for this report.

1.2.1 Detection

Detection may be by independent, on-board visual or electronic means, or by ground-based visual sightings or radar reports. Whatever the source, the pilot will immediately take precautionary measures to a degree dictated by the environment (hostile, neutral or friendly), and his foreknowledge of the likelihood of the 'target' being hostile. His preparation will usually include a build-up of total energy and initial checks of his weapons.

1.2.2 Identification

The rules in force in the theatre of hostilities will dictate the precise order of events. The pilot may adopt an offensive flight path if he is certain the target is hostile and may even acquire the target with his missile before positive identification. It would be more normal for a positive visual identification to be made before this stage was reached. However, it can be assumed that the pilot will be fully prepared before identification, 'just in case'.

1.2.3 Acquisition

This implies that the weapon system of one aircraft has been brought to bear on the other aircraft, and therefore, that all the envelope criteria for its release have been satisfied. This may happen on the first pass, as in a slashing attack, or after a protracted series of manoeuvres devoted to the solution of the angular and range problems. To describe the preliminary manoeuvres that precede acquisition the term used will be the 'development' or 'tactical' phase. Acquisition does not always take place after a tactical phase.

1.2.4 Tracking

This term implies a precise manoeuvre which is required to solve the delicate sighting problems associated with guns. It can be applied loosely to missiles although the precision required will clearly be less for the more advanced missiles with large acquisition envelopes. It is this, and the acquisition phase which are the subjects of this report.

1.2.5 Weapon Release

Although apparently a simple end to the preceding series of events, it should not be forgotten that the weapon system itself may well be affected by the motion of the aircraft on which it is mounted. This aspect will not be dealt with in this report. The further implication of this phase of air combat is that systems management appears at a most crucial moment in the pilot's working life. Although not a transonic phenomenon, the extra workload can have a more significant effect on the outcome of the engagement than some of those to be described; this will result if inadequate attention has been given to this aspect of cockpit design.

1.3 THE CONDUCT OF AIR COMBAT

The outcome of an air combat engagement depends upon the motivation, aggressiveness, skills and characters of the pilots almost as much as the performance and handling qualities of the fighters. Figure 1-7 shows, in algorithm form, some of the factors to be considered when a single fighter detects a potential threat during an otherwise routine patrol. The relevance of the various handling phenomena under consideration will be dealt with later. It can be seen that the algorithm is typical of the 'manoeuvring' to be found in any two-person game theory.

1.3.1 Multi-Aircraft Combat

In the 1-on-1 combat situation, because the fight is almost invariably a turning fight, both aircraft are generally at maximum usable C_L for a large proportion of the time. In a 2-on-1 or 2-on-2 situation it is normal for one of the offensive aircraft to be at a higher speed, relatively unloaded in terms of normal 'g'. The flight is conducted in a coordinated fashion with both members of the team in radio contact, and when the slower team member, who is turning at his limit, has attracted an offensive fighter from the opposing team his team mate should be in a position to return to the fight to carry out a high speed, low 'g', slashing attack. It is not possible to give this subject any more detailed treatment in this report; the size of the 2-on-2 algorithm may be gauged from the relatively simple 1-on-1 algorithm at Figure 1-7. The main influence of section tactics is that there is likely to be a greater difference between the total energies of opposing fighters than there is in 1-on-1 combat.

1.3.2 1-on-1 Aerial Combat

Considering, as the basis for aerial combat, the 1-on-1 fighter engagement, the fight has been shown to consist of five phases. Armament sighting may take place either immediately after the identification phase if conditions are right, during the manoeuvring phase if the manoeuvres are successful, or when the target tries to escape. The majority of actual kills have occurred very early when the offensive aircraft is able to make a slashing attack, gaining the element of surprise and retaining a high escape speed. An inferior aircraft may achieve a successful weapon release in this phase, but if he fails to achieve a kill because of

- inability to aim the weapon correctly,
- weapon system inadequacy or failure,
- target evasion, or
- countermeasures,

then the fight proceeds to the tactical development. If the aggressor knows his aircraft to be inferior he may conserve his energy and break out of the fight at this point.

In the tactics phase each aircraft is manoeuvred in the way thought by the pilot to be the best for the solution to his sighting problem while not allowing his own aircraft to become the target for the adversary's weapon. If, after two or three manoeuvres, say 60 to 90 seconds, neither pilot has achieved a significant reduction of his sighting errors then very often the fight is broken off. It will be apparent to both pilots that the engagement should be terminated while there is still sufficient fuel to take evasive action should a further attack be initiated. The pilot who leaves his break away manoeuvre until it is fuel dictated will be at a severe disadvantage if he is the first to reach this critical moment. The alternative outcome during a neutral tactical phase is a firing opportunity given away by the first pilot who makes an unforced error.

If however one aircraft is clearly gaining an advantage in the tactical phase, then the defensive aircraft will change its tactics either to those which will provide it with an opportunity to break out of the fight without penalty, or to those which create a stand-off situation for long enough for the superior aircraft to reach a minimum combat fuel state. In either situation the superior aircraft will continue to address the manoeuvring problem in an endeavour to enter the firing envelope of his weapon. If the counter-tactics of the defensive aircraft fail then the fight will enter the terminal phase.

The type of flying demanded for the offensive aircraft in the terminal phase will vary with the type of weapon system. For instance, with the advanced missile systems the tracking task is simply to keep the target within a cone of half angle 20° or so around the attacker's longitudinal fuselage datum (LFD), and in general this is a fairly easy task, the success or otherwise of which depends more upon aircraft performance than upon precision of control. On the other hand if spot harmonised cannons are employed at extreme range then it may be necessary to control the aircraft LFD to within ± 2 milliradians (mils) moving point ahead of the target manoeuvring in three planes. In the former case the target can be regarded as having no chance of avoiding the inevitable outcome but in the case of the latter, where the attacking aircraft must change from coarse manoeuvring flying to relatively delicate precision flying, the target has one final option. This is to upset the tracking solution by making short term, coarse, random alterations to its flight path, employing positive and negative 'g', sideslip, and bank which, when performed at a period of about 2 to 3 seconds, can conflict with the short period characteristics of the attacking aircraft/pilot combination.

1.4 PRECISION MANOEUVRING

There are, therefore, three general categories of air to air tracking:

- Target passive – attacker manoeuvring – surprise attack,
- Target and attacker manoeuvring – steady,
- Target evading – attacker manoeuvring – unsteady.

It can now be seen that buffeting and the other transonic phenomena being considered may affect combat aircraft in four ways.

(1) By affecting the ability of the pilot to extract the maximum performance from his aircraft by degrading the handling qualities at high C_L .

(2) By reducing the maximum performance obtainable, although the limit is not dictated by handling qualities degradation.

(3) By reducing the accuracy with which a tracking task may be accomplished, although adequate performance is available.

(4) By degrading the performance of the weapon system.

It is the first and third of these that will be considered, leaving aside the performance and weapon system aspects.

The precision manoeuvring task of tracking, unlike for instance an instrument approach, is not one that requires the flight path to be controlled in relation to a line in space. It is more a case of aligning the LFD in the vertical and horizontal planes (usually with an angular rotation to compensate for target crossing angle) in a manner that is correct for the characteristics of the weapon in use. It has been shown that the maximum allowable error in tracking may be large in the missile case, or very small in the cannons case. A number of factors will now be defined and their influence on precision manoeuvring discussed. Later some advanced control system concepts will be discussed in the same context.

1.5 THE TRANSONIC PHENOMENA INFLUENCING PRECISE MANOEUVRING

This report deals with the ability of a pilot to track a moving target accurately during manoeuvres. It is therefore most useful to consider the requirements of an aircraft equipped with a lead-computing gunsight and cannons that are 'spot' harmonised to provide minimum alignment error at between 1200 and 1800 feet range. The aiming marker is usually 2 mils (0.11°) in diameter. The pilot's tracking task is to maintain the aiming mark on a nominated point on the target; this is usually either the cockpit or the tail-pipe. Exactly where is less important than the fact that it must not vary, as random movement around the target will mean that the solution to the sighting problem from the gyro lead-computer will be inaccurate.

It is important that the aiming mark is held steady for at least one second before gun-firing commences and that the aim is not varied by more than 2 mils (0.11°) during firing. In the absence of any disturbances, given a good handling qualities aircraft and a target in steady flight, the average pilot has no difficulty in tracking to within 3.5 mils (.2°) and with practice this can be reduced to 2 mils (0.11°).

As shown in Figure 1-3, 50% of fights terminate at medium level and medium speed. The majority of tracking takes place in this region. The 'snap-shot' situation arising from a slashing attack at high speed is, however, very common in the opening phases of a combat engagement. Accuracy of tracking is no less essential in these attacks than it is after the tactical manoeuvring phase is over.

The phenomena defined are described in greater detail in Reference 1-3.

The onset of the phenomena under discussion is a function of the total aircraft shape. Due consideration should be given to the fact that during stores release in combat the change in the external shape of the aircraft may well bring about variations in the conditions required for the onset of an unwanted aircraft motion. This may be adverse or beneficial.

All of the phenomena to be described can occur in transonic flight. Some of them can be found at the lower Mach numbers, where air combat is usually conducted after a protracted engagement. They are usually the result of high angle of attack degradation of the otherwise satisfactory handling qualities which make the aircraft normally an adequate aiming platform for the weapon system in use.

1.5.1 Buffeting

The word buffet is all things to all men. Different disciplines will define buffet to satisfy their own criteria. For this chapter, from the fighter pilot's standpoint, it will be defined as: a vibration which is perceptible to the pilot to a degree that intrudes into his concentration on his manoeuvring task and may interfere with the precision of his control.

It is not important from the handling standpoint whether it comes from wing flow separation, separated flow striking part of the airframe, intake flow breakdown, stores interference, spoilers, airbrakes, bomb doors, or other devices that change the shape of the aircraft. It may, of course, be significant if the part of the structure that is vibrating is that where the pilot or the weapon is situated.

To the fighter pilot who knows his aircraft, buffet onset is a valuable source of information in moments of intense activity when he is not able to refer to his flight instruments. Of the many different buffet level criteria to be found from Reference 1-4 and others in this report the following is a summary which smooths out the variations. The 'g' values quoted are peak values.

Onset	± .035	to	.1	g_z	perception depends on workload/normal g
Light	± .1	to	.2	g_z	definitely perceptible
Moderate	± .2	to	.6	g_z	annoying
Severe	± .6	to	1.0	g_z	intolerable for more than a few seconds

Provided that there are no other effects such as loss of full control or random aircraft motions, light buffet usually has no adverse effect on manoeuvring, either coarsely or precisely. The average fighter pilot is so used to flying in this region that he may not even comment on it at the lower amplitudes. He will however feel annoyance and frustration when the buffet characteristics reach the level where his ability to track his target is affected: other effects on his performance may result from the arm mass feedback to the stick and his ability to see the target or his cockpit controls and instruments. At the intolerable level the motion becomes physically punishing, and full control is not possible as a result of the effect of the buffet on the pilot himself.

The significance of buffet in air combat depends upon the task. If flight in buffet gives a performance improvement then pilots will use this region during the tactical phase of combat. Tracking will also take place at quite high buffet levels, even with guns; but when the low frequency, high amplitude 'bouncing' buffet occurs then there is no further advantage to be gained from operating in this region.

In this general treatment of buffet there is no division of buffet into the transonic buffet and that associated with high angle of attack separation at low speeds. Indeed, whatever the cause, the effect in manoeuvring combat is largely the same.

To summarise, flight in the buffet region can affect the precise manoeuvring in combat in various ways. Gunsight performance may be affected, pilot performance may deteriorate and he may have difficulty in making control selections, and the aircraft performance itself may deteriorate as a result of the loss of optimum aerodynamic conditions giving an increase in drag and a reduction in lift.

1.5.2 Wing Rock

From the pilot's point of view, wing rock is a motion that he regards as a rolling motion. At low amplitude the roll oscillations will be tolerable and the motion accepted as a necessary evil if a performance improvement can be gained. When required to track precisely with a gyro gun-sight a yawing motion may become apparent and it is clear that in any but the most innocuous rolling oscillation tracking is impossible. A roll rate of about ±10°/second is regarded as the aiming limit; this is well inside the comfort limit.

For different aircraft it is possible to subdivide wing rock further into such categories as: pure wing rock, roll/yaw wing rock and plain Dutch roll. There are not yet hard and fast rules as to which is which, but in general the hard-edged pure wing rock will only be found at high Mach numbers, and a more sedate Dutch roll will be found at low Mach numbers.

When hard-edged pure wing rock is encountered at high Mach numbers, by the time the pilot has taken recovery action by reducing angle of attack, what started out as a turn to the left may end up as a turn to the right. Thus, not only is precise tracking impossible, there is also a severe tactical manoeuvring limit. This motion is characterised by its irregularity and an almost total lack of yawing motion.

The roll/yaw wing rock has a significant yawing content and the motion is usually symmetrical. Up to ± 50°/sec roll rates have been encountered and the amplitude may be up to ± 90° of bank or even divergent.

Unlike the previous two examples, pilots are often quite happy to tolerate a neutral Dutch roll motion, and although they may not be able to track accurately with guns it is conceivable that certain automatic missiles may function satisfactorily in this condition.

All these motions are affected by the Dutch roll damping and in Reference 1-5 it is indicated that there may be beneficial effects in some aircraft from an increase in the Dutch roll damping beyond the moderate buffet level. But it is not to be assumed that tracking errors will be smaller due to this effect as the degradation due to the buffet itself will become more significant.

1.5.3 Wing Drop (or 'Roll Off')

This is an uncommanded motion seen by the pilot as a divergence in roll and an incipient departure. Typically the roll rates are not high, being of the order of 10 20°/second. It is clearly beyond both the aiming limit and the tactical manoeuvring limit, and immediate recovery action is required in order to maintain full control.

1.5.4 Nose Slice (or 'Yaw Off')

This is an uncommanded motion seen by the pilot as a divergence in yaw and is also an incipient departure.

No aiming is possible after its onset, and indeed, in contemporary aircraft, by the time the pilot has recognised the symptoms, it is usually too late to prevent the incipient spin departure. This and wing drop are typical of the motions resulting when the pilot pulls back on the stick to get that last bit of turning performance out of the aircraft.

1.5.5 Nose Wander (or 'Snaking')

This is a yawing oscillation present in many aircraft during precise tracking throughout the flight envelope. Pilots often try to solve small azimuth errors in tracking by yawing the sight on to the target; thus any tendency to snake is often prone to excitation by the pilot himself. On the other hand, if it is self sustained, the pilot can often control the sight motion by exercising yaw control. The limit to which these techniques may be applied is about 10 mils (0.57°) of error. The sighting solution of the gunsight may also be affected, so the overall tracking accuracy will be degraded.

1.5.6 Pitch-Up

This phenomenon has been experienced at such low rates as to be described by the pilot merely as 'stick-lightening', and it can happen at such a high rate that the pitch control authority is exceeded and the angle of attack increases to the level at which one of the other high angle of attack phenomena is precipitated. If there are no lateral/directional effects resulting from the angle of attack excursions, and control authority is not exceeded, then pitch-up is an aggravating limitation on precise tracking, and a workload increasing phenomenon in tactical manoeuvring.

By itself it interferes with the pilot's control task and inevitably reduces the performance of the aircraft due to the drag increase. The real danger is that one or more of the previously mentioned high angle of attack phenomena may occur, resulting in a departure and a severe penalty tactically.

1.5.7 Departure

As this has been mentioned frequently, departure will be defined as an aircraft motion resulting from loss of control and which requires a finite time using specific control inputs for recovery to normal flight to be achieved. It is often the result of no action being taken at the onset of one of the motions described previously.

1.6 OTHER FACTORS INFLUENCING AIR COMBAT MANOEUVRING

In addition to the aircraft motion effects experienced in precise transonic manoeuvring, there are other relevant factors which it is appropriate to mention in this chapter. The very large number of subjects that can be discussed in this report reflects the 'Total System' nature of the concept of a manoeuvring combat aircraft.

1.6.1 Control Forces, Harmonisation, and Pilot Induced Oscillations

The stick force required to apply a given amount of aileron rarely changes in an aircraft with irreversible powered controls; similarly the rudder pedal force/deflection ratio is not usually variable. On the other hand it is customary to vary the stick force/deflection or stick force per 'g' through the medium of bob-weights, q-feel, Mach trim and so forth, in order to satisfy the various handling specifications. The result, although achieving conformity with the relevant handling criteria, rarely results in a consistent ratio between roll and pitch control feel — or 'harmonisation'. Pilots can, and do, adapt to this; tracking is a closed loop feedback exercise; but the danger is that before a pilot can reschedule the gain of his own tracking pitch inputs he will excite a Pilot Induced Oscillation (PIO) which rakes the target from nose to tail with the aiming mark.

A PIO in roll is also often seen with the aiming mark wandering from side to side of the target. It is in the suppression of this that the pilot will often 'freeze' his roll control and steer the aiming mark with his rudder.

1.6.2 Displays

Apart from the visual effects of buffeting, which are dealt with in Chapter 2, there are one or two obvious points to make about cockpit sighting displays.

It is essential for the pilot to be able to see both the target and the sight easily during the tactical development. Difficulties that have been experienced include loss of view of the sight either because of gyro saturation at high turn rates, or because of sun reflections. Even though equipped with a lead-computing sight, many pilots like to see, in addition, a fixed marker on the aircraft boresight to show where the longitudinal axis is pointing in space.

1.6.3 Workload

The total workload in a combat engagement is extremely high, both physically and mentally. The pilot has to solve the tactical problem, monitor his aircraft systems, manage his weapons system, and maintain an alertness for his own self-protection, all the while he is manoeuvring an aircraft that may suffer from one or more of the handling

deficiencies mentioned earlier. The optimisation of the controls and displays is of paramount importance to ensure that aircraft systems monitoring and weapons system management detract as little as possible from the effort that can be applied to the aircraft control, tactical solution, and self protection aspects of combat.

When the tracking phase of a combat is reached the only action that should be required is weapon release. Systems monitoring is usually suspended and the utmost concentration is applied to the weapon aiming task. The pilot is then exposed to two risks.

Firstly, when already close to a manoeuvring limit he may, by fractionally increasing his angle of attack, reach the point where control is lost through one of the phenomena described in Section 1.5. This is particularly so if a natural buffet warning is not available. It is of advantage to have automatic warning devices such as an audio-angle-of-attack indicator or rudder pedal shaker.

Secondly, he is exposed to the risk of a counter attack from the rear or the flank. When in a 2-on-1 combat the pilot's team-mate has the task of ensuring that this does not occur; in a solo engagement some automatic warning is highly desirable to preclude the possibility of a surprise attack.

1.7 ADVANCED CONTROL CONCEPTS IN TRACKING

It was stated in Section 1.4 that the precision task of tracking in air combat is one of aircraft attitude alignment while manoeuvring.

1.7.1 Automatic Flight Controls and Stability Augmentation

There are two advantages to be gained from the use of manoeuvre-demand or Command Augmentation Systems (CAS) and stability augmentation systems at high angle of attack in combat.

Firstly, by delaying or preventing departures the severe tactical penalty and aircraft loss from irrecoverable spins at low altitude can be eliminated or reduced.

Secondly, given the ability to use higher angles of attack without degradation of handling qualities, an enlargement of the usable tracking flight envelope is possible.

Much has been said about the use of manoeuvre demand systems, automatically scheduled to limit the aircraft to within a safe flight envelope. While improvement in automation of engine systems is to be highly commended the question of automatic manoeuvre limits requires further consideration. What will the limits be, who will set them, will they be set for highly skilled pilots or the average pilot and will the margins be small or large? The difference between success and failure in air combat may depend upon .1° of aircraft rotation. It would be most unfortunate if the skilled pilot, well acquainted with his aircraft, were denied this by the margins in a manoeuvre limiting flight control system. The additional penalty that these systems would impose is that when needed for coarse manoeuvring, some areas not suitable for the tracking task would be denied to the pilot. This begs the question of whether separate flight controls should be used for coarse manoeuvring and for precise tracking, as suggested in Reference 1-6.

1.7.2 Direct Lift Control and Direct Side Force Control

It would seem that these concepts could contribute to the overall combat manoeuvring task by enabling the offensive aircraft to acquire the defensive aircraft more quickly. That is, to place the target more quickly within the weapon envelope. As both concepts imply constant attitude, variable force (z, y) control, they are unlikely to improve the solutions of small tracking problems. Reference 1-6 has shown an initial favourable reaction to the concept of Direct Lift Control (DLC) and raises the question whether its introduction would merit a reappraisal of the modes of pilot flight path control. A more detailed treatment of this subject is given in Chapter 6.

1.7.3 Reaction Controls

The results of recent experiments are as yet unpublished, so the treatment given to this subject can only be circumspect. It is clear that additional control power can be either a good or a bad thing. The high angle of attack handling problems will be reached more easily, but greater control power is available for recovery. Also the separation effects on the controls themselves will be absent. This, however is not a dominant problem among all the others affecting the task. The real benefit to be gained from reaction controls would probably be the provision of high control power at very low speeds for rapid attitude change in an aircraft where this type of manoeuvre is acceptable.

1.8 DISCUSSION

Air combat manoeuvring is a complex and dynamic phase of flight. The pilot, in trying to achieve the aim of destroying his adversary, finds that his effectiveness may be governed by a number of high angle of attack phenomena:

- Loss of turning performance by aerodynamic effects,
- Loss of turning performance by handling deficiencies,
- Loss of accuracy through handling degradation,
- Reduction of pilot effectiveness by physiological effects,
- Weapon system degradation.

With the rapidly changing speeds and altitudes found commonly in vertically orientated modern combat, the manoeuvre limit may change from nose slide to wing rock and back again in the few seconds that it takes to execute a steep 'yo-yo' type of manoeuvre. It is not possible to point to one aircraft and say "that aircraft is limited in air combat by . . . . . ". Buffet, particularly, can be shown to impose a tracking limit when laboratory experiments are carried out, and, indeed, the same results would be obtained in aircraft were it not for the fact that buffet has been found to occur rarely in flight to that degree without the appearance of one or more of the other, more limiting phenomena. So although buffet can impose a precise manoeuvre limit in the way that has been described, pilots rarely refer to it as the most severe limiting factor for their aircraft.

To assess the relative importance of the phenomena from the stand point of tracking accuracy is not easy; they are all as bad as each other if they make the pilot miss the target. However, those which result in a lateral/directional departure must be regarded as the worst cases as they do not permit a rapid re-sighting of the target. Therefore the most serious phenomena could be said to be nose slice and wing drop. Next, the longitudinal departure, pitch-up, may be considered as fairly serious, although after recovery there may not have been a worsening of the look-angle from the attacker to the target.

Wing rock, buffet and nose wander – in that order – complete the list of phenomena in their order of relative importance. In each of these three cases the angular errors may be small, and refined weapon systems such as missiles or steerable guns may compensate for them.

1.9 CONCLUSIONS

In this chapter a broad outline of air combat manoeuvring has been given, and the influence of buffet and other transonic and subsonic phenomena has been discussed.

It has been stressed that an air combat fighter is a total system dependent upon the aircraft design and handling qualities, weapon system design and management, and the character and abilities of the pilot. Many of the points made are subjective and opinionative. The literature is not well stocked with information on the influence of buffet and the other phenomena on aircraft and pilots in actual combat; for the precise quantification of many of the factors actual trials combat flying is required.

It is important to separate the coarse tactical manoeuvring, fine weapon acquisition, and precise tracking phases of air combat. The requirements and limitations are not the same for each. It will require considerable flight combat research to identify which problems are of greatest importance in which area of flight.

To isolate essential areas of research, much preliminary work is required to determine the limitations that affect the aircraft performance, aircraft handling qualities, pilot performance, and weapon system functioning limitations, in mock combat research; it will not be possible to get the best results from sterile flight test techniques. Because much reliance must be placed on pilot opinion, it will be essential that test pilots, fully familiar with modern combat techniques, are employed in addition to sophisticated instrumented combat ranges and test aircraft.

CHAPTER 2

AIRCREW CAPABILITIES AND LIMITATIONS*

by

R.N.Slarve

2.0 INTRODUCTION

The pilot factors that can influence aircraft tracking precision during maneuvering flight are, in a general way, the same factors one can cite as being of importance to the successful completion of the overall flying mission. This chapter will deal only with those pilot factors such as vision and the man/machine interface known or thought to be important to successful mission completion for the specific mission segment of tracking precision during high load factor buffet. Aeromedical factors such as illness and dehydration are treated elsewhere and it will be assumed throughout that the aircrew members are physiologically "normal". In this Chapter the following symbology is used:

g		denotes vibrational acceleration in root mean square notation. $\pm 1\,g \cong \pm 9.8\ m/sec^2 \cong \pm 32.2\ ft/sec^2$
rms		root mean square
G		denotes sustained acceleration. $1\,G \cong 9.8\ m/sec^2$
Hz	=	cycles per second (Hertz)
g_z	=	vibration along the spinal axis
g_x	=	chest to back vibration
g_y	=	side to side (shoulder to shoulder) vibration

2.1 HUMAN PERFORMANCE EFFECTS OF ACCELERATION ENVIRONMENTS

Both sustained and vibratory accelerations are capable of producing stress effects upon the human operator which cause performance degradation. The literature reveals extensive investigation of these effects in limited experimental situations. However, to date, there is no proven generalized theoretical structure which allows prediction of flying performance degradation during actual flight conditions. This lack of total analysis is understandable when one considers the extreme complexities associated with attempting to identify and describe all the significant parameters that might be necessary to characterize the acceleration stimulus, physical boundary conditions (restraint system, etc.), experimental parameters (workspace geometry, human operator anthropometry, etc.), environmental conditions, and additional physical stresses such as temperature extremes. Furthermore, to quantify performance degradation, it becomes necessary to quantify a suitable performance index and completely describe important attributes of the performance situation that determine task complexity. This has not yet been done.

Both the synthesis and analysis approaches are being used to study the effects of accelerative forces on tracking performance. The synthesis approach consists of the analysis of the effects of these forces on elemental human operator functions such as perception and motor activities. Such data may make it possible to synthesize a tracking system performance model in the future. The analysis approach, on the other hand, uses both experimental and analytical methods to determine performance changes occurring in particular tracking situations. Specific work will be mentioned as appropriate in the following sections on vibration (g) and sustained acceleration (G).

2.1.1 Vibration/Buffet

It is well known that under many conditions of vibration, performance decrements can occur. The international community is in general agreement that the most important frequencies of concern to performance in vibration environments lie generally below 80 Hz, and that, for a constant vibration acceleration, humans are most sensitive to the region from 4 - 8 Hz for g_z (head to foot) and the region of 1 - 2 Hz for g_x (chest to back) and g_y (side to

* Dr Henning E. von Gierke and Col. George C.Mohr, USAF, MC, were of great assistance in reviewing and commenting on the draft of the chapter. Maj. Carlold B.Harrah, USAF, BSC assisted in adapting some of the data used and in editing the section on human operator analysis.

side) vibrations. (Figures 2-1 to 2-4, References 1-1 to 1-3.) For some military missions the acceleration values of these figures multiplied by a factor of 4 may be acceptable (Ref.2-4). However, it could be expected that performance will be marginal in this region. Curves for the region below 1 Hz have not yet been generally adopted, but recent data indicates that a standard similar to that proposed in Reference 2-5 and shown in Figure 2-5 is reasonable. In the area of performance degradation as applied to the flight environment, the region of 10 Hz and below is of greatest overall importance, with vibrations below 5 Hz associated with the largest tracking decrements (References 2-4, 2-6 and 2-7). The region of 1 Hz and below is of interest in the study of motion sickness as well as performance, but the short durations experienced in the specific environment discussed here and the high experience and acclimatization level of combat pilots would tend to minimize any possible motion sickness effects on mission success. There is no reliable data on the significance of rotary vibrations for human performance.

Buffet from the pilot's point of view may be defined as the onset of perceptible vibrations causing annoyance, task interference, or cueing. Figure 2-6 (Ref.2-8) is an example of one set of subjective response curves compared to tolerance curves for g_z as determined in the laboratory. The general slope of the curves can be compared to those in Figures 2-1 and 2-2. There is some obvious overlap of the data attributable to varying experimental techniques. In Figure 2-6 the perception level curve lies around .035 g rms (0.10g peak to peak). However, perception levels in the region of 0.01 g rms have been recorded. For g_x and g_y vibrations, the limits as depicted in Figures 2-3 and 2-4 are somewhat lower than for g_z (Figures 2-1 and 2-2) in terms of the acceleration levels. This compares well with the example of actual flight test data shown in Figure 2-7 (Ref.2-9) in which buffet onset, defined as a side vibration of .035 g_y peak to peak measured at the pilot's seat, coincides with the pilot's perception of buffet. The criterion of .035 g_y peak to peak buffet onset as used here was established from an average of 45 measurements, with a range of .01 – .06 g_y peak to peak, taken when buffet onset was indicated by the pilots during 16 flights with accelerometer readings taken below 70 Hz. For simultaneous g_z measurements, values as high as 0.10 g were recorded at the point of pilot-indicated buffet onset.

2.1.1.1 Performance Quantification

For US fighter-type aircraft, a few studies have shown that the buffet frequency transmitted to the pilot's seat is primarily due to the first wing bending mode in the range of 6 – 12 Hz (Ref.2-10). Furthermore, these studies have shown intensities up to 0.35 g rms in both the vertical (g_z) and lateral (g_y) axes. This frequency range and intensity combination can immediately induce severe tracking decrements which in some cases would not be compatible with good aircraft control if occurring in a single axis. To compound the problem, there is preliminary evidence that multiaxial vibration effects are related to the products of the decrements found in the single component axes rather than in an additive relationship (References 2-11 and 2-12). Figure 2-8 demonstrates this relationship based on results for 18 subjects and Figure 2-9 provides one example of how personal equipment (shoulder harness) can affect performance. In addition, random vibrations, especially at lower frequencies around 5 Hz, may cause degradations of 25% more than those indicated by sinusoidal vibration studies (Ref.2-13).

In considering any of the rather voluminous data available on tracking task performance under vibration conditions, and the various human operator – control – display relationships describing various degrees of degradation, it should be clearly recognized that the vast majority of the experiments usually considered only one axis or one frequency at a time under varying experimental configurations and also that the laboratories were generally not airborne. Thus, in most instances it is difficult to extrapolate specific conclusions to the flight environment in which there is a steady-state six degree-of-freedom acceleration capability with superimposed vibrations of a wide range and random nature. Nevertheless, it does not appear unreasonable to accept the general statements made above as being the primary area of interest for the precision tracking problem.

Attempts to derive general vibration performance curves for use by the aeronautical engineer have been less than ideal for the reasons cited above. Rustenburg (Ref.2-14), while recognizing the drawbacks of combining different studies, has derived performance curves normalized to 1 g rms and 1 Hz after deriving normalization constants from the basic data of several authors. The results of these calculations are shown in Figures 2-10 and 2-11. It should be noted that the data below 1 Hz are extrapolations and there is no time integral in these charts. However, these curves are generally compatible with Figures 2-1 and 2-3. Using this approach, a single number, H_c, or pilot tracking performance index, was developed to give a qualitative estimate of ride quality.

2.1.1.2 Vision

There is minimal visual degradation due to vibration at frequencies below 2 Hz. As the whole body moves with the seat there is negligible relative motion of the eye in respect to the viewed object, including instruments, and the eye is capable of compensatory tracking at these low frequencies (References 2-15 to 2-17). Above 3 Hz visual decrements begin to be measurable and in the region of 12 Hz a major peak in visual decrement occurs. There is another peak at 25 Hz and an additional peak at 60 – 90 Hz. The higher frequencies are not normally significant operationally as there is adequate attenuation usually present in the operational environment. However, the 12 – 25 Hz region can pose problems. Figure 2-12 summarizes the vibration frequencies of interest for various body areas. Relevant acceleration levels can be estimated from Figures 2-1 and 2-3.

One study of particular interest for the specific air combat maneuvering task compared visual acuity at varying eye-target distances. Figure 2-13 (Ref.2-18) shows the variation of visual efficiency or performance index (P.I.) (subjects compared to their control values) with frequency (or displacement) for 0.53 g_z rms amplitude as a function of viewing distance. The 1 meter and 4 meter results are of most interest as they represent cockpit display (dials, etc.) and far vision distances. The 1 meter distance is important if concurrent in-cockpit tasks are required as indicated in Figure 2-20. For the "far" vision condition, Figure 2-13 shows that the biggest decrement occurs at 20–25 Hz with a P.I. of .65 and that the visual efficiency is 70–80% in the 7–15 Hz range. This is probably not of great significance in and of itself for the task of seeing an opponent aircraft grossly. However, during tracking the visual decrement could interefere with the pilot's ability to obtain lead information from visual cues about his opponent's maneuvers, for example from wing tip motions associated with rolling maneuvers. This data should be interpreted with caution as it could be expected that the effects of vibration combined with sustained maneuvering G would be somewhat less than the effects of vibration alone. In addition, the vibration level of 0.53 g_z rms would probably be of more importance from the total manual control standpoint than as a pure acuity problem.

2.1.1.3 System Analysis

What does all this information mean to the aircraft designer? It seems fairly obvious that definitive data does not exist to fully compare the relative importance of buffet induced tracking degradations due to direct effects on the pilot's tracking ability under vibration conditions versus the aeronautical engineer's problem of achieving an aerodynamic configuration which can be aligned with a target. A simple, albeit facetious approach would be to take the position that buffet should be eliminated. The brief data presented here indicate that tracking decrements due to direct pilot manual control interference are of sufficient magnitude to justify continued engineering attention to buffet during critical target tracking maneuvers.

These considerations, of course, must be directed toward optimization of total system performance. Eney (Ref.2-10) and others have stated that personal interviews with pilots lead to a conclusion that the hindrance to performance commonly attributed to buffet actually involves other related and more critical phenomena. For example, a tendency of the airplane to encounter wing rock or nose wander (see Chapter 1) at a certain lift coefficient can be the deciding factor in determining the tracking decrement due to buffeting. Likewise the effects of acceleration are an important factor in the tracking problem (see Section 2.2) and the buffet environment cannot be assumed to be a constant factor throughout the air attack, i.e., it should be considered an intermittent occurrence dependent on the changing aerodynamic characteristics of the aircraft. Consequently, potential improvements or deteriorations in other aspects of the aircraft's stability and control should be considered simultaneously with any attempt to decrease the intensity of buffeting or to move the frequency spectrum to a mode that should not seriously affect human tracking performance, e.g., above 30 Hz.

A general preliminary goal could be to limit buffeting to 0.1 g rms in all axes at frequencies below 12 Hz from the point of view of tracking performance. Above 0.25 g rms, maintaining control in the general sense becomes more important. Engineering feasibility studies can help determine if this can reasonably be attained, and if the answer is negative, then perhaps the greater emphasis should be on the weapon system itself, i.e., sensors, compensating displays, etc. A combination of these approaches may well be the best solution.

2.1.1.4 Human Operator Analysis

The great majority of manned weapon systems are dynamic systems; the analysis and design of such systems require a dynamic description of the human operator controller. The development of dynamic descriptions for human controllers has been a scientific problem for more than twenty years. During this time, there have been numerous models proposed by numerous authors with varying degrees of verification and usefulness. Only two of these models have been verified to the point where they can be usefully applied in solving problems: (a) a linear time-invariant model proposed by McRuer (References 2-19 and 2-41) and (b) an optimum control model discussed by Kleinman (Ref.2-20). These two models have both been applied in a wide range of circumstances from simple laboratory control experiments to the analysis of manned weapons systems. Phatak (References 2-21 and 2-22), in work sponsored by the USAF Aerospace Medical Research Laboratory, has reported on the identifiability of the optimum control model for use in the analysis and design of manned weapon systems where threats may be a factor.

As mentioned earlier, both experimental and analytical methods are used for performance analysis. Shoenberger (Ref.2-15) provides a recent review of experimental work. One promising analytical approach based on control theory models is briefly described below.

An example of a human operator controller model with vibration input is shown in block diagram form in Figure 2-14 (Ref.2-23). The terms perceptual and motor remnant are used to describe the amount of tracking error and control output that cannot be correlated directly with either the tracking (display) or vibration inputs. Y_p represents the human operator's visual-motor dynamics and Y_c represents the controlled element dynamics. Perceptual remnant is that portion of the tracking error remnant thought to be attributable to visual system noise while the motor remnant is noise due to neuromuscular and proprioceptive feedback effects. Thus far human operator remnant modeling for vibration environments has not been satisfactory and the proportion of remnant due

to either motor or perceptual noise has not been quantified. However, it can be conjectured that vibration interferes in some way with visual and motor physiological mechanisms in addition to its direct mechanical effects on vision and on the arm/hand body segment.

Figure 2-15 (Ref.2-24) illustrates the significance of the remnant problem in vibration effects modeling. In this experiment four subjects were exposed to 0.28 g_y rms (lateral) vibration for two minutes while performing a single dimensional tracking task displayed on a cathode ray tube. The vertical ordinates of the two charts cannot be related directly to each other. However, it can be said in a general sense that more remnant is generated (note the logarithmic scale) with a spring stick than with a stiff stick during vibration and that the stiff stick appears to cause less decrement in the lower frequency range while the spring stick appears to have less decrement at 10 Hz. The solid triangles and circles on Figure 2-15 designate the tracking input and remnant baselines. This example is meant only to illustrate the modeling problem and does not constitute a basis for designating one type of stick as superior to another.

Hopefully, in the future, these modeling efforts can be combined with models of the controlled elements (such as an aircraft) and the actual control feedback values so that optimal control designs, including appropriate damping values, can be incorporated into systems required to operate under widely varying flight conditions.

2.1.2 Sustained Acceleration (G)

Well trained individuals wearing standard G suits are usually capable of safety tolerating approximately 7 G for 5–10 seconds, and this time can be extended to more than 30 seconds under well controlled conditions. However, significant decrements in tracking begin to occur in the range of 4–5 G with the standard US seat back angles of 13–19 degrees. Increased G tolerance as a result of increasing the seat back angle and raising the legs has been proposed since the 1930's (Ref.2-25) but until recently there was no necessity to specifically establish the relationship between seat back angle and performance under sustained G because aircraft structures were not designed for sustained acceleration maneuvers much above the human tolerance level for the 13 degree seat back angle.

A recent study at the USAF Aerospace Medical Research Laboratory demonstrated a two-fold increase in tracking performance using a two dimensional tracking task for a 65 degree reclined seat over a 30 degree seat at 8 G (Figure 2-16, (Ref.2-26)). Although the details of possible physiological costs such as a decreased efficiency of oxygen consumption under high G conditions have not yet been thoroughly evaluated, this data clearly demonstrates a potential maneuvering advantage and it can be surmised that an aircraft with this capability will have a consistent edge over conventional aircraft in combat.

The above simple description of acceleration tolerance and general performance capability is meant only to bracket the area of interest. Other methods of enhancing G tolerance and a detailed account of the physiology involved can be found elsewhere (References 2-25 and 2-27).

2.1.3 Combined Sustained Acceleration (G) and Vibration (g)

Of specific importance here, a search of the literature has provided only two references affording a reasonable exploration of tracking performance during G ± g. Piranian (Ref.2-28) has done an excellent investigation of 1.3, 2.5 and 5.0 G_z combined with 0, 0.07, 0.18, and 0.35 rms simultaneous g_z and g_y at 10 Hz. Figure 2-17 (Ref.2-28) summarizes the combined effects of buffet and sustained acceleration for six pilots using a centrifuge simulator incorporating an F-4B cockpit. It can be seen that for this experiment the effects of buffet over a 15 second tracking run were essentially negligible compared to the effects of G_z. These effects are not too surprising when one considers the smoothing effect on ± g that a sustained and steady + G should have when the sustained acceleration is greater than the vibration.

The other pertinent study by Dolkas (Ref.2-29) utilized 2.0 and 3.5 G with vibrations of 0, 0.35, 0.7, 1.16, 1.4, and 2.32 rms g_x at 11 Hz. The x axis was used as the study was related to rocket flight. However, it is of interest here in the event that tiltback seats are put into operational use. Figure 2-18 (Ref.2-29) summarizes the results at 3.5 G_x for two different stability augmentation system (SAS) modes and shows that vibration has a definite effect above 1.0 g_x. For the region below 1.0 g_x, this data agrees quite well with the g_z data presented above (Ref.2-28). These studies should be expanded to other frequencies. However, it would seem that the effect of sustained acceleration on tracking is of far more importance than vibration in the current operational environment.

2.2 OTHER ENVIRONMENTAL AND PILOT FACTORS

Factors, other than acceleration force fields, which may contribute to pilot performance degradation will now be considered.

2.2.1 Noise

The noise environment in US fighter cockpits ranges from 110 db to as high as '35 db during some phases of flight (Ref.2-30). A properly fitting helmet attenuates the noise presented to the ear by 10–25 db, depending on the type of helmet (Ref.2-31). This is adequate for the majority of flight environments when time weighting factors are considered.

Recent ground based studies compared the effect of 60 db noise and 100 db noise during vibration at 6 Hz, 0.07 rms g_z on horizontal and vertical tracking (Ref.2-32). For the 100 db noise level the tracking errors in this specific experiment were *decreased* approximately 10% from the tracking errors for the 60 db noise level when combined with vibration, although both noise and vibration independently causes increased tracking errors. The possible salutory effects of similar noise levels during actual combat maneuvering flight are not known, although it could be surmised that there would be little effect as arousal of the pilot should already be at a high level during combat. No noise data are currently available for this flight regime at this time.

2.2.2 Temperature

Reference 2-33 reports on study, similar to the one quoted above (Ref.2-32), which was done using combinations of noise (105 db), temperature (120°F), and vibration (5 Hz, 0.21 rms g_z). A two dimensional tracking test was used with a side arm controller and 4 minute exposures. The main findings are summarized in Figure 2-19. It is interesting to note that the tracking decrements due to vibration alone were slightly, but not significantly, larger than those occurring when all three stressors were combined and that the separate effects of noise and temperature were small, with the tracking performance for the single stressors being similar to those for the control runs. Temperature exposures for the runs were a minimum of one hour. Thus it appears, at least for these experimental conditions, that combined noise and heat do not cause additional decrements in tracking performance during vibration exposures. The separate effect of heat combined with vibration has not yet been studied.

2.2.3 Fatigue

No specific study on the influence of fatigue on combat performance during buffet is available. However, it may be generally assumed from daily experience and the many general studies of fatigue that tracking performance could be expected to be less efficient if the pilot is fatigued. Figures 2-1 and 2-3 reflect fatigue effects. A brief summary of approaches to pilot workload quantification as given by Bernotat (Ref.2-34) could be expanded to include fatigue effects. Figure 2-20 (Ref.2-35) illustrates a workload analysis for a 120 second simulated high acceleration air-to-air combat engagement. The complexity of tasks required for success would seem to be a good source for fatigue effects in the buffet environment.

2.2.4 Psychological Motivation

Motivation has long been known to be a prime factor in any human performance task. Of particular interest here would be the effect of hostile versus non-hostile conditions on a tracking requirement. Certainly the intellectual motivation to succeed in a hostile environment is at a high point. However, little is known in a quantifiable way about the possible deleterious effects of a very hostile air combat environment on performance, i.e., at what point and how much does an adverse physiologic reaction to the fear of failure overwhelm a pilot's abilities? Anecdotal data on pilot performance during severe combat stress is subject to tremendous variation and a definitive interpretation cannot be attempted here.

2.2.5 Personal Equipment

Personal equipment such as G-suits, pressure suits, thermal wear, armor, helmets, and restraints are known to have both positive and negative effects on performance in vibration environments, depending on the frequency and amplitude. One example is shown in Figure 2-9. All personal equipment such as helmets, masks, etc., should be tested to assure that no adverse vibration modes appear when subjected to the operational environment.

2.2.6 Man-Machine Interface/Control Dynamics and Configurations

The total system design, as it reflects the dynamic compatibility between the human operator and the hardware, must optimize system performance. With respect to the human operator, this dictates that every advantage be taken of man's high adaptability while, at the same time, acknowledging the inherent limitations of his sensory, information processing, and motor capabilities. For non-stressed situations, the human factors literature indicates extensive work has been done in man-machine interactions, especially as regards display/control design (Ref.2-36). However, it should be kept in mind that in stressful situations, as might exist in high performance aircraft, it becomes necessary to think in terms of how the man-machine interface is impacted by the stress. This is particularly obvious when considering direct vibration and/or accleration effects on control motions and display adequacy. The concept of interface stress-resistance must be kept in mind. An illustration of these interface effects was given earlier (Section 2.1.1.4 and Figure 2-15) in the discussion of vibration feedthrough to a spring stick as compared to a stiff stick.

2.3 BUFFET PROTECTION MEASURES

As stated above, the best protection against buffet is prevention. Various solutions to buffet protection, including active and passive seat isolators, have been proposed and investigated. All methods have drawbacks, depending on the frequency to be protected against.

Figure 2-21 (Ref.2-37) illustrates acceleration transmissibility curves for several seat and cushion configurations. It is seen that for all the configurations tested protection is afforded at high frequencies. However, at low or intermediate frequencies amplification is the rule. Although cushions and other elastic dampers are effective for increasing comfort and visual performance in the higher frequency ranges, they are not practical for use in current fighter aircraft because: (a) large displacements are required at low frequencies (for example, 12.5 cm at 2 Hz, 0.7 g rms); (b) bottoming out occurs at high levels of sustained G; and (c) excessively increased acceleration onset rates that can cause spinal injuries are experienced at the time of bottoming out during the ejection sequence. In addition, the Y axis would not be affected by cushions or other elastic dampers and there would be a problem with in-cockpit tasks due to the differences in phase angle between motions of the cockpit instruments and the pilot (Ref.2-38).

Calcaterra (Ref.2-39) has described an active isolation system in which feedback controls provide inputs to an electrohydraulic seat isolator. The system was shown to provide 80% vibration isolation at frequencies above 5 Hz. However, there is a considerable weight penalty involved with such a system and there is as yet no provision for Y axis motion isolation. This active isolator was tested to explore its effect on tracking performance. As shown in Figure 2-22 (Ref.2-38), it was found that, using a horizontal tracking task and vertical sinusoidal vibration, tracking performance was degraded at very low frequencies with the isolator and was essentially unchanged at the higher frequencies. Similar results were found for a vertical tracking task.

Thus it appears that the best vibration alleviation techniques currently available primarily involve adequate pilot restraints and seating design to minimize excessive relative cockpit-pilot motion and aircraft design improvements/modifications to prevent vibration/buffet onset. For example, strategically placing the pilot's seat at a structural vibration nodal point could minimize vibration effects by decreasing the amplitude of the pilot's motion.

2.4 CONCLUSIONS

The considerable literature on vibration effects on human performance is difficult to translate directly into useful generalized design parameters for maneuvering combat aircraft. Figure 2-23 briefly summarizes the state of knowledge of vibration effects.

There is preliminary evidence that the effects of buffet (vibration) on the pilot's tracking performance may be of minor importance in the presence of sustained acceleration. This evidence does not negate the need for continued research into the effects of vibration on other mission segments such as low altitude high speed flight or the need to further validate these preliminary findings.

Total system analysis is needed to determine the relative effects of buffet on the pilot per se versus the deterioration in handling qualities in the buffet region prior to the initiation of major design exercise to improve human combat tracking performance by buffet compensation.

CHAPTER 3

FLOW FIELD ASPECTS OF TRANSONIC PHENOMENA

by

B.Monnerie

3.0 INTRODUCTION

Chapter 1 described the difficulties a pilot may encounter in transonic maneuvering flight. Let us try to explain the origin of these problems by examining the aerodynamics of a wing in the transonic speed regime. What happens? What are the flow features? What are the means for understanding what happens? How can we predict what happens?

The results of numerous research studies on transonic flows conducted all over the world during the last twenty five years are used in this chapter. Many points are drawn from Reference 3-1, a quite recent comprehensive overall description of transonic maneuvering problems and a survey/evaluation of analytical methods prepared by Gentry and Oliver under contract to the US Office of Naval Research.

3.1 THE TWO-DIMENSIONAL CASE

Because of the complexity of transonic aerodynamic phenomena, it is useful to first examine the case of a two-dimensional airfoil. One can have a good idea of the phenomena by looking at the evolution of the pressure distribution on the airfoil when the free stream Mach number increases from low values to supersonic ones. Despite the fact that this evolution is quantitatively dependent on the type of wing section chosen, the main lines of what we observe are general.

We start at low free stream Mach numbers with an entirely subsonic flow distribution over the airfoil. There is a stagnation point near the leading edge, then the flow expands and accelerates to a maximum speed, and finally it recompresses and slows down near the trailing edge. For a free stream Mach number value called the critical Mach number, the speed of sound is reached at some point on the airfoil (Fig.3-1). For higher free stream Mach numbers a small supersonic zone develops in the region around this point. Initially the recompression can be isentropic but soon it must be made through a shock wave. This shock moves downstream as the free stream Mach number increases and, generally, its intensity increases simultaneously.

3.1.1 Drag Rise and Pitch Up

Without going into more details we can now understand two major difficulties encountered when an aircraft's speed approaches Mach 1. The first is the rapid increase in drag, called the drag divergence, associated with the development of the shock wave. The drag, starting at a low value in subsonic flight (the drag is zero for a perfect non viscous flow in the subsonic regime), increases rapidly when strong shock waves develop in the flow field.

The second difficulty is due to differences between the shock movements on the upper and lower surfaces of the airfoil at angles of attack when the free stream Mach number increases. For classical wing sections a shock first appears on the upper surface, but the one which appears later on the lower surface moves downstream faster as the Mach number increases and consequently reaches the trailing edge before the shock on the upper surface. Thus there is a loss of lift over the rear portion of the airfoil and a corresponding positive (nose up) pitching moment. At free stream speeds near Mach 1 the upper surface shock also reaches the trailing edge and the magnitude of the nose-up pitching moment decreases. This phenomenon occurs earlier – that is to say at lower Mach number – for higher angles of attack and the resulting pitching moment curve, for a given Mach number, shows a typical kink which is characteristic of a loss in longitudinal stability, named pitch-up and due to positive values of $dC_m/d\alpha$.

The explanation given above for the pitch-up occurrence does not expose the real reasons why the upper surface shock does not go regularly and rapidly downstream. The main reason is the occurrence of flow separation due to the fact that the boundary layer cannot bear the recompression imposed on it by the shock.

3.1.2 Different Types of Separated Flow Regions

Separation is one of the most important features of transonic flows. Most transonic troubles, and especially buffeting, are closely related to the presence of more or less extended regions of separated flow. Many types of separated flow regions may exist and Figure 3-2 presents the main ones:

- Airfoil A shows a shock free leading edge laminar separation. This separation is basically similar to that which can occur in an incompressible flow.
- Airfoil B depicts a total leading edge separation.
- Airfoil C has a turbulent boundary-layer separation produced by shock-recompression with subsequent re-attachment of the flow behind the bubble.
- On airfoil D the flow does not reattach behind the bubble.
- In the case of airfoil E there is a shock induced separation bubble with downstream flow reattachment. However, the turbulent boundary layer is sufficiently deenergized that it separates again before reaching the trailing edge.
- Airfoil F depicts several different separation effects occurring together, a combination which may occur with certain airfoil geometries.

3.1.3 Upstream Mach Number and Angle of Attack Effects

Figure 3-3 shows the evolution of the pressure distribution with Mach number and the corresponding flow patterns. The development of an aft separated region does not prevent the rearward movement of the shock but slows it down.

The typical evolution of the pressure distribution with angle of attack at a given Mach number is presented in Figure 3-4. As the angle of attack increases the shock first moves aft and becomes more intense. Due to the effects of the stronger shock, a bubble of increasing size is created, producing a thicker boundary layer and wake behind the trailing edge. When the bubble has extended to the trailing edge the shock moves forward. This situation can be obtained either by a downstream extension of the shock induced bubble or by a forward movement of the trailing edge separation region. For still larger angles of attack the flow separates at the leading edge. It should be noted that as soon as a bubble of some size has been created, the trailing edge pressure, previously at a constant level, begins to decrease. The lowest trailing edge pressure occurs when the bubble is largest. This phenomenon is used to detect noticeable separated regions and is named "trailing edge pressure divergence".

3.1.4 Shock Boundary Layer Interaction Problems and Reynolds Number Effects

In the previous two typical evolutions for increasing Mach number or angle of attack we have seen shocks, sometimes strong, moving on the airfoil. These shocks act directly on the boundary layer and the resulting effects depend on the boundary layer characteristics (thickness and shape factors) and the shock intensity.

In any case the boundary layer is thickened by the shock interaction. If separation does not occur, the effects are minor. However, if a separated region is formed, even if flow reattachment occurs downstream, the consequences can be important. The resulting boundary layer is greatly thickened and destabilized, and therefore is less able to overcome the trailing edge recompression. This explains why the effect of Reynolds number can be so large on transonic flows and why it is not easy to improve the situation by using transition devices. To accurately simulate the flight condition one must restore the correct boundary layer thickness and shape factor. For this reason it may be necessary to adjust the transition trips (type, position, size) for each particular flight condition (Mach number, Reynolds number, and angle of attack).

Figure 3-5 shows the effect of Reynolds number on the pressure distribution for a symmetrical airfoil at zero angle of attack. For the lowest Reynolds number there is a typical laminar shock boundary layer interaction with a quite large bubble. The recompression is spread out over nearly 40 per cent of the chord length. At a larger Reynolds number (0.66×10^6) the interaction region decreases. For still higher Reynolds numbers there is a turbulent shock boundary layer interaction without separation, and the pressure distribution becomes Reynolds number independent.

Reynolds number effects can be even more spectacular for cases where the flow is near separation when it reaches the trailing edge. In these situations the change in the shock position due to the upstream extension of the trailing edge separated region is affected by the Reynolds number. Therefore to study and understand what happens in flight it is very important to be able to perform wind tunnel tests at Reynolds numbers as close as possible to flight Reynolds numbers.

3.1.5 Flow Visualizations

As will be discussed later in this chapter, detailed theoretical evaluations of transonic viscous separated flows are beyond present capabilities. This is the reason why experimental investigation techniques are of considerable interest. Many types of techniques may be employed to obtain information, and these will be examined systematically

in connection with three-dimensional flows. In this section we discuss only those techniques which are more specific to two-dimensional flows, namely the optical methods. In these visualization techniques the variation with density of the air index of refraction is used to examine phenomena and characteristics in the air flow.

Several optical devices exist which allow visualizations wherein lines represent constant values of either:

- the density (interferometry)
- the gradient of density (Schlieren),
- the second derivative of density (direct shadow method).

Interferometry can be exploited quite easily to provide quantitative measurements in the flow field. This is an attractive method because the results are free of probe interference effects and concern the whole flow field. Figure 3-6 is an example of the quantitative use of an interferometer photograph (Ref. 3-2).

Figure 3-7 presents a series of Schlieren photographs showing the evolution of the shock position with Mach number for a NACA 0012 airfoil at angles of attack of 0 and 4 degrees (the pressure distributions over this airfoil at 4 degrees angle of attack are shown in Figure 3-1). The large separated region occurring at high Mach numbers is easily observed in the Schlieren photographs.

3.1.6 How to Delay the Transonic Troubles

The transonic troubles discussed in the previous sections can be delayed by modifying either the airfoil or the planform of the wing. Concerning the airfoil two possibilities exist:

- alter the airfoil shape, for airfoils of the same family with the same relative thickness distribution, by reducing its maximum thickness. Transonic similarity rules indicate that benefits can be expected from reduced thickness.
- use airfoil sections specially designed to overcome the difficulties. This is why much work is done to design new airfoil sections such as peaky profiles, supercritical profiles (see Figure 3-8) and shockless profiles (Refs 3-3 to 3-5).

The other way to delay the transonic problems is to modify the wing planform by using leading edge sweep. It is well known, both theoretically and experimentally (Ref. 3-6), that the transonic events are related to the Mach number normal to the leading edge ($M_\infty \cos\phi$ if ϕ is the sweep angle) and therefore occur at higher free stream Mach numbers if the wing planform has a swept leading edge.

3.2 THREE-DIMENSIONAL FLOWS

It is difficult to present general considerations on three-dimensional flows because nearly each case is a particular one due to the numerous parameters necessary to completely characterize a wing: aspect ratio, taper ratio, sweep angle, thickness, camber and twist distribution. Nevertheless, wings can be classified into main categories depending on one of the most important parameters – the mean sweep angle. The categories are: (a) wings with low sweep, including unswept wings; (b) swept wings, and (c) highly swept or slender wings. Typical values for the sweep angle for each category can be given, for example 5, 30 and 60 degrees, but it is impossible to establish precise limits for each category because for intermediate sweep angle values considerations of other parameters such as aspect ratio or angle of attack then determine the main characteristics of the air flow.

Concerning wings with low sweep, except for low aspect ratio and twisted wings they have flow patterns which are practically two-dimensional (Ref. 3-7). All that has been discussed in the previous sections apply to wings with low sweep.

3.2.1 Swept Wings

For swept wings the situation is much more complicated, involving an inextricable and apparently unpredictable mixture of shock waves, vortex systems, strong spanwise flows, boundary layer separation and reattachment. However, thanks to patient and numerous wind tunnel studies using pressure measurements as well as wall visualization techniques, a quite good quantitative understanding has been obtained in some cases.

The typical flow pattern for moderately swept wings at moderate angles of attack is shown in Figure 3-9. It is the basic three shock system. The forward shock, originating near the leading edge of the wing root, is oblique and goes downstream towards the tip. The rear shock, originating from the trailing edge of the wing root, goes upstream towards the tip. These two shocks meet and merge together to form a single stronger shock, the outboard shock.

For increasing angles of attack the forward shock moves downstream and the rear shock moves upstream so that the intersection point moves nearer the root section and the portion of the wing influenced by the outboard

shock increases. This is very important because, due to its strength, the outboard shock produces a flow separation generally extending to the trailing edge (airfoils C and D in Figure 3-2). Hence when the angle of attack increases the separated region behind the outboard shock spreads from the tip towards the root. For larger angles of attack the separation line moves forward to the leading edge (airfoil B in Figure 3-2) and the separated region tends to be organized into a vortex. Finally, the flow is completely separated and organized into a vortex originating from the wing apex.

The existence of large separated flow regions on the wing explains most of the transonic troubles:

- the force and moment curves are strongly perturbed, the lift gradient diminishes, the drag increases, and losses in longitudinal stability and large rolling moments may occur.
- the steadiness of the flow is completely altered because the separated flow regions are places where turbulence and vorticity are created in large quantities, producing high pressure fluctuation levels which excite the aircraft structure and provoke buffeting. Figure 3-10 shows the correlation between the increase with angle of attack of the pressure fluctuations measured with two KULITE gauges located near the trailing edge and the trailing edge static pressure divergence already mentioned in Section 3.1.3 as an indicator of flow separation. The intensity of the pressure fluctuations depends on the type of flow in the separated region and especially whether or not it is organized into a vortex. The factors affecting the existence and location of a vortex system are shown in Figure 3-9.

3.2.2 Highly Swept Wings

The three-dimensional flow pattern of wings in the highly swept or slender category is such that at low angles of attack the flow is already separated along the leading edge and rolled up to form a well organized coiled vortex sheet. Aft of this vortex the flow reattaches to the wing surface and the whole separation pattern is a very orderly one. No significant buffeting is caused except possibly at extremely high angles of attack, depending on the sweep angle and the leading edge sharpness, when the vortex core may burst over the wing surface.

3.2.3 Experimental Means of Study

The available understanding of the very complicated transonic three-dimensional flows is based almost completely on experimental work and it is useful to review the available investigation techniques. However, it must be pointed out again that experimental results are representative of what occurs in flight only if the flight Reynolds number is sufficiently well simulated in the tests.

The most accurate means of investigation is static pressure measurements. However, this is a heavy and expensive technique because a large number of measurement points are required and the wind tunnel model is sophisticated and time-consuming to construct. In addition, the interpretation of the resulting measurements is not always obvious and recourse to other means is needed.

A very efficient means of investigation is provided by flow visualization techniques. The idea behind these techniques is to reconstitute the flow structure on a wing by observing the path followed by particles deposited on the wing surface. Many processes have been used and they all give similar results. These techniques can be classified into two classes:

- those in which a viscous substance, generally with an oil base, is spread on the wing surface. An example is shown in Figure 3-11 where the results for two different wings can be compared (Ref. 3-8).
- those in which a fluid is injected through small holes in the wing surface. Figure 3-12 presents photographs obtained using this technique (Ref. 3-9).

The photographs in Figures 3-11 and 3-12 are for swept wings and illustrate what has been discussed previously about the three-dimensional flows for these wings.

Another source of useful information, especially for buffeting studies, is provided by unsteady measurements. Previous sections have discussed the use of unsteady static pressure measurements, but it should be noted that these are even more expensive than mean static pressure measurements because a special gauge is needed for each measurement point. However, they do furnish information of prime importance on the sources of buffeting. Skin friction gauges may also be useful. Figure 3-13 presents the typical evolutions of hot film signals from two locations on a wing as the angle of attack is continuously increased. It is clearly seen when the separated flow region moves over the two gauges.

3.3 PREDICTION METHODS

In previous sections it has been pointed out that viscous effects are of great importance in transonic flows and, particularly, all the phenomena which cause troubles and which we would like to be able to predict are due to viscous

effects. Since the direct solution of the Navier-Stokes equations is, up to now, completely out of reach for this purpose, we must resort to an indirect step-by-step solution. As a first step we try to predict the inviscid flow characteristics. Then, using these results, it will perhaps be possible to predict the viscous effects as is done for subsonic flows.

3.3.1 Inviscid Flows

Progress has been made since the publication of Reference 3-1, at least for two-dimensional flows, and several methods for transonic supercritical two-dimensional flow calculations have become operational. The time dependent or unsteady methods have been developed and have been improved in their efficiency to reach the steady limit by simplifying the terms containing the temporal derivatives (pseudo unsteady method of Reference 3-10) or by time splitting the finite difference operators (Ref. 3-11). These methods have the advantage of solving the exact equations of rotational non-isentropic flows and consequently giving shocks which verify the Rankine Hugoniot relations. However, the computation times remain very long and the methods cannot be used for routine design calculations but only for reference calculations for comparison purposes with the results of other methods.

In the mean time two other methods have successively become operational. The first one, proposed by Murman and Cole in Reference 3-12 and further developed in References 3-13 to 3-15, solves the transonic small perturbation equation by a relaxation technique. The second method treats the full potential equation after having made a conformal mapping of the flow field inside a circle (Garabedian and Korn, References 3-16 and 3-17, and Jameson, Reference 3-18). Both methods have been intensively tested, especially the second one for which a computer program has been published in Reference 3-17. Since the computation times for both methods are comparable, the second one, which uses the full potential equation, seems more attractive for an isolated airfoil. However, the first method is able to treat the case of an airfoil placed between two walls. The two methods often give quite similar results (Fig. 3-14) and agree generally well with experiments (Fig. 3-15).

It should be noted that work is being done to improve the accuracy and to decrease computation times in the solution of the perfect flow equations. In particular, better enforcement of the shock conditions has been obtained recently for the small perturbation relaxation method by Murman (Ref. 3-19). Figure 3-16 shows that this new treatment brings the small perturbation results closer to the more exact results of the unsteady method. This gives hope for obtaining good agreement with experimental data when viscous effects will be taken into account.

In conclusion, one can say that these methods constitute a tool which is able to favorably replace the Sinnott procedure for predicting supercritical pressure distributions.

For three-dimensional flows the situation is somewhat less advanced. Bailey and Steger (Ref. 3-20), Isom and Caradonna (Ref. 3-21), Ballhaus and Bailey (Ref. 3-22) and after them others (Refs 3-23 to 3-25) have succeeded in computing pressure distributions over three-dimensional wings using either the transonic small perturbation equation or the full potential equation. The first results are encouraging (Fig.3-17), but not enough comparisons are available to draw general conclusions. In other respects, it must be noted that the computation time is still too long for routine design calculations. In References 3-26 to 3-28 one will find recent general reviews of computational methods for two-dimensional and three-dimensional transonic flows. For lack of suitable transonic three-dimensional methods, subsonic three-dimensional ones such as the vortex lattice method or the Woodward method will give reasonably good results if significant supercritical flows are not present (Ref. 3-1).

3.3.2 Viscous Flows

The main problem in predicting transonic flow characteristics is the strong coupling between the inner boundary layer and the outer inviscid flow in a region of shock boundary layer interaction. Experimental pressure distributions through a shock are smooth while those computed for an inviscid fluid are steep. This is the reason why, in order to perform a boundary layer calculation, one must change the theoretical distribution obtained for an inviscid flow in a quite arbitrary manner. Using this technique Thomas and Redecker (Ref. 3-29) have succeeded in predicting buffeting limits with some success, but the generality of their results is questionable.

Work is being done to improve the situation by simultaneously calculating the boundary layer and the outer inviscid flow (Klineberg and Steger Reference 3-30). This approach appears promising, but more work needs to be done.

3.4 CONCLUSIONS

The brief review of transonic phenomena which has been presented in this chapter shows that most transonic troubles, and particularly buffeting, are due to the presence of more or less extended regions of separated flow. These are directly or indirectly related to the shock waves which form on the aircraft in the transonic speed regime.

From the theoretical point of view, prediction of transonic phenomena is probably one of the most difficult problems in aerodynamics. Although much progress has been made during the last five years in transonic flow

computations, considerable effort is still needed to be able to theoretically predict flows with separated regions as complicated as those shown in Figures 3-11 and 3-12. Thus the prediction of what will occur in flight still must rely on wind tunnel tests.

We have seen how the transonic phenomena are very dependent on Reynolds number. Consequently, the quality of current flight performance predictions is bounded by our capability to obtain realistic Reynolds numbers in existing wind tunnels. Taking into account the continuous increase in flight Reynolds number due to increasing aircraft size, there is a need for higher Reynolds number wind tunnels.

CHAPTER 4

DYNAMIC RESPONSE OF AIRCRAFT STRUCTURE

4.0 INTRODUCTION

As discussed in the previous chapters, buffeting and other transonic phenomena which degrade combat capability are caused by shock induced flow separation on components of the aircraft, usually on the wing. Separated flow is always associated with random fluctuating pressures. These pressures force the aircraft structure to respond, usually with pronounced peaks at its natural frequencies. The resulting induced structural vibrations produce unsteady air forces which interact with the separated flow, causing movements of the shock waves which further excite the structure.

The purpose of this chapter is to give some insight into the physical and mathematical problems associated with the response of elastic structures to random excitations and to provide some tools for calculating the vibration levels of any part of the aircraft, e.g., wing tip, wing root, pilot's seat, etc. The two frequently cited transonic phenomena in this context, "buffeting" and "wing rock", may be interpreted as low to medium frequency symmetric and low frequency antisymmetric aircraft responses to unsteady separated flow forces.

This chapter is composed of three main sections contributed by separate authors. Section 4.1 discusses the general dynamic system consisting of the aircraft structure, the aerodynamic driving forces due to separated flow, and the aerodynamic forces due to aircraft structural motion. A general so-called "buffeting flutter model", which takes into account the interactions between the separated and motion induced flows, is presented. Relaxations of this model with regard to the flow interaction and which lead to the familiar "forced vibration model" are explained.

Section 4.2 deals with the structural and aerodynamic quantities of the dynamic system with special emphasis given to the description of the aerodynamic forces. The state-of-the-art of similarity laws, scaling effects and wind tunnel testing are outlined.

Finally, Section 4.3 reviews methods for data processing of fluctuating pressure recordings and discusses techniques for response analysis for random excitation. Comparisons are presented of results from flight tests and predictions for a fighter type aircraft.

The aerodynamic forces must be considered as the "weak link" in any approach to predict buffet levels by structural response calculations. The fluctuating pressures in separated flow regions on a wing force the flow, both in the separated regions and in the attached regions by induction, to behave oscillatory. This produces high unsteady loads associated with oscillations of the flow separation lines of the shock positions and consequently exites the wing structure. Therefore, for unsteady buffet pressure measurements on wind tunnel models which are to provide the aerodynamic input for structural response calculations it is believed important

- to adequately simulate the expected stall progression flow pattern of the full size aircraft, and
- to use flexible models in order to obtain the flow hysteresis effects during limit cycle oscillations.

Naturally, careful selection has to be made of the essential similarity laws which are mainly given by the Mach number, Strouhal number, Reynolds number, Froude number, and mass density. The essential similarity laws must be obeyed in order to permit reliable extrapolations to full scale, which is mandatory. The technology seems to be well established for obtaining the correct structural dynamic characteristics in wind tunnel models used for this purpose.

Based on comparisons between predictions and flight test results, there is good cause to believe that the rigorous approach to predict buffet levels, by solving the full dynamic equations using random pressure measurements from wind tunnel tests, is the right way to treat the problem. However, further progress in improving wind tunnel modeling techniques is necessary.

4.1 THE DYNAMIC SYSTEM by R.J.Zwaan

In this section an overall description is given of analytical models of a flexible aircraft in buffeting conditions. This subject has been considered recently in a number of investigations, especially at the Royal Aircraft Establishment, United Kingdom (References 4-1 and 4-2).

4.1.1 DESCRIPTION OF THE DYNAMIC SYSTEM

The aircraft is considered to be in a flight condition in which the flow separates locally at one or both wings. The irregular flow is coupled with pressure fluctuations at the aircraft surface, perceptible inside and sometimes also outside the regions of flow separation. The pressure fluctuations excite the aircraft and its structure responds with an oscillatory motion, being in general the superposition of rigid-body motions and structural vibration modes, each with its own resonance frequency and its own pattern of nodes and antinodes.

Following here a common practice in aeroelastic analysis, the rigid-body modes together with the structural resonance modes as they would occur at zero speed are taken as generalised co-ordinates to describe any arbitrary time-dependent displacement $w(x)$ of the aircraft in a body-fixed axis system:

$$w(x, t) = \sum_{n=1}^{N} f_n(x) q_n(t) . \tag{4-1}$$

In this expression $f_n(x)$ denotes the mode shape of the n-th mode and $q_n(t)$ is the generalised co-ordinate indicating the contribution of the n-th mode in the total displacement w.

The action of each degree of freedom is associated with inertia forces and, as far as structural deformations are involved, with structural stiffness and damping forces. The aerodynamic forces on the aircraft surface are distinguished into forces which depend on the oscillatory motion of the aircraft and forces which are independent of the motion. All these forces are in a dynamic equilibrium for each degree of freedom. This equilibrium can be expressed mathematically by the following differential equations:

$$M_n \ddot{q}_n(t) + D_n \dot{q}_n(t) + \omega_n^2 M_n q_n(t) + F_{D_n}(\dot{q}_1(t) \ldots . \dot{q}_N(t)) + F_{K_n}(q_1(t) \ldots . q_N(t)) = P_n(t) ,$$

$$n = 1 \ldots . N \tag{4-2}$$

where

M	generalised mass
D	structural damping
ω	resonance frequency
$\omega^2 M$	structural stiffness
F_D	motion-dependent aerodynamic damping
F_K	motion-dependent aerodynamic stiffness
P	motion-independent aerodynamic force

A derivation of Equation (4-2) is not given here, but reference is made to current literature on aeroelasticity (References 4-3 to 4-5) and to the AGARD Manual on Aeroelasticity (Ref. 4-6).

Equation (4-2) shows that the structural forces are linear with the generalised co-ordinates q_n, which remains valid as long as the q_n's are fairly small. The aerodynamic forces F_D and F_K may be nonlinear. As a consequence of the specific choice of resonance modes to act as degrees of freedom, there is no coupling between the inertia and stiffness forces. The only coupling is of an aerodynamic nature. This is illustrated in Figure 4-1 for a system with two degrees of freedom, showing that the aerodynamic forces generated by the one mode can also excite the other one, and conversely. However, if the resonance frequencies are well separated the aerodynamic coupling can be neglected, so that the system works as two one-degree-of-freedom systems.

The resonance mode shapes and the corresponding values of M_n, D_n and ω_n can be determined by calculations and in ground vibration tests. Methods to do so are indicated in Section 4.2. These values pertain normally to the 1 g condition. However, they may change at high C_N values, especially the values of the structural damping, due to an accommodated settlement of the structure.

4.1.2 ANALYTICAL MODELS FOR BUFFETING AIRCRAFT IN SEPARATED FLOW

The major difficulty in analysing buffeting problems by using Equation (4-2) is the fact that appropriate

knowledge about the aerodynamic forces is still lacking. Previous chapters should have made it clear that the nature of separated flow is very complicated and that the influence of parameters like Mach number and angle of attack, which do not depend on aircraft osillatory motions, is far from completely understood. In this chapter the primary discussions concern the influence of aircraft motions due to flow separation, especially separation occurring on wings and tail surfaces. A proper understanding of the flow mechanisms involved in separation is also incomplete. An adequate aerodynamic theory is not available to describe this mechanism, and there do not exist generally accepted model testing procedures that yield the data to represent the aerodynamic forces in Equation (4-2).

As a consequence of this uncertainty at the present time an analytical model for a buffeting aircraft in separated flow of which the general applicability has been proven in practice does not exist. So far two types of analytical models have been proposed, the forced vibration model and the buffeting flutter model, of which the first one has been applied already in a number of investigations. In the following sections both models are discussed.

4.1.2.1 Forced Vibration Model

The motion-dependent forces F_D and F_K in Equation (4-2) are considered to be linear with motion and to be unaltered by the separated flow, i.e., they have the same values as in attached flow. The assumption of linearity requires that the amplitudes of the aircraft motions should be small.

The motion-independent force P is a function of time only and is generated by flow separation. It has a random character, i.e., the force is the result of pressure fluctuations at the aircraft surface which are more or less ordered in time and space. The random fluctuations need not be confined to the separated flow region itself. If the separated flow extends over significant parts of the wing surface, including especially part of the trailing edge, the circulation along the whole wing span may become fluctuating, being perceptible also outside the separated flow region.

This model is basically the same model as that commonly used in gust analysis, except that the aerodynamic excitation in the latter case is provided by atmospheric turbulence.

Description of the pressure fluctuations, which are considered usually as stationary Gaussian random processes, is possible in terms of correlation functions (time domain), spectral density functions (frequency domain), and root mean square values. Definitions of these quantities are given in Section 4.3.2 (see also Reference 4-7).

A simple example is discussed here to illustrate the effect of random pressure fluctuations on the aircraft response.

Consider a mechanical system with one degree of freedom, e.g., a wing bending mode. Applying the spectral density formulation, Equation (4-1) takes the form:

$$\Phi_q(\omega) = |H(\omega)|^2 \Phi_p(\omega) \tag{4-3}$$

in which the transfer function $H(\omega)$ is given by

$$H(\omega) = [-\omega^2 M + i\omega D + \omega_f^2 M + i\omega F_D(\omega) + F_K(\omega)]^{-1} \tag{4-4}$$

$|H(\omega)|$ shows a peak near $\omega = \omega_f$, of which the width is mainly governed by $D + F_D(\omega)$. Φ_q and Φ_p are the power spectra of the structural response and the pressure fluctuations respectively, both as functions of the frequency ω. Denoting the bending mode shape by $f(x)$, in which x represents the co-ordinates on the wing surface. Φ_p is defined by the following double integral:

$$\Phi_p(\omega) = \int_{\substack{\text{wing}\\\text{surface}}} f(x_1)\,dA_1 \int_{\substack{\text{wing}\\\text{surface}}} f(x_2)\,\Phi_{p_1p_2}(\omega; x_1, x_2)\,dA_2 \tag{4-5}$$

$\Phi_{p_1p_2}$ is the cross-spectrum of pressure fluctuations at the points x_1 and x_2. The correlation in time is represented by $\Phi_{p_1p_2}$ as a function of ω and the correlation in space for a certain value of ω is represented by $\Phi_{p_1p_2}$ as a function of x_1 and x_2.

If in the pressure fluctuations at all points of the wing surface a certain frequency ω_0 is distinctly dominating, the cross-spectrum $\Phi_{p_1p_2}$ and consequently also the power spectrum Φ_p will take a narrow-band form centered at that frequency. In the limiting case of a perfect correlation in time the spectra of the pressure fluctuations would contain only one frequency. On the other hand, if no frequency dominates, the spectrum of Φ_p is wide-band. In practice Φ_p will be somewhere between these cases. In wind tunnel investigations it has been found sometimes that for low sweep wings in subsonic flow the existence of a peak can be related to the dimensions of the separated flow region (Ref. 4-8). For swept wings in transonic flow correlation has been found with oscillating fore-and-aft shock motions (Ref. 4-9).

The consequences of the type of input spectrum Φ_p on the resulting aircraft motion are illustrated in Figure 4-2. Considering once again the model represented by Equations (4-3) and (4-4), the aircraft structure acts like a filter with a resonance frequency near ω_r. Due to the peak in $|H(\omega)|$ a peak in the output spectrum Φ_q also appears.

A significant response of the aircraft structure is to be expected when ω_0 and ω_r coincide. This may happen in practice when the wing oscillation has some sort of regulating influence on the fluctuations in the separated flow. Such a process is discussed in the next section. Besides the correlation in time the magnitude of Φ_p is also governed by the spatial correlation of the pressure fluctuations at the wing surface. Outside the separated flow region the fluctuations are mainly due to wing oscillations, so that the cross-spectrum $\Phi_{p_1p_2}$ between points x_1 and x_2 will be narrow-band. However, if one of the points is shifted into the region of separated flow, the cross-spectrum will become more wide-band. Furthermore, the spatial correlation is weighted by the mode shape $f(x)$, as is indicated by Equation (4-5). Figure 4-3 illustrates that the action of pressure fluctuations, and consequently the contribution of $\Phi_{p_1p_2}$ to Φ_p, is most effective in regions well away of the nodal lines.

So far the forced vibration model has been employed several times to analyse results of model tests and flight tests (References 4-1 and 4-9 to 4-11). The main purpose is to extract information about the motion-dependent and motion-independent aerodynamic forces from the measured pressure fluctuations at the wing surface and the measured model or aircraft responses. In one particular case full-scale predictions have been given on the basis of wind tunnel results (Ref. 4-2). Applications of the forced vibration model are discussed extensively in Sections 4.2 and 4.3. If experimental information about the motion-dependent forces is absent, calculation methods commonly used in flutter investigations (lifting-surface theory) may be applied. Examples can be found repeatedly in the mentioned references.

4.1.2.2 Buffeting Flutter Model

The relatively scarce experimental results of model tests concerning the aerodynamic forces in Equation (4-2), especially for transonic flow, do not always confirm the correctness of the forced vibration model. Both wind tunnel and flight test results have shown (Ref. 4-8) that at buffet onset the damping force $D + F_D$ increases rapidly from its attached flow value and falls off again at C_N values corresponding to moderate buffeting. A typical result derived from Reference 4-8 is shown in Figure 4-5. These results obviously invalidate the assumption in the forced vibration model that the motion-dependent forces are considered to be unaltered by flow separation. In Reference 4-1 the suggestion is made that when the amplitudes of the aircraft oscillations increase, some mechanism in the flow induces a larger ordering of the pressure fluctuations in time, so that as a consequence the power spectrum Φ_p becomes more narrow-band. When the amplitudes are large enough the driving force P has gone over essentially into F_D and F_K, so that the total aerodynamic force depends in a deterministic way on aircraft motion. The relationship is nonlinear in general so that a disturbance in motion will result in a limit-cycle oscillation. Because this model closely resembles the model used to describe conventional flutter in the case of attached flow, the motion may be typified as buffeting flutter (Ref 4-5). The difference with the forced vibration model is made clear once more by the block-diagrams in Figure 4-4.

The considerations concerning the buffeting flutter model find their origin probably in the ample experience with flow past fixed and oscillating circular cylinders and also objects with irregularly shaped cross-sections, where the amplitudes of the oscillating motion transverse to the flow direction have a distinct synchronising influence on the vortex shedding in the wake. In turn the vortices exert regulated forces on the oscillating object, so that the motion becomes in fact self-excited when the oscillation amplitude is large enough and develops generally into some limit-cycle oscillation.

At transonic speeds such a regulating mechanism may be amplified by the coupling of up- and down-stream shock motion, shock-induced separation and wing oscillatory motion.

No applications of the buffeting flutter model are known to exist in recent investigations. The point is that application of this model in its pure deterministic form might even be unrealistic. The forced vibration model and the buffeting flutter model actually are two extremes, between which any practical case may be supposed to lie.

As an illustration, Figure 4-6 shows a typical result, derived from Reference 4-1, concerning the influence of a pitching motion on wing load fluctuations for a low speed wind tunnel model. The oscillating motion of the wing causes a peak in the load spectrum, but the point to be noted is that the energy content at neighbouring frequencies has been decreased.

Although the continuous transition from the forced vibration model to the buffeting flutter model with increasing amplitude has been described here by words, a mathematical description of the dynamical system would be necessary in order to proceed to further investigations and possibly to arrive at an unification of both models.

4.2 STRUCTURAL AND AERODYNAMIC QUANTITIES OF THE DYNAMIC SYSTEM, SIMILARITY LAWS, AND MODEL TESTING by P.W.Hanson

4.2.1 SURVEY

The dynamic system under discussion is quite complex and although buffet phenomena have received much attention from investigators, the state-of-the-art to definitively predict analytically or experimentally the complete structural response and handling characteristics as the buffet boundary is penetrated leaves much to be desired. (Reference 4-12 presents a reasonably complete bibliography and summarizes briefly information available on buffet loads on airplanes to about 1959. From the mid-fifties to the mid-sixties much buffet loads research, particularly in the United States, was oriented toward missiles and space launch vehicles configurations. Reference 4-13 lists many reports pertinent to this work.)

One of the characteristics of this area of research or study is a lack of generally accepted definitions of terms, expressions, and phenomena. There can be, therefore, a sort of "communication gap" among investigators in this field unless care is taken to define the expressions and concepts of the phenomena being discussed. At the risk of some repetition of material in other chapters of this report, a brief review of certain aspects of the "dynamic system" being discussed here will first be presented. The important structural and aerodynamic quantities of the system will then be discussed. A theoretical model will be presented which relates these quantities to each other, and then they will each in turn be considered in terms of the state-of-the-art of determining the quantities, and in terms of areas where further research is needed. The similarity laws and scaling relationships applicable to determining buffet structural response will then be presented and areas where simplification is required or may be permissible will be mentioned. Finally, the various types of model tests pertinent to predicting response of the aircraft structure to buffet flow will be discussed.

4.2.2 PERSPECTIVE OF THE DYNAMIC SYSTEM

The "dynamic system" consists of two parts – a flexible aircraft structure, and an unsteady aerodynamic force field that acts on, or interacts with, the aircraft structure to produce undesired motions, either in terms of dynamic structural deformations, "rigid body" movements, or a combination of both. The unsteady aerodynamic force field may exist without the presence of the aircraft (i.e., atmospheric turbulence) or may be the result of the presence of the aircraft. The latter is the case to be discussed here. These unsteady (generally random) aerodynamic forces are caused by flow separation from the aircraft surface, either due to high incidence or due to shock-boundary layer interactions; or by turbulent wakes from upstream surfaces or protuberances. The flow that produces these unsteady aerodynamic forces is termed "buffet flow".

The aircraft response to buffet flow (buffeting) may be categorized as local (i.e., panel vibration), structural (whole surface deformations – wing, fuselage, tail surfaces), and "rigid body". The rigid body response to buffet flow will be discussed in Chapters 5 and 6 on Stability and Control. The discussions here will mainly be concerned with structural response to unsteady flow fields that are the result of the presence of the aircraft, i.e., response of the aircraft to atmospheric (or wind tunnel) turbulence is minimal compared to the response to buffet flow. This is not to say that local response is not important. Local panel response is believed to have caused the destruction of the first unmanned Mercury-Atlas launch vehicle, and on airplanes, panel response can be a source of noise discomfort and skin fatigue.

Two areas of buffet flow or buffeting are of interest – the "buffet onset" flight conditions, and the level of intensity of structural loads and rigid body motions as the penetration into the buffet region (in terms of increasing angle of attack or Mach number) continues. Buffet onset will be addressed later in Part III of this report. In the following sections attention will be confined primarily to the response of the structure as the buffet boundary is penetrated.

4.2.3 STRUCTURAL AND AERODYNAMIC QUANTITIES OF THE DYNAMIC SYSTEM

Certain fundamental quantities of the dynamic system have to be determined or considered to predict aircraft buffet loads from either theoretical/empirical methods or from scaled model tests. It may be instructive therefore to consider briefly a theoretical model that relates structural response to the random aerodynamic forces of buffeting flow.

4.2.3.1 Theoretical Model Depicting Important Aerodynamic and Structural Quantities

For illustrative purposes consider a wing (or other surface) flying at constant altitude with constant velocity under flight conditions that are producing buffet flow. The only aerodynamic forces considered present in addition to the random component are damping forces proportional to the velocity of the bending vibrations of the wing. Little loss of generality results from neglecting the aerodynamic inertia and "spring" forces, since such forces usually

are small compared with their structural counterparts. Under these conditions a set of differential equations which govern the bending vibration characteristics of the system may be written

$$M_n\ddot{Z}_n(t) + C_n\dot{Z}_n(t) + \omega_n^2 M_n Z_n(t) = qS\int_0^1 c_L(\xi, t)h_n(\xi)d\xi \quad (n = 1, 2, 3, \ldots) \tag{4-6}$$

where

ξ	nondimensional spanwise coordinate
$Z_n(t)$	deflection of a point (say the tip) in n^{th} bending mode
t	time
C_n	generalized damping coefficient in n^{th} bending mode, including aerodynamic and structural components
M_n	generalized mass in n^{th} bending mode
ω_n	natural circular frequency in n^{th} bending mode

The right hand side of Equation (4-6) is the generalized random aerodynamic load expressed in coefficient form. The function $c_L(\xi, t)$ is the random section lift coefficient and S, q, and $h_n(\xi)$ are, respectively, reference area, free stream dynamic pressure, and mode shape of the n^{th} bending mode referred to unity at the tip. Using the method of generalized harmonic analysis which was first applied to the analysis of buffeting many years ago (Ref. 4-14), Equation (4-6) can be solved approximately for the mean square tip deflection

$$y(t)^2 = q^2S^2\sum_{n=1}^{\infty}\frac{\Pi\,\omega_n}{4M_n^2\omega_n^4\left(\frac{C}{C_{cr}}\right)_n}C_{L,n}(\omega_n) \tag{4-7}$$

where

$\left(\frac{C}{C_{cr}}\right)_n$	generalized damping coefficient, fraction of critical damping for the n^{th} mode
$C_{L,n}(\omega_n)$	power spectrum of effective random aerodynamic list coefficient for the n^{th} mode
S	reference area

It has been assumed that the system has small damping and reasonably well separated natural frequencies so that all contributions to the total response are small except in the neighborhood of resonant frequencies. Thus, modal coupling is considered negligible so that the total response can be considered a linear superposition of single-degree-freedom responses.

In buffeting studies on elastic structures, usually the acceleration or bending moment at some point on the structure is desired rather than the deflection of the structure. By using Equation (4-7) and a set of coefficients which relate the acceleration in the n^{th} bending mode at a point to the tip amplitude in that mode an expression for the acceleration may be obtained

$$a^2(\xi_0)_T = S^2q^2\sum_{n=1}^{\infty}\frac{k_n}{M_n^2}\frac{1}{\left(\frac{C_a}{C_{cr}}+\frac{C_s}{C_{cr}}\right)_n}\hat{C}_{L,n}(k_n) \tag{4-8}$$

where

$a(\xi_0)_T$	total root-mean-square acceleration at a particular location
k_n	reduced frequency ratio for n^{th} natural vibration mode, $k_n = \frac{b\omega n}{V}$ where b reference length, mean wing chord V free stream velocity
$\left(\frac{C_a}{C_{cr}}+\frac{C_s}{C_{cr}}\right)_n$	sum of aerodynamic and structural damping in n^{th} vibration mode, fraction of critical damping
$\hat{C}_{L,n}(k_n)$	power spectrum of effective random aerodynamic lift coefficient expressed as a function of reduced frequency, $\hat{C}_{L,n}(k_n) = \frac{V}{b}C_{L,n}(\omega_n)$

Thus, the acceleration is dependent on the aerodynamic excitation force in the form of the power spectrum of effective random aerodynamic lift coefficients, the aerodynamic and structural damping, the generalized mass and reduced frequency of each vibration mode of significance. The manner in which these quantities are usually determined will now be discussed.

4.2.3.2 Unsteady Aerodynamic Excitation Forces

Although there has been some apparent success in calculating the buffet onset conditions for relatively large aspect ratio wings at moderate angles of attack (Reference 4-15, for instance) the situation is quite different for the prediction of buffet load intensities in fully developed buffet flow, particularly for fighter aircraft wings with large sweep angles and small aspect ratio operating at high angles of attack at high Mach numbers. The problem is primarily the lack of an appropriate aerodynamic theory for calculating the random aerodynamic excitation forces, $\hat{C}_{L,n}(k_n)$, in the theoretical model just discussed. For this reason investigators have generally turned to wind tunnel tests for the unsteady pressure distributions needed to provide the buffet aerodynamic excitation forces for the dynamic analysis. The information required to fully describe the random aerodynamic forces are the magnitude and frequency spectrum of the unsteady pressures, their locations and effective area of coverage on the surface, and a pattern of spatial correlation which can be represented by cross-correlation or cross-spectra functions. Although there have been numerous investigations dealing with turbulent boundary layers, separated flow, and shock-boundary layer interaction (References 4-16 to 4-18, for example) the studies have generally been oriented toward measurement of intensities of pressure fluctuations beneath attached turbulent boundary layers at supersonic speeds with very limited analysis of power spectra and spatial correlation data applicable to the separated flow found on a maneuvering high performance figher wing. Most such studies in the past have dealt with the flow over space launch vehicles and missiles. Some of the more immediately applicable studies are reported in References 4-2 and 4-19 to 4-21. One of the more detailed recent studies of aircraft buffet flow during transonic maneuvers is discussed in Reference 4-9. Comparisons are given in Reference 4-19 of root mean square pressure coefficients, $\Delta C_{p_{rms}}$ (root mean square fluctuating pressure divided by free stream dynamic pressure), measured on a "rigid" wind tunnel model and those measured on the full scale airplane wing at two corresponding locations. An example of these comparisons is shown in Figure 4-7. The model pressures were generally somewhat higher than the full scale pressures. A sample comparison of model and full scale pressure spectral shape taken from Reference 4-19 is shown in Figure 4-8. It was concluded that the model and airplane spectral shapes agreed reasonably well for most of the test conditions. The disparities were apparently greatest at the lower end of the spectrum. Some other conclusions of this study pertinent to the unsteady aerodynamic excitation forces are: (1) at high angles of attack the flow over the wing was quite complex, being influenced strongly by vortices from the leading edge, "snag", and wing tip; (2) disturbances seemed to emanate from multiple sources simultaneously and propagate in a complex manner; (3) the fluctuating pressure spectra frequently exhibited peaks at frequencies believed to be associated with the vortices; and (4) maximum fluctuating pressure coefficients were generally of the order of $\Delta C_{p_{rms}} = 0.2$.

Digressing for a moment to the wind tunnel model/full scale rms pressure coefficient comparisons, one may speculate on several reasons for the differences. There is, of course, always the nagging doubt about Reynolds number effects, tunnel turbulence and wall effects. Then, there is the difference in the manner in which the variation of unsteady pressure with angle of attack is achieved. (The mean angle of attack in the tunnel is essentially steady, whereas in flight, particularly at the higher speeds, the angle of attack is continuously changing.) A more fundamental question is whether the unsteady aerodynamic excitation forces on a rigid (nonmoving) wing are the same as those on an identical but flexible (responding) wing. That is, does the tendency of the flexible wing to move with the driving force tend to reduce those forces relative to the forces acting on a nonmoving surface? Some definitive experiments are needed to answer this question. J.G.Jones in Reference 4-1 discussed in some detail the interpretation of fluctuating pressures associated with separated flow measured on nonmoving and responding wings for evaluation of the unsteady aerodynamic excitation forces, and in Reference 4-22, L.E.Ericsson presents a semi-empirical analysis that uses static experimental data as an input to attempt to explain some of the dynamic effects of shock-induced flow separation.

4.2.3.3 Aerodynamic and Structural Damping

Another factor needed to predict quantitatively the response of the structure to buffet flow is the total system damping which can be broken down into two components – aerodynamic and structural, neither of which can be readily determined explicitly at buffet flight conditions. The aerodynamic damping is itself a function of flight condition (density and velocity), mean angle of attack, and oscillation frequency (Ref. 4-23). A simplified relationship between these parameters and the aerodynamic damping ratio $\frac{C_a}{C_{cr}}$ developed in Reference 4-23 for a wing oscillating in the fundamental bending mode is

$$\frac{C_a}{C_{cr}} = \frac{\Pi \rho V F_e \cos \bar{\alpha} \int_0^L [h_1(y)]^2 dy}{2\omega_1 M_e} \tag{4-9}$$

where

ρ	free stream density
V	free stream velocity
$\bar{\alpha}$	mean angle of attack about which oscillation occurs
ω_1	first natural frequency

M_e	equivalent mass
c	local chord
$h_1(y)$	first bending mode shape
L	wing span
F_e	effective value of aerodynamic damping coefficient

It has been common practice in scaling buffet loads from one flight condition to another to assume that, other factors being equal, the aerodynamic damping ratio is proportional to (ρV) and sufficiently greater than the structural damping so that the structural damping is negligible (References 4-24 and 4-25 for example). Under these assumptions it may be seen from Equation 4-8 that for a particular mode the root mean square acceleration response is proportional to the square root of the dynamic pressure. If, on the other hand, it is assumed that the only significant damping is structural, then the rms response is directly proportional to the dynamic pressure. The true case, of course, is somewhere between these two extremes. The relative magnitudes of aerodynamic and structural damping is subject to some contradiction in the literature. There is some experimental evidence that at least for long slender bodies, such as launch vehicles, the rms buffet response is inversely proportional to the square root of total damping as indicated in Equation 4-8. For example, Figure 4-9 is based on results from Reference 4-26 where the total damping of a launch vehicle aeroelastic buffet model was varied electromagnetically under wind-on conditions. The relative changes in rms buffet bending moment, σ_Δ/σ, with relative changes of total damping

$$\left[\frac{\frac{C_a}{C_{cr}} + \frac{C_s}{C_{cr}} + \frac{\Delta C_s}{C_{cr}}}{\frac{C_a}{C_{cr}} + \frac{C_s}{C_{cr}}}\right]^{1/2}_n$$

for the first bending mode of one configuration and the first three bending modes of a second configuration are shown to follow reasonably well the curve defined by

$$\left[\frac{1}{\frac{C_a}{C_{cr}} + \frac{C_s}{C_{cr}}}\right]^{1/2}$$

Figure 4-10 from Reference 4-24 showing the variation of rms wing root bending moment with density at constant Mach number (measured on an F-86A fighter) indicates the response to be proportional to $(q)^{1/2}$ so that the damping must be primarily aerodynamic in nature. Figure 4-11 from Reference 4-25 compares rms bending moments measured on geometrically identical model wings made from aluminum and from magnesium with calculated values scaled from bending moments measured on a geometrically identical but much stiffer wing made from steel. The experiment was designed so that some of the many parameters which are of importance in buffeting such as Mach number, Reynolds number, and reduced frequency were held essentially constant so that other factors, such as effects of damping on scaling relationships, could be evaluated. The data are presented for three different scaling relationships used to scale the data from the steel model: in Figure 4-11(a) both aerodynamic damping (calculated after Reference 4-23) and structural damping (measured under no-wind conditions) were used in the scaling relationship; in Figure 4-11(b) aerodynamic damping only was used; and in Figure 4-11(c) only structural damping was used. It was concluded that the prediction based on aerodynamic damping only, which apparently contained compensating inaccuracies, provided values of buffeting loads which were closer to the measured values than those predicted by the more complete analysis including both structural and aerodynamic damping. There is other evidence (References 4-27 to 4-29, for example) to suggest that wing damping of solid metal wind tunnel models is predominantly structural. It is apparent tha the character of system damping in buffet flow needs further study.

Attention will now be turned to some of the more common means of determining damping. Analytical methods of determining aerodynamic damping are almost exclusively confined to empirical means based on measurements or based on aerodynamic theories applicable to attached subsonic or supersonic flow that bears little relation to flow experienced beyond the buffet boundary. Structural damping is usually measured under "no-wind" conditions by various methods, as is total damping under flight or wind-on conditions. The aerodynamic damping is taken to be the difference between "wind-on" and "wind-off" damping. It is worth mentioning that both structural and aerodynamic damping may very well be amplitude dependent so that in deducing aerodynamic damping from total damping measurements care should be taken that wind-on and wind-off measurements are made at the same amplitude or that the variation with amplitude is established.

Various methods of determining damping are presented in the literature (References 4-23 and 4-30 to 4-33, for example). Reference 4-31 contains a general review of experimental techniques that are discussed in some detail. A complicating factor in the measurement of damping under separated flow conditions, however, is the random response of the model, i.e., the damping generally must be measured as statistical means averaged over many cycles. A recently devised technique (Ref. 4-33) known as "random-dec" appears to be particularly attractive for determining

total damping under either full scale or wind tunnel model buffet flow conditions. Basically, the method extracts the damped sinusoidal response of the structural vibration modes from the total structural response to either an externally applied force or, more importantly, to the random buffet excitation forces. By averaging the measured response over a number of time-sweeps that are started at a given response amplitude, the response of the system to a "step input" is determined. (The measured response of the system can be considered to be composed of the response to a step, an impulse, and a random force. The response to an impulse and to a random force average to zero.) Damping is obtained in the same way as from a free vibration decay since the decrement or "random-dec signature" is representative of the free vibration decay curve which would be obtained if the structure were displaced to the selected amplitude and suddenly let go. For single-degree-of-freedom linear systems excited by white noise, the random-dec signature is identical in form to the autocorrelation function, but for multi-degree-of-freedom systems and nonlinear systems, it differs in that troublesome cross-products which occur in the autocorrelation of closely coupled modes are absent. Real systems, of course, contain many modes and several techniques can be used to reduce the response to an effective single-degree-of-freedom system for each mode of interest. Figure 4-12 (Ref.4-33) shows an example of two forms of analysis from which damping measurements may be made. Figure 4-12(a) shows the spectral density for an isolated mode obtained by Fast Fourier Transform of the time history of the response of a flat plate to thick turbulent boundary layer flow. The difficulty of determining damping by measuring the band-width of the half-power point is obvious. Figure 4-12(b) shows the random-dec signature for the same data set with damping measurements obtained from the well-known equation

$$\xi = \frac{1}{2\Pi N} \ln \frac{Y_2}{Y_1} \quad .$$

Note the consistent values of ξ_{sys} for N = 1, 2, and 3. It is concluded in Reference 4-33 that for systems with modes closely spaced in frequency, application of the technique is not so straightforward and that further work is needed to define the limitations and precision of measurements for such cases.

4.2.3.4 Generalized Mass

The final modal factor to be determined for the determination of buffet response from application of dynamic relationships such as Equation (4-8) is the generalized mass. (The reduced frequency, k , is simply a function of modal frequency.) Mass effects appear in the structural analysis of dynamic systems in the form (for a planar system)

$$M_n = \iint m(x, y)\, h_n^2(x, y)\, dx\, dy \qquad (4\text{-}10)$$

where

M_n	generalized mass associated with mode n
x, y	physical coordinates
$h_n(x, y)$	normalized deflection at x, y
$m(x, y)$	mass per unit area at x, y

The integral can be evaluated for each mode by using either a known mass distribution and mode shape which have been determined experimentally or analytically; or the generalized mass can be determined directly by experimental means if the structure exists. A widely used method (Ref. 4-34) considers the change in frequency caused by the addition of a small mass. Briefly, if the generalized stiffness of the n^{th} vibration mode is defined as

$$K_n = M_n \omega_n^2$$

where ω_n is the natural frequency of the n^{th} structural mode, and if it is assumed that the addition of a small known mass, ΔM , does not change the generalized stiffness, then

$$K_n = (M_n + \Delta M\, h_{n,\Delta}^2)\, \omega_{n,\Delta}^2$$

where

$h_{n,\Delta}$	ratio of modal deflection at point where incremental mass is added to deflection at station for which generalized mass is desired
$\omega_{n,\Delta}$	natural frequency of n^{th} mode with added mass ΔM

therefore

$$(M_n + \Delta M\, h_{n,\Delta}^2)\, \omega_{n,\Delta}^2 = M_n \omega_n^2$$

or

$$M_n = \frac{\Delta M\, h_{n,\Delta}^2}{\left(\frac{\omega_n}{\omega_{n,\Delta}}\right)^2 - 1}$$

For each mode, ΔM is known and $h_{n,\Delta}$, ω_n and $\omega_{n,\Delta}$ are measured. In practice, it is convenient to plot $\Delta M\, h_{n,\Delta}^2$ as a function of

$$\left(\frac{\omega_n}{\omega_{n,\Delta}}\right)^2 - 1$$

for various values of ΔM. The slope of this curve, evaluated over the linear portion near zero, is the generalized mass. Difficulty may be experienced in applying the method if the modes are not well separated or if the damping is large. The author of Section 4.2 is not aware of any recent significant advances that have been made in this area.

4.2.4 SIMILARITY LAWS AND SCALING RELATIONSHIPS

The similarity laws and scaling relationships for predicting from wind tunnel model tests the response of the full-scale airplane structure (in terms of root mean square accelerations, bending moments, etc.) to buffet flow conditions will now be discussed. The similarity requirements will first be considered on the basis of what is necessary to predict quantitatively the response of specific aircraft configurations as contrasted to requirements for "trend studies". Then suitable relaxations of these requirements dictated by practical considerations and a more liberal interpretation of scaling relationships to meet less stringent objectives will be discussed.

4.2.4.1 Relative Importance of Similarity Laws

In principle, a model that meets the similarity requirements for flutter testing will also be suitable for direct scaling of buffet response to full scale values. (However, there are considerations, to be discussed later, in addition to similarity requirements that make the design and construction of a dynamically scaled aeroelastic buffet model more difficult than a similar flutter model.) Discussions of the basic requirements for achieving dynamic similarity of model and full scale aircraft abound in the literature (References 4-35 to 4-38, for example) and will only be reviewed here briefly as they apply to transonic buffet loads studies. The similarity requirements are generally deduced by applying the Buckingham II theorem of dimensional analysis or by examining the appropriate governing equations in non-dimensional form. For a flexible body completely immersed in a fluid with relative motion between the body and the fluid these procedures result in independent nondimensional parameters which may be thought of as ratios of the potentially significant inertia, viscous, elastic, and gravity forces that act on the body and fluid. The more important ones to be considered are:

(1) $\dfrac{V}{a}$ Mach number, M

(2) $\dfrac{b\omega}{V}$ reduced frequency, k

(3) $\dfrac{m}{\rho b^2}$ mass density ratio

(4) $\dfrac{\rho V b}{\mu}$ Reynolds number

(5) $\dfrac{V^2}{bg}$ Froude number

where

a	fluid free stream speed of sound
V	fluid free-stream velocity
ρ	fluid free-stream density
μ	fluid free-stream dynamic viscosity
g	acceleration due to gravity
b	characteristic length
ω	characteristic oscillation frequency
m	body mass per unit length

These five basic independent dimensionless parameters result from several assumptions regarding characteristics of the body and the fluid, i.e.: (1) the fluid is compressible and behaves as a perfect gas but the velocity range is low enough so that effects of kinetic heating are insignificant; and (2) the body is completely immersed so that surface tension effects may be ignored. Implicit in the five basic parameters is another, the ratio of the specific

heat of the fluid, γ, and if dissipative forces are considered a further parameter, the ratio of structural damping to critical damping, C_s/C_{cr}, may be added. From these basic similarity parameters other dependent ratios relating model quantities to full scale quantities may be derived. If these dimensionless parameters have the same values for the model and the full scale aircraft and the mass, stiffness, and to a lesser degree the damping distributions are the same for the model and full scale aircraft, then the flexible and rigid body response or behavior of the model will be similar to the aircraft providing the model is geometrically similar to the aircraft, orientation to the airflow is similar to that of the aircraft, and the model supported in a manner that does not significantly affect the model response or behavior.

The simultaneous satisfaction of all the similarity parameters in a single model or test is not practical. The degree to which the various parameters may be ignored or approximated is a function of the test objective and the available tunnel performance. For example, if the purpose of the test is to determine buffet response at high angles of attack at relatively low speeds the Mach number need not be the same, whereas, for response at high speeds the model and airplane Mach numbers should definitely be simulated. The gravitational parameter is not usually simulated except for studies where static deflections or aeroelastic deformations are important. Full scale values of Reynolds number are quite difficult to achieve because of wind tunnel performance limitations and the conflicting requirements of other similarity parameters. Viscous flow phenomena, including boundary layer type, thickness, and separation conditions are influenced in varying degrees by the value of the Reynolds number, and so this parameter would appear to be somewhat more significant for buffet studies than for flutter tests. Although the locations of local shocks and the commencement of local separated flow may be Reynolds number dependent in varying degrees depending on the particular aerodynamic configuration, there is some experimental evidence to suggest that the integrated effects on the structural response and even on total lift may be small. For example, in Reference 4-20 which compares buffet pressures measured in flight with wind tunnel data (Reynolds number range approximately 3–20 million), it is concluded that for a sharp unswept wing at Mach numbers to 0.7 Reynolds number effects were small. Figures 4-13 and 4-14 taken from Reference 4-39 provide some further evidence from wind tunnel/flight comparisons. The data are from measurements made on a complete dynamically scaled aeroelastic buffet model being flown on a cable mount system at model Reynolds numbers of 0.87 to 1.33 million compared to flight values of 20 to 28 million. (The Reynolds numbers mentioned on page 10 of Reference 4-39 are, in fact Reynolds number per foot rather than absolute values as stated.) Figure 4-13 compares the model and full scale variation of normal force coefficient, C_N, with angle of attack well beyond the buffet boundary. The model and airplane values are seen to agree reasonably well except for the 72 degree sweep case. Figure 4-14 compares model and airplane buffet onset (in terms of normal force coefficient) and buffet boundary penetration as a function of Mach number. Again, the model predicted buffet boundary agrees well with flight values except for the high sweep condition. Thus, although the locations of local shocks and commencement of separated flow may have been different for the airplane and model, their integrated effects on the structural response apparently were small, at least for the lower sweep cases. Reynolds number effects on aerodynamic simulation are discussed extensively in Reference 4-40. Just how much the Reynolds number requirements may be relaxed for buffet flow conditions has not been conclusively established in the literature, and further studies are needed. For the present, because of wind-tunnel performance limitations, practical model fabrication considerations, and the overriding importance of testing the model at a mass-density ratio comparable to that of the airplane, no attempt normally is made to simulate Reynolds number in high speed flutter models and the same compromise has to be made for high speed buffet response models. From similar considerations the gravitational parameter (Froude number) is usually ignored.

The total damping is certainly an important parameter in structural response buffet tests. Unfortunately, modeling technology has not advanced to the point where it is possible to simulate full scale structural damping (even assuming it is known) so attempts are usually limited to keeping the model structural damping to reasonably small fractions of critical damping. The rationale is that the structural damping is a relatively small part of the total damping and therefore its significance is lessened. This assumption is not always valid, of course. For example the buffet boundary may be quite close to the flutter boundary in which case the aerodynamic damping might be very small indeed.

The ratio of specific heats similarity parameter is generally automatically satisfied when the model tests are conducted in air. (The satisfaction of this parameter provides similarity in the compressible behavior of the gas under adiabatic conditions and is necessary for exact similarity of the flow pattern.) However, tests in gases heavier than air offer several advantages including easier model construction, higher Reynolds numbers, and lower tunnel power requirements (see Reference 4-41 and 4-42, for example), and there is evidence that it is not always necessary to satisfy this condition for Mach numbers less than about 1.4. (Freon-12 is routinely used in the NASA Langley Research Center Transonic Dynamics Tunnel for flutter and buffet response tests.) However, for tests where local shock location is critically important the parameter can be significant.

For buffet model response studies with the objective of predicting full scale buffet loads quantitatively the mass density and reduced frequency similarity parameters are as important as they are in flutter proof-tests, and much effort is made to have these parameters the same for model and full scale aircraft. At best, however, the parameters are strictly satisfied in a single model only for the tunnel/flight conditions chosen as the design point. It is generally assumed that the slight deviations from these parameters caused by testing at conditions not far removed from the design point do not significantly affect flow-response similarity and that the resulting model measurements

at a particular velocity (or Mach number for high speed tests) may be scaled to other altitudes or densities by application of suitable scaling relationships

4.2.4.2 Scaling Relationships for Structural Response

Once a geometrically similar model has been constructed so that the stiffness and mass distributions are similar to the full scale aircraft, and the values of stiffness and mass are reasonably close to the values dictated by the similarity parameters, for the model measurements to be useful to predict full scale structural loads the necessary buffet response scaling relationships must be known. The theoretical buffet model which relates the various important structural and aerodynamic quantities (Equation (4-8) in Section 4.2.3.1) may serve as a basis for developing a scaling relationship for root-mean-square buffet acceleration. Taking the subscript r to indicate airplane-to-model ratio, and subscripts M and A to refer to model and airplane quantities respectively, Equation (4-8) may be written

$$a^2(\xi_o)_{T,A} = b_r^4 q_r^2 \frac{1}{m_r^2} \sum_{n=1}^{\infty} k_{n,r} \left[\frac{\left(\frac{C_a}{C_{cr}} + \frac{C_s}{C_{cr}}\right)_{n,M}}{\left(\frac{C_a}{C_{cr}} + \frac{C_s}{C_{cr}}\right)_{n,A}} \right] [\hat{C}_{L,n}(k_n)]_r \, a^2(\xi_o)_{n,M} \qquad (4\text{-}11)$$

where the generalized mass, M_n, has been replaced by the physical mass ratio, m_r (since the full-scale and model shapes are optimally identical).

For a dynamically scaled aeroelastic buffet model that meets the similarity requirements so that it responds in vibration modes similar to those of the aircraft the terms $k_{n,r}$ and $[\hat{C}_{L,n}(k_n)]_r$ optimally will be unity when the model is tested at design point flow conditions. Because of variations of the speed of sound in the wind tunnel with respect to the speed of sound in flight the actual reduced frequency, $k_{n,r}$, will vary slightly from unity and, therefore, the term will be retained for increased scaling accuracy since it is readily measurable. Although the power spectrum of the effective random aerodynamic lift coefficient ratio, $[\hat{C}_{L,n}(k_n)]_r$, is a function of reduced stiffness, for small variations it is assumed to remain at unity. At the scaling design point flow conditions, the damping term in brackets in Equation (4-9) will normally be very near unity for dynamically scaled aeroelastic models with relatively low structural damping. However, this is not true for model test conditions removed from the design point, or for tests in flow conditions where the aerodynamic damping is relatively small, unless the model and airplane structural damping are identical. The value of the damping term may be evaluated by measuring the model aerodynamic damping and structural damping, calculating the airplane aerodynamic damping from the relationship– $\left(\frac{C_a}{C_{cr}}\right)_{n,A} = \left(\frac{\rho V b^2}{m \omega_n}\right)_r \left(\frac{C_a}{C_{cr}}\right)_{n,m}$ (see Reference 4-23, for example) and estimating or measuring the airplane structural damping. The reduced frequency ratio, $k_{n,r} = \frac{b_r \omega_r}{V_r}$, is generally taken to be the same for all modes (although in practice there is usually some variation in frequency ratio, ω_r, for the various modes). Equation (4-11) may therefore be written

$$a^2(\xi_o)_{T,A} = b_r^4 q_r^2 k_r \frac{1}{m_r^2} \sum_{n=1}^{\infty} \frac{1}{(C_T/C_{cr})_{r,n}} a^2(\xi_o)_{n,M} \qquad (4\text{-}12)$$

where

$$\left(\frac{C_T}{C_{cr}}\right)_{r,n} = \frac{\left(\frac{C_a}{C_{cr}} + \frac{C_s}{C_{cr}}\right)_{n,A}}{\left(\frac{C_a}{C_{cr}} + \frac{C_s}{C_{cr}}\right)_{n,M}} .$$

An expression similar to Equation (4-12) can be derived for the airplane root-mean-square buffet bending moment at a particular location

$$\sigma^2(\xi_o)_{T,A} = b_r^6 q_r^2 k_r \sum_{n=1}^{\infty} \frac{1}{(C_T/C_{cr})_{r,n}} \sigma^2(\xi_o)_{n,M} \quad . \qquad (4\text{-}13)$$

Actually it is not generally possible to measure directly the bending moment $\sigma(\xi_o)_{n,M}$ or acceleration $a(\xi_o)_{n,M}$ buffet response of the model in a particular mode. Rather, the total response at a particular location $\sigma(\xi_o)_M$ is measured and the "modal composition" of the indicated response is estimated from power spectra. Several conditions are inferred in this application of the scaling relationships: (1) the "natural vibration modes" of importance in the total response can be identified, are well separated, and are lowly damped; (2) the total measured model response can be treated as a summation of individual modal responses,

that is $$\sigma^2(\xi_o)_M = \sum_{n=1}^{\infty} \sigma^2(\xi_o)_{n,M}$$

and (3) the structural and aerodynamic damping of the modes are known or can be estimated. Further, it should be noted that Equations (4-12) and (4-13) relate measurements made on the model at a particular location to full scale values at the same location. If full scale maximum response values are desired (as is usually the case) and for some reason the measurements are made on the model at a location different from that where the maximum bending moments or accelerations occur or if a distribution of the loads is desired from a single location measurement, then a measurement location "sensitivity factor" must be determined for each contributing vibration mode. This may be accomplished in principle by calculating the bending moment and/or acceleration distributions due to inertia loading per unit deflection for motion in each mode.

4.2.5 MODEL TESTING

Rigorous application of buffet scaling relationships such as Equations (4-10) and (4-11) is seldom possible so that certain simplifying assumptions are usually required, depending on the type and purpose of the test. There are basically two different methods of quantitatively predicting aircraft buffet response: (1) measure buffet accelerations or strains on a dynamically scaled aeroelastic model (References 4-39 and 4-43, for example) and (2) measure the pressure fluctuations on a nominally rigid model and then calculate the dynamic response when these pressures act on the flexible structure (Reference 4-2, for example). Each method has its advantages and disadvantages. The practical application of these and other relationships will now be discussed for several types of buffet studies.

4.2.5.1 Dynamically Scaled Aeroelastic Models

The most direct approach for predicting full scale buffet response loads with a minimum of scaling assumptions is the measurement of the buffet responses of a reduced size dynamically scaled aeroelastic model supported in wind tunnel flow that accurately simulates the airflow over the airplane in a manner such that the model and airplane degrees of freedom and inertia loads are properly related. In theory, buffet response predictions based on this approach should be the most accurate of the several methods to be discussed. In practice, it is impossible to meet all the above requirements and certain assumptions still are required concerning the significance of the effects of parameters over which little control can be exercised. For instance, pitch rate effects are usually assumed to be negligible for rates applicable to a maneuvering aircraft. Also, it is usually necessary to assume that wind-on mode shapes are essentially the same as wind-off shapes, that there are no significant differences in model and airplane mode shapes that are important in the buffet response, and that the model and airplane structural damping in a particular mode is independent of vibration amplitude, temperature, and flow conditions. A major disadvantage of the approach is the complex and costly modeling requirements, but some conditions or circumstances make the dynamically scaled aeroelastic model test the desirable approach. For instance, when a complete flutter model is required or is desirable for flutter proof tests to minimize expensive flight flutter testing, the extra expense required to make the model suitable for buffet loads testing (primarily due to strength and instrumentation considerations) may be acceptable. The approach may also be desirable when components other than the wing are considered to be buffet critical. When a maneuvering aircraft "penetrates the buffet boundary" each part of the aircraft experiences its own boundary. Although attention is usually focused on the wing response as a function of increasing angle of attack, for example it is possible that an all movable horizontal tail, suddenly deflected for an abrupt pull-up maneuver, may be the first component to experience buffeting conditions. In fact, there have been several instances where the design loads on tail surfaces have been exceeded due to buffeting. Although the horizontal tail is normally considered to be the critical tail component, during recent wind-tunnel buffet studies on a fighter airplane it was found that the critical components at high angles of attack were the vertical tails which were vibrating primarily in a torsion mode. Of course, when buffeting flow is encountered anywhere on the aircraft the entire structure responds, with the load or acceleration intensities varying over the aircraft according to its structural characteristics. The highly maneuverable high performance fighter, typically flown well into the buffet boundary, and subject to buffet flow due to shock-boundary layer interaction, high angle of attack, and wake impingement presents a formidable challenge to predict the response characteristics. It has generally been found that even for these conditions, the critical consideration is not the wing buffet loads but rather (1) vibrations which subject fire control, navigation and reconnaissance equipment, instruments, and crew to a more severe operational environment and increase fatigue; (2) degradation of performance through increased drag and decreased lateral stability which detracts from tracking capability; and (3) as mentioned previously, excessive structural loads on tail and control surfaces.

When complete aircraft buffet response acceleration and load predictions are required, the dynamically scaled aeroelastic model test would seem to offer the best hope of obtaining suitable data. This technique has been evaluated in Reference 4-39 by comparing the scaled buffet bending moments and accelerations measured on a 1/8-scale flutter model of a variable-sweep fighter airplane with those measured in a flight buffet research program (Ref. 4-44). The model was "flown" on a cable mount system with a lift balancing device which counteracted the lift in excess of the model weight, thus allowing the model to be flown under conditions simulating high load factors (neglecting inertia and rate effects, of course). Figure 4-15 is a schematic representation of the system which was designed to provide a relatively constant low level spring rate so that the model could respond in rigid and elastic body dynamic motions with a minimum of restraint.

Figure 4-16(a) compares the airplane buffet response with model-predicted values (using scaling relationships shown in Equations (4-12) and (4-13)) of wing and horizontal tail rms bending moments and rms accelerations at the center of gravity. The data are typical in that the full scale buffet bending moments on the wing and horizontal tails and the c.g. buffet accelerations predicted from the model data agreed well with airplane values at all Mach numbers at a wing sweep angle of 26°. At a wing sweep angle of 50° the agreement was reasonably good at all Mach numbers tested for the wing bending moments, but the correlation of the model and airplane c.g. accelerations and horizontal tail bending moments was not as good at the higher Mach numbers. At 72° sweep, Figure 4-16(b), both the airplane and model data exhibit a large degree of randomness at extremely low levels of buffet response which make evaluation of the correlation difficult.

Figure 4-17 shows sample comparisons of the model and airplane wing and horizontal tail bending moment response spectra. For the horizontal tail the model response is primarily in the horizontal tail first symmetry bending mode with secondary response in the fuselage vertical bending mode. Unpublished airplane spectra indicate that the primary response varied between horizontal-tail bending and fuselage vertical bending depending on flight condition and whether the right or left tail was being considered. For the wing the model and airplane spectra are almost identical with the response of both being primarily in the first symmetrical bending mode. It is this characteristic of wing buffet response that makes possible the use of much simplified models (to be discussed next) under certain conditions to estimate full scale wing response. Except for the wing, however, power spectral density analyses of the model response to buffet flow showed that the indicated modal composition of the total measured response was dependent on the type and location of the measurement, wing sweep angle, Mach number, and, in some cases, the depth of penetration into the buffet region.

4.2.5.2 Stiff but Responding Models

In the dynamically scaled aeroelastic model approach to predicting absolute values of full scale buffet loads the reduced stiffness and mass density similarity ratios and the stiffness and mass distributions are satisfied by design so that, assuming an adequate model, the modal response of the model is identical to that of the full scale airplane. Therefore, all the quantities needed in Equation (4-11) to scale model response loads to full scale values are either identically unity or can be explicitly measured or calculated except for full scale structural damping. Variants of this approach may be used to gain insight into the buffet phenomena, to investigate the validity of certain assumptions made in theoretical modeling, and to estimate relative intensity levels and boundary penetration characteristics of different geometrical configurations. For instance, considerable information may be deduced about wing buffet onset conditions and the relative rise in response intensity with buffet boundary penetration by measuring the wing bending moment response of conventional "semi-rigid" wind tunnel models (References 4-24, 4-45, and 4-46). This method may be valid when the conventional wind tunnel model wing first bending mode is similar in shape and scaled frequency to that of the full-scale aircraft and the model structural damping is reasonably low. One must also assume the response of the wing is in the first bending mode only, and that the responses of other components of the structure are isolated and do not influence the response of the component being evaluated. The use of this type of model is generally restricted to wing buffet studies – primarily for buffet onset, but in some instances for load intensities as the buffet boundary is penetrated or the aerodynamic configuration changed. Buffet onset predictions have generally been good using this technique. The prediction of absolute buffet loads on wings has met with varying degrees of success, likely depending on the relative magnitudes of model structural and aerodynamic damping, mass density ratio, and tunnel turbulence levels. The method has been used since the early fifties but wind tunnel/flight correlation buffet loads data are sparse. Figures 4-18(a) and 4-18(b) from Reference 4-24 and Figure 4-18(c) from Reference 4-47 are indicative of results achieved using this technique.

A refinement of this approach that makes use of "stiff" conventional models to predict maximum flight penetration buffet boundaries is suggested in Reference 4-46. The basic hypothesis is that the tunnel turbulence or unsteadiness (which must be known in terms of unsteady pressure or flow angle power spectra) can be used as a given level of aerodynamic excitation to calibrate the model response at the wing fundamental frequency, and hence to derive buffeting coefficients from buffet strain measurements on the wing. Figure 4-19 from Reference 4-8 illustrates a recent test of this hypothesis. The method is discussed fully in Chapter 7 on Buffet Definition and Criteria.

4.2.5.3 "Rigid" Buffet Pressure Models

Both the dynamically scaled aeroelastic model approach and tests on "stiff" but responding models make use of measurements of model response to predict full scale buffet characteristics. A completely different approach makes use of measurements of buffet fluctuating pressures on "rigid" models to predict analytically the full scale buffet loads on the flexible aircraft. The term "rigid" is meant to imply that no significant model response mode occurs at frequencies in the vicinity of the scaled frequency at which buffeting intensity is to be predicted on the full scale aircraft. The method, briefly outlined here, will be discussed in some detail in Section 4.3 of this chapter. Basically the method entails (1) the measurement of the unsteady pressure distribution on the rigid model in terms of root-mean-square pressure levels on prescribed areas, power and crosspower spectral density functions and correlation functions; (2) definition of the dynamic characteristics of the aircraft analytically or by vibration tests; (3) combining pressure and modal displacement data to yield the buffet forcing function; and (4) applying the forcing function to the elastic system to compute the required buffet response loads and displacements. The practical application of the method requires many assumptions at each stage, particularly in the generation of the buffet forcing function, and requires that an estimate of the aerodynamic damping be available. This approach has been used (Ref. 4-2) to

calculate buffeting at low speeds of a slender wing with a leading-edge vortex. A modification to this approach has been used in Reference 4-48 to calculate the buffet response of a swept wing fighter at transonic speeds. A 1/10 scale conventional wind tunnel model was used in this series of tests designed to learn as much about the buffet flow field as possible. Here the "rigid" model did have scaled frequencies near those of the full scale airplane which implies an assumption that any wing motion effects on the buffet flow were the same for model and full scale airplane. Figure 4-20 from Reference 4-48 compares predicted and measured acceleration responses at Mach number of 0.79 and 0.92. Predicted spectra are shown for two different modal damping distributions. One distribution was obtained from the sum of the structural and aerodynamic damping (obtained from velocity versus damping flutter solutions) in each of 20 wing modes used in the analysis. The other was obtained from a constant damping ratio of 0.05 used for all 20 modes. The manner in which the damping was considered is seen to have little effect on the spectra compared to the differences between the measured and predicted responses. The authors of Reference 4-48 conclude that the agreement is reasonable and note that the specific method employed is considered a "first generation" approach to which refinements in technique may be added.

4.3 RESPONSE ANALYSIS FOR RANDOM EXCITATION* by C.Hwang

4.3.1 SURVEY

In a transonic maneuver, the flight attitude of the aircraft changes continuously. As a result, the so-called steady pressures on the lifting surfaces change with time. The steady state pressures are essentially deterministic, i.e., their distribution is dependent only on flight condition parameters such as the Mach number and altitude, the angle of attack, the pitch rate, the flap settings, etc. An exception is that load redistribution may occur due to shock oscillations even though the flight condition remains unchanged. In addition to the steady state pressures, fluctuating dynamic pressures also exist which may excite the aircraft and cause instability. In aircraft buffet, as the separated flow develops on the wing surface, the magnitudes of the dynamic pressures increase substantially. It is not uncommon for the pressure power spectral density (PSD) to increase 20 db or more in a wide frequency range as the local flow becomes separated. The dynamic pressures are random in nature, i.e., even though their overall amplitudes and frequency content are predictable under a given condition, their explicit time histories cannot be predicted. This section deals with the processing and analysis of random buffet pressure data and also the analysis of the aircraft's response to excitation by the random pressure loads.

4.3.1.1 Buffet Pressure and Aircraft Response Data

In aircraft buffet test, the steady state pressure data may be acquired using regular pressure taps. The dynamic pressures on the aircraft wing and other surfaces may be measured by miniaturized differential pressure transducers featuring a diaphragm sensor and semiconductor gages. The detail instrumentation and recording techniques, as well as test results obtained in recent aircraft buffet test programs, are described in Chapter 9 on Buffet Flight Test Techniques.

In order to illustrate the nature of the random pressures and the response data, as well as the analytical techniques used in processing these data, typical time history plots based on flight test results are presented in Figures 4-21 to 4-23. The data were acquired during flight tests of a Northrop F-5A single seat fighter at Mach number $M_0 = 0.925$ and an altitude of 10,668 m (Ref. 4-49). Specifically, four time histories of dynamic pressure transducer outputs for the F-5A aircraft with all flaps retracted are shown in Figure 4-21. In the figure, the elapsed time in seconds is indicated at the top of the plot. Also indicated is the instantaneous angle of attack. Pressure Transducer Number 4 was located at a 85% semi-span and 90% chordwise position on the top surface of the right wing. The data shows a substantial decrease in pressure (increase in lift) as the angle of attack was increased. This is consistent with the flow behavior prior to and during the development of a shock-induced separation wake on the airfoil surface. The remaining traces of Figure 4-21 give the steady state and low-frequency pressure data for a 85% semi-span location on the bottom surface of the right wing. The three traces are for 20%, 60% and 90% chordwise positions. Transducer Number 19, 20, and 21 respectively.

Typical dynamic pressure data with steady state pressure components filtered out are shown in Figure 4-22. The three pressure transducers (Nos 1, 2, and 3) were located at 85% semi-span and 20%, 40%, 60% chordwise positions. Typical response data in the form of normal and longitudinal accelerations at the center of gravity (CG) and normal accelerations at the wing tip are given in Figure 4-23. These plots indicate that the buffet pressure and response data are random and non-stationary. This point will be discussed in subsequent paragraphs.

4.3.2 PROCESSING OF RANDOM DATA

In a transonic maneuver, the flow field surrounding the buffeting aircraft is transient and highly nonlinear. The dynamic pressures exerted on the aircraft are random. Nevertheless, certain statistical and spectral properties based

* The major contents of this section were obtained in the process of performing work under Contract NAS2-6475 sponsored by NASA Ames Research Center.

on the temporal and spatial correlations of the local dynamic pressures may be determined. The spectral processing transforms the random pressure (and response) data into functions and expressions which are better subject to analysis. The processing techniques used for aircraft buffeting studies are described briefly in this section.

The real time random pressure data are usually recorded in PCM or FM format. (See Chapter 9 which reviews buffeting flight test recording techniques.) The flight data tapes are processed directly in an analog fashion, or they are converted into digital data tapes for further processing. Some modern analog processing equipments are actually hybrid machines, i.e., a digital technique is used for intermediate data storage within the processors. In either case, the basic theory of processing the random data is the same.

4.3.2.1 Temporal and Spatial Correlations of Random Data

Under certain conditions (to be described later), one or more sets of random data, obtained within a finite time span, may be used to generate the correlation and spectral functions. Consider a single random function $x(t)$ observed over time span $(0, T)$. The auto-correlation function of $x(t)$ is:

$$R_x(\tau) = \lim_{T\to\infty} \frac{1}{T}\int_0^T x(t)\, x(t+\tau)\,dt \,. \tag{4-14}$$

The auto-correlation function $R_x(\tau)$ has a time parameter τ. The mean value of μ_x may be computed in terms of the auto-correlation function as τ approaches infinity (or a very large time span in a practical case):

$$\mu_x = \sqrt{R_x(\infty)} \,. \tag{4-15}$$

The auto-correlation function establishes the influence of the basic function value at any time over values at a future time. The variation of $R_x(\tau)$ with respect to the parameter τ is determined by the frequency make-up of the random data $x(t)$. A well known relation between the auto-correlation function and the power spectral density (PSD) function is that the Fourier transform of the auto-correlation function yields the one-sided PSD of the same basic function:

$$\phi_x(\omega) = \frac{1}{\pi}\int_{-\infty}^{\infty} R_x(\tau)\, e^{-i\omega\tau} d\tau \,. \tag{4-16}$$

The PSD function $\phi_x(\omega)$ may be defined as the mean square value of a function $x(t)$ within a narrow frequency range $\Delta\omega$:

$$\phi_x(\omega) = \lim_{\Delta\omega\to 0} \lim_{T\to\infty} \frac{1}{\Delta\omega T}\int_0^T x^2(t, \omega, \Delta\omega)\,dt \tag{4-17}$$

where $x(t, \omega, \Delta\omega)$ is the time function of $x(t)$ as processed by a narrow band filter with center frequency ω and bandwidth $\Delta\omega$. A typical auto-correlation function (not normalized) and the corresponding PSD function for a set of pressure data measured near the wing tip of the F-5A aircraft during a buffet test are shown in Figures 2-24 and 2-25 respectively. The time interval T during which the data were collected was 8.20 seconds. The wing location at which the pressure data were measured was under separated flow so that the PSD level was high as compared to the unseparated flow case. This point will be explained later.

In buffet pressure measurements, the time variation of the pressure acquired at a fixed station is random. Of interest is the interrelationship between the random pressure data acquired at two distinct stations. This interrelationship is examined by the cross-correlation function. The cross-correlation function is a measure of whether the two sets of random data are working in unison (perfectly correlated), are physically unrelated (zero correlation), or are somewhere in between. For two random time functions, $x(t)$ and $y(t)$, the cross-correlation function is defined as:

$$R_{xy}(\tau) = \lim_{T\to\infty} \frac{1}{T}\int_0^T x(t)\, y(t+\tau)\,dt \,. \tag{4-18}$$

Similar to the case of the auto-correlation, the Fourier transform of the cross-correlation function yields the cross spectral density function of the two random functions $x(t)$ and $y(t)$. The one-sided cross spectral density function $\phi_{xy}(\omega)$ is defined as:

$$\phi_{xy}(\omega) = C_{xy}(\omega) \quad i\, Q_{xy}(\omega) \tag{4-19}$$

$$C_{xy}(\omega) = \lim_{\Delta\omega\to 0} \lim_{T\to\infty} \frac{1}{\Delta\omega T}\int_0^T x(t, \omega, \Delta\omega) y(t, \omega, \Delta\omega)\,dt \tag{4-20}$$

$$Q_{xy}(\omega) = \lim_{\Delta\omega\to 0} \lim_{T\to\infty} \frac{1}{\Delta\omega T}\int_0^T x(t, \omega, \Delta\omega) y^{0}(t, \omega, \Delta\omega)\,dt \tag{4-21}$$

where $i = \sqrt{-1}$. $C_{xy}(\omega)$ and $Q_{xy}(\omega)$ are called the co-spectral density and quadrature spectral density functions, respectively. $y^0(y, \omega, \Delta\omega)$ represents the band-pass-filtered functions of $y(t)$ with a 90° phase shift. The relation between $\phi_{xy}(\omega)$ and $R_{xy}(\tau)$ is:

$$\phi_{xy}(\omega) = \frac{1}{\pi}\int_{-\infty}^{\infty} R_{xy}(\tau)e^{-i\omega\tau}\,d\tau . \tag{4-22}$$

The auto and cross-spectral density functions of the buffet pressures are essential inputs for aircraft response computations. This point will be explained in Section 4.3.3. Furthermore, to determine whether the random time functions $x(t)$ and $y(t)$ are caused by the same physical source, or whether a certain degree of correlation exists between the two sets of data, the coherence function $\gamma_{xy}(\omega)$ is applied. It is defined as follows:

$$\gamma_{xy}^2(\omega) = \frac{|\phi_{xy}(\omega)|^2}{\phi_x(\omega)\,\phi_y(\omega)} \leq 1 . \tag{4-23}$$

Figure 4-26 presents the various spectral functions as defined in Equations (4-18), (4-22), and (4-23) corresponding to the random pressure data measured at two neighboring stations at the 85% semi-span location on the F-5A wing. The correlation function is shown in the lower right corner of the figure. The modulus and phase angle of $\phi_{xy}(\omega)$ are presented on the left hand side of the figure, while the coherence function is shown at the upper right corner. The phase angle plot indicates that the two sets of pressure data are mostly in phase within the covered frequency range (4–60 Hz). The value of the coherence function is fairly high. These observations indicate that the dynamic pressures are possibly caused by a single physical source (shock or turbulent shear flow, etc.).

For cases where the buffet pressures at two locations are known to be caused by the same source, it is expected that their auto-correlation functions and auto power spectra would be of the same general shapes. A plausible model of the correlation function for measurements at any two locations, x and y, was proposed in Reference 4-48 (Equations 5-8, p.43) as:

$$R_{xy}(r, \tau) = \sigma_x\,\sigma_y\,\exp(-\delta|r|)\rho_0(\tau - \tau') \tag{4-24}$$

where σ_x and σ_y denote the rms values (with zero mean), r is the distance between the two locations, δ is the spatial decay coefficient, τ is time, τ' relates to the time of convection of the pressure from one point to the other and ρ_0 denotes the normalized auto-correlation function. Based on the above assumption of identical or near-identical auto-correlation functions (different only in amplitude), the phase angle θ of the cross spectral density ϕ_{xy} and the cross-correlation coefficient $\rho_{xy}(r, \tau')$ may be expressed as follows:

$$\theta = -2\pi f\tau' \tag{4-25}$$

$$\rho_{xy}(r, \tau') \simeq \exp(-\delta|r|) \simeq \gamma_{xy}(r, f) . \tag{4-26}$$

In Equation (4-26), γ_{xy} is the square root of the coherence function as defined in Equation (4-23). Apparently, γ_{xy} is assumed to be independent of frequency f. Based on Equation (4-26), the spatial decay constant δ may be determined. Processing of flight test data indicates that the above condition was true only for limited locations for certain flight maneuvers. For instance, based on dynamic pressure data obtained from the F-5A aircraft ($M_0 = 0.925$, $h = 10{,}668$ m), contours on the wing surface of equal γ_{xy} for Station Number 2 (85% semi-span, 40% chordwise location) can be plotted, as shown in Figure 4-27. The contours are plotted only in the wing region where the convection effect was observed, and the approximate formulation of Equation (4-26) was applicable.

4.3.2.2 Stationarity of Random Data

In a random process, a measure of the consistency of the data is determined by the stationarity of the data. For a single set of random data, the mean value $\mu_x(t_1)$ and the auto-correlation function $R_x(t_1, t_1 + \tau)$ are computed based on a given sampling time t_1. [$R_x(t_1, t_1 + \tau)$ may also be written as $R_{xx}(t_1, t_1 + \tau)$.] If these two functions remain unchanged when the sampling time t_1 is varied, then the original function $x(t)$ is called weakly stationary. In a more exact sense, if all the moments and joint moments [e.g., $R_{xxx}(t_1, t_1 + \tau_1, t_1 + \tau_2)$] are independent of the sampling time t_1, then the data are called strongly stationary. The definition of stationarity may be extended to more than one set of random data (see for instance, p.71 in Reference 4-7). Strictly speaking, only stationary random data may be processed into meaningful correlation functions and auto and cross spectral functions as they are described in this section.

The stationarity of the random data is essentially a measure of whether the basic physical phenomenon which causes the random process remains unchanged (with respect to time) during the process. For instance, in transonic wind tunnel testing of a scaled model, as long as the model attitude and the tunnel flow conditions remain unchanged, the random buffet pressure acquired are stationary or nearly stationary. On the other hand, in a typical transonic flight maneuver (which may last from 12 to 30 seconds), where the aircraft's angle of attack and other flight condition parameters change continuously, the resulting pressure data obtained in a long time span (relative to the maneuver

time) are non-stationary. An approximate method dealing with the nonstationary random data assumes that the random function(s) may be divided into a finite number of time segments. Within each time segment, the random data may be represented by the product of a deterministic function and a stationary random function. The complete random function is then called segmentwise stationary. This method may be applied to the response analysis of a buffeting aircraft, the details of which will be discussed later in Section 4.3.4.

4.3.2.3 Digital Techniques and Error Estimate in Spectral Processing

The pressure and response data of an aircraft in a transonic maneuver are acquired by transducers and other instruments in a continuous fashion (i.e., in analog format). In order to have the data processed by a digital computer, the analog data have to be digitized. To accomplish this, the analog data are transcribed at regular sampling time intervals and the results are recorded on a digital tape. The sampling rate and the total number of samples to be processed are determined by such factors as the data length, the performance specifications of the instrumentation and recording system, the capacity and allowable processing time of the digital equipment, as well as the requirements of the spectral data (frequency range and resolution, acceptable range of standard error, etc.) to be obtained from the digital tapes.

In determining the sampling rate, a major consideration is the aliasing error introduced in digitization. Briefly, the spectral data cut-off frequency (Nyquist frequency) is determined by the sampling time interval h:

$$f_c = \frac{1}{2h} \quad . \tag{4-27}$$

The cut-off frequency is usually selected in such a way that it is equal to one and one-half or two times the maximum frequency of interest. After f_c has been selected, and if the analog data are not properly filtered prior to or during digitization, then the frequency components higher than f_c may be erroneously introduced into the working frequency range and mixed with the genuine spectral data. The error thus introduced is called the aliasing error. More detailed descriptions of the problem are contained in special texts on digital processing (for instance, References 4-7 and 4-50).

In Equations (4-16) to (4-18) and (4-20) to (4-22) dealing with the correlation and power spectral density functions, it is assumed that the basic random data cover an infinite time span and that their Fourier components are integrable within the time span. In reality, test data are available only in a finite time span so that truncations of the integrals are necessary. The effect of the truncation is to impose a so-called boxcar function $u_{T'}(\tau)$ to the integrand. The boxcar function is defined as:

$$\begin{aligned} u_{T'}(\tau) &= 1 , \quad |\tau| \leq T' \\ u_{T'}(\tau) &= 0 , \quad |\tau| > T' . \end{aligned} \tag{4-28}$$

It is noted that T', the truncated half time span, is different from the data time span T used in Equations (4-14), (4-17), etc. With the above definition, the truncated integral of Equation (4-16) for the one-sided PSD is:

$$\hat{\phi}_x(\omega) = \frac{1}{\pi} \int_{-\infty}^{\infty} u_{T'}(\tau)\, R_x(\tau) e^{-i\omega\tau}\, d\tau . \tag{4-29}$$

The truncation causes the true PSD $\phi_x(\omega)$ of the random data to be masked by a spectral window of the type $(\sin \chi/\chi)$. It can be shown that the truncated PSD and the true PSD functions are related by the following equation:

$$\hat{\phi}_x(\omega) = \int_{-\infty}^{\infty} \phi_x(\omega)\, 2\, \frac{\sin(\omega - \omega')T'}{\omega - \omega'}\, d\omega' \tag{4-30}$$

where ω' is a dummy circular frequency and T' is the truncated half time span. The error introduced by Equation (4-30) in spectral processing is called the leakage error. In digital processing, the PSD leakage error is dependent on the finite lag time $T_m (= T')$ of the correlation functions. ($T_m = mh$, where m is the maximum lag value and h is the sampling time increment used in correlation function computation.) The undesirable leakage in digital spectral processing using truncated data may be minimized through the use of special compensating windows. The windows commonly used for this purpose are the Hann window and the Hamming window (see, for instance, Reference 4-7). The application of these windows may be affected through the modification of either the real time digital data or the computed PSD function (with bandwidth $B_e \approx 1/mh$). The statistical error in PSD processing is defined as the normalized standard error ϵ, which is the ratio of the standard deviation of the PSD estimate from the sample record to the standard deviation of the true PSD function. Based on variance computation, it can be shown that without compensation:

$$\epsilon \approx (B_e T)^{-1/2} \tag{4-31}$$

where B_e is as defined above and T is the time span. Thus, the requirements of stationarity (i.e., small T), a high degree of frequency resolution, a broad frequency range, and a minimum normalized standard error pose conflicting conditions on the processed data. It is then important to weigh these factors and to determine the most appropriate time span, sampling rate, and resolution frequency(s) for spectral processing.

Reference 4-49 reports on an error study made during the spectral processing of buffet data by varying the processing parameters. The dynamic data at a 33% semi-span, 80% chordwise position were processed in two ways. Firstly, the PSD data were generated using a low frequency digital tape covering a time span T of 4.096 seconds. The low frequency tape had a frame rate of 1000 per second. The effective resolution frequency B_e used in the process was 0.9766 Hz. The normalized standard error was then

$$\epsilon \approx (B_e T)^{-1/2} = 0.500 .$$

The PSD's for the same data recorded on a higher frequency digital tape were also generated. The high frequency tape had a frame rate of 5000 per second. The cut-off frequency of this tape was 2500 Hz. With $T = 4.920$ seconds, $B_e = 9.766$ Hz, the normalized standard error was:

$$\epsilon \approx (B_e T)^{-1/2} = 0.144 .$$

The PSD data obtained from the high and low frequency tapes are plotted in Figure 4-28. (Only the low frequency portions of the high frequency PSD are plotted. In the range of comparison, both the low frequency and high frequency digital tape data are not affected by their respective processing filters.) Referring to Figure 4-28 and allowing for the lack of certain details in the high frequency PSD in the low frequency region, the high frequency and low frequency PSD's are considered consistent in magnitude and spectral trend.

4.3.3 AIRCRAFT TRANSFER FUNCTIONS AND RESPONSE POWER SPECTRAL DENSITIES

The aircraft transfer functions are computed in the frequency domain. In determining the input forces, the dynamic buffet pressure data are processed through Fourier transforms. The results are used to generate the modal forces as functions of frequency. Based on the aircraft transfer function and the modal force data, the PSD of aircraft responses may be computed.

4.3.3.1 Aircraft Transfer Functions

Within the frequency band of interest, the aircraft response functions usually are computed using a modal approach. For this purpose, the basic elastic modes of the aircraft are generated and are used as the normal modes in the response formulation. The frequency response functions are determined for deflection, acceleration, control point load, shear, bending moment, torque, and stress at specified locations. In this section, the basic building blocks used in the aircraft response analysis are described.

The aircraft is represented by a system of control points with concentrated masses. The control point masses and intermediate masses are calculated such that the mass and inertia properties of the system are matched with those of the aircraft. The control point and intermediate masses are used to derive the coupled mass matrix for a dynamically equivalent system.

The oscillatory aerodynamic influence coefficients (AIC's) are computed based on unsteady aerodynamic theory assuming airfoil lifting surfaces (thin or considering thickness) and slender bodies, or some other unsteady aerodynamic theories. The AIC's relate the control point deflections whose derivatives are the downwash velocities. Aerodynamic forces are expressed in terms of AIC's for motion in a matrix form. The resulting AIC's are functions of planform, Mach number, and reduced frequency.

The basis of the lifting surface theory is found in the aerodynamic integral equation that relates the pressures on the surface to the downwash at the surface. A number of solutions to these integral equations by collocation methods are available. The methods are based on certain approximate treatments of the kernel of the integral equation. Tail downwash due to wing lift should be taken into account. The AIC's for the fuselage due to motion are usually derived from the slender-body theory which employs the momentum theory of Munk and Jones.

Considering structural damping in the form of modal damping coefficients g_f, the dynamic equation of the aircraft and the corresponding modal transfer function matrix may be formulated as shown below:

$$\begin{bmatrix} -\omega^2[M_{FF}] + [M_f\omega_f(\omega_f + ig_f\omega)] & -\omega^2[M_{RF}]^T \\ -\omega^2[M_{RF}] & -\omega^2[M_{RR}] \end{bmatrix} \begin{Bmatrix} \{q_F\} \\ \{q_R\} \end{Bmatrix} = \begin{Bmatrix} [X_1]^T\,[A]\{\bar{p}\} \\ [T]^T\,[A]\{\bar{p}\} \end{Bmatrix} \qquad (4\text{-}32)$$

$$[H(\omega)] = \begin{bmatrix} -\omega^2[\bar{M}_{FF}] + [M_f\omega_f(\omega_f + ig_f(\omega)] & -\omega^2[\bar{M}_{RF}]^T \\ -\omega^2[\bar{M}_{RF}] & -\omega^2[M_{RR}] \end{bmatrix}^{-1} \quad (4\text{-}33)$$

where:

$[\bar{M}_{FF}]$, $[\bar{M}_{RF}]$, $[\bar{M}_{RR}]$ = generalized mass plus aerodynamic matrices. F refers to the flexible modes and R refers to the rigid body modes.

$\{q_F\}$ = free-free modal coordinates

$\{q_R\}$ = rigid body modal coordinates

$\{\bar{p}\}$ = Fourier transforms of the measured pressures

M_f = generalized masses

ω_f = non-zero natural circular frequencies

g_f = modal damping coefficients

$[X_1]$ = flexible modal matrix

$[T]$ = rigid body modal matrix

$[A]$ = subareas associated to pressure transducers

Assuming that no aeroelastic coupling exists between the rigid body modes and the free-free modes, the aircraft transfer function matrix may be rewritten as follows:

$$[H(\omega)] = \begin{bmatrix} -\omega^2[M_{FF}] + [M_f\omega_f(\omega_f + ig_f(\omega)] & 0 \\ 0 & Z_R(\omega) \end{bmatrix}^{-1} . \quad (4\text{-}34)$$

Considering the symmetrical response of the buffeting aircraft, $Z_R(\omega)$ is a (2 x 2) matrix corresponding to the downward displacement and the pitch angle. The elements of $Z_R(\omega)$ are.

$$Z_{11}(\omega) = -\frac{1}{2}\rho V^2 S\left[-\frac{\omega^2 c}{2V^2}\left(\frac{4m}{\rho Sc} - C_{z\dot{\alpha}}\right) + \frac{i\omega c}{V} C_{z\alpha}\right] \quad (4\text{-}35)$$

$$Z_{12}(\omega) = -\frac{1}{2}\rho V^2 S\left(\frac{i\omega c}{2V}\right)\left(\frac{4m}{\rho Sc} + C_{zq}\right) \quad (4\text{-}36)$$

$$Z_{21}(\omega) = -\frac{1}{2}\rho V^2 Sc\left(-\frac{\omega^2 c}{2V^2} C_{m\dot{\alpha}} + \frac{i\omega}{V} C_{m\alpha}\right) \quad (4\text{-}37)$$

$$Z_{22}(\omega) = -\frac{1}{2}\rho V^2 Sc\left(\frac{\omega^2 c^2}{4V^2} i_B + \frac{i\omega c}{2V} C_{mq}\right) \quad (4\text{-}38)$$

where:

$i_B = 8(\rho Sc^3)^{-1} B$

B = aircraft moment of inertia about the y-axis

The detailed derivation of the impedance matrix $Z_R(\omega)$ and the definitions of the aerodynamic derivatives in Equations (4-35) to (4-38) may be found in Reference 4-51. The computation of rigid body responses (symmetrical and anti-symmetrical) during buffet using the above described approach has not been carried out extensively. The difficulty is mostly due to the lack of precisely defined buffet pressure modal forces and the uncertainty of the aircraft transfer functions in large-amplitude motions.

4.3.3.2 Aircraft Response Power Spectral Densities

The auto and cross spectral density functions of the buffet pressures are described in Section 4.3.2. The dynamic equation of the aircraft (Equation (4-32)) uses the Fourier transform of the buffet modal forces to determine the modal responses in terms of the flexible and rigid body modes. Under certain conditions relating to the spatial correlation of the pressures, the Fourier transform of the pressures may be used to compute the modal force PSD matrix of the buffet pressures. Otherwise, the correlation functions are to be used to generate the pressure PSD matrix $\varphi(\omega)$. In either case, the following equation may be used to determine the modal force PSD matrix:

$$[\phi_p(\omega)] = [X]^T [A] [\phi_{p_r p_s}(\omega)] [A] [X] \quad (4\text{-}39)$$

where r and s are the location subscripts for the pressures, and [X] is the transform matrix which is composed of submatrices X_i and T shown in Equation (4-32). For a stationary case, the aircraft response PSD is defined below:

$$\phi_w(\omega) = [Y]^T [H(\omega)] [\phi_p(\omega)] [H^*(\omega)]^T [Y] \quad (4\text{-}40)$$

where [Y] is the transfer matrix to convert the modal amplitudes to responses.

4.3.4 PROCESSING AND EVALUATION OF FLIGHT TEST DATA

As described in the previous sections, the dynamic buffet pressures exerted on the aircraft are complex in both temporal and spatial make-ups. These pressure data are processed into auto and cross PSD functions which are the inputs for aircraft response computations. The available aircraft frequency transfer functions used in the computations are linear functions. They are independent of the pressure input amplitude, and the interaction between the buffet pressure forces and the aeroelastic response of the aircraft is ignored. Because of these factors, present-day analytical computations of aircraft buffet response are imprecise and approximate at their best. On the other hand, the analytical processing and computation, and the subsequent correlation with buffet flight test results, may shed light as to the detailed mechanisms of aircraft buffet responses. These tasks can be productive to the structural dynamicists and designers who are interested in combating and alleviating the buffeting problem.

4.3.4.1 Difference Between Gust Response and Transonic Buffet Response

In gust penetration, the air turbulence encountered by the aircraft is random in nature. The spectral make-up and the rms values of turbulence, measured for random velocities in three directions in space, are a complicated matter. Yet, because of extensive work on the subject covering meteorological data gathering, analytical processing and flight testing, the gust penetration problem (including prediction and design) is much better understood as compared to the aircraft buffeting problem.

The driving force in gust penetration is the random air velocity encountered by the aircraft. The random normal and lateral air turbulence velocities (with proper phase relationships considering the dimensions and geometry of the aircraft) are usually treated together with the respective induced velocities generated by the vibration and oscillation of the aircraft structure.

In the case of aircraft buffeting, the driving forces are the dynamic pressures applied on the exposed surfaces of the aircraft. In this manner the driving forces are separately defined as against the aeroelastically induced pressures and air velocities. These separate identities do not mean that the buffet forces and the aircraft motions do not interact with each other. On the contrary, the interaction of the buffeting forces and the oscillating aircraft can be a significant problem for which only some preliminary research work has been carried out. The analysis described in Section 4.3.3 ignores this interaction problem.

4.3.4.2 Buffet Response Considered as a Segmentwise Stationary Random Phenomenon

As mentioned previously, transonic maneuvers are dynamic in nature, and the local buffet pressure and response data are nonstationary in a strict sense. Within a short time interval (1 or 2 seconds) when no drastic change in local physical behavior takes place, the data may be considered random and near-stationary so that spectral processing techniques may be applied. In this section auto power spectra of pressure and responses for a buffeting aircraft are presented in a systematic manner corresponding to various phases (or time segments) of a transonic maneuver.

For data acquired in a transonic maneuver of the F-5A aircraft (Run 5, Flight 825, $M_0 = 0.925$, $h = 10{,}668$ m, $\delta_n/\delta_f = 0°/0°$), five time segments were chosen for spectral processing. Each time segment represented 1.025 seconds. Roughly the five time segments were classified as follows:

Designation	*Starting Time*	α *Initial*	*Description*
A	334.0	2.2°	Initiated wind-up turn. Shock appeared at localized area.
B	335.03	4.1°	Buffet onset.
C	336.06	7.8°	Separation region expanded.
D	337.09	12.3°	Separated flow covered the complete wing surface.
E	338.12	13.9°	Recovery initiated.

In Figures 4-29 to 4-31 five PSD plots, corresponding to the time segments A through E noted above, are shown for three measurements. Figure 4-29 presents the PSD plots for Pressure Station No.1 (85% semi-span, 20% chordwise location). Figure 4-30 shows the corresponding PSD plots for an inboard station (Station No.23, 47% semi-span, 40% chordwise location). In Figure 4-31 the PSD plots for the center of gravity normal acceleration are presented. For these results it should be mentioned that starting at Time Segment C some low frequency aircraft vibrations appeared. These were characteristic of wing rock. The vibrations, though comparatively small, are reflected in the acceleration PSD plots (Fig.4-31). The low frequency data in these plots lack precision because of the wide spectral frequency coverage (up to 1000 Hz) and the fixed frequency bandwidth used in processing the digital data. This problem can be alleviated when variable resolution frequency is used to process the response data. In the following section the analytical correlation aircraft response using the segmentwise stationary approach is described.

4.3.4.3 Analytical Correlation of Aircraft Response Power Spectral Density Data

In order to improve the analytical correlation of aircraft response results, the major portion of a transonic maneuver can be divided into a number of segments. In each segment, the buffet pressure data can be assumed to be stationary. The aircraft can then be subjected to the consecutive application of the buffet loads, and the cumulative dynamic effects are subsequently reflected in the time-varying response PSD. The detailed formulation of the segmentwise stationary approach and the computation flow diagram are given in Reference 4-49.

This approach has been applied to flight test data for the F-5A aircraft with the following set of parameters:

Flight number	871, Run 2
Mach number	0.925
Altitude	10,668 m (35,000 ft.)
Flap settings	(4°/12°)
Low frequency digital tape frame rate	1000 per sec
Time increment	0.002 sec
Frequency increment	0.488 Hz
Spectral frequency range	1.4 – 20.0 Hz

Typical real-time pressure data for this run were shown previously in Figure 4-22. Altogether, dynamic pressure data covering the time span from 073.00 to 082.10 seconds were used. The data, assumed to be perfectly correlated, were divided into four equal time segments. The computation was carried out using the rigid body plunging mode and the first three symmetrical flexible modes. The pitch mode was not included because of lack of tail surface dynamic loads data. Corresponding to this flight condition, the natural frequency and damping ratio of the aircraft's short period move were 0.3947 Hz and 0.245, respectively.

Figure 4-32, shows the mean square values of the rigid body (plunging) mode (f_R) and three flexible mode forces (f_1, f_2 and f_3) for the four equal time segments of the transonic maneuver. Only the contributions within the frequency range of 1.4 to 20.0 Hz were taken into account in computing the mean square values. The relatively high modal forces in the second time segment reflect the shock oscillations at buffet onset. (See, for instance, Figure 4-22, the data for which were acquired in the same test run as the data described here.) The modal forces diminish in the third time segment and then reach their highest values in the fourth time segment when the angle of attack was at its maximum values.

Based on preliminary data such as shown in Figure 4-32, the nonstationary response PSD's for two stations at the right wing tip and for the CG were computed for specific times increments, one within each of the four time segments. These results are presented in Figures 4-33 to 4-35. Also plotted are the corresponding segmentwise stationary PSD's based on the flight test response data. For the two right-hand wing tip stations (Figures 4-33 and 4-34), the computed response PSD's are too high in the first time increment. This is believed due to the higher damping (of the Coulomb type) at the initial phase of the maneuver which was not accounted for in the computation. The correlation is more satisfactory for the third time increment and also for the fourth time increment when wing rock occurred. For the CG acceleration results, Figure 4-35, the computed response PSD is low in the first time increment because more spectral energy was due to wing vibrations, as explained above. For the later time increments, with some exceptions, somewhat better correlations between the computed and flight test PSD data are realized. In general, the correlation of analytical and flight test response PSD data is more satisfactory using the segmentwise stationary approach as compared to the approach where a major portion of the transonic maneuver is considered stationary.

4.3.4.4 Separation of Genuine Buffet Pressure and Induced Pressure Due to Structural Vibration and Rigid Body Motion

A subject of interest in a buffet test program is the magnitude of the induced aerodynamic forces (as a function of frequency) relative to the overall dynamic pressure force during buffet. In this section the computed induced aerodynamic pressure data, based on the measured buffet pressure distribution, and the responses of the F-5A aircraft are discussed.

Assuming that the buffet pressure distribution has perfect spatial correlation, it is possible to separate the genuine pressure p_b due to flow separation from the measured pressure p_m. The separation of the two pressures is accomplished by the computation of the Fourier transforms of the pressure induced by wing motion, p_i, in a uniform flow using flight test wing motion data. In this manner, the relative magnitude of the induced pressure at the top surface of the wing to the measured oscillatory pressure p_m at different tranducer locations as a function of frequency may be determined as follows:

$$\zeta = \beta|p_i|/|p_m| = |1 - p_b/p_m|. \qquad (4\text{-}41)$$

In Equation (4-41), β represents the percentage of the induced pressure attributed to the top surface. In cases where no specific β data are available, β is assumed to be equal to 0.5. Using this approach, the pressure ratio can be plotted versus frequency, as shown in Figure 4-36 for Transducer Locations 1, 4, 18 and 23 whose semi-span and chordwise positions on the F-5A wing were (85% b/2, 20% C), (85% b/2, 90% C), (33% b/2, 80% C), and (47% b/2, 40% C), respectively. In Figure 4-36, the peaks in the pressure ratio correspond either to a resonance frequency which induced a large deflection at that transducer location, or a frequency at which there was a very low value of the measured pressure. In general, the ratio ζ is less than 0.3. In other words, the genuine buffet pressure p_b dominates in most frequency ranges while the induced pressure is less significant in the response computation. The top plot of Figure 4-36 shows the ζ values for Transducer No.1 where the relative amplitude of the induced aerodynamic pressure yields a very high peak, the details of which are:

$f = 7.324$ Hz

$\zeta = 1.086$

$p_m = (-7.31 + i5.81)$ N/M^2, $\quad |p_m| = 9.31$ N/M^2

$\beta p_i = (-2.12 - i9.92)$ N/M^2, $\quad \beta|p_i| = 10.14$ N/M^2

$p_b = (-5.18 + i15.73)$ N/M^2, $\quad |p_b| = 16.56$ N/M^2.

This highest peak occurs near the second eigen frequency where the location of Transducer No.1 has a large deflection. For this case, even though ζ is greater than unity, $|p_b|$ is still 1.6 times the value of $\beta|p_i|$ while the two complex pressure vectors βp_i and p_b are out of phase.

4.4 CONCLUDING REMARKS

This chapter has discussed the two analytical models which have been proposed for a buffeting aircraft in separated flow: the forced vibration model and the buffeting flutter model. At the time insufficient evidence exists as to which model is most adequate for transonic buffeting analysis. The regulating interaction of shock motion, shock-induced separation and wing motion needs further investigation. Therefore, future research on transonic buffeting should include evaluations of both models and an attempt to develop a continuous description of the transition between the models.

The important structural and aerodynamic quantities associated with a flexible aircraft responding to buffet flow conditions, requirements for simulating or calculating the response with the aid of wind tunnel models, required scaling relationships, and test methods have also been discussed relative to the state-of-the-art and to considerations, assumptions, and idealizations that are usually required. Some examples of contradictory evidence in the literature regarding some of these assumptions and idealizations have been cited to indicate areas where further research is required, and some recent results obtained by investigators using several prediction techniques have been compared with measured flight buffet loads.

A significant advancement in buffet analysis techniques was made in the early fifties with the application of the methods of generalized harmonic analysis, and there have since been notable contributions to the understanding of buffet phenomena. However, the state-of-the-art to definitively predict analytically or experimentally the complete structural response and handling characteristics as the buffet boundary is penetrated leaves much to be desired. Although some progress has been made in theoretical methods for predicting buffet onset conditions, particularly at subsonic speeds, no adequate theoretical method exists for calculating the unsteady aerodynamic excitation forces in fully developed separated flow at transonic speeds. The determination of these excitation forces from wind tunnel model tests for subsequent use in structural response calculations requires many assumptions that need to be validated. A fundamental question that needs to be resolved is whether the unsteady aerodynamic excitation forces on a rigid (non-moving) wing are the same as those on an identical but flexible (responding) wing, or at least what are the conditions under which they may be considered the same. The practical significance of Reynolds number effects on separated flow in terms of the effects on structural and rigid body response needs to be determined. The effect of rate-of-change of angle of attack on buffet load intensity needs further study. A systematic study of the aerodynamic damping variation occurring with approach to, and penetration of, buffet boundaries is needed along with better means of measuring damping under these conditions.

In spite of these uncertainties several prediction techniques have been shown to give results that compare favorably with flight data for certain categories of buffeting, most notably wing buffet onset and, to some extent, buffet load intensity. However, experience has shown that even well beyond the buffet boundary the critical consideration is not usually the wing buffet loads but rather the excessive loads on tail surfaces; vibrations which subject fire control, navigation equipment, instruments, and crew to a more severe operational environment and increase fatigue problems; and degradation of performance through increased drag and decreased lateral stability which detracts from tracking capability.

None of the various approaches to the prediction of buffet response accelerations and loads is completely satisfactory, each having its own advantages and disadvantages. A complication factor for all methods is the extreme configuration dependency of the various buffeting excitation forces that occur on the aircraft.

Regarding the uncertainty of model/flight comparisons, the fact that buffeting essentially is a random process leads to difficulty in comparing flight buffet loads from a maneuvering aircraft to those predicted from wind tunnel tests. For example, high-load-factor flight data sample lengths of buffet loads as a function of angle of attack are usually too short to provide the stationarity of the data required in scaling relationships. In addition, the aircraft is not usually maneuvered in such a way that Mach number and density remain constant (as in the usual wind tunnel test) while the angle of attack is increased to values well beyond the buffet boundary. In other respects one must also take account of the lack of Reynolds number simulation and the tunnel turbulence and wall effects. Until the important parameters can be separated and better controlled, the possibility must be recognized that the degree of correlation between predicted and measured flight buffet response characteristics may be fortuitous.

The prediction of maneuvering aircraft buffet structural response is obviously a fertile field for imaginative research.

CHAPTER 5

STABILITY AND CONTROL STATUS FOR CURRENT FIGHTERS

by

W.G.Williams and J.L.Lockenour

5.0 INTRODUCTION

The task of putting the weapon on the target involves the dynamic interaction of a very complex closed-loop system, all elements of which must work in concert. Schematically, this system may be represented as in Figure 5-1. Because the total system dynamics are vital to the success of the task, the performance must ultimately be evaluated for the total closed-loop system. Additionally, the individual elements are separately evaluated and, due to the complexity of the problem, research and development efforts typically concentrate on the individual elements.

The element labelled "Airframe Dynamics" includes the aerodynamic performance, stability and control characteristics. Since the flight envelope of a fighter aircraft, in terms of speed, altitude and normal acceleration, is usually extremely large (see Figure 5-2), these characteristics vary dramatically. The remaining elements of the system must adjust accordingly, compensating for these changes if the task of weapon delivery is to be successful. If severe limitations exist in any one of the elements, total system performance will not be adequate.

Complicating the problem is the task-dependency of the desired control dynamics. For instance, air-to-ground bombing requires precise flight path or velocity vector control, whereas air-to-ground gunnery requires precise attitude control. In addition, air-to-air and air-to-ground tasks require both gross, abrupt "all-out" maneuvers (of an open-loop precognitive sense) by the pilot and tight closed-loop precision tracking. Because of these two basic facts, relatively complex stability and/or control augmentation systems are typically employed on advanced fighter aircraft.

There are many subsystems that influence the tracking precision during maneuvering flight. The fire control/display system has dynamic response characteristics peculiar to its particular type (i.e., lead computing, director, etc). The pilot acts to minimize the displayed error between the target and the sighting recticle by manipulating the various cockpit controls available to him. His control inputs are fed to the airframe/control/augmentation system combination. The important consideration is the response of the aircraft or gunsight reticle to the pilot's control inputs; the dynamic response characteristics of each individual element are not important in themselves. For example, a high performance stability augmentation system can compensate for a bare airframe instability. There are, however, basic aircraft response limits due to such factors as aerodynamic flow separation, maximum control surface authority, and maximum control surface (hydraulic system) rates which must be recognized.

This chapter discusses the current state-of-the-art of stability and control technology for maneuvering and precision tracking. Basic aerodynamics and aerodynamic stability and control, flight control system concepts, and methods of prediction and analysis are covered. In this chapter the following symbology is used:

AADP	aileron alone divergence parameter, $C_{n_\beta}\left[1 - \frac{C_{n_{\delta_A}}}{C_{l_{\delta_A}}}\frac{C_{l_\beta}}{C_{n_\beta}}\right]$
AR	aspect ratio
BW	bandwidth
C*	C-star longitudinal response parameter
CEP	circular error probable
C_l	rolling moment coefficient
$C_{l_{\delta_A}}$	coefficient of rolling moment due to aileron deflection; aileron effectiveness
C_{l_β}	coefficient of rolling moment due to sideslip; dihedral effect
$C_{l_{\delta_{sp}}}$	coefficient of rolling moment due to spoiler deflection; spoiler effectiveness
C_m	pitching moment coefficient
$C_{m_{\delta_E}}$	coefficient of pitching moment due to elevator deflection; elevator effectiveness
C_n	yawing moment coefficient
$C_{n_{\delta_A}}$	coefficient of yawing moment due to aileron deflection
C_{n_β}	coefficient of yawing moment due to sideslip; directional stability
$C_{n_{\beta_{dyn}}}$	dynamic directional stability, $C_{n_{\beta_{dyn}}} = C_{n_\beta} - \frac{I_{zz}}{I_{xx}} C_{l_\beta} \sin\alpha$ [one definition]

C_{n_p}	coefficient of yawing moment due to roll rate
C_{RR}	$1 - \frac{C_{n_{\delta_A}}}{C_{l_{\delta_A}}} \frac{C_{l_\beta}}{C_{n_\beta}}$
$\bar{c}$	mean aerodynamic chord
c.g.	center-of-gravity
DEP	deflection error probable
F_s	pitch stick force
HUD	head up display
I_{xx}	moment of inertia about roll axis
I_{yy}	moment of inertia about pitch axis
I_{zz}	moment of inertia about yaw axis
K_p	pilot gain
M_q	pitching moment due to pitch rate
n_z	normal acceleration
n_{z_α}	normal acceleration sensitivity
p	roll rate
PIO	pilot induced oscillation
REP	range error probable
$t_{1/2}$	time to one half amplitude
α	angle of attack
β	angle of sideslip
δ_A	aileron deflection
δ_e	elevator deflection
δ_{tl}	horizontal tail deflection
$\delta_{LE_{FLAP}}$	leading edge flap deflection
δ_s	stabilizer deflection
δ_{s_p}	spoiler deflection
Δ	increment
ζ_3	damping ratio of second-order control system lag
ζ_{sp}	short period damping ratio
θ	pitch angle
θ_c	pitch command
θ_e	pitch attitude error
$\dot{\theta}$	pitch rate
$\ddot{\theta}$	pitch acceleration
Λ	wing sweep back angle
τ_1	time constant of control system lead
τ_2	time constant of control system lag
τ_{p_1}	time constant of pilot's lead
τ_{p_2}	time constant of pilot's lag
τ_{θ_2}	airframe lead time constant in θ/F_s transfer function
ω_3	undamped natural frequency of second order control system lag
$\omega_{n_{sp}}$	short period undamped natural frequency
ω_θ	pitch frequency
ω_ψ	yaw frequency

5.1 AERODYNAMIC STABILITY AND CONTROL LIMITATIONS

The primary stability or control characteristics which have caused serious limitations in the gross maneuvering capability for some contemporary fighters have been pitch up, roll reversal and wing rock with the closely associated phenomena of nose wander, nose slice (yaw divergence) and wing drop. Buffet intensity levels have also contributed to maneuvering and tracking degradation.

5.1.1 Buffet Onset

Earlier configurations, particularly those of low sweep, experienced a rapid progression from buffet onset to severe buffet and stall as the angle of attack increased. Accordingly, for these aircraft buffet onset served as a warning of an impending stall and the pilot could reduce the angle of attack or load factor before entering stall conditions. With most present-day fighters, buffet onset no longer serves this purpose since a wide "g" range often exists between buffet onset and the maximum usable lift, with considerable maneuvering being done in buffet. For example, Figure 5-3 shows the relationship of buffet onset to maximum usable lift in the high subsonic and transonic range for an F-4E aircraft with maneuvering flaps. This figure clearly indicates that the presence of buffet "per se" does not establish a maneuvering limit. Other factors, such as those discussed in the following sections, may establish this limit.

5.1.2 Pitch Up

Pitch up is normally related to a statically unstable longitudinal relationship indicated by lift and pitching moment data. It can usually be predicted from wind tunnel test results such as the example test data for a fighter model shown in Figure 5-4. In this example an unstable static stability region is shown in the 0.6 to 0.8 lift coefficient range. The elevator control power required to trim often rapidly decreases as the angle-of-attack is increased in the pitch up region. The rapid change in pitching moment with lift coefficient, unless immediately counteracted, by the pilot, would cause the aircraft to continue pitching up. If the aircraft was not artificially augmented, this characteristic could lead to loss of control. A less severe pitch up would probably preclude precise tracking in the angle-of-attack range where the instability occurred. Pitch up might drive the aircraft into an unstable lateral-directional region (yaw divergence) from which a stall and/or spin could be entered, if the unstable longitudinal

characteristic is very severe. Generally, the cause of pitch up with increasing angle of attack is related to one of three basic phenomena: (a) the wing center-of-pressure moving forward due to flow separation starting at the wing tips and then moving inboard and forward; (b) the effect of the wing wake on the horizontal tail as the tail is first immersed in the wing wake and then emerges; and (c) increased downwash at the horizontal tail for a high tail location.

Pitch up on the F-104 aircraft with its high T tail location occurs at the angle of attack where the wing tip vortices shed off the rather short span wing pass through the plane of the horizontal tail. These counter-rotating vortices induce a strong downwash field between them which inputs a sudden large down-load on the tail, causing pitch up.

Pitch up can be caused by a pitching moment variation with speed as well as with angle of attack. A change in longitudinal stability and/or longitudinal control effectiveness with Mach number can occur in the transonic region as illustrated in Figure 5-5. This characteristic makes it difficult to maintain control in a high "g" decelerating turn and, if severe, can cause pitch up into the yaw divergence regime. If less severe it will still degrade precision tracking. This phenomenon is also known to pilots as "dig-in".

5.1.3 Roll Reversal

Under conditions of high "g" at high angle of attack, the roll control effectiveness of ailerons or spoilers is reduced due to flow separation and due to changes in the lateral-directional characteristics. This decrease in roll power can be predicted by wind tunnel tests. The decrease in roll effectiveness as angle of attack is increased is generally more gradual for ailerons than for spoilers. An example is shown in Figure 5-6 for a variable sweep fighter at 30° leading edge sweep where ailerons and spoilers were separately tested on the same configuration.

Roll reversal is a response phenomenon for which a lateral cockpit control deflection results in a (steady state) roll opposite to the intended direction. This occurrence is not due solely to the decrease in aerodynamic effectiveness of the lateral control devices but is also determined by the amount of yaw resulting from the lateral control deflection, the lateral-directional stability relationship and, for rapid maneuvers, the inertia characteristics. An "effective" lateral control power expression for the "static" condition where inertia effects are ignored is:

$$C_{l_{\delta_A\,\text{effective}}} = [C_{RR}]\, C_{l_{\delta_A\,\text{aero}}} = \left[1 - \frac{C_{n_{\delta_A}}\, C_{l_\beta}}{C_{l_{\delta_A}}\, C_{n_\beta}}\right] C_{l_{\delta_A\,\text{aero}}}$$

Roll reversal occurs at conditions where the bracketed quantity $[C_{RR}]$ passes through zero. The value of C_{RR} can change very rapidly as angle of attack increases and consequently roll reversal can suddenly occur. An example is seen in Figure 5-7, where wind tunnel data for the F-4 was used to calculate the roll characteristics for +30°/−0° aileron deflection at a Mach number of 0.9 versus angle of attack. It can be seen that at an angle of attack of about 15° the effective roll power rapidly decreases and becomes negative while the aerodynamic roll power remains positive and does not decrease significantly.

$[C_{RR}]$ is a rough approximation to the $\left(\frac{\omega_\phi}{\omega_d}\right)^2$ parameter where $\frac{\omega_\phi}{\omega_d}$ is the ratio of the numerator and denominator second order terms in the roll rate to lateral control input transfer function. An estimate of this ratio which includes inertia terms gives a more accurate value for $[C_{RR}]$.

The effects of flexibility, particularly for outboard located ailerons, may serve to further reduce the roll effectiveness and lower the angle of attack at which roll reversal occurs.

5.1.4 Inertia Coupling

Inertia coupling in the form of gyroscopic effects will affect the pitch and yaw divergence boundaries during high roll rate maneuvers, and may result in autorotation or cross coupling such as a pitch response to a rudder input. This effect was first described in 1950 and an interesting history is presented in Reference 5-6.

High roll rate maneuvers are the most common cause of inertia coupling, and the divergences are normally associated with long slender aircraft which have pitch inertias much larger than their roll inertias, as is generally true of present high speed aircraft including fighters. The trend in inertia characteristics presented in Figure 5-8 from Reference 5-7 shows that high performance, high Mach number fighters will have inertia characteristics for which roll coupling may be a problem.

The Phillips stability diagram (Fig.5-9), taken from Reference 5-8, illustrates the relationship between roll rate (p) and pitch (ω_θ) and yaw (ω_ψ) frequencies. The stability boundaries are altered by the longitudinal and lateral-directional damping as indicated in the figure.

In most present day configurations the pitch divergence condition is rarely seen due to the larger aerodynamic stability in the pitch axis compared to the stability in the yaw axis. However, advanced concepts which employ relaxed (decreased) static longitudinal stability are being proposed for fighter aircraft. The YF-16 employs this concept and the inertia coupling pitch divergence phenomena was carefully considered in its design.

5.1.5 Wing Rock

As does buffet, wing rock begins with low intensity levels, often at the point of buffet onset, and builds up ultimately to a yaw divergence with an accompanying increase in the buffet level. This is not surprising since the lateral-directional instabilities of wing rock are primarily due to flow separation, as is buffet. Before yaw divergence (nose slice) occurs the earlier experienced characteristics may be nose wander, or wing drop, pure wing rock or roll/yaw wing rock (a rocking motion exciting the Dutch roll mode). Wing rock occurring before the limiting yaw divergence seriously degrades maneuvering handling qualities and can make precision tracking impossible. Yaw divergence may be expected at the angle of attack at which the Dutch roll frequency goes to zero. The non-dimensionalized coefficient expression related to the Dutch roll frequency is referred to as C_{n_β} dynamic. Several approximations to this parameter are being used; a common one is:

$$C_{n_\beta}\ \text{dynamic} = C_{n_\beta} - \frac{I_{zz}}{I_{xx}} C_{l_\beta} \sin \alpha .$$

Generally it is expected that those configuration features which increase the angle of attack at which C_{n_β} dynamic diminishes to zero will also improve the wing rock characteristics occurring before the yaw divergence. The use of leading edge flaps has been shown to improve C_{n_β} dynamic. An example is a modified F-4E aircraft, for which the resulting improvement in lateral-directional characteristics, including C_{n_β} dynamic is shown in Figure 5-10. Another concept to improve high angle of attack stability is employed on the YF-16 and YF-17 fighters and involves large forebody strakes. Properly designed strakes coupled with leading edge flaps can provide significant improvements in the high angle of attack lateral-directional characteristics. Figure 5-11 presents data obtained for a research configuration used in the development of the YF-16 aircraft. A comparison is shown of characteristics for configurations without flaps or strakes, with strakes, and with strakes and flaps. The significant improvements in directional and lateral stability at the high angle of attack (25°) condition are illustrated. These improvements serve to keep C_{n_β} dynamic positive up to very high angles of attack.

Since a purely longitudinal maneuver is rarely if ever encountered, another approach to determine the stability or departure boundary assesses simultaneously the dynamic directional stability (C_{n_β} dynamic) and the Effective Roll Reversal concept previously discussed. Reference 5-11 by Weismann compares C_{n_β} dynamic with AADP (Aileron Alone Divergence Parameter). In this reference the definitions are:

$$C_{n_\beta}\ \text{dynamic} = C_{n_\beta} \cos \alpha \quad \frac{I_{zz}}{I_{xx}} C_{l_\beta} \sin \alpha$$

and:

$$\text{AADP} = C_{n_\beta}\,|C_{RR}| = C_{n_\beta}\left[1 \quad \frac{C_{n_{\delta_A}}\, C_{l_\beta}}{C_{l_{\delta_A}}\, C_{n_\beta}}\right].$$

The boundaries shown in Figure 5-12 were established by evaluating the response due to a small sideslip disturbance using a six-degree-of-freedom computer simulation of the equations of motion for an aircraft in a high "g" maneuver.

A thorough understanding of the flow phenomena occurring during the progressive stages of wing rock is not generally available. However, several factors are thought to be involved. Flow separation on the wings is one factor and is very sensitive to angle of attack and sideslip. Consequently, slight asymmetries may result in significantly greater areas of flow separation on one wing than on the other. At transonic speeds the usual subsonic leading or trailing edge separation is present as is shock-induced separation. These phenomena will interact. The deflection of wing mounted controls or high lift maneuvering devices will affect the extent of separation and the location and strength of shock waves. Vortices, whether generated deliberately as with the prototype vortex-lift fighters or as a natural consequence of high angle of attack wing-body aerodynamics, will have a definite effect on the wing flow and the rolling moments due to asymmetric lift. For many configurations, the vortices shed by the nose or forward fuselage are particularly sensitive to small flow asymmetries.

As the angle of attack is increased an unstable leading edge vortex will form at the wing tip and move forward, up the wing leading edge. The point at which the vortex comes off the leading edge is very sensitive to sideslip. Small sideslip angles can cause significantly different separation patterns and, therefore, can result in asymmetric lift distributions with associated rolling moments.

In addition to problems originating with the wing flow field, the flow field in the vicinity of the horizontal and vertical tail is subjected to such phenomena as severe separation due to fuselage blanking, asymmetric downwash due to asymmetric wing lift, vortex interference and low dynamic pressure from the wing wake, and vortex bursting.

5.2 CURRENT FLIGHT CONTROL CONCEPTS

Flight control technology has evolved from straight mechanical stick-to-control-surface connections to the current

high-authority closed-loop electrical controls. Total fly-by-wire systems without mechanical backup have recently been tested in the USAF Survivable Flight Control System (SFCS) Advanced Development Program and on the YF-16 Lightweight Fighter Prototype. These aircraft have employed a "response command" (typically called a Command Augmentation System, CAS) flight control system. Such systems allow the designer great flexibility in optimizing the vehicle's flying qualities for the various mission tasks and for suppressing the effects of uncommanded aircraft responses to external disturbances.

The results of recent flying qualities tests of particular importance to fighter aircraft design will be discussed in the following sections.

5.2.1 Longitudinal Short Period Response

The design of fighter aircraft longitudinal control systems is complicated by the fact that these systems must provide satisfactory control both for abrupt high-g maneuvers and for precision tracking. In addition, the control characteristics best suited for air-to-ground gunnery differ from those which are optimal for air-to-ground bombing.

The flying qualities design criteria of Reference 5-12 require the aircraft's short period characteristics to fall within the region shown in Figure 5-13. These boundaries are based on classical aircraft systems for which the short period poles are easily identified and meaningful. With highly augmented or higher order systems it is usually possible to define an equivalent set of classical characteristics which closely approximate, in the time domain, the more complex response. This "equivalent system" approach is somewhat artful and not widely accepted for generalized criteria application. An additional criteria, first proposed by H.N.Tobie et al in Reference 5-13, has been extensively used recently by controls engineers. This criteria is known as C^* and is shown in Figure 5-14. The parameter C^* is defined by:

$$C^* = n_{z_{pilot}} + K\dot{\theta} \ .$$

The C^* parameter is primarily influenced by the pitch rate ($\dot{\theta}$) at low speeds and by the normal acceleration at the pilot's station at high speeds. The thought behind this parameter is that C^* corresponds to the primary controlled variable of concern to the pilot throughout the speed regime. This criteria is the subject of some controversy as to its general validity; for example, Reference 5-14 reports significant lack of correlation of system "goodness" with the original criteria. Its use is motivated primarily by the ease of checking the acceptability of a response with the time history envelope and also by the correspondence between the criteria and contemporary system feedback design. A block diagram of an advanced longitudinal control system typical of the TWeaD and Survivable Flight Control System programs (Reference 5-15 and 5-16, respectively) is shown in Figure 5-15. The $\dot{\theta}$ feedback is used to provide stability and the n_z feedback is employed to increase the speed of response. In the design of such systems, extensive ground-based simulation is normally used in conjunction with the C^* and other criteria to obtain satisfactory dynamics.

The most recent longitudinal response criteria proposed by the Cornell Aeronautical Laboratory in Reference 5-17 uses a closed-loop pilot-model formulation of a pitch attitude tracking task as shown in Figure 5-16. The suggested flight control system plus airframe design requirements are placed on the overall $\theta/\theta_c(s)$ transfer function characteristics, and limits are then set on the low frequency droop, peak resonance, and bandwidth (BW) as shown by Figure 5-17.

Several recent investigations (References 5-18 to 5-20) have concentrated on "task optimized control". Reference 5-20 has shown that, within the requirements of Figure 5-13, air-to-air gunnery accuracy can be improved by a factor of two. The importance of high short period damping is emphasized in References 5-18 and 5-20 for air-to-ground gunnery; both reports recommend damping ratios of 0.5 to 0.7 or greater for this task which basically involves pitch attitude control. Reference 5-21, however, investigated air-to-ground bombing with free fall weapons (a velocity vector control task) and found that pitch attitude control dynamics which were objectionable to the pilot but which gave more responsive velocity vector control resulted in significantly improved weapon impact accuracies (Fig.5-18). The zero static margin, low damped configurations, although acceptable for small perturbation precision flight path control, were unsafe in the abrupt recoveries following a dive bombing pass. Precise "g" control was extremely difficult and the aircraft tended to over-rotate and be subjected to overstress conditions. It is, therefore, very obvious that control task differences must be considered if optimum flight control designs are desired.

5.2.2 Longitudinal Stick Force

The primary combat maneuvering stick force parameter is F_s/g. The change of stick force with normal acceleration should be linear and should have the proper gradient; classically a minimum of 3 #/g. In the design of advanced fighters, two additional considerations are becoming important. These aircraft have the ability to sustain high load factors and therefore even a gradient of 3 #/g can result in relatively high stick forces at the maximum maneuver conditions. Reference 5-22 reports that for precision pitch control a real problem occurs for pilots if steady force levels of 30 lbs or greater must be held, and also that these high longitudinal force levels cause difficulty in control about the roll axis because of the force disharmony.

One of the major longitudinal axis improvements noted in the control augmented TWeaD F-4 aircraft (Ref.5-15) was the reduction in "stick force lightening" at high normal accelerations (Fig.5-19). Because of the "lightening",

pilots were reluctant to go beyond the linear portion of the F_s/g curve in the standard F-4. The TWeaD system allowed the pilots to utilize more of the F-4's available normal acceleration capability.

5.2.3 Trim Rate

Reference 5-23 reports that combat pilots often use longitudinal trim to relieve the precision control and harmony difficulties noted in the previous section. The trim rate for most contemporary fighters, however, is considered inadequate. Here again it is suggested that a two mode trim system with high rates for combat and a lower rate for cruise might be necessary. Parallel trim is preferred to series trim. With parallel trim, the stick position reflects the control surface position and is an indication to the pilot of the remaining available control authority.

A neutral speed stability mode has been investigated in the flight tests reported in Reference 5-15. This specific control system mechanization essentially eliminates the need to trim. The concept has proven to be satisfactory especially for accelerating air-to-ground dive attacks where conventional trimming will continually upset the tracking solution. Positive speed stability, however, is classically considered an essential ingredient for satisfactory flying qualities in the landing approach regime and even for cruise flight under manual control. In these flight tasks, the stick force cue occurring with a change in airspeed is important to the pilot.

5.2.4 Pilot Induced Oscillations (PIO)

PIO's remain a very complex problem with many possible causes and the occurrence is, therefore, often difficult to predict a priori. Reference 5-14 discusses several example PIO's demonstrated with the use of variable stability aircraft and Reference 5-24 presents a good discussion of PIO prediction through analysis. The causes of PIO's are usually either linear pilot/vehicle coupling or limit cycles induced by nonlinear elements in the control loop. The high speed, potentially catastrophic, cases are the ones which first come to mind and naturally attract the most attention. An example of a dramatic PIO occurrence, shown in Figure 5-20, was recorded during flight test development of the T-38 aircraft.

In terms of air-to-air and air-to-ground precision tracking, however, noncatastrophic PIO's can result and these are extremely degrading to task accomplishment. This phenomenon normally occurs in situations where the pilot's gain is driven to high levels by the demanding nature of the task. As the loop gain increases, the control loop will be driven toward instability. The effect of the pilot's gain in driving the aircraft's short period roots to the imaginary axis is shown in Figure 5-21. This same phenomenon was recently demonstrated in an inflight refueling evaluation using a matrix of configurations set up on the Variable Stability T-33 aircraft (Ref.5-26). The task was probe/drogue refueling and as the pilot approached the drogue basket his internal gain would of necessity increase and a PIO would develop. Aircraft control was no real problem until the task became sufficiently demanding.

5.2.5 Lateral-Directional Response

Again, as in the longitudinal case, there appears to be a difference between the preferred response characteristics for air-to-ground gunnery and for air-to-ground bombing; that is between attitude control and velocity vector control tasks. Reference 5-20 reports that the best gunnery results were obtained with Dutch roll frequencies and damping ratios well above the Level 1 requirements of Reference 5-12. For bombing, however, Reference 5-21 shows that high damping does not result in the best impact accuracy scores (see Figure 5-22).

5.2.6 Roll Control

Rapid and precise control of aircraft bank angle is a general requirement for any classically controlled fighter aircraft. Three parameters are typically involved in measuring roll control "goodness": (1) the roll response, currently measured by the bank angle achieved at a certain number of seconds following an aileron input (ϕ_t); (2) the roll mode time constant (τ_R); and (3) the roll control sensitivity, or response per pound of stick force.

The roll control characteristics required by current design criteria for fighter aircraft in combat are:

(1) Roll Response: $\phi_t \geq 90^\circ$ in 1.3 seconds

(2) Roll Time Constant: $\tau_R \leq 1.0$ second

(3) Roll Sensitivity: less than 15° in 1 second per pound of lateral stick force.

The maximum roll control power in general, however, is established by requirements at low speeds and/or abnormal flight conditions; for example, landing gust upsets and single engine control. In the case of an aircraft performing air-to-ground weapon delivery the lateral control power can be dictated by control requirements during a 4 to 6 g dive pullout with asymmetric stores. Therefore, many conditions must be checked during the design and test phases on an aircraft development to assure satisfactory roll control power.

Reference 5-12 requires that the roll mode time constant be less than 1.0 second in combat flight phases. Several recent studies have shown that a much more responsive system is very desirable. References 5-18, 5-19 and

5-27 all recommend an optimum τ_R in the vicinity of 0.2 seconds. Typical results from a ground based air combat simulation are shown in Figure 5-23. A rapidly responding roll mode, although beneficial for precision tracking, is not satisfactory for other flight phases such as cruise. Thus a situation occurs where selectable flight control system gains would be beneficial for task-optimized flying qualities. In addition, although no lower limit is given by current specifications for the roll mode time constant, it is intuitively certain that too abrupt a roll response would be undesirable.

5.2.7 Adverse Yaw

Adverse yaw is characterized by excessive aircraft yaw resulting from a roll maneuver. The cause may be due to the yawing moment from aileron and/or spoiler deflections, the dynamic derivative C_{n_p} or inertia coupling since the aircraft tends to roll about a body or principal axis rather than about stability axis and consequently angle of attack tends to become sideslip during large roll maneuvers. The difficulty may be eliminated by geometric changes affecting the aerodynamics, by the use of a mechanical or electrical roll/yaw interconnect, or by a combination of both. The interconnect may involve a fixed gain relationship between aileron and rudder deflections. Automatic systems may vary the gain based upon $\dot{\beta}$ and/or $p\alpha$ (roll rate times angle of attack).

The F-4 aircraft has such a large spin-inducing yaw-due-to-lateral-control characteristic at high angles of attack that for indicated angles of attack above nineteen units "rudder rolls" are normally employed. In most aircraft, however, the bank angle-to-rudder control loop is of poor quality. Advanced control systems are being designed to automatically utilize the rudder as a roll control surface at high angles of attack. Thus increasing emphasis is being placed on the bank angle to rudder response characteristics of aircraft. The F-4, for example, requires about 300 lbs of pedal force for full rudder deflection in some flight conditions; the F-105 is considered ideal with about 52 lbs pedal force for full rudder deflection. The amount of improvement potential in this area is indicated in Figure 5-24 from Reference 5-28 which shows the increased bullet stream yaw rate response that can be obtained with the F-4.

5.2.8 Gun Angle

The relationship between the gun angle, the velocity vector, and the roll command angular velocity vector is very important to the gunnery task. In Reference 5-29 it is shown (see Figure 5-25) that the flight control system can be used to improve the bullet stream response of the Viggen aircraft. The improved response is obtained by forcing the aircraft to roll about an axis slightly below the gun line. This results in a bullet stream response that is at all times in the same direction as the desired aiming error correction. It is also stated in Reference 5-29 that the preferred gun angle for air-to-air combat is slightly above the wing zero lift line.

5.2.9 External Disturbances

High maneuverability for an aircraft usually requires a relatively large wing and low wing loading. Such characteristics lead to configurations which are sensitive to gust upsets and turbulence. An air-to-ground attack aircraft also encounters wind shear layers at low altitudes during a diving attack.

Intelligent augmentation system design, however, can minimize the gust sensitivity of an aircraft about all axes. Command augmentation systems, for instance, can be designed with high bandwidth feedback loops which will, within limits, suppress all but the commanded responses. The desired lower control bandwidths are obtained by using prefilters on the input signals so that the system response is compatible with the control bandwidth of the pilot.

The new high muzzle velocity, 20 30 millimeter, rapid fire cannons can potentially cause significant upset moments when installed in contemporary aircraft. Recoil forces like those shown in Figure 5-26, if not passing directly through the aircraft's center of gravity, can result in very significant upsetting moments. To overcome the effects of these disturbances, either response command control systems or direct trigger-to-control-surface interconnects are usually employed. Although efforts are made to eliminate the moment disturbance, the direct force inherently remains. For instance, if the gun line is to the right of the c.g., a trailing edge left rudder deflection can cancel the yawing moment but a net side force will remain. This effect is very similar to one of the schemes used to obtain direct side force control as discussed in Chapter 6.

5.2.10 Velocity Response to Controls

The acceleration/deceleration responses of a fighter aircraft, particularly an air superiority aircraft, to throttle movements, use of afterburner, speedbrake deflections, etc., are probably one of the more important but least well understood areas in the aircraft control field. Several studies have investigated the relative effectiveness of various means for generating thrust/drag control, but the manner of tactical utility of these systems has not been addressed.

5.3 METHODS OF PREDICTION AND ANALYSIS

5.3.1 Analytical Methods for Aerodynamic Stability and Control Characteristics

The ability to adequately determine, by analytical means, the stability and control characteristics of maneuvering fighter aircraft can be most readily assessed by considering the prediction techniques currently available. These are thoroughly presented and discussed in the USAF Stability and Control Datcom (Ref.5-30). For the most part, proven methods are based on steady motion and potential flow theory, with viscous cross-flow effects and skin friction also taken into account. Such methods work well for aircraft configurations which can be broken down into largely independent aerodynamic components, with each making its own contribution to the stability derivatives. However, as was pointed out by H.H.B.M.Thomas in 1961 (Ref.5-31), the expanding speed range of fighter aircraft has led to more highly swept wings of lower aspect ratio, relatively larger fuselages, and close-coupled configurations for which mutual interference effects have become much more important. At speeds above the critical Mach number, shock-induced flow separation compounds the problem and the complexity of the analytical methods, which are further aggravated by the unsteady flow effects and the large combined angles of attack and sideslip encountered during combat maneuvering. There are no generalized prediction techniques by which these highly nonlinear characteristics can be accurately determined. Currently, the only feasible solution is to obtain experimental data for the specific configurations and flight conditions under consideration.

5.3.2 Wind Tunnel Predictions for Aerodynamic Stability and Control Characteristics

Presently, the developmental and substantiation testing for fighter configurations are primarily concentrated in wind tunnel static tests using rigid models for force, moment and pressure data. The force and moment data are obtained across the flight envelope, but are normally limited to approximately 30° angle of attack at high subsonic speeds and above. The takeoff and landing configuration is examined at low speed. Pressure data are primarily obtained to verify the wing pressure distribution at cruise conditions. Analytical means are used to apply "flexibility" corrections to the rigid body data to account for the effects of dynamic pressure and airloads on the flexible structure. Flexible models are tested to verify flutter boundaries. Dynamic derivative testing, by free or forced oscillation methods, is sometimes done at subsonic and transonic speeds. Spin modes and spin recovery are investigated with special models in a spin tunnel. Departure and very high angle of attack characteristics, upwards to 90°, are examined at low speed. Departure may also be investigated using tethered model tests during which the longitudinal and lateral-directional modes are controlled by separate pilots and the "thrust" is provided by a cable attached to the model (i.e., a "tethered" model) in a large low speed tunnel. A recent development is the use of "drop models" to investigate departure, spin and spin recovery. With this technique, large models (up to approximately three-tenths scale) are dropped from a carrier aircraft or helicopter at altitude and are controlled remotely from the ground. Parachute recovery is used. The YF-16 and YF-17 aircraft are being analyzed using this technique.

5.3.3 Analysis of Bare Airframe Characteristics

Digital computer programs are generally utilized in the analysis of bare airframe characteristics. The aerodynamic stability and control characteristics in derivative form, along with inertias and flexibility corrections, are put in the digital programs which represent linearized equations-of-motion, often broken down into uncoupled modes. Transfer functions representing aircarft responses to control or disturbance inputs are determined. These response characteristics can be compared with the requirements of handling qualities specifications such as MIL-F-8785B. Additionally, a digital "simulation" may be employed with coupled nonlinear six degree-of-freedom equations of motion. This simulation is particularly useful if proper accounting of the "inertia-relief" effects is required, and is the primary method for investigating roll-coupling and the loads occurring in design maneuvers.

5.3.4 Flight Control System Design

There are three main tools currently used for flight control system design: (1) computer analysis; (2) piloted simulation; and (3) flight test.

Standard analysis techniques involve modeling the airframe dynamics and the flight control system and subsequently testing the combination for its stability and response dynamics. The total system characteristics can then be compared with the variety of existing design criteria, such as those discussed in Section 5.2, to determine the system "goodness". In addition, analytical pilot models (transfer functions) are often used to close the controlled variable feedback loop and to test the pilot-in-the-loop stability. In one scheme, called "Paper Pilot" (References 5-32 and 5-33), the analytical pilot parameters are adjusted to optimize a performance functional and a predicted Cooper-Harper pilot rating (Ref.5-34) for the aircraft is obtained.

At the present time, ground-based flight simulators are being used extensively for flight control system design purposes. The primary reasons for this use are the lack of generalized design criteria for the complex flight control systems of current fighters and the high visual/motion fidelity of contemporary simulation facilities. For the study of one-on-one air combat, facilities such as the one at the NASA Langley Research Center (shown in Figure 5-27) can be used (Ref.5-35). These tools are excellent for design integration purposes because actual fighter pilots can be used to explore the interactions of controllers, displays, switchology, control modes, etc., in a realistic combat

environment. Centrifuges such as the one at the Naval Air Development Center at Warminster, Pennsylvania (shown in Figure 5-28) have also been used to study the effects of sustained load factor and buffet on tracking precision. It has been determined, however, that the use of such a device for general handling qualities investigations is limited because of the false motion cues inherent in the gondola rotations necessary to change the acceleration vector.

Finally, the ultimate flight control system evaluation is made in actual flight tests. Recent tests have been conducted using the Variable Stability T-33 aircraft to study flight control system design (Ref.5-26). These tests included realistic one-on-one tracking and gross maneuvering tasks. Also, the TWeaD and Survivable Flight Control System programs (References 5-15 and 5-16, respectively) conducted similar flight control system tests.

5.4 CONCLUSIONS

The maximum useable maneuvering capability of present fighter aircraft is often limited to "g" levels below the maximum aerodynamic lift capability by stability, control and handling qualities degradations. In addition, handling qualities degradations often prohibit precision tracking although gross maneuvering may still be possible. Automatic flight control systems (stability augmentation and command augmentation) are being employed to correct many of the bare airframe deficiencies and additional capability is being provided by advancements in the fire control systems.

CHAPTER 6

STABILITY AND CONTROL POTENTIAL FOR FUTURE FIGHTERS

by

J.L.Lockenour and W.G.Williams

6.0 INTRODUCTION

The preceding chapter discussed the complex closed-loop dynamic system which present-day fighters represent for accomplishing the tasks of air-to-ground and air-to-air combat. Particular emphasis was placed on transonic conditions since a significant amount of combat occurs in this speed regime. Advanced stability and control concepts aimed at further improving maneuvering and precision tracking are presented in this chapter. The proposed concepts will further complicate an already complex dynamic system. This complexity will demand an even more exact knowledge of the system dynamics and the aerodynamics involved, thus requiring the use of more advanced and in-depth analysis and prediction methods. This chapter discusses the proposed new modes of control, methods of generating the required forces and moments necessary to produce the motions, flight control system concepts to implement the maneuvering modes, and the additional impact of pilot factors. Methods of prediction and analysis are also presented, and recommendations are made regarding the concepts and areas of analysis which are considered to be most important for research support.

In this chapter the following symbology is used:

AMDA	advanced maneuvering demonstrator aircraft	DSFC	direct side force control
C_L	lift coefficient	fps	feet per second
$C_{L_{max}}$	maximum lift coefficient	H	altitude
C_m	pitching moment coefficient	L/D	lift to drag ratio
C_{m_0}	pitching moment coefficient at zero lift	RSS	relaxed static stability
C_Y	side force coefficient	TE	trailing edge
$\bar{c}$	mean aerodynamic chord	T/W	thrust to weight ratio
CEP	circular error probable	X	aircraft center of gravity position
DLC	direct lift control	δ_H	horizontal tail deflection

6.1 FUTURE FIGHTER FLIGHT CONTROL MODES

Substantial improvement in air-to-air and air-to-ground mission performance is expected with the application of new active control concepts aimed at providing uncoupled degrees of freedom, improved vehicle response characteristics, precision control for tracking, and direct control of the vehicle's attitude and velocity vector. Uncoupled motion capability provides direct translation control, with drag modulation providing velocity variations in the forward direction. Obtaining an uncoupled motion capability with optimized response characteristics requires a complex blending of control and thrusting forces which realistically can only be accomplished using fly-by-wire techniques. Discussed in the following sections are the expected advantages of several concepts and modes of operation currently being proposed or developed.

6.1.1 Direct Force Control

Direct force control may consist of direct lift, direct side force, and drag modulation modes and, with these capabilities, the potential for a fuselage aiming mode. Direct lift and direct side force provide vertical and lateral translation capability without vehicle rotation. Proposed concepts additionally aim to provide the translational motions with improved response time and damping characteristics. Direct force control is expected to improve fighter effectiveness not only in maneuvering, convergence and tracking tasks for air-to-air combat, but also in air-to-ground weapon delivery, terrain following, inflight refueling and take-off and landing. In the air-to-air role direct

lift control and direct side force control (DLC/DSFC) are expected to provide rapid translational jinking and thus permit evasion without visual cues, rapid load factor and attitude control, and precision tracking. In air-to-ground weapon delivery better survivability is expected due to shorter exposure times with more precise low level offset bombing and due to the capability to counter steady cross winds and/or provide gust alleviation. The fuselage aiming mode, an adjunct to most DLC/DSFC concepts, permit control of the fuselage position in angle of attack and sideslip, thus providing improved gun aiming ability and increased time on target.

DSFC was investigated in 1971 when a particular mechanization was evaluated in flight using the Variable Stability NT-33A aircraft. (Ref.6-1) This research vehicle was also used in support of the AX development (Ref.6-2), and the A-9A aircraft has DSFC capability for the air-to-ground role. In the variable stability T-33 study a factor of two improvement in weapon delivery accuracy, in terms of Circular Error Probability (CEP), was found for DSFC compared to the best conventional control configuration tested. Figure 6-1 shows some of the study results, in this case pilot rating and CEP with and without DSFC. Reference 6-3 reports on a ground simulation study of the air-to-ground task which also found similar payoffs for DSFC, as shown in Figure 6-2. These studies assumed that a fixed reticle gun/bomb sight was used.

Drag modulation, or control of the magnitude of the aircraft's velocity vector, can result in a tactical advantage by forcing an enemy overshoot or preventing an offensive overshoot. Concepts aimed at rapid and accurate speed control will also improve control/precision in formation flying and inflight refueling.

6.1.2 Flight Propulsion Control Coupling

The concept which ties together aerodynamics, propulsion and active control to provide one or more of the capabilities in direct lift, high lift, direct side force, and drag modulation is termed "flight propulsion control coupling". The total system is so configured that the pilot's command input to obtain a desired response is appropriately fed to the control and/or thrusting components so as to obtain the response optimized to a preestablished performance criteria. This criteria may involve maximum maneuvering capability, minimum fuel consumption, minimum structural stressing or some other performance goal. The thrust vectoring concept employed on the Kestrel/Harrier aircraft represents the existing capability regarding the integration of aerodynamic and engine thrust coupling for lift and drag control. For this aircraft thrust vectoring can be used either at relatively small deflections to increase turn rate performance at a given speed (as shown in Figure 6-3) or at larger deflections as a very effective speed brake (as shown in Figure 6-4).

6.1.3 Maneuver Enhancement Control

Conventional aircraft generate increased lift by a rotation (pitching) of the entire vehicle to a higher angle of attack. The direct lift concept discussed previously provides lift without rotation. For maximum maneuver response these two modes can be blended as illustrated in Figure 6-5. Proper blending can provide a quickened vehicle flight path response with reduced pitch rate overshoot. The initial reduction in load factor, occurring when conventional (aft) control surfaces are deflected, is eliminated. In addition to the quicker response, there is potential for greater maximum lift since the DLC capability should provide more flexibility to achieve a configuration optimized for the high lift aerodynamics.

6.1.4 Maneuver Load Control

As part of the general concept of maneuver load control an aircraft's wing geometry may be optimized either to maximize lift or to minimize structural loads (e.g., wing root bending). The latter may allow an expansion of the flight envelope (e.g., low altitude, high speed) without the usual requirements for additional structural weight.

6.1.5 Relaxed Static Stability (RSS)

Relaxed or reduced static longitudinal stability can improve an aircraft's performance by increasing the maximum lift capability and reducing the trim drag at cruise or in maneuvering flight. This concept involves a reduction in the bare airframe's stability to very low levels, most often even to an unstable condition, and the provision of stability by active controls. Due to the usual aft shift in an aircraft's aerodynamic center as the Mach number increases from subsonic to supersonic values, the maximum lift capability of present day configurations at supersonic speeds is often control power (trim) limited. This effect can be minimized by allowing a bare airframe instability at subsonic speeds.

Figure 6-6 shows the typical relationship of lift coefficient and pitching moment coefficient plotted for two different moment reference points (corresponding to two different center-of-gravity locations), one stable and one unstable. For simplicity in this example, the zero lift pitching moment coefficient (C_{m_0}) is assumed zero. For the unstable configuration, if trimmed with an aft horizontal tail a positive (up) lift would occur on the tail, thereby additing to the total lift. The stable configuration requires a down load on the tail and consequently the total lift is reduced. The trimmed drag is improved for the unstable configuration since no components of the aircraft are causing negative lift contributions. For non-zero values of C_{m_0}, the argument is still valid, if incremental lift contributions are considered.

The effect of RSS was examined in a study performed by McDonnell-Douglas and reported in Reference 6-5. A lightweight fighter weighing approximately 17,000 pounds and having a thrust-to-weight ratio of approximately 1.6 was evaluated for a range of center-of-gravity locations. Figure 6-7 shows that for a 6% negative static margin an increase in the maximum sustained turn rate at Mach number 1.2 of nearly 15% is achieved when compared to the turn rate with a conventional 4% positive static margin.

If only static trim requirements are evaluated it appears that the use of relaxed static stability with active control stabilization may reduce the horizontal tail size requirement, as indicated in Figure 6-8 from Reference 6-6. The picture is not so clear, however, if the effects of a gusty environment are considered. Figure 6-9 from the study reported in Reference 6-7 indicates the effect of gust inputs on required horizontal tail deflections at both landing approach and combat conditions.

6.2 METHODS OF GENERATING FORCES AND MOMENTS

The maneuvering concepts and modes of operation discussed in the preceding sections are only realizable if means for developing the required forces and moments are provided. The following sections discuss several potential concepts for generating these forces that are presently being postulated for future fighter applications.

6.2.1 Direct Lift

The direct lift concept provides vertical translation capability without aircraft rotation. Low levels of direct lift can be achieved with very rapid response rates. Usually the deflection of a single control surface will produce a moment in addition to the desired lift force and consequently compensation must be made if the aircraft's attitude is not to be disturbed. Thus most direct lift systems would require the coupling of several devices installed at different locations on the aircraft.

6.2.1.1 Horizontal Canards

Horizontal canards may be coupled with symmetrically deflected flaperons and/or the horizontal tail. With this arrangement, a moment balance may be obtained so that all surfaces are positive (up) lifting surfaces in contrast to the flaperon/horizontal tail direct lift arrangement which requires incremental down loads on the horizontal tail. A modification proposed for the F-4 aircraft incorporates such a canard arrangement (see Figure 6-10).

6.2.1.2 Variable Incidence Wing

This concept allows a significant part of the major lifting surface of the aircraft the freedom to be rotated with respect to the aircraft fuselage. Aerodynamically, this is similar to the operation of an all-moveable horizontal tail such as that on the F-111 aircraft and, indeed, a lightweight fighter might employ variable incidence wings of nearly the same size as this tail. Collective deflection of the wings, coupled with a tail deflection to balance the pitching moment, would provide direct lift and differential deflection of the wings would provide a rolling moment. A proposed configuration employing this concept is the McDonnell-Douglas AMDA (Advanced Maneuvering Demonstrator Aircraft) shown in Figure 6-11. This vehicle is described in Reference 6-8.

6.2.1.3 Vectored Thrust

Engine thrust may be vectored by nozzle deflections so as to provide a significant component of lift. If the engine nozzles are placed at the trailing edge of the wing or incorporated in part of the trailing edge flap, the exhaust jet may induce a large additional circulation over at least part of the wing (similar to a jet flap) and large induced aerodynamic lift gains may be possible.

6.2.2 Direct Side Force

The direct side force concept provides lateral translation capability without banking or sideslipping (by rudder control) the aircraft. As with the direct lift concept, the coupling of devices located at different places on the aircraft is usually required for a moment balance.

6.2.2.1 Vertical Chin Canard(s)

These surfaces may be coupled with a vertical rudder and the deflections of all surfaces may be adjusted to balance both rolling and yawing moments. This arrangement is incorporated in the proposed McDonnell-Douglas modified F-4 and AMDA designs shown in Figures 6-10 and 6-11.

6.2.2.2 Split Flap Vertical Tail

Split flaps on the wing may be asymmetrically deflected to provide balancing of the rolling and yawing moments induced by deflections of a vertical rudder which is used for side force control. This concept is employed on the A-9 close air support aircraft.

6.2.2.3 Differential Horizontal Canard

Proper positioning of horizontal canards can result in a configuration for which the canard/body flow field interaction will cause usable levels of side force when the canards are differentially deflected. Rudder deflection then augments the side force while balancing the yawing moment. Results from a USAF/AFFDL sponsored wind tunnel investigation (Ref.6-9) of this approach for a canard-wing-horizontal tail configuration are indicated in Figure 6-12. If this low speed side force capability could be maintained to transonic speeds, side acceleration levels of approximately one "g" for a moderately sized, lightweight fighter can be expected. Most significant are the good linearity of the side force and the fact that the capability is maintained to high angles of attack.

6.2.3 High Lift (High L/D and High $C_{L_{max}}$)

Generally, the methods discussed under direct lift in Section 6.2.1 can also be utilized to obtain high lift capability. The canard arrangement tested on the F-4 aircraft showed a significant lift improvement, particularly when coupled with the slotted leading edge flaps (a variable camber approach) as shown in Figure 6-13 from Reference 6-10. High lift for a configuration employing a variable incidence wing can be optimized, given the freedom to adjust the wing/body incidence relationship. The vectored thrust concept, particularly when coupled with supercirculation, can result in significant gains with respect to the lift polar for an unaugmented configuration.

6.2.3.1 Variable Contour Wing

In this concept the wing is contoured to the best shape for the flow conditions experienced in maneuvers and therefore the contour varies from the cruise shape. Several presently flying fighter configurations employ leading and/or trailing edge flap deflections when in maneuvering flight (e.g., F-4E with slats, YF-16, and YF-17). Until recently, high lift systems on most aircraft were only employed in the takeoff and landing flight phases. Improvements in the application of variable camber are expected to involve methods to provide smooth contours upon deflections (e.g., flexible surfaces); optimized deflections as a function of parameters related to the actual flow conditions the wing is experiencing, including Mach number, angle of attack, and dynamic pressure; and aeroelastic tailoring to adjust the camber and twist under loads.

6.2.3.2 Jet Flap

In this concept a gas flow, usually obtained from the engines, is exhausted down from the trailing edge of the wing, often with variable deflection angle and flow rate capability. Though some component of the increased lift is due to the vectoring of the exhaust flow, the primary lift augmentation is due to the increased circulation (super circulation) about the wing. The change in trailing edge pressures with a jet flap is also expected to modify the wing shock location. As mentioned previously, a hybrid concept involves a short span, high momentum jet flap and is referred to as vectored thrust supercirculation.

6.2.3.3 Vortex Lift Enhancement by Blowing

Since inducing a longitudinal flow in a vortex core can enhance its strength and stability, the concept of blowing into the wing leading edge vortex is being studied as a method to increase the lift and delay the vortex breakdown. Several approaches may be involved, e.g., spanwise leading edge flap blowing and issuing a jet from the fuselage oriented along and behind the wing leading edge.

6.2.3.4 Variable Sweep

Several aircraft which employ the variable sweep concept are in service. For these, the wing sweep position is nominally selected to minimize the drag at 1 "g" conditions (except for the landing mode) and, therefore, is a function of Mach number. Studies have shown that an optimized polar can be obtained for maneuvering flight, given the freedom to vary wing sweep during the maneuver. Figure 6-14, from Reference 6-11, shows the improvement in the L/D ratio for a research configuration at a Mach number of 0.8 when the wing leading edge sweep is varied from 30° to 20°.

6.2.3.5 Advanced Airfoil and Wing Body Designs

Under study are many concepts aimed at providing a total integrated configuration having high lift and high L/D capability. These include configurations with advanced transonic airfoils, the use of large forebody stakes, and other designs wherein the wing is not considered as the only significant lifting component. Increased emphasis is being placed on fuselage lift, e.g., the blended body designs.

6.2.4 Drag Modulation

Although kinetic energy is sacrificed when drag-producing "brakes" are deployed, a tactical advantage is sometimes achieved with their use. Decelerations can be obtained from speed brakes or spoilers, and inflight thrust reversing or thrust vectoring can provide the capability for a variation in drag levels. Figure 6-15 from Reference 6-12

shows a comparison of the deceleration capabilities for a typical speed brake and for a thrust reverser at two thrust-to-weight ratios.

6.2.5 Directional Stability Improvements

Ultimate maneuvering capability is most often limited by a degradation in the aircraft's lateral-directional stability and control characteristics. Maximum capability is particularly dependent upon maintaining directional stability to high maneuvering angles of attack. This will be accomplished by the development of configuration concepts which minimize flow separation, prevent rapid changes in flow conditions, and provide more nearly symmetric wing and forebody flow conditions while in sideslips. The prevention of asymmetric vortex shedding from the nose is required. High angle of attack stability improvements have been shown to occur with blowing along the leading edge and with well designed, properly positioned horizontal canards. The large forebody strake arrangement on aircraft like the YF-16 and YF-17 serves to strengthen and position the vortex at high angles of attack. A segmented leading edge flap may linearize the flow characteristics by fixing vortices at specific spanwise locations and simultaneously provide optimized deflections across the wing span to prevent flow separation during maneuvering.

6.3 ADVANCED FLIGHT CONTROL SYSTEM CONCEPTS

The current thrust of flight control technology is in two major areas: (1) digital flight control hardware and (2) control law development for the various modes discussed in Section 6.1.

With the recent successful flight tests of total fly-by-wire systems in an F-4 and the YF-16, the next logical step is to employ a digital computer as the "brain" of the control system. The primary advantage gained with a digital system is the ability to tailor the control laws in order to optimize the performance for each mission task. This concept is known as "multimode" flight control. As was pointed out in Chapter 5, the total system dynamics which are preferred in one task may not be appropriate for another. Therefore, multimode flight control is required for effective mission perfomance in each task.

A digital flight control system has been successfully flown on an F-8 aircraft by the NASA Flight Research Center at Edwards AFB, California, and the Swedish Saab A-37 Viggen is slated to have a digital command augmentation system. The US Air Force Flight Dynamics Laboratory (AFFDL) is installing a digital multimode control system in an A-7 aircraft and also is working with the USAF Avionics Laboratory on an integrated avionics/flight control digital program called DAIS (Digital Avionics Integrated System). Studies are also underway at the AFFDL to investigate an integrated flight control/propulsion control system. This concept would allow the blended use of both aerodynamic control surfaces and propulsion system controls of engine thrust, nozzle angle, jet flap, blow-out doors, etc., to obtain the desired pilot-commanded response of the aircraft.

The recent developments in direct force control, as described in Section 6.1, have greatly broadened the horizons of the flight control designer. The use of direct lift, side force, and drag modulation control along with the more conventional moment controllers has made it possible to decouple responses or to generate any form of blended response, of course within the configuration's control power constraints. The control laws for the best use of direct force modes are not yet fully determined, and the true payoff/cost effects of these capabilities are not fully known.

Control Configured Vehicle (CCV) fighter studies have shown that significant flow interference occurs with the deflection of forward mounted horizontal or vertical canards. Therefore there will be upsetting disturbances about other axes associated with these controllable canards. The use of any kind of gain-scheduled mechanical interconnect to sufficiently remove the effect of such disturbances will probably not be feasible and a command augmentation system, which attempts to negate all but the desired command response, will be required.

6.4 PILOT FACTORS

As pointed out in Chapters 2 and 5, there are many factors which influence the pilot's ability to control the vehicle in a combat task. Only the three most important factors will be discussed in this section: the displays, the controller, and the seat.

6.4.1 Displays

The air combat task is a "head-out-of-the-cockpit" effort with the pilot's concentration being devoted to the target aircraft. For this primary reason, heads up displays (HUD) are used not only for presenting the aiming reticle but also for providing useful flight control information such as range to target, height above the ground, and airspeed. Especially for air combat, the effect of displaying energy management information is also being explored.

The use of various computing gunsight schemes can have a very dramatic effect on the closed-loop stability of the tracking solution. Lead computing, tracer line, and director gunsights all involve sensing or computational delays.

A variety of compensation techniques such as damping and quickening or lead, are employed to provide a smoother track. However, these techniques create an error between the indicated and actual firing solution during transient maneuvers, and "settling time" is required before accurate aiming solutions are obtained. Therefore, the dynamics of the fire control/display subsystem must be taken into account when analyzing the total tracking accuracy control problem.

6.4.2 Controllers

Fly-by-wire flight control systems have now made it practicable to consider controllers other than center sticks, since any device which can generate an electrical signal can be used to control the aircraft. With additional considerations such as sustained high load factors and tiltable seats, the possible use of sidesticks or other controllers becomes attractive if not mandatory. The rigid sidestick shown in Figure 6-16 is being used in the YF-16 prototype program. Quadraplex sensors provide electrical signals to the flight control system proportional to the applied stick force.

The type of controller (rigid or motion, sidestick or centerstick, etc.) directly influences the response to control force gradients that are most desirable. In addition, the cues available to the pilot through the controller and the quickness with which a control input can be made are affected by the controller type and these, to some degree, influence the total system characteristics that are desirable.

6.4.3 The Seat

A recent development which markedly influences a pilot's ability to function under high load factors is the reclined seat or high acceleration cockpit shown in Figure 6-17. The seatback angle may be fixed, driven as a function of load factor or have discrete multiple position settings. Test data for this concept (Ref.6-13) shows that in a sustained 8 "g" maneuver, tracking performance is improved by a factor of 2 over that for a conventional upright seat position (see Figures 2-16 and 6-18). This data was obtained in centrifuge tests and a flight article will probably be tested in the near future.

6.5 METHODS OF PREDICTION AND ANALYSIS

6.5.1 Analytical Methods for Aerodynamic Stability and Control Characteristics

Preliminary estimates will continue to be calculated using techniques such as those in the USAF Stability and Control Datcom. Computerization of these methods, such as DigiDatcom, will greatly speed up the analysis process. Expansion of the methods to include the highly nonlinear characteristics occurring in high "g" combat maneuvers is needed. The most promising approach to the development of analytical methods of desired generality is an empirical approach guided by theory. Such a technique has been used successfully numerous times in the past, and provides, in addition to the prediction methods themselves, a fuller understanding of the dominant flow phenomena.

6.5.2 Wind Tunnel Predictions for Aerodynamic Stability and Control Characteristics

The scope and type of testing outlined in Section 5.3 will continue and will be augmented with additional testing. For the new fighter concepts, an increase in the number of devices employed over a greater operating range is expected and consequently the number of variables will increase substantially and the total amount of testing required will increase proportionally. The relaxation of stability levels makes it even more important that a solid degree of certainty is achieved as to the exact nature of the aerodynamic stability and control characteristics, since the aerodynamic margins for error are smaller when active "controls" provide the "stabilizing" function. It is expected that the rapidly driven control surface of some possible future fighter designs will experience unsteady aerodynamic effects and dynamic overshoots of surface loads. These effects will have to be determined experimentally. Dynamic derivatives will be more important and experimental values will have to be obtained.

The use of flexible wind tunnel models to obtain data on interactions of flexible performance, stability and control characteristics is being investigated. Composite materials are being studied and developed for the construction of flexible wind tunnel models. How to handle the effect of "inertia relief" with the tunnel simulation is yet to be resolved. High model strength in addition to scaled flexibility is required since the high "g", high angle of attack conditions are most important to combat maneuvering capability.

6.5.3 Analysis of Vehicle Response Characteristics

Since future fighters are expected to employ active control concepts as an integral part of their design, bare airframe handling qualities characteristics are not very meaningful. Six degree-of-freedom simulations with the automatic flight control system included in the simulation will be a necessity and will be used to determine responses to control or disturbance inputs as well as to investigate roll coupling and the loads occurring in design maneuvers. The size of the simulations will greatly exceed present requirements because of the increased number of devices, potential for more complex and nonlinear aerodynamics, increased impact of dynamic aeroelastic effects, and the additional complexity of the flight control system. The present lack of generalized handling qualities design criteria

for vehicles employing these new control modes will increase the reliance on piloted ground simulation studies and the use of analytical techniques which employ reliable mathematical models of the pilot.

6.5.4 Remotely Piloted Vehicles

Scale free flight models, remotely piloted from the ground will play an increasing role in the future; The use of "drop models", discussed in Section 5.3, may be expanded and these may become powered. Ultimately, complete powered scale vehicles, omitting maybe only the pilot, will be used in complex fighter developments as a means of demonstrating a high risk concept without the attendant risk to a pilot.

6.5.5 Flying Qualities Analysis

The primary current emphasis in new analytical flight control analysis techniques is the development of multi-loop pilot models. In all real flight tasks the pilot manipulates more than one control at a time (two axis center stick, rudder pedals, throttle, and trim) and/or reacts to a variety of motion, visual and control feel cues with each controller. In order to adequately model the pilot in a complex control task, all of the important input and output variables of the pilot must be included. In addition, in an air combat task, the pilot's control technique is influenced by such factors as tactics, situation (close or long range to target), and spatial position (high altitude or close to the ground). Sometimes the pilot operates as a closed loop controller, for example when he is the attacking tracker, and at other times, as is the case for most defensive evasive maneuvers, he operates in an open loop fashion.

At the present time, however, there is simply insufficient experimental data for the development of a multiloop pilot model. Past experience has indicated that results of engineering value can be obtained when significant simplifications are made. Hopefully, the same trend will hold true for multiloop pilot modeling.

6.5.6 Simulation

As stated in Section 5.3, the development of flight simulators is quite advanced. Existing facilities range from simple fixed base cockpits with only instrument displays to those with large amplitude motions, wide field-of-view color visual displays, and generators of other cues such as sound and g-greyout. A more sophisticated simulator, of course, gives a more precise representation, but such facilities are costly to build, maintain and operate.

To insure cost effective utilization of the spectrum of simulation capability, one must know what degree of sophistication is necessary to solve the problem at hand. One could, therefore, obtain a greater number of sufficiently satisfactory answers at less cost. To properly match the simulator to the problem, one will likely have to consider the task (landing, air combat, etc.), aircraft type, problem (pilot-induced oscillation, speed stability in the approach, etc.), and the extent of the variables to be studied. The intent of this last item is illustrated by the time histories in Figure 6-19 taken from Reference 6-14 which show that for a well behaved aircraft the lack of motion cues in the simulation does not completely prevent the completion of a landing flare maneuver. However, if the aircraft is statically unstable or somewhat more difficult to control, then the lack of motion cues can totally prevent the pilot from performing a flare and touchdown in the simulator.

Typically, simulation investigations have relied largely on the evaluations of the subject pilots as the measure of "goodness" of the flight control system. Some studies have used quantitative measures of performance, but there is no consistent set of meaningful parameters. It is, therefore, difficult to compare the results of one study with another.

6.5.7 Flight Test

The technology of parameter identification shows promise for improving stability and control flight testing. The methods can be used to identify only the airframe's stability derivatives or the total airframe/flight control/augmentation system dynamics. Improved parameter identification methods will be used for analysis of dynamic maneuvers. The use of parameter identification in conjunction with a flight test data telemetry system should greatly speed up the costly flight test programs for new aircraft.

Flight testing can also be improved using the new air combat maneuvering ranges (ACMR's) which were originally created for training purposes to allow safe and effective means for ACM training. An important feature of these ranges is the capability to incorporate computer generated weapon trajectories and hit/kill calculations. The same equipment obviously has the capability to determine the mission effectiveness advantage of one test aircraft over another. For example, the decision making process for fighter prototype "flyoffs" could be greatly enhanced by ACMR test data. Also, the payoff of any flight control system improvement for a given aircraft, say the F-4, could be determined by flying the modified F-4 against a standard model.

6.6 RECOMMENDATIONS

Several new concepts and modes of control for improving fighter maneuvering capability have been reviewed in

preceding sections. Analysis and prediction techniques required in the development of advanced fighters incorporating these concepts were also discussed. Research and development efforts are needed in these areas so that the payoff/cost relations can be determined and the useful concepts can transition to operational systems.

This section discusses further several technical areas specifically outstanding in their potential for payoff in systems application and in need of research support.

6.6.1 Vehicle Dynamics and Tracking Control

Increased combat maneuvering capability, including precision tracking and weapon delivery, requires improvements in: (1) gross maneuvering characteristics; (2) vernier vehicle control, i.e., small amplitude direct lift and/or side force; and (3) additional precision tracking provided by a controllable gun/gun sight. Work is required especially on the following aspects.

Future highly maneuverable aircraft will incorporate active flight control technology with blended control of components which are very closely coupled aerodynamically. The ultimate viability of any concept will be highly dependent upon the tractability of the stability and control characteristics which result from the complex aerodynamic interactions. Less margin for error in the estimation of vehicle characteristics can be tolerated for these aircraft which incorporate bare-airframe instabilities. The effects of nonlinearities become magnified and dynamic phenomena uncommon to more conventional designs may result, e.g., pitch coupling. Development of configurations having the necessary superior basic aerodynamic and inertial characteristics is needed.

In addition to direct lift and direct side force control now under study, control of the axial force vector will give complete direct force control. This means the coupling of aerodynamic surfaces and, more importantly, engine thrust (both magnitude and direction). Flight propulsion/control coupling is a critical technology area. Presently there are no requirements on the "speed control" dimension of flight control or handling qualities in the development of fighter aircraft. The importance of speed control in gaining or maintaining a position of tactical advantage in an air combat engagement needs to be measured, criteria for levels and rates need to be established, and control characteristics need to be defined.

Additional vernier tracking can be provided by developments in trainable guns and computing gun sights or by incorporating other flexibility in the gun and its dynamics. The tracking reticle dynamics are an integral part of the pilot/flight control/airframe/gun system when designing for air combat.

6.6.2 Parameter Identification

The application of newer parameter identification techniques, such as the Newton-Raphson method, for extracting stability and control derivatives from flight test results is needed. It will be particularly valuable when the methods can be applied to nonsteady-state maneuvers with a high degree of confidence. Presently, steady-state maneuvers, with controls pulsed so as to excite individual modes with minimum excitation of the other modes are being analyzed with parameter identification techniques. Success of the analyses has been mixed. A reliable method, refined to the point that the average engineer is capable of performing the analysis, is very much needed.

6.6.3 Optimal Control Techniques

Optimal control techniques have been applied to the design of flight control systems in recent studies. These studies have been limited in scope, with the control tasks and system degrees of freedom narrowly defined. Application of these techniques to the combined airframe/flight control system is a promising area for future work.

6.6.4 Flight Control in Preliminary Design

CCV (Control Configured Vehicle) is an aircraft design concept which provides for the inclusion of flight control system functional capability as part of the configuration development of a new aircraft. To date, however, the major design studies which have been undertaken involve a retrofit to an existing aircraft. This, of course, very greatly constrains the design. The development and exercising of a preliminary design technique for CCV is very much needed.

6.6.5 Multiloop Pilot Models

Most flight control tasks involve multi-input, multi-output pilot operation. An analytical model which is representative of the operating characteristics of a real pilot for specific critical control tasks would be very useful for early design purposes. Such a pilot model could be used with the mathematical models of the airframe and control/augmentation system for an early assessment of the total system closed-loop stability.

6.6.6 Flight Simulation

Flight simulation is extensively used today as an engineering tool from preliminary design through flight test to

operational usage. There is a real need for an understanding of the extent of simulation capability necessary (to assure credible answers) for each specific engineering application.

6.6.7 Digital Multimode Flight Control

The acceptance of fly-by-wire control system technology has brought with it the feasibility of employing a central digital computer and, therefore, the ability to change the control laws to fit the primary mission tasks. The conceptual and hardware technologies are available and the next step is to integrate and test such a system.

6.6.8 Generalized Criteria

Advances in technology, such as fly-by-wire, flight computers, new controllers, and control modes, have been rapid and it has not been possible for the development of generalized design criteria or requirements to keep pace. The result has been the use of relatively inefficient trial-and-error methods of design evaluation. The accumulation and correlation of data on advanced systems is necessary in order to guide the development of the next generation aircraft.

6.7 CONCLUSIONS

Highly reliable, fly-by-wire, active flight control technology has opened the door for the achievement of good control capability in highly maneuverable fighter aircraft. The blending of control modes by the flight control system will permit the operation of aircraft with its motion free of the constraints of classical aircraft dynamics. There is potential for optimized response characteristics which will improve both gross maneuvering and precision tracking. The unconventional handling characteristics exhibited by aircraft with these systems may require readaptation by the pilot, and the specification of desirable handling qualities with these modes will become necessary. Research and development efforts are required in flight control systems, fire control, energy management, and flight control/propulsion system coupling as well as in prediction and analysis methods. The automatic systems reasonably cannot be expected to compensate for inordinate deficiencies in the basic aerodynamic stability, control and performance characteristics. Development of aerodynamic configurations having desirable, tractable characteristics is necessary in spite of their anticipated highly complex aerodynamic interactions.

CHAPTER 7

BUFFET DEFINITION AND CRITERIA

7.0 INTRODUCTION

The presence of separated flow regions either on an aircraft's wing, tailplane, or fuselage or in cavities and bomb bays provides a sufficiently large energy source to disturb the airframe. Accordingly, the performance of the aircraft may be limited by such disturbance-induced vibrations or by the degradations in handling characteristics which may accompany them. The highly undesirable rigid body motions of aircraft at angles of attack above separation onset are referred to in the longitudinal axis as "bouncing", "pitch up" and "porpoising", and in the lateral-directional axes as "wing rocking", "wing dropping" and "nose slicing". These phenomena belong to the flight mechanics problem area and have a direct effect on aircraft controllability and the pilot's ability to hold an accurate flight path. A detailed discussion of these handling qualities problems has been presented in previous chapters.

Flow separation phenomena which cause flexible mode vibrations of the structure influence the aircraft's "ride qualities" and are referred to as buffeting. Both rigid and flexible aircraft motions of this kind may degrade the combat capability of an aircraft. Buffeting may not be considered necessarily as a flight limit but it always gives an indication that more adverse phenomena, especially affecting lateral-directional motions, may occur whenever the angle of attack or Mach number are further increased.

This chapter concentrates only on buffet. In Sections 7.1 and 7.2 two individual contributions summarize buffet definitions and criteria used for wings and tails and for bomb bays.

Besides the rigorous approach of solving the complete dynamic response equations, as described in Chapter 4, there are powerful methods to predict wing buffet penetration levels based on certain criteria from rigid model wind tunnel testing. All the methods take into account deviations from linear behavior or kinks in the curves of particular aerodynamic quantities plotted either versus angle of attack or Mach number. The most frequently used quantities are lift, pitching moment, trailing edge pressure (based on the work of H.H.Pearcy), and root wing bending moment (based on the work of D.G.Mabey). In particular, correlations between rms wing root bending moments measured on rigid wind tunnel models and buffet levels on full scale aircraft, referred to as "onset", "light", "medium", and "heavy" buffet, have been established. The degree of unsteadiness in the separated flow is highly dependent on the nature of the flow separation, which is characterized by the type of leading edge or trailing edge separation as well as the spanwise stall departure. Interacting with a shock wave the flow separation can cause essential differences in buffet sensitivity between low and highly swept wings.

In addition to the main discussion on wing buffet in Section 7.1, general views are also presented on tail buffet, which usually is due to an excitation by the wing wake. In less frequent cases flow separation on the tail itself or flow separation on an aft-fuselage region have been identified as the cause for inconvenient or even unacceptable tail oscillations.

Finally, Section 7.2 contains a comprehensive description of the state-of-the-art of predicting open bomb bay buffet. Conclusions and Summary Remarks are presented in each of the two main sections rather than combined at the end of this chapter.

7.1 WING AND TAIL BUFFET* by D.G.Mabey

This Section presents a cautious examination of the physical processes at work above the buffet boundary on aircraft, when the boundary layer has separated. We still really know very little about these processes but it is hoped that Section 7.1 may stimulate further research and questioning, and more precise measurements of buffet onset and the severity of buffeting.

The prediction of buffeting is a difficult and controversial topic. Any presentation would evitably involve a degree of selection, and the author of Section 7.1 accepts responsibility for this. The references provided an up-to-date introduction to some of the more important papers. In Section 7.1 the following notation is used:

---

* This Section is based on a Specialists Lecture titled "Beyond the Buffet Boundary", presented at the Royal Aeronautical Society on 5 December 1972 and published in the Aeronautical Journal in April 1973.

c	wing chord (m)
$C_B = C_B(M,)$	buffeting coefficient — wing root strain signal/kinetic pressure (arbitrary units)
C_B', C_B''	dimensionless buffeting coefficients defined in Equations (7-3) and (7-4)
C_L	lift coefficient
f	frequency Hz(c/s)
$F(h)$	contribution to p^2/q^2 in frequency band Δf
$\sqrt{nF(n)}$	$p/q(\epsilon)^{1/2}$
K	transformation factor Equation (7-3)
L	typical dimension
l	bubble length (m)
n	frequency parameter fL/V
p	pressure fluctuation in a band Δf at frequency f (N/m^2)
p	rms pressure fluctuations (N/m^2)
p^2/q^2	$= \int_{\log n=-\infty}^{\log n=\infty} nF(n)d(\log n)$
q	kinetic pressure $\frac{1}{2}\rho V^2$ (N/m^2)
R	Reynolds number — based on aerodynamic mean chord
V	free stream velocity (m/s)
x	distance from leading-edge (m)
α	angle of incidence or angle of attack (°)
ϵ	analyser bandwidth ratio ($\Delta f/f$)
Λ	sweep angle (°)
ρ	free stream density (kg/m^3)

7.1.1 DEFINITIONS

We must first establish what we mean by buffeting. Buffeting is defined as the structural response to the aerodynamic excitation produced by separated flows. In the example sketched in Figure 7-1, there is a large area of separated flow on the wing. This provides the excitation which at a given point may be characterised by the rms level, the frequency spectrum (we shall see that the spectrum is often fairly flat at low frequencies), the degree of correlation in space and time, and the length scale. The pressure fluctuations excite a response of the structural modes which we call buffeting. The aircraft structure acts as a selective filter for the excitation so that spectra of buffeting always contain pronounced peaks at structural frequencies. In the example sketched in Figure 7-1 both the wing and the tailplane are excited. Rigid body modes may also be excited, such as "wing rocking", "wing dropping" or "nose slicing", but these are at much lower frequencies and can be regarded as aircraft handling problems, of great importance but outside the scope of this chapter. Buffet onset is often defined as the first appearance of a significant area of separated flow, although aerodynamicists often argue about how large the area must become before it is significant. (This is one of the uncertainties inherent in the theoretical methods for the prediction of buffet onset now being developed. These methods are briefly discussed in the Appendix, Section 7.1.7.) The onset of buffeting in flight is even more difficult to specify, for much of our present data are based on pilot impressions, which may be inaccurate if the pilot sits on or close to a node of the predominant modes being excited. Most pilots expect wing buffeting to provide a warning of more serious phenomena such as stall, pitch up or wing-drop, and are unhappy with aircraft which do not provide such a warning, unless an automatic visual or audio warning system is fitted.

The term buffeting was apparently first introduced into aeronautical literature when a structural failure occurred to the tail of a Junkers monoplane in 1930 (Ref.7-1). This failure was attributed by the British accident investigation to buffeting of the tailplane excited by flow separations on the wing. The flow separations on the wing were caused by an encounter with a severe gust and the German investigation attributed the accident directly to the structural failure of the wing caused by the gust (Ref.7-2). This incident emphasises again that buffeting often occurs in critical flight situations, when limit loads are being approached or when the aircraft is approaching lateral or longitudinal stability boundaries.

A consistent, dimensionless representation of excitation spectra is required when comparing measurements made at different flow densities and velocities. We shall adopt the notation suggested by T.B.Owen (Ref 7-3) and represented in Figure 7-2. Here we have a frequency parameter

$$n = fL/V$$

where f = frequency (Hz)

V = velocity (m/s)

and L = typical dimension (m).

We also have a buffet level

$$p/q\sqrt{\epsilon} = \sqrt{nF(n)}$$

where p = pressure fluctuation in a band Δf at frequency f

and $\epsilon = \Delta f/f$ = analyser bandwidth ratio.

7.1.2 BUFFETING CRITERIA FOR FIGHTER AND TRANSPORT AIRCRAFT

Figure 7-3 illustrates how buffeting criteria, expressed in terms of C_L — M boundaries, can influence the choice of wing loading for fighter and transport type aircraft. The boundaries presented for onset, light, moderate and heavy buffeting are based on some unpublished RAE measurements (Ref.7-4). (These boundaries are derived by a method outlined later.)

A typical fighter aircraft (with a wing leading-edge of sweep angle 42°) will cruise well below the buffet onset boundary, but will frequently perform 5g manoeuvres which take it well beyond the buffet boundary to the moderate buffeting, or even to the heavy buffeting contour. For a fighter aircraft the moderate buffeting limit is sometimes taken as the highest level at which guns or missiles can be aimed successfully, whereas the heavy buffeting limit is that at which the aircraft becomes useless as a weapon platform, but is still controllable. For a fighter, frequent buffeting loads can seriously influence the fatigue life of the structure, for they are considerably larger than the loads caused by turbulence.

In contrast a typical transport aircraft (with the wing leading-edge of sweep angle 27°) may cruise at about 0.1 in C_L below the buffet onset boundary. On infrequent occasions the aircraft may encounter a strong gust* which carries the aircraft beyond the buffet boundary, right up to the moderate buffeting level. The steady load achieved during the excursion into buffeting is probably more serious than the buffeting loads, which may be little larger than those associated with the atmospheric turbulence encountered during every flight.

Buffeting on fighter and transport aircraft only determines the extent of the penetration beyond the buffet boundary if there are no other handling limitations, such as wing rocking, wing dropping, pitch-up or stalling. We will return to this point later in this chapter.

7.1.3 CLASSIFICATION OF WING FLOWS AND BUFFETING

A broad classification of wings with separated flows that excite buffeting will be useful as a framework for our discussion, even if the classification suggested is incomplete (Fig.7-4).

Wings with low angles of sweep are characterised beyond the buffet boundary at subsonic speeds by leading-edge or trailing-edge separations. These separations form bubbles on the wing which usually excite heavy buffeting. At transonic speeds the presence of strong shock waves nearly parallel with the leading-edge add to the difficulties of predicting the flow, so that we give this flow a prediction rating of 10. (These prediction ratings are arbitrary and not used in any calculations, an increase in prediction rating represents increased difficulty of prediction.) Swept wings are characterised by a combination of mixed flows (Ref.7-6) which are difficult to predict. The separated flows on a swept wing at transonic speeds may include shock waves (which vary in intensity across the span), bubbles (from the leading-edge or the trailing-edge) and vortices. Thus a small increase in Mach number may dramatically alter the position of a shock wave or the reattachment point of a bubble. Similarly an increase in unit Reynolds number or a change of the roughness band used to fix transition on the model in wind tunnel tests may completely alter the character of the shock wave/boundary layer interaction (References 7-7 and 7-8). These difficulties seem to justify a prediction rating for swept wings of 100, an even higher rating would be appropriate for a variable geometry wing.

Slender wings with sharp leading-edges are characterised by a simple vortex type of flow, which prevails over the complete speed range from subsonic to supersonic speeds. This unified type of flow is a powerful argument for the application for supersonic aircraft (Ref.7-9). The vortices, which produce significant non-linear lift, have a well defined, small scale structure and we shall see that they do not produce severe buffeting unless vortex breakdown occurs at high angles of attack outside the normal flight envelope. In addition the vortices on slender wings

* The gust of 12.5 m/s selected in this example would have a wavelength of about 33 m (Ref.7-5).

with sharp leading-edges are relatively insensitive to wide variations in Reynolds number. Hence slender wings are given a prediction rating of 1.

These prediction ratings are, of course, arbitrary, but they reflect real differences between the flows, which will now be considered in greater detail.

7.1.3.1 Unswept Wings

The character of the excitation caused by leading-edge separation bubbles on unswept wings may be inferred (Ref.7-10) from the simplified model for a bubble suggested by Norbury and Crabtree in Reference 7-11 (Fig.7-5). In the constant-pressure region of the bubble, we would expect the excitation caused by low frequency fluctuations in the separation point to be relatively small, whereas in the reattachment region, where the rate of pressure recovery is high, the excitation should be much higher. Thus the excitation might be expected to reach a maximum in the middle of the reattachment region. These inferences from the mean static pressure distributions are broadly confirmed by the measurements, although the excitation attenuates both upstream and downstream of the reattachment region owing to the influence of the shear layer.

The spectrum of surface pressure fluctuations for a boundary layer approaching separation in an adverse pressure gradient may be divided into high-frequency and low-frequency components (Ref.7-12). The high-frequency pressure fluctuations are similar to those found under a boundary layer in zero pressure gradient (Ref.7-13) and are generated in the small scale inner region of the boundary layer associated with the law of the wall. The low-frequency pressure fluctuations are generated in the large-scale outer region associated with the law of the wake, and increase in intensity as the outer region of the boundary layer thickens. Between separation and reattachment, measurements suggest that the low-frequency pressure fluctuations continue to increase steadily as the separated boundary layer thickens, until a point is reached where the mixing layer turns towards the surface and the mean pressure starts to increase*. Somewhere close to the reattachment point, the measurements for a wide range of bubble flows show a maximum value of the rms pressure fluctuation coefficient of

$$p/q \text{ between } 0.10 \text{ and } 0.04 .$$

The spectra also show a marked similarity if the frequency parameter n is based on the bubble length l, for a peak pressure fluctuation is found when

$$n = fl/V = 0.5 \text{ to } 0.8 . \qquad (7\text{-}1)$$

This probably implies a feed-back process between conditions at the reattachment and separation points. Equation (7-1) will be inappropriate when there is a strong, coherent disturbance in the wake (e.g., a Kármán vortex street) or if there are acoustic resonances (as there may be in cavities). The measured pressure fluctuations always cover a broad band of low frequencies, rather than a single discrete frequency as given by Equation (7-1), probably because the velocity of the eddies in the shear layer varies with the eddy size.

Leading-edge bubbles may be important for aircraft with sharp leading-edges, for which we have some good excitation measurements (Fig.7-6). Leading-edge bubbles were formed on the centre section of the Bristol 188 aircraft (Ref.7-15) and on a Venom aircraft with a sharp leading-edge (Ref.7-16). Figure 7-6 shows that the rms excitation at two points on the Bristol 188 increases gradually from separation ($x/l = 0$), reaches a maximum of

$$p/q = 0.10$$

just upstream of the reattachment point ($x/l = 1.0$), and then decreases. The frequency parameter n based on the bubble length has a maximum at about $n = 0.7$ and correlates the spectra quite well at $x/c = 0.85$, where most of the measurements are taken in the region of rapid pressure recovery ($x/l = 0.94$). The peak level is about $\sqrt{nF(n)} = 0.006$. (The parameter n does not work so well at $x/c = 0.50$, where some of the measurements are taken in the constant steady pressure region ($x/l = 0.56$).) Measurements of pressure fluctuations on a Venom aircraft also conform to the general pattern shown in Figure 7-6(a) and show no significant variation in the rms pressure fluctuations or the spectra over the Mach number range from $M = 0.3$ to 0.6. Only a small Reynolds number effect on the low-speed pressure fluctuations was measured between the aircraft and a model (Ref.7-16). Some pressure fluctuation measurements on aerofoils with round leading edges recently published (Ref.7-17) suggest similar rms levels and a peak frequency parameter of about 0.8 to 1.0.

Equation (7-1) helps us to discriminate between the excitation frequencies associated with long and short bubbles because of the large change in the bubble length between the two flows. A long bubble covers a significant area of the aerofoil chord and, from Reference 7-18, because

---

* Bradshaw has shown that the flow in the reattachment region is dominated by a rapid reduction in eddy size as the shear layer is divided into two halves. The lower half of the shear layer moves upstream from reattachment, the upper half moves downstream. It seems reasonable that this sudden reduction in eddy size should be accompanied by a sudden reduction in excitation at low frequencies.

$$l/c = O(1)$$

the pressure fluctuations will be at comparatively low frequencies which can excite the structural modes; e.g., for a long bubble on a wing with a chord of 3 m moving at 70 m/s, the excitation frequency would be

$$O(12\ Hz).$$

(Typical wing fundamental bending frequencies are 10 Hz for a small aeroplane and 2 Hz for a large aeroplane.) A short bubble only influences a small area of the wing, but, in addition, because

$$l/c = O(0.01)$$

these pressure fluctuations will be at such high frequencies that they are unlikely to excite structural modes; e.g., for a short bubble on a wing with 3 m chord moving at 70 m/s, the excitation frequency would be

$$O(1200\ Hz).$$

Flight tests on the Venom with a sharp leading-edge (Ref.7-16), and the canard control of the XB-70 (Ref.7-19), showed that buffet onset corresponded with the formation of a long bubble. The buffeting then increased steadily as the bubble extended downstream, until the reattachment point approached the trailing-edge and the trailing-edge pressure diverged. This point corresponded with heavy buffeting. Hence the local pressure fluctuations within a long bubble must be quite strongly correlated.

The character of the excitation caused by a spoiler of height h (Fig.7-6(b)) closely resembles that caused by a leading-edge bubble. The excitation increases steadily from separation and reaches a maximum of

$$p/q = 0.05$$

just upstream of reattachment. The peak frequency parameter n for the spoiler is about 0.9 in the experiments of Fricke, rather than 0.7 for the leading-edge bubble. The experiments of Fricke (Ref.7-20), in air, and of Greshilov (Ref.7-21), in water, give peak frequency parameters of about 0.9 and 0.8 although the bubble lengths are respectively 16 h and 5.5 h. The coincidence of the frequency parameters based on bubble length confirms that this is a useful parameter for comparing the spectra of the pressure fluctuations generated by bubble flows.

The character of the rms pressure fluctuations and spectra caused by bubbles is largely independent of the origin of the bubble (Ref.7-10). Thus, in particular, the maximum pressure fluctuations occur just upstream of reattachment for

leading-edge bubbles,
bubbles downstream of spoilers,
bubbles downstream of steps,
bubbles upstream of steps,
bubbles downstream of sudden expansions in pipes,
bubbles within shallow cavities (Fig.7-7).

Thus the data correlations presented in Reference 7-10 have application to a wide class of flows.

The prediction of the onset and severity of buffeting is of crucial importance at transonic speeds. In this speed range, the mixed subsonic/supersonic flows and the different regimes of shock/boundary layer interaction can modify the model for bubble flows described here, at least near the shock. However, downstream of the shock, an approximately constant average pressure is often observed in the separated flow region, followed by a rapid rise to reattachment. Coe's investigation (Ref.7-22) of the loads on launch vehicles included some measurements at subsonic and transonic speeds of the mean and fluctuating static pressures caused by a separation bubble downstream of a step in a body of revolution (Fig.7-8). Both the mean and fluctuating pressure distributions aft of the step correspond very well in general character with the low-speed pressure distributions over the complete speed range from M = 0.60 to 1.19, although the maximum fluctuating pressure falls steadily from

$$p/q = 0.06 \text{ at } M = 0.80$$

to

$$p/q = 0.03 \text{ at } M = 1.19.$$

This fall in the pressure fluctuations is probably due to the improved stability of the mean bubble flow because of the reduction of upstream influence from the reattachment region as the region of supersonic flow expands. (The base-pressure fluctuations on a body of revolution also fall from subsonic to supersonic speeds and a similar explanation may be applicable (Ref.7-23).) The mean pressure distribution suggests that the length of the bubble does not change significantly from M = 0.60 to 1.19, so that, within this speed range, there is probably no major change in the internal structure of the bubble.

The apparent universality of the pressure fluctuations caused by bubble flows at subsonic speeds is also well illustrated in Figure 7-8 which includes the pressure fluctuations measured (Ref.7-24) behind a two-dimensional step at $M = 0.33$ as well as those measured (Ref.7-22) behind a step on a body of revolution at $M = 0.80$. The similarity at subsonic speeds between both the rms pressure fluctuations and the spectra for the two different experimental configurations and Reynolds numbers is good.

Recently some interesting measurements of the excitation on a two-dimensional lifting aerofoil at transonic speeds were made by Moss and Mundell and reported in Reference 7-25 (Fig.7-9). The condition selected for this aerofoil ($M = 0.82$, $\alpha = 6.7°$) is just beyond buffet onset. Although the trailing-edge pressure has not yet diverged, there is a short separation bubble on the aerofoil (with a length of about $l = 0.1\ c$) immediately downstream of the shock-wave. The position of the bubble was inferred from the shape of the mean pressure distribution, because it could not be seen in oil flow tests. (The interpretation of oil flow tests on two-dimensional aerofoils is often difficult because there are no telltale inflexions in the streak lines as there are on swept wings.)

The excitation measurements along the chord are presented from two frequency parameters

$$n = fc/V = 0.08 \text{ and } 0.8 .$$

At a frequency parameter of $n = 0.08$, a typical value for wing structural modes, there is a large local increase in excitation in the vicinity of the shock wave. This local excitation decreases rapidly downstream of the shock wave but then shows a small local maximum in the vicinity of the reattachment region, before decreasing again. This variation in low-frequency excitation must be caused by the coupling of the shock wave motion (at separation) with the development of the bubble and with conditions at reattachment. In contrast, at a frequency parameter of $n = 0.8$, a typical value for wing panel modes, the excitation increases progressively downstream from the shock position, reaches a maximum close to the reattachment line and then falls rapidly as in the other bubble flows discussed in this section.

To find how the excitation develops, the angle of attack may be increased at constant Mach number. The separation bubble then extends rapidly towards the trailing-edge and the trailing-edge pressure diverges, while the shock wave starts to move upstream slowly. Thus the area of the aerofoil influenced by both the low frequency and high frequency excitation increases, and a progressive increase in buffeting would be expected. It should be noted that as the bubble extends rapidly in length from about $l = 0.1\ c$ to $l = 0.5\ c$, the predominant bubble frequency parameter will fall from $n = 8$ to $n = 1.6$, so that there should be a large increase in excitation in a frequency range centred on this lower value.

7.1.3.2 Swept Wings

Figure 7-10 shows the complex separated flow on a typical model with swept wings at a Mach number of 0.80. These sketches illustrate some of the features which make buffet prediction difficult for swept wings and justify the prediction rating of 100 allotted in Figure 7-4. At buffet onset there are at least three shockwaves on the wing and a small shock induced separation bubble (with a length of perhaps 0.05 c) immediately downstream of the strongest shock wave, which runs roughly parallel with the leading-edge. At moderate buffeting there are complex shock patterns on the wing, areas of separated flow and areas with attached flow having a strong spanwise velocity component. (Great care is always necessary to achieve an optimum transition fix for the boundary layer under high lift conditions like this at transonic speeds.)

Pressure fluctuations are presented for a single point P on the wing; Figure 7-11 shows the variation of rms pressure fluctuations with the angle of attack. An attempt is made to explain this variation, but it is speculative because of the difficulty of discriminating between local events at P and what is happening simultaneously elsewhere on the wing. A local Mach number of 1.0 is reached at a small angle of attack at a point on the wing near the leading-edge and close to the tip. A local region of supersonic flow then develops as the angle of attack increases. This supersonic region is terminated by a shock wave, which oscillates upstream and downstream. The pressure fluctuations at P first increase slowly with the angle of attack (point A, $\alpha = 1.8°$) because of the combined effect of the shock oscillation and the pressure fluctuations caused by an attached boundary layer growing under an increasingly adverse pressure gradient (Ref.7-12). As the terminal shock wave approaches and passes the transducer position (point B, $\alpha = 5.0°$) the pressure fluctuations increase rapidly; the major part of this increase must come from the shock wave oscillation. Shortly after point B the boundary layer separates at the terminal shock, and the terminal shock then starts to move forward and buffeting is detected by the wing-root strain gauges. (Thus the wing-root strain gauges give a measure of the integrated excitation on the wing.) When the terminal shock moves upstream of the pressure transducer the local pressure fluctuations fall rapidly to a minimum at about $\alpha = 6°$ because the point P is no longer influenced directly by the shock oscillation. The pressure fluctuations then increase to a maximum (point C, $\alpha = 7.2°$), when the reattachment line crosses the pressure transducer, just as on the aerofoil (Fig.7-9). The local pressure fluctuations then decrease as the bubble extends downstream, although the wing buffeting, which is the response to the total excitation on the wing, continues to increase steadily from moderate to heavy.

The spectra of the pressure fluctuations provide additional information. Figure 7-12 shows that at point A, well below the buffet onset, the increase in pressure fluctuations is above the frequency range of wing modes. At the point B, with the terminal shock oscillating across the transducer, the peak pressure fluctuations become larger and move to lower frequencies, within the range of wing modes. At the point C, this peak is lower, because the shock is upstream of the transducer. However we notice at point C that there is an increase in pressure fluctuations at high frequencies ($n > 0.5$). This may be associated with the separation bubble downstream of the shock. By analogy with the low-speed results, we might expect to find a second peak in the spectra at $n = 5$ to 10 with this short length of bubble ($l \triangleq 0.1$ c) but the present measurements did not extend much beyond $n = 1.0$.

This is obviously only a simplified account of the development of the excitation, using data from a single point on a wing. A complete description of the excitation all over a wing (including rms levels, spectra and correlations) would be difficult to achieve. Extensive computing facilities would also be needed to utilize this data. Hence few measurements of excitation are currently available for swept wings at transonic speeds. However, we can learn a great deal about the wing behaviour from buffeting measurements, and these are discussed in Section 7.1.4.

7.1.3.3 Slender Wings

The fluctuating normal force measurements of Farnshaw and Lawford (Ref.7-26) (Fig.7-13) show that slender wings with sharp leading-edges can operate up to quite high angles of attack (and hence achieve reasonably high lift coefficients) without experiencing strong excitation. Although these tests were made at low Reynolds number ($R = 0.2 \times 10^6$ to 0.4×10^6), the flow characteristics of wings with sharp leading-edges are insensitive to wide changes in Reynolds number, primarily because the separation lines are fixed.

Recent measurements on the Concorde by BAC/Aerospatiale confirm that the level of excitation is light and almost identical with that measured on a 1/30 scale model (Ref.7-27) (Fig.7-14). Hence we may be confident that Reynolds number effects on the excitation of slender wing configurations with sharp leading-edges are insignificant.

The excitation is also light on slender wings with round leading-edges. However on slender wings with round leading-edges, large-scale effects have been observed, particularly at subsonic speeds. A well documented example is the scale effects on the development of the leading-edge separations observed on the FD2 research aircraft (see References 7-28 and 7-29, and Figure 12 in Reference 7-30).

Although the level of excitation on slender wings is small, the level of buffeting attained is of interest because a slender-wing aircraft must fly above the buffet boundary on every take-off and landing, and thus acquire a large number of loading cycles during its operational life. The buffeting on rigid models of slender wings can be detected by sensitive semiconductor strain gauges (Ref.7-31). Measurements on two different rigid models conformed to the same pattern. Buffeting increases after the formation of the vortices and then reaches a plateau (Fig.7-15). This plateau is obtained because, although the area influenced by the vortices is increasing, the vortices are moving away from the wing. A sudden further increase in buffeting occurs when the vortex breakdown point moves across the trailing-edge, but it is unlikely that a slender wing aircraft would be required to operate in this region. An unusual feature of these buffeting measurements was that the third symmetric mode predominated, rather than the fundamental (as discussed in Section 7.1.4). Thus these measurements could not be used with confidence to predict the level of buffeting, quite apart from uncertainties about the appropriate damping coefficient. The solution found to this problem was to test an aero-elastic model for a rather similar configuration.

The buffeting on this aeroelastic model was readily detected by wire strain gauges (Ref.7-31), even though the tests were restricted to low equivalent airspeeds because of the danger of overloading and destroying a valuable aeroelastic model. (Most aeroelastic models are designed for flutter testing under zero lift conditions.) The buffeting on the aeroelastic model was also predominantly in the second and third structural modes, confirming the results for the rigid models. This response is probably caused by the excitation being localized to a comparatively small area under the vortices, rather than being distributed across the span as for unswept and swept wings. The level of buffeting extrapolated to full scale from this model was estimated to be small but just measurable. This prediction has recently been confirmed in flight.

In flight most of the buffeting is in the second and third structural modes. At the low values of EAS at which the aircraft flies above the buffet boundary there is little aerodynamic damping in these modes so that we may reasonably assume constant damping. The wing-tip acceleration A will then vary with V^2 at a constant angle of attack. Hence the curve of

$$A/V^2 \text{ versus } \alpha$$

derived from the flight measurements at constant weight closely resembles that measured on the model (Fig.7-15) at constant kinetic pressure.

The level of buffeting has also been calculated by Mitchell (Ref.7-32), using as the excitation the pressure fluctuations measured at 14 points on the 1/30 scale model (Ref.7-27). Mitchell had to make rather sweeping assumptions about the correlations of the pressure fluctuations, and also to assume values of total damping appropriate to the motion, but he succeeded in predicting almost exactly the buffeting levels recently measured in flight.

Many readers will be disappointed that the correlation of the pressure fluctuations in these vortex flows has not been discussed. This is primarily because there are so few correlation measurements available. The most complete set available to the author are those for a model of the BAC 221, a slender wing research aircraft. Figure 7-16 shows a typical example, with vortex breakdown about halfway between the apex of the wing and the trailing-edge (Ref.7-27). The contours of excitation have a maximum value underneath the point at which the vortex bursts. Using this point as reference we can then observe the correlation of the pressure fluctuations at the frequency selected. The clear impression given by all the contours of correlation is of a definite wave pattern. It is possible to show, by time delay techniques, that the contours are caused by the convection downstream of a fixed wave pattern associated with the vortex burst.

7.1.4 BUFFET ONSET AND THE SEVERITY OF BUFFETING

In Reference 7-33 Huston et al suggested a method for predicting the onset of buffeting and flight buffeting loads from measurements of unsteady wing-root strain made on rigid wind tunnel models with unswept and swept wings. Thus buffeting tests could be made simultaneously with routine force measurements. The similarity relations suggested are shown in Figure 7-17.

The method assumes that the reduced frequencies of the wing fundamental mode are about the same for the model and the aircraft, i.e.,

$$fc_{model}/fc_{aircraft} \simeq 1 .$$

In practice a variation in reduced frequency parameter from 0.7 to 1.6 seems to be acceptable, at least for measurements of buffet onset (Ref.7-29), probably because the buffet excitation spectra are always comparatively smooth (e.g., Figure 7-12, Curves B and C).

7.1.4.1 Onset of Buffeting

The measurement of unsteady wing-root strain is generally accepted as the most consistent and reliable method of assessing buffet onset from model tests (References 7-29, 7-34 and 7-35) and many tunnel/flight comparisons of buffet onset are available (References 7-29 and 7-35). There is generally a fair correlation between the tunnel and flight buffet onset boundaries over an extreme range of wing planforms and thickness distributions. Tunnel results obtained by this method are usually somewhat pessimistic, particularly at subsonic speeds, but are extremely useful for project studies and comparative tests.

7.1.4.2 Alleviation of Buffeting

The measurement of unsteady wing-root bending moments has been widely used for comparative tests to assess the alterations in wing buffeting produced by changes in wing design (References 7-36 to 7-38). Figure 7-18 shows three typical examples. The first part of Figure 7-18 shows how the addition of a slat to the leading-edge of a 35° swept wing of constant chord delays the build up of buffeting to much higher wing angles of attack (Ref.7-36).

Measurements are only given for a Mach number of 0.65 because it is difficult to design a leading-edge profile which gives a satisfactory compromise over a wide speed range from $M = 0.50$ to 0.90. Hence a variable geometry leading-edge, as proposed in the "RAE VAM" principle, may yet be used to optimize wing buffeting characteristics. A full discussion of these aspects of leading-edge design is given in Reference 7-36. The second part of Figure 7-18 shows how the addition of a slat to a 1/20 scale model of the Phantom aircraft raised the buffet onset boundary, a somewhat smaller improvement was obtained in flight (Ref.7-34) (Fig.7-26). The third part of Figure 7-18 shows how the buffet onset boundary of a wing with its quarter chord line swept 45° was improved (Ref.7-37). The addition of carefully streamlined bodies to retard the downstream movement of the terminal shock raised the lift coefficient for buffet onset by about 0.2 for Mach numbers of 0.6 to 0.8 and by about 0.40 at a Mach number of 0.90. The addition of small boundary layer fences to the noses of these bodies produced a further increase in buffet onset lift coefficient of about 0.2 at subsonic speeds (where there were probably shock and/or vortex type separations close to the leading-edge) but no further increase at $M = 0.90$ (where the separation were probably shock-induced further downstream on the wing).

An interesting flight investigation on the F-104 aircraft of the alleviation of buffeting achieved by the deflection of leading-edge and trailing-edge flaps is described in Reference 7-39.

7.1.4.3 Alternative Methods of Defining Buffet Onset

The improvements in wing buffeting caused by the postponement or alleviation of flow separations can sometimes be associated with changes in the mean forces and pressures on the wing, particularly for low angles of sweepback where the buffeting is generally heavy*. Thus Figure 7-19 shows that the slats which delay heavy buffeting on

* For moderate or highly swept wings this is a much more difficult process. The term "kinkology" has been applied for these methods of determining improvements in buffet

the 35° swept wing (Ref.7-36) also improve $C_{L_{max}}$ from about 1.0 to 1.3. The slat also delays the divergence of the trailing-edge static pressure at a typical wing station (2y/b = 0.50).

When dynamic wing buffeting tests are made in wind tunnels with low levels of flow unsteadiness the onset of buffeting is normally well defined. However if the flow unsteadiness at the wing fundamental frequency exceeds the levels specified in Reference 7-40, interpretation of the wing-root strain measurements may be difficult, and incorrect answers can be obtained. When the wing-root strain measurements are ambiguous a critical assessment of the overall forces may identify buffet onset. The examples which follow represent a bad failure of the dynamic method in some early tests in an unsteady tunnel ($\sqrt{nF(n)} = 0.008$), and are not typical of what is readily achieved in a tunnel with low unsteadiness.

Figure 7-20 shows a comparison of the buffet onset boundary for a typical wing with low sweepback with two criteria for the onset of flow separations (Ref.7-29). The breaks in the C_D vs C_l^2 curves correspond quite well with the onset of flow separations derived from surface flow visualisation. This boundary also compares fairly well with the buffet boundary at subsonic speeds ($M < 0.80$) but at transonic speeds the buffet boundary is manifestly too high. In contrast the breaks in the C_l vs α curves occur at such a high C_l over the complete Mach number range that they give too high a level for buffet onset. This observation is in accordance with the recent experiments of Ray and Taylor on a large number of wings (Ref.7-34). On a three-dimensional wing the initial onset of separation and loss of lift on one area of the wing may be associated with a compensating increase in lift on another area of the wing, so that there may be no breaks in the C_l vs α curves at buffet onset. Nevertheless Bore has obtained some success with particular wings in using breaks in the C_l vs α curves to obtain buffet onset boundaries (Ref.7-41).

Figure 7-21 shows the same buffet boundary compared with the trailing-edge pressure divergence boundaries. We see that every spanwise position on the wing gives a different divergence boundary, but that the boundary for 2y/b = 0.82 gives reasonably good agreement with the onset of flow separations at high subsonic and transonic speeds as Pearcey suggested (Ref.7-42). This station is recommended because many swept wings are designed so that the flow first separates at about 2y/b = 0.80. Indeed at transonic speeds the combination of wing taper, leading-edge sweep and thickness distribution will often ensure the onset of flow separations in this area, unless flow separations can be deferred by modifications to the wing planform, the wing section or the wing twist distribution. For this wing the flow separations extend rapidly downstream from the leading-edge (at subsonic speeds) or from the terminal shock wave (at transonic speeds) and hence trailing-edge pressure divergence correlates reasonably well with buffet onset. The leading-edge separations on highly swept wings at transonic speeds generally extend rapidly to the trailing-edge so that trailing-edge pressure measurements can assist the interpretation of buffeting measurements on these wings (Ref.7-43). If the flow separations extend slowly downstream from the leading-edge, we have seen that trailing edge pressure divergence will occur significantly later (References 7-16 and 7-19) than buffet onset.

Observation of the wing tip vortices can help to define the buffet onset boundary, if the initial flow separations are close the wing tip. This technique has been rarely exploited, but during buffet tests in the RAE 3 ft x 3 ft tunnel (Ref.7-29) close agreement was obtained on several models between the angle of attack at buffet onset derived from measurements of unsteady wing-root strain and the angle of attack at which the cores of the wing tip vortices disappeared from the Schlieren apparatus.

When the wing flow is attached, the boundary layer near the wing tip is concentrated into the core of the wing tip vortex, and is clearly visible in a Schlieren system with a horizontal knife-edge. However, if there is a separation on the outboard wing section, the vortex core rapidly diffuses and it is difficult to distinguish on the Schlieren system. The change between these types of flow is well defined on the Schlieren but not very well reproduced on photographs. The critical angle of attack is repeatable to ±1° and small asymmetries between the onset of separation on port and starboard wings can be identified.

7.1.4.4 Severity of Buffeting

We must now return to the scaling of the buffeting loads from the model to the aircraft, which presents serious difficulties (Fig.7-17). Huston assumed that any difference between the mode shapes of the rigid model and the flexible aircraft would be insignificant and this is probably a fair assumption. He also assumed that it would be fairly easy to establish the total damping coefficient appropriate to the model and flight experiments but experience proves this hope is not well founded. Huston showed that for a given Mach number and angle of attack, if

$$\text{Wing-root strain} \propto \text{air density}$$

then the damping of the motion was predominantly structural and constant. Structural damping (generally denoted by g/2 = % critical) seems to predominate on nearly all rigid wind tunnel models (References 7-44 and 7-45) and remains constant from zero lift to heavy buffeting conditions. In contrast, if

$$\text{Wing-root strain} \propto (\text{air density})^{1.2}$$

Huston showed that the damping of the motion was predominantly aerodynamic. Huston suggested that this law

would be followed in flight if the aerodynamic damping (generally denoted by γ % critical) was unaltered by the onset of flow separations. However there are few reliable flight experiments, and no conclusive tests on aeroelastic models in wind tunnels to verify this law. The measurements of Jones (Ref.7-45) suggest that in flight at constant density and velocity, but with varying angle of attack, the basic assumption of a constant damping coefficient equal to the attached flow value may be in error. Figure 7-22(a) shows the variation of total apparent damping coefficient with normal force coefficient for a small fighter aircraft (Ref.7-46). At buffet onset the total damping coefficient increases rapidly from its attached flow value, 3% critical, to 16% critical and then falls again to about 4% of critical in the region of moderate buffeting. No convincing explanation of this phenomena has yet been given and it is not known yet whether this behaviour is peculiar to this aircraft, or typical of most swept wing aircraft.

A similar variation of total damping with lift coefficient has been derived at least once before (Ref.7-37) during wind tunnel buffeting tests of a rigid model over a limited Mach number range from $M = 0.93$ to 1.00. Figure 7-22(b) shows that the structural damping of this model was low and the same for all configurations tested ($g/2 = 0.4\%$ of critical damping). For the clean wing the total damping of the fundamental mode remained about 2% from low lift until well beyond buffet onset, then increased slowly to about 3% and then decreased again. (This variation is rather larger than we would expect for a rigid model, although Wornom and Davies observed a variation from 3% to 1.5% which could be related with the lift on the model (Ref.7-44).) In contrast, for the same wing structure and frequency, but with the aerodynamics altered by the addition of bodies and fences, the damping started at low lift coefficients at the same level as the clean wing (2%) but then increased rapidly to 6% at buffet onset ($C_L = 0.7$). The damping reached a maximum of 8.5% at $C_L = 0.08$ and then fell to about 4% at $C_L = 0.9$ to 1.0. The author of the original report thought that this change in damping was caused by the change in the flow produced by the wing modifications and not by any peculiar variation of structural damping. Figure 7-22(c) shows a similar variation of total damping for another improved configuration of the same wing at a Mach number of 0.98. Once again, a large increase in the total damping seems to occur before buffet onset. If variations of damping coefficient of this kind are going to occur in flight or tunnel experiments it will be impossible to utilize the simple relations for the severity of buffeting previously suggested (Fig.7-17).

One attempt to escape this dilemma is to by-pass the uncertainties associated with the damping in flight and to use the buffeting measurements on rigid wind tunnel models with constant damping to derive dimensionless buffeting coefficients which can then be compared directly with the buffet penetration achieved in flight (Ref.7-30) on aircraft for which we do not know the damping coefficients. Many assumptions are implicit in this method, but it works reasonably well. The basic hypothesis is that the tunnel unsteadiness (which must be known) can be used as a given level of aerodynamic excitation to calibrate the model response at the wing fundamental frequency, and hence to derive buffeting coefficients from the buffeting measurements. These buffeting coefficients are a measure of the generalised force in the wing fundamental mode due to any distribution of pressure fluctuations on the wing. Past experience with nine aircraft models suggests that levels of buffeting coefficient obtained in this way can be identified appropriate to the maximum flight penetration of buffeting for both transport and fighter type aircraft. The method is illustrated by a typical example (Ref.7-29), (the same model as discussed in Figures 7-20 and 7-21).

Figure 7-23 shows the curve of unsteady wing-root strain signal at the wing fundamental frequency, f_1, plotted against angle of attack. If these signals are divided by the appropriate kinetic pressure $q = \frac{1}{2}\rho V^2$, we have, if the flow is insensitive to changes in Reynolds number,

$$\text{Wing-root strain signal}/q = C_B(M, \alpha) \tag{7-2}$$

where $C_B(M, \alpha)$ is a dimensional function of Mach number M and is independent of q at a given M and angle of attack, if the total damping of the wing fundamental mode is constant (Ref.7-45). Before the onset of flow separations on the model, most of the curves in Reference 7-29 and numerous tests in other wind tunnels (Ref.7-34) show that $C_B(M, \alpha)$ is constant and equal to $C_B(M, \alpha = 0)$. This is the portion of the model response caused by the tunnel unsteadiness $\sqrt{nF(n)}$ at the appropriate Mach number and the same frequency f_1. We now scale all the measurements so that the level $C'_B(M, \alpha = 0)$ represents the tunnel unsteadiness and the model response to that unsteadiness. Thus

$$C'_B(M, \alpha = 0) = \sqrt{nF(n)} = 1/K \cdot C_B(M, \alpha = 0) \tag{7-3}$$

where K is a constant scaling factor. The subsequent increase in $C'_B(M, \alpha)$ as the angle of attack increases gives a measure of the integrated pressure fluctuations arising from the wing buffet pressures and of the model response to this excitation. Having used the tunnel unsteadiness $\sqrt{nF(n)}$ to establish a datum buffeting scale, this signal must now be subtracted to give the true buffeting level in the absence of tunnel unsteadiness. If the tunnel unsteadiness does not exceed the criteria in Reference 7-40 there should be no correlation between the tunnel unsteadiness and the wing buffeting and so we can calculate a corrected buffeting coefficient

$$C''_B(M, \alpha) = \sqrt{C'_B(M, \alpha)^2 - C'_B(M, \alpha = 0)^2}\,. \tag{7-4}$$

The angle of attack at which $C''_B(M, \alpha)$ first differs from zero is buffet onset. Contours of buffeting coefficients are then readily obtained as a function of Mach number and angle of attack or lift coefficient. For the seven fighter

aircraft models heavy buffeting corresponds with

$$C''_B = 0.012 \text{ to } 0.016 .$$

For the fighter aircraft there is considerable scatter from the flight buffet onset boundary to the $C''_B = 0.004$ contour. Hence for fighter aircraft the following buffeting criteria are suggested:

Buffet onset	$C''_B = 0$
Light buffeting	$C''_B = 0.004$
Moderate buffeting	$C''_B = 0.008$
Heavy buffeting	$C''_B = 0.016 .$

For the two transport aircraft models the buffeting limit corresponds with $C''_B = 0.006$.

Figure 7-24 illustrates a recent test of this hypothesis for a fighter aircraft. The model was similar to the one considered in Figure 7-23 but the tunnel unsteadiness was much lower ($\sqrt{nF(n)} = 0.002$) and the Reynolds number much higher ($R \triangleq 4 \times 10^6$). Buffet onset in the new flight tests (carefully derived from wing-tip accelerometers) agrees well with the light buffeting contour

$$C''_B = 0.004$$

and the maximum flight penetration corresponds with the heavy buffeting contour

$$C''_B = 0.016 .$$

Figure 7-25 shows sketches based on typical oil flow photographs taken on this model at Mach numbers of 0.70 and 0.90 at the light, moderate and heavy buffeting levels, and we note the progressive development of the areas of separated flow as the buffeting coefficient increases.

The correlations established between buffeting contours and maximum flight penetration are somewhat surprising because it might reasonably be expected that the severity of buffeting in flight would be based on the dimensional level of vibration (either estimated by the pilot or measured by an accelerometer), rather than a dimensionless buffeting coefficient. There are two alternative explanations for the correlations established. Either

(1) the severity of wing buffeting is not really the limiting factor so that pilots of fighter or strike aircraft tend to fly right up to a handling boundary, such as pitch-up, stalling or wing dropping. This handling boundary might coincide with the heavy buffeting contour. Or

(2) the pilot may instinctively include in his assessment of buffeting a 'q' factor, as he tends to do in the application of steady loads to the aircraft.

If he does introduce a 'q' factor, pilot-defined boundaries for light, moderate and heavy buffeting at constant altitude would tend to be uniformly spaced above the buffet onset boundary where Mach number effects are small, and would correspond with constant values of pressure-fluctuation coefficients measured in the tunnel and hence of buffeting coefficients, C''_B (see Figure 14 in Reference 7-16 for the Venom aircraft with a sharp leading-edge).

The pilots of transport aircraft generally sit further from the nodal points of the wing fundamental mode than do pilots of fighter or strike aircraft and would not wish to approach a handling boundary, even if sufficient thrust were available. Thus for transport aircraft the maximum penetration coefficient $C''_B = 0.006$ seems more reasonable than the value of 0.016 for fighter aircraft. This limit for maximum flight buffet penetration for transport aircraft of $C''_B = 0.006$ is based on measurements for only two models at low Reynolds numbers and may need to be revised as additional tunnel/flight comparisons become available for this class of aircraft

The heavy buffeting contour can be given a general physical significance because the buffeting coefficient ought to be of the same magnitude as the fluctuating normal force coefficient if the flow over most of the wing is separated and the excitation is well correlated across the wing. The measurements of Polentz on aerofoils (Ref.7-47) show a maximum normal force coefficient at low frequencies of about 0.010 to 0.020 which brackets the heavy buffeting contour of 0.016. Similarly Figure 7-13 shows that the maximum fluctuating normal force coefficient at a particular low frequency parameter $n = 0.05$ for a family of slender wings varies from about $\sqrt{nG(n)} = 0.008$ to 0.010 for $\Lambda = 45°$ to $\sqrt{nG(n)} = 0.014$ to 0.019 for $\Lambda = 70°$. These high values of normal force coefficient are obtained when vortex breakdown occurs on the wings irrespective of which way the models are tested and therefore irrespective of the details of the vortex flow (Ref.7-26).

One recent application of this method utilized buffeting measurements made by Hanson on an aeroelastic model of a variable geometry fighter aircraft*; the original report repays careful study (Ref.7-48). The aeroelastic model

* The author acknowledges the use of additional information, kindly given by Mr Hanson, which is not included in Reference 7-48.

was tested in Freon 12 in the NASA Langley Transonic Dynamics Tunnel. The model was flown on wires and achieved an almost exact duplication of the aircraft modes and dampings for the different wing sweep angles. As expected, the response measured by the wing-root strain bridge was predominantly in the wing fundamental mode, at about 16 Hz model scale (Figure 8a of Reference 7-48), and the damping was predominantly aerodynamic.

Figure 7-26 shows the buffeting coefficients C_B' derived from these wing-root strain measurements and the tunnel flow unsteadiness level (Figure 1b of Reference 7-48). Different transformation factors, K , are required for the port and starboard wings, and for every Mach number, because the damping of the fundamental mode is predominantly aerodynamic and varies with kinetic pressure q . These values of K reduce the buffeting measurements to single, well defined curves of C_B' vs C_N . The angles of attack selected for the onset, light and moderate buffeting contours correspond with $C_B'' = 0$, 0.004 and 0.008 respectively, as derived from tests on ordinary sting-supported wind tunnel models tested in air.

Figure 7-27 shows a comparison of the buffeting contours derived from the model tests and the buffet onset and maximum penetration achieved in flight. In the tunnel tests the maximum penetration was not limited by wing buffeting, but instead either by a limiting tail deflection (the aeroelastic model must fly trimmed) or by a roll instability which the "pilot" could not control. Similarly in flight no manoeuvres were aborted due to the severity of buffeting, but only due to the attainment of the "g" and "α" limits mentioned in the report. For $\Lambda = 26°$ and $50°$ the flight buffet onset boundary agrees fairly well with the buffet onset contour $C_B'' = 0$ derived from the tunnel tests. For $\Lambda = 70°$ the flight buffet onset boundary is between the buffet onset contour $C_B'' = 0$ and the light buffeting contour $C_B'' = 0.004$. Above buffet onset the flight and tunnel contours look similar and support the broad conclusion that maximum flight penetration would have corresponded fairly well with the heavy buffeting contour $C_B'' = 0.016$, if this could have been achieved on the aeroelastic model. Even with the severe restrictions applied to the aeroelastic model by the tail deflection and the roll instability, maximum levels of $C_B'' = 0.010$ and 0.013 were achieved for $\Lambda = 26°$ and $70°$ respectively.

These results from an aeroelastic model flown on wires may reasonably be viewed as a severe, and yet fairly satisfactory, test of the hypothesis originally advanced in Reference 7-30 on the basis of tests on ordinary wind tunnel models supported by stings. It should be noted that buffeting tests on an ordinary sting-supported model of the aircraft would not have been limited by tail loads or a roll instability, and could probably have been made at higher Reynolds numbers. (The test Reynolds numbers quoted on page 10 of Reference 7-48 are in fact Reynolds numbers/ft so that the model Reynolds numbers are comparatively low.)

It is interesting to note that in both the flight and tunnel tests reported in Reference 7-48 rapid increases in angle of attack excited less severe buffeting than slow increases in angle of attack. This effect has been noticed previously in flight tests of other combat aircraft. Although part of the delay can be attributed to the finite time taken by the structure to respond to the aerodynamic excitation (as discussed by Zbrozek and Jones in Reference 7-5), there is some evidence that there may well be, in addition, a transient effect on the development of the flow separations, if the rate of change of the angle of attack is high.

7.1.5 TAIL BUFFETING

Although tail buffeting has occurred on many other aircraft since the classic investigation cited previously (References 7-1 and 7-2), few of these investigations are well documented. A useful survey of the literature available up to 1959 was included in a paper by Seal (Ref.7-49).

Tail buffeting may be excited either by the wing wake or, less frequently, by local separations on the tailplane. Tailplane buffeting normally occurs at the first symmetric bending frequency, but may occur at the first antisymmetric bending frequency in conjunction with the first fuselage torsional bending frequency. Although tailplane buffet onset may be measured by the application of tail-root strain gauges on rigid models, the severity of the buffeting cannot be determined with confidence. This is because the fuselages modes and stiffnesses on rigid models are unrepresentative to those on the real aircraft. Hence dynamic models must be used in which the fuselage modes are correctly represented. References 7-48 and 7-50 provide interesting examples of this technique of measuring tail buffeting loads.

Examples of tail buffeting induced by the wing wake are less serious now because of the care with which tailplane positions are selected. Some of the factors which influence tail position, including buffeting, are discussed in Reference 7-51. The tailplane position selected is inevitably a compromise between many mutually conflicting requirements (e.g., longitudinal stability at high speeds and low lift coefficients and at low speeds and high lift coefficients, or even by noise alleviation constraints) and hence tail buffeting can normally be anticipated somewhere within the flight envelope. Tail buffeting need not necessarily be harmful, e.g., on one aircraft buffeting on the T-tail provided a natural warning of the wing stall (Ref.7-52). Tail buffeting excited by wing flow separations will be sensitive to any devices which alter these separations, such as vortex generators, flaps or engine nacelles. A possible hazard which has occurred on combat aircraft is tail buffeting excited by the carriage of pylon-mounted external stores under the wing. Preventing the flow separations by increasing the gap between the store and the wing or by reducing the thickness/chord ratio of the pylons also eliminates this type of tailplane buffeting.

Local flow separations, and tail buffeting, caused by inadequate sealing between the lower and upper surfaces of tailplanes have been eliminated by improving the sealing. Local flow separations may also occur at transonic speeds, particularly with T-tailplanes, so that carefully designed bullets may be required to reduce the buffeting to acceptable levels.

Accurate representation of local flow separations on tailplanes in wind tunnel tests may be difficult because of the low Reynolds number of the flow on the tailplane relative to the flow on the wing. For particular tests high Reynolds numbers may be obtained by a separate model of the tail unit, but this precludes a simultaneous investigation of the tail buffeting excited by the wing flow.

7.1.6 CONCLUDING REMARKS

The main themes of Section 7.1, and related to Figure 7-4, can be reiterated as follows: (1) For bubble flows, which occur in many different situations, the largest excitation is found just upstream of the reattachment point; (2) For slender wings with sharp leading-edges the buffeting is light, but just measurable, exactly as predicted from wind tunnel tests 8 to 10 years in advance of flight; and (3) For swept wings the complex nature of the flows and wing performance assessment are best examined by buffeting measurements on rigid models, despite their limitations. In the future these buffeting measurements will be supplemented by extensive measurements of the excitation of the type presented in Reference 7-53 (which should be read in conjunction with Reference 7-35).

For older aircraft with swept wings we frequently find significant differences between wind tunnel predictions and flight measurements of the buffet onset boundary. Figure 7-28 shows a typical example (Ref.7-35). There are large differences between the buffet onset boundaries for the clean wing and the wing with slats at subsonic speeds, but only relatively small errors at transonic speeds. In contrast there is now evidence (References 7-54 and 7-55) from modern aircraft with swept wings that our simulation is in error even at transonic speeds. Our inability to produce the correct flows is probably due to our failure to reproduce sufficiently high Reynolds numbers. Hence if we are to guarantee the buffeting limits of future aircraft with advanced wing designs (not merely buffet onset but also maximum penetration), new high Reynolds number facilities, suitable for buffeting tests, will have to be provided. Buffeting tests will place constraints on these facilities in terms of levels of flow unsteadiness (Ref.7-40) and in terms of running times. Running time considerations are briefly discussed in the Appendix, Section 7.1.7

If ground based high Reynolds number facilities suitable for buffeting tests are provided, the aerodynamicist will no longer be able to attribute discrepancies between tunnel predictions and flight performance to the inadequate simulation of Reynolds number. We shall then see a demand for far more searching flight tests in order to establish if the separations obtained in the wind tunnel are being duplicated in flight. The experiments of Jones (Ref.7-46) and Hollingsworth (Ref.7-35) may be cited as typical of the most detailed research of this type so far achieved in flight, but even these tests were not sufficiently detailed. They revealed differences between the developments of the separations on the model and in flight, but not the origin of these differences, or how the differences could be removed. If we are to explain these differences we shall have to measure the static pressure distributions over the wings, the development of the boundary layer upstream of separation and downstream of reattachment, as well as the fluctuating pressures and the wing response.

These flight experiments will be difficult and might even justify the allocation of special aircraft. A few really detailed comparisons of the separated flows obtained on wind tunnel models and on aircraft will probably make the most significant single contribution to the achievement of safe flight beyond the buffet boundary.

7.1.7 APPENDIX — THE FUTURE OF BUFFETING RESEARCH

We have seen that buffet onset is closely linked with the onset of flow separations so that there seems a reasonable chance of ultimately being able to predict the buffet onset boundary for a given wing using boundary layer prediction methods. Thomas (Ref.7-56), Magnus and Yoshihara (Ref.7-57), and Redeker (Ref.7-58) have already suggested methods which indicate the type of approach which might be exploited. It will be essential to combine refin methods of predicting three-dimensional turbulent boundary layers (Ref.7-59) with recent improvements in potential transonic flow theory (Reference 7-60 may be cited as a typical example). If these optimistic hopes are fulfilled, the predictions of the calculation methods must be checked fully, either by tests on a wind tunnel model over a wide range of Reynolds number, or by comparisons with flight experiments for which both the pressure distribution and the boundary-layer development are available.

When the integrity of these methods is established, they will be applied to much more advanced wing designs incorporating rear-loaded sections, for which two buffet onset boundaries will be obtained at transonic speeds. The buffet onset at high lift will be caused by boundary-layer separation on the upper surface of the wing and the buffet onset at low lift will be caused by separations on the lower surface. The existence of two buffet boundaries for rear-loaded sections has already been demonstrated (Ref.7-61). We do not yet know how the severity of buffeting on rear-loaded wings will compare with that on conventional wings. However it seems likely that at transonic speeds the forward movement of the terminal shock may be less rapid and hence the buffeting may be less severe than on conventional wings.

No boundary-layer theory is valid beyond separation, so that above the buffet boundary we shall still have to rely on model tests in wind tunnels for the prediction of steady and fluctuating pressures. Some deficiencies are already apparent in the simulation for existing aircraft in our present transonic tunnels (Ref.7-54). These deficiencies may be more serious with advanced wing designs, unless the Reynolds number available can be increased (Ref.7-55).

The buffeting coefficients selected from tests on conventional models in type A flow situations, at low Reynolds number (1×10^6 to 4×10^6) as appropriate for maximum penetration in flight, may well include a scale effect on the development of the separations (Ref.7-62). With advanced wing designs, in type B flow situations, the character of the scale effects may be different from those on conventional wings, requiring different buffeting coefficients from those previously established. This justifies the inclusion of comparative buffeting tests on advanced and conventional wing designs over a wide range of Reynolds numbers.

It is imperative that the high Reynolds number intermittent transonic tunnels now being considered should provide a running time sufficiently long to measure buffeting reasonably accurately. Wing buffeting measurements at a fundamental frequency of 150 Hz in the BAC 4 ft x 4 ft wind tunnel at Warton, England were possible in a running time as short as 10 seconds, so this would be a reasonable target running time for a tunnel with a 1 m x 1 m working section. In contrast, a larger model with a fundamental frequency of only about 30 Hz suitable for a 5 m x 5 m working section would require a running time of about 50 seconds to ensure comparable accuracy*, which is dependent primarily upon the number of cycles of buffeting. Hence there is a manifest advantage of building a small, highly pressurized tunnel for buffeting measurements for a given Reynolds number.

An incidental advantage of selecting a small, highly pressurized tunnel is that it would probably be easier to obtain low levels of flow unsteadiness in the working section, particularly at low frequencies, because of the small scale of any disturbances in the maximum section, working section or diffuser. If these new intermittent facilities are to be used successfully for buffeting tests they must achieve levels of flow unsteadiness at least equal to those in the best continuous facilities now in operation (Ref.7-40).

Rigid models will be used exclusively for buffeting tests in these new facilities, because of the difficulty of constructing sufficiently strong aero-elastic models for prolonged tests under lifting conditions. Even with rigid models static aero-elastic distortion may require the model wing to differ from the aircraft shape by up to 0.4° twist (Ref.7-63). At present buffeting tests of aero-elastic models of swept wings under lifting conditions are confined almost exclusively to the NASA Langley Transonic Dynamics Tunnel (with a working section of 16 ft x 16 ft) which can be operated with air or Freon 12. Although operation with Freon 12 allows the aerodynamic damping to be more readily simulated, there is some evidence that its inadequate simulation of the specific heat ratio may produce incorrect data at high lift at transonic speeds (Ref.7-64). However, one buffeting test in this tunnel, using Freon 12, has given a good prediction for the wing-root strain on a dynamic model of a variable geometry aircraft (Ref.7-48).

Kilgore et al have shown that the problems caused by static aeroelastic distortion should be less severe in cryogenic transonic tunnels (Ref.7-65). In cryogenic tunnels the kinetic pressure may be held constant while the Reynolds number is increased at constant Mach number by reducing the free stream static temperature. This appears an attractive concept for obtaining high Reynolds numbers at transonic speeds. However the concept poses many problems (in terms of possible changes in stiffness, structural damping and fatigue life) which may prevent its application for routine buffeting tests.

7.2 BOMB BAY BUFFETING by J.Becker

The term "bomb bay buffeting" is used in this section to characterize the specific dynamic behaviour of an aircraft when excited by forces of random and harmonic nature due to flow separation in open bays or cavities, and the term "bomb bay buffet" is used for the excitation itself. The dynamic response of an aircraft is the result of the interaction of the random buffet flow, additional flow on the oscillating aircraft components, and the structure. As a consequence, the flight mechanics behaviour will be influenced by the generated rigid body oscillations, the aircraft's ride qualities will be impaired by elastic motions, and local structural stresses will be produced by the harmonic pressure fluctuations of high frequency.

A cavity or open bomb bay is by no means a dead air region. Large fluctuations in its pressure field may occur and, depending both on the level of the unsteady pressure field in the bay and in the surrounding region and on the elastic behaviour of the aircraft, high vibration levels may be generated in the aircraft's components. There are only a few publications concerning this specific buffeting problem (References 7-66 and 7-69 to 7-72). However, at the AGARD Structures and Materials Panel Meeting in 1962 in Paris, J.E.Rossiter gave an elaborate review and covered almost all the important aspects associated with the bomb bay buffet phenomenon (Ref.7-66). Since then some additional investigations have been performed, especially taking into account several features such as the influence of the attitude of the aircraft and the alleviation of pressure fluctuations (References 7-67 and 7-68).

The intent of Section 7.2 is to summarise all significant properties, including details on the effects of cavity

* Unless we accept the repetition of 5 x (10 second) runs for every combination of Mach number, angle of attack and total pressure.

geometry, Mach number and Reynolds number on the mean and unsteady pressure distributions in the bay, as well as the effects of installations for the reduction of strong pressure fluctuations. In this Section the following notation is used:

A	bay area
C_P	generalized cross power spectrum of the pressure fluctuation
C_D	generalised cross power spectrum of the displacement
P	mean pressure coefficient
D	matrix of generalized structural damping
f	frequency
F(n)	spectrum of the nondimensional fluctuation
$\hat{F}(\omega)$	Fourier transform of the generalized pressure fluctuation
h	spoiler height
H	generalized admittance matrix
K	generalized stiffness matrix
L	bay length
M	matrix of generalized masses
n	frequency parameter f L/V
p	pressure fluctuation
p	RMS pressure fluctuation
$\left(\frac{p}{q}\right)^2$	$= \int_{-\infty}^{\infty} F(n)\,dn$
P	generalized pressure fluctuation
$P_{I.D}$, $P_{I.S}$	generalized aerodynamic damping and stiffness matrix
q	kinetic pressure
R	Reynolds number based on bay length
S	generalized power spectrum of the pressure fluctuations
V	free stream velocity
Z	amplitude of motion
Z	RMS amplitude
x, y	coordinates
ϵ	bandwidth ratio $\Delta f/f$
δ	boundary layer thickness
ρ	free stream density
ϕ	amplitude of modal modes
RMS	root mean square

7.2.1 THE MEAN FLOW OVER CAVITIES

7.2.1.1 Characteristic Flow Shapes

The length to depth ratio primarily determines the flow pattern occurring in the interior and the vicinity of a cavity. Considering the flow development in a two dimensional bay (Fig.7-29(a)), the front edge first causes the air flow to separate and in the case of a bay with a length/depth ratio not smaller than about 6, the accelerated flow will reattach at a point along the roof of the cavity. After reattachment, the flow decelerates to the rear wall region and again separates just ahead of the rear wall. Downstream of the cavity the boundary layer may reattach again or a turbulent wake will exist.

The reattachment and the separation points move together in the case of a deeper cavity (Fig.7-29(b)) and if the length/depth ratio is further decreased, the reverse flow in front of the rear wall enlarges until a captive eddy builds up (Fig.7-29(c)).

The flow pattern in three dimensional cavities is almost the same as that in two dimensional cavities, even if the width is much smaller than the length. But the flow shape over a three dimensional cavity is not restricted to clearly separated internal and external streamlines as in the two dimensional case. Air is drawn into the eddy and escapes in a trailing vortex system shed from the eddy.

Frontal spoiler installations extremely change the flow pattern and the flow becomes totally separated (Fig.7-29(d)).

7.2.1.2 Mean Pressure Distributions

According to the flow behaviour, the bay is generally divided into two regions, the front part with negative and the rear part with increasing positive mean static pressures. Figure 7-30 presents results from different measurements (References 7-66 and 7-67) for the two different types of flow patterns which can occur in cavities. Although the results are not entirely compatible due to different Mach numbers and length/width ratios, general conclusions can be drawn. For the very shallow type of cavity the pressure changes due to reattachment and separation along the bottom of the bay are easily observed. At length/depth ratios of about 6, depending on the Mach number, the two pressure rises have merged and at length/depth ratios smaller than 6 the pressure is almost constant along the bottom, indicating that reattachment had not occurred. A remarkably large change in mean pressure for varying length/depth ratios of the cavity from about $4 \leq L/D \leq 10$ is seen, and this causes the overall drage to rise abruptly.

Drag measurements demonstrate the remarkable effect of a critical length/depth ratio (Ref.7-73). The mean pressures in the cavity, and consequently the critical length/depth ratio are influenced to some degree by the following parameters (Ref.7-73):

- length/width ratio,
- attitude of the aircraft,
- external installations such as open bomb bay doors,
- Mach number,
- boundary layer ahead of the cavity.

The critical length/depth ratio decreases at the length/width ratio increases (Ref.7-66). This is evident since the reducing effect of the side walls on the pressure distribution, as shown in Reference 7-66, is more pronounced in narrow cavities.

An increase in angle of attack reduces the mean static negative pressures in the front part of the bay, whereas the positive pressures at the rear part are increased (Fig.7-31). The effect of sideslip is more complicated, and general tendencies can not be stated for different angles of sideslip (Ref.7-67). The pressures in cavities without bomb bay doors are relatively high for high angles of attack. The pressure peaks are remarkably reduced through the effect of bomb bay doors, as shown by the impressive example from the investigation presented in Reference 7.66. However, it is questionable whether the reduction shown in Reference 7-66 would be as great in high subsonic flows.

J.E.Rossiter (Ref.7-66) reported on the effect of Mach number on mean pressures in cavities in subsonic flows. A reasonable decrease in the pressures at the rear of simple shallow rectangular cavities occurs as the Mach number is increased (Fig.7-32). In supersonic flows the same types of flow patterns as in subsonic flows occur, as indicated by the investigations of McDearmon (Ref.7-72) and Charwat (Ref.7-71). But there is a remarkable change in the critical length/depth ratio from about 6 up to 10.

The condition of the boundary layer ahead of the cavity is another significant parameter, since a thick boundary layer decreases the pressure peak at the rear part of the bay. With frontal spoilers the characteristic flow pattern is completely changed. The negative pressures vary negligibly, but the high pressure is strongly weakened. The low pressure region is enlarged up to 0.9 L for small angles of attack. A small high pressure region exists only in the rear part. Different spoiler installations for the bay configuration in the investigation of Reference 7-67 are shown in Figure 7-33. The spoiler influence generally grows with increasing spoiler area and the number of spoilers. The number of spoilers is more important than the spoiler area. Configuration 3 in Figure 7-33 is more effective than Configuration 9. Configurations 8 and 5 are the optimum for the reduction of the high pressure. Additional enlargement of the area is useless and meaningless (Ref.7-67). The most efficient spoiler arrangement (5 spoilers, spoiler height $h/L = 0.0366$, and spoiler width $d/L = 0.018$) leads to mean pressure reductions of about 50%.

7.2.2 THE FLUCTUATING PRESSURE DISTRIBUTION

7.2.2.1 Characteristic Features of the Unsteady Pressure Field

The behaviour of the unsteady pressure fields in the surrounding region of cavities was previously studied in wind tunnel investigations by different authors (References 7-66 to 7-70) using unsteady pressure measurement techniques. Little information is known about measurements under flight conditions (References 7-66 and 7-74), and extrapolation of wind tunnel results to flight conditions is therefore the most important next step. Scaling parameters for the random component of the pressure fluctuations have been investigated by Owen and reported in Reference 7-69.

The following general features of the flow characterize the fluctuations in bays:

(1) The actual flow in and around cavities is highly unsteady and consists of both random and periodic components.

(2) The power spectral density of the fluctuating pressures is used for their description. Typical spectra of the unsteady pressure field near the rear of a cavity are shown in Figure 7-34.

(3) As in the discussion on the mean pressure behaviour, there are specific criteria which are significant for the deep, medium and shallow types of bays.

(4) A spectrum characteristic of a randomly varying quantity describes the fluctuating pressure distribution for a shallow cavity ($L/D = 10$) at $M = 0.4$.

(5) Periodic pressure fluctuations are superimposed on the random signal as the depth of the bay is increased ($L/D = 6$, $M = 0.9$ and 0.9). The periodic components are indicated by small peaks in the spectrum for a cavity of medium depth.

(6) Very deep cavities are characterized by a spectrum with marked periodic components and a relatively smaller random level.

(7) As in the mean flow description, length/depth ratios in the vicinity of the critical ratio are important. The corresponding spectra of the mixed random and periodic type have the relatively highest levels of random pressure fluctuations.

(8) Mach number generally alters the frequency and increases the magnitude of the periodic buffeting component.

(9) Boundaries for the different types of flow regimes can be defined. As shown in Figure 7-35, the mixed random-periodic type of flow occurs predominately near the critical length/depth ratio (L/D = 6), depending upon the Mach number. The boundaries shown in Figure 7-35 cannot generally be used, because the boundary layer thickness, which varies for different configurations, plays an important role and will change both the random and the periodic pressure levels.

(10) The strong effect of the boundary layer thickness ahead of the bay is shown in Figure 7-36. The level of the spectrum will be reduced with increasing thickness.

(11) A variation in the cavity width primarily changes the periodic component of the spectrum (Fig.7-37), and hardly influences the random level.

(12) The effect of Reynolds number, as demonstrated by its influence on RMS pressure fluctuations (Fig.7-38), is of minor importance.

7.2.2.2 Shallow Cavities

In general the pressure fluctuations are mainly random for the shallow type of cavity. It is convenient to use the root mean square values of the pressure to describe these random distributions. However, RMS values should be used only for low speed results, since the small periodic components (the peaks in the spectrum) of the fluctuations increase with increasing Mach number, as shown previously.

Different measurements indicate that the fluctuating pressures increase from the front to the rear of a cavity and decrease rapidly behind the cavity. The increase in the front part is due to the growth in turbulence in the boundary layer while it is separated. A slight reduction occurs in the centre of the cavity, caused by reattachment. The increase in fluctuating pressures associated with the growing turbulence of the rear separation is remarkable. The high level of pressures behind the cavity may be associated with intermittent venting of high pressure separation to the low pressure region behind the cavity (Fig.7-39).

The effect of increasing angle of attack of the cavity is mainly a reduction in the strong increasing pressure fluctuations at the rear end. Sideslip partly compensates for the reduction caused by angle of attack. The pressures behind the cavity are hardly changed, except for the case of positive angle of attack and sideslip.

The effect of Mach number on the RMS values of the pressure fluctuations in shallow cavities (Fig.7-40) is an increase in the magnitude of the pressure at the rear end as the subsonic Mach number is increased, together with a decrease along the center of the cavity. Behind the cavity there is little change up to M = 0.9 but a large decrease in the RMS pressure fluctuations for a supersonic flow (M = 1.2 in Figure 7-40).

7.2.2.3 Deep Cavities

A periodic pressure fluctuation with one predominant frequency is the characteristic feature of the separated flow in clean deep cavities (L/D < 2), as indicated by the pressure peaks in Figure 7-34. The other peaks occur at frequencies which are partly integer multiples, and partly not simple multiples (secondary frequencies), of the dominant frequency. These secondary frequencies lie on a set of curves (Fig.7-45) together with the dominant frequencies, which jump from one value to another as the Mach number increases.

The following entirely empirical equation was derived for these curves:

$$f = \frac{V}{L} \frac{(m - \gamma)}{(1/K + M)}, \quad m = 1, 2, 3 \ldots, \quad \gamma = 0.25, \quad K = 0.6$$

from which a periodic time T can be formulated.

$$T = \frac{1}{(m - \gamma)} \left[\frac{L}{K \cdot V} + \frac{L}{a} \right]$$

which indicates that the periodic fluctuation is initiated through a vortex travelling from the front of the cavity at a speed K · V until it is one quarter of a wavelength behind the rear wall and a pressure wave leaving the rear wall at that moment and travelling upstream with sonic speed and which then initiates the whole process again. This mechanism, resembling the "edge tone" phenomenon (Ref.7-66), is modified since the periodic pressure fluctuations are changed by the existence of different modes of standing pressure waves (resonance). The jumps in the dominant

frequencies are therefore caused by amplification due to the vicinity of resonance frequencies. Results of an investigation suggest that the magnitude of the pressure fluctuations is proportional to ρV^4 (Ref.7-66), but it should be evident that for every configuration new measurements need to be made.

7.2.3 ALLEVIATION OF BAY BUFFETING

Based on analysis of results from several wind tunnel investigations, the following fundamental recommendations can be made for the reduction of strong pressure fluctuations in and around cavities. In general, alleviation is by taking into account specific goemetric relations for the dimensions of the cavity and for additional installations.

7.2.3.1 Choice of Length/Depth Ratio

A length/depth ratio of about 6 should be avoided for clean cavities without special alleviation installations. The flow changes from shallow to deep type cavities and the random component of the pressure fluctuations are strongest near this critical length/depth ratio (Fig.7-34). Furthermore, a change in aircraft attitude will cause the flow to change intermittently from the shallow to the deep type, and this is disadvantageous.

7.2.3.2 Modifications of Bay Construction

A rectangular cavity without installations reaching beyond the cavity depth and without rounding of the side wall corners is preferred, since the level of RMS pressure fluctuations is increased by open bay doors (Ref.7-68) and the levels of the spectra for modified bays exceed the values for a clean rectangular bay (Ref.7-66).

Rounding the rear corner of the bay and fitting fairings ahead of the rear bulkhead will reduce markedly the intensity of pressure fluctuations. However, these methods are not very efficient at high subsonic speeds.

A bay with a length/depth ratio near the critical value may be split into components using baffles, a method which has been found to be effective. (Ref.7-66)

7.2.3.3 Spoiler Installations Ahead of the Bay

Several properties of the flow caused by spoilers ahead of the cavity turn out to be very beneficial and the installation of spoilers is the most efficient way to reduce strong pressure fluctuations. In detail, the beneficial effect of spoilers is due to the increase in the effective boundary layer thickness and consequently the decrease in the magnitude of both the random and periodic components of unsteady pressure distributions in and around a cavity.

For bays with length/depth ratios near the critical value, the spoiler installation will cause the flow to remain of the shallow-cavity type. Furthermore, an effective reduction in the periodic component of the pressure fluctuations is achieved.

The results of measurements on a cavity with frontal spoilers in subsonic flow (Ref.7-68) for a shallow cavity indicate that

- the level of random fluctuations can be reduced up to 50%.
- a configuration similar to Number 5 shown in Figure 7-33 seems recommendable. (5 or more spoiler elements $h/\delta = 5$) due to the relatively high efficiency at all angles of attack and sideslip.
- the width of the spoiler elements should be $d/\delta = 2.5$, although a small decrease in width is possible without a large reduction in efficiency.

The effect of different spoiler arrangements is shown in more detail in Figure 7-41 by the spectra of the pressure fluctuations at different cavity locations for different spoiler configurations (see Figure 7-33). As might be expected from its length/depth ratio of 10 (shallow type of cavity), the clean configuration spectra are essentially flat for all X/L stations and have a gradual decrease at higher frequencies. The pressures in the rear part of the bomb bay are greatly reduced by the use of spoilers. However, in the front part of the bay, up to $X/L = 0.5$, the influence of spoilers is negligible in the low frequency range. The difference in efficiency for the three spoiler configurations is quite small.

The influence of either angle of attack or sideslip on the pressure fluctuations for a bay with a No.5 spoiler configuration is a small increase in the fluctuations. With a high angle of attack ($\alpha = 15°$) , sideslip increases the spectrum level in the front part of the cavity and decreases the level near the rear part (Fig.7-42). The relatively high efficiency of a spoiler configuration similar to No.5 in Figure 7-33 at all angles of attack and sideslip is shown in Figure 7-43 using, for the purpose of illustration, the integral value of the RMS pressure fluctuations. The influence of the number of spoilers and spoiler height is shown in Figure 7-44.

7.2.4 BUFFETING OF THE AIRCRAFT

The aeroelastic response of an aircraft structure to an unsteady loading at the bomb bay is now considered. Energy from both the random and the periodic pressure fields in the bay will be extracted by the aircraft at frequencies corresponding to the normal modes of vibration. The random fluctuations will cause excitation of the lowest frequencies, corresponding to the vertical and lateral flexible modes of the fuselage, whereas the periodic components tend to excite the higher frequency modes, for example the local structural modes.

7.2.4.1 Equations of Motion

Numerical treatment of the problem is by the well known generalized harmonic analysis which is also used in connection with general wing buffeting calculations. Generally, the equations of motion are usually formulated by a modal approach which includes the effects of all components of the airplane's motion as rigid body motions and structural deformations.

The motion of the airplane is expressed by the equation

$$Z_S(x, y, t) = \sum_i \phi_{iS}(x, y) q_i(t) \quad \text{for the lifting surfaces}$$

and more simply

$$Z_f(x, t) = \sum_i \phi_{if}(x) q_i(t) \qquad \text{for the fuselage}$$

where $\phi_i(x, y)$ are rigid modes (for example, $\phi_1 = 1$ and $\phi_2 = x$) and modal shapes (for example, natural modes) of the free-free airplane. The complete equations of motion by the Lagrangian formulation become

$$M\ddot{q} + Dq + Kq + P_{1D}q + P_{1S}q = P_B(t) \tag{7-5}$$

where

M = matrix of generalized masses, $M_i = \int \phi_i^2 \, dm$

D = matrix of the generalized structural damping

K = matrix of the generalized stiffness

Generalized aerodynamic stiffness and damping are introduced, mainly due to the displacement of the lifting surfaces since the fuselage contribution is generally small

P_{1D} = generalized aerodynamic damping

P_{1S} = generalized aerodynamic stiffness

With the assumption of small angles of attack, lifting surface theory is used for the prediction of the generalized aerodynamic damping and stiffness (Ref 7-77)

$P_B(t)$, the right hand side of Equation (7-5) repesents the generalized forces of the different mode shapes which are derived by integration of the bay pressure fluctuations, $p(t)$. Mainly terms of the vertical fuselage modes ϕ_{jf} will exist and the associated generalized forces can be defined by

$$P_j(t) = \iint_{(A)} p(x, y, t)\phi_{jk}(x) \, dx dy$$

where A is the area associated with non-negligible pressure fluctuations in and around the bay. Through generalized harmonic analysis the power spectrum, S_j, can be expressed directly in terms of generalized exciting forces (References 7-75 and 7-76)

$$S_j(\omega) = \lim_{T \to \infty} \frac{1}{2T} \left| \int_T^T P_j(t) e^{-i\omega t} dt \right|^2$$

Using the expression of $q(t)$ in Fourier integral form,

$$q(t) = \int_{-\infty}^{\infty} q(\omega) e^{i\omega t} \, d\omega$$

and substituting into the equations of motion yields, in matrix notation,

$$[-M\omega^2 + iD\omega + P_{1S} + i\omega P_{1D}]\{q(\omega)\} = \{\bar{P}(\omega)\}$$

where $\hat{F}(\omega) = \int_{-\infty}^{\infty} P(t)e^{-i\omega t}\,dt$ is the Fourier Transform of $P(t)$. The Fourier spectrum $q(\omega)$ is then derived from

$$q(\omega) = [-M\omega^2 + iD\omega + P_{LS} + i\omega P_{LD}]^{-1} F(\omega)$$

and the power spectral density of the response $Q(\omega)$ is then related to the excitation spectrum by

$$Q(\omega) = \left| [-M\omega^2 + iD\omega + P_{LS} + i\omega P_{LD}]^{-1} \right|^2 \cdot S(\omega)$$

or

$$Q(\omega) = |H(\omega)|^2 \cdot S(\omega)$$

where $H(\omega)$ is the generalized admittance matrix.

The mean square value of the response may be found from

$$q^2(t) = \int_{-\infty}^{\infty} Q(\omega)\,d\omega$$

where the RMS value of the motion of the aircraft at all points of the structure is derived by using

$$z(x, y, t) = \sum_i \phi_i(x, y) \cdot q_i \ .$$

The response problem is treated completely by the introduction of the cross spectral density. The relation between displacement response cross spectral density C_D and pressure loading cross spectral density C_P is, in matrix notation,

$$C_D(\omega) = H^*(\omega) A \cdot C_P \cdot A H^T(\omega)$$

The elements of the cross spectral density matrix $A \cdot C_P \cdot A$ are defined as the Fourier transform of the convolution integral of the generalized buffet forces. The asterisk denotes the complex conjugate. The diagonal elements of the left hand matrix are displacement power spectral densities and the off diagonal terms are displacement cross power spectral densities.

7.2.4.2 Scaling Effects

The most decisive step in the appliecation of measured wind tunnel buffet loadings occur in their extrapolation to flight conditions and the following considerations are important in this regard

The magnitude of the almost random pressure fluctuations in bays with medium length/depth ratios is proportional to the free stream kinetic pressure. The scale of the frequency f is proportional to the free stream velocity V and inversely proportional to the bay length L (Ref.7-69). The following definition therefore holds for the energy spectra.

$$\left(\frac{p}{q}\right)^2 = \frac{1}{2\pi}\int_0^{\infty} F(\omega)\frac{V}{L}\,d\omega = \int F(n)\,dn$$

with the nondimensional frequency $n = f\frac{L}{V}$ and with the definition of $F(\omega)$ as the Fourier transformation of $F(t)$.

$$F(\omega)e^{i\Phi(\omega)} = \int_0^{\infty} F(t)e^{-i\omega t}\,dt$$

Using the scale factors, the thickness effect of the boundary layer ahead of the measured model cavity should be taken into account.

The periodic components which are apparent, especially for deep cavities, should be scaled using the following relations for the frequencies and magnitudes (see Section 7.2.2.3 and Reference 7-66)

$$f = \frac{V}{L}\,\frac{(m - \gamma)}{(1/K + M)} \qquad (m = 1, 2, 3 \ldots)$$

l/D	K	γ
1	0.61	0.25
2	0.66	0.25
4	0.57	0.25
6		0.38

In regions of a spectrum with slowly varying ordinates (random character) the RMS value of the pressure fluctuation p is related to the power spectral density F(n) by the expression

$$\frac{p_\epsilon}{q\sqrt{\epsilon}} = \sqrt{nF(n)} \qquad \text{where } \epsilon = \text{bandwidth of the analyser}$$

The magnitude of the periodic component may then be defined as

$$\left(\frac{p}{q}\right)^2 = \epsilon\left[\left(\frac{p_\epsilon}{q\sqrt{\epsilon}}\right)_1^2 - \left(\frac{p_\epsilon}{q\sqrt{\epsilon}}\right)_2^2\right]$$

where

index 1 refers to the peak of the periodic component
index 2 refers to the general level around the peak

7.2.5 SUMMARY REMARKS

Bomb bay buffet influences the flight mechanics and ride qualities of an aircraft. Open bays of shallow, medium and deep type are distinguished by distinct mean and fluctuating pressure distributions caused by different kinds of flow separations. A remarkably large change in mean pressures occurs for bays with a length/depth ratio of about 6, and this is a critical length/depth ratio. Drag rises abruptly for bomb bays with a length/depth ratio near the critical value. The mean pressure levels are strongly reduced with increasing Mach number, and suitably installed frontal spoilers can reduce the mean pressure by about 50%.

Pressure fluctuations have maximum levels in bomb bays with near critical length/depth ratios. Smaller, mainly periodic, oscillations occur in deep cavities and relative low, random type, fluctuations exist in very shallow bays. Fluctuation decreases take place with increasing angle of attack, Mach number and Reynolds number. Spoiler installations are recommended for efficient alleviation of bay buffet.

The prediction of buffeting intensities of the aircraft due to bay buffet is achieved by a dynamic response calculation, the starting point of which is the measurement of unsteady bay pressure distributions. Generalized harmonic analysis is then applied, introducing generalized structural and aerodynamic inertia, stiffness and damping and generalized spectra of the buffet excitation. Using this method mean values of the amplitudes and accelerations at any position on the aircraft may be predicted.

CHAPTER 8

BUFFET ANALYSIS

by

P.J.Butkewicz

8.0 INTRODUCTION

An important feature of transonic flow over wings is the occurrence of buffeting which is usually more severe than at lower speeds due to the larger aerodynamic forces involved. Buffet is the aircraft response to time varying aerodynamic loads associated with unsteady flow separation. For the transonic regime, separation with associated buffet is closely connected with the shock-boundary layer interaction, which can either trip the boundary layer or result in early separation due to the increased susceptibility of the post shock boundary layer in an adverse pressure gradient.

The boundaries of the buffet regime are not rigorously defined and the resulting uncertainty is particularly troublesome for theoretical prediction. Generally, buffet onset occurs when significant separation is present on a wing, corresponding to such indicators as small fluctuations (± 0.05 g) in normal acceleration at the aircraft c.g., pressure divergence over portions of the trailing edge, or pilot opinion. The upper buffet limit is a function of the type of aircraft and its mission. For instance, a transport aircraft would be limited by structural considerations and passenger comfort, while a fighter would more likely be limited by handling qualities problems.

The methods available for transonic buffet analysis are reviewed in this Chapter. The analysis methods are divided into two groups: experimental model testing including associated empirical prediction methods, and semi-empirical or theoretical procedures which require flow field calculations to some extent. Due to the complexity of the transonic flow about wings experiencing unsteady separation, wind tunnel testing is the primary tool for obtaining detailed information about the buffet intensity. But even for model testing, a serious problem exists in applying the results to full scale due to improper boundary layer modeling at the relatively low test Reynolds numbers.

The need for buffet prediction in the early design stages led to the development of semi-empirical methods, some requiring inviscid flow field calculations. At the present time only one method, that due to Thomas, is amenable to a theoretical calculation based on a simplified flow model. The model assumes a steady flow and a decoupling between an inviscid flow field and a boundary layer. Even after ignoring the unsteady viscous-inviscid interaction, a formidable problem remains in solving the inviscid transonic flow field, particularly in three dimensions (see Figure 3-9 in this Report from Reference 8-1). The semi-empirical and theoretical methods are limited to the prediction of buffet onset.

8.1 EXPERIMENTAL BUFFET ANALYSIS

Due to the complex flow field associated with wings (particularly swept wings) and wing sections in transonic flow, methods for predicting buffet onset and intensity have been based primarily on experimental testing. Wind tunnel tests can be used initially to determine buffet characteristics and these tests can be followed by flight test correlations. The various empirical or semi-empirical methods available have for their data base either wind tunnel or flight test results, and in some cases possibly both.

8.1.1 Estimation of Buffet from Wind Tunnel Tests

In order to evaluate the buffet characteristics of a wing, generally both static aerodynamic forces and fluctuating quantities are measured and analyzed. The variety of buffet detection procedures based on wind tunnel tests are indicated in Figure 8-1 (from Reference 8-1). These methods give predictions of buffet onset that vary in accuracy and reliability over a range of geometric configurations and test conditions. The relative merit of some commonly used methods are discussed in this section.

The most widely applicable and generally useful experimental buffet analysis method is the measurement of the unsteady wing root bending moment. It is considered to be a consistent and reliable method for predicting buffet onset (Ref.8-2) and for providing a way to measure the severity of buffet intensity beyond onset. Although somewhat

pessimistic for predicting buffet onset at subsonic speeds, correlations between wind tunnel and flight test results have been fairly good for a wide range of wing planforms and thickness distributions (Ref.8-2). In addition, the method is convenient since buffet data can be obtained at the same time that the usual force measurements are made during rigid wind tunnel model tests.

Although in general wing root strain measurements provide the most useful indication of buffet onset, there are conditions for which these measurements are difficult to interpret or where they can lead to incorrect predictions. For instance, for wind tunnels having high levels of flow unsteadiness or noise, difficulties can arise if the flow unsteadiness at the wing fundamental frequency exceeds a certain level (see Reference 8-2). At tests at NASA Langley (Ref.8-3) it was found that the well-defined plateau level and pronounced divergence ...e bending moment curves which might be expected (see Figure 7-23) does not occur for wings having significant thickness-induced flow fields when tested at high subsonic Mach numbers. These wings experience buffet onset at lift coefficients approaching zero, and the wind tunnel noise is high (tunnel noise, which increases with increasing Mach number, is observed as the output of the bending moment gauge which is insensitive to model incidence), interpretation of the bending moment measurement results for them is even more difficult.

A commonly used buffet indicator is the divergence of the pressure measured near the trailing edge. This divergence indicates the presence of flow separation. For wings on which separation occurs first at the trailing edge (aft loaded airfoils) or for wings on which a separation bubble forms at the shock or leading edge and grows rapidly enough, the trailing edge pressure divergence correlates reasonably well with buffet onset, provided that a judicious choice is made for the spanwise station at which the pressure is measured. As indicated in Figure 7-21 there is a large variation in the pressure divergence boundaries obtained for different spanwise measurement locations. For the wing shown in Figure 7-21 the best measurement location for buffet onset predictions at high subsonic and transonic speeds is approximately 80% of the semi-span, a location which tends to be a good choice for swept wings (Ref.8-2).

For certain flow conditions on a wing, the interpretation of the trailing edge pressure divergence as an indicator of buffet onset can result in an erroneous prediction. An example is provided from the results of tests on the canard of the XB-70 aircraft. Although a long bubble formed on the canard at buffet onset, by the time the reattachment point had reached the canard trailing edge and, consequently, a pressure d...ergence had occurred, the canard was undergoing heavy buffet (Ref.8-4). On the other hand Peake et al (Ref.8-5) point out that for a shock-closed bubble interaction on the aft portion of an airfoil, a thickened wake is formed which will cause a pressure divergence in the absence of buffet onset.

The interpretation of steady aerodynamic force data is often employed to predict buffet onset conditions. Several criteria based on steady force data are shown in Figure 8-1. Consider the criterion based on a break in the lift curve (C_L vs α) shown as Method 3. When applied to wings having low sweepback, the lift curve break gives values for buffet onset which are too optimistic over a wide Mach number range (Ref.8-6), as illustrated in Figure 7-20. Similar results were obtained for a large number of wings by Ray and Taylor (Ref.8-3). However, as shown in Reference 8-3 a fair correlation appeared to exist for cambered wings having high buffet-free lift coefficients, and Bore (Ref.8-2) used the criterion successfully in a particular application. The generally unimpressive accuracy of the lift-curve-break criterion may result because the initial onset of separation and the associated loss of lift on one part of a wing can be offset by increased lift on another part, thereby giving no net change in lift at buffet onset (Ref.8-2).

A somewhat more consistent buffet onset criterion based on steady force measurements appears to be the break and pronounced reversal in the slope of the axial force curve (Method 10 on Figure 8-1). This criterion was shown by Ray and Taylor (Ref.8-3) to give good results for a variety of wings and to be particularly useful in certain cases when the wing bending moment method was indecisive. However, this criterion also must be used with caution since, as Ray and Taylor point out, erratic axial force characteristics can result from shock systems on a wing which are not sufficiently strong to separate the boundary layer.

Due to the possibility of obtaining inadequate or misleading information if only one buffet onset criterion is investigated, it is necessary to analyze data from several different measurements and to apply various complementary buffet criteria for a given test in order to have a reasonable chance of accurately predicting buffet onset. A typical test might include measurements of the wing root bending moment, lift and axial force coefficients, and trailing edge pressure coefficients and also the use of oil flow photographs. The first indicator listed would in general carry the most weight and the next two would be required primarily if the bending moment results should be inconclusive. Oil flow photographs provide an overall view of the flow on the wing, indicating the extent of the separated region.

The measurement of wind tunnel model buffet intensity and the scaling of model loads to loads on the real aircraft present particular difficulties. The most widely reported method for measuring buffet intensity is the wing root bending technique which is reviewed by Mabey (Ref.8-2). A major problem concerns the total damping coefficient which seems to be constant and composed mainly of structural damping for the rigid wind tunnel model but which appears to be variable and composed mainly of aerodynamic damping for the flexible aircraft. Mabey (Ref.8-7) suggests eliminating this difficulty by introducing dimensionless buffeting coefficients which are a measure of the generalized force in the wing fundamental mode due to any pressure fluctuations on the wing. By using the wind tunnel flow unsteadiness to calibrate the model response at the wing fundamental frequency, the derived buffeting coefficient can then be applied to relate the rigid model buffet measurements to the full-scale, flexible aircraft which has an unknown damping coefficient (Ref.8-2).

8.1.2 Procedures and Instrumentation in Wind Tunnel Testing for Buffet

Buffet wind tunnel testing should be conducted in a two phase program. The first phase should consist of flow visualization runs to obtain an understanding of the flow patterns and to aid in finalizing the locations for the model instrumentation. The second phase then should be the conduct of those tests required to obtain the quantitative pressure, acceleration, strain and force data.

In a typical flow visualization test, oil flow and tuft pattern photographs should be taken to define regions of two-dimensional flow, flow interferences, and shock wave locations. One wing should be equipped with oil orifices along its semi-span, and the other wing should be provided with a tuft grid. Both wings should be painted an appropriate color to contrast with the oil and tuft colors. As a minimum, flow patterns should be obtained at the critical test points.

Following the flow visualization tests, the dynamic instruments are installed on the model. This instrumentation consists of fluctuating pressure transducers (microphones), accelerometers and strain gauges. Strain gauges are installed on the wing and on the horizontal tail to measure the bending and torsional strains induced during buffet. In addition to an accelerometer located at the model c.g., a pair of high frequency accelerometers should be located near the wing tip to measure the bending and torsion acceleration responses to buffet pressure. Figure 8-2 shows the locations and types of instrumentation on a typical model and Figure 8-3 shows the detailed sensor locations on the wing (both figures from Reference 8-8). All wing mounted transducers should be recessed in the wing to preserve a smooth wing contour.

The dynamic sensors used in a typical fighter model for buffet tests are described as follows:

(1) *Microphones* –

Range 25 psi (pressure difference); accuracy ± 1%; natural frequency 125,000 Hz.

(2) *Accelerometers* –

Range ± 1000 g; sensitivity 3.3 mv/g; resonant frequency 2900 Hz.

(3) *Strain Gauges*

(a) Two-element rosettes (2 per Wheatstone bridge of measure torsion) 350 ohms.

(b) Uniaxial gauges (4 per Wheatstone bridge to measure bending) 350 ohms.

Vibrations tests should be performed after the installation of the sensors to determine the vibration modes and frequencies since these might influence the buffet data measured on the model.

8.1.3 Scale Effects in Wind Tunnel Buffet Prediction

In applying wind tunnel results to predict buffet boundaries for the full scale aircraft, a persistent problem (which is often blamed to some extent for the discrepancies between wind tunnel and flight test results) lies in the inability to match the test Reynolds number with that for the flight condition. The principal viscous effect for transonic airfoils is the interaction of the shock wave and the boundary layer on the upper surface. The magnitude of the scale effect has been shown to depend on whether the airfoil is a conventional thin, lightly loaded section or a relatively thick, aft loaded section (Ref.8-9). The flow field for the former case, which is characterized by a bubble formation behind the shock, is regulated by the conditions near the shock but mainly in the inviscid region adjacent to the separation bubble. Consequently, the shock induced flow field is fairly insensitive to scale effects (see examples in Reference 8-9).

On the other hand, aft loaded airfoils which have adverse pressure gradients over the rear, upper surface tend to experience rear separation. Since rear separation is sensitive to the boundary layer thickness and the velocity profile, the upstream shock-boundary layer interaction directly influences the rear separation and modulates the rate and magnitude of the developing separated flow. At the usual wind tunnel test Reynolds numbers, rear separation on aft loaded airfoils usually occurs, thereby introducing significant scale effects.

Turning from two-dimensional airfoils to three-dimensional models, scale effects can cause greater difficulties in reconciling the test results with the characteristics of the full-scale flow field. Not only may the flow separation locations differ for test and full-scale, but also the development of the separation regions may differ (References 8-2 and 8-10). Haines (Ref.8-10) discusses the problem of scale effects and gives examples illustrating the importance of these effects. He also points out shortcomings in the experimental procedure of using transition strips for artificially influencing boundary layer thickness at the shock wave or trailing edge location.

8.1.4 Flight Test Verification of Buffet Boundaries

Flight testing is the only way to evaluate the accuracy of buffet predictions. There appear to be two principal methods used for indicating buffet onset during flight tests: measurement of fluctuating responses of accelerometers positioned at the aircraft c.g. or in the wing tips, and pilot opinion. For the first method, a fluctuation of + 0.05 g

in normal acceleration at the c.g. would be a typical threshold level for buffeting. The second method is naturally less exact and tends to be pessimistic compared with wind tunnel measurements (Ref.8-6). If the pilot's seat is located on or near a node of the predominant modes being excited by the pressure fluctuations, buffet onset could be missed (Ref.8-2). However, for fighter-type aircraft, good agreement has been found between the pilot's awareness of buffet onset and the fluctuating response of an accelerometer located at the aircraft's c.g. (Ref.8-11).

In order to develop dependable prediction methods, detailed flight test data are required. To date only a small amount of detailed flight test data, with variable quality, has been obtained. Detailed comparisons with wind tunnel test results are possible only if the flight tests incorporate static pressure surveys, measurements of boundary layer development before separation and after reattachment, fluctuating pressure readings, and dynamic wing root strain measurements. For swept wings, as indicated in Section 8.1.3, flight and wind tunnel results show the possibility of different flow developments which may not be due to Reynolds number effects alone. A body of good flight test data would be valuable for comparison purposes when high Reynolds number wind tunnels become available and buffet tests are made in them.

8.1.5 Empirical Buffet Onset Prediction Methods – Correlations with Airplane Geometry

The desirability of having a simple method for making rapid buffet predictions during the early stages of an aircraft design led to the development of buffet onset prediction methods based on correlations between aircraft geometry parameters and experimental test results. Clearly this method could not be expected to have great accuracy, but the choice of the proper combination of parameters can result in sufficiently accurate preliminary predictions. Two examples of this type of prediction method are discussed in this section: one for airfoils and the other for wings.

Outman and Lambert (Ref.8-12) observed that the pressure distributions over the aft 30% of several airfoils were nearly constant up to a certain Mach number, beyond which wide deviations occurred. The flow separation causing the pressure deviations is a function of the adverse pressure gradient over the rear airfoil surface, which in turn is significantly linked to the inclination of the surface. A correlation was found between the Mach number of buffet onset determined experimentally and the angle between the free stream and a line connecting the trailing edge to the 70% chord location on the upper surface. The criterion of Outman and Lambert was applied in Reference 8-11 to seven aircraft having unswept wings and was found to give consistently optimistic results.

A more recent and elaborate geometry correlation method, developed by Lindsay (Ref.8-13), incorporates three wing parameters: aspect ratio, sweep angle, and taper ratio. The data base consisted of flight test results for 24 different aircraft. Also, wind tunnel tests using NACA 6-series airfoils provided data for estimating the required airfoil section properties. The method is limited to predicting the buffet onset normal force coefficient, C_{NB}, for Mach numbers of 0.6 and 0.7 and the Mach number for zero-lift buffet (or the minimum normal force coefficient for buffet).

The procedure for calculating C_{NB} consists of first predicting the buffet onset lift coefficient for the wing root section, knowing the section thickness and camber, and then correcting this value for sweep and aspect ratio using empirical functions. The Mach number for zero-lift buffet is found directly from graphs provided in the report. For a typical case shown in Reference 8-13, the calculated values of C_{NB} were found to have an accuracy of $\pm 10\%$. However, the method is sensitive to the degree of similarity of the aircraft configuration to those used in obtaining the correlations. If the difference is too great, useful results would not necessarily be obtained.

8.2 BUFFET ANALYSIS REQUIRING FLOW FIELD CALCULATIONS

Although wind tunnel testing is at present the most accurate and reliable means for predicting buffet boundaries for aircraft, there exist several methods for predicting buffet which can be used in the earlier design stages, thereby reducing the time and expense of wind tunnel testing. The prediction methods considered in the following sections are all based to some extent on correlations between wind tunnel tests and calculated flow field quantities. One buffet onset prediction method, using the procedure reported by Thomas (Ref.8-14), requires only theoretical flow field calculations.

8.2.1 Flow Field Calculation Methods

8.2.1.1 Inviscid Flow

Two-dimensional transonic flow fields can be calculated using either empirical or theoretical methods. Developed first and frequently used in buffet prediction calculations, the empirical method of Sinnott (Ref.8-15) requires as inputs both a subsonic potential flow solution and an empirically determined sonic flow solution. (Calculation methods applicable to both two- and three-dimensional, subsonic inviscid flows are thoroughly surveyed in Reference 8-1). Wind tunnel test correlations are used to give the supersonic flow region and the location of the terminating shock wave. The advantage of the Sinnott method is that it combines simplicity and speed while yielding reasonable pressure distributions, provided the particular airfoil is not too different from those on which the correlations are based.

The theoretical flow field calculation methods which have been developed are based on finite difference procedures but use different forms of the governing equations. In one approach, the problem is formulated using the time dependent, hyperbolic form of the conservation equations (Ref.8-16). After applying a finite difference matching procedure, a converged solution is obtained for large values of time and this is the required solution. In another approach, the problem is formulated in terms of the steady, mixed elliptic-hyperbolic form of the equations with the flow field mapped to the interior of a circle. The corresponding finite difference equations are solved using a relaxation technique (References 8-17 and 8-18). In both cases the embedded shock wave appears automatically in the solution although there is a question of whether or not the latter method properly handles the shock jump condition (Ref.8-13). The finite difference methods have produced good results, but the nonsteady approach requires from 4 to 8 times more computing time than the relaxation method (40 minutes versus 5 - 10 minutes, approximately, Reference 8-19).

Recently the relaxation approach has been extended to three-dimensions using the small disturbance equations in the physical coordinate system (References 8-20 and 8-21). In addition to the added computer storage and increased calculation time requirements, which can increase one or two orders of magnitude, further complications relate to the treatment of the vortex wake of the lifting wing and the matching of the finite difference grid network to the three-dimensional surface. The calculation procedure is limited to thin wings of low sweep at small angles of attack.

8.2.1.2 Boundary Layer

There are several established boundary layer calculation methods suitable for those buffet prediction methods requiring them. Both integral and finite difference methods have been used, integral methods being used more frequently. Integral methods are faster and relatively simple but involve some empiricism and give little detail about the flow field. On the other hand, the finite difference methods involve comparatively long computing times but do give a detailed description of the boundary layer.

Boundary layer calculations in the applicable buffet prediction methods are required to find the location of the flow separation. The flow separation criterion used depends on the boundary layer calculation method and on whether the flow is two or three-dimensional. Only two-dimensional separation is discussed here because criteria for the three-dimensional case are not well defined (Ref.8-22). (An example of a three-dimensional boundary layer calculation in a buffet prediction calculation is given in Section 8.2.3.) For integral calculation methods the separation criterion relates to the critical value of the shape parameter based on the velocity profile. The critical value of the shape factor is obtained from correlations with test data and this fact introduces an element of uncertainty in the criterion. For the finite difference methods, the velocity profile is calculated, thus allowing the separation point to be found directly as the location of vanishing shear stress.

8.2.2 Semi-Empirical Buffet Prediction Methods

There are several buffet onset prediction methods which require an inviscid flow field calculation. The simplest and least accurate method is based on the crest critical criterion for which one merely inspects the Mach number at the crest (position on the airfoil upper surface where the slope is parallel to the free stream). In general, as the local Mach number approaches one, drag divergence begins and consequently buffeting occurs.

Two other methods requiring an inviscid flow field calculation involve correlations between the pressure upstream of the shock and the trailing edge pressure divergence. The first, due to Gadd (Ref.8-23), provides an empirical buffet boundary curve, based on a plot of pressure upstream of the shock versus shock location. The second method, due to Sinnott and Osborne (Ref.8-23), involves an empirical buffet boundary curve based on a plot of Mach number (or pressure) upstream of the shock versus a geometric parameter of the wing section. The correlations for both methods show a fair amount of scatter but both criteria can be used to make preliminary buffet onset predictions.

A more elaborate semi-empirical prediction method requiring a boundary layer calculation was developed at Dornier (Ref. 8-24). This method discovered a correlation between buffet intensity as indicated by the wing root bending moment and a calculated, dimensionless coefficient C_{BI} based on the fraction of the local chord l_A over which the flow is separated. It is assumed that fluctuations in the wing root bending moment are proportional to the product of the local lift fluctuation and the corresponding distance from the wing root integrated over the wing. Further, l_A is assumed to be proportional to the root-mean-square value of the local lift fluctuations.

For the calculations made in Reference 8-24 to obtain C_{BI}, the inviscid solution was obtained using the method of Murman and Cole as modified by Krupp (Ref.8-25) (steady small disturbance equations are solved using line relaxation). A modified version of a procedure due to Küchemann (Ref.8-26) was used to extend the calculations for three-dimensional effects. The boundary layer was calculated using the three-dimensional entrainment method of Cumpsty and Head as extended by Redeker to compressible flows (Ref.8-27).

After comparison of calculated curves with buffet boundary curves (lift coefficient versus buffet onset Mach number) from flight and wind tunnel tests, it was found that $C_{BI} = 0.1$ is the criterion for light buffet. Other

comparisons of measured and calculated buffet curves indicated good agreement for the slopes of the curves. It was also found that the method's assumption of a linear relationship between C_{BI} and the root-mean-square value of the bending moment is valid only for small to moderate values of C_{BI}.

8.2.3 Method of Thomas and its Extensions

A buffet onset prediction method suitable for theoretical analysis was developed by Thomas (Ref.8-14) and applied to two different flow models. The first, associated with Pearcey and referred to as model A, is for conventional airfoils which tend to experience a bubble formation triggered by the shock-boundary layer interaction (Ref. 8-14). For increasing Mach number or angle of attack, the bubble grows rapidly until the reattachment point reaches the trailing edge, causing the bubble to burst. When the trailing edge pressure is disturbed, the overall flow field is altered (Ref.8-9).

The other flow model, referred to as model B, was introduced to characterize thicker, aft loaded airfoils which display a significant pressure rise from the shock to the trailing edge and which, therefore, have a tendency, for rear separation. Since the boundary layer development downstream of the shock is sensitive to the shock pressure jump and the associated boundary layer thickening, an increasing shock strength will lead to more severe aft separation until eventually separation will occur at the shock. For model B the Thomas method admits only the case in which no separation bubble occurs at the shock (Ref.8-27).

The procedure for the Thomas method is to calculate the flow separation position by means of separate inviscid flow field and boundary layer calculations. In the original paper (Ref.8-14), buffet onset was assumed to occur when the separation point and the shock location coincided. However, for model B airfoils the criterion was later modified and became linked to separation at the 90% chord point (Ref.8-27). The calculations for obtaining the separation position are repeated for a range of Mach numbers in order to obtain the buffet boundary curve for a particular wing section.

Clearly, the Thomas procedure conforms to model B airfoils. The rationale in applying it to model A airfoils as well (boundary layer theory cannot account for separating-reattaching flow) is that the separation point was found to jump suddenly from the trailing edge to the shock wave at a particular Mach number when using standard boundary layer calculations. The jump in separation point, according to Thomas (Ref.8-27), is associated with the bursting of the separation bubble and consequently with buffet onset. This sudden jump is the reason for retaining the original buffet criterion for model A. Even for model B the calculation procedure is closely applicable only for slightly separated flows since the inviscid flow field surface pressures become less accurate as the severity of the separation increases. At buffet onset the extent of the separation region is probably not too great although the limitations of the method are not firmly established.

For the boundary layer calculation in the Thomas method, provision must be made for inputting the shock jump pressure. Experimental investigations by Gadd (Ref. 8-28) of weak shock-boundary layer interactions on a flat plate showed that the shock caused a thickening of the boundary layer and the corresponding formation of compression waves in the exterior flow field. The net effect was to cause the shock pressure rise to be spread over 3 to 5 local boundary layer thicknesses. Thomas assumed a linear pressure rise over a distance of four boundary layer thicknesses (Ref. 8-27).

In applying the Thomas method to other than straight wings with uniform section properties, certain modifications are required. For moderately swept wings the same calculation procedure could be used provided that the free stream conditions are replaced with those normal to the wing leading edge. Then the Mach number and lift coefficient for buffet onset (C_{l_B}) can be restored to streamwise values using the cosine law (Ref. 8-27). If the wing sweep is large, this approach gives results which are too optimistic. Few calculations have been made following the Thomas procedure and using three-dimensional inviscid and/or boundary layer calculations.

Gentry and Oliver (Ref.8-1) have presented buffet predictions for swept wings based on the Thomas procedure and accounting for spanwise wing loading. The Woodward program with compressible flow corrections was used to provide a plot of the aircraft lift coefficient (C_L) versus an arbitrary sectional lift coefficient (c_l). Root and pressure peak sections were used. In turn this plot was used as the intermediary between the sectional buffet boundary curve (c_l vs. M_B) and the aircraft buffet boundary curve (C_L vs. M_B).

In order to account for the viscous effects of spanwise flow for highly swept wings, Redeker (Ref. 8-27) extended the three-dimensional boundary layer calculation method of Cumpsty and Head to compressible flow and used it in a buffet onset calculation. Flow separation was judged to occur when streamlines near the wing surface became parallel to the wing leading edge. Similar to the two-dimensional case, the buffet onset condition was assumed to occur when the separation line reached the 90% chord location of any wing section.

8.2.4 Comparison of Some Buffet Prediction Methods

Flight test results for the Bell X-1 aircraft, as reported in Reference 8-11, have been used more widely than any other flight data for comparison with buffet onset prediction methods. The X-1 aircraft had an unswept wing

of aspect ratio 6 and taper ratio 0.5. The buffet boundary comparison compiled from References 8-1 and 8-11 is shown in Figure 8-4. The predictions based on the four empirical and semi-empirical methods (curves Nos 3 to 6) show pessimistic results, with the predicted buffet onset boundary for the crest critical criterion, the simplest method, least resembling the experimental curve in slope and position. The two curves in Figure 8-4 labeled Thomas Result are from the original Thomas paper (Ref. 8-14) and were calculated using the semi-empirical Sinnott method for the inviscid flow field and the integral method due to Walz for the boundary layer calculation (method II of Reference 8-29. The Dornier program also uses this method).

Gentry and Oliver (Ref.8-1) applied the Thomas procedure to the X-1 aircraft using a modified version of the Sinnott method for the inviscid calculation and three different methods for the boundary layer calculation: the NASA Lewis integral program, the Cebeci and Smith finite difference method, and the Dornier integral program. The results are plotted together in Figure 8-5 (from Reference 8-1), where C_{N_A} is the force coefficient normal to the chord at buffet onset. It is not clear why the results using the more exact finite difference boundary layer calculation or the equally exact NASA program are in poorer agreement with the flight test experiment data than those using the original Dornier program. As Thomas remarked in Reference 8-27, more comparisons with experimental results are needed in order to thoroughly evaluate the calculation procedure.

Junke et al (Ref.8-24) also compared their prediction method with X-1 flight test data. Figure 8-6 taken from Reference 8-24 compares the calculated and experimental buffet onset boundaries. The calculated results, however, do not include the case for $C_{BI} = 0.1$, which was later determined to be the value for buffet onset. The trend of the other calculated curves indicates that the $C_{BI} = 0.1$ curve would probably be in good agreement with the experimental data.

8.3 CONCLUDING REMARKS

For detailed investigations of buffet, particularly beyond buffet onset, wind tunnel testing with rigid models is likely to remain the principal investigative tool for the immediate future. An exact theoretical formulation of the transonic buffet problem is beyond current analytical capabilities. However, the Thomas method may prove to be useful in preliminary and intermediate design, particularly with refined three-dimensional flow calculation components. The ultimate usefulness of this analytical buffet prediction method is linked to the availability and quality of computer codes for the flow calculations. Unfortunately there appear to be shortcomings in this regard at the present time. Gentry and Oliver (Ref. 8-1), who worked with a variety of programmed inviscid flow and boundary layer calculation methods, discovered that the codes are not available in a readily compatible form, are usually cumbersome for systematic studies, sometimes show low levels of programming proficiency, and have little internal program documentation.

Many investigators engaged in buffet analysis have pointed out the need for detailed and reliable wind tunnel and flight tests in which measurements are made of pressure distributions, fluctuating pressures, boundary layer development (particularly before separation and following reattachment), and wing response, Such results could serve two important functions. They would allow evaluations of theoretical calculation procedures by means of detailed comparisons, and they would indicate the influence of scale effects in the flow development on models.

CHAPTER 9

BUFFET FLIGHT TEST TECHNIQUES

by

P.J.Butkewicz

9.0 INTRODUCTION

Transonic maneuverability has evolved as one of the primary measures of the combat performance capability of modern fighter aircraft. Buffet flight testing thus can be viewed as the final field trials which yield the qualitative and quantitative performance data and which indicate the degree of success attained by the designer. From an operational standpoint such testing is essential since it relates the pilot's opinion of the aircraft's maneuvering qualities with the engineering data. Finally, buffet flight testing is an invaluable source of data (fluid dynamics, structures, stability and control, etc.) which design engineers can use to correlate analytical and wind tunnel results.

In the past, buffet flight testing consisted primarily of obtaining pilot opinion data on buffet onset and the relative buffet intensity, and measurements of the normal load factor at the center of gravity. Consequently such tests related buffet onset to the pilot's tolerance of load factor vibrations, and other aircraft structural characteristics and only weakly to the air flow separation phenomena. Current buffet flight testing has progressed to an advanced state such that highly accurate engineering data are obtained and a more thorough understanding of the flow fields, shock interactions, air loads, structural responses, etc., is gained.

This Chapter discusses both buffet instrumentation and flight test techniques. Data reduction and analysis techniques were discussed in Section 4.3 of Chapter 4.

9.1 BUFFET INSTRUMENTATION

Flight test instrumentation must be of sufficient quantity to provide information on aerodynamics, accelerations, structural dynamics, aircraft and flight parameters, and flow visualization. Details of the instrumentation installed for buffet tests of a F-106A aircraft (and which are typical for general buffet flight tests) are given in the Appendix (Section 9.4 from Reference 9-1). In this Appendix the buffet instrumentation is discussed at length, including type, location, accuracies, ranges, etc. Table 9-1 and Figures 9-1 and 9-2 present some of these details. Sample oscillograph output traces, from an actual flight test are shown in Figure 9-3 from Reference 9-1. In this figure the aircraft structural filtering effect is clearly seen by the differences in the normal accelerations measured at the wing tips and at the aircraft c.g. Figure 9-3 also shows that the wing static pressure divergence indication of flow separation/buffet onset is in excellent agreement with the buffet onset indication from the wing tip accelerometers.

In general, flight instrumentation for buffet tests should include static pressure taps; total pressure and boundary layer rakes; accelerometers; strain gauges; aircraft attitude sensors; high speed camera and wing tufts; and a cockpit event marker. In the case of buffet flight testing of an operational aircraft, allowable instrumentation modifications may be limited (due to outside constraints), and close coordination must be maintained between the test engineer and the modification facility to assure optimum installation locations.

Particular attention must be paid to the application of wing tufts for flow visualization and for the mounting of the camera. In many programs it has been necessary to use tufts of various colors as well as to paint the wing various colors before satisfactory results were achieved. Tufts are generally applied with either high strength pressure sensitive tape or epoxy glue compounds. A typical tuft grid pattern on a wing is shown in Figure 9-4 (Ref.9-1). To aid in obtaining the best possible photographs, a small television camera, having the same field of view of the wing, can be mounted near the movie camera. The television receiver screen is placed in the cockpit and monitored by the pilot. To avoid distortion of the television picture, the camera should be well isolated from other electrical "noise". Also, both the television and movie cameras should be equipped with automatic "f" stop capability.

In the event that buffet flight tests are to be performed with an aircraft dedicated to research, or an operational aircraft having a new wing, far more comprehensive instrumentation may be incorporated. A good example of the latter is the USAF/NASA Transonic Aircraft Technology (TACT) Program. In this program, an existing aircraft was modified to incorporate an advanced supercritical wing. During the manufacturing/modification process 168 static

TABLE 9-1

Buffet Boundary Instrumentation

MR No.	Measurement Requirement	Recorder*	Range	Resolution	Accuracy	Frequency Response (Hz)
1	Airspeed	P	50 – 700 kt	1 kt	2 kt	–
2	Altitude	P	0 – 50,000 ft	20 ft	100 ft	–
3	Fuel Remaining	T	0 – 10,000 lb	100 lb	300 lb	–
4	Engine RPM (N_3)	T	1 – 100%	0.25%	1.00%	–
5	Data Correlation Mod IRIG B	D, P, T	hr, min, & sec	1 sec	0.1 sec	–
6	Pilot's Event Marker	C, P, T				
7	Normal Acceleration, Cockpit Display	D	0 – 7 g	0.1 g	0.2 g	5
8	Outside Air Total Temperature	P	−60 + 190°F	0.5°	2.0°	1
9	Rudder Position	T	−25 + 25 deg	0.2 deg	1.0 deg	10
10	Right Elevon Position, Inboard Actuator	T	−33 + 10 deg	0.2 deg	1.0 deg	10
11	Left Elevon Position, Inboard Actuator	T	−33 + 10 deg	0.2 deg	1.0 deg	10
12	Right Elevon Position, Outboard Actuator	T	−33 + 10 deg	0.2 deg	1.0 deg	10
13	Angle of Attack	D, T	0 + 50 deg	0.5 deg	1.0 deg	2
14	Angle of Sideslip	D, T	−10 + 10 deg	0.5 deg	1.0 deg	2
15	Pitch Rate	T	± 20 deg/sec	0.2 deg/sec	2.5 deg/sec	2
16	Normal Acceleration, Right Wing Tip 95% Span, Spar 7	T	−5 + 10 g	0.05 g	0.2 g	70
17	Normal Acceleration, Right Elevon Trailing Edge 50% Span	T	−5 + 10 g	0.05 g	0.2 g	70
18	Normal Acceleration, Right Elevon Trailing Edge 95% Span	T	−5 + 10 g	0.05 g	0.2 g	70
19	Normal Acceleration, Left Wing Tip 95% Span, Spar 7	T	−5 + 10 g	0.05 g	0.2 g	70
20	Normal Acceleration, Aircraft cg	T	0 – 7 g	0.05 g	0.2 g	70
21	Lateral Acceleration, Cockpit Floor	T	± 0.5 g	0.05 g	0.01 g	20
22	Normal Accleration, Cockpit Floor	T	0 – 7 g	0.05 g	0.2 g	70
23	Longitudinal Acceleration, Aircraft cg	T	−1 + 1 g	0.05 g	0.1 g	35
24	Pitch Attitude	T	−90 + 90 deg			10
25	Roll Attitude	T	−180 + 180 deg			10
26	Right Wing Spar 2 Strain, Bending Response	T	0.5 to 1.0 mv/v			35†
27	Right Wing Spar 3 Strain, Bending Response	T	0.5 to 1.0 mv/v			45†
28	Right Wing Spar 4 Strain, Bending Response	T	0.5 to 1.0 mv/v			60†
29	Right Wing Spar 5 Strain, Bending Response	T	0.5 to 1.0 mv/v			80†
30	Right Wing Spar 6 Strain, Bending Response	T	0.5 to 1.0 mv/v			110†
31	Not Used					
32	Right Wing Upper Surface Differential Pressure, 58% Span, 50% Chord	T	± 2.5 psid	0.05 psi	0.15 psi	5
33	Right Wing Upper Surface Differential Pressure, 58% Span, 65% Chord	T	± 5.0 psid	0.05 psi	0.3 psi	5

* Recorders: C – Tuft Camera, D – Cockpit Display, R – Photo Panel, and T – Tape.
† Subcarrier oscillator limits system frequency response.

(Continued)

TABLE 9-1 (Continued)

MR No.	*Measurement Requirement*	*Recorder**	*Range*	*Resolution*	*Accuracy*	*Frequency Response (Hz)*
34	Right Wing Upper Surface Differential Pressure, 58% Span, 80% Chord	T	± 5.0 psid	0.05 psi	0.3 psi	5
35	Right Wing Upper Surface Differential Pressure, 58% Span, 95% Chord	T	± 7.5 psid	0.05 psi	0.3 psi	5
36	Right Wing Lower Surface Differential Pressure, 58% Span, 95% Chord	T	± 7.5 psid	0.05 psi	0.3 psi	5
37	Reference Pressure in Actuator Compartment	T	0 to 15 psia	0.4%	±1%	5
38	Left Wing Upper Surface Tuft Film	C	–	–	–	–
39	Lateral Acceleration, Fin Tip	T	−2 to +2 g	0.05 g	0.2 g	35
40	Lateral Acceleration, Upper Aft Rudder	T	−2 to +2 g	0.05 g	0.2 g	35
41	Right Wing, Upper and Lower Skin ΔT, Spar 2	T	± 60°C	10°C	10°C	1
42	Right Wing, Upper and Lower Skin ΔT, Spar 6	T	± 60°C	10°C	10°C	1
43	Pilot's Voice	T	–	–	–	–

* Recorders: C – Tuft Camera, and T – Tape.

pressure taps, 25 dynamic pickups, and 36 boundary layer rake tubes were installed in the wings and 30 static pressure taps were installed along the fuselage centerline. In addition, standard buffet instrumentation (i.e., accelerometers, strain gages, tufts/camera, nose boom, etc.) were also installed. Figures 9-5 and 9-6 show the instrumentation locations used. Instrumentation of this extent is considered to be the current state of the art.

In addition to the on-board data recording equipment and, perhaps, telemetry, a certain minimum standard for cockpit displays is required to ensure the expeditious completion of a buffet flight test plan such as that presented in Table 9-2 from Reference 9-2. The normal cockpit instrument for indicated airspeed/Mach number is usually adequate, but consideration should be given to the large pressure errors which may occur at high α and high 'g' The cockpit altimeter, particularly in wind-up turn tests, should not be subject to large lags. Clearly a 'g' meter and an α gage are required and, even though unreversible powered flying controls may be in use, aileron and rudder deflection indicators are required. The aircraft may have structural side force limits, in which case these should be calculated before each test condition is flown and a sideslip gage or lateral accelerometer provided to allow the pilot to monitor the side force during possible yaw divergence or wing-rock. Other test aids found to be of value are a voice recorder, a nose camera to record horizon motion, and an event button for the pilot to record subjectively significant times on the data traces for later identification and explanation.

9.2 FLIGHT TEST TECHNIQUES

In buffet flight testing, the schedule should incorporate that sequence of aircraft configurations and Mach-altitude conditions which will provide the most rapid collection of critical data based on (1) the time required to attain the desired aircraft configuration and test condition; and (2) the aircraft modification time required for the subsequent configurations. Considerations in planning the test schedule should include such factors as maneuvering flap deflections, external stores on and off, and the Mach-altitude envelope. Table 9-2 is illustrative of a typical test schedule flown during a buffet flight program.

Flight test maneuvers normally take the form of wind-up turns, wing level pull-ups, or steady "g" turns. Wind-up turns are flown to the maximum usable lift coefficient or the structural limit of some aircraft component, i.e., 4–5 g's for wing flaps and slats. Typical wind-up turns commence about 3000 feet above the nominal altitude and at the required Mach number. The aircraft is rolled into a left or right turn and the load factor is increased until the desired buffet level is attained. Altitude and Mach number excursions should be held to a minimum, and lateral or directional controls should not be used during the data collection period. Data gathered under such flight conditions exhibit minimum scatter, and quantitative parameter levels can be developed using existing averaging techniques. Figures 9-7 (Ref.9-3) and 9-8 (Ref.9-1) show typical aerodynamic data obtained during buffet flight testing.

TABLE 9-2

Buffet Flight Test Plan

Flight Conditions and Flap Deflections Tested							
Flight No.	*Configuration*	*Altitude* Feet	*Mach No.*	δ_n Deg.	δ_f Deg.	*Takeoff* *Weight* lbs	*Takeoff* *C.G. Percent Mac*
650	Clean Wing Tips	25,000	0.85, 0.90	9	0, 4	13,265	14.0
652		35,000	0.90	9	0, 4	13,273	13.9
654		25,000 35,000	0.80, 0.85, 0.90 0.80, 0.85	9 9	0, 4 0, 4	13,273	13.9
655		25,000 35,000	0.80, 0.85, 0.90 0.80, 0.85	9 9 9	0, 4 0 0, 4	13,273	13.9
656		25,000 35,000	0.85 0.80, 0.85, 0.90 0.80, 0.85, 0.90	9 9 9	0 8 8	13,273	13.9
657		25,000 35,000	0.80, 0.85, 0.90 0.80, 0.85, 0.90	0 0	0, 8 0, 8	13,273	13.9
658		25,000 35,000	0.70 0.70, 0.80, 0.85, 0.90 0.80, 0.85, 90	0 0 0	0 4 4	13,273	13.9
659		25,000 35,000	0.70 0.70, 0.80, 0.85, 0.90 0.80, 0.85, 0.90	18 18 18	4 4 0	13,265	14.0
660		25,000 35,000	0.70 0.70, 0.80, 0.85, 0.90	13 13	0, 4 0, 4	13,265	14.0
661		25,000 35,000 35,000	0.70 0.75 0.70, 0.80, 0.85, 0.90	13 13 13	8 0 8	13,265	14.0
662	Tip Tanks	25,000 35,000	0.80, 0.85, 0.90 0.80, 0.85, 0.90	0 0	8 8	13,454	14.55
663		25,000 35,000	0.80, 0.85, 0.90 0.80, 0.85, 0.90	0 0	8 8 flap gap scaled	13,484	14.44
664		35,000 35,000	0.80, 0.85, 0.90, 1.20 0.80, 0.85, 0.90	0 0	0 4	13,474	14.34
665		25,000 35,000	0.80, 0.85, 0.90 0.90, 1.10	0 0	0, 4 0	13,474	14.34

Many aircraft have 'Q' and Mach scheduled longitudinal control system devices which either provide stick/surface deflection ratio changes or give nominal trim changes with variations in altitude and speed. If these devices function during a buffet/wing rock test as a result of an altitude change or a Mach number excursion they can cause residual changes in the longitudinal trim which may upset the test in progress, thus negating the pilot's attempts to keep the control positions constant. Often it may be advantageous to disconnect these devices, particularly if the sources for their actuation include pressure and static vents which are subjected to flow variations during wing rock or buffet associated flow separation.

9.2.1 Pilot Workload During Buffet Flight Tests

Pilot workload can be high during buffet flight tests because of the rapidity with which events succeed each other. After carrying out his instrumentation trim checks, the pilot sets up his start conditions according to the aircraft's specific excess power characteristics and the type of maneuver to be conducted. Taking a wind-up turn as the most active test the following sequence of actions is typical. The pilot first notes the 'g' and side force limitations for the run to be conducted, making allowances for slight excursions that may occur from the desired test condition. At 2 to 3 thousand feet above the test height the aircraft is rolled into the turn and power is increased as the 'g' or angle of attack is increased to the required value. Speed is maintained constant by varying the bank angle. Height, speed, g, angle of attack and side force are monitored by the pilot and subjective features of the run are noted for future recording. The instrumentation is evented and the nose camera is turned on if appropriate. The pilot concentrates on maintaining fixed cockpit control positions during the critical recording period and monitors his flight path to ensure that any aircraft motions do not nullify the preplanned recovery. When at an altitude of 2 to 3 thousand feet below the nominal height the wings are levelled and the pull-out conducted within the aircraft's limitations, the instrumentation and camera being switched off. The total elapsed time will be about 20–30 seconds. During the subsequent climb for the next run, fuel loading is noted and more leisurely comments are recorded while the aircraft is repositioned. This is the basic sequence of events and it can be added to as necessary by the requirements to maintain a specific buffet level or to inject rudder pulses and aileron pulses at specific angles of attack. As the demands of the flight test may reduce the 'look-out' that the pilot can maintain, high quality collision avoidance ground radar is essential, and in a particularly demanding trial a chase look-out aircraft may be used.

As with all high angle of attack testing various considerations are worthy of note. A test flight of 10 to 15 buffet/wing-rock runs can be physically demanding to the pilot and the flight should be scheduled to cater for this by alternating high and low 'g' runs where possible.

9.3 CONCLUSIONS

The performance of buffet flight testing is the final ingredient in determining quantitative and qualitative aircraft maneuvering performance, and is the sole source of full-scale aircraft data used for direct comparisons with analytical or empirical predictions.

Buffet flight test instrumentation has been steadily improved such that highly accurate engineering data now can be obtained. With future improvements in the instrumentation hardware and software, a corresponding improvement in the quantity and quality of flight test data can be expected.

Buffet flight test techniques currently used are adequate for such testing. With the newer emerging fighter aircraft having a thrust-to-weight ratio of the order of one, altitude loss during wind-up turns is minimized, and adequate time is available for data acquisition at the desired steady state flight conditions.

9.4 APPENDIX – INSTRUMENTATION DETAILS (FROM REF.9-1)

The instrumentation system described in this Appendix was designed to provide quantitative data pertinent to the buffet phenomena and its effect on the F-106A airframe. Accelerations, bending-responsive wing strain gage bridge measurements, wing pressures, flight parameters, and aircraft attitudes were monitored and recorded. Table 9-I presents the complete measurements list. Measurement locations are shown in Figure 9-1.

The instrumentation system consisted of three major subsystems: sensing, signal conditioning, and recording. A block diagram representation of the signal flows and the equipment interfaces is presented in Figure 9-2.

9.4.1 Sensing Subsystem

9.4.1.1 Pressure Transducers

Static pressure distribution on the right-hand upper wing surface was monitored at four locations. These locations were at 15 percent intervals from 50 to 95 percent of the wing chord at the 58 percent wing semi-span station. Plastic tubing routed the surface pressures from the pick-up points to the transducer installation in the right-hand outboard elevon actuator fairing. The five differential pressure transducers were referenced to ambient pressure in

the actuator fairing through a common manifold. Ambient pressure in the fairing was monitored by an absolute pressure transducer.

Preliminary evaluations of the data gave rise to a question on whether the frequency response of the pressure survey was adequate for buffet determination purposes. A check was made on the transducer with the most damping due to line length, i.e., the upper-surface 50 percent location transducer. This check revealed a frequency response in excess of 20 Hz.

9.4.1.2 Aircraft Control Surface Transducers

Elevon position was monitored using the production feedback potentiometers located on the inboard actuators. A linear position potentiometer was installed on the right-hand elevon outboard actuator. An angular position potentiometer coupled to the rudder hinge pin was installed to measure rudder angular displacement.

9.4.1.3 Aircraft and Flight Parameter Transducers

A Convair-design nose boom was installed on the production nose cone. The nose boom housed dual pitot static systems and vane-driven precision potentiometers for angle of attack and angle of sideslip measurements. The angle of attack measurement had a range of −5 degrees to +45 degrees. The angle of sideslip measurement had a range of ±15 degrees.

The instrumentation pitot-static system was completely separate from the production system and drove sensitive indicating instruments located on the photo panel.

Pitch and roll attitudes were measured by a cageable vertical gyro installed on an equipment shelf below the instrumentation platform in the forward missile bay. Measurement ranges were: pitch attitude ± 90 degrees, and roll attitude ±180 degrees.

Pitch rate was derived from the turn rate transmitter, which was part of the aircraft's stability augmentation system. The range of the derived pitch rate was ± 20 deg/sec.

9.4.1.4 Strain Gage Bridges

Strain gage bridges were located on Spars 2 through 6 of the right wing at the wing root. Strain gage elements were placed on the upper and lower wing surface at the centerline of each spar. The strain gage elements at each spar were wired as fully active bridge circuits to provide maximum output and linearity. Since temperature differences can be expected between the upper and lower wing surfaces, thermocouples were installed on these surfaces at Spars 2 and 6. The thermocouples were iron-constantan and were wired to provide a voltage output proportional to the temperature differential of the wing surfaces.

9.4.1.5 Accelerometers

Eleven accelerometers where installed on the aircraft at the center of gravity, pilot station, wing tips, right-hand elevon, vertical tail tip, and rudder. Two normal accelerometers were located at the aircraft's center of gravity: one drove a remote indicator in the cockpit and the other was used for the tape recorder signal.

When the accelerometer data were first analyzed using standard playback techniques, it was difficult to correlate the pilot's callouts with the aircraft response measurements. It was suspected that the accelerometer mounts were adding noise to the data and modifying the measurements of the actua. aircraft's motions. To eliminate this potential source of error, the normal and longitudinal accelerometers at the center of gravity were moved to more rigid locations. Data analysis revealed that although relocation made some difference, the mounting location was not the basic problem. The problem was eventually solved by selective filtering of the signals and by amplifying the accelerometer playbacks.

9.4.2 Signal Conditioning Subsystem

Three units made up the signal conditioning subsystem: signal conditioner unit, time code generator, and subcarrier oscillators. These units served to amplify, convert, multiplex, or otherwise condition the transducer voltages for recording on magnetic tape, photo panel, or visual displays in the cockpit.

9.4.2.1 Signal Conditioner Unit

The signal conditioner unit contained all the circuits necessary to standardize the signal amplitudes to 5 volts peak to peak. Voltage gain and impedance buffeting was accomplished by high-gain integrated circuit operational amplifiers in conjunction with a thermally regulated differential amplifier input stage. Negative feedback was employed to stabilize the gain impedance and to reduce the susceptibility to power supply variations. Resistive balance circuits were incorporated on all bridge inputs to obtain a null voltage for static conditions.

Instrumentation power was developed in the signal conditioner and including 5 v dc transducer excitation, −15 v dc outside air total temperature indicator excitation, + 5 v dc time display excitation, and ± 15 v dc amplifier excitation.

The signal conditioner could be placed in the calibration mode by a switch on the unit for checkout or by a remote control switch on the pilot's control panel for inflight calibration. When placed in the calibration mode, the 5 v excitation was removed from the transducers, the signal conditioning amplifier inputs were switched to substitute bridges or voltage sources within the unit, and the excitation was stepped from full scale to half scale to zero scale. Each step of the calibration cycle was two seconds in duration and was initiated from the 1 pulse per second (pps) signal from the Convair time-code generator. The calibration cycle could be stopped at any step by moving the mode switch from the automatic to the manual position.

9.4.2.2 Time-Code Generator

The Convair time-code generator controlled all timing functions throughout the instrumentation system. An accurate time base was derived from a highly stable oven-controlled 1.0 MHz crystal oscillator.

The 1.0 MHz reference was divided to provide binary coded decimal outputs for remote display of minutes and seconds in the cockpit and on the photo panel, an IRIG B amplitude-modulated 1 kHz carrier time format for recording on tape, and a 1 pps time reference for framing the photo panel camera and stepping the calibration cycle in the signal conditioner.

The counting circuits of the time code generator were transistor-transistor logic integrated circuits which provided a high reliability and a small package size.

9.4.2.3 Subcarrier Oscillators

Subcarrier oscillators accepted the standardized voltages from the signal conditioner and converted the signals to frequency-modulated carriers. The carrier frequencies were multiplexed into four composite signals. Each composite signal was amplified by a wide-band amplifier that provided impedance matching and voltage gain prior to interfacing with the tape recorder electronics.

9.4.3 Recording Subsystem

The recording subsystem consisted of four units: photo panel, tape recorder, wing tuft camera, and cockpit display and control panel. All recording units were controlled remotely from the pilot's control panel.

9.4.3.1 Photo Panel

The photo panel was installed in the aft missile bay to record airspeed, altitude, outside air temperature, time display, and the pilot's event marker light. A 35 mm camera filmed the indicator deflection at a rate of one frame per second. The camera shutter framing was controlled by the 1 pps signal from the time-code generator to assure a direct timing relationship with other recording units.

9.4.3.2 Tape Recorder

The airborne magnetic tape recorder was installed in the forward missile bay. This recorder used one-inch tape and had a 14-track direct record capability conforming to IRIG standards. The data recorded on tape consisted of four tracks of composite frequency-modulated data, one track of the 50 kHz reference frequency, and one voice track. The recorder was operated at 15 inches per second (ips) and could be started and stopped remotely. Significant performance characteristics of the recorder were the following:

Reel size (NARTB hub)	10.5 inches
Recording time at 15 ips (using 1 mil tape)	60 minutes
Wow and flutter, uncompensated	± 0.35%
Temperature operating range	−54 to + 71°C
Shock (with shock mount)	15 g, any axis
Reference frequency	50 kHz

9.4.3.3 Wing Tuft Camera

The wing tuft camera was installed in the vertical tail of the aircraft. Maximum wing coverage was accomplished by remoting the lens system through a flexible six-foot fiber optics bundle to a clampable swivel ball joint. The camera was boresighted for optimum wing coverage rotating the swivel and clamping it in place.

A neon light interval to the camera provided an event mark on the side of the film between the sprocket holes. This pilot-controlled event mark permitted correlation of the tuft camera data with other recorded data. The 16 mm camera contained a 400-foot film spool and operated at a frame rate of 12 frames per second.

A pattern of white tufts on a black wing was used. The six-inch tufts were fabricated from 1/8-inch nylon shroud lines with the ends treated to prevent fraying.

Considerable difficulty in achieving satisfactory photographic results was encountered with this system. Pictures from Flights 1 and 2 were satisfactory. On Flight 3, with no known changes other than local atmospheric differences (which qualitatively were judged to be brighter), pictures with the aircraft in a rolled attitude were unusable. A filter was added for Flight 4. Pictures from this flight were totally unusable. For Flight 5, colored film was used. To improve contrast, the black paint was removed and the white tufts were replaced with red tufts. This resulted in satisfactory pictures when the aircraft was in a rolled attitude, but too much glare when the aircraft was in level flight. On viewing the film, it was noted that the red tufts showed well against the blue background of the insignia. Based on this observation, the wing was painted blue for Flight 6. An additional set of white tufts were also added. The results were the same as those on Flight 5. It was concluded that to achieve satisfactory film coverage, it would be necessary to have an automatic f stop capability for the lens.

9.4.3.4 Cockpit Display and Control Panel

The pilot's interface with the instrumentation system was through the cockpit display and control units. Control of instrumentation power, recording systems, and inflight calibration was accomplished at the instrumentation cockpit control panel located in the right console at normal position of the Homing Point Selector panel. Push-to-test indicator lights were placed above each switch to indicate that a switch had been moved to an active circuit. An additional control panel for uncaging the attitude gyro was located just aft of the instrumentation control panel on the right-hand console fairing.

Aircraft normal acceleration at the center of gravity was displayed to the pilot. The indicator was located in the lower left-hand quadrant of the instrument panel. Angle of attack and angle of sideslip were displayed to the pilot by two meter movements located on a panel fitting over the face of the multi-mode storage tube.

A digital time display with a readout in minutes and seconds was located over the airspeed indicator on the left-hand side of the pilot's instrument panel. This display was driven directly from the time-code generator and allowed the pilot to time-correlate events.

Voice recording was obtained from the microphone side of the intercom system. This pickup point provided a "hot" mike so that the pilot had a direct line to the tape recorder and did not have to key the mike to annotate the recording.

The armament trigger switch on the right-hand control stick was wired as an event marker. Actuation of this switch caused an event mark on all recording media.

CHAPTER 10

LIMITATIONS IN THE CORRELATION OF FLIGHT/TUNNEL BUFFETING TESTS

by

D.G.Mabey

10.0 INTRODUCTION

Chapters 4 and 7 presented review of methods of defining the onset and severity of buffeting on an aircraft in flight from tests of wind tunnel models and included correlations with flight test results. This Chapter expands the summary remarks made in those Chapters in explanation of some of the differences observed between flight and tunnel tests.

The differences between flight/tunnel comparisons of buffeting are often lumped together on the charge sheets as "Reynolds number effects". However, it is probable that the charge sheet should be much longer and include uncertainties in both the flight and wind tunnel tests, in addition to genuine Reynolds number effects. The review in this Chapter may encourage research workers to attempt a more critical evaluation of flight and tunnel test data.

In this Chapter the following notation is used:

b	wing span	δ	boundary layer thickness (mm)
c	wing chord (m)	ρ	free stream density (kg/m^3)
C_L	lift coefficient		
g/2	structural damping (% critical)		
M	Mach number		
q	kinetic pressure $\frac{1}{2}\rho U^2$ (N/m^2)		
R	Reynolds number		
S	Wing area (m^2)		
U	free stream velocity (m/s)		
x	distance from leading-edge (m)		
α_w	angle of attack of wing (o)		
γ	aerodynamic damping (% critical)		

10.1 UNCERTAINTIES IN FLIGHT EXPERIMENTS

10.1.1 Measurements of Mach Number and Angle of Attack

While we must accept that the flight buffeting characteristics of an aircraft are in one sense the "correct" ones, we must also recognise that flight buffeting data will inevitably be somewhat scattered and imprecise relative to tunnel measurements. The highest attainable accuracies for Mach number and angle of attack, which may be obtained in a flight experiment only with special instrumentation, are given in the table below. The table also gives somewhat optimistic estimates for the corresponding accuracies from tunnel tests.

	Flight	*Tunnel*
Mach number M	± 0.005	± 0.002
Angle of attack α_w	At 10° ± 0.4°	± 0.05°

Manifestly flight buffeting data can never be as precise as tunnel data in regions where the buffeting characteristics are changing rapidly with Mach number and angle of attack, as they generally do at transonic speeds.

10.1.2 Measurement of Buffeting

Wing-tip accelerometers and wing-root strain gauges are now widely used for correlation of flight and tunnel buffeting experiments, and generally give reasonably consistent results. However, it is difficult to maintain a steady buffeting condition in flight, e.g., in a steeply banked turn, and so the length of the record available for analysis is usually less than 10 seconds. Even with a small fighter aircraft the wing frequency will not be much higher than 12 Hz so that only about 120 cycles of the buffeting signal will be available for analysis.

A flight experiment must cover a wide range of altitude (say from 5,000 to 30,000 ft) at constant Mach number if a serious attempt is to be made to establish the scaling laws appropriate for the buffeting. Many flight buffeting measurements have been made over a narrow altitude range (say from 30,000 to 35,000 ft) and thus do not allow sufficient variation in air density to establish the scaling laws.

Many of the early buffeting experiments relied heavily upon the pilot's impressions of buffeting. This was unfortunate because a pilot's impression of the onset of buffeting may be prejudiced by the cockpit position. Thus if the cockpit is at a node of a vibration mode being excited, the pilot may be unaware of the extent of the buffeting. In addition, his assessment of the severity of buffeting may be prejudiced by his other problems, such as controlling the aircraft to prevent a structural failure or to avoid an attack by an enemy aircraft. Hence early buffeting data (e.g., on the Bell X-1 aircraft) should be used with some caution as a basis for flight/tunnel comparison.

10.1.3 Visualisation of Areas of Separated Flows

At low speeds it is usually possible to arrange a limited programme of flow visualisation with tufts to establish the pattern of the stall development. However, at transonic speeds tuft photographs showing the growth of separated regions are rarely attained because of the expense of the flight development programme and the difficulty of interpreting the motion of a tuft in the presence of a shock wave and a separation.

With specially instrumented aircraft, mean pressure measurements at a series of points may be used to infer more precisely the position of shock-waves and separations. Fluctuating pressure measurements may also give a direct indication of the excitation. However, the selection of points available for these measurements is generally severely compromised by the need to avoid spars or control surfaces. Where such measurements are attempted it is advisable to cover as wide a range of altitude as possible, at least at the Mach number of most interest (generally between $M = 0.60$ and 0.85 for a fighter aircraft), in order to detect any significant variation in the separation development with either kinetic pressure (q) or Reynolds number. There is some evidence from flight tests on wings of combat aircraft with moderate sweep angles (say between 35° and 45°) that significant Reynolds number effects can persist even at fullscale, but it is difficult to separate these from the effects of static aeroelastic distortion.

The establishment of the shock and separation patterns in flight is an essential condition for any valid flight/tunnel comparison.

10.2 UNCERTAINTIES IN TUNNEL EXPERIMENTS

10.2.1 Influence of Tunnel Characteristics on Model Buffeting

A wind tunnel may influence model buffeting in at least two different ways.

(1) If the tunnel flow unsteadiness is high, buffet onset may be difficult to detect and the severity of buffeting may be altered (see Reference 10-1 and the brief discussion in Chapter 7).

(2) If the model is operating at a high lift coefficient at transonic speeds (say $C_L = 0.6$ at $M = 0.90$), shockwaves from the wing may intersect the walls of the working section. Manifestly, if this happens the tunnel corrections (to Mach number, lift coefficient and angle of attack) will become large and unpredictable. Even if the wing shock waves do not reach the walls, there may still be significant, unpredictable corrections. The tunnel constraint corrections may also be somewhat uncertain at low lift coefficients at transonic speeds, but at least they are then comparatively small.

10.2.2 Measurement of Buffeting

Wing-root strain gauges are widely used to measure buffeting on wind tunnel models. The most serious difficulties encountered concern the value of the total damping appropriate to the wing fundamental mode, which on a rigid model is generally quite small ($\gamma + g/2 = 1$ to 2% of critical) and predominately structural (see Figure 5 in Reference 10-2). The dampings are thus almost completely unrepresentative of the values which are appropriate in flight where they are generally much larger ($\gamma + g/2 = 6$ to 10% of critical) and predominately aerodynamic.

The structural damping on a rigid wind tunnel model may vary both with the static lift on the model ($qS\,C_L$) and with the amplitude of the wing motion (typified by the wing-tip acceleration). It is extremely difficult to separate these effects, either by tests with the wind on or by tests with the wind off.

10.2.3 Visualisation of Areas of Separated Flow

Generally wind tunnel tests provide adequate information about the areas of separated flows which excite buffeting on the model, as long as sufficient tunnel time can be made available.

The surface oil flow technique is most widely used and can be applied successfully both in continuous and intermittent facilities (Ref.10-3). From time to time tufts have been used on large models in low speed tests to permit a direct comparison with tuft motion in flight (Ref.10-4).

Pressure plotting on model wings, including the measurement of trailing-edge pressures, is also commonly used to supplement or replace visual observation of separated flows.

10.2.4 Transition Fixing and Reynolds Number Effects

One of the major uncertainties in any model buffeting test is probably the choice of the roughness band used to fix transition. On a two-dimensional aerofoil, if the roughness size is too small, then there may well be a laminar boundary layer/shockwave interaction completely different from what would occur at fullscale with a turbulent boundary layer/shockwave interaction. In contrast, if the roughness size is excessively large, the boundary layer will be excessively thick and the aerofoil lift curve slope will be reduced, even at zero lift. Similarly boundary layer separation will occur at a lower angle of attack than with the correct roughness height.

In buffeting tests on three-dimensional wings the situation is more difficult than on an aerofoil. On a wing the roughness band should be graded across the span, but usually a single roughness height is selected to cover a wide range of Mach number (say from $M = 0.6$ to 1.2) and angle of attack (say from $\alpha = -2^\circ$ to $+12^\circ$). This roughness band can really only be optimised at one point on the wing for a particular combination of unit Reynolds number, Mach number and angle of attack. For buffeting tests the best course is probably to select the optimum roughness size for a condition near buffet onset at the most important Mach number*. The effectiveness of the roughness should always be checked at this position. Of the methods available to detect transition, the most convincing, and easiest to apply, is perhaps the sublimation technique. Acenapthene, for example, is widely used for sublimation tests in continuous tunnels at transonic speeds. Reports of wind tunnel buffeting tests rarely quote this crucial information about the effectiveness of the roughness used, although it can profoundly influence the validity of a flight/tunnel comparison of buffeting.

Buffeting measurements obtained by varying the unit Reynolds number over a somewhat limited range (say from 80% to 120% of the original Reynolds number) may themselves help to indicate if the roughness band chosen is adequate. If the effect of a wider variation in Reynolds number is to be measured (say from 180% to 220% of the original) the roughness height should always be reduced to ensure that transition is not overfixed. Again, reports of wind tunnel tests in which Reynolds number was varied over a wide range rarely state if the roughness band was changed.

It should be noted that most of the published buffeting measurements refer to tests on wings with Type 'A' flow separation†, for which it is important to ensure that the boundary layer thickness upstream of the shock is as representative of fullscale as possible. On advanced wings with Type 'B' flow separation**, it is important to aim for representative boundary layer thicknesses both at the shock and the trailing-edge. Hence the selection of a roughness trip with a Type 'B' flow separation is crucial. Some wind tunnel tests with Type 'B' flow separations have been made without any roughness band (Ref.10-6). For this particular test the "peaky" pressure distribution at the nose at the design condition (M, α) created a small bubble which was laminar at separation but which reattached as a thin turbulent layer. This test technique may give a good representation of fullscale for the boundary layer thickness at the terminal shock and at the trailing-edge. Tests without a roughness band may sometimes aid the selection of an optimum roughness band even in a Type 'A' flow situation.

As an illustration of the difficulty of assessing the effects of different boundary layer thicknesses in tunnel/flight comparisons we may refer to a careful investigation of buffeting made on the McDonnell Douglas F-4 Aircraft (Ref.10-7).

Figure 10-1 (based on Figure 22 of Reference 10-7) shows the local pressure coefficient close to the trailing-edge plotted against the wing angle of attack for a Mach number of 0.80. The tunnel results are given at spanwise

* This roughness will usually be somewhat higher than that required at small angles of attack.

† Type 'A' flow separation (Ref.10-5) is a separation behind the terminal shock on a wing which extends downstream towards the trailing-edge as the angle of attack increases at constant Mach number. Scale effects should normally be comparatively small with Type 'A' flow separations.

** A Type 'B' flow separation (Ref.10-5) extends forward from the trailing-edge as the angle of attack increases; it may be associated with another separation and reattachment upstream on the wing. Scale effects may be large with Type 'B' flow separations.

stations of 80 and 90% b/2, the flight results are only available at the intermediate station at 86% b/2. At low angles of attack the tunnel measurements give about $C_p = +0.02$ whereas the flight measurements give $C_p = -0.04$. This difference indicates a relatively thicker boundary layer at the trailing-edge in the flight experiment than in the tunnel test! If the boundary layer in the flight tests really was thicker than in the tunnel tests, one tentative explanation might be a relatively poor surface finish in the leading-edge region on the test aircraft. But transition was fixed by a roughness band on the model! At high lift coefficients, above the buffet boundary, the rate of divergence of the trailing-edge pressure appears about 20 times more rapid in the tunnel experiment than in flight, which should indicate a more rapid growth in the flow separations. (Actually the variation in flight looks so small as to be suspect.) However, the premature onset of flow separations in the tunnel experiment is well attested by the large scale effect on the buffet boundaries already noted in Chapter 7 in the discussion on Figure 7-28.

Figure 10-2* shows the upper surface pressure distributions measured at $M = 0.90$ and $\alpha_w = 8°$ on the inner wing on a 1/10 scale model of the F-4 aircraft at two Reynolds numbers (3.8×10^6 and 7.6×10^6) and in flight (at a Reynolds number of 44×10^6). Considering first the pressures measured on the model, at the higher Reynolds number both of the shocks are appreciably further downstream, although the trailing-edge pressure is virtually unaltered. Hence we may regard this as a genuine scale effect within the wind tunnel experiment, even though the roughness band was unchanged. Comparing the model test result at $R = 7.6 \times 10^6$ and the flight data at $R = 44 \times 10^6$, we see again a further displacement downstream of the shock system in the flight experiment, consistent with a further genuine scale effect. However, the trailing-edge pressure on the inboard wing is apparently lower in the flight experiment than in the tunnel. This suggests that the boundary layer thickness is higher in flight, just as at the outboard station at $M = 0.80$ (Fig.10-7).

Whatever is the explanation of these anomalies, Figures 10-1 and 10-2 certainly emphasise the need for a critical assessment of the differences between tunnel and flight comparisons of buffeting.

10.2.5 Differences between Models and Aircraft

We have implied that the separation boundaries for a wing are closely related with the boundary layer thickness distribution. It follows that the model should represent any feature on the aircraft which can influence the boundary layer development. Unfortunately some of the features which influence the boundary layer on an aircraft are themselves of the same scale as the boundary layer. For example, the height of vortex generators on an aircraft might be only twice the local boundary layer thickness, δ, but scaling vortex generators correctly, even for a 1/10 scale model, poses serious questions. Even boundary layer fences, which are generally significantly higher than vortex generators (say from 5δ to 10δ), often do not control the separation development the same way on the model as on the aircraft. Thus to obtain a broadly similar separation development on a model of an early version of the Harrier aircraft, the boundary layer fence on the model had to be displaced inboard by about 3% relative to the position on the aircraft. This effect was most significant at moderate subsonic speeds, where the fences were controlling shock and/or vortex type separations close to the leading-edge.

There are a host of other details on an aircraft wing which are difficult to represent on model wings such as surface roughness, badly fitting inspection panels or doors, pitot-static tubes and aerials. In addition, gaps occur around the control surfaces on aircraft, and flow through these gaps will have a strong influence on the local boundary layer development, particularly near the trailing-edge. Again, it is most unusual for gaps to be represented on wind tunnel models. A further minor source of scatter may be the failure to repesent in a tunnel model the varying mass distribution caused by fuel usage.

Leading-edge slats and trailing-edge flaps are used to enhance the performance of combat aircraft. It is difficult to provide sufficient strength to represent these accurately on a model, and if they are represented inaccurately the boundary layer development will be altered. (The design of these surfaces for the model may well be severely constrained by the need to achieve static aeroelastic distortions comparable to those which occur on the aircraft.)

There is evidence from wind tunnel tests that alterations in tail setting generally have no significant influence on the buffeting of model wings. However, in flight, buffeting measurements are always made with the aircraft trimmed, and hence it is essential to present tunnel buffeting measurements either in terms of wing angle of attack or wing lift coefficient or of the trimmed lift coefficient. During the early project stages, wind tunnel wing buffeting tests are often made tail-off because the wing buffeting measurements may then be readily compared with the corresponding static force measurements. However, during the final project stages it may be advisable to make the wing buffeting measurements with the tailplane close to a trimmed manoeuvre condition.

10.3 DISCUSSION

Many uncertainties inherent in both flight and wind tunnel measurements of buffeting have been presented in this Chapter. Hence it is essential that differences between flight and tunnel predictions of buffeting should not be attributed directly to Reynolds number effects, without a critical evaluation of all the evidence.

* Figure 10-2 is based on data kindly provided by P.J.Butkewicz of the USAF Aeronautical Systems Division, Wright-Patterson Air Force Base, Ohio. More extensive information is given in Reference 10-8.

The ultimate criterion for any successful buffet prediction must be that the separation developments on the aircraft and the model should be identical. The chances of achieving this objective vary considerably with the aircraft planform. Referring to the planforms shown in Figure 7-4, for slender wings with sharp leading-edges the attainment of this objective can almost be guaranteed. Hence the Reynolds number effects are inherently small and a prediction rating of 1 is appropriate. With unswept wings significant Reynolds number effects must be expected, and a prediction rating of 10 is appropriate. With swept wings large Reynolds number effects must be expected, particularly at subsonic speeds, and a prediction rating of 100 is appropriate.

There are good grounds for expecting that reliable theoretical methods may be found in the future to predict buffet onset boundaries (see the Appendix to Section 7.1). These should give good estimates for the genuine Reynolds number effects on buffet onset. (The theoretical methods presently available, and cited in the Appendix to Section 7.1, all predict much larger Reynolds number effects than can be measured in wind tunnel tests.)

In contrast to the optimistic outlook with respect to the theoretical prediction of buffet onset, the outlook is pessimistic for the theoretical treatment of buffet severity. This is essentially because boundary layer theories are only valid up to the separation point. At moderate buffeting we may have, say, 50% of the wing surface flow separated, a condition not amenable to treatment by boundary layer theory. In addition, the wing trailing-edge pressure will generally have diverged (at least over part of the span) so that the circulation, and hence the potential flow, will be uncertain. It can never be legitimate to ignore the presence of this separated flow on the potential flow pressures.

A recent paper (Ref.10-9) presented a theoretical method to predict the fluctuating pressures at the foot of an oscillating shock at supersonic speeds. The method involves the perturbation of the mean inviscid pressure field by the small pressure fluctuations in the attacked turbulent boundary layer upstream of the shock. The method cannot predict the pressure fluctuations in the separation bubble downstream of the shock. It seems likely that the method would be difficult to apply at transonic speeds, where the shock wave oscillation would be influenced by tunnel flow unsteadiness and disturbances propagated upstream from the wake through the subsonic flow regions.

One recent semi-empirical attempt to predict the severity of buffeting is suggested in Reference 10-2. Methods of this kind may ultimately help in making rough estimates of the severity of buffeting on swept wings, and should be compared to measurements of unsteady wing-root strain on a wide range of configurations to check their reliability.

10.4 CONCLUSIONS

Some possible sources of discrepancies between flight and tunnel measurements of buffeting have been discussed. The single, most serious cause of discrepancies is probably the failure to represent on the model the development of flow separations on the actual aircraft.

The best way to improve future predictions is to test as large a model as possible (and representative of gaps, surface roughness, etc.) at as high a Reynolds number as possible, and then to insist on an extensive flight programme.

CHAPTER 11

INFLUENCE OF CONFIGURATION FACTORS ON BUFFETING*

by

H.Max

11.0 INTRODUCTION

This Chapter presents data regarding the effects on an aircraft's buffet boundaries and the buffet intensities as influenced by geometrical configuration parameters, Reynolds number, Mach number, external stores and supercritical wing layout. The geometrical parameters considered are the wing aspect ratio, taper ratio, sweep angle, relative maximum thickness of the wing root section, and relative maximum camber of the wing section. An extensive bibliography (References 11-1 through 11-72) is contained in the References Section of this report to indicate the scope of theoretical and experimental information available on this subject.

For studying the effects of individual parameters on the buffet behaviour and for obtaining a broad spectrum of validating results, not only are experimental data taken into consideration but also theoretical methods (References 11-1 and 11-2) are used to define "light buffet" boundaries. The theoretical methods are based on the assumption that there is a linear relationship between the buffeting intensity and the region of the separated air flow. The effects of geometrical configuration parameters were calculated, plotted and then corrected by experimental data if possible. The effects of external stores and supercritical wing layout are shown only by some examples since generalized data are not available. To indicate the relative usefulness of the configuration geometrical parameter data presented in the earlier sections of this Chapter, comparisons are made for nine different aircraft and these show good agreement between estimated and measured buffet boundaries.

Due to the different test techniques, data processing and analysis methods which are used to obtain buffet boundaries, experimental data cannot be generalized with great accuracy and consequently it is not possible to predict the buffet behaviour of an aircraft in the design stage as accurately as necessary. It is very difficult to isolate the influence of aircraft geometrical parameters by analysing measured buffet data obtained from wind tunnel or flight tests, because of the fact that, very often, the dispersions in the measurements are higher than the effects of the parameters being considered. Furthermore, a satisfactory statistical analysis of buffet boundaries is not possible due to the limited number of test results.

There are very few parametric studies (References 11-3 to 11-6), which give the effects of various parameters on the buffet behaviour of aircraft and these cover only a small part of the possible spectrum for the different parameters. Buffet boundaries measured in wind tunnels or in flight are normally established by the first deviation of a certain measurement (wing bending moment, normal acceleration, etc.) registered by the different instruments (see Chapters 5 and 8). Taking into account the sensitivity of the sensors and the structural and aerodynamic damping, measured "buffet-onset" is equivalent to "lift buffet", an intensity which can be calculated by the method of Reference 11-2 (see also Reference 11-7). Consequently for the information presented in this Chapter computed results were used to obtain the basic influences of various parameters on the buffet boundaries and then experimental results were used to correct the calculated plots, when necessary and possible.

In this Chapter the following notation is used:

c	wing chord	ζ_{25}	sweep angle at 25% of chord
t/c	relative maximum thickness of wing root section	Λ	aspect ratio
$C_{L_{LB_{Ref}}}$	lift coefficient for "light buffet" of the basic wing ($\Lambda = 4.0$; $\lambda = 0.5$; $Re = 1.5 \times 10^6$; f/c = 0)	$\Delta_f C_{L_{LB}}$	influence of manoeuvering flaps on buffet boundary
M	free stream Mach number	$C_{L_{LB}}$	lift coefficient for "light buffet"
λ	c_{tip}/c_{root} = taper ratio	f/c	relative maximum camber of wing section
		Re	Reynolds number

* Dipl.-Ing. H.J.Proksch, Dornier GmbH, was of great assistance in collecting and preparing data for this Chapter and in reviewing and commenting on the draft of the report.

$\Delta_1 C_{L_{LB}}(\lambda)$ influence of taper ratio on buffet boundary

$\Delta_2 C_{L_{LB}}(\Lambda)$ influence of aspect ratio on buffet boundary

$\Delta_3 C_{L_{LB}}(f/c)$ influence of camber on buffet boundary

$\Delta_4 C_{L_{LB}}(Re)$ influence of Reynolds number on buffet boundary

η_v leading-edge flap deflection

η_k trailing-edge flap deflection

11.1 INFLUENCE OF GEOMETRICAL CONFIGURATION PARAMETERS

11.1.1 Sweep and Thickness

The effect of wing thickness on buffet boundaries is shown in Figure 11-1 for two different wing sweep angles. The plots represent a large number of flight test results which were converted by a theoretical method to a Reynolds number of 1.5×10^6 (see References 11-1 and 11-2). The tendencies shown in Figure 11-1 are as follows:

The influence of wing thickness decreases with increasing sweep and decreasing Mach number.

Higher airfoil thicknesses as (t/c = 9% to 12%) have to be accompanied by increased wing sweep angles in order to achieve a buffet-free flight corridor.

For smaller airfoil thicknesses (t/c = 4% to 6%) the buffet boundaries tend to occur at lower lift coefficients with increasing wing sweep angles.

Figure 11-2 presents buffet boundaries plotted versus Mach number for various values of airfoil thickness and wing sweep. Calculated results (shown by dashed lines) were corrected using the experimental data shown in Figure 11-1. There is a remarkable difference between the calculated and corrected plots, especially in the higher Mach number region for the smaller airfoil thickness (t/c = 4%). For this parameter combination the limitation of the theoretical method was reached and the assumed linear relationship between the buffet intensity and the region of separated air flow was no longer valid. Flight test results for highly swept wing configurations are presented in Figure 11-3 and show the same tendencies as described above.

11.1.2 Taper Ratio

The effects of taper ratio on buffeting, due to the change in the effective angle of attack over a span, for different thickness ratios and Mach numbers are shown in Figure 11-4. The influence of different Reynolds numbers occurring across the span on buffet boundaries has been neglected. Compared to the inaccuracies of the measured data and the limitations of the theoretical method used to obtain these results, this influence would seem to be small. The main trends shown in Figure 11-4 are the following:

The influence of taper ratio on the "light buffet" boundaries is nearly independent of the airfoil thickness and has only a small dependency on Mach number.

Decreasing the taper ratio ($\lambda \rightarrow 0$) shifts the buffet boundaries to higher lift coefficients.

Test results of the influence of taper ratio on the buffet behaviour of aircraft seem to be very rare, and therefore no corrections to the theoretical data have been made.

11.1.3 Aspect Ratio

The theoretical method (References 11-1 and 11-2) used for the "light buffet" boundary calculations in this Chapter is only quasi-three dimensional, and special three dimensional air flow phenomena, such as the appearance of a forward and/or rearward shock, cannot be treated. Due to the fact that the relation of forward, rearward and outboard shocks is nearly independent of the wing span, it is only for small aspect ratios that the three dimensional air flow phenomena have their strongest effect. For these reasons the plots in Figure 11-5, showing the effect of aspect ratio on the lift coefficient for light buffet as a function of airfoil thickness and Mach number, tend to be less exact for smaller aspect ratios.

Experimental test data (from References 11-4 and 11-8 to 11-10) are compared with computed values in Figure 11-5(b), and it can be seen that even for higher aspect ratios only approximate effects of aspect ratio can be obtained from the computed results. It should be noted that due to the relatively high dispersion of the measured data, the small effect of aspect ratio on the lift coefficient for "lift buffet" was difficult to determine. In addition, the effect of aspect ratio on the buffet boundaries of wings is small even when computed using the theoretical curves. The influence of other parameters is much higher.

The tendencies shown in Figure 11-5 are as follows:

For lower Mach numbers ($M \approx 0.85$) the buffeting boundaries occur at higher lift coefficients for increasing aspect ratios.

For higher Mach numbers (M = 0.9 to 0.95) the contrary trend exists.

11.1.4 Camber

Theoretical results for the influence of camber on buffet boundaries of wings are not available, but estimations are possible using the method of Reference 11-2. In addition there are very limited experimental test data (References 11-4 to 11-6) which allow an analysis of the isolated camber effect. Therefore Figure 11-6 only shows, as an example, the effect of camber on the lift coefficient for "light buffet" for three different wings. The tendencies are as follows:

- The buffeting boundaries occur at higher lift coefficients with increasing camber.
- With increasing thickness the camber effect tends to be smaller.

11.2 INFLUENCE OF OTHER FACTORS

11.2.1 Reynolds Number

Since test results for the effect of Reynolds number on buffet boundaries are known from the literature, this influence has been calculated using a theoretical method (References 11-1 and 11-11). As an example the effect is shown in Figure 11-7 for one wing at three Mach numbers. The trends are as follows:

- The "light buffet" boundaries occur at higher lift coefficients with increasing Reynolds number.
- The influence of Reynolds number is stronger for higher Mach numbers (M = 0.9 and 0.95) than for a lower Mach number (M = 0.85).

11.2.2 Supercritical Wing Layout

The pressure distribution on conventional airfoils at higher Mach numbers leads to the formation of a strong shock wave which produces a strong positive pressure gradient at the airfoil surface. This may cause separation of the boundary layer and consequently a large increase in drag, severe airfoil buffeting, and stability and control problems. The special shape of supercritical airfoils prevents the termination of the supersonic flow in a strong shock wave and reduces the adverse pressure rise behind the shock wave, giving a positive effect on the buffet behaviour of wings. Therefore a supercritical wing layout will permit efficient flight at speeds up to Mach 1.0.

Careful integration of supercritical airfoils into aircraft configurations can delay the Mach number for buffet onset at a given lift coefficient and increase the maximum lift coefficient for buffet onset at a given Mach number. As an example, Figure 11-8 shows the buffet boundaries for the T-2C aircraft with conventional and supercritical wings. The supercritical wing improved the maneuvering g-margin as measured by the altitude increment between the design cruise altitude and the buffet boundary altitude, at constant Mach number. It also improved the low-speed cruise margin but slightly reduced the over-speed buffet margin as measured by the Mach number increment between the design cruise Mach number and the high-speed buffet boundary Mach number, at constant altitude.

11.2.3 External Stores

The author of this Chapter does not know of any statistical data showing the effect of external stores on buffet boundaries of aircraft. Due to flow field interference effects of external stores, their influence on buffet boundaries depends strongly on their size and their location on the aircraft. As a first approximation, based on wind tunnel and flight test results of a ground attack aircraft, it can be stated that the maximum buffet-free lift coefficient at a constant Mach number for an aircraft with pylon-mounted stores is decreased by about $\Delta C_{L_{B,0}} \approx 0.1$ to 0.2. Further work is needed before a more generalized statement can be made.

11.3 INFLUENCE OF AIRCRAFT PARAMETERS ON BUFFET INTENSITY

The "light buffet" boundary is one of the few boundaries, with respect to Mach number effects, which can be calculated and/or measured with high accuracy in the design stage of an aircraft and which can be reproduced in flights of the real aircraft. After the appearance of this first Mach number effect, other transonic phenomena may occur, as discussed in Chapter 1 of this report (for example, "wing rock", "nose wander", etc.). These normally establish the real active and/or passive maneuvering limits of the aircraft. In most practical cases the buffet intensity like "moderate" or "heavy", does not limit the maneuvering capability of the aircraft. Thus the following discussion of the influence of aircraft parameters on buffet intensity relates only to certain aspects of increased Mach number effects.

Wing sweep, thickness, camber and Mach number are the main parameters affecting buffet intensity. The influence of wing sweep on the increase in buffet intensity is shown in Figure 11-9 for a wing with an 8% thickness. For all Mach numbers shown, larger sweep angles reduce the rise in buffet intensity with increased lift coefficient. Thus with respect to buffet intensity, aircraft with higher swept wings have better buffeting characteristics.

The effect of thickness on buffet intensity is presented in Figure 11-10(a). For Mach numbers between 0.7

and 0.75 the slope of the curve of buffet intensity versus lift increases with increasing thickness. At higher Mach numbers the tendency is reversed. Figure 11-10(b) indicates the influence of camber on the increase of buffet intensity for NACA 65-series airfoils. At all Mach numbers higher camber decreases the slope of the buffet intensity versus lift curve.

Plots of buffet intensity versus increasing lift, at constant Mach numbers, show Mach number effects on buffet intensity as indicated in Figure 11-10(c). It can be seen that for lower Mach numbers buffeting will begin at higher lift values but the slope of the curve of buffet intensity versus lift is much steeper.

The effects of taper ratio, aspect ratio and Reynolds number on the increase in buffet intensity with lift seem to be small, as indicated by calculations and limited experimental test data (Ref.11-4).

11.4 ESTIMATION OF "LIGHT BUFFET" BOUNDARIES AND COMPARISON WITH EXPERIMENTAL DATA

The information presented earlier in this Chapter can be used to estimate the "light buffet" lift coefficient for a given wing at specific transonic Mach numbers and Reynolds numbers. The estimation method is based on the following equation:

$$C_{L_{LB}}(\xi, t/c, \lambda, \Lambda, f/c, M, Re) = C_{L_{LB_{Ref}}}(\xi, t/c, \lambda = 0.5, \Lambda = 4.0, f/c = 0, M, Re = 1.5 \times 10^6) + \\ + \Delta_1 C_{L_{LB}}(\lambda) + \Delta_2 C_{L_{LB}}(\Lambda) + \Delta_3 C_{L_{LB}}(f/c) + \Delta_4 C_{L_{LB}}(Re)$$

which can be written, in a more simplified form, as:

$$C_{L_{LB}} = C_{L_{LB_{Ref}}} + \Delta_1 + \Delta_2 + \Delta_3 + \Delta_4$$

where $C_{L_{LB_{Ref}}}$ is determined from Figure 11-2 and the Δ increments 1 to 4 are obtained from Figures 11-4 and 11-7.

Figure 11-11 presents "light buffet" lift coefficients for nine different wings calculated by this method and also shows corresponding experimental test results. The comparisons in these examples indicate the validity of the estimation techniques.

11.5 CONCLUSIONS

The information presented in this Chapter shows that it is absolutely necessary to promote further theoretical and experimental studies on buffeting. Due to the numerous geometric and aerodynamic parameters which influence the buffet boundaries, future work should be oriented so as to:

- Isolate more specifically the effects of the various parameters.
- Broaden the spectrum of the various parameters.
- Obtain a better understanding of the physical process of buffeting.

To reach these goals it is necessary:

- In the experimental field to perform systematic parameter studies in order to generalize test results more precisely.
- In the theoretical field to develop real three-dimensional methods for calculating transonic pressure distributions and boundary-layer behaviour.

With better theoretical and experimental information it should be possible not only to determine the "light buffet" boundary of an aircraft in the design stage more accurately, but also to ascertain the aircraft's behaviour beyond this boundary.

CHAPTER 12

IMPROVEMENT OF AIRCRAFT BUFFET CHARACTERISTICS

by

G.Bucciantini

12.0 INTRODUCTION

During the course of an aircraft design or from prototype flight testing some unexpected buffet problems may arise, or the buffet limits may appear appreciably lower than estimated. In this case the designer has to undertake prompt and proper provisions for aircraft modifications. It is worth remarking that, being a question of transonic problems, even very small changes may lead to significant aerodynamic effects.

Therefore, the task is extremely delicate and requires experience, accurate analysis of the phenomena, proper selection of the measures to be attempted and careful appraisal of all the consequent effects. A series of provisions which can be taken to improve the buffet characteristics are presented in this Chapter, and some practical application cases are described.

12.1 METHODS OF BUFFET ESTIMATION

For passenger-carrying transport airplanes the buffet limit corresponds to the start of buffet perception by the pilot, whilst for fighters buffet penetration is accepted. At present the buffet phenomena, originated by flow separation, cannot be treated through purely theoretical means due to their complexity; therefore, all the relevant investigations are based on wind tunnel measurements or flight tests.

From wind tunnel testing much information for buffet estimation can be obtained, like kinks in the aerodynamic coefficients, wing trailing edge static pressure divergence, wing or tail root bending moment fluctuations (Ref.12-1), unsteady pressure measurements (Ref.12-2), flow anomalies visualization, etc. From flight testing similar data are obtainable (References 12-2 to 12-5), besides the acceleration level at some significant points (e.g., pilot seat, c.g., wing and tail tips, etc.).

12.2 WING BUFFET

Some systematic wind tunnel tests focusing the influence, on the buffet limits, of wing geometry variations (sweep, aspect ratio, airfoil thickness and camber, etc.) have recently appeared in the literature (References 12-5 to 12-9) and can give to the designer, in the initial phase of the project, the trend of the buffet characteristics versus the wing main geometric parameters (see Chapter 11). This Chapter reports and describes, with some application cases, a series of possible changes to the wing design, without significant planform and section variations, which can improve, perhaps considerably, the buffet characteristics.

These provisions can be made, without major structural changes, in the advanced stage of the project development or during the flight tests, when the main lines of the aircraft configuration are frozen.

12.2.1 Maneuver Slats and Flaps

Papers have already appeared in the literature (References 12-7, 12-10 and 12-11) dealing with the improvement of the buffet limits from small deflections of slats (or nose flaps) or/and flaps, and some quantitative information are furnished. In Figures 12-1 to 12-5 some typical results are presented, which can give to the designer an indication of what can be achieved with these kinds of provisions.

In Figure 12-6 a carpet plot is presented, derived from wind tunnel tests on a variable sweep fighter model, which gives the order of magnitude to the buffet limit increment which can be achieved through properly designed maneuver devices. It has to be remarked that, especially for the maneuver slats, the design optimization is extremely delicate since shock induced separation in the ducts may deteriorate drastically the buffet characteristics and provoke divergence phenomena, like pitch-up, wing drop, etc.

In Figures 12-7 and 12-8 for two sweep angles an example is given on how small modifications to the slat duct can cause sensible gains in the buffet limits. In this case the change consisted of a fixed leading edge redesign with a reduction in the curvature variation at the slat duct exit where large negative pressure peaks caused shock-induced separations in transonic flow. The change was beneficial not only in raising the buffet limits but also in eliminating the premature pitch-up, the deterioration of the lateral characteristics and the drag penalty due to the above mentioned flow separation.

As far as variable camber is concerned (e.g., the wing of the Northrop P-530), its effect is treated in Chapter 11.

12.2.2 Strakes

A provision for increasing the usable lift, adopted in some recent projects having moderate wing sweep and aspect ratio (Northrop F-5E, P-530, General Dynamics YF-16, Lockheed F204 "Lancer", Mitsubishi XT-2, etc.), is a highly swept leading edge extension at the wing root, named a "strake". If properly designed, the strake generates a vortex, due to its highly swept and sharp leading edge, which magnifies the negative pressures and stabilizes the flow on the main wing upper surface, delaying the separation and therefore raising the buffet onset. The delay in buffet onset may be accompanied by a reduction in buffet intensity.

The influence of strakes on the buffet characteristics is indicated in Figures 12-9 to 12-11 for typical swept wing configurations.

12.2.3 Aerodynamic Fixing (Notch, Sawtooth, Fence, etc.)

The provision of simple aerodynamic fixes, usually taken to overcome the deterioration of the aerodynamic behaviour at high angles of attack, can also increase the buffet limits since the produced vortices delay the flow breakdown. Of course the location of these devices has to be selected at the origin of the flow separation.

Very little information has been published in the technical literature on the effects of these devices on the buffet characteristics, and it is highly desirable that systematic research be undertaken in this field.

In Reference 12-12 the effect of fences and sawteeth on the buffet limits of the Harrier is described.

12.2.4 Vortex Generators

Usually vortex generators are employed to eliminate flow separation, both at low speed (high angle of attack) and in transonic flow (shock induced separation). With these devices, problems like pitch-up, wing drop/rock, loss of control effectiveness, etc., are therefore treated. It has been ascertained that vortex generators also may have an important influence on the maximum usable lift dictated by post-buffet flight steadiness, as it is asserted in Reference 12-12 regarding the Harrier. In this case the vortex generators, combined with the remaining whole repertory of BLC devices (sawteeth and fences), were intentionally applied in the design stage to raise to the maximum the lifting capability of the wing without the weight penalty inherent in possible leading edge devices. The final configuration, optimized by systematic tests in a transonic wind tunnel on a 1/10 scale model (Ref.12-13), presents an extreme degree of sophistication with vortex generators of tapered form, graded incidences to the local surface velocity directions, "low drag scheme" etc.

In Figure 12-12 the case of the transonic fighter FIAT G91Y is shown where vortex generators have been applied on the wing to eliminate a light wing drop which occurred within a narrow Mach range at the upper end of its transonic flight regime. The provision proved successful, with consequent overall improvement, even for the maximum usable lift.

Figure 12-13 shows the influence of vortex generators on the buffet onset for the Grumman Gulfstream (Ref.12-14).

The extreme sensitivity of positioning (chordwise, spanwise, etc.) and geometry (corotating, counterrotating, spacing, dimensions and setting of the single elements, etc.) of vortex generators on the relevant aerodynamic effects is well known, (Ref.12-15), and careful attention is necessary if they are employed for buffet problems. There are not, however, systematic quantitative data available on the effect of vortex generators on the buffet characteristics of an aircraft, and proper research on this topic is needed.

12.2.5 Extrapolations from Wind Tunnel to Full Scale

The buffet limits derived from wind tunnel tests, once corrected for the interference of the model sting, for possible differences between the model geometry and the geometry of the aircraft, etc., have to be extrapolated to full scale by taking into account several effects, like Reynolds number, aeroelastic deformations, etc.

As far as Reynolds number is concerned, its favorable effect generally decreases with increasing Mach number in the transonic range. In Figures 12-14 and 12-15 the variations with Reynolds number of the buffet limits for

fighter configuration models, as measured in a pressurized wind tunnel according to the Mabey method (Ref.12-1), are presented. Good agreement (for buffet onset) between wind tunnel and flight test results is also mentioned in Reference 12-12.

In Figures 12-16 and 12-17, for two typical fighter configurations, the effects of wing aeroelastic deformations on buffet onset and penetration are presented.

12.3 TAILPLANE BUFFET

Tailplane buffet, more frequent for the horizontal tail, is provoked, as for wing buffet, by flow separation and its subsequent evolution. However, unlike wing buffet, the flow separation originates generally outside of the tailplane itself, e.g., from the wing wake, the afterbody, the cockpit, etc.

The actions to be taken in case of tailplane buffet must begin first in identifying and possibly removing the buffet sources outside the tailplane. If the problem is due to the wing wake, changes can be made on the wing by providing vortex generators, fences, etc., or on the tail by changing the vertical displacement, anhedral or dihedral, etc. If the separation is provoked by the fuselage shape, local fuselage contour changes can be made or changes can be applied on the tail by providing root strakes, vortex generators, profile variations, etc. An example of the use of vortex generators to cure a sort of tailplane buffet due to flow separation at the fuselage afterbody is that of the jet-fighter FIAT G-91 (Fig.12-18).

Another typical example of horizontal tail buffet, and of the successful solution of the problem, is the case of the FIAT G91Y fighter (Fig.12-19). In this case the buffet, associated with a deterioration of the lateral-directional characteristics, was occurring in the high transonic range and was ascertained to be caused by fuselage flow separation below and aft of the tailplane root. Proper transonic wind tunnel tests did provide an understanding of the phenomenon and allowed the necessary provisions to be taken.

In Figure 12-20 the separation area on the fuselage afterbody of the original configuration is shown, and in Figure 12-21 is shown the final modification which consisted of local area ruling associated with a boattail angle reduction and a small cut-out at the elevator root. In Figure 12-22 the maximum deviation from the mean value of the bending moment of the horizontal tail root is indicated, as measured in a wind tunnel, and in Figure 12-23 the corresponding in-flight measurements are shown from accelerometers on the stabilizer tips. As can be seen, the situation has been normalized and made similar to that of the G91T trainer.

Figure 12-24 shows the effect of the change on the directional stability, which appears completely restored. The modification brought beneficial effects also on the fuselage base pressures and on the aerodynamic drag, as can be seen in Figures 12-25 and 12-26, which indicate the strong intercorrelation of the aerodynamic phenomena having the same origin (flow separation, in this case).

12.4 CONCLUSIONS

Examples have been presented in this chapter which show that relatively conventional state-of-the-art means (such as maneuvering flaps, slats, vortex generators, etc.) can be applied to improve adverse flow qualities should buffeting or handling qualities problems arise on existing aircraft. Newer aircraft in the earlier design stages can have more advanced means to improve high lift characteristics, such as wing strakes, maneuvering canards and pre-programmed variable camber for transonic maneuvering. Of course these devices are more sophisticated and would have to be carefully integrated into the overall aircraft design and thoroughly tested in wind tunnels.

Proceeding one step further into the future, advanced aircraft may incorporate such concepts as variable camber, thin supercritical airfoils, boundary layer control, jet flaps, spanwise blowing, etc. as well as new aircraft configuration concepts. Such ideas would be incorporated into an aircraft design to improve the high lift potential of the aircraft and not as a means to improve buffet per se. However, applications of such devices would, most likely, strongly affect the buffet characteristics.

CONCLUSIONS AND RECOMMENDATIONS

CONCLUSIONS

Operating combat aircraft in the flight regime where transonic flow occurs, especially in high angle of attack flight, leads to Mach number effects which deteriorate the performance and the handling qualities of the aircraft. Varying degrees of buffet are encountered which affect the pilot only after reaching a certain intensity. The foregoing chapters which summarized the state of the art regarding the buffeting phenomena have provided an insight into numerous facets which necessarily must be taken into consideration in the overall transonic maneuvering problem. It is readily apparent that the aerodynamic-structural force/response interdependencies, when coupled with the man-machine interaction, result in a formidable total system problem. Yet in an aerial combat situation, the intense drive of the pilot to be the victor greatly overshadows the deteriorating aircraft aerodynamic characteristics and the aircraft will be flown to near the point of departure. Based on prior tracking experience, light to moderate levels of buffet do not necessarily substantially detract from the tracking task, and the maneuvering demands are maintained until serious handling qualities problems (severe wing rock, nose slice, tail buffet, etc.) restrict further maneuvering and provide the actual maneuvering limit. Nevertheless, buffet onset is one of the factors which must be considered in the design of an aircraft as it usually preceeds or is an indicator of an adverse flow separation leading to more serious handling qualities problems.

The ability analytically to predict buffet onset and intensity levels during the design stage and rigorously to predict their effects on maneuvering aircraft performance is currently unsatisfactory. However, buffet onset can be estimated and measured on wind tunnel models in the design phase of an aircraft: methods on how to do this and parameters which influence and improve the buffet behavior are discussed extensively in this report.

RECOMMENDATIONS

As implied by the development of this report, numerous technical disciplines must be subject to intensive applied research and where state of the art advances are obtained, they must further be examined to determine their applicability to the total maneuvering system problem. As a starting point, however, areas of work in each discipline must be started and maintained keeping in sight the end goal of developing practical, workable methodology. Areas in which work could be immediately pursued are discussed in the following paragraphs.

(1) Because of pilot opinion, supported by preliminary experimental evidence, that the effects of buffet (vibration) on the pilot's tracking performance may be of minor importance in the presence of sustained acceleration effects, a total system analysis is needed to determine the relative importance of the effects of buffet and loss of handling qualities on pilot and total aircraft system performance during maneuvering flight.

(2) Since buffeting and other transonic flow difficulties are induced by flow separation which is complicated by shock-boundary layer interactions and because precise evaluation is not currently possible, a continued effort to improve steady and unsteady three-dimensional viscous flow field and separation prediction methods is required.

(3) The Thomas method for predicting buffet onset should be improved through the incorporation of the most advanced inviscid and viscous aerodynamic prediction programs available. Predictions should be performed for a wide range of aircraft and compared with wind tunnel and flight test data to determine the ranges of applicability of the method.

(4) Due to the lack of satisfactory analytical methodology, the prediction of transonic flow difficulties relies on wind tunnel measurements. The improvement of measurement quality requires a better knowledge of perturbing effects (i.e., wall effects, noise and turbulence, sting support, etc.) and better simulation of flight Reynolds numbers. Wind tunnel testing should employ the best possible available techniques and new techniques, and should include flow visualization in addition to the standard measurements (forces, moments, pressures, etc.).

(5) Special emphasis should be put on the understanding of high speed stall progression. On new aircraft these investigations should include comparisons and correlations of theoretical predictions, wind tunnel model test results, and controlled flow separation on wind tunnel models.

(6) Buffet flight tests should be performed on the new advanced configurations now becoming operational. Where aircraft are multiseated, acceleration measurements should be made at all crew stations. Wind tunnel correlations with flight test results should be performed to understand better the relationships between the wing root bending moment and other buffet measurements, especially at the pilot station.

(7) Adequate structural response methods are currently available which predict response for known forcing functions. However, the random aerodynamic driving forces and structural response forces interact, and work should be pursued to identify this interaction, scaling effects, and the relationship between the separated flow and the oscillating aerodynamic forces.

(8) Development of future fighter systems which minimize adverse dynamic characteristics, particularly wing rock, will be enhanced by understanding the basic and interacting phenomena on existing and emerging fighters. The phenomena include aerodynamic flow fields, structural response, and coupling with stability and command control augmentation systems. Special attention should be given to interacting effects on advanced fighters configured with canards, special direct lift or sideforce controls, in-flight thrust vectoring, powered boundary layer control and other force producers intended to improve performance and maneuverability.

(9) Due to the numerous geometric and aerodynamic parameters influencing the buffet boundaries, future work should be performed to isolate the effects of the various parameters more clearly, to broaden the spectrum of the various parameters, and to give a better understanding of the physical process of buffeting. To reach this it is necessary to perform experimental systematic parameter studies in order to generalize test results more precisely.

REFERENCES

1-1	Fellers, W.E. Patierno, J.	*Fighter Requirements and Design for Superiority Over Threat Aircraft at Low Cost*, AIAA Paper No.70-516, 1970.
1-2	Herbst, W.B. Krogull, B.	*Design for Air Combat*, AIAA Paper No. 72-749, 1972.
1-3	Burris, W.R. Lawrence, J.T.	*Aerodynamic Design and Flight Test of US Navy Aircraft at High Angles of Attack*, AGARD-CP-102, November 1972.
1-4	Bore, C.L.	*Post-Stall Aerodynamics of the 'Harrier' GR1*, AGARD-CP-102, November 1972.
1-5	Jones, J.G.	*The Dynamic Analysis of Buffeting and Related Phenomena*, AGARD-CP-102, November 1972.
1-6	Hall, G.W.	*A Flight Test Investigation of Direct Side Force Control*, AFFDL-TR-71-106, September 1971.
2-1		*International Organization for Standardization, ISO/DIS 2631*, 28 April 1972.
2-2		*United States MIL-STD 1472A*, 15 May 1970.
2-3	Magid, E.B. Coermann, R.R. Ziegenruecker, G.H.	*Human Tolerance to Whole Body Sinusoidal Vibration*, Aerospace Medicine, 31: 915-924, November 1960.
2-4	von Gierke, H.E.	*Physiological and Performance Effects on the Aircrew During Low Altitude High Speed Flight Missions*, AMRL-TR-70-67, November 1971. Aerospace Medical Research Laboratory, Wright-Patterson AFB, Ohio.
2-5	Allen, G.R.	*Initial Proposals to ISO for Vibration Exposures below 1 Hz, with Some Modifications to DIS 2631 below 2 Hz*, April 1973. Unpublished proposal to ISO/TC 108.
2-6	Schoenberger, R.W.	*Human Performance as a Function of Direction and Frequency of Whole-Body Vibration*, AMRL TR-70-7, October 1970. Aerospace Medical Research Laboratory, Wright-Patterson AFB, Ohio.
2-7	Guignard, J.C.	*AGARDograph No.151*, Chapter 6, pp.46-66, November 1972, Advisory Group for Aerospace Research and Development.
2-8		*Ten Years of Human Vibration Research*, Human Factors Technical Report D3-7888, The Boeing Company, Wichita, Kansas, August 1969.
2-9	Titiriga, A., Jr	*F-5A Transonic Buffet Flight Test*, AFFDL-TR-69-110, Wright-Patterson AFB, Ohio.
2-10	Eney, John A.	*Buffet in Air Combat Maneuvering, Problem Definition*, NAIC AM-7040, 23 September 1970. Department of the Navy, Naval Air Development Center, Johnsville, Warminster, Pa., USA.
2-11	Lovesy, E.J.	*Some Effects of Dual-Axis Heave and Sway Vibration upon Compensatory Tracking*, Royal Aircraft Establishment Technical Memorandum EP 484, July 1971.
2-12	Lovesy, E.J.	*An Investigation into the Effects of Dual Axis Vibration, Restraining Harness, Visual Feedback, and Control Force on a Manual Positioning Task*, Royal Aircraft Establishment Technical Report 71213, November 1971.

2-13	Dupuis, H. Hortund, E. Louda, L.	*Random Vibrations of a Limited Frequency Range Compared with Sinusoidal Vibrations with Regard to its Effect on Man*, SAM-TT-G-1155-0373, Brooks AFB, Texas. Source: "Ergonomics", 1972, Vol.15, No.3,237 265 (German).
2-14	Rustenburg, John W.	*Development of Tracking Error Frequency Response Functions and Aircraft Ride Quality Design Criteria for Vertical and Lateral Vibration*, Aeronautical Systems Division TR-70-18, January 1971, Wright-Patterson AFB, Ohio.
2-15	Shoenberger, R.W.	*Human Response to Whole-Body Vibration*, Perceptual and Motor Skills, Monograph Supplement 1-V34, 1972.
2-16	von Gierke, H.E. Clarke, N.P.	*Effects of Vibration and Buffeting on Man*, Chapter 10, Aerospace Medicine, editor Randel, H.W., 2nd editor, Williams and Wilkins, 1971.
2-17	Lange, K.O. Coermann, R.R.	*Visual Acuity Under Vibration*, Human Factors, pp.291-300, October 1962.
2-18	O'Briant, C.R. Ohlbaum, M.K.	*Visual Acuity Decrements Associated with Whole Body ±1 Gz Vibration Stress*, Aerospace Medicine, 41 : 1; 79-82, January 1970.
2-19	McRuer, D. et al.	*Human Pilot Dynamics in Compensatory Systems*, Air Force Flight Dynamics Laboratory Report No. AFFDL-TR-65-15, July 1965.
2-20	Kleinman, D.L. et al.	*A Control Theoretic Approach to Manned-Vehicle Systems Analysis*, IEEE Trans. on Auto. Cont., Vol. AC-16, pp.824-832, 1971.
2-21	Phatak, A.V. Mehra, R.K. Day, C.N.	*Identification of the Optimal Control Model for the Human Operator*, Ninth Annual Conference on Manual Control, 23-25 May 1973, MIT.
2-22	Phatak, A.V. Mehra, R.K. Day, C.N.	*Application of System Identification to Modeling Human Controller under Stress Conditions*, to be published in the IEEE Automatic Control Special Issue on System Identification, December 1974.
2-23	Allen, W.R. Jex, H.R. Magdaleno, R.E.	*Vibration Effects on Manual Control Performance*, Paper No.122 presented to 8th Annual NASA – University Conference on Manual Control, Ann Arbor, Michigan, May 1972. (Systems Technology, Inc., Hawthorne, California.)
2-24	Allen, W.R. Jex, H.R. Magdaleno, R.E.	*Manual Control Performance and Dynamic Response During Sinusoidal Vibration*, Aerospace Medical Research Laboratory TR 73-78, Wright-Patterson AFB, Ohio.
2-25	Howard, P. Gillies, J.A.	A Textbook of A. ation Physiology, Chapter 23, Pergamon Press, London, 1965.
2-26	Rogers, D.B.	*Effect of Modified Seat Angle on Air to Air Weapon System Performance under High Acceleration*, Aerospace Medical Research Laboratory, TR-73-5, July 1973, Wright-Patterson AFB, Ohio.
2-27	Christy, R.L.	*Effects of Radial, Angular, and Transverse Acceleration*, Chapter 9 in Randel, Aerospace Medicine, Williams and Wilkins, Baltimore, 1971.
2-28	Piranian, A.G.	*The Effect of the Individual and Combined Stresses of Vibration and Sustained G on Pilot Performance*, Unpublished report, to be presented to AGARD, Aerospace Medicine Panel, April 1974, US Naval Air Development Center, Warminster, Pa.
2-29	Dolkas, C.B. Stewart, J.D.	*Effect of Combined Linear and Oscillatory Acceleration on Pilot Attitude Control Capabilities*, NASA TN D-2710, March 1965, Ames Research Center, Moffett Field, Ca.
2-30	Cole, John	Personal Communication, data in preparation, Aerospace Medical Research Laboratory, Biodynamic Environment Branch.
2-31	–	USAF Regulation 161 35, *Hazardous Noise Exposure*, 27 July 1973.

2-32	Sommer, Henry, C. Harris, S.C.	*Combined Effects of Noise and Vibration on Human Tracking Performances and Response Time*, Aerospace Medicine, 44 : 3, 276-280, March 1973.
2-33	Grether, W.F. et al.	*Effects of Combined Heat, Noise, and Vibration Stress on Human Performance and Physiological Functions*, Aerospace Medicine, 42:10, 1092-1097, October 1971.
2-34	Bernotat, R.K. Wanner, J.	*Pilot Workload*, in AGARD CP-106, *Handling Qualities Criteria*, June 1972.
2-35	Sinnett, J.M. Asiala, C.F.	*Advanced Fighter Concepts Incorporating High Acceleration Cockpits, Volume IV Pilot Performance Analyses*, AMRL TR 72-116, July 1973, Wright-Patterson AFB, Ohio.
2-36	Van Cott, H.P. Kinkade, R.G. editors	Human Engineering Guide to Equipment Design, 1972.
2-37	Radke, A.O.	*The Application of Human Engineering Data to Vehicular Seat Design*, Bostrom Research Laboratories Report No.117, October 1956.
2-38	von Gierke, H.E. Carmichael, J.B., Jr	*Biodynamic Applications Regarding Isolation of Humans From Shock and Vibration*, presented at ASME Colloquium on *Isolation of Mechanical Vibrations, Impact and Noise*, Cincinnati, Ohio, September 1973.
2-39	Calcaterra, P.C. Schubert, D.W.	*Research on Active Vibration Isolation Techniques for Aircraft Pilot Protection*, AMRL-TR-67-138, October 1967, Wright-Patterson AFB, Ohio.
2-40	Swisher, G.H.	*A Review of Human Operator Models with Application to Tracking under Environmental Stress*, Aerospace Medical Research Laboratory TR-72-48, February 1973, Wright-Patterson AFB, Ohio.
2-41	McRuer, D.T. Krendel, E.S.	AGARDograph No.188, *Mathematical Models of Human Pilot Behavior*, Advisory Group for Aerospace Research and Development, Brussels, 1974.
3-1	Gentry, A.E. Oliver, W.R.	*Investigation of Aerodynamic Analysis Problems in Transonic Maneuvering*, Douglas Aircraft Co, Rpt MDC J 5264-01, Vol.I, September 1971.
3-2	Delery, J. Laval, P. Chattot, J.J.	*Etude Expérimentale et Théorique de l'Ecoulement Transsonique Autour d'un Demi-Profil*; 10ème Colloque d'Aérodynamique Appliquée de la AAAF; Nov. 1973 (to be published in the *Recherche Aéronautique* Journal).
3-3	Pearcey, H.H.	*The Aerodynamic Design of Section Shapes for Swept Wings. Advances in Aeronautical Sciences*, Vol.3; Proceedings of the second International Congress in Aeronautical Sciences, 1962.
3-4	Vincent de Paul, M.	*Experimental Research on Supercritical Wings Profiles*; AGARD CP 35 Transonic Aerodynamics, September 1968.
3-5	Nieuwland, G.Y. Spee, B.M.	*Transonic Shock Free Flow, Fact or Fiction?* AGARD CP 35 Transonic Aerodynamics, September 1968.
3-6	Rogers, E.W.E. Hall, I.M.	*An Introduction to the Flow about Plane Swept-Back Wings at Transonic Speeds*, Journal of the Royal Aeronautical Society, Vol.64, August 1960.
3-7	Moss, G.F.	*Some Notes on the Aerodynamic Problems Associated with the Phenomenon of Buffeting*. Tech. memo aero 1293, February 1971.
3-8	Vanino, R. Wedemeyer, E.	*Wing Tunnel Investigations of Buffet Loads on Four Airplane Models*. AGARD CP 83, April 1971.
3-9	Monnerie, B. Charpin, F.	*Essais de Buffeting d'une Aile en Flèche en Transsonique*. 10ème Colloque d'Aérodynamique Appliquée de la AAAF; Nov. 1973 (to be published in the *Aérodynamique et Astronautique* Journal).
3-10	Magnus, R. Yoshirara, H.	*Steady Inviscid Transonic Flows over Planar Airfoils. A Search for a Simplified Procedure*, NASA C.R. No.186, 1972.

3-11	MacCormack, R.W. Paullay, A.J.	*Computational Efficiency Achieved by Time Splitting of Finite Difference Operators;* AIAA Paper 72-154, 1972.
3-12	Murman, E.M. Cole, J.D.	*Calculation of Plane Steady Transonic Flows.* AIAA J., Vol.9, No.1, January 1971.
3-13	Murman, E.M. Krupp, J.A.	*Solution of the Transonic Potential Equation Using a Mixed Finite Difference System.* Proc. Sec. Int. Conf. Num. Meth. in Fluids Dynamics, Lecture Notes in Phys, Vol.8, Springer Verlag, 1971.
3-14	Krupp, J.A.	*The Numerical Calculation of Plane Steady Transonic Flows Past Thin Lifting Airfoils.* Rep. D 130-12958-1, Boeing Sci. Res. Lab. Boeing Co, June 1971.
3-15	Krupp, J.A. Murman, E.M.	*The Numerical Calculation of Steady Transonic Flows Past Thin Lifting Airfoils and Slender Bodies.* AIAA Paper, No. 71-566, June 1971.
3-16	Garabedian, P. Korn, D.	*Analysis of Transonic Airfoils.* Com. Pure and Appl., Vol.XXIV, pp.841-51, 1971.
3-17	Bauer, F. Garabedian, P. Korn, D.	*Supercritical Wing Sections,* Lecture Notes in Economics and Math. Systems, 66, Springer-Verlag, 1972.
3-18	Jameson, A.	*Transonic Flow Calculations for Airfoils and Bodies of Revolution.* GRUMMAN Report 390, 71-1, 1971.
3-19	Murman, E.M.	*Analysis of Embedded Shock Waves Calculated by Relaxation Methods.* – AIAA Computational Fluid Dynamics Conference, Palm Springs, Cal., 1973. – AIAA Journal, Vol.12, No.5, May 1974.
3-20	Bailey, F.R. Steger, J.L.	*Relaxation Techniques for the Three-Dimensional Transonic Flow about Wings.* AIAA Paper 72-189, January 1972.
3-21	Isom, M.P. Caradonna, F.X.	*Subsonic and Transonic Potential Flow over Helicopter Rotor Blades.* AIAA Paper 72-39, June 1972.
3-22	Ballhaus, W.F. Bailey, F.R.	*Numerical Calculation of Transonic Flow about Swept Wings.* AIAA Paper 72-677, 1972.
3-23	Rohlfs, S. Vanino, R.	*A Steady Relaxation Method for Two and Three-Dimensional Transonic Flows.* EUROMECH 40, September 1973.
3-24	Albone, C.M.	*A Method for Computing Transonic Flow about Lifting Swept Wings.* Communication to EUROMECH 40, September 1973.
3-25	Lomax, H. Bailey, F.R. Ballhaus, W.F.	*On the Numerical Simulation of Three-Dimensional Transonic Flow with Applica- to the C-141 Wing.* NASA TND-6933, 1973.
3-26	Murman, E.M.	*Computational Methods for Inviscid Transonic Flows with Embedded Shock Waves. Numerical Methods in Fluid Dynamics.* AGARD Lecture Series No, No.48, 1972.
3-27	Yoshimara, H.	*A Survey of Computational Methods for 2D and 3D Transonic Flows with Shocks. Advances in Numerical Fluid Dynamics.* AGARD Lecture Series No.64, 1973.
3-28	Taylor, T.D.	*Numerical Methods for Predicting Subsonic, Transonic and Supersonic Flow.* AGARDograph No.187, 1974.
3-29	Thomas, F. Redeker, G.	*A Method for Calculation the Transonic Buffet Boundary Including the Influence of Reynolds Number.* AGARD Conference Proceedings No.83, 1971.
3-30	Klineberg, J.M. Steger, J.L.	*Calculation of Separated Flows at Subsonic and Transonic Speeds.* Proceedings of the third international conference on numerical methods in fluid mechanics. Springer-Verlag, 1972.
4-1	Jones, J.G.	*A Survey of the Dynamic Analysis of Buffeting and Related Phenomena.* RAE Techn. Rep. 72197, 1973.

4-2	Mitchell, C.G.B.	*Calculation of the Buffeting on a Slender Wing Aircraft at Low Speed.* RAE Techn. Rep. 68165, 1968.
4-3	Bisplinghoff, R.L. Ashley, H.	*Principles of Aeroelasticity.* J.Wiley, New York, 1962.
4-4	Försching, H.	*Dynamic Aeroelastic Calculations of Aircraft Based on Ground Vibration Test Data.* Progr. in Aerosp. Sci., Vol.11. Pergamon Press, Oxford, 1970.
4-5	Fung, Y.C.	*The Theory of Aeroelasticity.* J.Wiley, New York, 1955.
4-6	Mazet, R. (Gen. Editor)	*Manual on Aeroelasticity.* Vol.III. AGARD Publication, London, 1968.
4-7	Bendat, J.S. Piersol, A.G.	*Measurement and Analysis of Random Data.* John Wiley & Sons, Inc., New York, 1971.
4-8	Mabey, D.G.	*Beyond the Buffet Boundary.* Aeron. J., Vol.77, pp.201-215, April 1973.
4-9	Moss, G.F.	*Some Notes on the Aerodynamic Problems Associated with the Phenomenon of Buffeting.* RAE Techn. Memo Aero 1293, 1971.
4-10	John, H.	*Buffeting – Critical Review of Methods to Predict the Buffet Penetration Capability of Aircraft.* MBB UFE 1091 (Ö), March 1974.
4-11	Hwang, Ch. Pi, W.S.	*Transonic Buffet Behaviour of Northrop F-5A Aircraft.* Paper presented at the 38th AGARD Structures and Materials Panel Meeting, April 1974.
4-12	Seal, Diana M.	*A Survey of Buffeting Loads.* ARC, CP No.584, 1962.
4-13	Anon.	*Buffeting During Atmospheric Ascent – NASA Space Vehicle Design Criteria (Structures).* NASA SP-8001 (Revised) 1970.
4-14	Liepmann, H.W.	*On the Application of Statistical Concepts to the Buffeting Problem.* Jour. Aero. Sci., Vol.19, No.12, pp.793-800, 822, December 1952.
4-15	Thomas, F. Redeker, G.	*A Method for Calculating the Transonic Buffet Boundary Including the Influence of Reynolds Number.* In AGARD Conference Proceedings No.83 – *Facilities and Techniques for Aerodynamic Testing at Transonic Speeds and High Reynolds Numbers*, 1971.
4-16	Bies, David Alan	*A Review of Flight and Wind Tunnel Measurements of Boundary Layer Pressure Fluctuations and Induced Structural Response.* NASA CR-626, 1966.
4-17	Coe, Charles F. Keskey, Arthur J.	*The Effects of Nose Cone Angle and Nose Cone Bluntness on the Pressure Fluctuation Measured on Cylindrical Bodies at Transonic Speeds.* NASA TM X-779, 1963.
4-18	Stahl, W. Hartmann, K. Schneider, W.	*Force and Pressure Measurements on a Slender Delta Wing at Transonic Speeds and Varying Reynolds Numbers* in AGARD Conference Proceedings No.83, April 1971.
4-19	Lemley, C.E. Mullans, R.E.	*Buffeting Pressures on a Swept Wing in Transonic Flight-Comparison of Model and Full Scale Measurements.* AIAA Paper No. 73-311, AIAA Dynamics Specialists Conf., Williamsburg, Va., March 19 – 20, 1973.
4-20	Rose, R. Nicholas, O.P.	*Flight and Tunnel Measurements of Pressure Fluctuations on the Upper Surface of the Wing of a Venom Aircraft with a Sharpened Leading Edge.* Brit. ARC CP No.1032 – 69.
4-21	Krishnamoorthy, V.	*Measurements of Pressure Fluctuations on the Surface of a Delta Wing.* ARC CP No.767, 1965.
4-22	Ericsson, Lars E.	*Dynamic Effects of Shock-Induced Flow Separation.* AIAA Paper No.73-308, AIAA Dynamics Specialists Conf., Williamsburg, Va., March 19 – 20, 1973.
4-23	Rainey, A. Gerald	*Measurement of Aerodynamic Forces for Various Mean Angles of Attack on an Airfoil Oscillating in Pitch and on Damping in the Stall.* NACA TR 1035, 1957.

4-24	Huston, Wilber B. Rainey, A. Gerald Baker, Thomas F.	*A Study of the Correlation Between Flight and Wing-Tunnel Buffeting Loads.* NACA RM L55E16b, 1955.
4-25	Rainey, A. Gerald Byrdsong, Thomas A.	*An Examination of Methods of Buffeting Analysis Based on Experiments with Wings of Varying Stiffness.* NASA TN D-3, 1959.
4-26	Hanson, Perry W. Doggett, Robert V., Jr	*Aerodynamic Damping and Buffet Response of an Aeroelastic Model of the Saturn I Block II Launch Vehicle.* NASA TN D-2713, 1965.
4-27	Davis, Don D. Wornom, Dewey E.	*Buffet Tests of an Attack-Airplane Model with Emphasis on Analysis of Data from Wind-Tunnel Tests.* NACA RM L57H13, 1958.
4-28	Mabey, D.G.	*Measurements of Wing Buffeting on a Scimitar Model.* ARC CP No.954, 1967.
4-29	Mabey, D.G.	*Comparison of Seven Wing Buffet Boundaries Measured in Wind Tunnels and in Flight.* CP No.840, Brit. ARC, 1966.
4-30	Hanson, Perry W. Doggett, Robert V., Jr	*Wind-Tunnel Measurements of Aerodynamic Damping Derivatives of a Launch Vehicle Vibrating in Free-Free Bending Modes at Mach Numbers from 0.70 to 2.87 and Comparisons with Theory.* NASA TN D-1391, 1962.
4-31	Bratt, J.B.	*Wind Tunnel Techniques for the Measurement of Oscillatory Derivatives.* Manual of Aeroelasticity, Part IV, Chapter 5, AGARD, 1961.
4-32	Keller, Anton C.	*Vector Component Techniques: A Modern Way to Measure Modes.* Sound and Vibration, Vol.3, No.3, pp.18-26, March 1969.
4-33	Cole, Henry A., Jr	*On-Line Failure Detection and Damping Measurement of Aerospace Structures by Random Decrement Signatures.* NASA CR-2205, 1973.
4-34	de Vries, G.	*Sondage des Systèmes Vibrants par Masses Additionelles.* Recherche Aéronautique, No.30, 1952.
4-35	Bisplinghoff, R.L. Ashley, Holt Halfman, Robert L.	*Aeroelasticity.* Addison-Wesley Pub. Co.
4-36	Scruton, C. Lambourne, N.C.	*Similarity Requirements for Flutter Model Testing.* Manual of Aeroelasticity, Part IV, Chapter 6, AGARD, 1960.
4-37	Calligeros, John M. Dugundji, John	*Similarity Laws Required for Experimental Aerothermoelastic Studies.* Massachusetts Institute of Technology TR 75-1, 1959.
4-38	Molyneaux, W.G.	*Scale Models for Thermo-Aeroelastic Research.* Brit. ARC CP 579.
4-39	Hanson, Perry W.	*Evaluation of an Aeroelastic Model Technique for Predicting Airplane Buffet Loads.* NASA TN D-7066, 1973.
4-40	Anon.	*Facilities and Techniques for Aerodynamic Testing at Transonic Speeds and High Reynolds Number.* AGARD Proceedings No.83, Fluid Dynamics Panel Specialists' Meeting, Göttingen, Germany, 26–28 April, 1971.
4-41	Chapman, D.R.	*Some Possibilities of Using Gas Mixtures Other than Air in Aerodynamic Research.* NACA TR 1259, 1956.
4-42	von Doenhoff, A.E. Braslow, A.L. Schwartzberg, M.A.	*Studies of the Use of Freon-12 as a Wind-Tunnel Testing Medium*, NACA TN 3000, 1953.
4-43	Doggett, Robert V., Jr Hanson, Perry W.	*An Aeroelastic Model Approach for Prediction of Buffet Bending Loads on Launch Vehicles.* NASA TN D-2022, 1963.
4-44	Friend, Edward L. Monaghan, Richard C.	*Flight Measurements of Buffet Characteristics of the F-111A Variable-Sweep Airplane*, NASA TMX-1876, 1969.

4-45	Pearcey, H.H.	*A Method for the Prediction of the Onset of Buffeting and Other Separation Effects from Wind Tunnel Tests on Rigid Models.* AGARD Rep. 223, 1958.
4-46	Mabey, D.G.	*An Hypothesis for the Prediction of Flight Penetration of Wing Buffeting from Dynamic Tests on Wind Tunnel Models* CP No.1171, Brit. ARC, 1971.
4-47	Davis, Don D., Jr Huston Wilber B.	*The Use of Wind Tunnels to Predict Flight Buffet Loads.* NACA RM L57D25, 1957.
4-48	Mullans, R.E. Lemley, C.E.	*Buffet Dynamic Loads During Transonic Maneuvers.* AFFDL-TR-72-46, 1972.
4-49	Hwang, C. Pi, W.S.	*Investigation of Northrop F-5A Wing Buffet Intensity in Transonic Flight*, NASA Contractors Report, April 1974.
4-50	Otnes, R.K. Enochson, L.	*Digital Time Series Analysis*, Wiley-Interscience, Inc., New York, 1972.
4-51	Etkin, B.	*Dynamics of Flight*, John Wiley & Sons, Inc., New York, 1959.
5-1	Rold, A.	*Development of the Saab-Scania Viggen*, Canadian Aeronautics and Space Journal, June 1972.
5-2	–	*Aerodynamic Stability and Control Characteristics Interim Report*, Rpt No. MDC A1571, 1 March 1972.
5-3	Goodson, K.W.	*Wind Tunnel Investigation at High Subsonic Speeds of the Effects on Static Stability Characteristics of Various Modifications to a Swept-Wing Fighter-Type Airplane Model*, NACA RM L57A31, Langley Aero Laboratory, April 1957.
5-4	McAllister, J.D. et al.	*Wing Roll Control Devices for Transonic High Lift Conditions*, AFFDL-TR-69-124, General Dynamics/Ft Worth, January 1970.
5-5	Ray, E.J. Hollingsworth, E.G.	*Subsonic Characteristics of a Twin-Jet Swept-Wing Fighter Model with Maneuvering Devices*, NASA TN-D-6921, NASA Langley Research Center, January 1973.
5-6	Pinsker, W.J.G.	*The Theory and Practice of Inertia Cross Coupling*, Aeronautical Journal of the RAE, Bedford, England, August 1969.
5-7	Jackson, V.R.	*Control System Design for Maximum Effectiveness*, AIAA Paper #70-342, General Electric, Binghamton, New York.
5-8	Pinsker, W.J.G.	*Charts of Peak Amplitudes in Incidence and Sideslip in Rolling Maneuvers due to Inertia Cross Coupling*, RAE Report No. Aero. 2604.
5-9	Gentry, A. Oliver, W.	*Investigation of Aerodynamic Analysis Problems in Transonic Maneuvering*, McDonnell-Douglas Report MDC-J5264-01, September 1971.
5-10	–	Private Communication: Mr D.B.Benepe, General Dynamics, Ft Worth Division, to Mr W.B.Williams, AFFDL/FGC, March 1974.
5-11	Weissman, R.	*Preliminary Criteria for Predicting Departure Characteristics/Spin Susceptibility of Fighter-Type Aircraft*, AIAA Paper #72-984, USAF/ASD, September 1972.
5-12	–	*Military Specification, Flying Qualities of Piloted Airplanes*, MIL-F-8785B (ASG), 7 August 1969.
5-13	Malcom, L.G. Tobie, H.N.	*New Short Period Handling Quality Criteria for Fighter Aircraft*, The Boeing Company Report D6-17841 T/N, October 1965.
5-14	Neal, T.P. Smith, R.E.	*An In-Flight Investigation to Develop Control System Design Criteria for Fighter Airplanes*, AFFDL-TR-70-74, December 1970.
5-15	Rubertus, D.P.	*Tactical Weapon Delivery (TWeaD) Flight Control System*, Presented at the 1972 Avionics Section Meeting, American Ordnance Section, AFFDL, November 1972.

5-16	Kisslinger, R.L. Wendl, M.J.	*Survivable Flight Control System Interim Report No.1, Studies Analysis and Approach (Supplement for Control Criteria Studies)*, AFFDL-TR-71-20, Supp 1, May 1971.
5-17	Chalk, C.R. et al.	*Revisions to MIL-F-8785B (ASG), Proposed by Cornell Aeronautical Laboratory Under Contract F33615-71-C-1254*, AFFDL-TR-72-41, April 1973.
5-18	Quinlivan, R.P.	*Multimode Flight Control Definition Study for Precision Weapon Delivery*, AFFDL-TR-71-39, June 1971.
5-19	Quinlivan, R.P.	*Multimode Flight Control Definition Study*, AFFDL-TR-72-55, May 1972.
5-20	Quinlivan, R.P. Tye, G.	*Multimode Control for Air-to-Air and Air-to-Ground Gunnery*, Presented at Sixteenth Symposium of Guidance & Control Panel of AGARD, June 1973.
5-21	–	*An In-Flight Investigation of the Influence of Flying Qualities on Precision Weapons Delivery*, Presented at the Sixteenth Symposium of the Guidance & Control Panel of AGARD, June 1973.
5-22	Jackson, V.R.	*Control System Design for Maximum Effectiveness*, AIAA Paper No.70-342, March 1970.
5-23	Stapleford, R.L. et al.	*Outsmarting MIL-F-8785 (ASG)*, STI-TR-190-1, System Technology Inc., August 1971.
5-24	Ashkenas, I.L. Jex, H.R. McRuer, D.T.	*Pilot-Induced Oscillations: Their Cause and Analysis*, STI-TR-239-2, System Technology, Inc., June 1964.
5-25	Hall, G.W.	*In-Flight Investigation of Longitudinal Short Period Handling Characteristics of Wheel-Controlled Airplanes*, AFFDL-TR-68-91, August 1968.
5-26	Boothe, E.M. Chen, R.I.N. Chalk, C.R.	*A Two Phase Investigation of Longitudinal Flying Qualities for Fighters*, AFFDL-TR-74-9, March 1974.
5-27	–	*Vought Air Combat Technology Series, Flying Qualities Analysis, Vol.8, The Effects of Lateral Control Sensitivity and Roll Time Constant Upon Air Gunnery*, Rpt # 2-53362/3R-50903, July 1973.
5-28	–	*Flight Control/Fire Control to Achieve Effective Air/Air Gunnery without Range or Angle Trackers*, General Electric ACS 10,406.
5-29	Bailey, D.G. Mobarg, Milton	*A Simplified Criterion for Optimization and Evaluation of Combat Aircraft Lateral Aiming Performance*, Honeywell Document T-413, September 1971.
5-30	Finck, R.D.	*USAF Stability and Control Datcom*, 1960, revised 1972.
5-31	Thomas, H.H.B.M.	*State-of-the-Art of Estimation of Derivatives*, AGARD Report # 339, 1961.
5-32	Anderson, R.O.	*A New Approach to the Specification and Evaluation of Flying Qualities*, AFFDL-TR-69-120, June 1970.
5-33	Dillow, J.D.	*The 'Paper Pilot' – A digital Computer Program to Predict Pilot Rating for the Hover Task*, AFFDL-TR-70-40, March 1971.
5-34	Harper, R.P., Jr Cooper, G.E.	*A Revised Pilot Rating Scale for the Evaluation of Handling Qualities*, CAL Report # 153, September 1966.
5-35	Ashworth, B.R. Kahlbaum, W.M., Jr	*Description and Performance of the Langley Differential Maneuvering Simulator*, NASA TN D-7304, June 1973.
6-1	Hall, G.W.	*A Flight Test Investigation of Direct Side Force Control*, AFFDL-TR-71-106, September 1971.

6-2	Hall, G.W. Weingarten, N.C. Lockenour, J.L.	*An In-Flight Investigation of the Influence of Flying Qualities on Precision Weapons Delivery*, AIAA Paper # 73-783, August 1973.
6-3	–	*An Investigation of Direct Side Force Control for Improving Maneuver Capability of Attack Aircraft*, Boeing Report D180-140004-1, October 1971.
6-4	Attinello, J.S.	*Thrust Vectoring – A new Dimension in Flight Maneuvering*, Paper presented at Air-to-Air Combat Analysis & Simulation Symposium, Kirtland AFB, New Mexico, March 1972.
6-5	–	Private Communication: McDonnel Douglas, St Louis, and Mr W.G.Williams, AFFDL/FGC, February 1974.
6-6	Herbst, W.B.	*Advancements in Future Fighter Aircraft*, Paper presented at 43rd AGARD Flight Mechanics Panel Symposium, 1 –4 October 1973.
6-7	Watson, J.H. Roberts, R.O.	*Control Power Criteria and Requirements for Control Configured Vehicles*, General Dynamic Convair Rpt RR-FW-1265, December 1971.
6-8	–	*Advanced Fighter Technology Entry Set*, article in Aviation Week, 29 August 1973.
6-9	–	Private Communication: Mr C.Anderson, General Dynamics, Ft Worth Division, to Captain Strahota, AFFDL/FGB, February 1974.
6-10	Bennett, D.	*Program Summary for Control Configured Vehicle Concepts Applied to Fighter Aircraft*, McDonnel Douglas Rpt No MDC AZ140, February 1973.
6-11	McAllister, J.D. et al.	*Wing Roll Control Devices for Transonic High Lift Conditions*, AFFDL-TR-69-124, General Dynamics Ft Worth, January 1970.
6-12	Ross, H. Frenzl, W.	*Design Features for Air Combat*, Paper presented at 43rd AGARD Flight Mechanics Panel Symposium, 1 –4 October 1973.
6-13	Kulwicki, P.V. Sinnett, J.M.	*The High-G Approach*, McDonnell Douglas Rpt MDC AZ169, February 1973.
6-14	Bray, R.S.	*Vertical Motion Requirements for Landing Simulation*, NASA TM X-62,236, August 1972.
7-1	–	*Technical Report on the Accidents Investigation Sub-Committee on the Accident to the Aeroplane G-AAZK at Meopham, Kent on 21 July 1930.* RM 1360, January 1931.
7-2	Blenk, H.	*Ueber neuere englische Arbeiten zur Frage des Leitwerkschüttelns* ZEM 24, 1933, 21-24, also English translation NACA TM 669.
7-3	Owen, T.B.	*Techniques of Pressure Fluctuation Measurements Employed in the RAE Low Speed Wind Tunnels*, AGARD Report 172, 1958.
7-4	Mabey, D.G. Moss, G.	RAE unpublished.
7-5	Zbrozek, J.K. Jones, J.G.	*Transient Buffet Loads on Wings*, Journal of Sound and Vibration, Vol.5, No.2, pp.197-214, 1967.
7-6	Rogers, E.W.E. Hall, I.M.	*An Introduction to the Flow about Plane Swept-Back Wings at Transonic Speeds*, Journal of Royal Aeronautical Society, Vol.64, pp.449-464, 1960.
7-7	Green, J.E.	*Some Aspects of Viscous-Inviscid Interactions at Transonic Speeds, and their Dependence on Reynolds Number*, AGARD CP 83, 1971.
7-8	Blackwell, J.A.	*Preliminary Study of the Effects of Reynolds Number and Boundary Layer Transition Location on Shock Induced Separation*, NASA TN D 5003, 1969.

7-9	Küchemann, D. Weber, J.	*An Analysis of Some Performance Aspects of Various Types of Aircraft Designed to Fly over Different Ranges at Different Speeds.*
7-10	Mabey, D.G.	*Analysis and Correlation of Data on Pressure Fluctuations in Separated Flow.* AIAA Journal, August/September 1972.
7-11	Norbury, J.F. Crabtree, L.F.	*A Simplified Model of the Incompressible Flow past Two-Dimensional Aerofoils with a Long Bubble Type of Separation*, RAE TN Aero 2352, June 1955.
7-12	Bradshaw, P.	*'Inactive' Motion and Pressure Fluctuations in Turbulent Boundary Layers*, NPL Aero Report 1172, October 1965. (Also published as ARC 27338).
7-13	Lilley, G.M.	*On Wall Pressure Fluctuations in Turbulent Boundary Layers*, ARC 24241, November 1962.
7-14	Bradshaw, P. Wong, F.Y.G.	*The Reattachment and Relaxation of a Turbulent Shear Layer.* Journal of Fluid Mechanics Vol.52, part p 1, pp.113-135, 1972.
7-15	Lawford, J.A. Beauchamp, A.R.	*Low Speed Wind Tunnel Measurements of Pressure Fluctuations on the Wing of a Twin Jet Aircraft (Bristol 188).* ARC R&M 3551, 1968.
7-16	Rose, R. Nicholas, O.P.	*Flight and Tunnel Measurements of Pressure Fluctuations on the Upper Surface of the Wing of a Venom Aircraft with a Sharp Leading-Edge.* ARC CP 1032, November 1967.
7-17	Heller, H.H. Bliss, D.B. Widnall, S.E.	*Incipient Stall Detection through Unsteady-Pressure Monitoring on Aircraft Wings*, Journal of Aircraft, Vol.9, No.2, pp.186-188, February 1972.
7-18	Crabtree, L.F.	*The Formation of Regions of Separated Flow on Wing Surfaces, Pt II Laminar Separation Bubbles and the Mechanism of the Leading-edge Stall*, RAE Report Aero 2578, July 1957, also in Pt 2 of ARC R&M 3122, 1959.
7-19	Jenkins, J.M. et al.	*Flight Measurements of Canard Loads, Canard Buffeting and Wing Tip Hinge Moments on the XB70 Aircraft Including Comparisons with Predictions.* NASA TN D5359, August 1969.
7-20	Fricke, F.R. Stevenson, D.C.	*Pressure Fluctuations in a Separated Flow Region.* Journal of the Acoustical Society of America, Vol.44, No.5, pp.1189-1201, November 1968.
7-21	Greshilov, E.M. Evutshenko, A.V. Lyamshev, L.M.	*Spectral Characteristics of the Wall Pressure Fluctuations Associated with Boundary Layer Separation Behind a Projection on a Smooth Wall*, Soviet Physics – Acoustics. Vol.15, No.1, pp.29-34, July–September 1969.
7-22	Coe, C.F.	*The Effects of Some Variations in Launch Vehicle Nose Shape on Steady and Fluctuating Pressures at Transonic Speeds.* NASA TM X 646, March 1962.
7-23	Mabey, D.G.	*Some Measurements of Base Pressure Fluctuations at Subsonic and Supersonic Speeds.* RAE TR 70 148, August 1970, (also published as ARC CP 1204, 1972).
7-24	Mohsen, A.M.	*Experimental Investigation of the Wall Pressure Fluctuations in Subsonic Separated Flows.* Boeing Co. Report D6-17094, AD669214, January 1967.
7-25	Moss, G.F. Mundell, A.R.G.	RAE – unpublished.
7-26	Earnshaw, P.B. Lawford, J.A.	*Low Speed Wind Tunnel Experiments on a Series of Sharp-Edge Delta Wings.* R&M 3424, August 1964.
7-27	Keating, R.F.A.	RAE – unpublished.
7-28	Dee, F.W. Nicholas, O.P.	*Flight Determination of Wing Flow Patterns and Buffet Boundaries for the Fairey Delta Aircraft at Mach Numbers between 0.4 and 1.3 and Comparison with Wind Tunnel Tests.* R&M 3482, 1964.
7-29	Mabey, D.G.	*Comparison of Seven Wing Buffet Boundaries Measured in Wind Tunnels and In Flight.* ARC CP 840.

7-30	Mabey, D.G.	*An Hypothesis for the Prediction of Flight Penetration of Wing Buffeting from Dynamic Tests on Wind Tunnel Models.* ARC CP 1171, 1971.
7-31	Mabey, D.G.	*Measurements of Buffeting on Slender Wing Models.* ARC CP No.954, 1967.
7-32	Mitchell, C.G.B.	*Calculations on the Buffeting on a Slender Wing Aircraft at Low Speeds.* Proceedings of the Symposium on Structural Dynamics, Loughborough University, March 1970.
7-33	Huston, W.B.	*A Study of the Correlation between Flight and Wind Tunnel Buffet Loads.* AGARD Report 121, April 1957. (Also published as ARC 20704.)
7-34	Ray E.G. Taylor, R.T.	*Buffet and Static Aerodynamic Characteristics of a Systematic Series of Wings Determined from a Subsonic Wind Tunnel Study.* NASA TN D 5805, 1970.
7-35	Hollingsworth, E.G. Cohen, M.	*Comparison of Wind Tunnel and Flight Test Techniques for Determining Transonic Buffet Characteristics on the McDonnell Douglas F-4 Airplane.* AIAA Paper No. 70-584, 1970.
7-36	Moss, G.F. Haines, A.B. Jordan, R.	*The Effect of Leading-Edge Geometry on High Speed Stalling.* AGARD CP 102, November 1972. (Also published as RAE TR 72099.)
7-37	Cornette, E.S.	*Wind Tunnel Investigation of the Effects of Wing Bodies, Fences, Flaps and Fuselage Addition on Wing Buffet Response of a Transonic Transport Model.* NASA TN D 637.
7-38	Sutton, F.B.	*A Buffet Investigation at High Subsonic Speeds of Wing-Fuselage-Tail Combinations having Swept Back Wings with NACA Four Digit Thickness Distributions, Fences and Body Contouring.* NASA Memo 3-25-59A, 1959.
7-39	Friend, E.L. Sefic, W.V.	*Flight Measurements of Buffet Characteristics of the F-104 Airplane for Selected Wing-Flap Deflections.* NASA TN D6943, August 1972.
7-40	Mabey, D.G.	*Flow Unsteadiness and Model Vibration in Wind Tunnels at Subsonic and Transonic Speeds.* ARC CP 1155, 1971.
7-41	Bore, C.L.	*Post Stall Aerodynamics of the "Harrier" GR1.* AGARD CP 102, November 1972.
7-42	Pearcey, H.H.	*Simple Methods for the Prediction of Wing Buffeting Results from Bubble Type Separations.* NPL Aero Report 1024, June 1962.
7-43	Mayes, J.F. Lores, M.E. Barnard, H.R.	*Transonic Buffet Characteristics of a 60 Degree Swept Wing with Design Variation.* AIAA Paper 69-793 (1969) also Journal Aircraft 1, pp.523-530 (1970).
7-44	Davis, D.D. Wornom, D.E.	*Buffet Tests of an Attack Airplane Model with Emphasis on Data from Wind Tunnel Tests.* NACA RML57 H13, February 1958.
7-45	Mabey, D.G.	*Measurements of Wing Buffeting on a Scimitar Model.* ARC CP 954, 1966.
7-46	Jones, J.G.	*The Dynamic Analysis of Buffeting and Related Phenomena.* AGARD CP 102, November 1972.
7-47	Polentz, P.P. Page, W.A. Levy, L.L.	*The Unsteady Normal Force Characteristics of Selected NACA Profiles at High Subsonic Mach Numbers.* NACA RM A 55 002, May 1955.
7-48	Hanson, P.W.	*Evaluation of an Aeroelastic Model Technique for Predicting Aircraft Buffeting Loads.* NASA TN D 7066, February 1973.
7-49	Seal, D.M.	*A Survey of Buffeting Loads.* RAE Structures Report 252 August 1959. (Also published as ARC CP 584, 1962.)
7-50	Rigby, R.N. Cornette, E.S.	*Wind-Tunnel Investigation of Tail Buffet at Subsonic and Transonic Speeds Employing a Dynamic Elastic Aircraft Model.* NASA TN D 1362, September 1962.

7-51 Byrnes, A.L. Hensleigh, W.E. Tolve, L.A. — *Effects of Horizontal Stabilizer Vertical Location on the Design of Large Transport Aircraft.* AIAA Paper 65-331, July 1965.

7-52 Soderman, P.T. Aiken, T.N. — *Full-scale Wind-Tunnel Tests of a Small Unpowered Jet Aircraft with a T-tail.* NASA TN D 6573, November 1971.

7-53 Lemley, C.E. Mullans, R.E. — *Buffeting Pressures on a Swept Wing in Transonic Flight – Comparison of Model and Full-Scale Measurements.* AIAA Paper 73-311, March 1973.

7-54 Cahill, J.F. — *Simulation of Full Scale Flight Aerodynamic Characteristics by Tests in Existing Transonic Wind Tunnels.* AGARD CP 83-71.

7-55 Haines, A.B. — *Possibilities for Scale Effect on Swept Wings at High Subsonic Speeds: Recent Evidence from Pressure Plotting Tests.* Paper 14 AGARD CP 83, 1971.

7-56 Thomas, F. — *Die Ermittlung der Schüttelgrenzen von Tragflügeln in Transsonischen Geschwindigkeitsbereich* WGLR Yearbook 1966 (1967) pp.126-144.

7-57 Magnus, R. Yoshihara, H. — *Flow Over Airfoils in the Transonic Regime – Prediction of Buffet Onset.* AFFDL TR 7016 Vol.I, March 1970.

7-58 Redeker, G. — *Die Berechnung der Schüttelgrenzen von Pfeilflügeln.* AVA Paper 71/21, October 1971.

7-59 Myring, D.F. — *An Integral Prediction Method for Three-Dimensional Turbulent Boundary Layers in Incompressible Flow.* RAE Technical Report 70147, 1970.

7-60 Bailey, F.E. Sieger, J.L. — *Recent Techniques for the Prediction of Three-Dimensional Flows about Wings.* AIAA Paper No. 72-189, January 1972.

7-61 Peake, D.J. et al. — *The Transonic Performance of Two-Dimensional Jet Flapped Aerofoils at High Reynolds Numbers.* AGARD CP 83, 1971.

7-62 Pearcey, H.H. Osborne, J. Haines, A.B. — *Interaction between Local Effects at the Shock and Rear Separations – a Source of Significant Scale Effects in Wind Tunnel Tests on Aerofoils and Wings.* NPL Aero 1071 (ARC 30477) September 1968.

7-63 Evans, J.Y.G. Taylor, C.R. — *Some Factors Relevant to the Simulation of Full Scale Flows in Model Tests and to the Specification of New High Reynolds Number Transonic Tunnels.* AGARD CP 83, 1971.

7-64 Treon, S.L. Hofstetler, W.R. Abbott, F.T. — *On the Use of Freon-12 for Increasing Reynolds number in Wind Tunnel Testing of Three-Dimensional Aircraft Models at Subcritical and Supercritical Mach Numbers.* AGARD CP 83, 1971.

7-65 Kilgore, R.A. Adcock, J.B. Ray, E.J. — *Flight Simulation Characteristics of the Langley High Reynolds Number Cryogenic Transonic Tunnel.* AIAA Paper 74-80, February 1974.

7-66 Rossiter, J.E. — *The Effect of Cavities on the Buffeting of Aircraft.* AGARD SMP, Paris, 1962.

7-67 Lück — Der Einfluss von Spoilern vor dem Lastraum auf die statischen Drücke im Lastenraum der VAK 191 B VFW Kurzbericht Ea-120, Nov. 1967.

7-68 Carra — VAK 191 B. *Bomb Bay Buffeting Wind Tunnel Results.* Fiat Report VAK-F-67108, December 1967.

7-69 Owen, T.B. — *Techniques of Pressure-Fluctuation Measurements Employed in the RAE Low Speed Wind-Tunnels.* AGARD Report 172, March 1958.

7-70 Roshko, A. — *Some Measurements of Flow in a Rectangular Cut-Out.* NACA Techn. Note 3488, 1955.

7-71 Charwat, A.F. — *An Investigation of Separated Flows.* J. Aero Sci 28 (6 & 7), June and July 1961.

7-72	McDearmon, R.W.	*Investigation of the Flow in a Rectangular Cavity in a Flat Plate at a Mach Number of 3.55*, NASA TN D 523, September 1960.
7-73	Tillmann, W.	*Additional Measurements of the Drag of Surface Irregularities in Turbulent Boundary Layers*, NACA Technical Memo 1299, January 1951. Translation of ZWB Untersuchungen und Mitteilungen Nr. 6619, December 1944.
7-74	Skingle, C.W.	*Measurements of Fluctuating Pressures in and Behind the Bomb Bay of a Canberra Aircraft*. ARC-CP-1025, April 1968.
7-75	Otnes, R.K. Enochson, L.	*Digital Time Series Analysis*. John Wiley & Sons, London 1972.
7-76	Bendat, J.S. Piersol, A.G.	Random data: *Analysis and Measurement Procedures*. John Wiley & Sons, London 1971.
7-77	Laschka, B.	Zur Theorie der harmonisch schwingenden tragenden Fläche bei Unterschallströmung Z. Flugwiss. 11, 1963.
8-1	Gentry, A.E. Oliver, W.R.	*Investigation of Aerodynamic Problems in Transonic Maneuvering*, Vol.1, McDonnell Douglas Report MDC-J5264-01, 1971.
8-2	Mabey, D.G.	*Beyond the Buffet Boundary*, Aeronautical Journal, pp.201-215, April 1973.
8-3	Ray, E.J. Taylor, R.T.	*A Subsonic Wind Tunnel Study to Determine the Buffet and Static Aerodynamic Characteristics of a Systematic Series of Wings*, NASA Langley Working Paper 537, January 1968 (incorporated in NASA TN D5805, 1970).
8-4	Jenkins, J.M. DeAngelis, V.M. Friend, E.L. Managhan, R.C.	*Flight Measurements of Canard Loads, Canard Buffeting, and Wing Tip Hinge Moments on the XB-70 Aircraft Including Comparisons with Predictions*, NASA TN D5359, August 1969.
8-5	Peake, D.J. Yoshihara, H. Zonars, D. Carter, W.	*The Transonic Performance of Two-Dimensional Jet Flapped Aerofoils at High Reynolds Numbers*, AGARD-CP-83-71, April 1971.
8-6	Mabey, D.G.	*Comparison of Seven Wing Buffet Boundaries Measured in Wind Tunnels and in Flight*, Aeronautical Research Council CP No.840, September 1964
8-7	Mabey, D.G.	*An Hypothesis for the Prediction of Flight Penetration of Wing Buffeting from Dynamic Tests on Wind Tunnel Models*, Aeronautical Research Council, CP No. 1171, 1971.
8-8	Mullans, R.E. Lemley, C.F.	*Buffet Dynamic Loads During Transonic Maneuvers*, AFFDL-TR-72-46, July 1972.
8-9	Pearcey, H.H. Osborne, J. Haines, A.B.	*The Interaction Between Local Effects at the Shock and Rear Separation*, AGARD CP No.35, September 1968.
8-10	Haines, A.B.	*Possibilities for Scale Effect on Swept Wings at High Subsonic Speeds*, AGARD CP-83-71, April 1971.
8-11	Gadeberg, B.L. Ziff, H.L.	*Flight-Determined Buffet Boundaries of Ten Airplanes and Comparisons with Five Buffeting Criteria*, NACA RM A50I27, 1951.
8-12	Outman, V. Lambert, A.A.	*Transonic Separation*, Journal of Aeronautical Sciences, Vol.15, No.11, November 1948.
8-13	Lindsay, T.L.	*A Procedure for Estimating Buffet Onset Normal Force as Affected by Wing Geometry*, Naval Ship Research and Development Center, Technical Note AL-70, June 1968.

8-14	Thomas, F.	*The Determination of the Buffet Boundaries of Aerofoils in the Transonic Regime*, Aircraft Research Association Library Translation No.19, 1969.
8-15	Sinnott, C.S.	*On the Prediction of Mixed Subsonic/Supersonic Pressure Distributions*, Journal of the Aerospace Sciences, October 1960.
8-16	Magnus, R. Yoshihara, H.	*Inviscid Transonic Flow Over Airfoils*, AIAA Journal, Vol.8, No.12, December 1970.
8-17	Garabedian, P. Korn, D.	*Analysis of Transonic Airfoils*, Comm. P. and Appl. Math, Vol.XXIV, 1971.
8-18	Jameson, A.	*Transonic Flow Calculations for Airfoils and Bodies of Revolution*, Grumman Report 390-71-1, 1971.
8-19	Yoshihara, H.	*A Survey of Computational Methods for 2D and 3D Transonic Flows with Shocks*, Convair Report GDCA-ERR-1726, December 1972.
8-20	Bailey, F.R. Steger, J.L.	*Relaxation Techniques for Three-Dimensional Transonic Flow about Wings*, AIAA Paper 72-189, 1972.
8-21	Ballhaus, W. Bailey, F.	*Numerical Calculation of Transonic Flow about Swept Wings*, AIAA Paper 72-677, 1972.
8-22	Hahn, M. Rubbert, P.E. Mahal, A.S.	*Evaluation of Separation Criteria and Their Application to Separate Flow Analysis*, AFFDL-TR-72-145, January 1973.
8-23	Pearcey, H.H.	*The Aerodynamic Design of Section Shapes for Swept Wings*, Advances in Aeronautical Sciences, Vol.3, The MacMillan Co., New York, 1962.
8-24	Jünke, E. Moeken, B. Proksch, H.J.	*Estimation of Buffet Intensity*, Dornier GmbH, Friedrichshafen, Germany, 1973 (Paper presented at EUROMECH 40, Transonic Aerodynamics, September 10–13, 1973, Stockholm).
8-25	Krupp, J.A. Murman, E.M.	*Computation of Transonic Flows Past Lifting Airfoils and Slender Bodies*, AIAA Journal, Vol.10, No.7, July 1972.
8-26	Küchemann, D.	*A Simple Method for Calculating the Span and Chordwise Loading on Straight and Swept Wings of any Given Aspect Ratio at Subsonic Speeds*, ARC R & M No. 2935, 1956.
8-27	Thomas, F. Redeker, G.	*A Method for Calculating the Transonic Buffet Boundary Including the Influence of Reynolds Number*, AGARD CP-83-71, 1971.
8-28	Gadd, G.E.	*Interactions Between Shock Waves and Turbulent Boundary Layers*, ARC R & M No. 3262, 1962.
8-29	Walz, A.	*Boundary Layers of Flow and Temperature*, The M.I.T. Press, Cambridge, Mass., 1969.
9-1	Emerson, E.R.	*F-106A Transonic Buffet Flight Test*, AFFDL TR 70-87, June 1970.
9-2	Titiriga, A.	*F-5A Transonic Buffet Flight Test*, AFFDL TR 69-110, December 1969.
9-3	Cohen, Marshall	*Buffet Characteristics of the Model F-4 Airplane in the Transonic Flight Regime*, AFFDL TR 70-56, April 1970.
10-1	Mabey, D.G.	*The Influence of Flow Unsteadiness in Wind Tunnel Measurements at Transonic Speeds*. LaWs Paper No.38, RAE unpublished.
10-2	Jünke, E. Moeken, B. Proksch, H.J.	*Estimation of Buffet Intensity*. Dornier Report, presented at Euromech 40, September 1973.

10-3	Vanino, R. Wedemeyer, E.	*Wind Tunnel Investigation of Buffet Loads on Four Airplane Models.* AGARD CP-83-71 Paper 34-1, 1971.
10-4	Issacs, D.	*Wind Tunnel Measurements of the Low Speed Stalling Characteristics of a Model of the Hawker Siddeley Trident 1C.* RAE TR 68-108 R & M 3608, 1968.
10-5	Pearcey, H.H. Osborne, J. Haines, A.B.	*Interaction between Local Effects at the Shock and Rear Separations – a Source of Significant Scale Effects in Wind Tunnel Tests on Aerofoils and Wings.* NPL Aero 1071 (ARC 30477) September 1968.
10-6	Yoshihara, H. Falta, H.	*The Aerodynamic Design and Test of an Attack Type Configuration at Supercritical Flow Condition.* US A1 905070, September 1972.
10-7	Hollingsworth, E.G. Cohen, M.	*Comparison of Wind Tunnel and Flight Test Techniques for Determining the Transonic Buffet Characteristics in the McDonnell Douglas F-4 Airplane.* AIAA Paper 70-584, 1970.
10-8	Grose, G. et al.	*Investigation of Scaling Effects in Transonic Wind Tunnel Testing.* AFFDL-TR-72-60, June 1972.
10-9	Plotkin, K.V.	*Shock Wave Oscillation Driven by Turbulent Boundary Layer Fluctuations.* AIAA Paper 73-662 July 1963.
11-1	Jünke, E. Moeken, B. Proksch, H-J.	*Estimation of Buffet Intensity.* Paper presented at: Euromech 40, Stockholm, Sweden, 1973.
11-2	Proksch, H-J.	*Ermittlung der Buffeting-Grenzen von Kampfflugzeugen.* Dornier-Bericht EA-101/2916, 1973.
11-3	Coe, C.F.	*Buffeting Forces on Two-Dimensional Airfoils as Affected by Thickness and Thickness-Distribution.* NACA RM A53K24, 1954.
11-4	Ray, E.J. Taylor, R.T.	*Buffet and Static Aerodynamic Characteristics of a Systematic Series of Wing Determined from a Subsonic Wind-Tunnel-Study.* NASA TN D 5805, 1970.
11-5	Vanino, R. Welte, D.	*Tragflügelentwurf für transonische Strömungen.* ZTL FAG 4 Do 405, 1970.
11-6	Polentz, P.P Page, W.A. Levy, L.L.	*The Unsteady Normal Force Characteristics of Selected NACA Profiles at High Subsonic Mach Numbers.* NACA RM A55C02, 1955.
11-7	Mabey, D.C.	*An Hypothesis for the Prediction of Flight Penetration of Wing Buffeting from Dynamic Tests on Wind Tunnel Models.* ARC CP 1171, 1971.
11-8	Gadeberg, L.B. Ziff, H.L.	*Flight Determinated Buffet Boundaries of Ten Airplanes and Comparisons with Five Buffeting Criteria.* NACA RM A50I27, 1950.
11-9	Lindsay, T.L.	*A Procedure for Estimating Buffet Onset Normal Force as Affected by Wing Geometry.* Nav. Air TN AL-70, 1968.
11-10	Mabey, D.C.	*Comparison of Seven Wing Buffet Boundaries Measured in Wind-Tunnel and Flight.* ARC CP No.840, 1966.
11-11	Thomas, F. Redeker, G.	*A Method for Calculating the Transonic Buffet Boundary, Including the Influence of Reynolds Number.* DFVLR-Bericht No.0663, 1971.
11-12	Baker, T.F. Johnson, W.E.	*Flight Measurements at Transonic Speeds of the Buffeting Characteristics of the XF-92A Delta Wing Research Airplane.* NACA RM H54L03, 1955.
11-13	Ayers, T.G.	*Supercritical Aerodynamics Worthwhile Over a Range of Speeds.* Astronautics & Aeronautics, August 1972.
11-14	Hollingsworth, E.G. Cohen, M.	*Comparison of Wind-Tunnel and Flight Test Techniques for Determining Transonic Buffet Characteristics on the McDonnell-Douglas F-4 Airplane.* AIAA Paper No. 70-584, 1970.

11-15	Briggs, D.W.	*Flight Determination of the Buffeting Characteristics of the Bell X-5 Research Airplane at 58.7° Sweepback.* NACA RM L54C17, 1954.
11-16	Aiken, W.S. See, J.A.	*Strain Gage Measurements of Buffeting Loads on a Jet-Powered Bomber Airplane.* NACA RM L50J06, 1951.
11-17	Baker, T.F.	*Results of Measurements of Maximum Lift and Buffet-Intensities During Flight-Investigation of the Northrop X-4 Research Airplane.* NACA RM L53G06, 1953.
11-18	Baker, T.F. Martin, J.A. Scott, B.J.	*Flight Data Pertinent to Buffeting and Maximum Normal-Force Coefficient of the Douglas X-3 Research Airplane.* NACA RM H57H09, 1957.
11-19	Bore C.L.	*A New Method for Estimating Buffet Boundaries from Wind-Tunnel Data.* HSA Project Office Note 981, 1966.
11-20	Bore, C.L.	*Post Stall Aerodynamics of the "Harrier" GR1.* AGARD CP 102, 1972.
11-21	Burris, W.R. Hutchis, D.E.	*Effect of Wing Leading-Edge Geometry on Maneuvering Boundaries and Stall Departure.* AIAA Paper No.70-904, 1970.
11-22	Butkewicz, P.J.	*On Airflow Separation and Buffet Onset During Fighter Aircraft Maneuvering.* AGARD CP 102, 1972.
11-23	Corner, A.H. Payne, M.M.	*Tabulated Pressure Coefficients and Aerodynamic Characteristics Measured on the Wing of the Bell X-1 Airplane in Level Flight at Mach Numbers from 0.79 to 1.00 and in a Pull-Up at Mach Number of 0.96.* NACA RM L50H25, 1950.
11-24	Charpin, F.J.	*Buffeting Test.* La Recherche Aerospatiale No.664, pp.9-16 1968.
11-25	Cohen, M.	*Buffeting Characteristics of the Model F-4 Airplane in The Transonic Flight Regime.* AFFDL-TR-70-56, 1970.
11-26	Cornette, E.S.	*Wind Tunnel Investigation of the Wing Buffet Response of a Variable Wing-Sweep Model at Subsonic and Transonic Speeds.* NASA TM X-443, 1961.
11-27	Damstrom, E.K. Mayes, J.F.	*Transonic Flight and Wind-Tunnel Buffet Onset Investigation of the F-8-D Aircraft.* AIAA Paper 70-341, 1970.
11-28	Dee, F.W. Nicholas, P.O.	*Flight Determination of Wing Flow Patterns and Buffet Boundaries for the Fairy Delta 2 Aircraft at Mach-Numbers between 0.4 and 1.3 and Comparison with Wind-Tunnel Tests.* RAE TR 64012, 1962.
11-29	Emerson, E.R.	*Buffet Characteristics During Transonic Maneuvers of the F106A Delta Wing Interceptor.* AFFDL-TR-70-87, 1970.
11-30	Friend, E.L. Monaghan, R.C.	*Flight Measurements of Buffet Characteristics of the F-11A Variable Sweep Airplane.* NASA TM X-1876, 1969
11-31	Friend, E.L. Sefic, J.W.	*Flight Measurements of Buffet Characteristics of the F-104 Airplane for Selected Wing Flaps Deflections.* NASA TN D 6943, 1972.
11-32	Gentry, A.E. et al.	*Investigation of Aerodynamic Analysis Problems in Transonic Maneuvering.* Volume I, Douglas Aircraft Company, AD-737 293, 1971.
11-33	Humphreys, M.D.	*Transonic Aerodynamic Characteristics of an NACA 64 A 006 Airfoil Section with a 15% Chord Leading-Edge Flap.* NACA RM L53G23, 1953.
11-34	Husk, D.I.	*The Influence of the major Design Parameters upon the Buffet Boundaries of a Wing.* '4th AGARD SMP-Meeting, July 1962.
11-35	Huston, W.B.	*A Study of the Correlation between Flight and Wind-Tunnel Buffet Loads.* AGARD Rep.411, 1957.
11-36	Huston, W.B.	*Measurements and Analysis of Wing and Tail Buffeting Loads on a Fighter Airplane.* NASA Rep. 1219, 1955.

11-37	Igoe, W.B.	*Wind-Tunnel Buffeting Measurements on Two Wing Endplate Airplane Configurations.* NASA TM X-1454, 1967.
11-38	Igoe, W.B. Capone, F.J.	*Subsonic Longitudinal Aerodynamic Characteristics of a 1/30-Scale Canard Airplane having a Wing with an Aspect Ratio of 6.* NASA TN-X-668, 1962.
11-39	Igoe, W.B.	*Longitudinal Aerodynamic Characteristics of a 1/30-Scale Subsonic Canard Airplane Model, having a Wing with an Aspect Ratio of 3.6.* NASA TN-X-669, 1962.
11-40	James, A.B.	*Preliminary Study of Effects of Reynolds-Number and Boundary Layer Transition Location on Shock-Induced Separation.* NASA TN-D-5003, 1969.
11-41	Jones, J.G.	*The Dynamic Analysis of Buffeting and Related Phenomena.* AGARD CP 102, 1972.
11-42	Jünke, E.	*Verfahren zur Berechnung von turbulenten Grenzschichten an schiebenden Flügeln.* Dornier AV-EA/P-0206/73, 1973.
11-43	Kantor, M.	*Estimation of the Buffet Onset Boundary for Straight and Swept-Wing Airplanes.* Bureau of Aeronautics, Navy Dep. Washington DC, TM 1-53, 1956.
11-44	Liepmann, H.W.	*Parameters for Use in Buffeting Flight Tests.* Douglas Aircraft Company, Rep. No. SM-14631, 1953.
11-45	Lorenz-Meyer, W. Wedemeyer, E.	*Windkanalmessungen zur Bestimmung des Schüttelverhaltens en vier Flugzeugmodellen.* AVA Bericht 71 C 02, 1971.
11-46	Mabey, D.C.	*Measurements of Buffeting on Slender Wing Models.* ARC CP No.917, 1966.
11-47	Mabey, D.C.	*Measurements of Wing Buffeting on a Scimitar Model.* RAE TR 66 160, 1966.
11-48	Mabey, D.C.	*Beyond the Buffet Boundary.* Aeronautical Journal, April 1973.
11-49	Margolin, M. Chung, J.G.	*F-105 F Transonic Buffet Study and Effect of Maneuvering Flaps.* AFFDL-TR-69-37, 1969.
11-50	Mayer, J.P. Valentine, G.M.	*Flight Measurements with the Douglas D-558-II Research Airplane, Measurements of Buffet-Boundaries.* NACA RM L50E31, 1950.
11-51	Mayer, J.F. Loree, M.E. Barnard, H.R.	*Transonic Buffet Characteristics of a 60° Swept Wing with Design Variation.* AIAA Paper No.69-793, 1969.
11-52	McWherter, R.C.	*Prediction of Buffet Onset for Aircraft.* AGARD FDP-Meeting, Izmir, Turkey, 1973.
11-53	Moeken, B. Vanino, R.	*Transonische Strömung und Buffeting an Tragflügeln von Kampfflugzeugen.* Dornier Bericht 72/28 B, 1972.
11-54	Moss, G.F. Haines, A.B. Jordan, R.	*The Effect of Leading Edge Geometry on High Speed Stalling.* AGARD CP 102, 1972.
11-55	Nelson, W.H. McDevitt, J.B.	*The Transonic Characteristics of 22 Rectangular, Symmetrical Wing Models of Varying Aspect Ratio and Thickness.* NACA TN 3501, 1955.
11-56	Nyberg, S.E.	*Correlation of Some Transonic Wind-Tunnel Test Data to Flight Test Results for Two Slender Wing Airplanes.* AGARD CP-83-71, 1971.
11-57	Pearey, H.H.	*A Method for the Prediction of the Onset of Buffeting and Other Separation Effects from Wind-Tunnel Tests on Rigid Models.* AGARD Rep. 223, 1958.
11-58	Phillips, W.P. Taylor, R.T.	*Longitudinal Aerodynamic Characteristics at Mach Numbers from 0.28 to 2.5 of a Multipurpose Tactical Airplane Configuration having Variable Sweep Wings.* NASA TM X-840, 1963.

11-59	Polhamus, E.C. King, T.J.	*Aerodynamic Characteristics of Tapered Wings having Aspect Ratios of 4, 6 and 8, Quarter-Chord-Lines Swept Back 45°, and NACA 631 A 012 Airfoil Sections.* NACA RM L51C26, 1951.
11-60	Purser, P.E. Wyss, J.A.	*Review of Some Recent Data on Buffet Boundaries.* NACA RM L51E02 a, 1951.
11-61	Ray, E.J.	*Buffet Studies.* NASA SP-178, 1972.
11-62	Ray, E.J.	*Techniques for Determining Buffet Onset.* NASA TM-X-2103, 1970.
11-63	Ray, E.J. McKinney, L.W. Carmichael, J.G.	*Maneuver and Buffeting Characteristics of Fighter Aircraft.* AGARD CP 102, 1972.
11-64	See, J.A. Aiken, W.S.	*Buffeting-Load Measurements on a Jet-Powered Bomber Airplane with Reflexed Flaps.* NACA RM L51E24a, 1951.
11-65	Squire, L.C.	*Experimental Investigation of the Characteristics of Cambered Gothic Wings at Mach-Numbers from 0.4 to 2.0.* ARC R & M 3310, 1961.
11-66	Staudacher, W.	*Verbesserungen der Manöverleistungen im hohen Unterschall.* DGLR-Mitteilung 73-04, 1973.
11-67	Sutton, F.B.	*A Buffet Investigation at High Subsonic Speeds of Wing-Fuselage-Tail Combinations, having Sweptback Wings with NACA Four Digit Thickness Distributions, Fences and Body Contouring.* NASA MEMO 3-23-59 A, 1959.
11-68	Thomas, F.	*Ermittlung der Buffeting-Grenzen von Tragflügeln.* Dornier-Bericht Ae 65/6, 1965.
11-69	Titiriga, J.A.	*F-5A Transonic Buffet Flight Test.* AFFDL-TR-69-110, 1969.
11-70	Vancamp, J.	*Transonic Wind-Tunnel Tests of the 0.07 Scale F-100 D Force Model to Obtain Buffet Data at Mach Numbers from 0.6 to 0.95.* North American Rockwell Report NA 68-257, 1968.
11-71	Vanino, R.	*Sonderprobleme im transonischen Bereich.* Dornier-Bericht EA-375/1917, 1969.
11-72	William, D.	*Buffet Boundary.* Fairchild Hiller EF Rep. 274, 1968.
12-1	Mabey, D.G.	*An Hypothesis for the Prediction of Flight Penetration of Wing Buffeting from Dynamic Tests on Wind Tunnel Models.* RAE Technical Report 70189 (ARC CP 1171), 1970.
12-2	Jones, J.G.	*The Dynamic Analysis of Buffeting and Related Phenomena.* AGARD-CP-102, 1972.
12-3	Damstrom, E.K. Nayes, J.F.	*Transonic Flight and Wind Tunnel Buffet Onset Investigation of the F-8D aircraft.* J. Aircraft, Vol.8, No.4, 1971.
12-4	Hollingsworth, E.G. Cohen, M.	*Comparison of Wind Tunnel and Flight Test Techniques for Determining Transonic Buffet Characteristics of the McDonnell Douglas F-4 Airplane.* J. Aircraft, Vol.7, No.6, 1970.
12-5	Mayes, J.F. Lores, M.E. Barnard, H.R.	*Transonic Buffet Characteristics of a 60° Swept Wing with Design Variations.* J. Aircraft, Vol.7, No.6, 1970.
12-6	Vanino, R. Wedemeyer, E.	*Wind Tunnel Investigation of Buffet Loads on Four Airplane Models.* AGARD-CP-83-71, 1971.
12-7	Ray, E.J. McKinney, L.W. Charmichael, J.C.	*Manoeuvre and Buffet Characteristics of Fighter Aircraft.* AGARD-CP-102, 1972.

12-8	Jünke, E Moeken, B Proksch, H.J.	*Estimation of Buffet Intensity*. EUROMECH 40, 1973.
12-9	Proksch, H.J.	*Ermittlung der Buffeting-Grenzen von Kampflugzeugen*. Dornier EA-101/2779, 1973.
12-10	Staudacher, W	*Verbesserung der Manoeuvreleistungen im hohem Unterschall*. DFLR Vortrag-summer 72-126, 1973.
12-11	Butkewicz, P.J.	*On Airflow Separation and Buffet Onset During Fighter Aircraft Manoeuvering* AGARD-CP-102, 1972.
12-12	Bore, C.L.	*Post-Stall Aerodynamics of the "Harrier" GR1*. AGARD-CP102, 1972.
12-13	Bore, C.L.	*Aerodynamics of the Harrier Wing, with Particular Reference to Stability and Control*. Hawker Siddeley Aviation Ltd, Research Note RN 54, November 1970.
12-14	Waaland, I.T. Curtis, E.J.	*"Gulfstream II" Aerodynamic Design*. SAE 670242, 1967.
12-15	Lachmann, G.V.	*Boundary Layer and Flow Control*, Vol.2, Chapter 4.5, Pergamon Press Ltd., 1961.

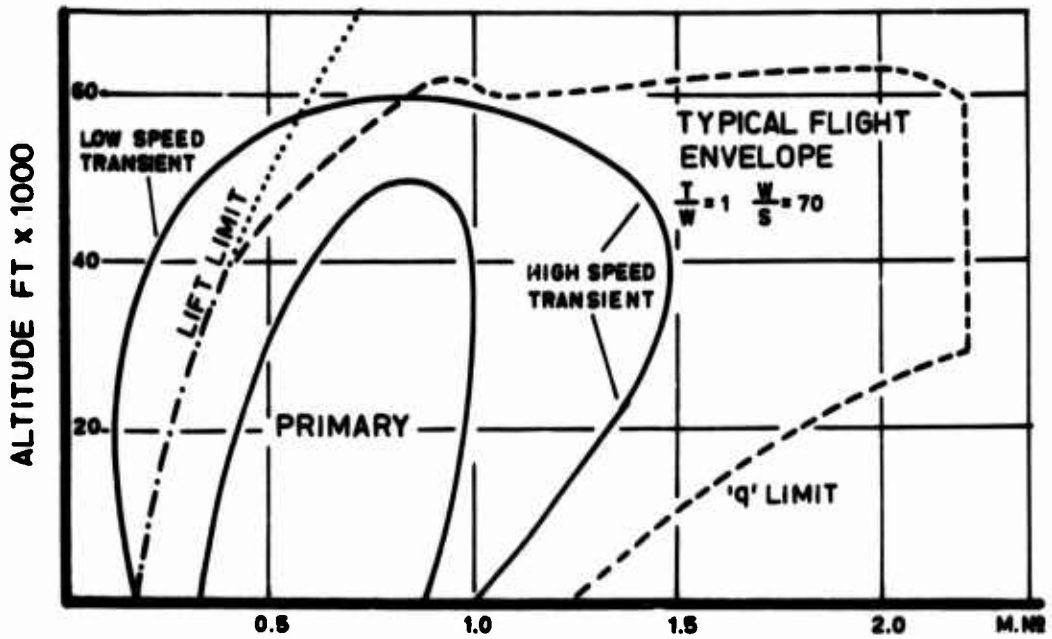

Fig. 1-1 Typical air combat arena

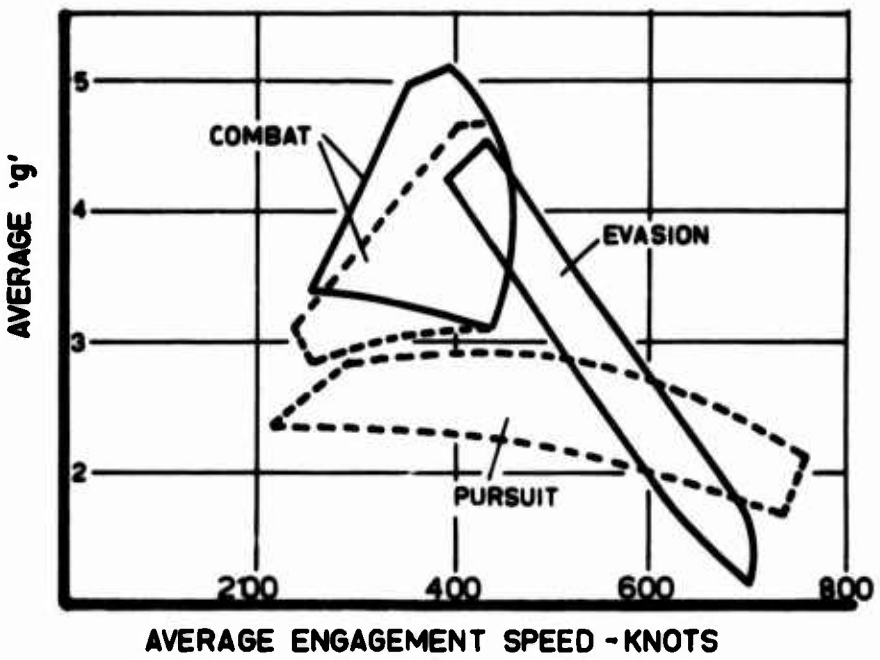

Fig. 1-2 Variation of battle arena in simulated air combat

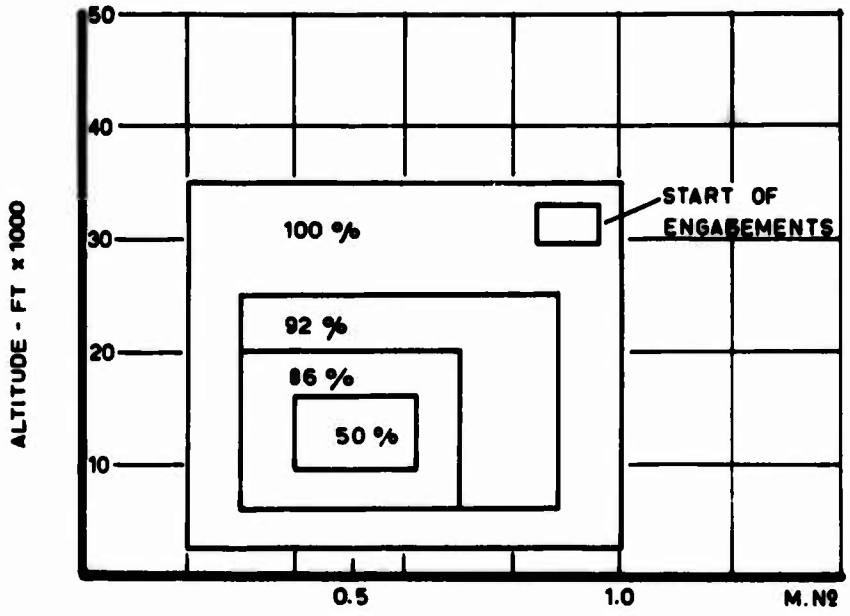

Fig.1-3 Combat termination regions – from flight test

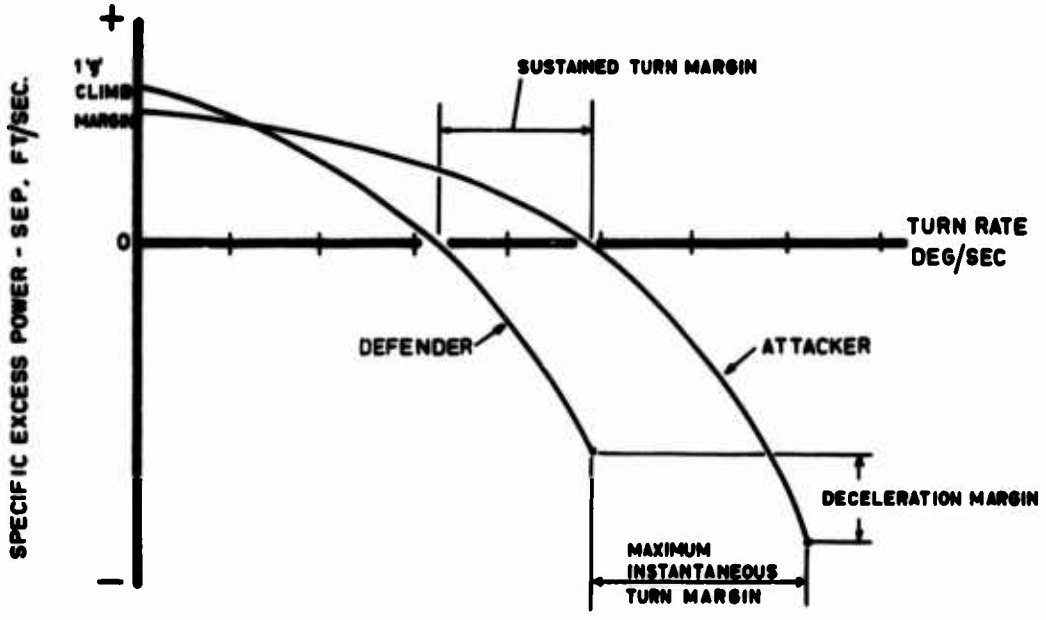

Fig.1-4 Variation of turn advantage with SEP at typical combat speed and altitude

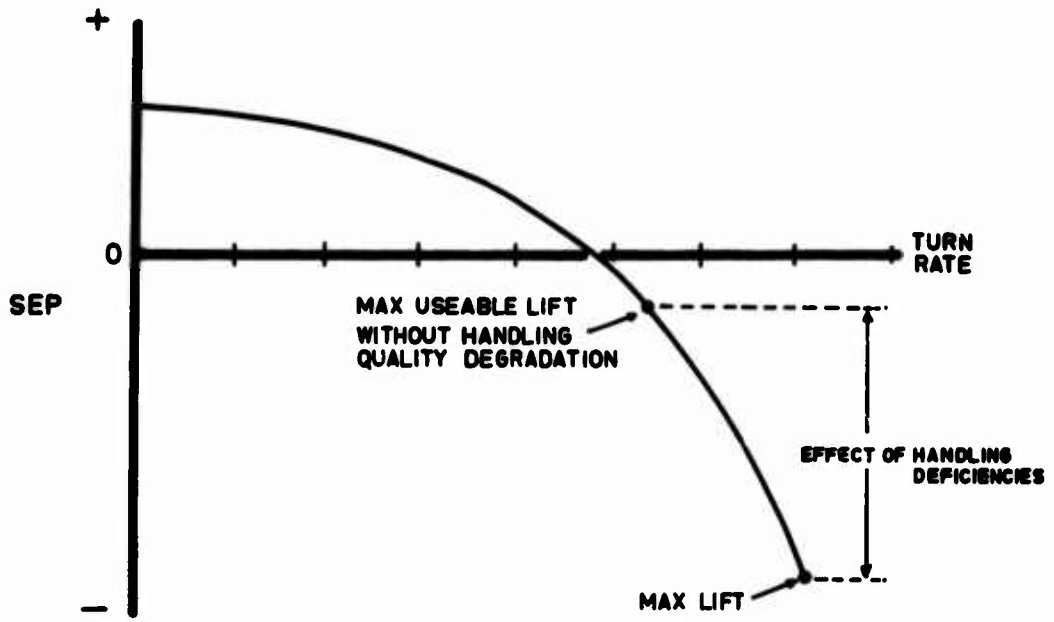

Fig.1-5 Effect of handling qualities on turn performance

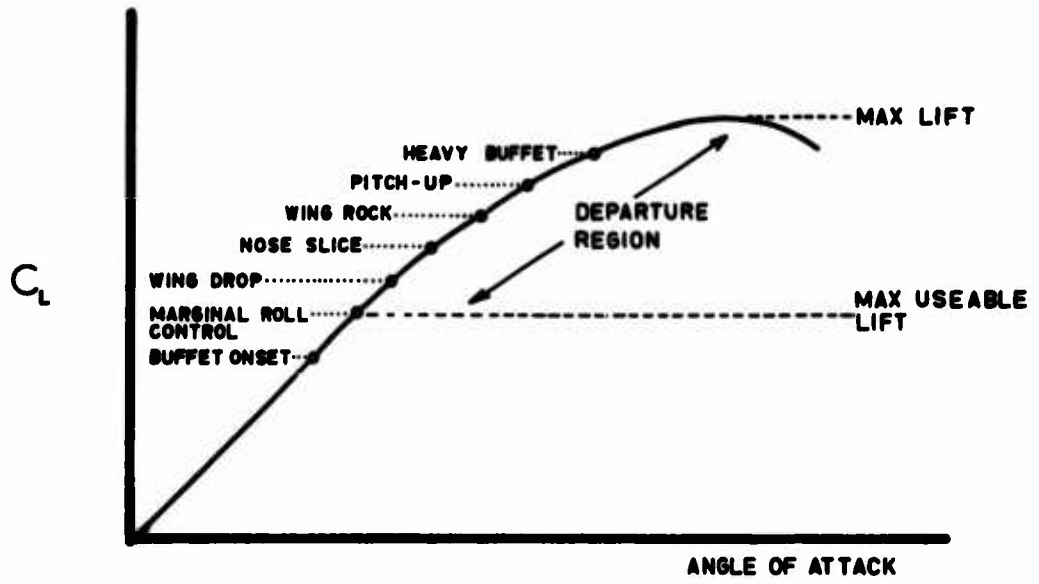

Fig.1-6 Effect of handling qualities deficiencies on useable lift

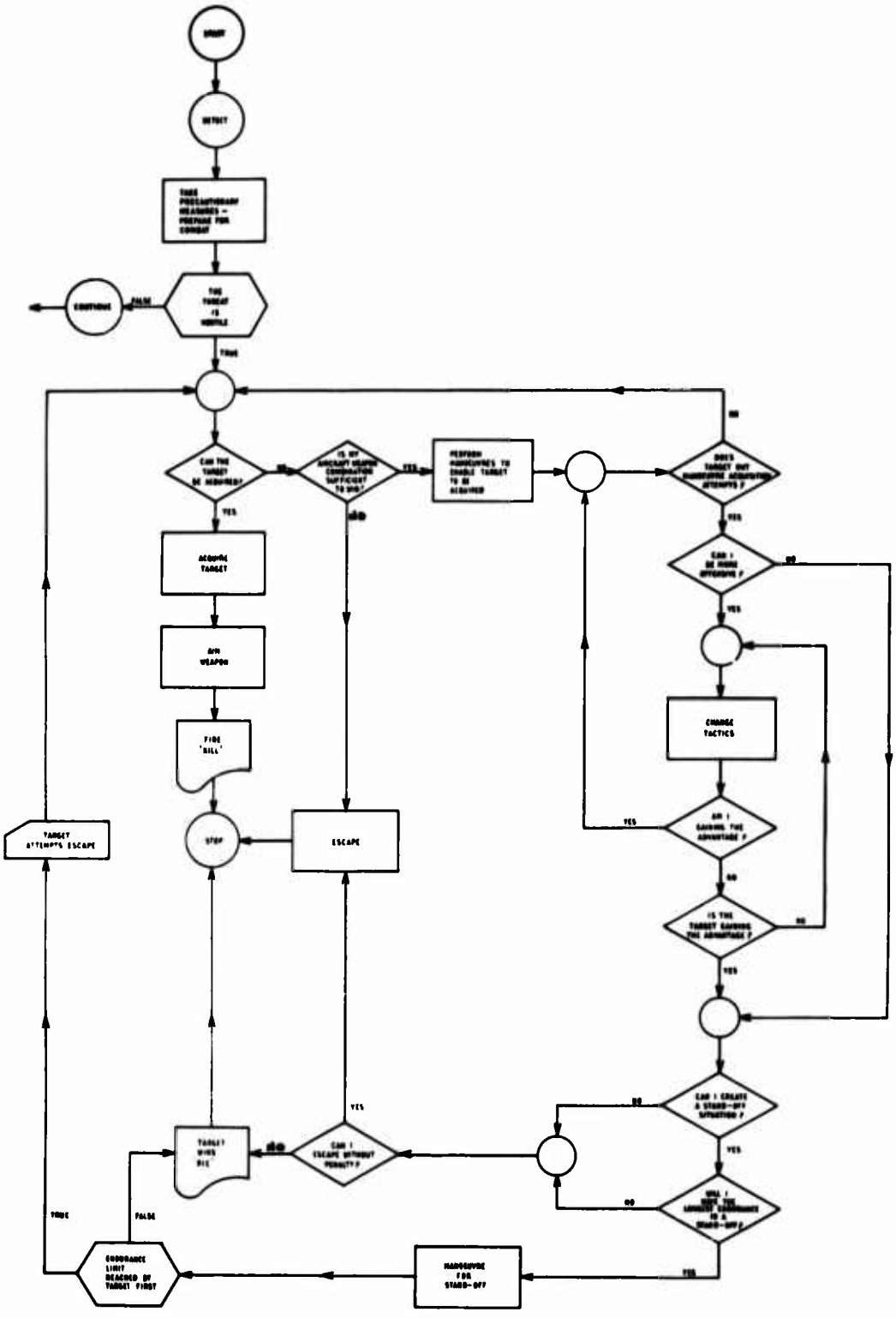

Fig.1-7 Simplified algorithm of 1-ON-1 air combat

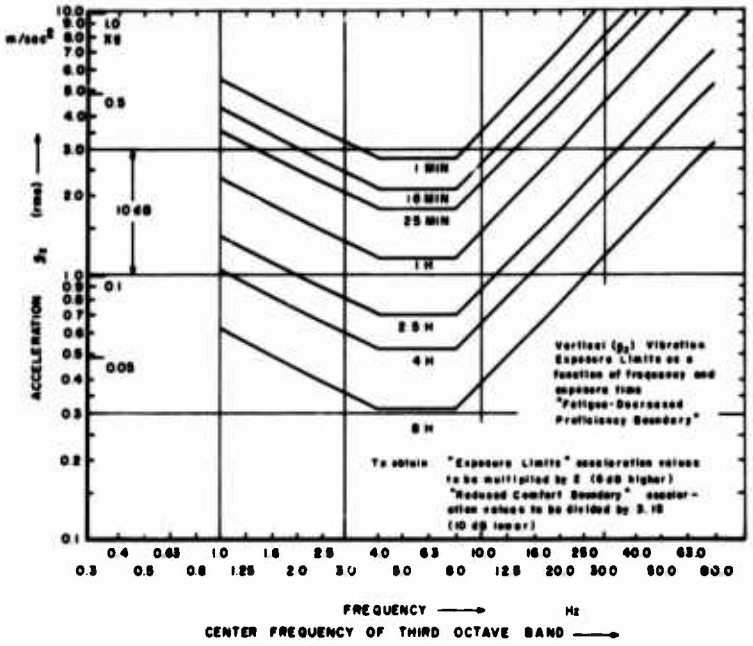

Fig.2-1 Vertical (g_z) vibration exposure criteria as a function of frequency and exposure time. The "fatigue-decreased proficiency" boundaries are shown*. (Ref.2-2)
*To obtain "exposure limits" multiply values by 2. For some military missions a factor of 4 is considered acceptable

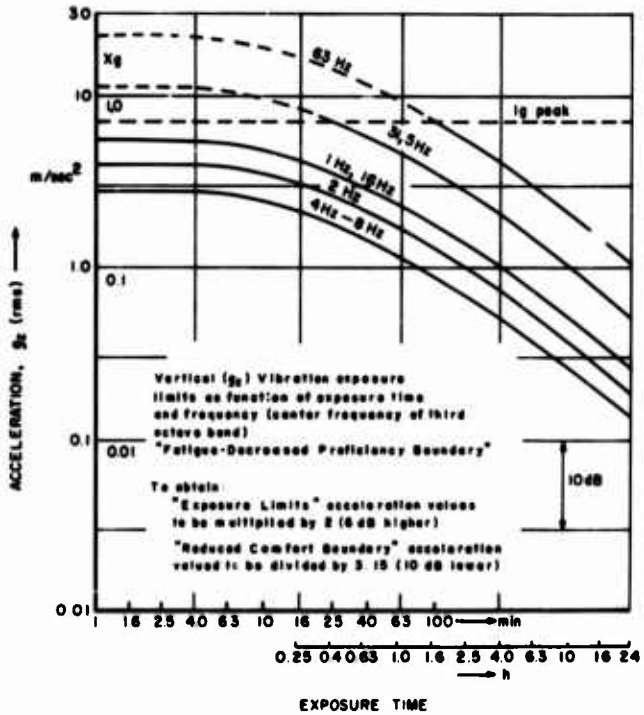

Fig.2-2 Vertical vibration exposure criteria as a function of exposure time and frequency*. (Ref.2-2)
*To obtain "exposure limits" multiply values by 2. For some military missions a factor of 4 is considered acceptable

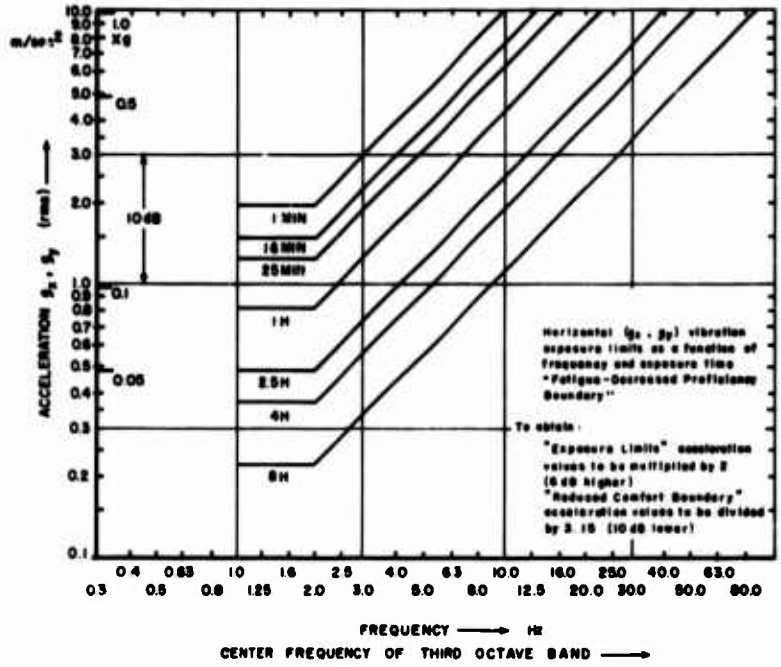

Fig.2-3 Horizontal (g_x, g_y) vibration exposure criteria as a function of frequency and exposure time. The "fatigue-decreased proficiency" boundaries are shown*. (Ref.2-2).
*To obtain "exposure limits" multiply values by 2. For some military missions a factor of 4 is considered acceptable

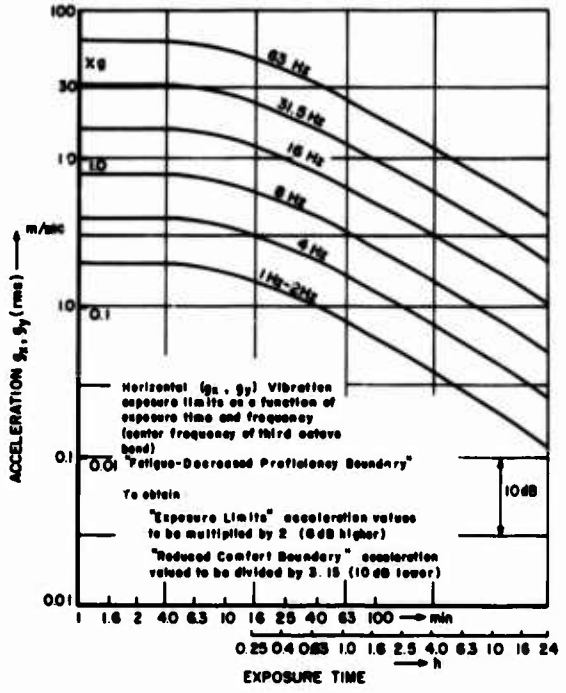

Fig.2-4 Horizontal vibration exposure criteria as a function of exposure time and frequency*. (Ref.2-2)
*To obtain "exposure limits" multiply values by 2. For some military missions a factor of 4 is considered acceptable

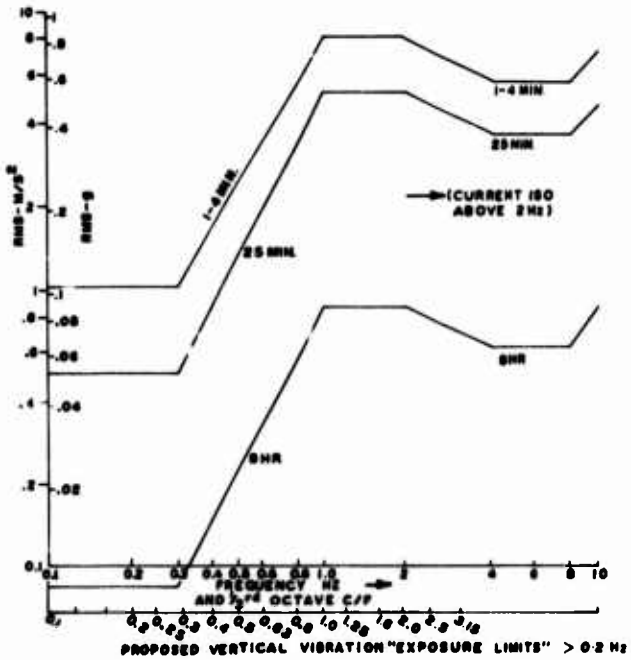

Fig.2-5 Proposed low frequency vertical (g_z) vibration exposure criteria . (Ref.2-5)

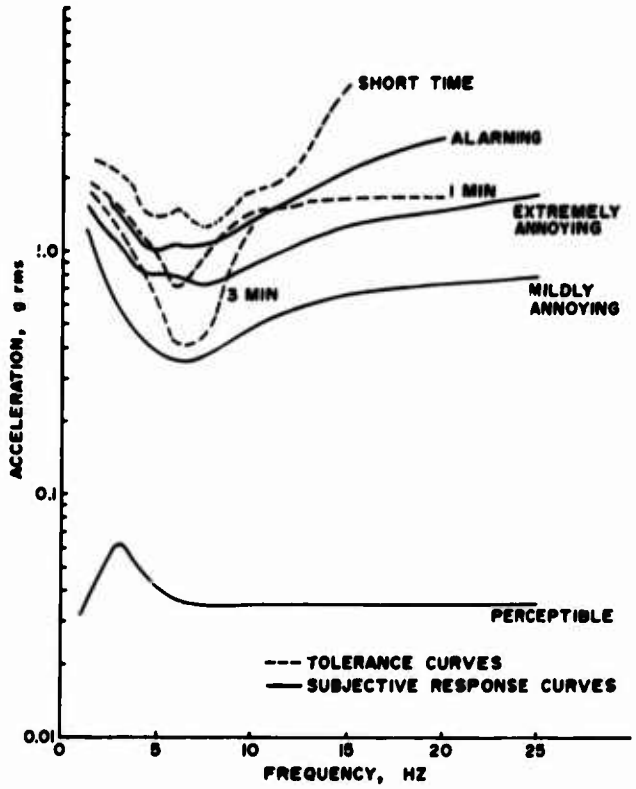

Fig.2-6 Subjective response curves (Chaney, 1964) compared to short-time, 1-minute and 3-minute tolerance curves (Magid, Coermann, and Ziegenruecker, 1960). (Adapted from Reference 2-8).

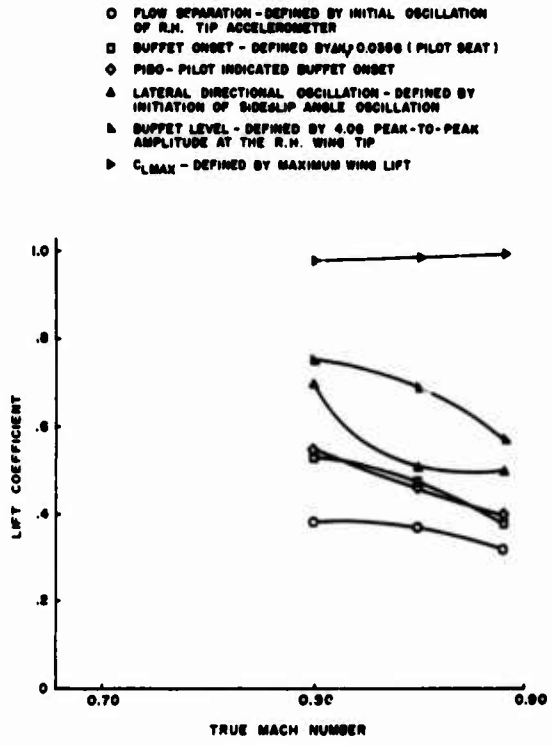

Fig.2-7 Buffet flight test data (Ref.2-9)

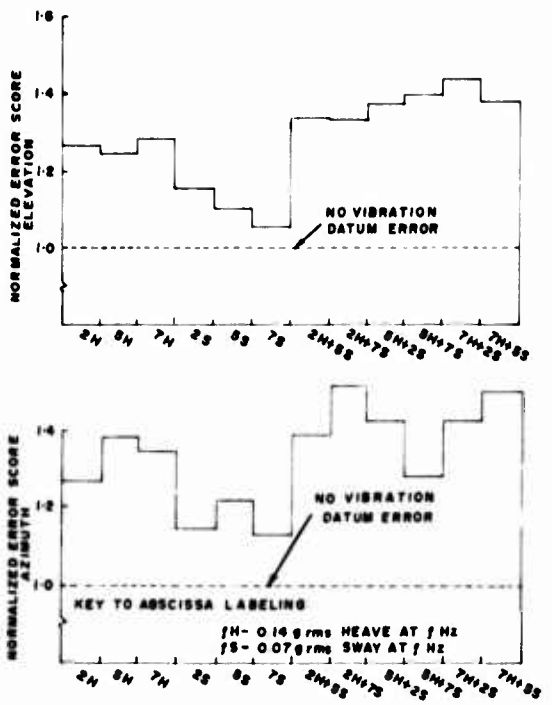

Fig.2-8 Average normalized compensatory tracking error scores for 18 subjects without restraining harness. (Adapted from Reference 2-11)

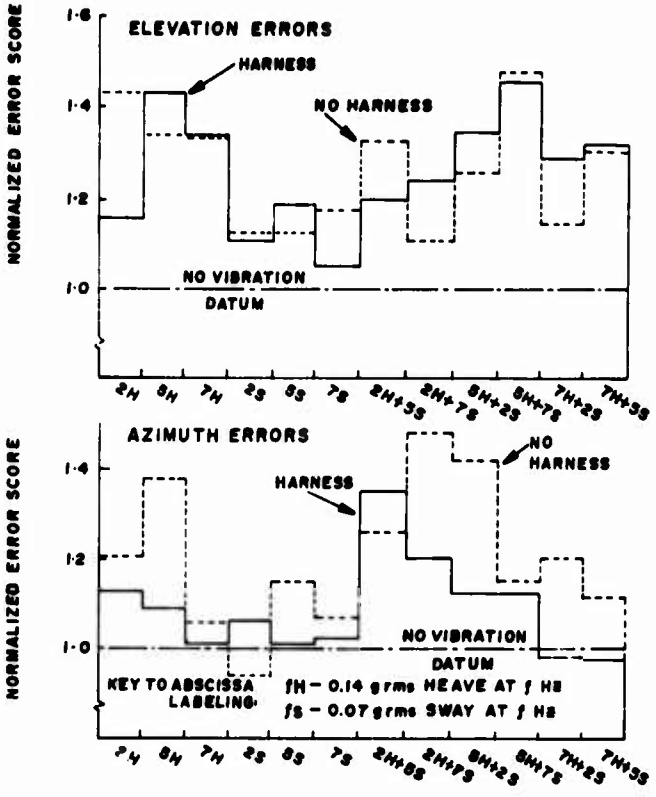

Fig.2-9 Average normalized compensatory tracking error scores for 3 subjects with and without harness. (Adapted from Reference 2-11)

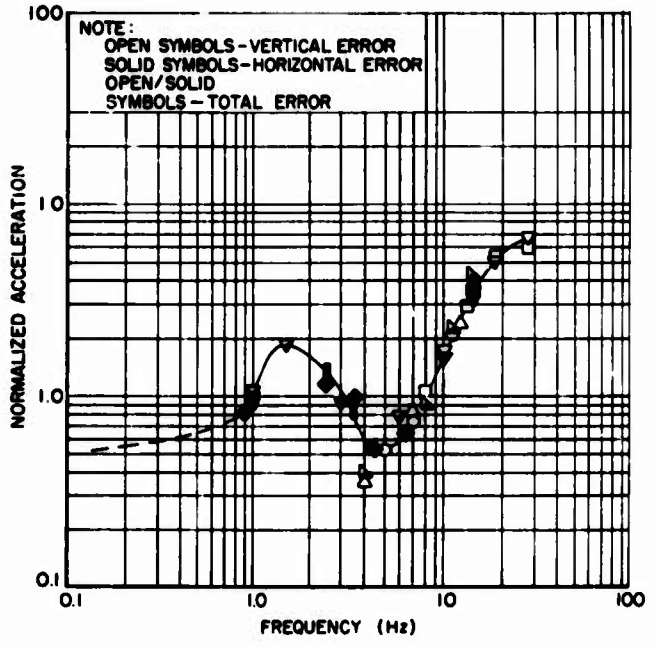

Fig.2-10 Normalized constant relative tracking error curve for vertical vibration. (Ref.2-14)

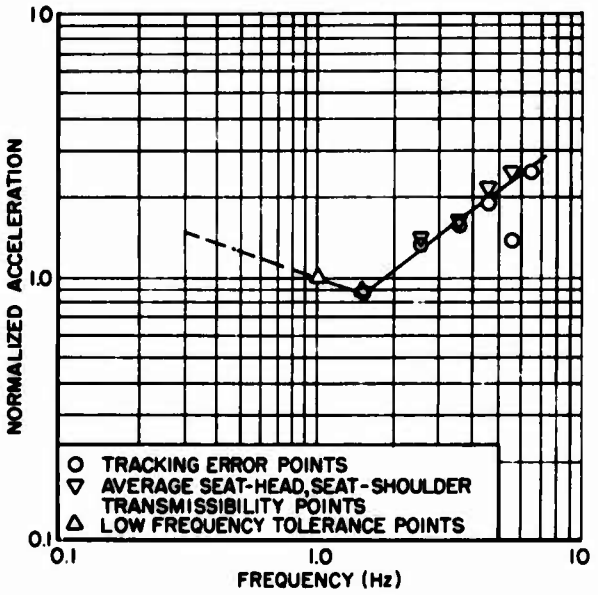

Fig.2-11 Normalized constant relative tracking error curve for lateral vibration. (Ref.2-14)

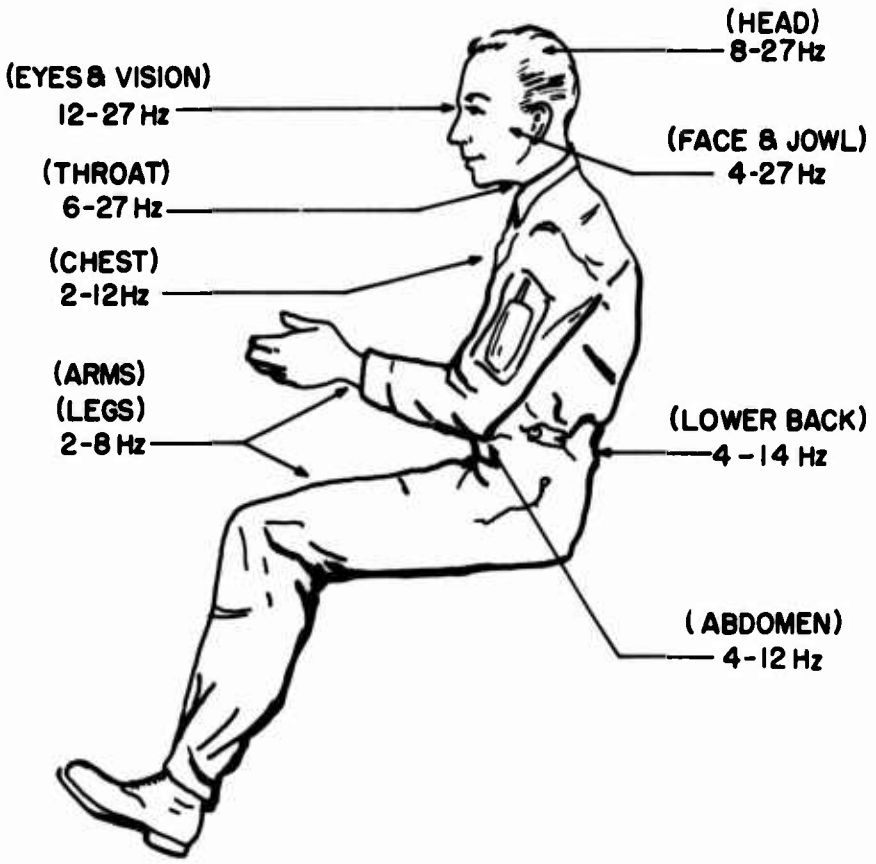

Fig.2-12 Concentrations of disturbing sensations and ranges of frequencies. (Ref.2-8)

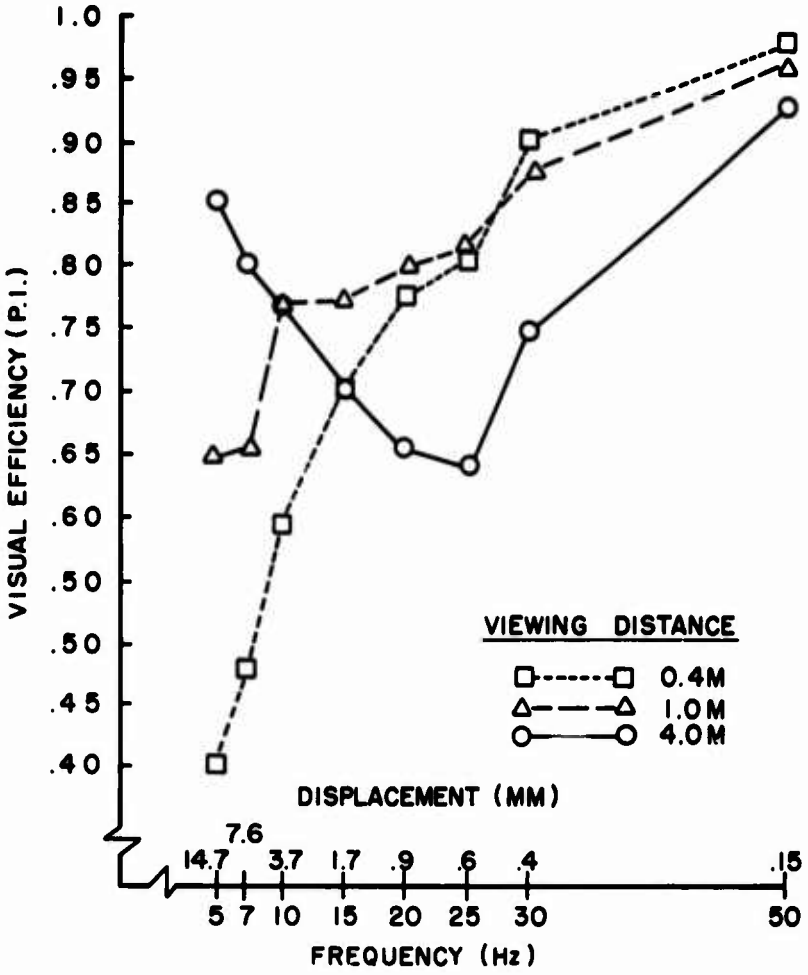

Fig.2-13 Visual efficiency at $0.53g_z$ rms as a function of frequency (or displacement) and viewing distance. (Ref.2-18)

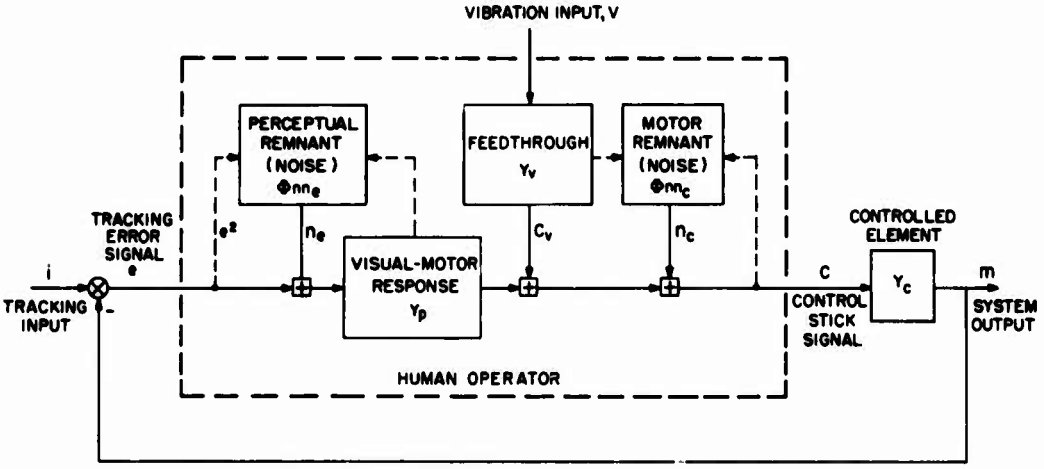

Fig.2-14 Measurement model structure. (Ref.2-23)

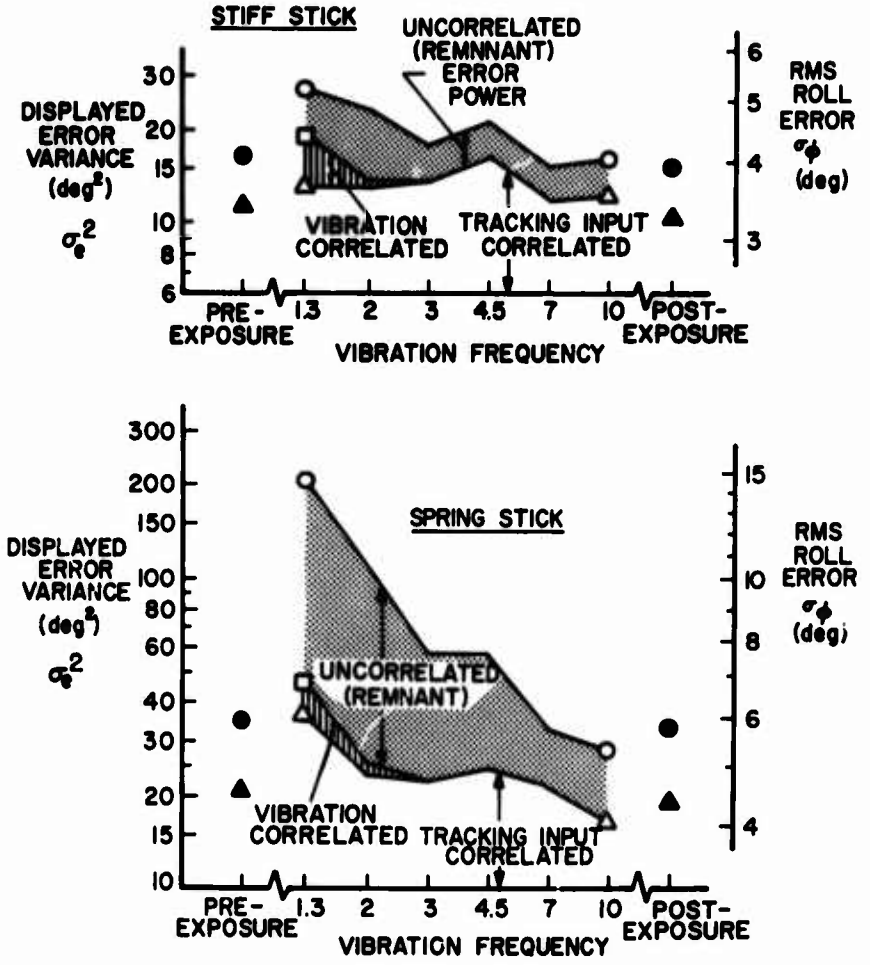

Fig.2-15 Displayed error variance components averaged over subjects for 0.28 g_y rms. (Ref.2-24)

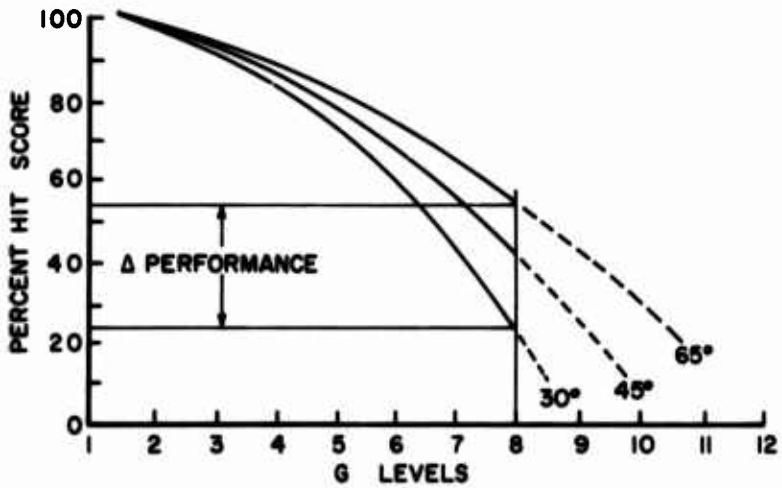

Fig.2-16 Best fit polynomials by seat angle during G (30 sec G pulse). (Ref.2-26)

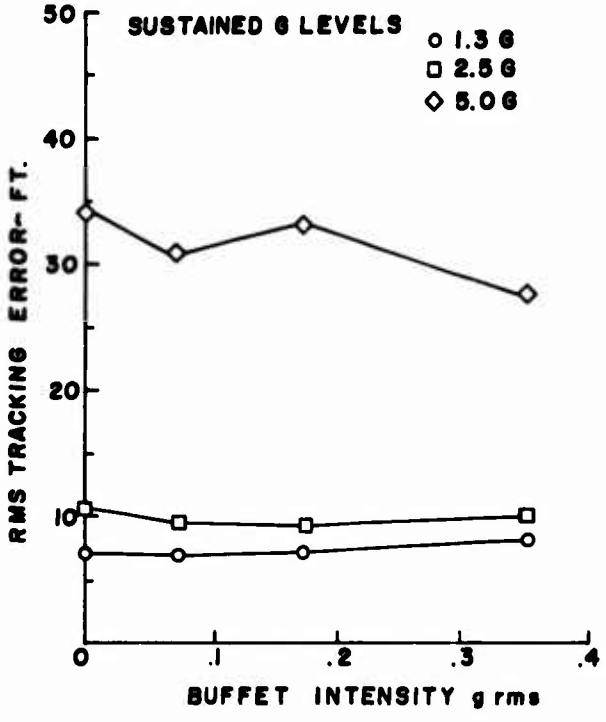

Fig.2-17 Combined buffet tracking scores for sinusoidal vibration at 10 H_z . (Adapted from Reference 2-28)

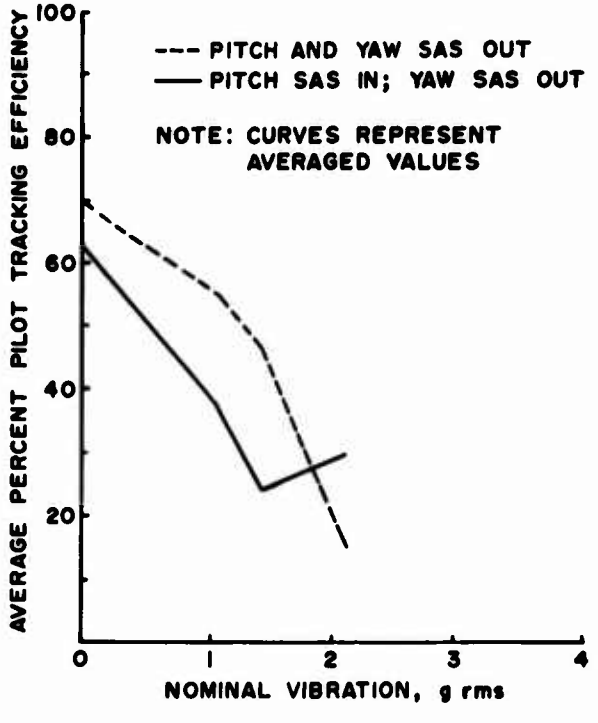

Fig.2-18 Tracking efficiency under combined g_x on G_x stress. Vibration at 11 H_z was combined with a nominal 3.5 G_x steady acceleration. (Adapted from Reference 2-29)

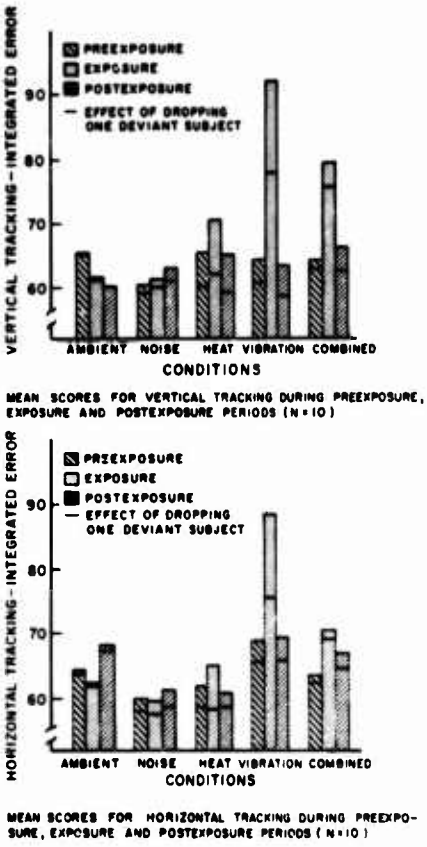

Fig.2-19 Effects of noise, heat and vibration on tracking performance (Ref.2-33)

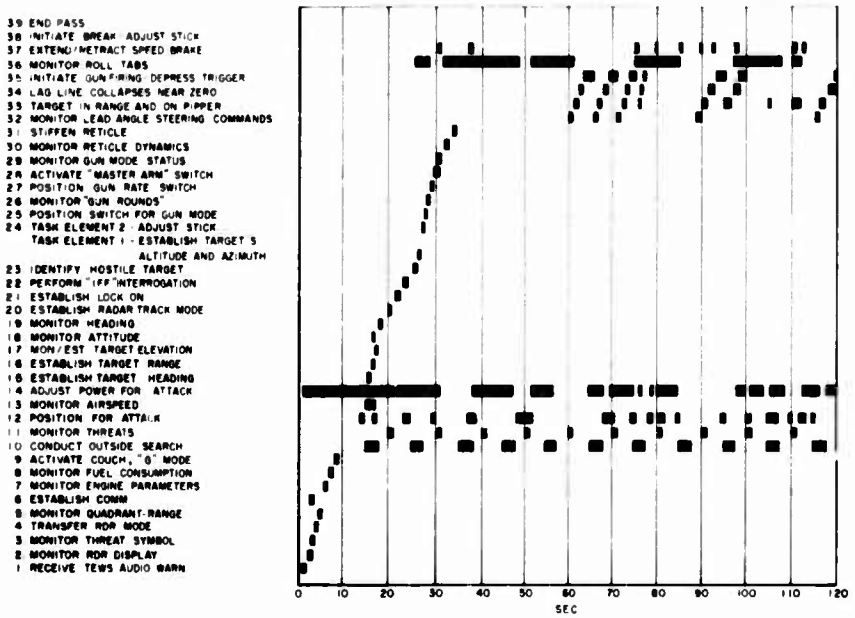

Fig.2-20 Simulated high acceleration fighter pilot workload at high G's. (Ref.2-35)

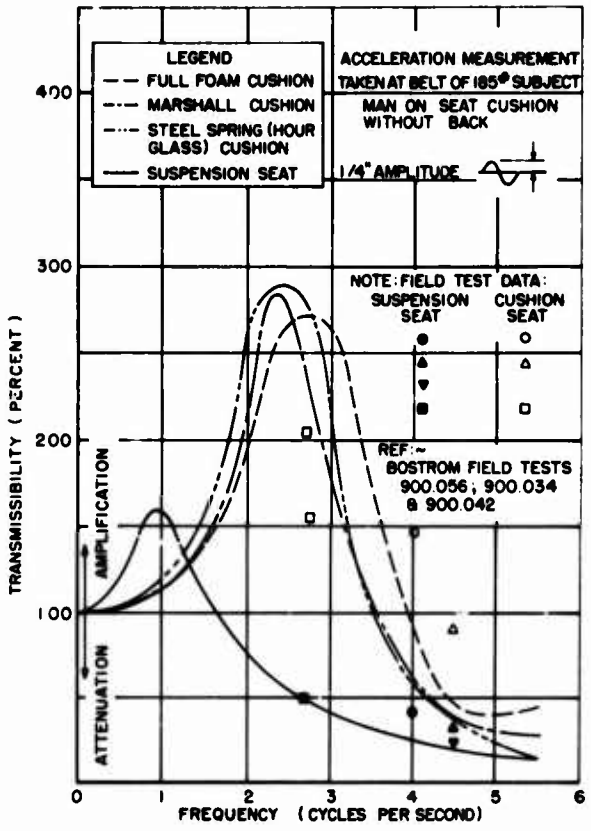

Fig.2-21 Acceleration transmissibility of several seat and cushion configurations. (Ref.2-37)

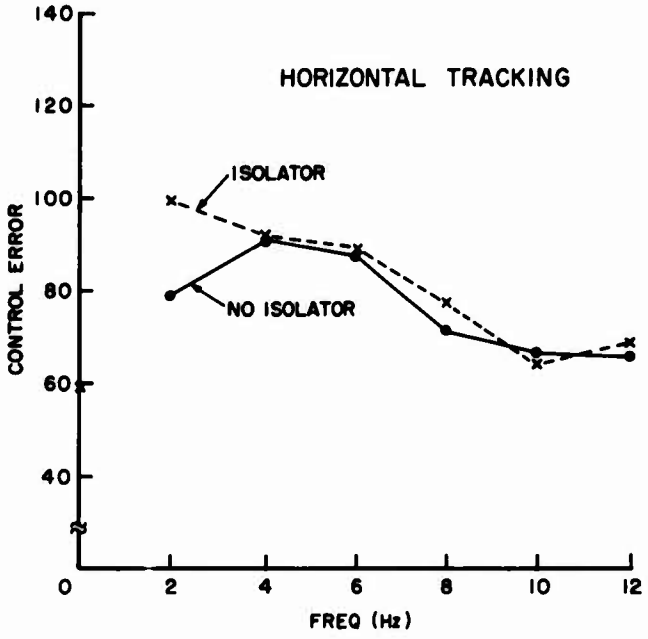

Fig.2-22 Comparison of tracking task errors with and without active isolation under 0.28 g_z rms. (Ref.2-38)

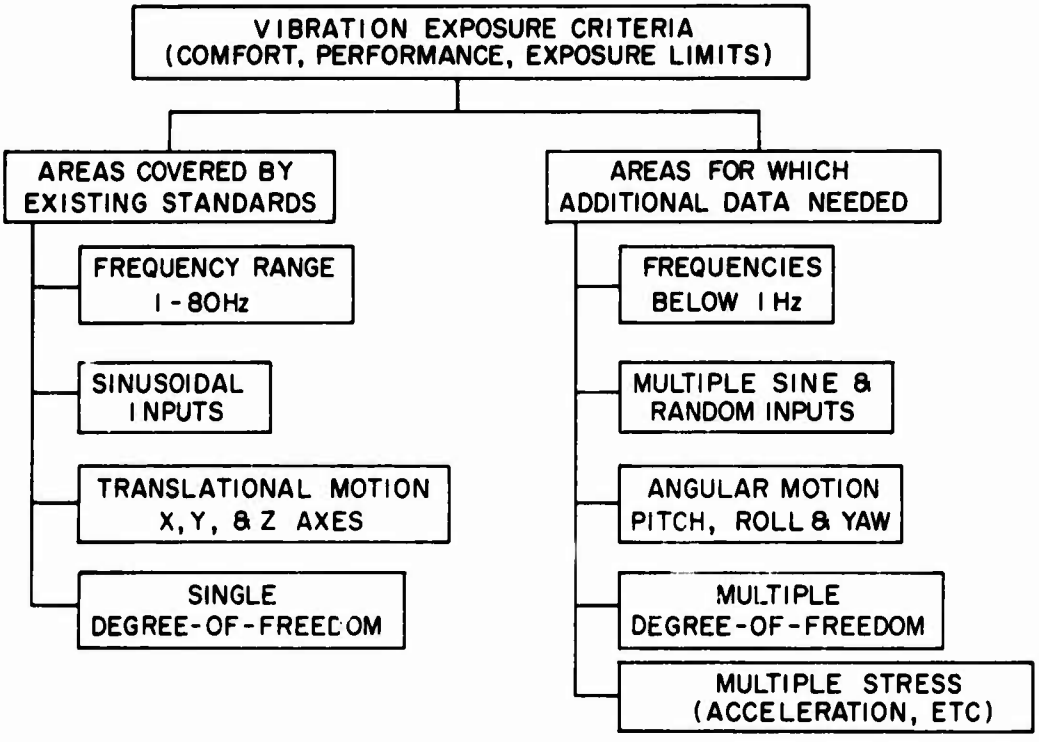

Fig.2-23 Summary of vibration effects knowledge

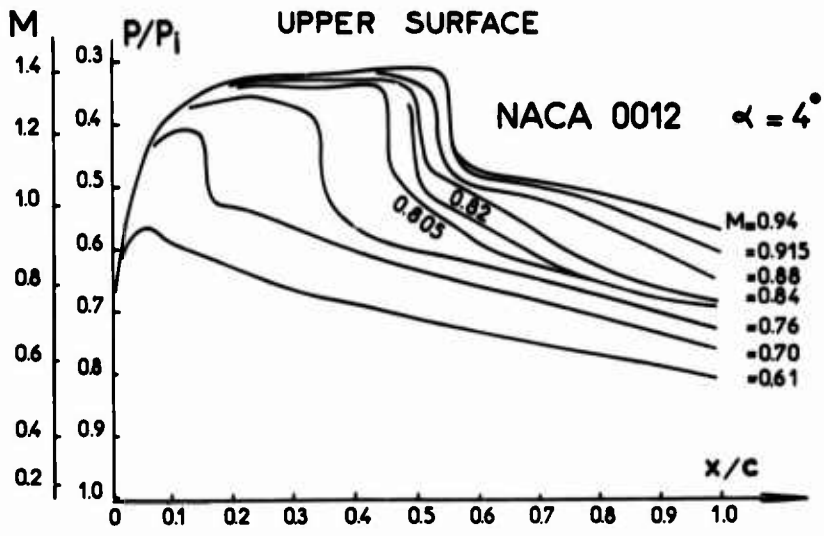

Fig.3-1 Effect of increasing Mach number on the pressure distribution for a symmetrical airfoil

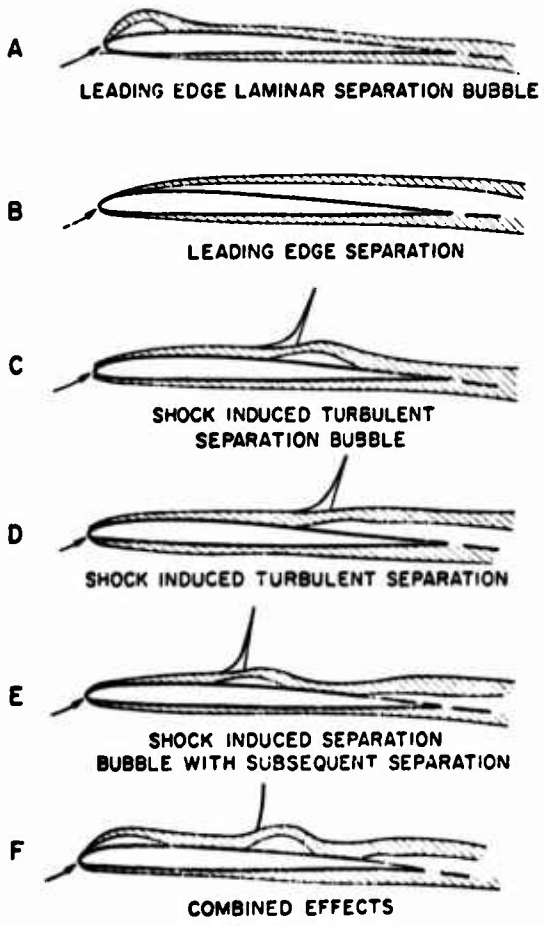

Fig.3-2 Airfoil separation characteristics (Ref.3-1)

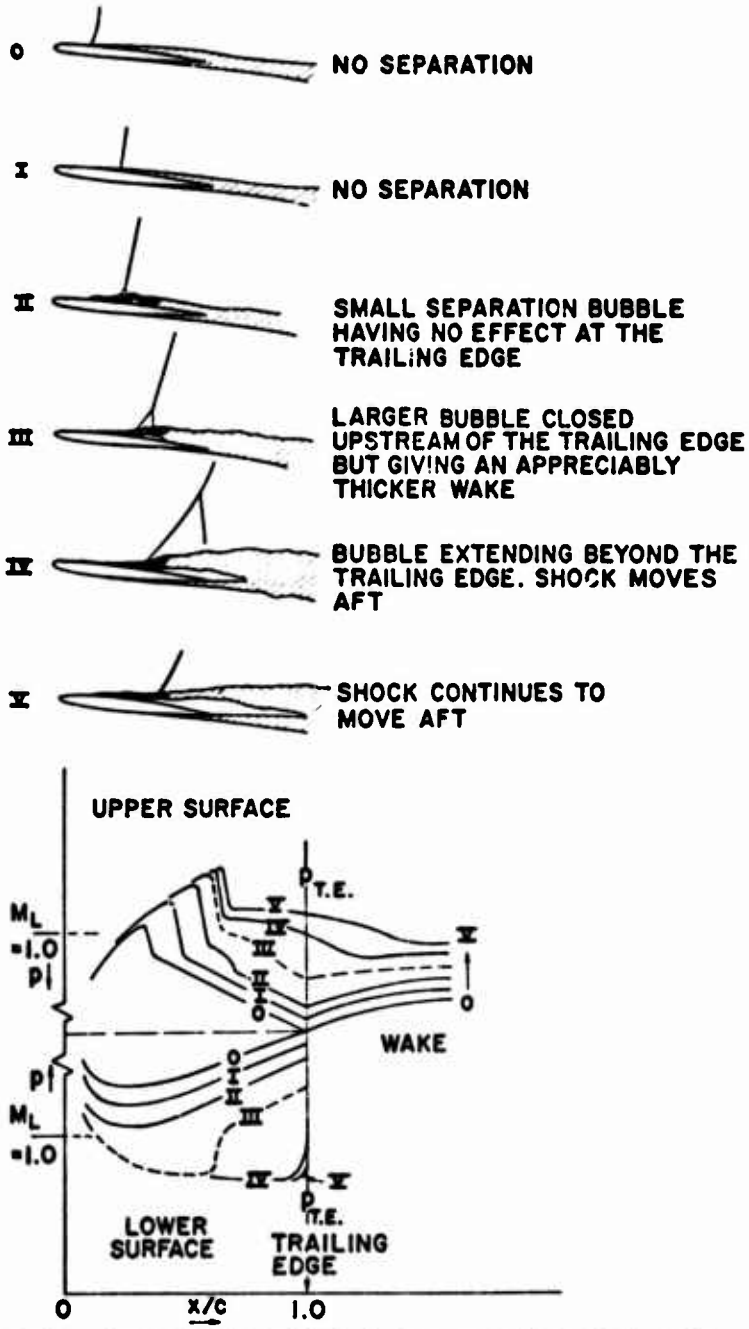

NOTE: THE ORDINATE OF PRESSURE FOR THE LOWER SURFACE IS A MIRROR IMAGE OF THAT FOR THE UPPER SURFACE.

Fig.3-3 High-speed flow separation with Mach number increasing and α constant (Ref.3-1)

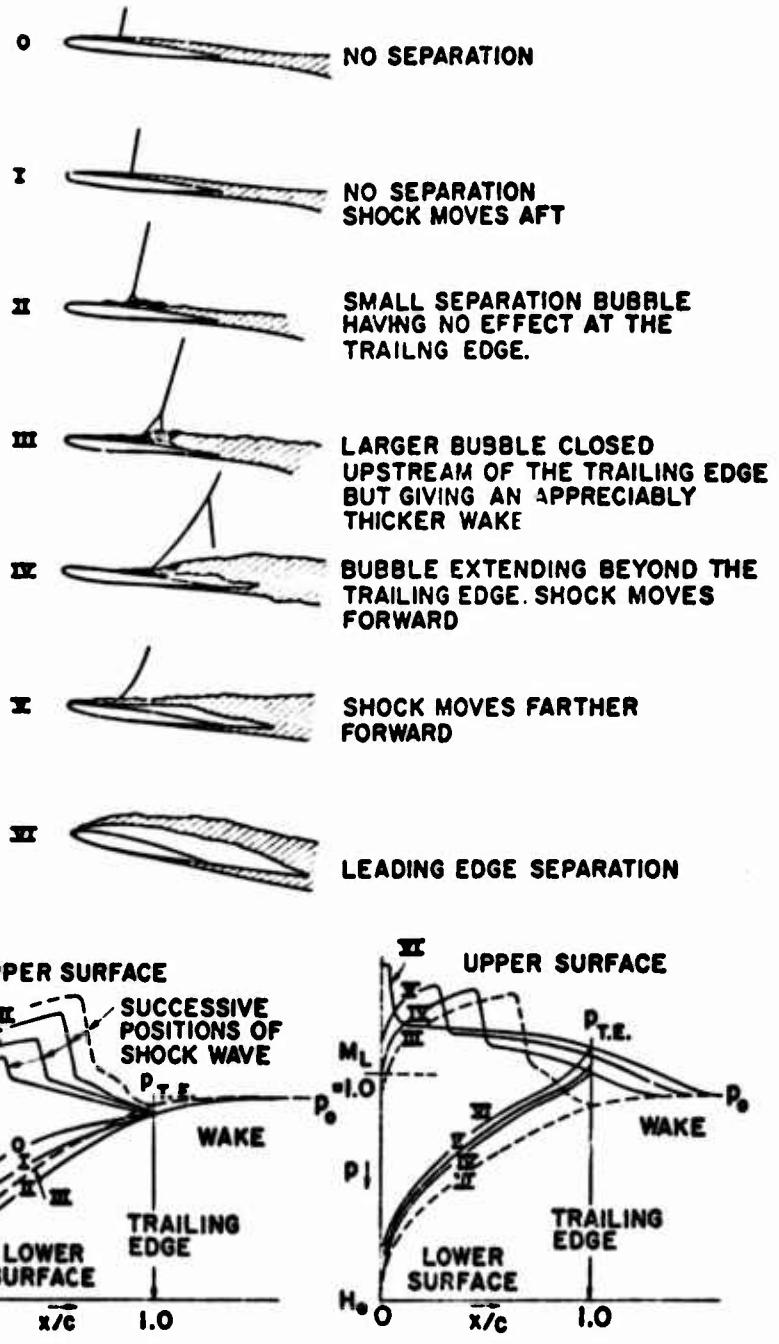

Fig.3-4 High-speed flow separation with α increasing and Mach number constant (Ref.3-1)

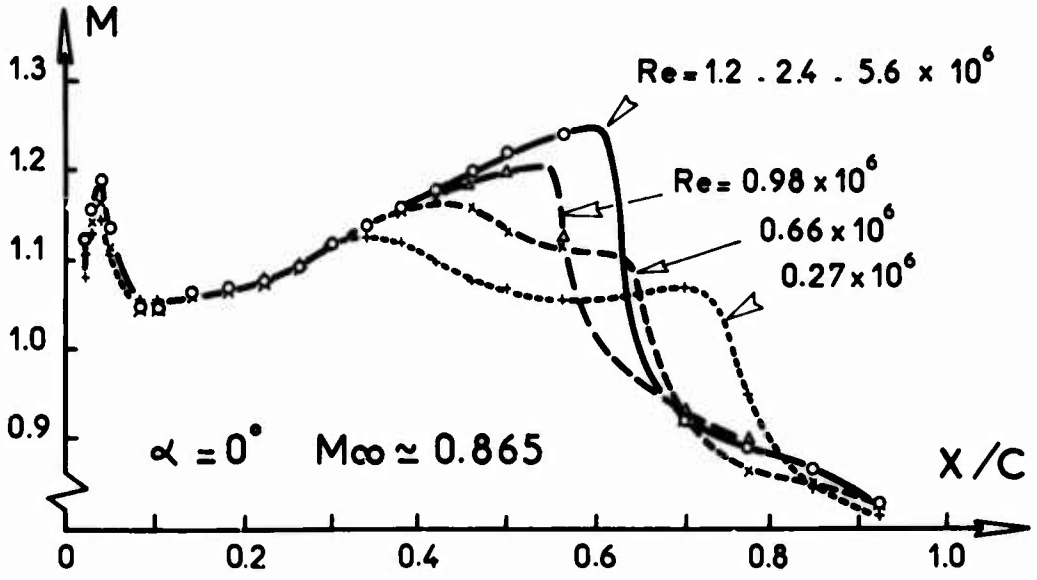

Fig.3-5 Reynolds number effect on a symmetrical peaky airfoil pressure distribution at 0 degree angle of attack

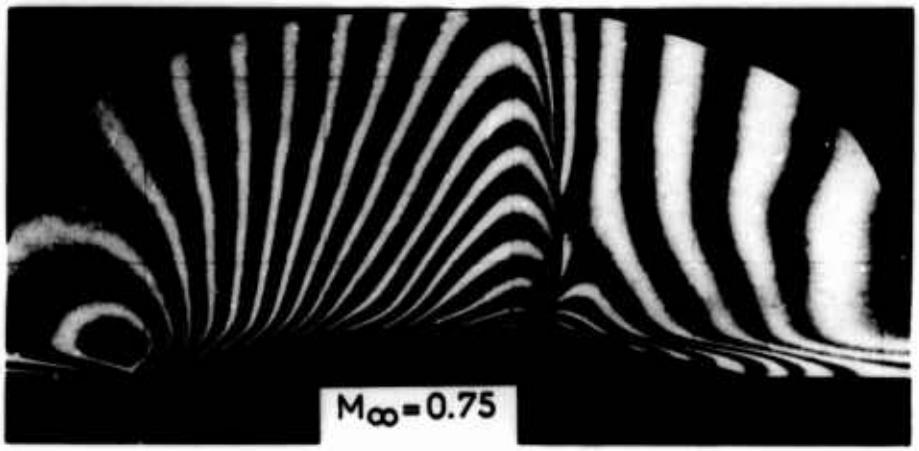

Photograph by ONERA

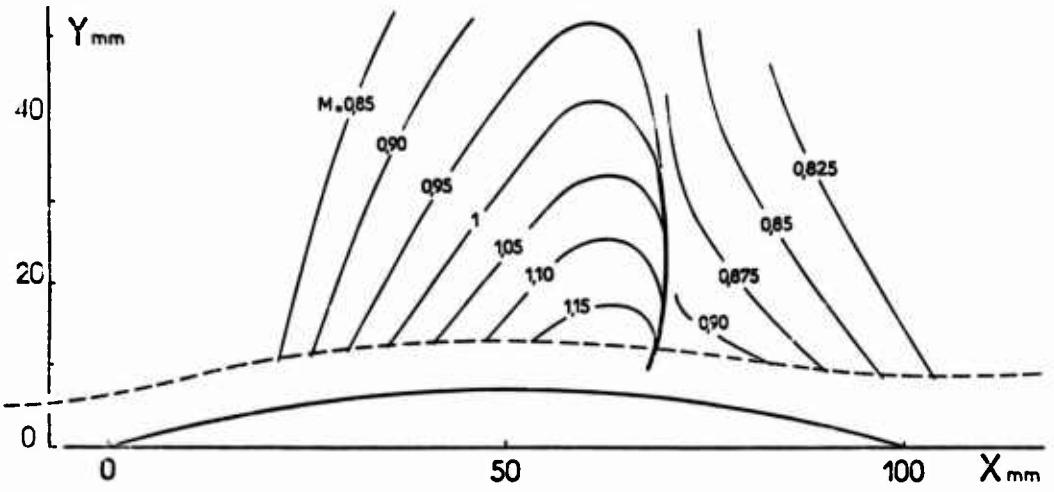

Isomach lines

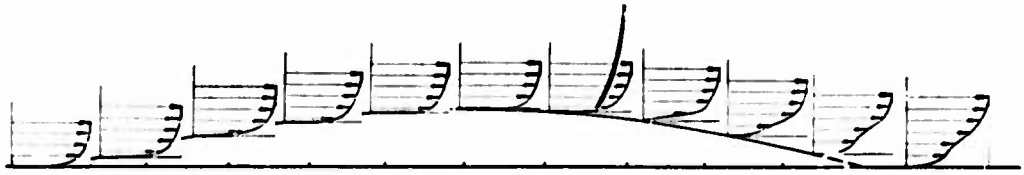

Boundary layer profile

Fig.3-6 Shock boundary layer fundamental study by means of quantitative use of interferometer photographs (circular arc shaped wall)

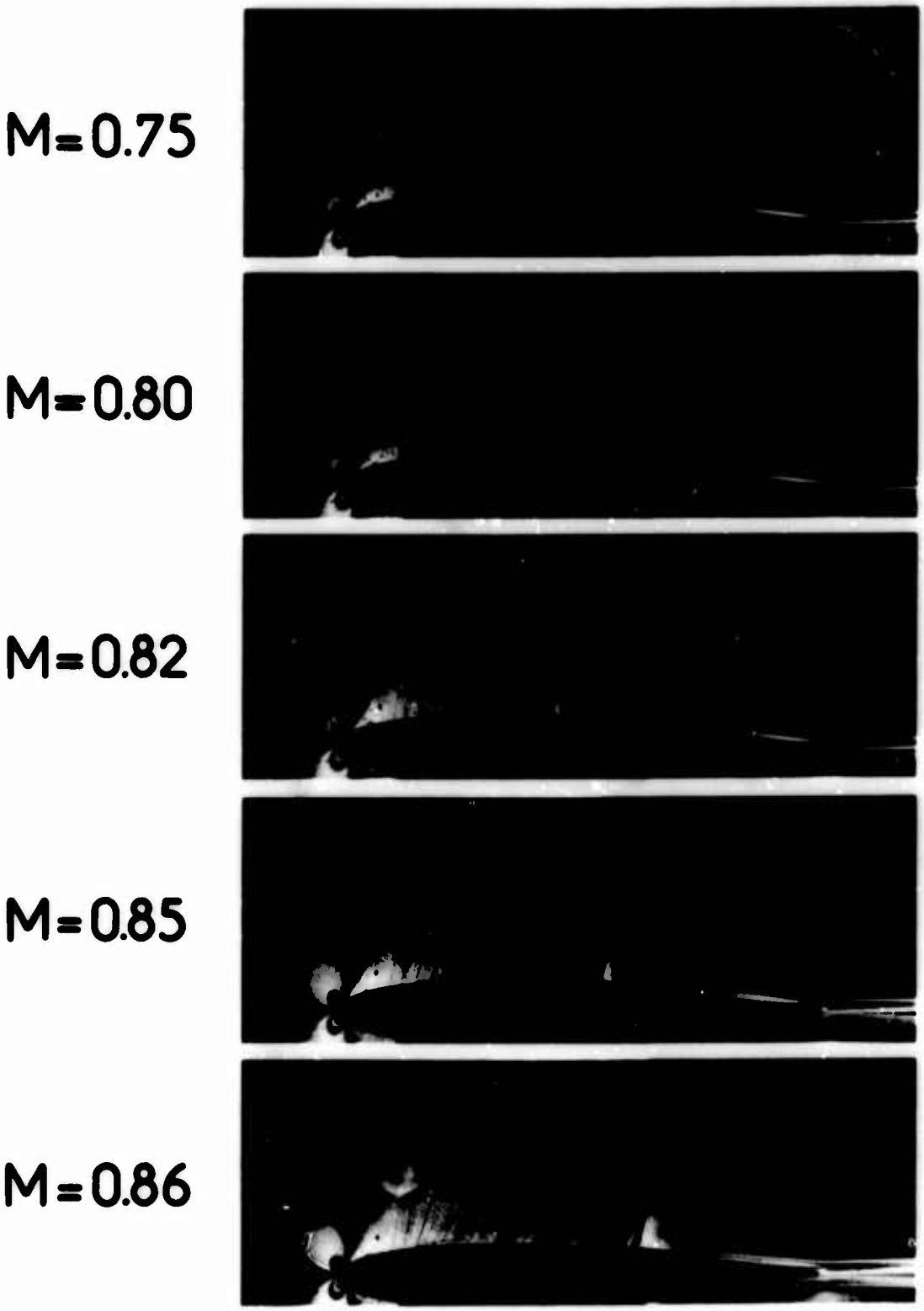

A. NACA 0012 airfoil , $\alpha = 0°$

Fig.3-7 Schlieren photographs showing the rearward movement of the shock for increasing Mach numbers. Photographs by ONERA.

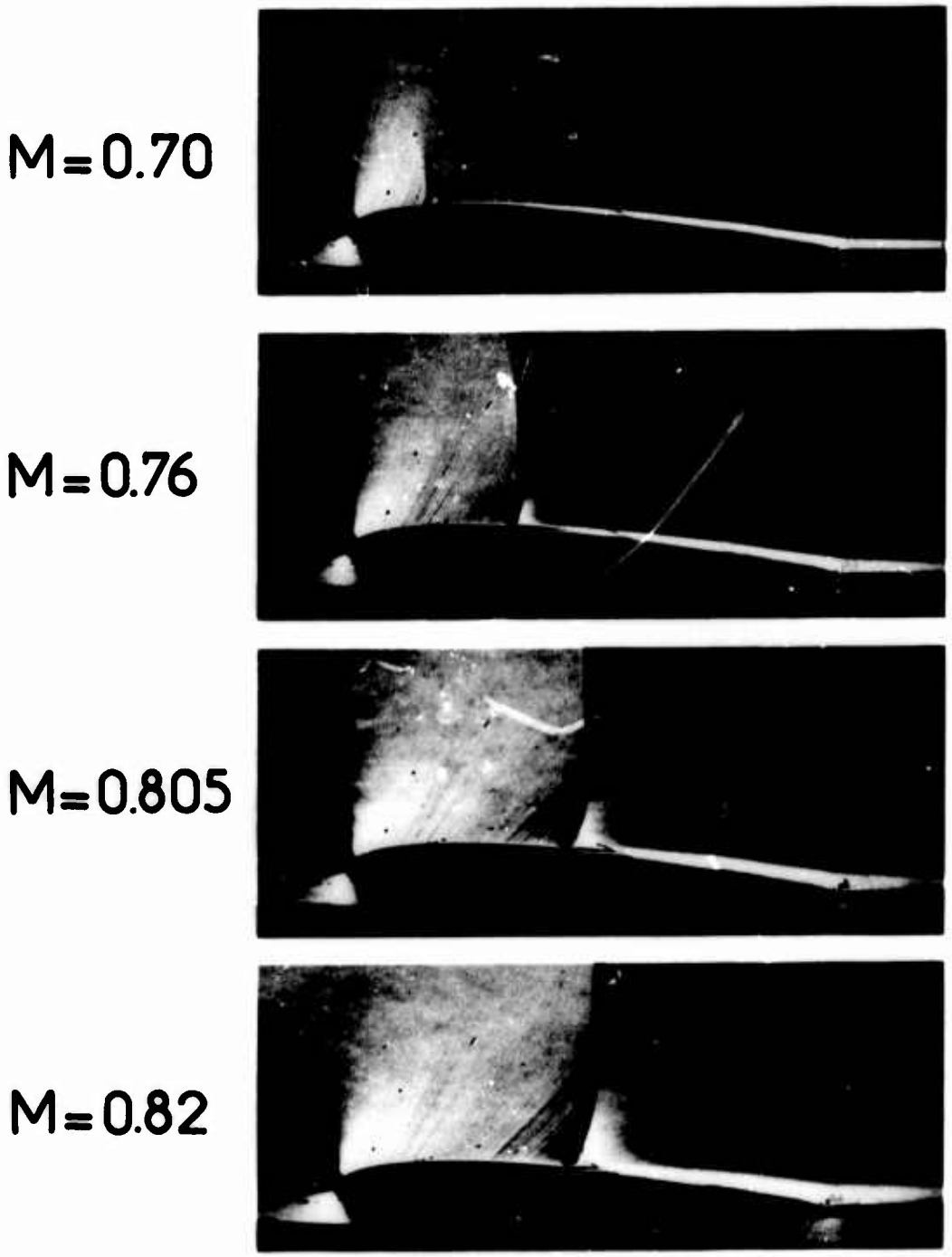

Figure 3-7 (continued). Photographs by ONERA

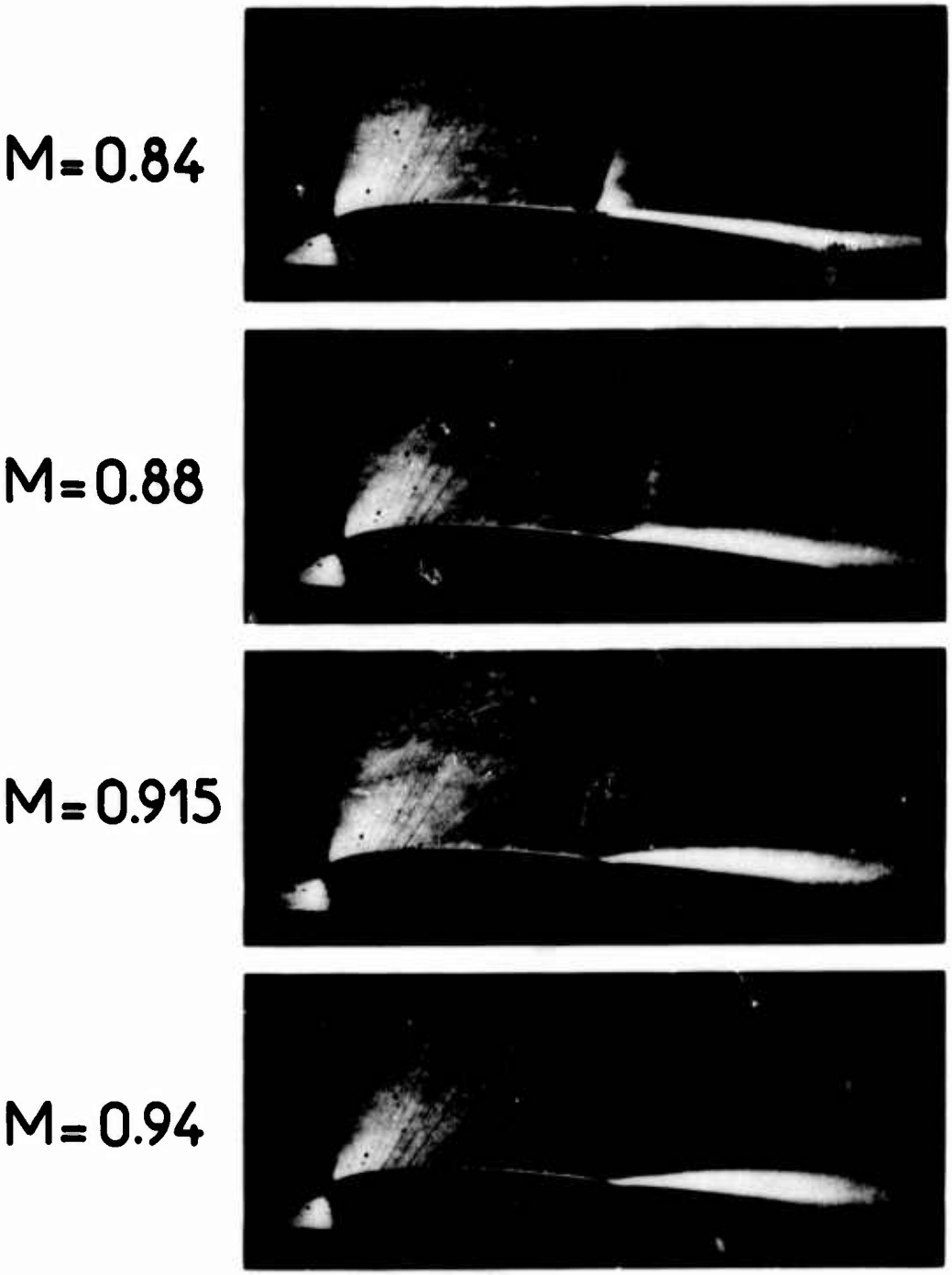

Figure 3-7 (concluded). Photographs by ONERA.

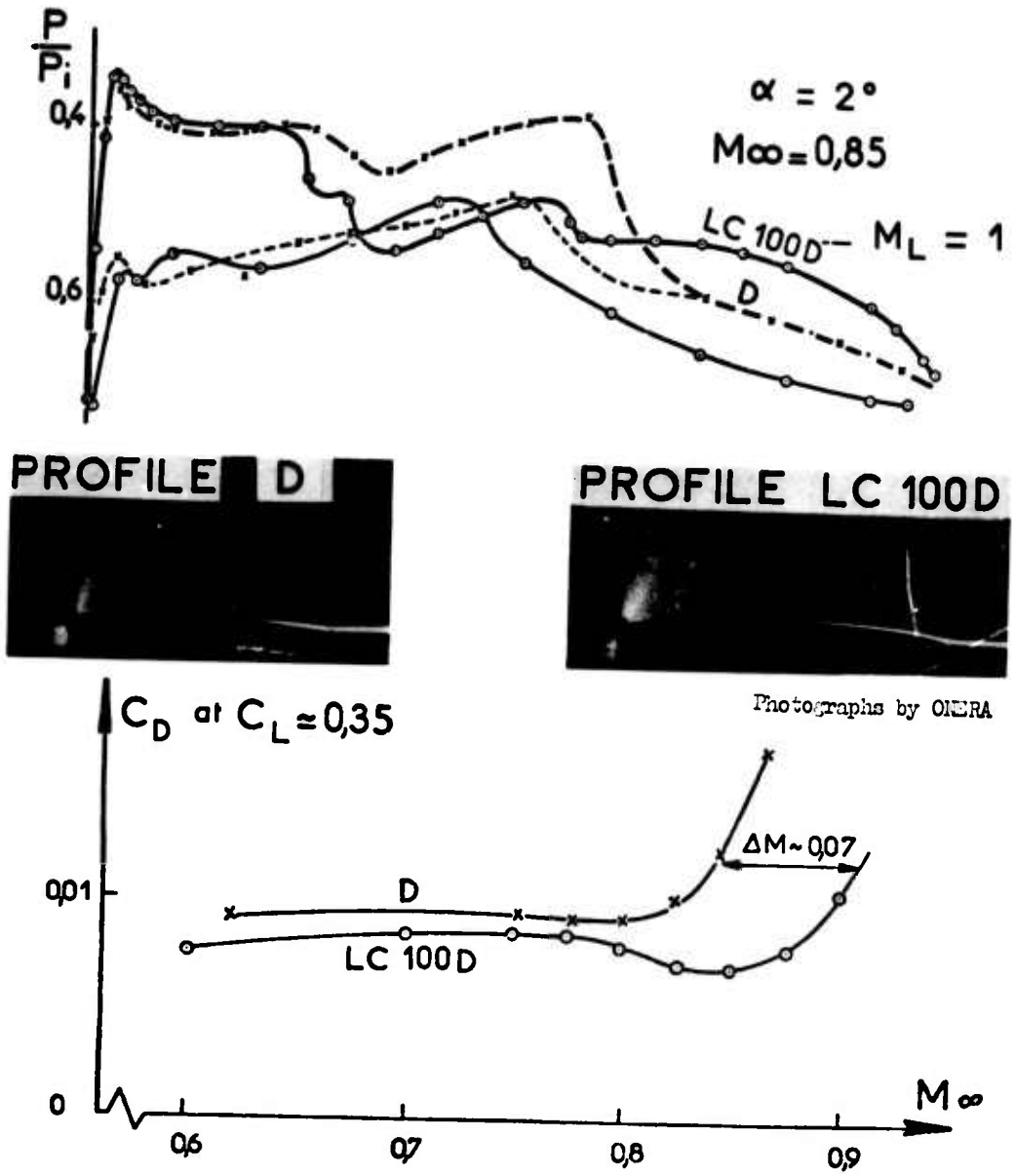

Fig.3-8 Example of drag divergence Mach number increase by use of rear loading. (Profile D is a peaky airfoil profile LC 100 D is a cambered airfoil having the thickness law of profile D)

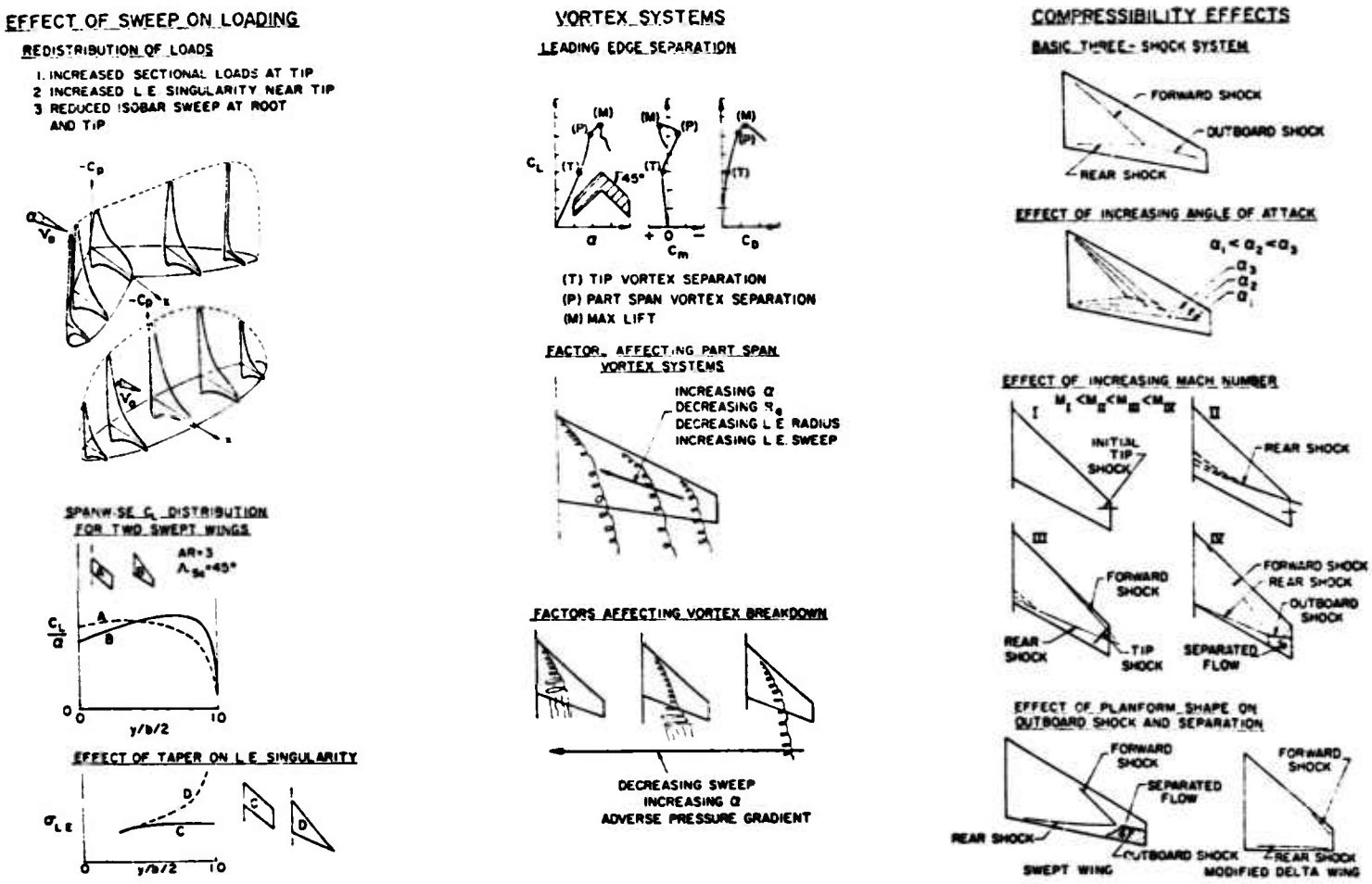

Fig.3-9 Three-dimensional wing characteristics (Ref.3-1)

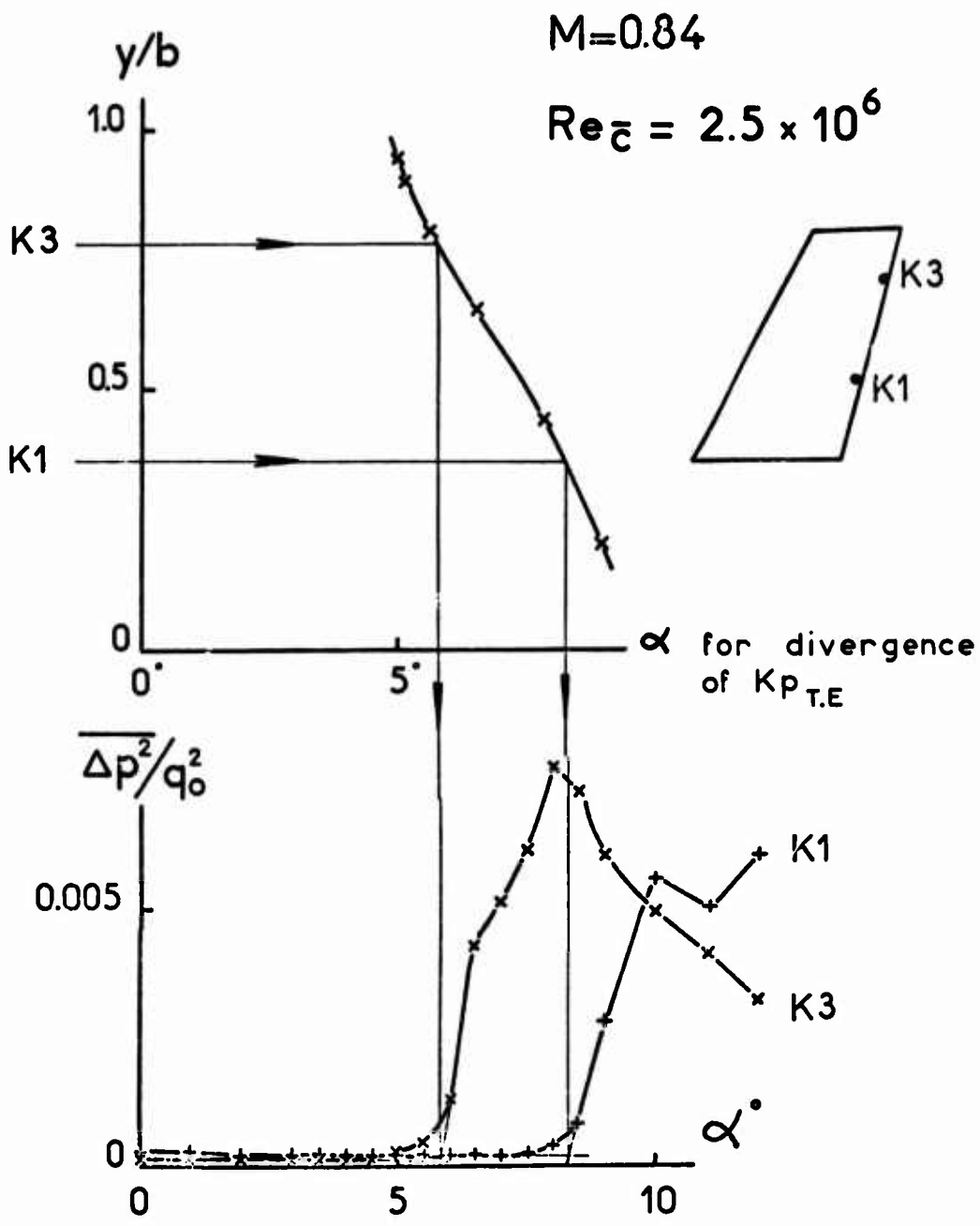

Fig.3-10 Correlation between static pressure divergence and increases in pressure fluctuations

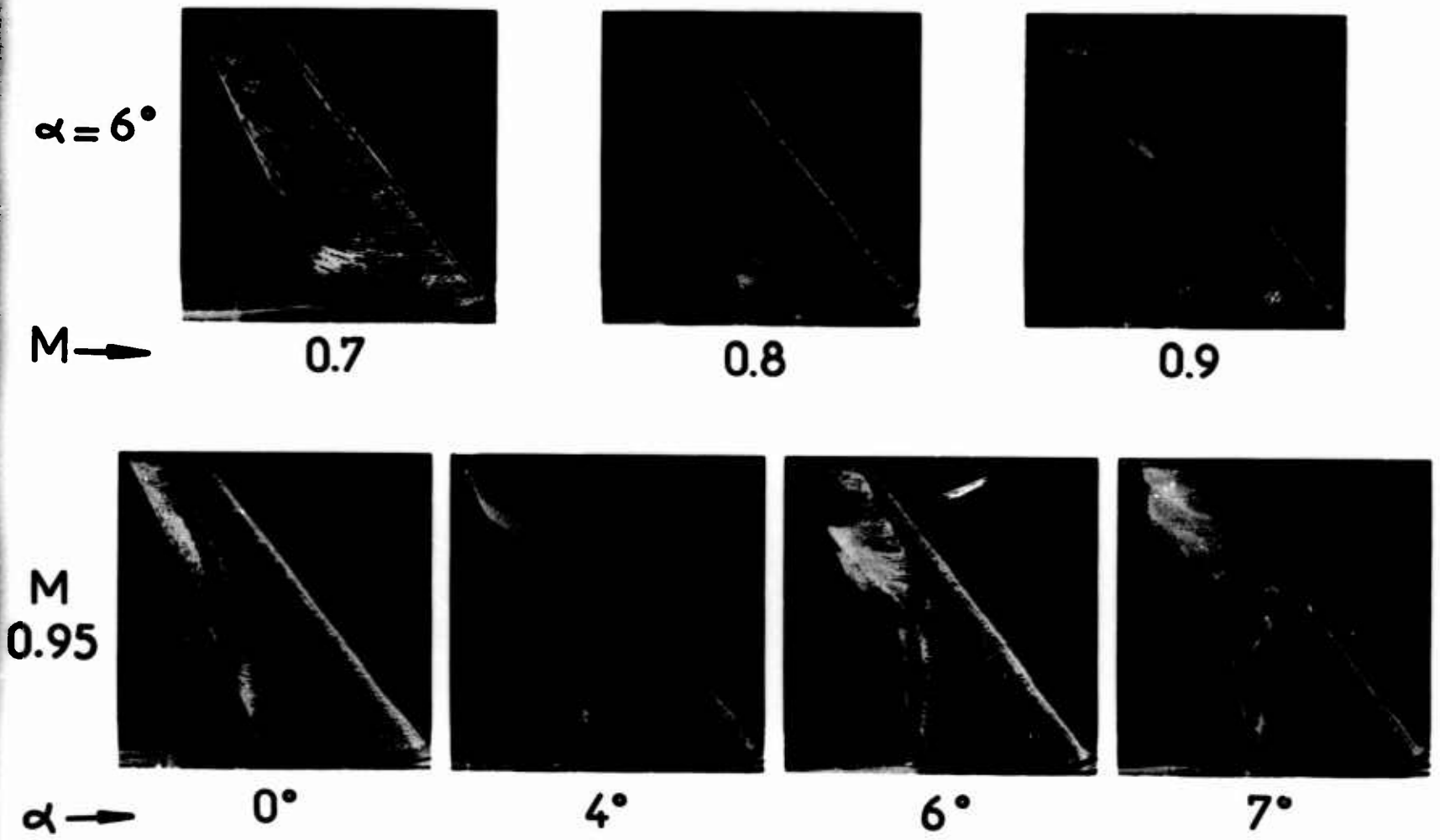

Fig.3-11a Oil flow photographs (wing sweep angle 35 degrees, wing aspect ratio 4.8). Photographs by DFVLR

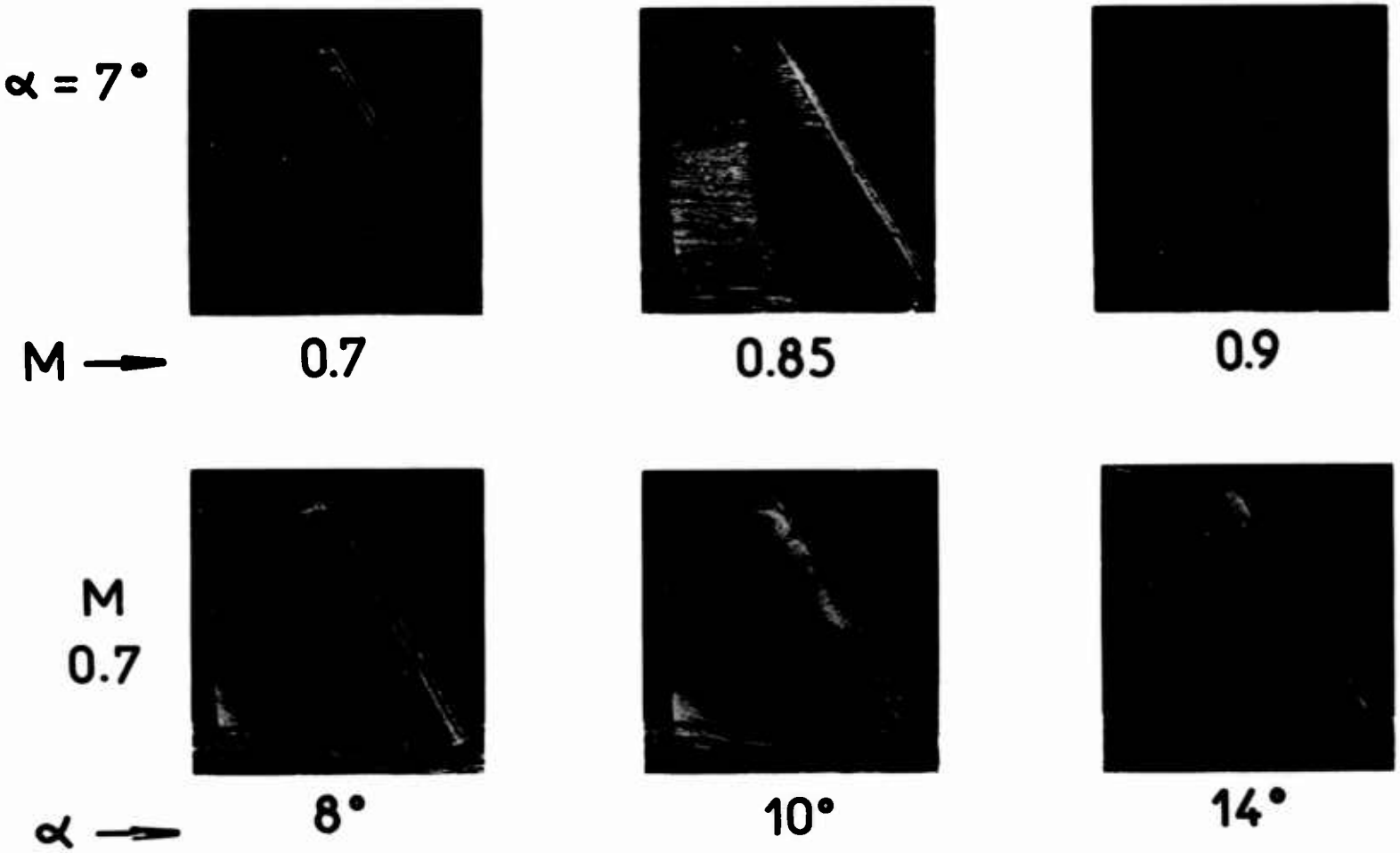

Fig.3-11b Oil flow photographs (wing sweep angle 25 degrees, wing aspect ratio 3). Photographs by DFVLR

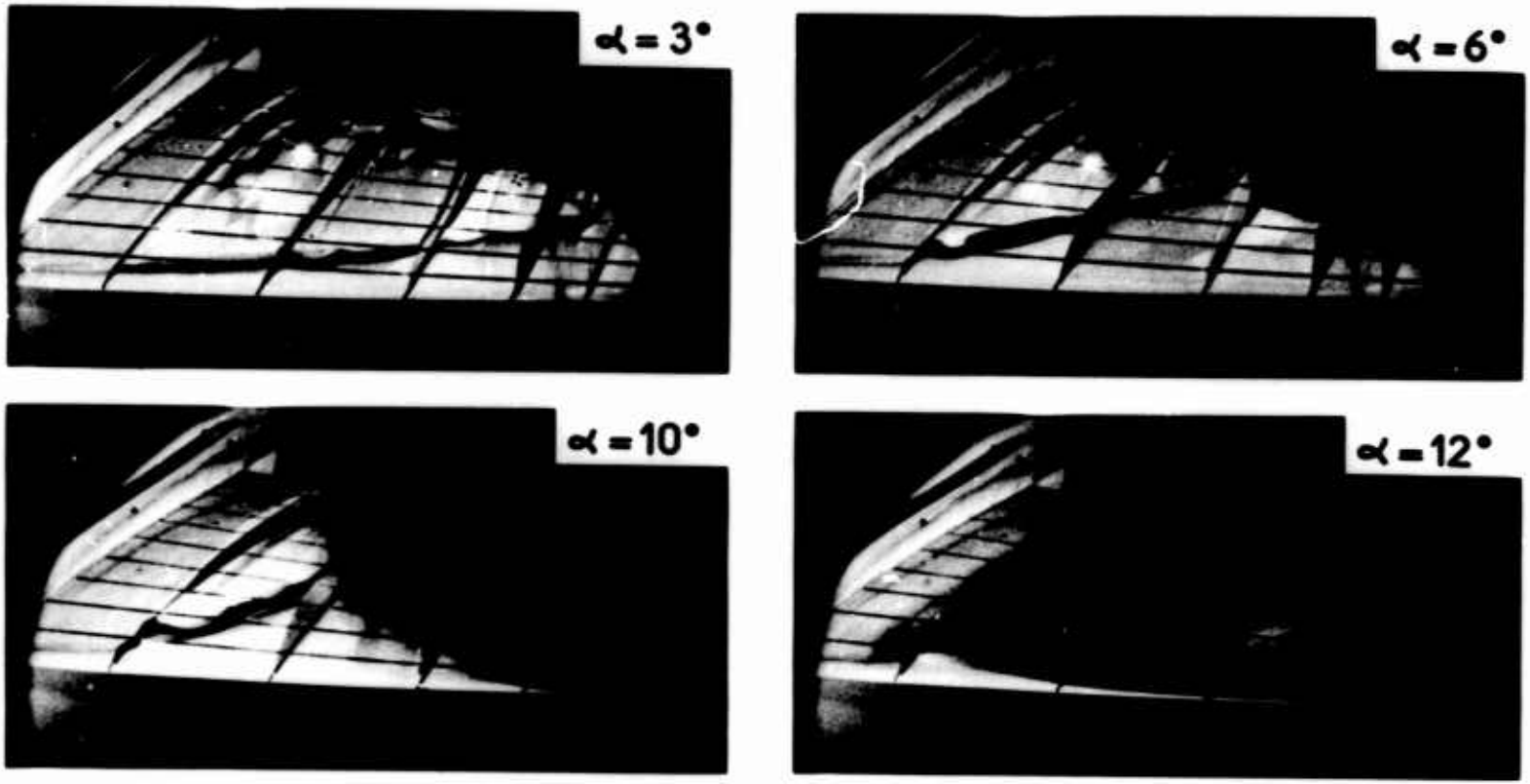

Fig.3-12 Surface flow vizualizations (wing sweep angle 30 degrees, wing aspect ratio 3.8). Photographs by ONERA.

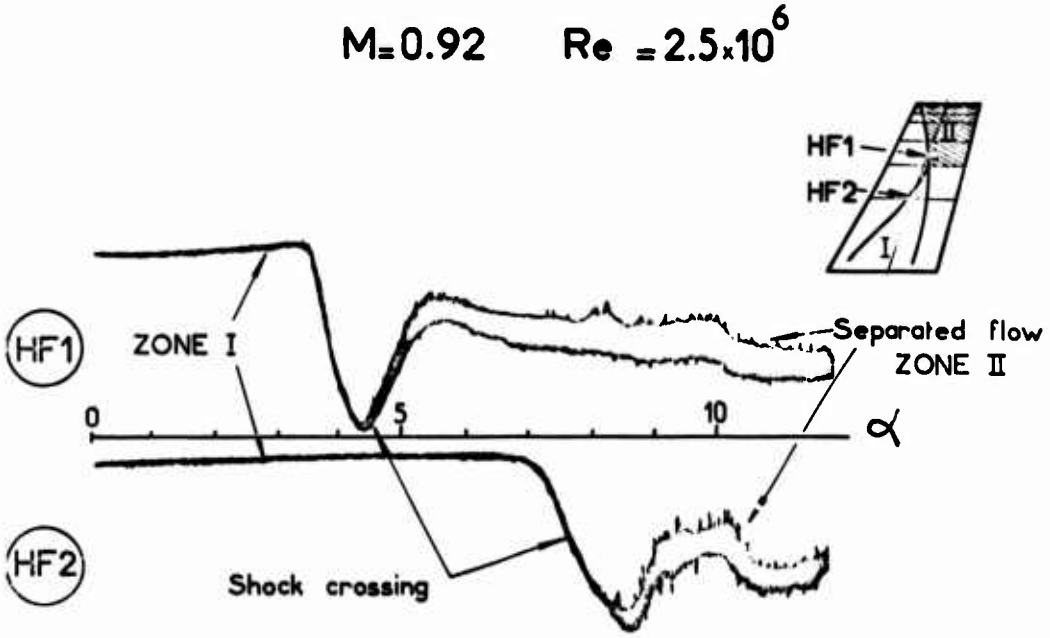

Fig.3-13 Evolution of hot film signals with wing angle of attack

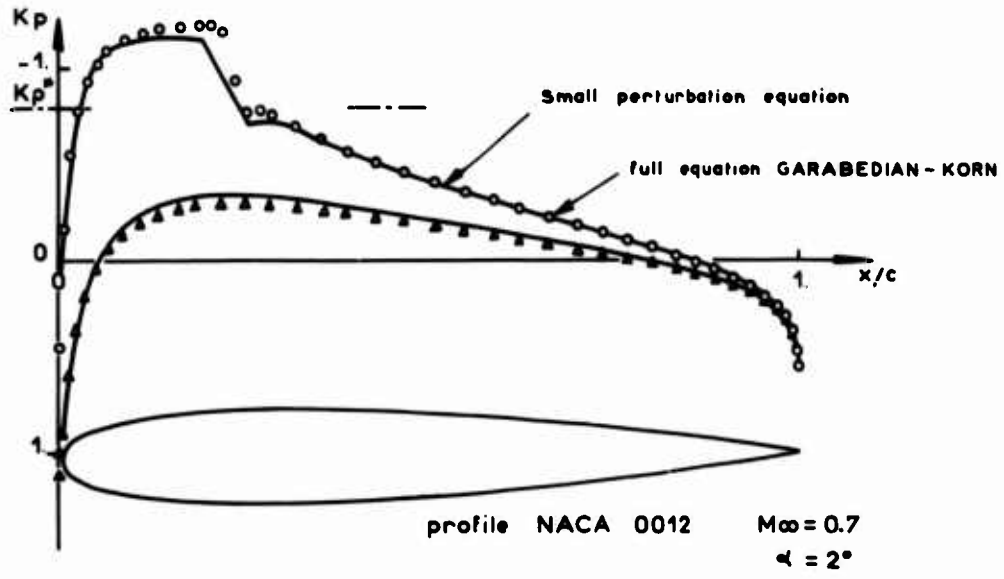

Fig.3-14 Comparison between the small perturbation method and the GARABEDIAN-KORN method

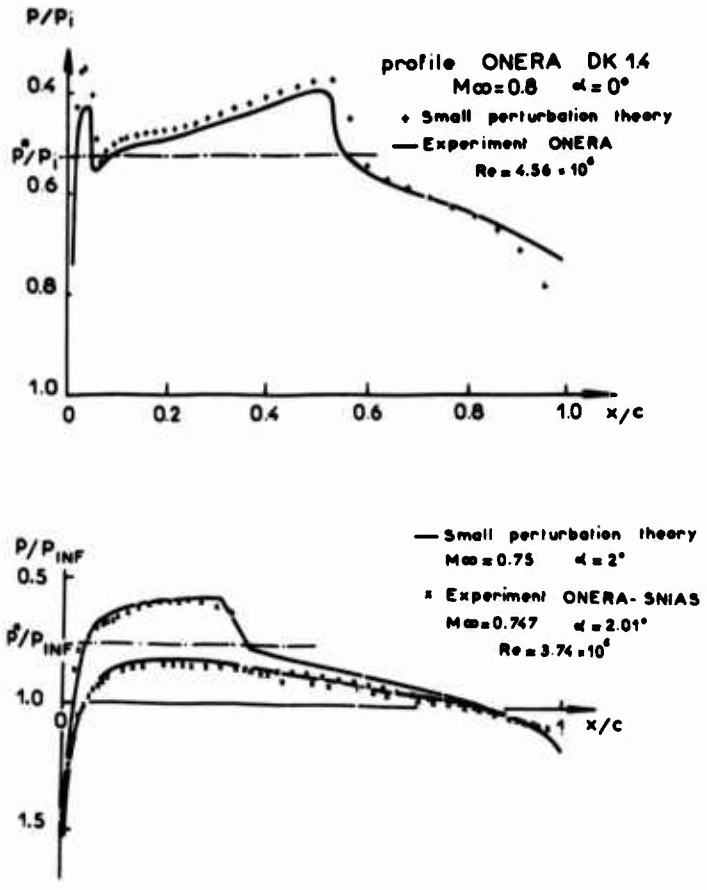

Fig.3-15 Comparison between experimental results and the transonic small perturbation method

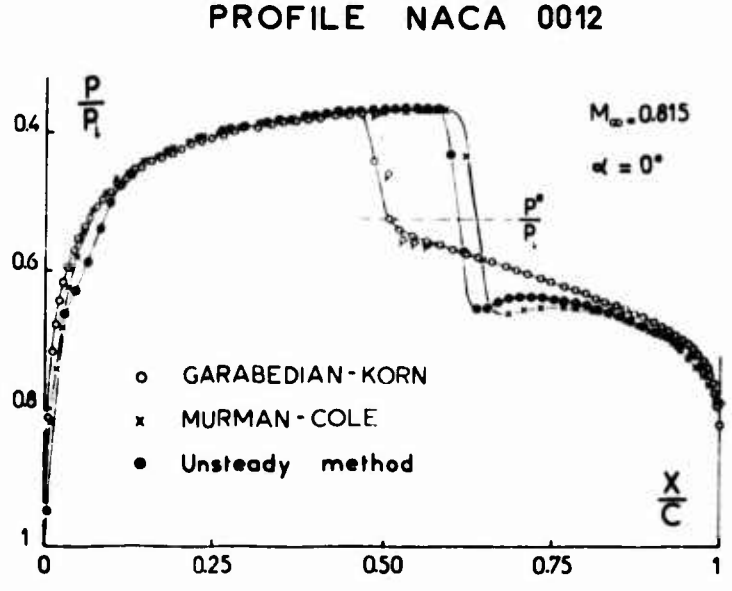

Fig.3-16 Small perturbation method results with an improved numerical scheme

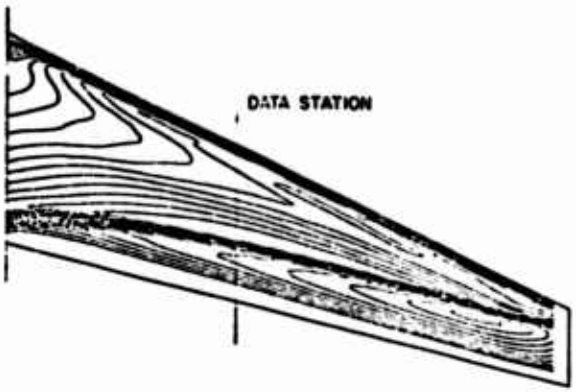

Fig.3-17a Calculated upper surface isobars for simulated C-141 wing at M = 0.825 (ref.3-25)

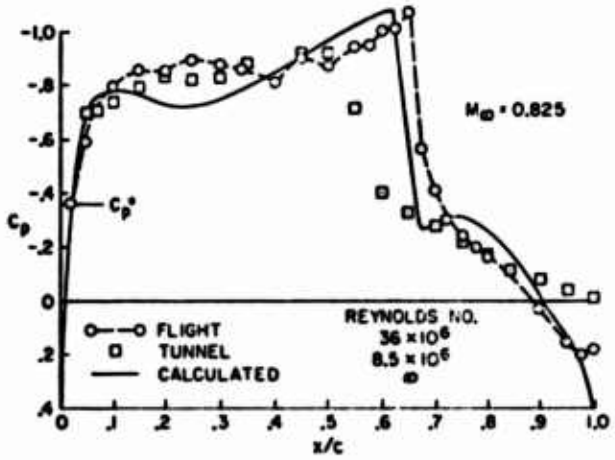

Fig.3-17b Wind tunnel, flight and computed upper surface pressure coefficient distribution for C-141 wing at y/b = 0.4 (Ref.3-25)

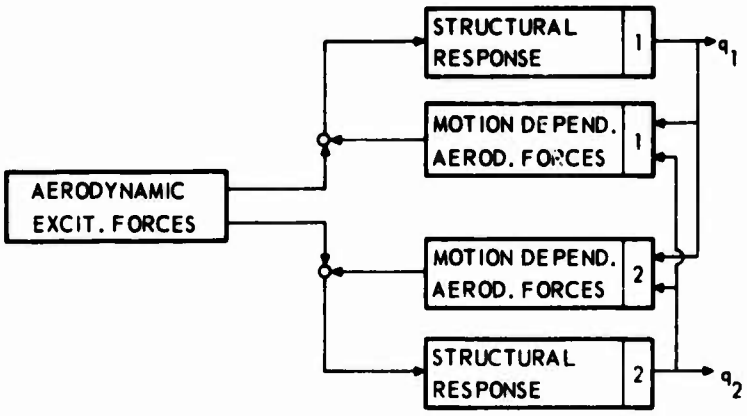

Fig.4-1 Example of dynamic system with two resonance modes as degrees of freedom

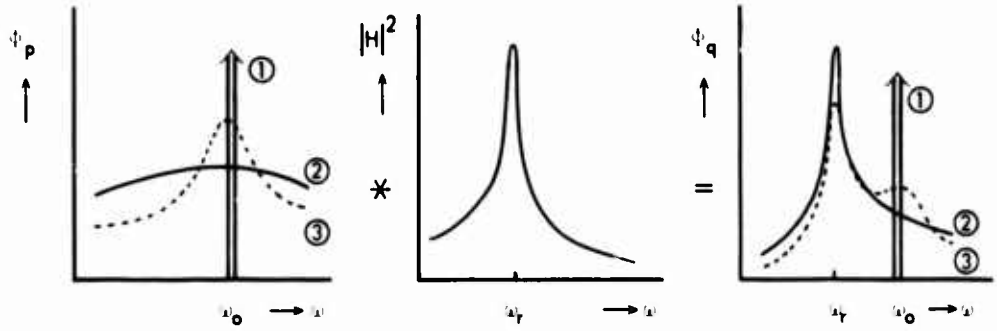

Fig.4-2 Relation between input and output spectrum for structurally responding system

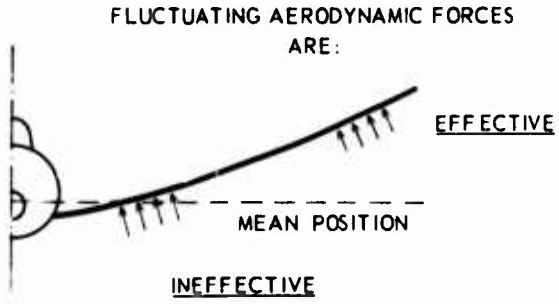

Fig.4-3 Influence of mode shape on generalized aerodynamic force

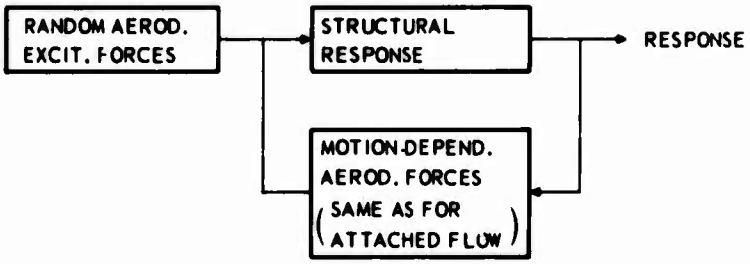

A. STRUCTURAL RESPONSE TO RANDOM AERODYNAMIC EXCITATION

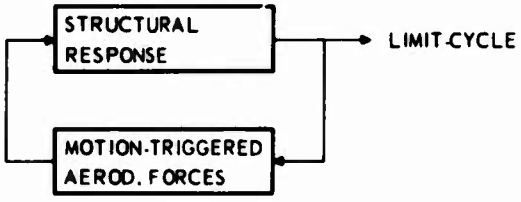

B. BUFFETING FLUTTER

Fig.4-4 Difference between two analytical models

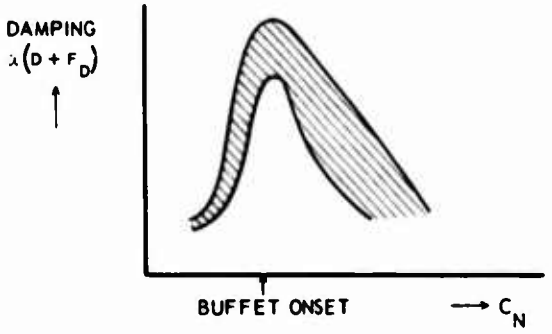

Fig.4-5 Variation of damping of bending mode with C_N. (Ref.4-8)

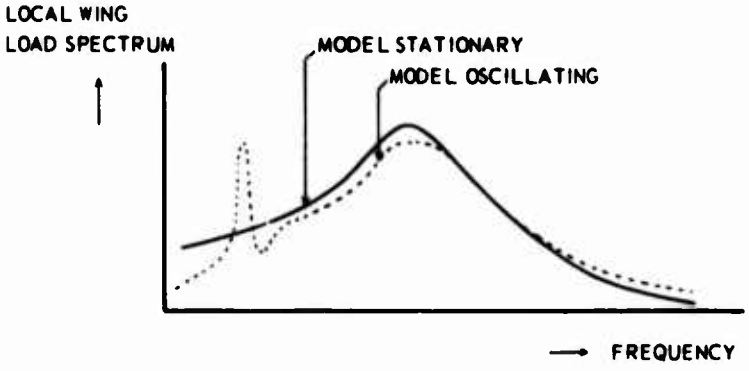

Fig.4-6 Influence of model oscillations on wing load spectrum. (Ref.4-1)

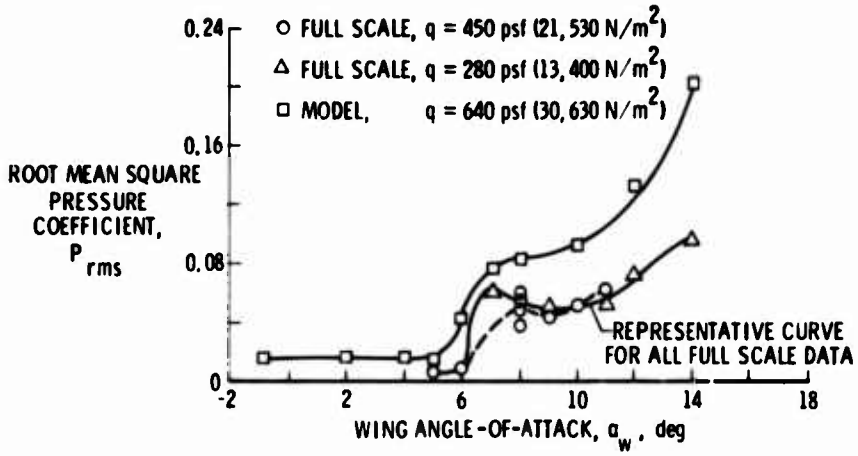

(a) M = 0.9, 90 percent chord, 86 percent semispan.

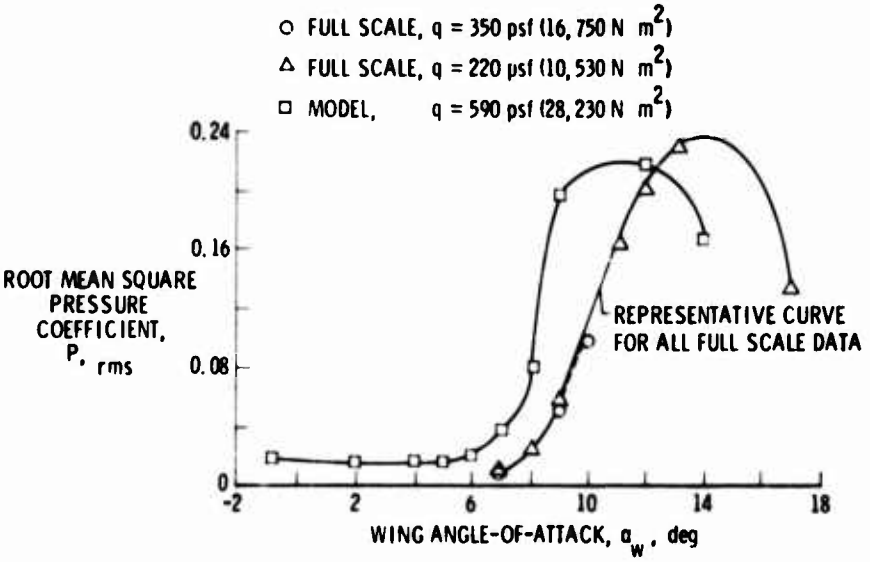

(b) M = 0.8, 90 percent chord, 78 percent span.

Fig.4-7 Comparison of model and full-scale rms pressure coefficient variation with angle of attack. (Ref.4-19)

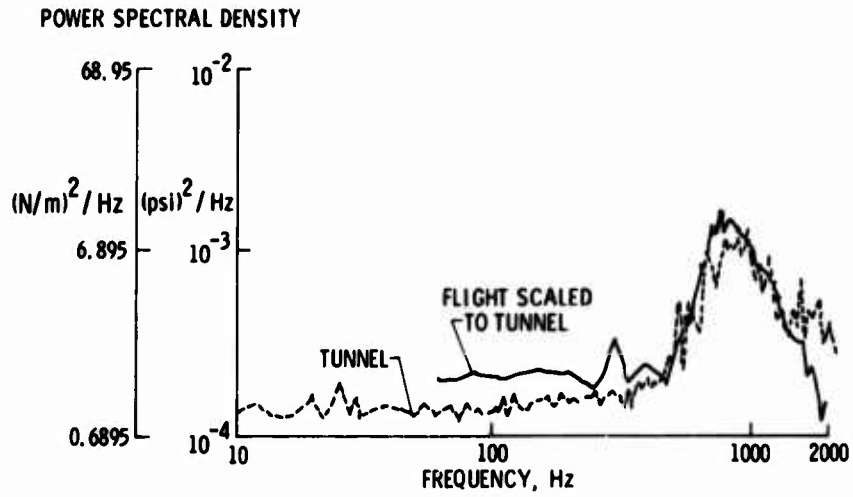

Fig.4-8 Comparison of model and full-scale pressure spectral shape (Mach 0.85, wing angle of attack 10 deg., transducer 18). (Ref.4-19)

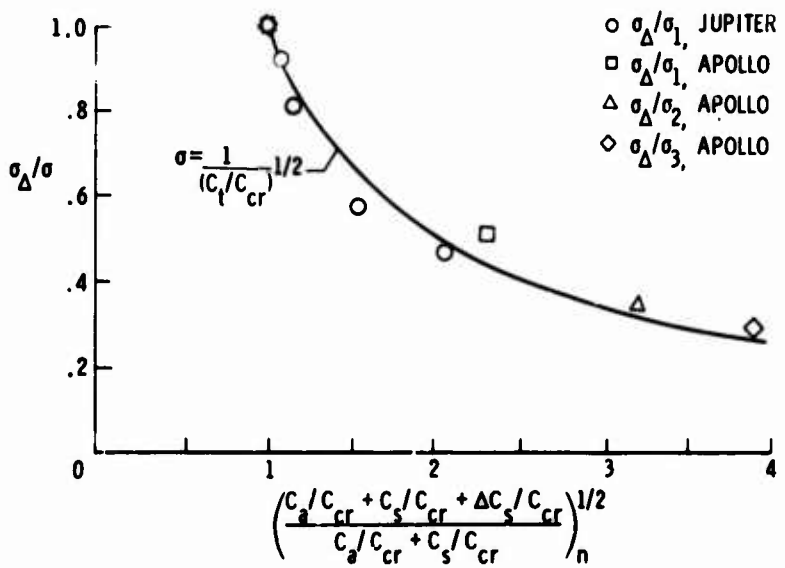

Fig.4-9 Effect of increase in structural damping on model buffet response at M = 0.9, angle of attack 0 deg. (Ref.4-26)

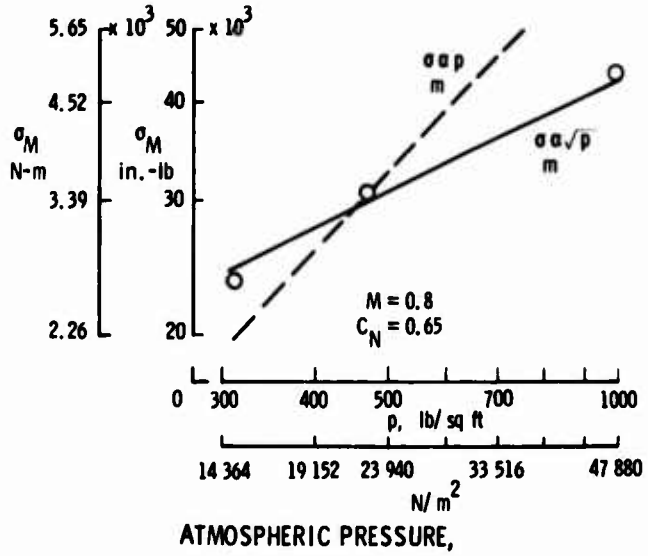

Fig.4-10 Variation of buffet loads with altitude (Ref.4-24)

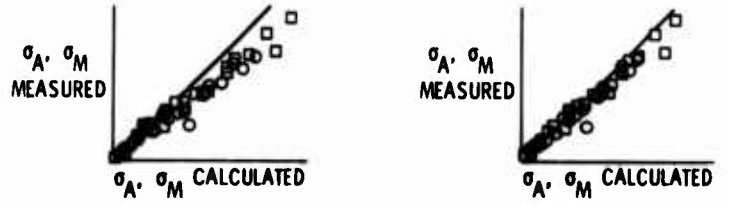

(a) Aerodynamic and structural damping.

(b) Aerodynamic damping only.

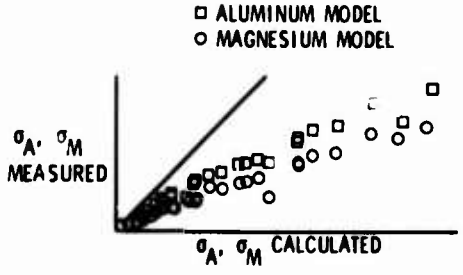

(c) Structural damping only.

Fig.4-11 Comparison of measured and calculated roots-mean-square bending moments (Ref.4-26)

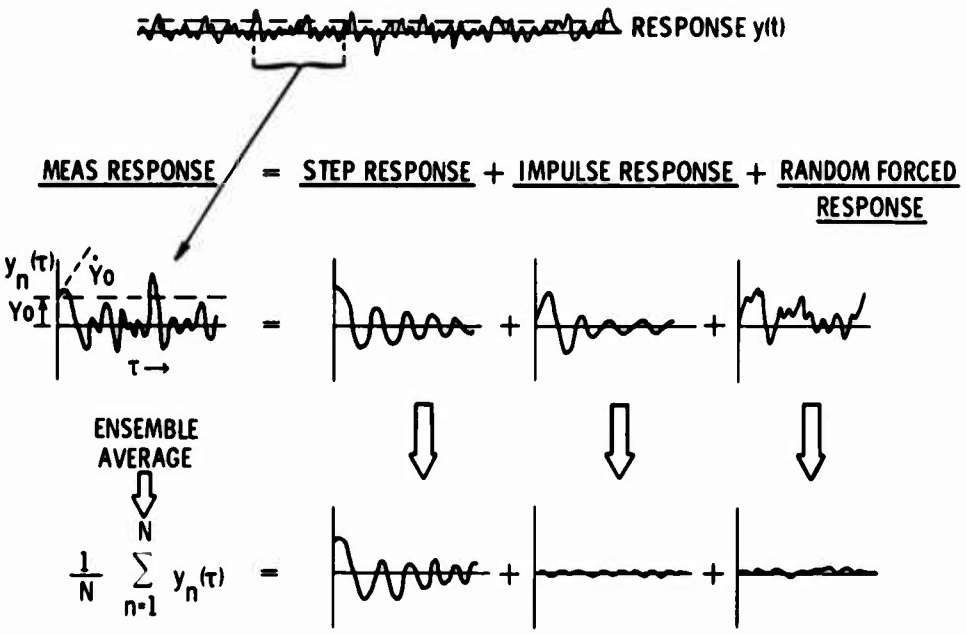

(a) Basic concept.

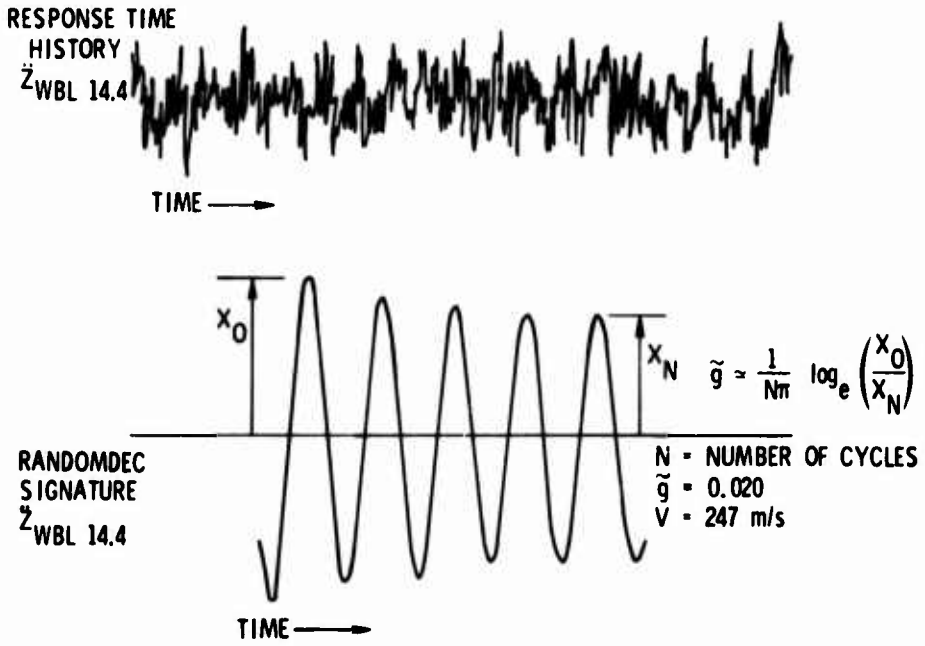

(b) Example of application.

Fig.4-12 Random-dec technique for determining damping (Ref.4-33)

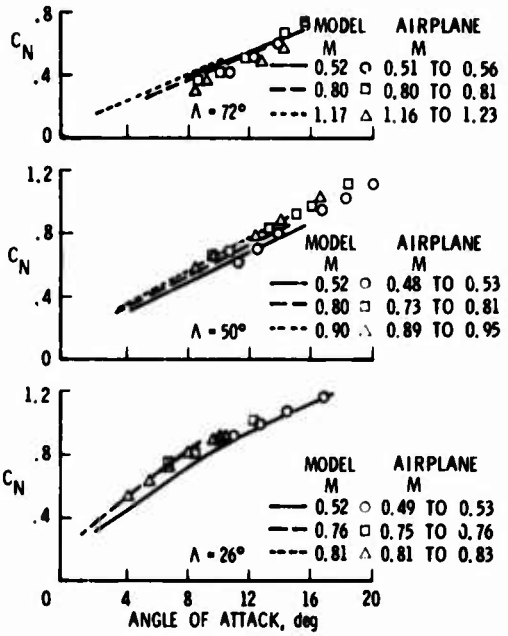

Fig.4-13 Comparison of model and airplane C_N variation with angle of attack (Ref.4-39)

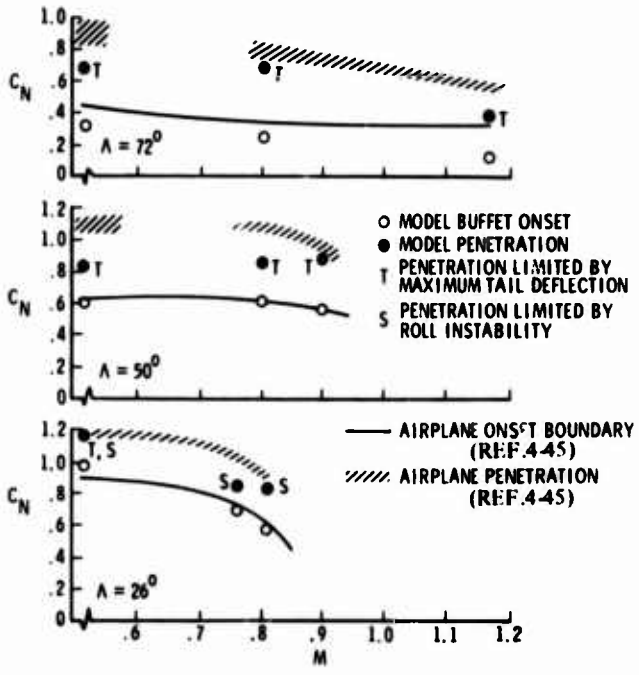

Fig.4-14 Comparison of model and airplane buffet onset and boundary penetration (Ref.4-39)

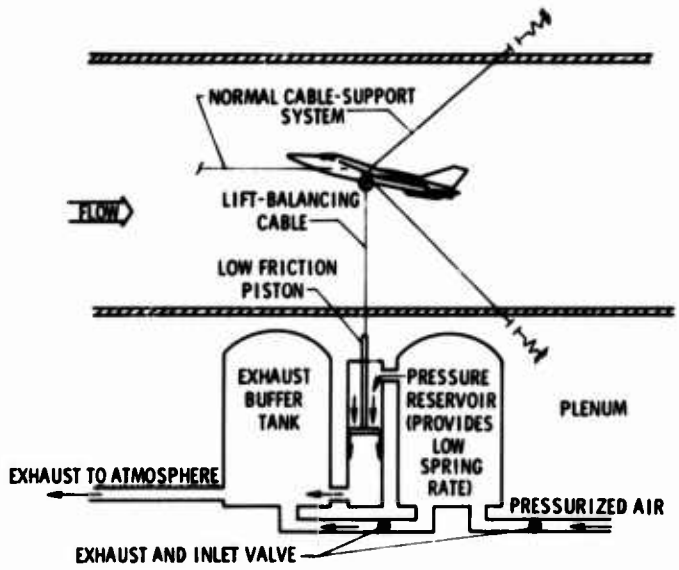

Fig.4-15 Lift-balancing device for testing models at high load factors (Ref.4-39)

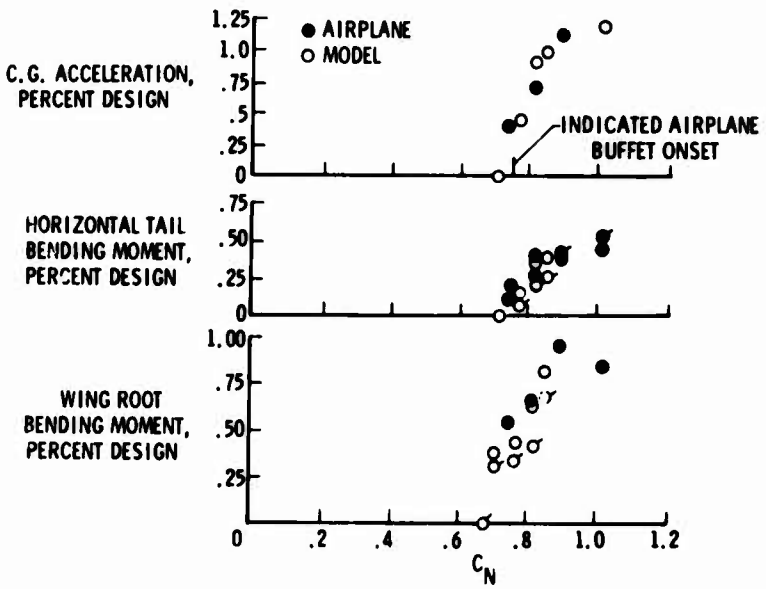

(a) $M_M = 0.76$; $M_A = 0.76$ to 0.75; 26° wing sweep.

Fig.4-16 (a) Comparison of airplane buffet response and buffet response predicted from model data normalized on airplane design loads. (Ref.4-39)

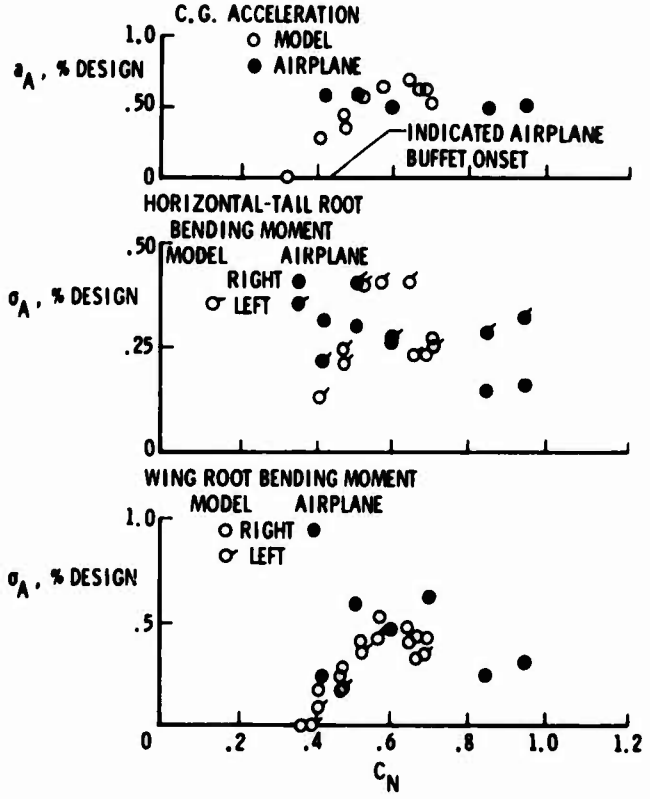

(b) $M_M = 0.52$; $M_A = 0.56$ to 0.51; 72^o wing sweep.

Fig.4-16 (b) Comparison of airplane buffet response and buffet response predicted from model data normalized on airplane design loads. (Ref.4-39)

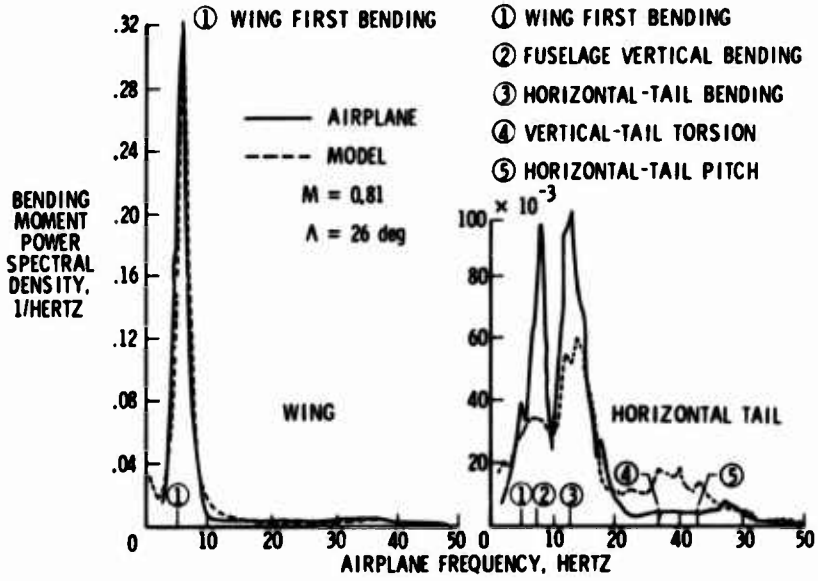

Fig.4-17 Sample comparisons of model and airplane response spectra for wing and horizontal tail. M = 0.81, 26° wing sweep. Spectra normalized on rms level. (Ref.4-39)

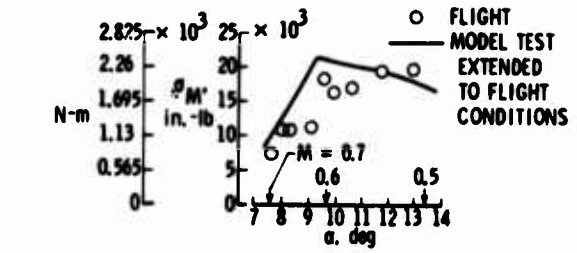

(a) X-3 airplane (Ref.4-24)

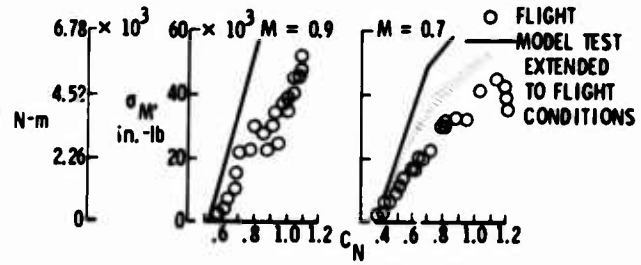

(b) D-558-II airplane (Ref.4-24)

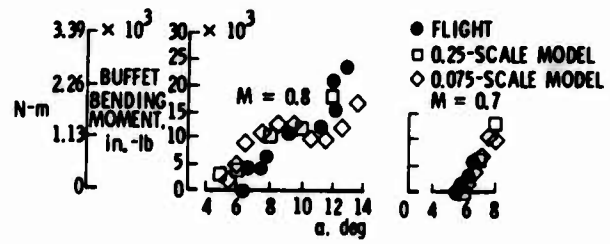

(c) X-1E airplane (Ref.4-47)

Fig.4-18 Comparisons of measured and scaled buffet loads

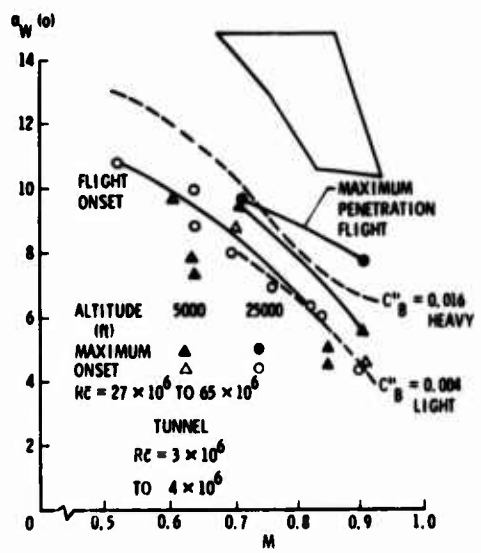

Fig.4-19 Aircraft buffeting penetration boundaries and model buffeting contours. (Ref.4-8)

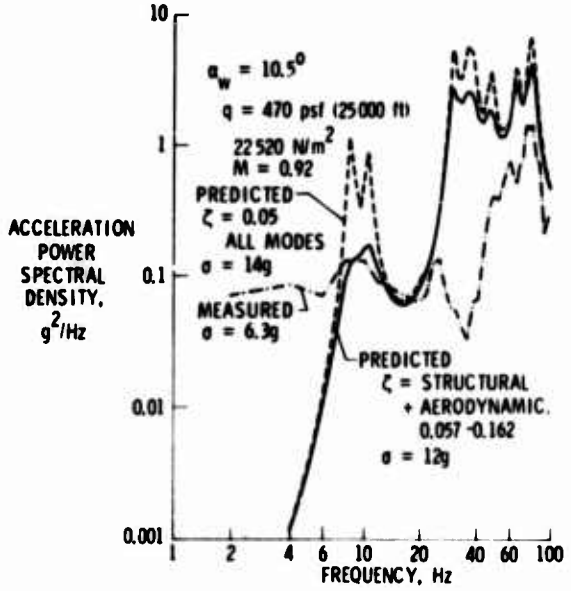

(a) Mach 0.92.

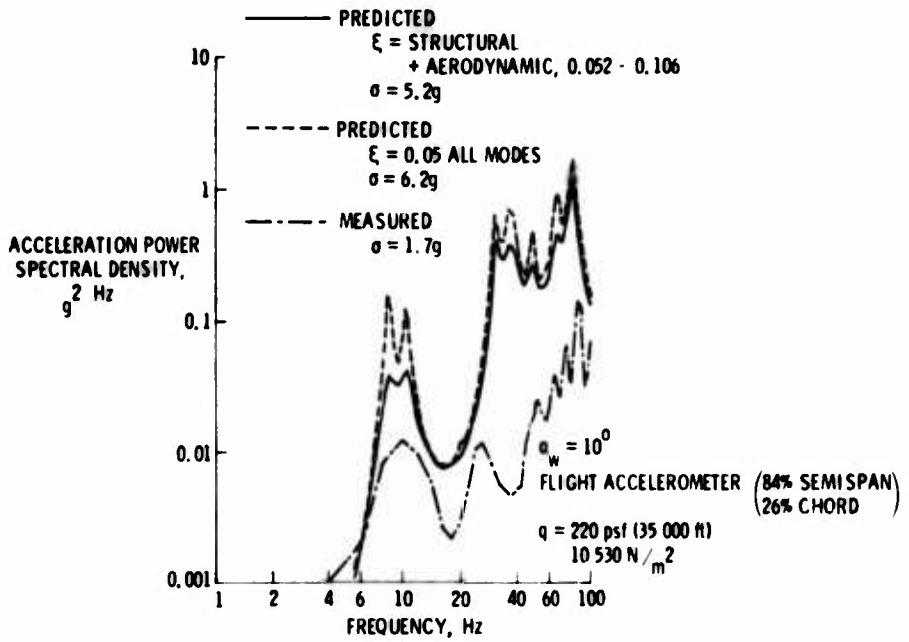

(b) Mach 0.79.

Fig.4-20 Comparison of predicted and measured acceleration response. (Ref.4-48)

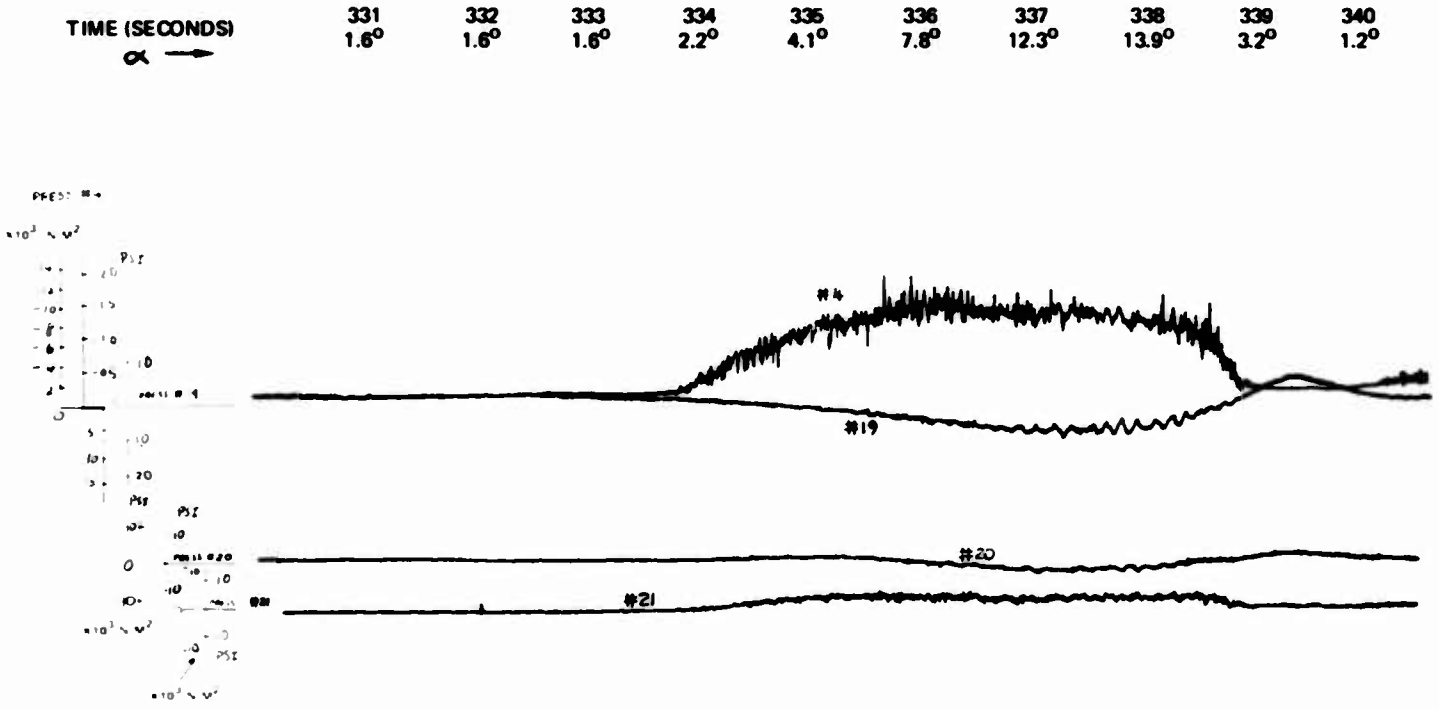

Fig.4-21 Typical wing top and bottom surface pressure histories of flight 825, run 5. $M_o = 0.925$, h = 10,668 m, $\delta_n = 0°$, $\delta_f = 0°$

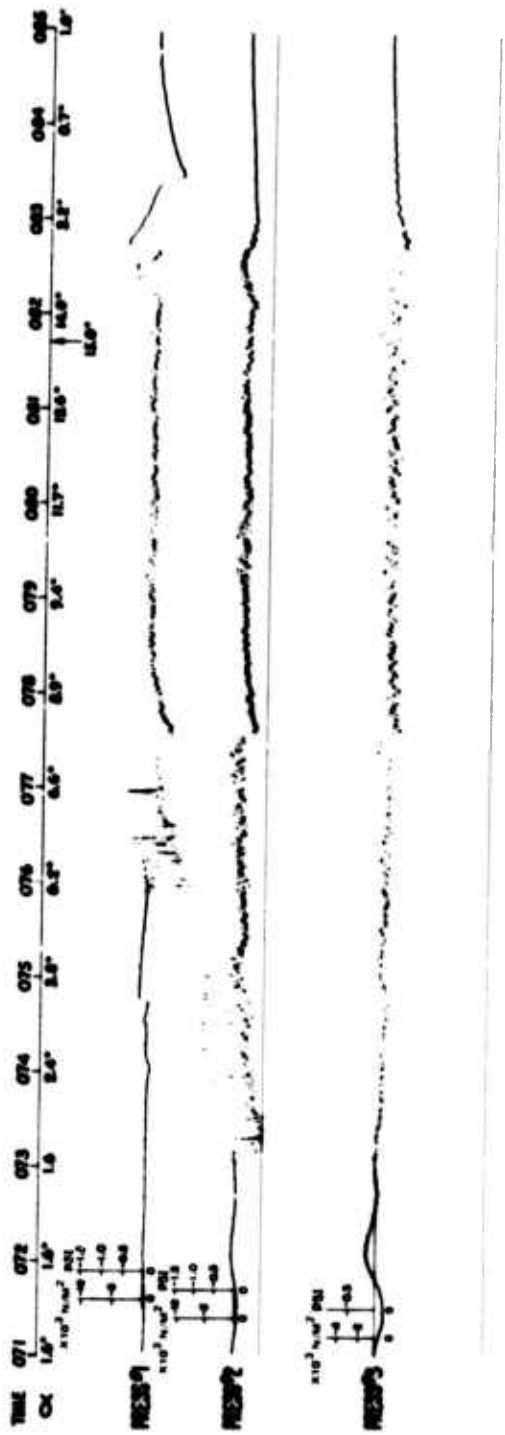

Fig.4-22 Oscillographs of pressure station numbers 1, 2, 3, recorded in run 2, flight 871. $M_o = 0.925$. $h = 10.668$ m. $\delta_n = 4°$. $\delta_f = 12°$

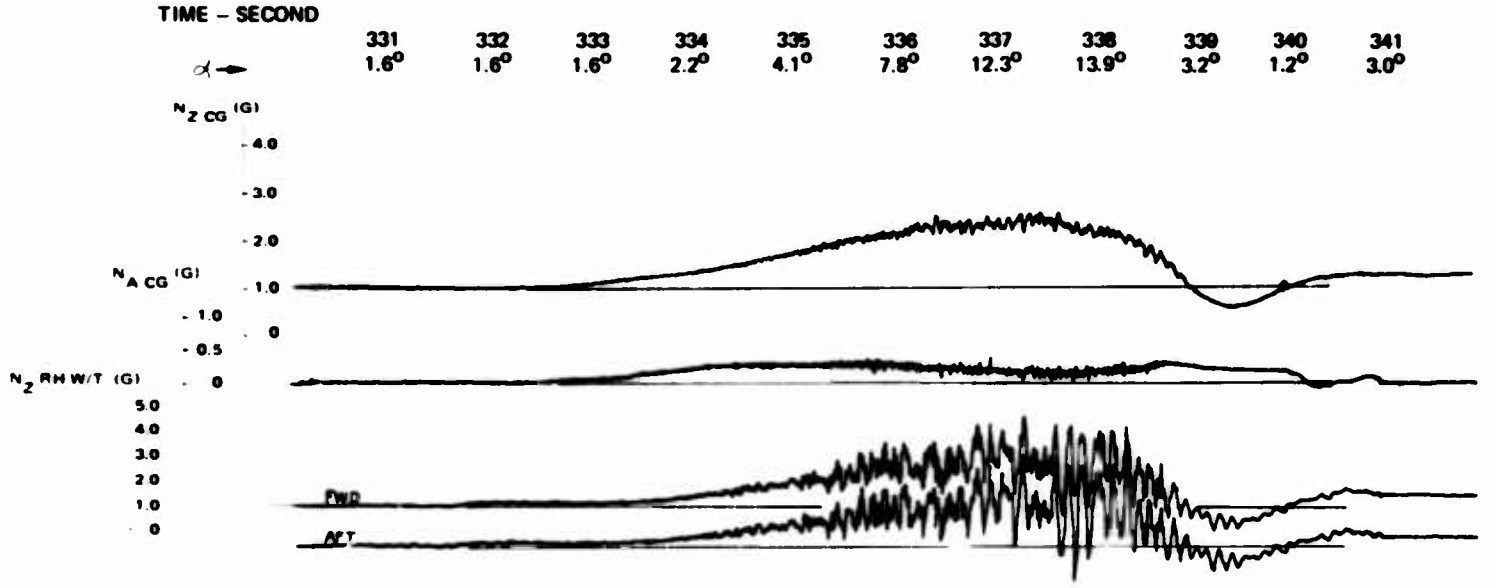

Fig.4-23 CG and right wing tip (forward and aft) acceleration time histories of flight 825, run 5, M_o = 0.925, h = 10,668 m, $\delta_n = 0°$, $\delta_f = 0°$

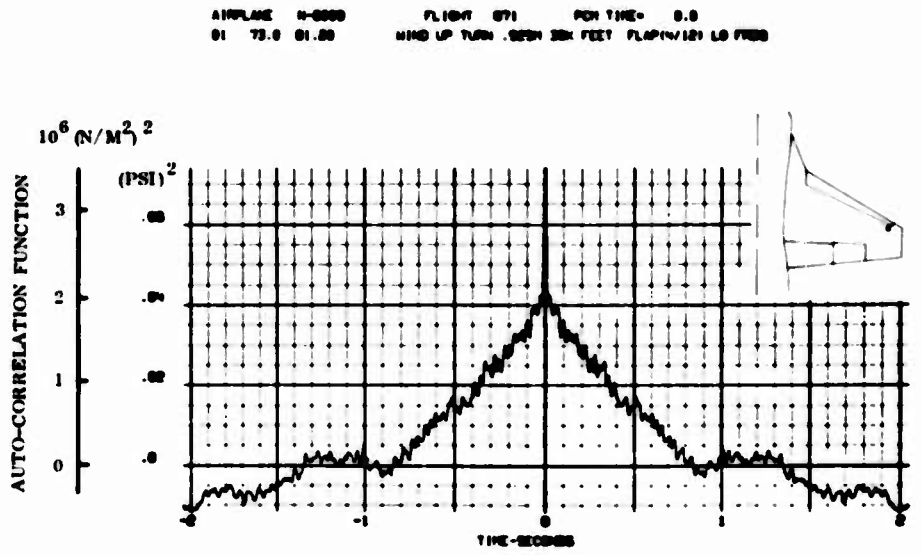

Fig.4-24 Auto correlation function of the dynamic pressure at station no. 1 (85% semi-span, 20% C). M_0 = 0.925, h = 10,778 m

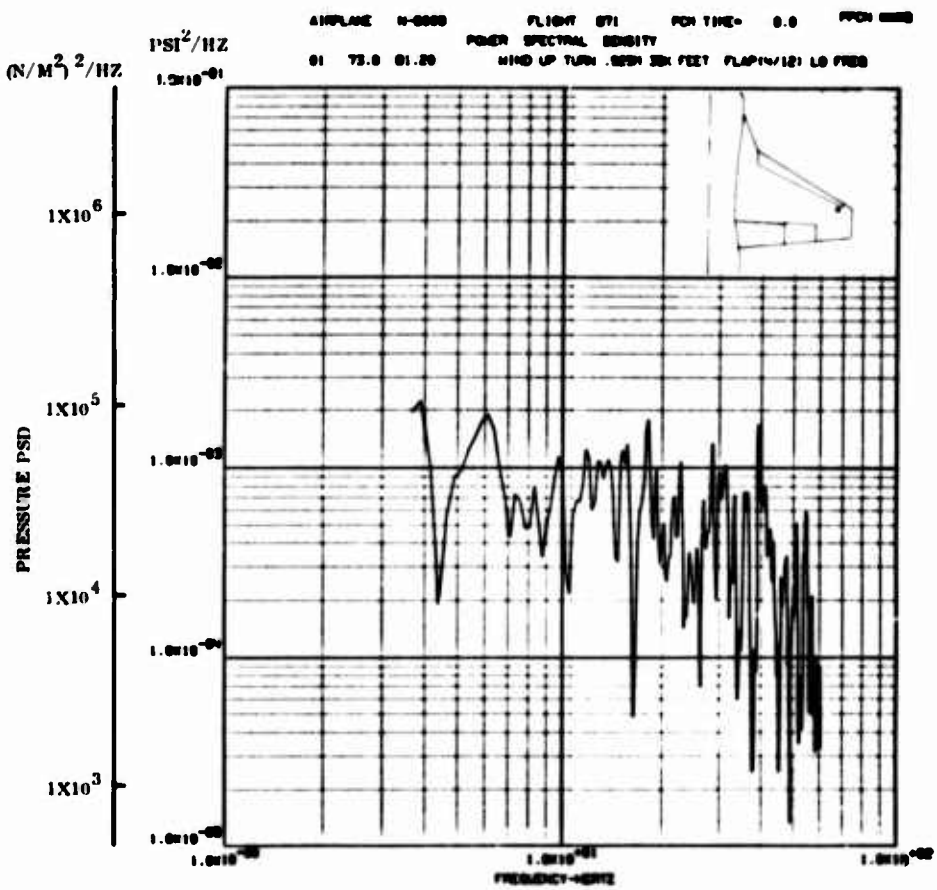

Fig.4-25 PSD function of the dynamic pressure at station no. 1 (85% semi-span, 20% C). M_0 = 0.925, h = 10,778 m

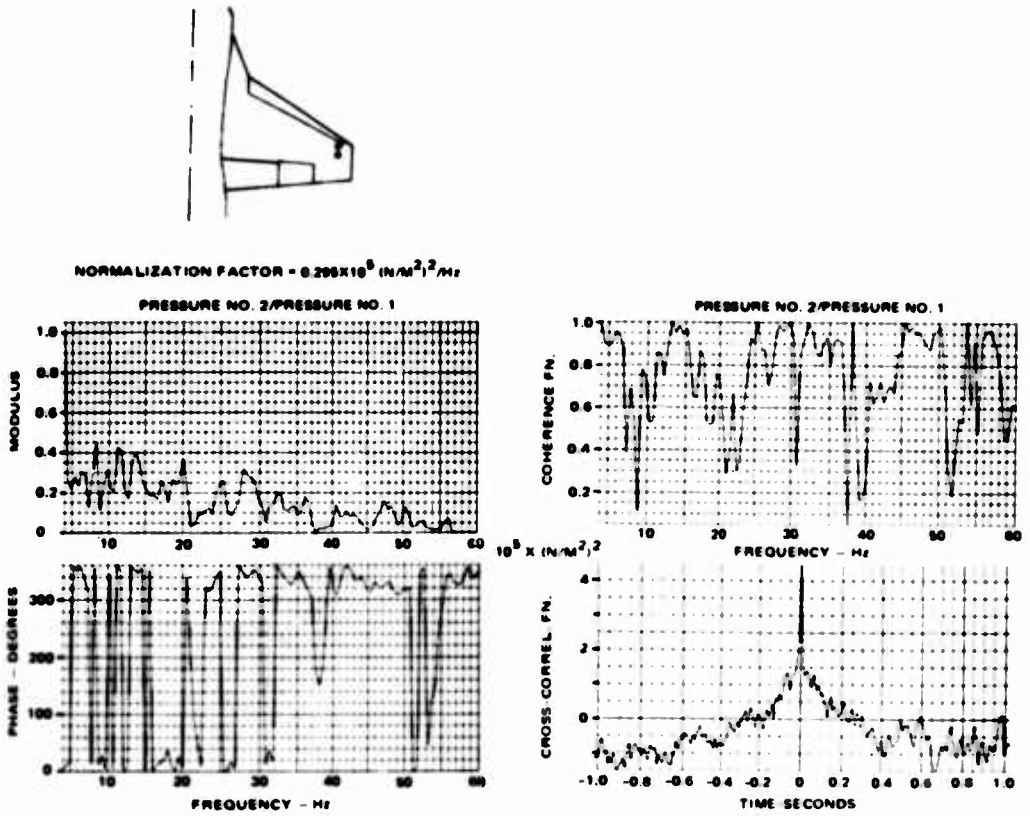

Fig.4-26 Correlation between the pressure transducer pair (1,2). $M_\infty = 0.925$, h = 10,668 m, $\delta_n = 4°$, $\delta_f = 12°$

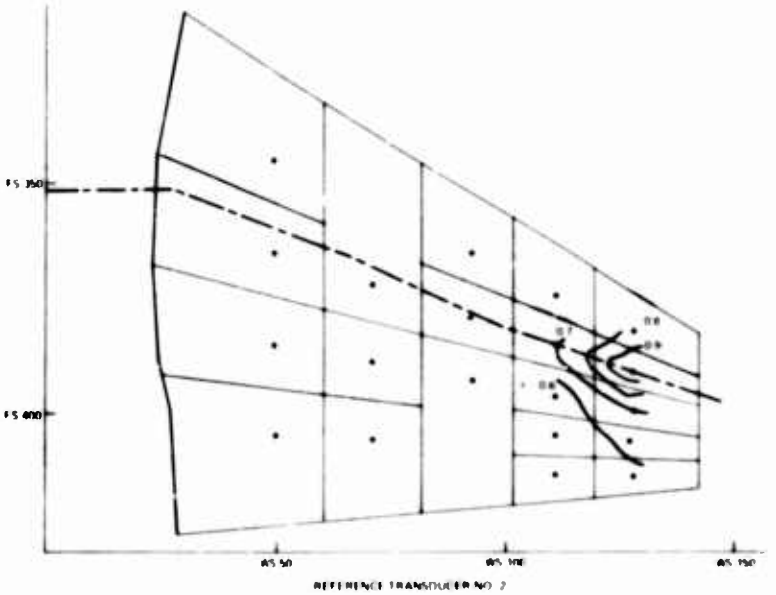

Fig.4-27 Contours of mean square root values of coherence function γ_{xy} for buffet pressures obtained in run 2, flight 871, $M_\infty = 0.925$, h = 10,668 m, $\delta_n = 4°$, $\delta_f = 12°$

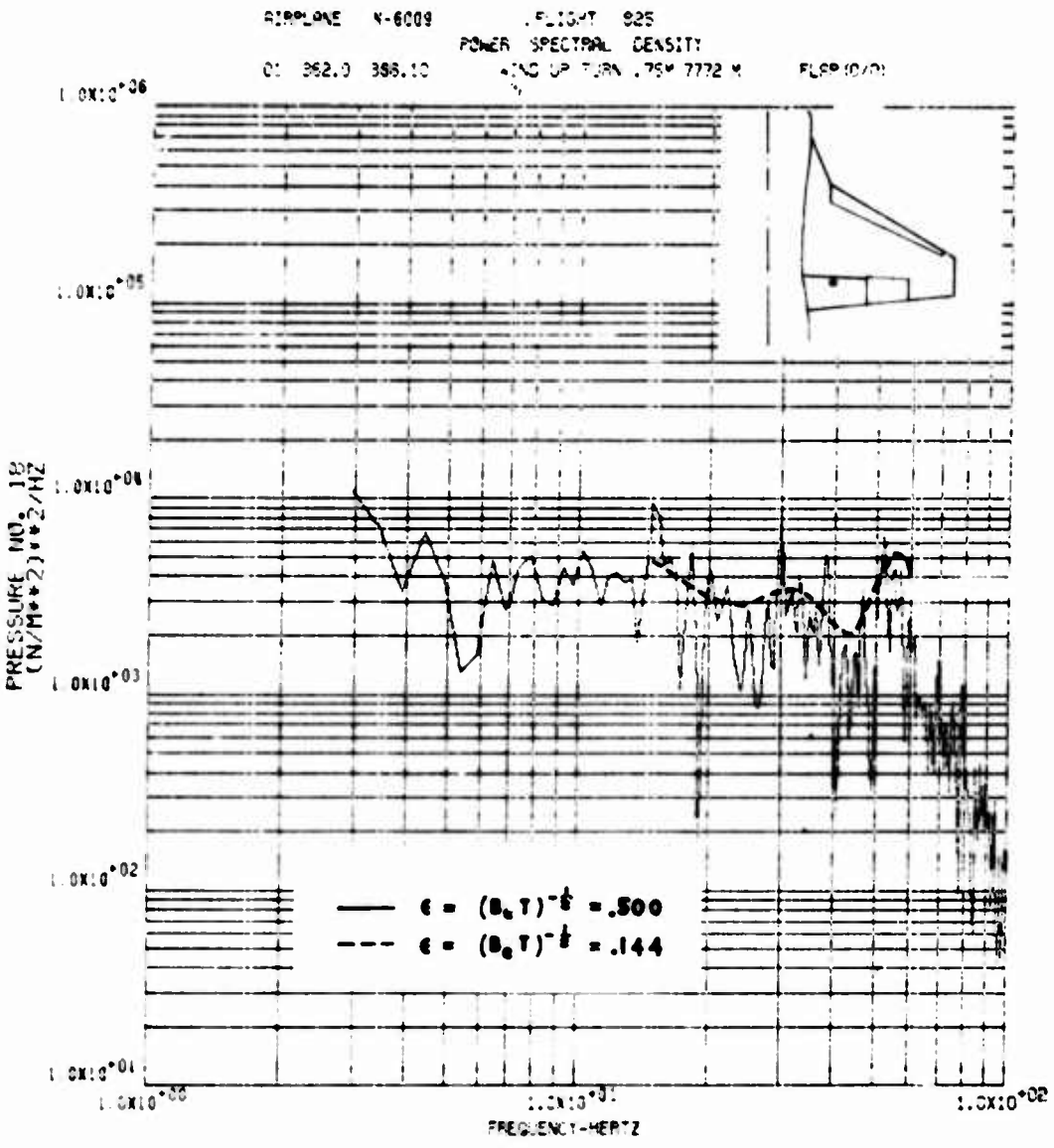

Fig 4-28 Low frequency PSD plot of pressure no. 18. $M_0 = 0.75$, h = 7,772 m, $\delta_0 = 0°$, $\delta_f = 0°$

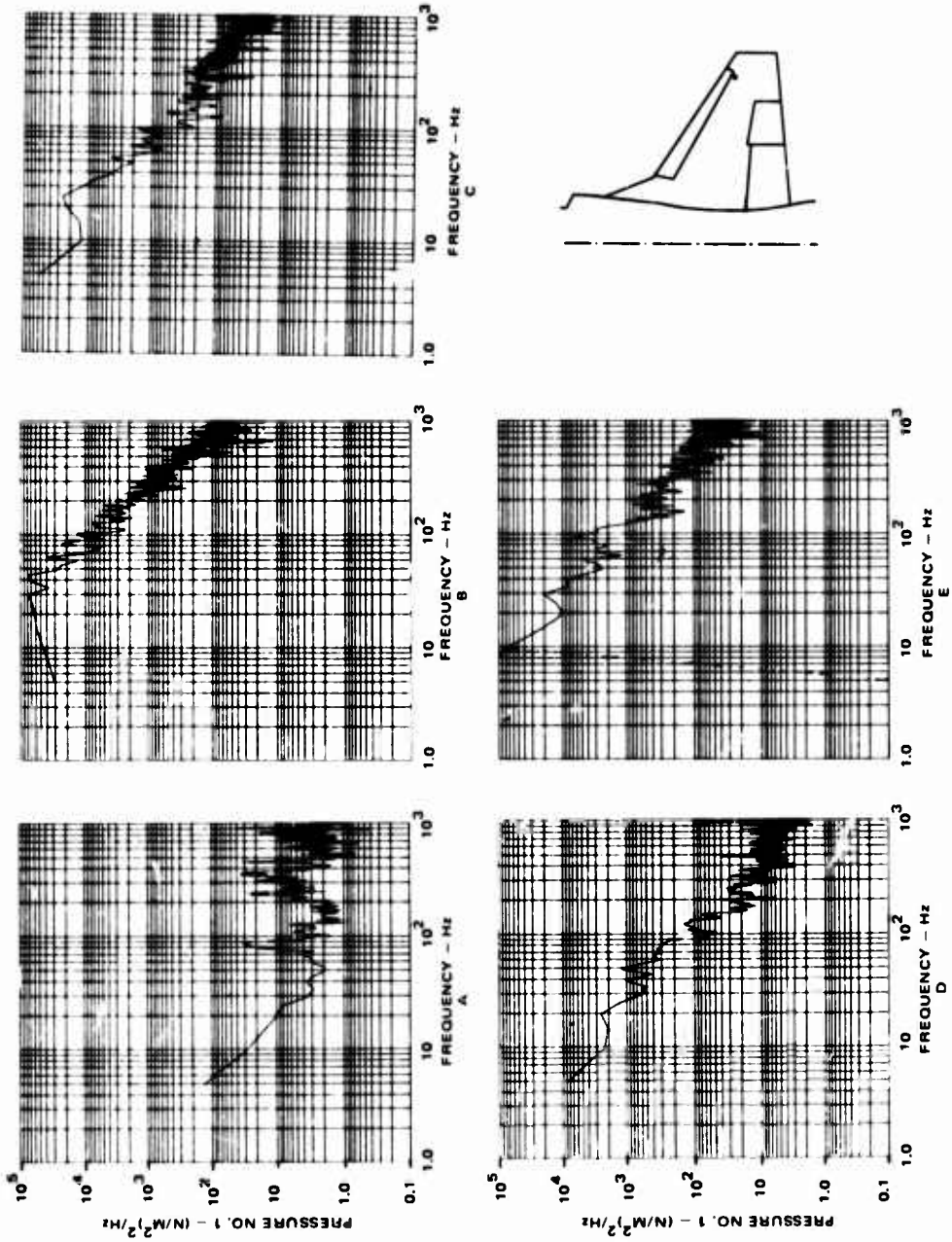

Fig.4-29 PSD's of pressure no. 1 based on various segments of real time data. $M_o = 0.925$, h = 10,668 m. $\delta_n/\delta_f = 0°/0°$

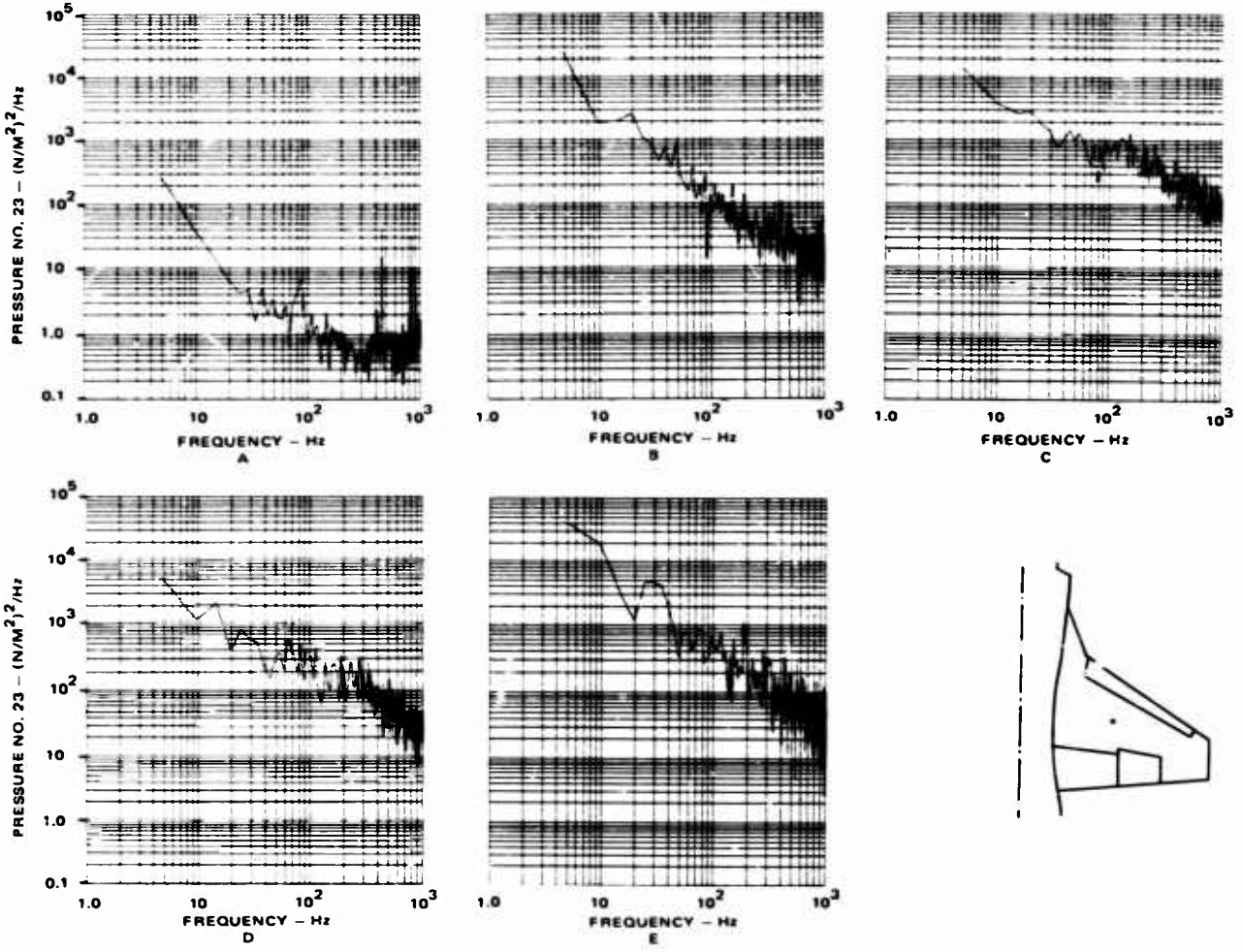

Fig.4-30 PSD's of pressure no. 23 based on various segments of real time data, $M_o = 0.925$, h = 10,668 m, $\delta_n/\delta_f = 0°/0°$

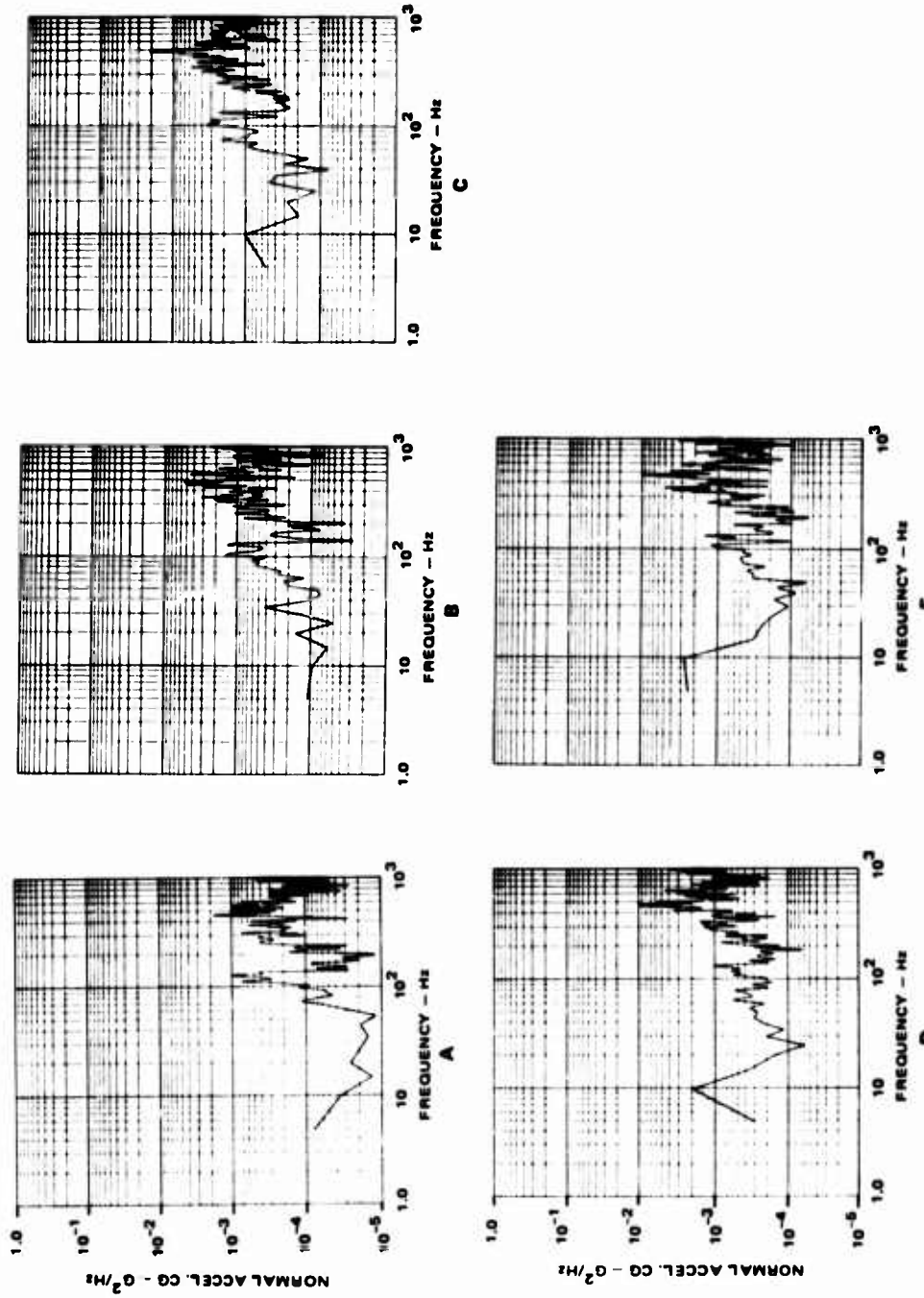

Fig.4-31 PSD's of CG normal acceleration based on various segments of real time data, $M_o = 0.925$, h = 10,668 m, $\delta_n/\delta_f = 0°/0°$

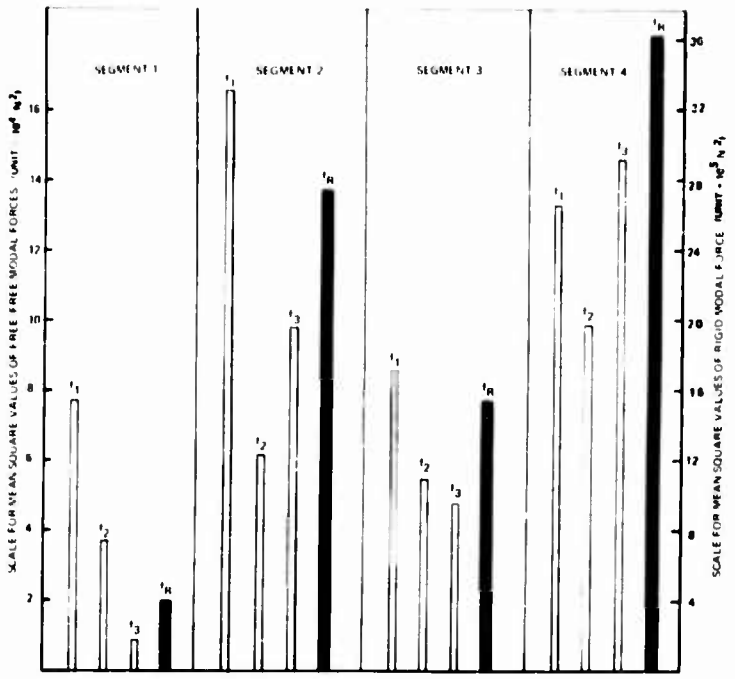

Fig.4-32 Mean square values of the modal forces corresponding to the four time segments of the transonic maneuver, run 2, flight 871, $M_o = 0.925$, h = 10.668m, $\delta_n = 4°$, $\delta_f = 12°$

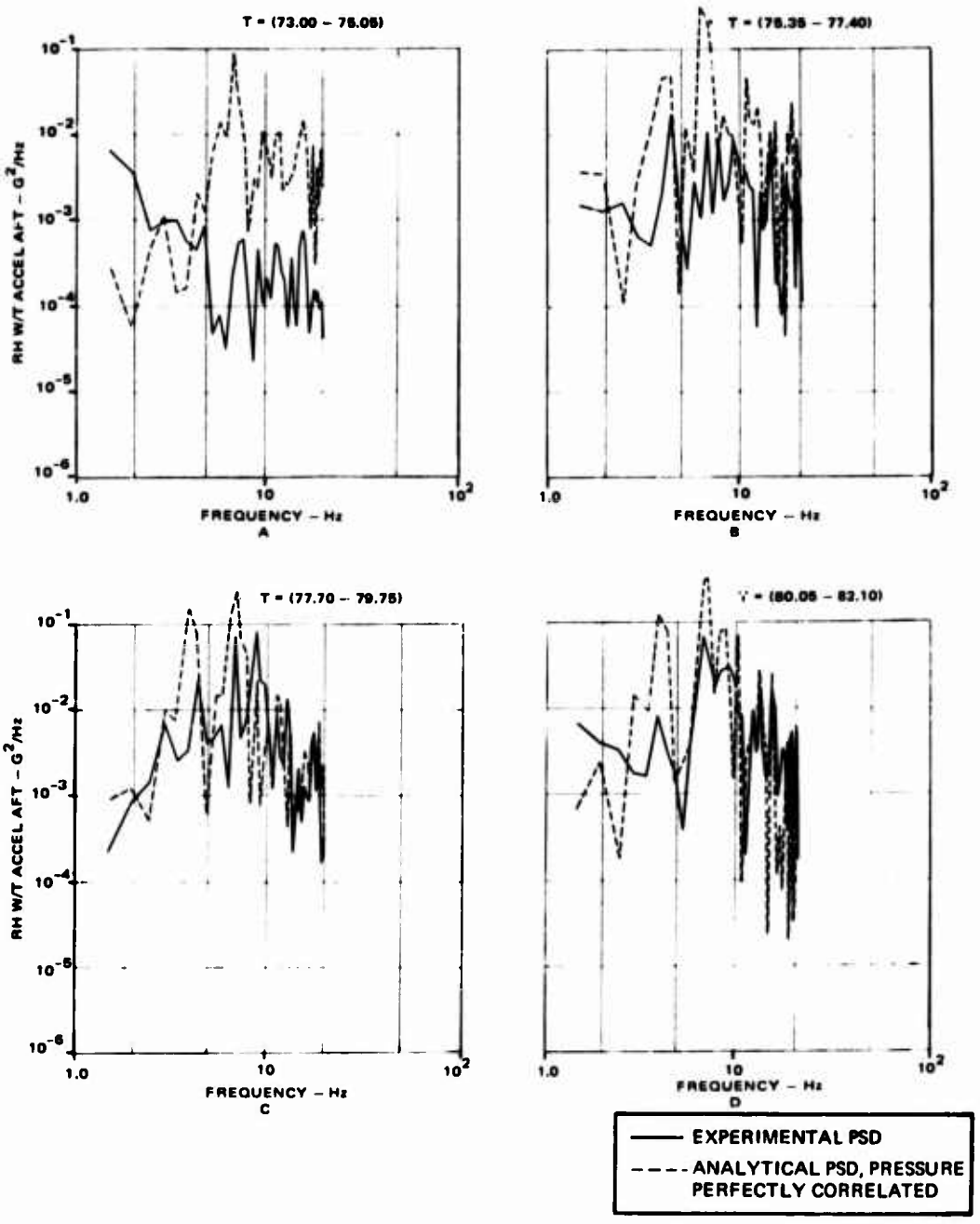

Fig.4-33 Time varying PSD's of right hand wing tip (aft) acceleration — experimental and analytical results. $M_0 = 0.925$, h = 10,668 m, $\delta_n = 4°$, $\delta_f = 12°$

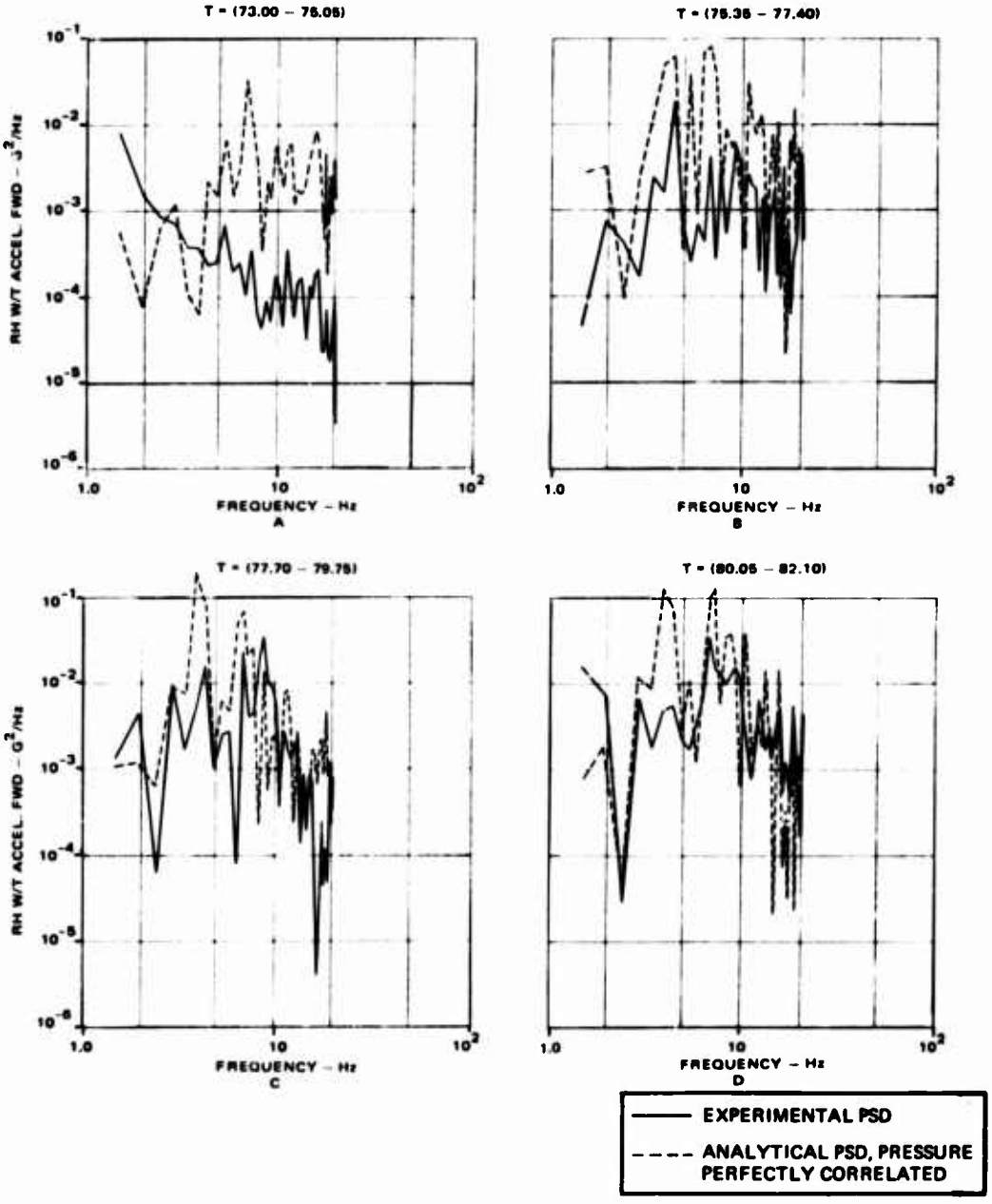

Fig.4-34 Time varying PSD's of right hand wing tip (forward) acceleration – experimental and analytical results, $M_0 = 0.925$, h = 10,668 m, $\delta_n = 4°$, $\delta_f = 12°$

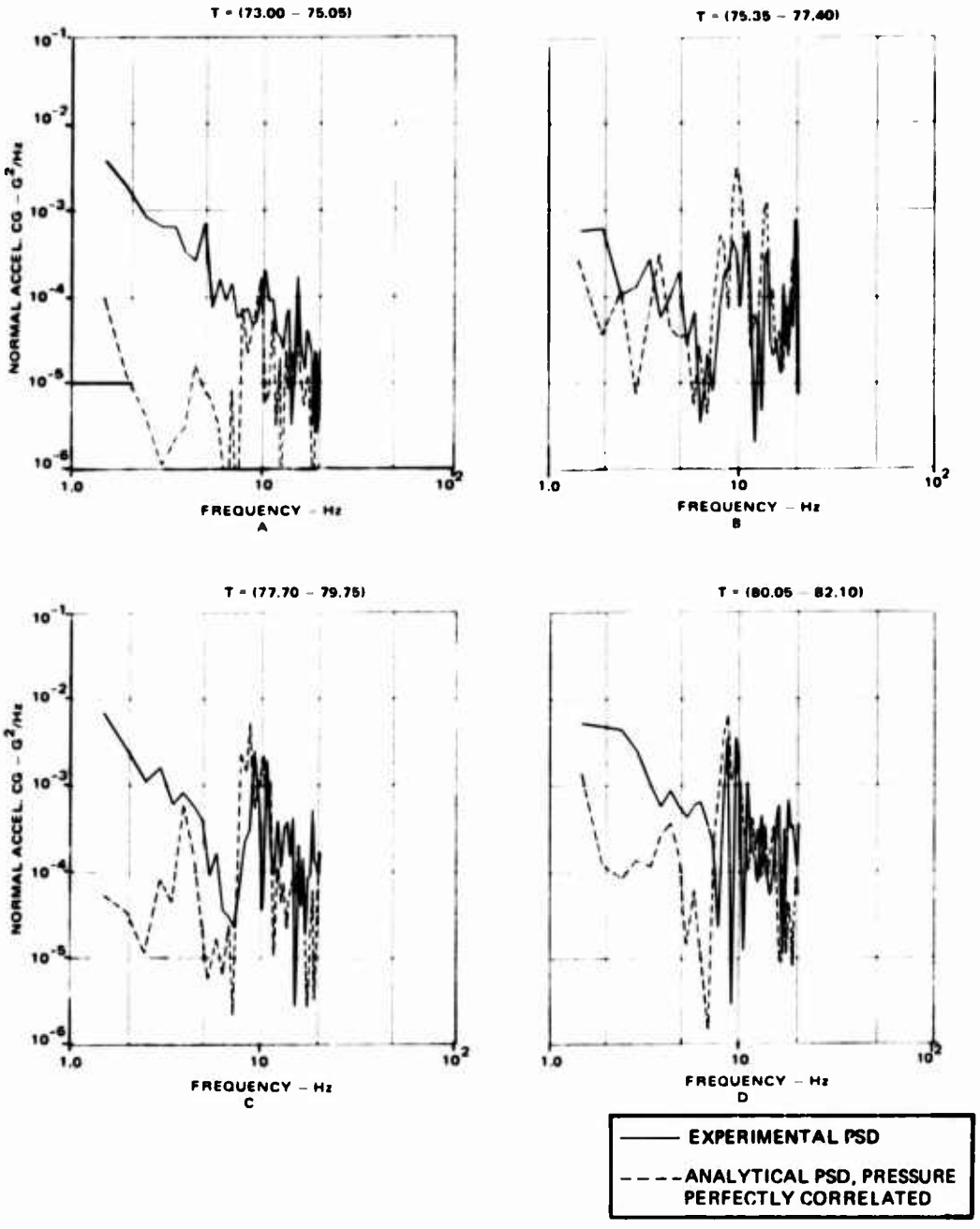

Fig.4-35 Time varying PSD's of CG acceleration — experimental and analytical results. $M_0 = 0.925$, h = 10,668 m, $\delta_n = 4°$, $\delta_f = 12°$

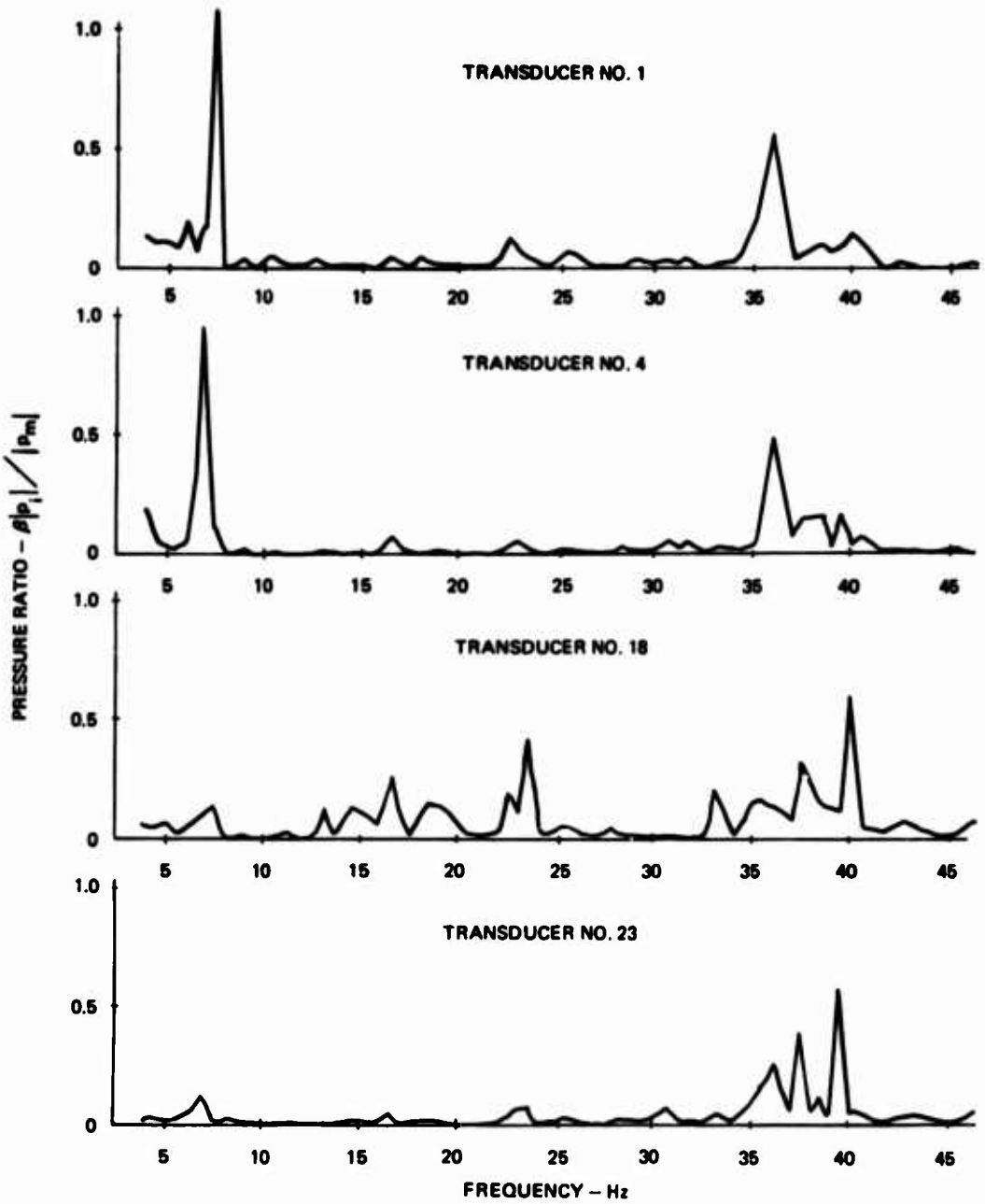

Fig.4-26 Relative magnitude of induced aerodynamic pressure to measured pressure acting on F-5A wing top surface, $M_0 = 0.75$, h = 7,772 m, $\delta_n = 0°$, $\delta_f = 0°$

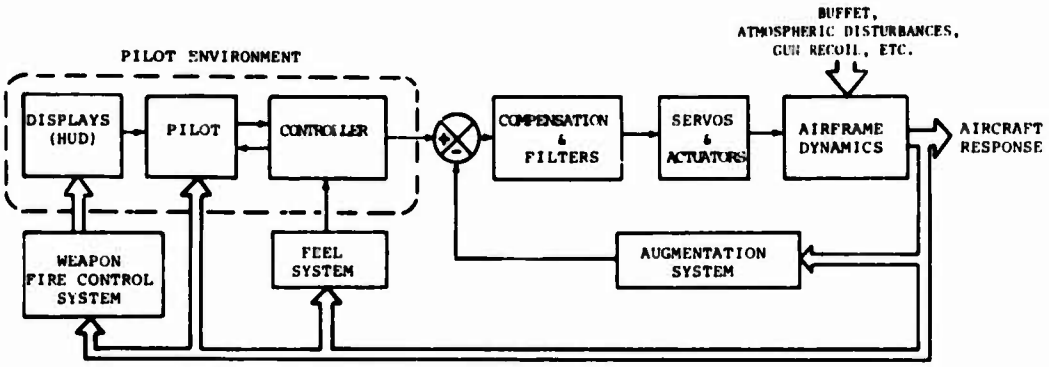

Fig.5-1 Total dynamic system

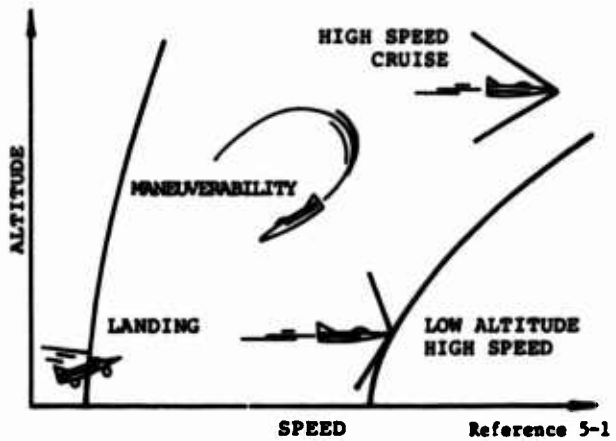

Fig.5-2 Fighter flight envelope

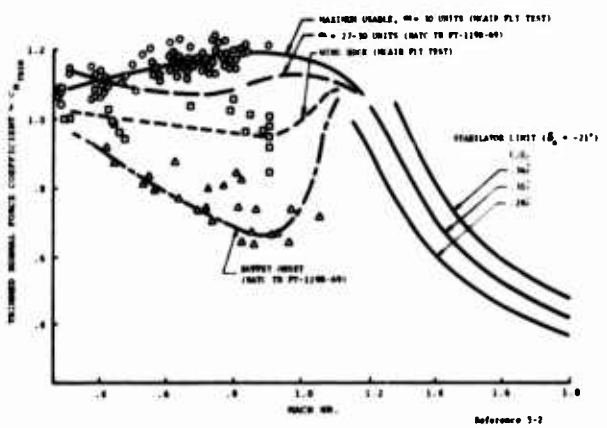

Fig.5-3 Normal force characteristics of the F-4E with two position leading edge slats

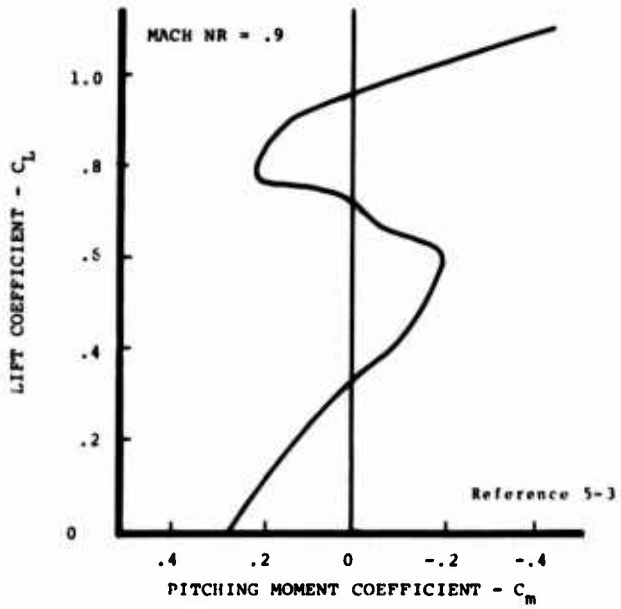

Fig.5-4 Tunnel test indication of pitch up

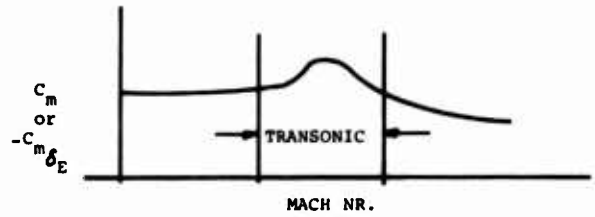

Fig.5-5 Variation with Mach number of longitudinal stability or control

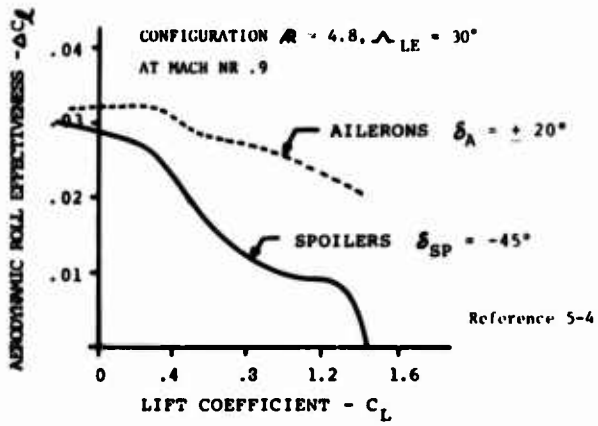

Fig.5-6 Comparison of roll effectiveness, ailerons versus spoilers

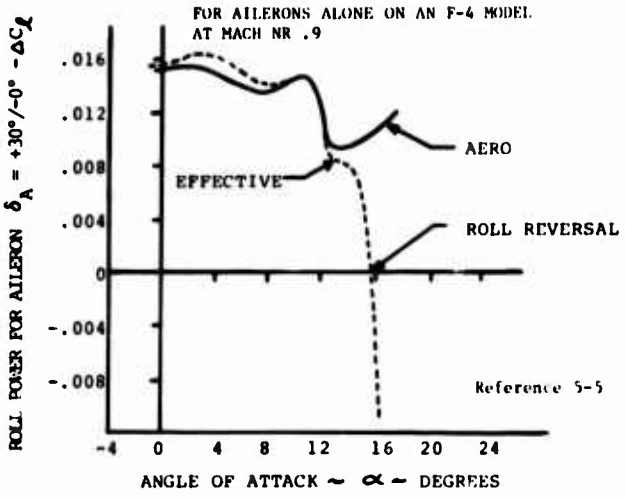

Fig.5-7 Effective versus aero roll power

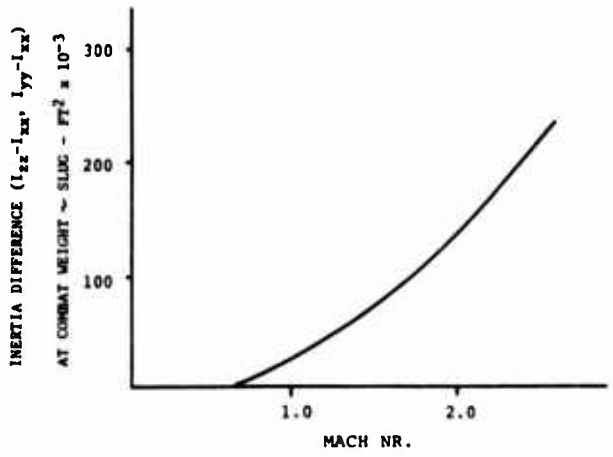

Fig.5-8 Combat aircraft inertia trends

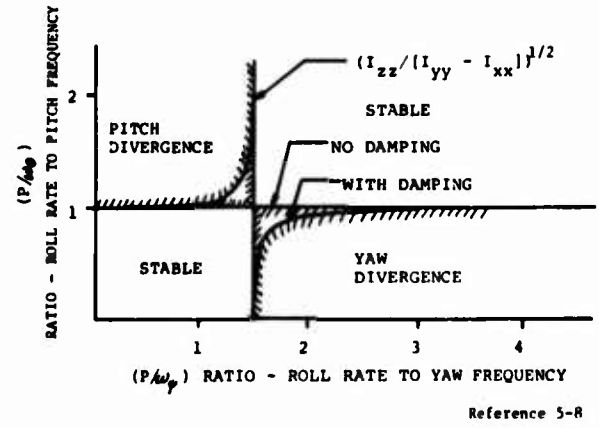

Fig.5-9 Phillips stability diagram

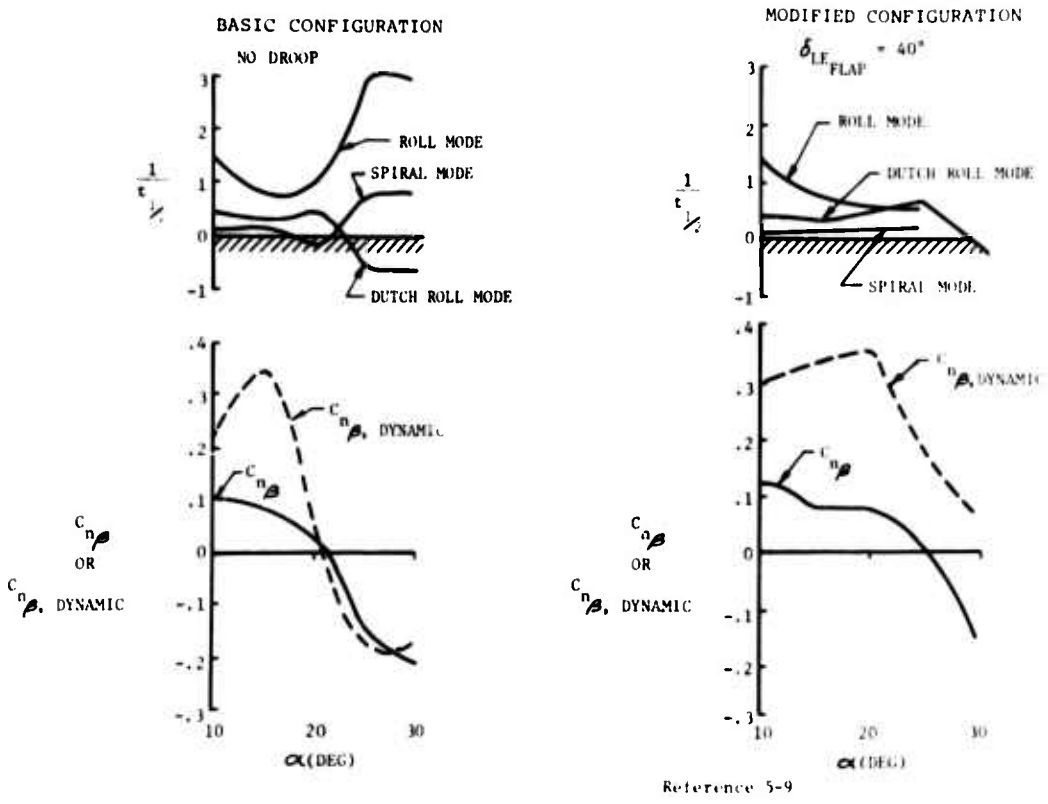

Fig.5-10 Effect of leading edge droop on lateral-directional characteristics of the F-4E

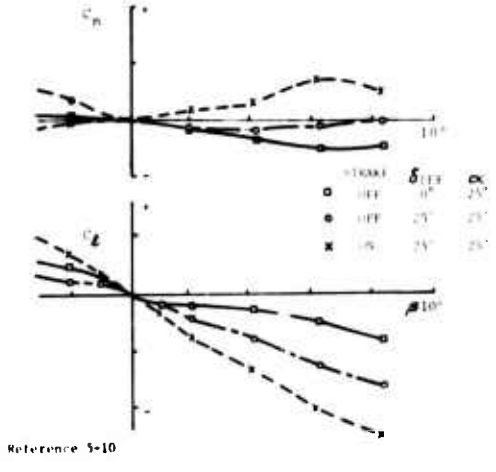

Fig.5-11 Effects of strakes and leading edge flaps on high angle of attack lateral-directional stability

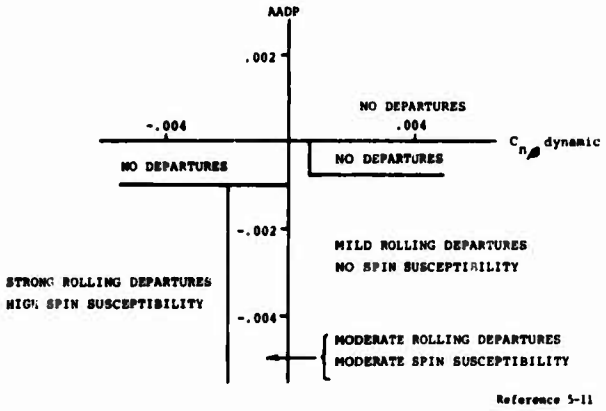

Fig.5-12 Weissman criteria for predicting departure/spin susceptibility

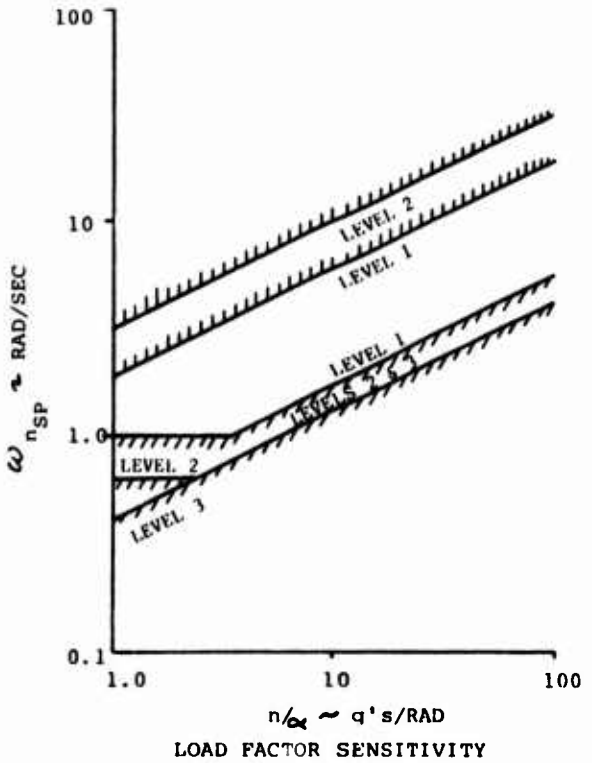

Fig.5-13 Short period frequency requirements

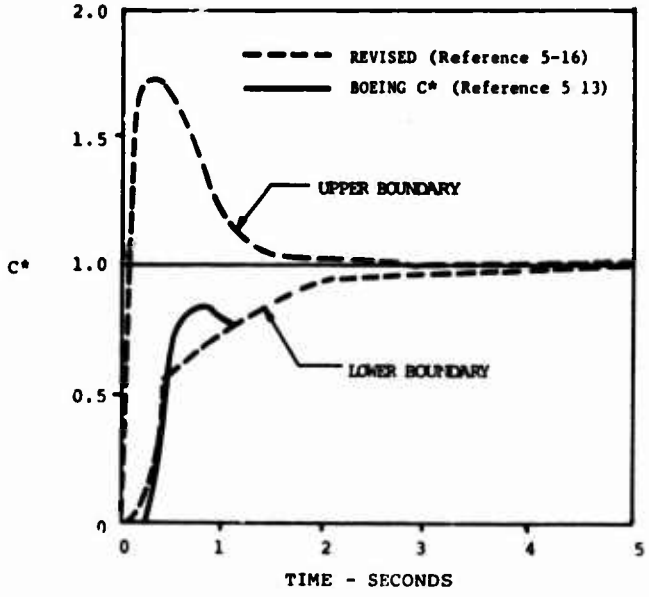

Fig.5-14 C* time history criterion

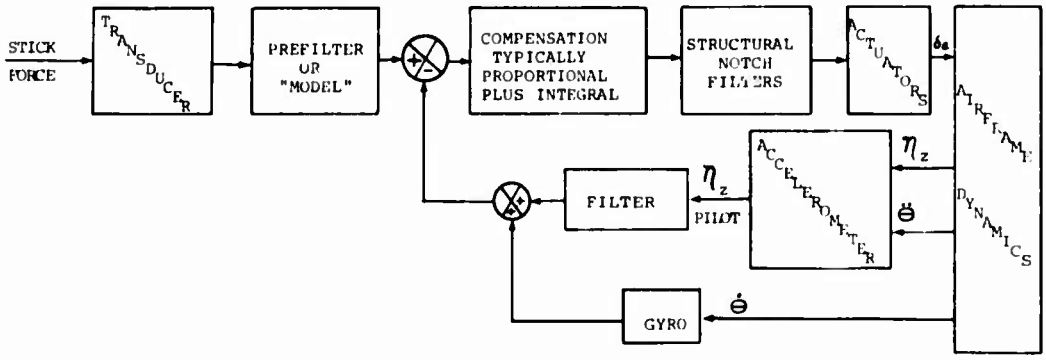

Fig.5-15 Typical longitudinal flight control system

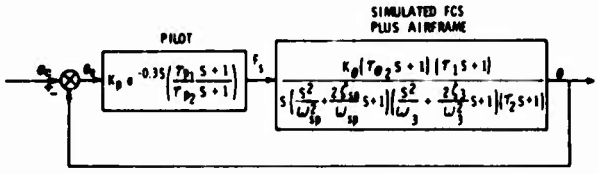

Fig.5-16 Mathematical model of pitch attitude tracking

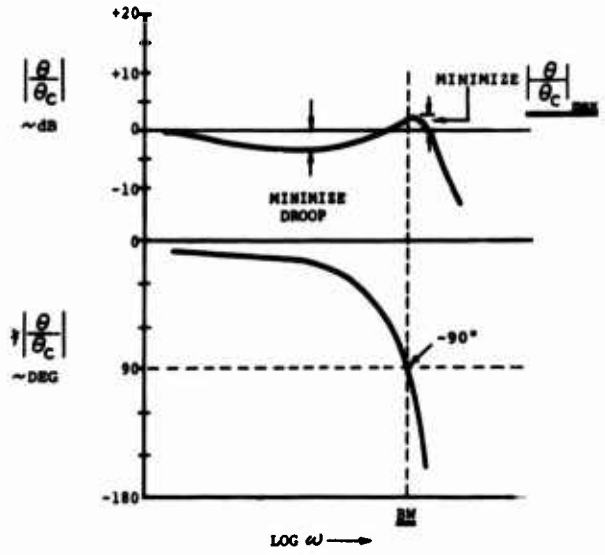

Fig.5-17 Tracking performance parameters

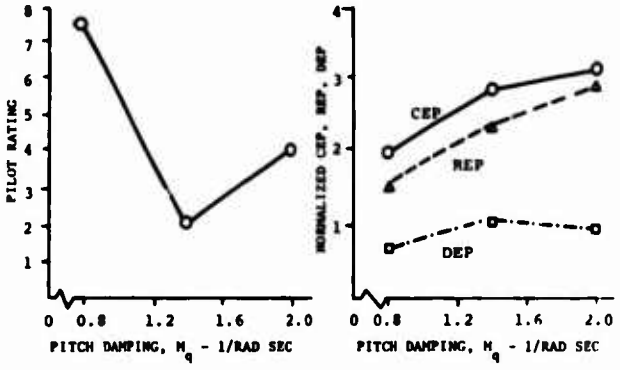

Fig.5-19 Stick force versus G

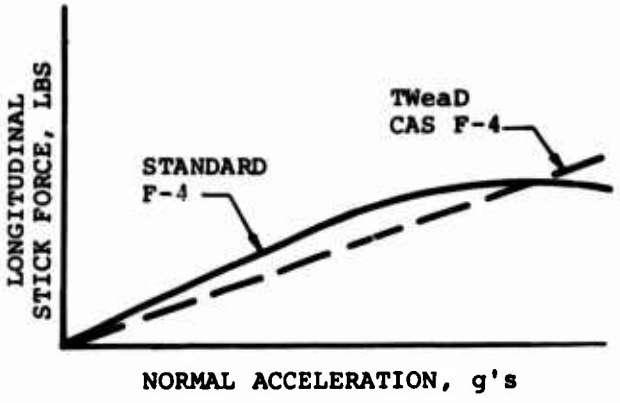

Fig.5-18 Pitch damping and static margin variations

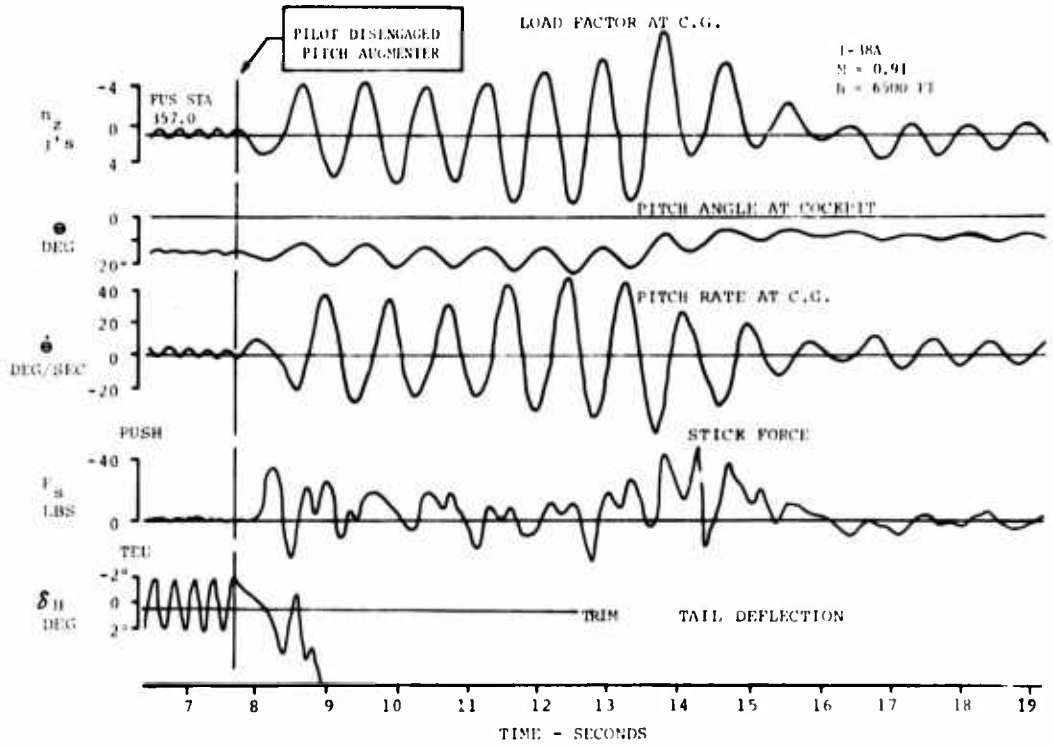

Fig.5-20 P.I.O. time history

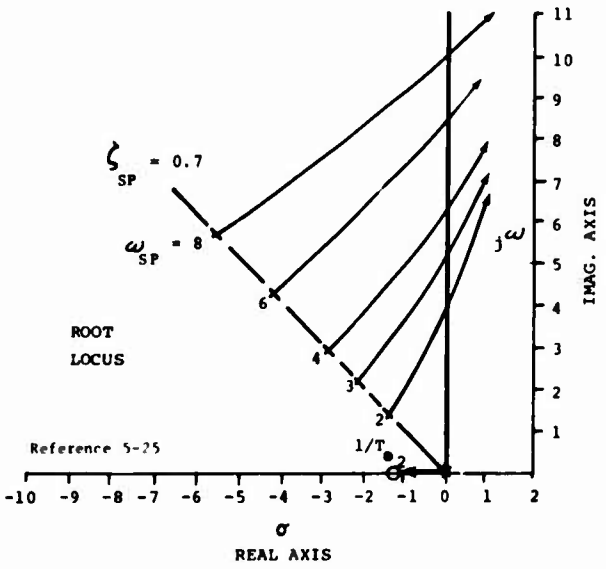

Fig.5-21 θ/δ_e transfer function with a pure gain pilot closing the attitude loop

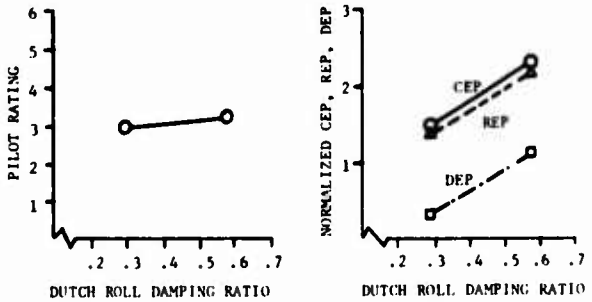

Fig.5-22 Effect of dutch roll damping ratio

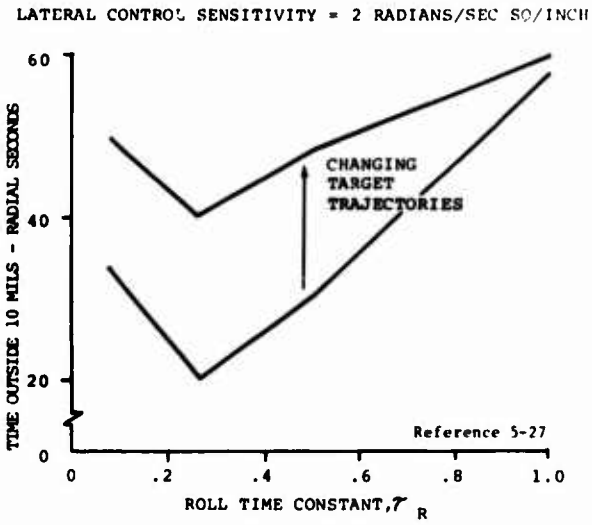

Fig.5-23 Effect of roll time constant on tracking

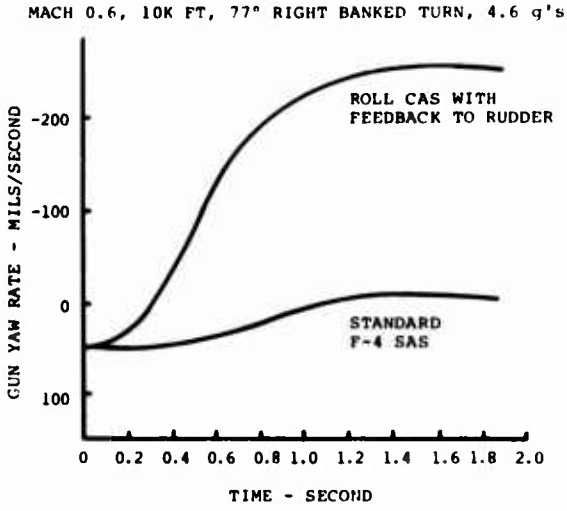

Fig.5-24 Yaw rate response to ½ left stick

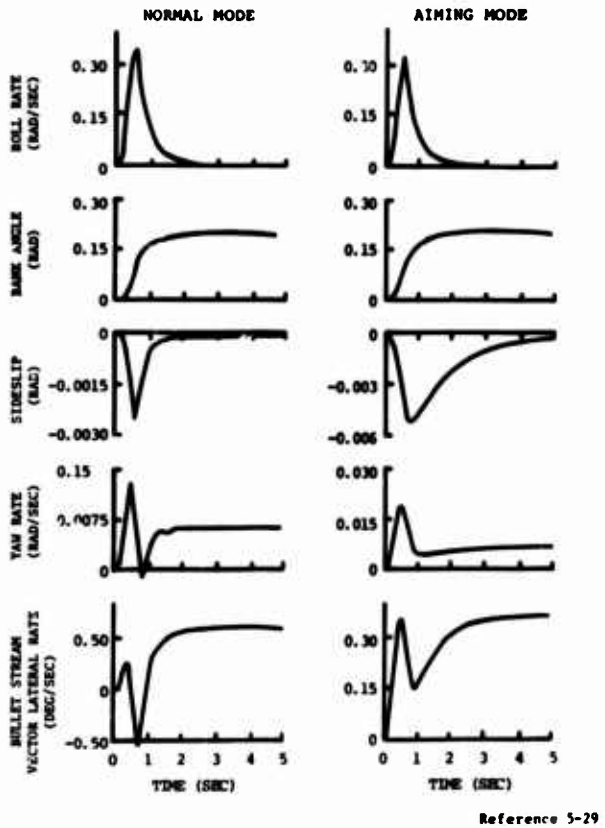

Fig.5-25 Bullet stream lateral rate response, normal and aiming modes

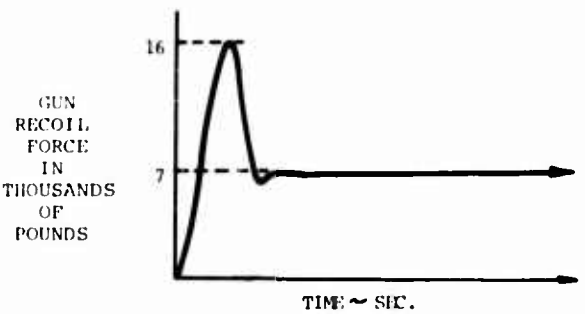

Fig.5-26 Gun recoil force time history

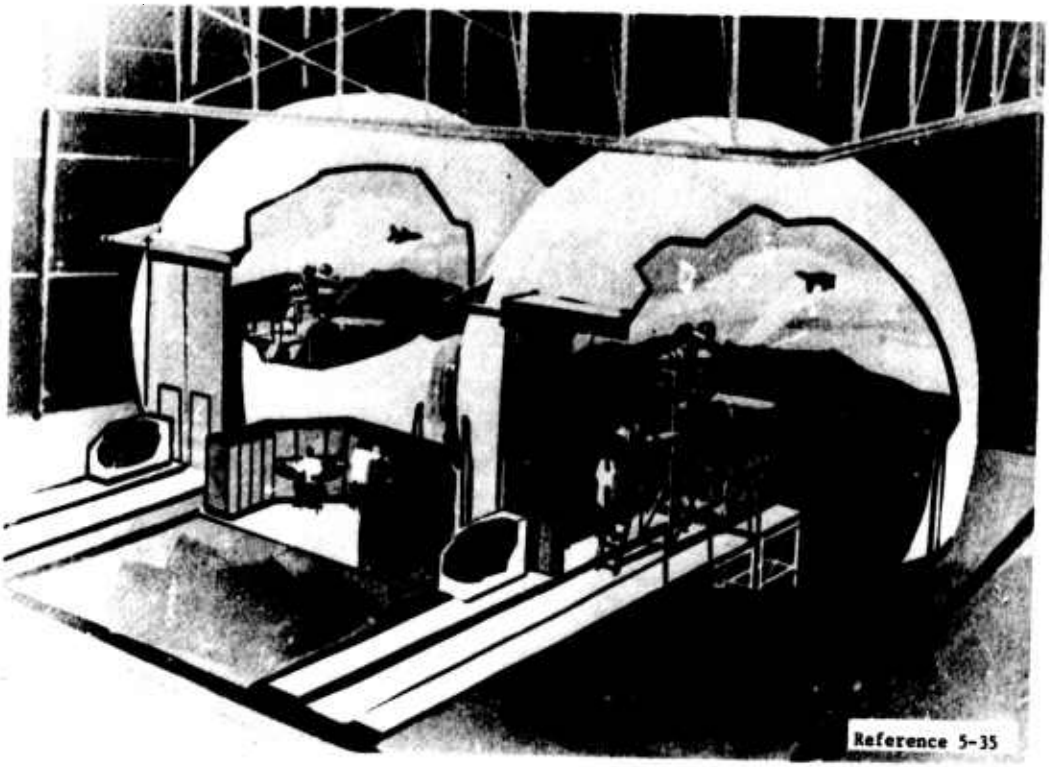

Fig.5-27 Differential maneuvering simulator at NASA Langley Research Center

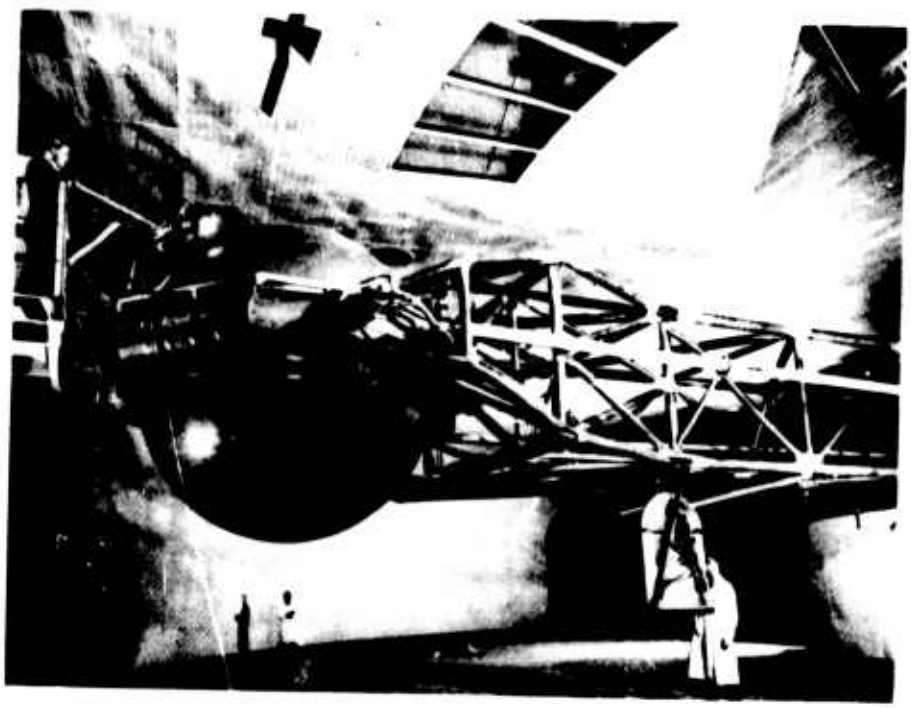

Fig.5-28 NADC centrifuge at Warminster, PA.

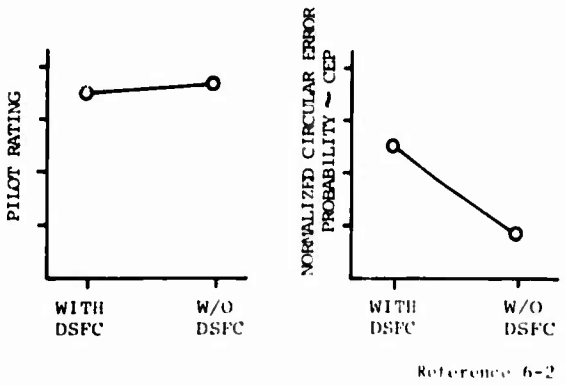

Fig.6-1 Flight simulation evaluation-effect of DSFC on aiming error

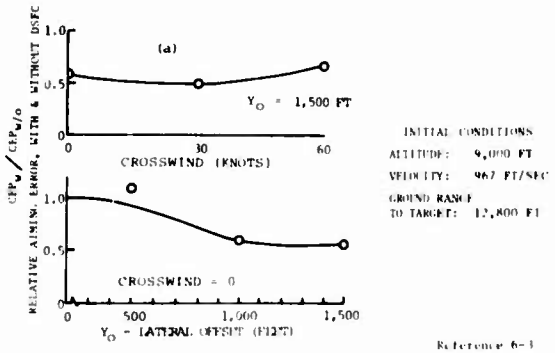

Fig.6-2 Ground simulation evaluation-effect of DSFC on aiming error

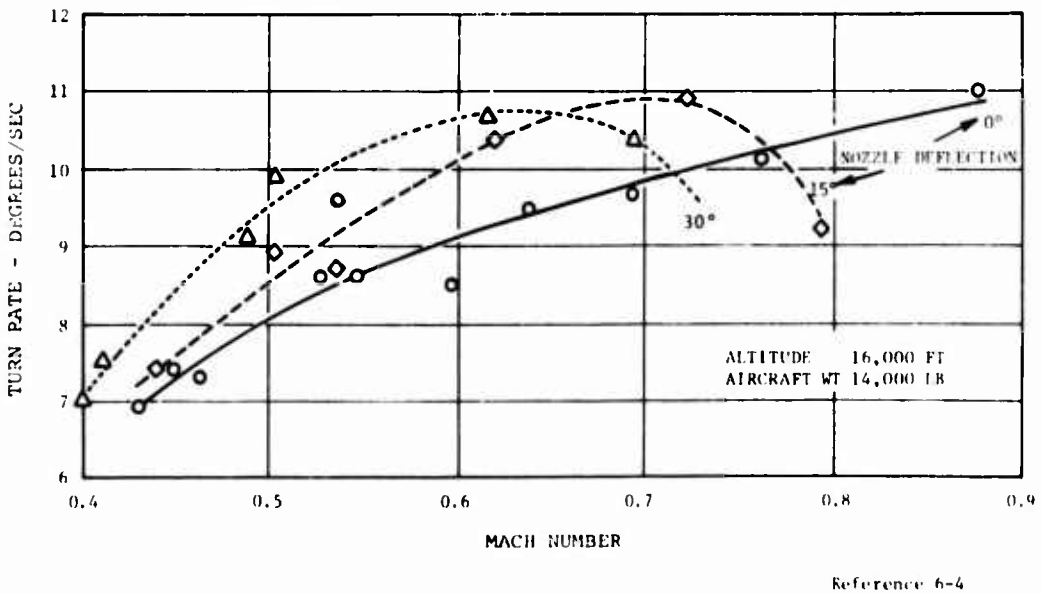

Fig.6-3 Kestrel turn rate performance

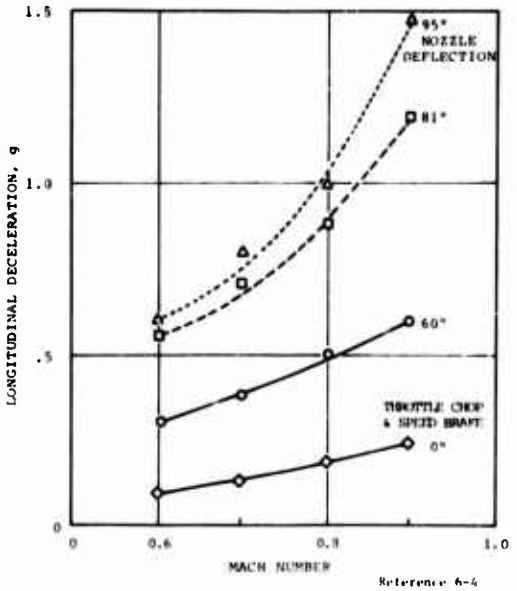

Fig.6-4 Kestrel deceleration performance

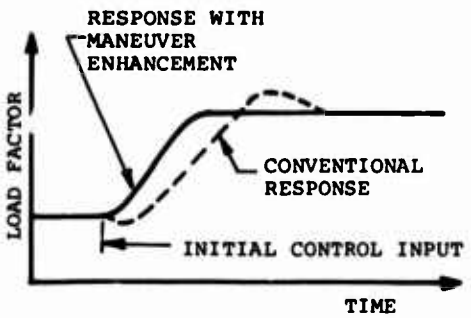

Fig.6-5 Optimized response with maneuver enhancement control

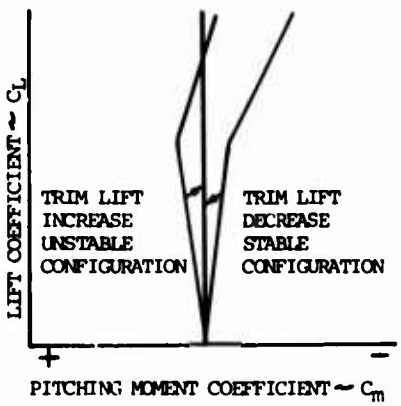

Fig.6-6 RSS effect on trimmed lift

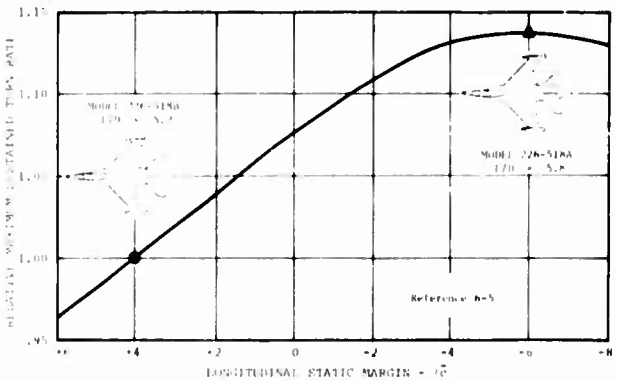

Fig.6-7 Effect of static margin on sustained turn rate-study fighter at Mach number 1.2

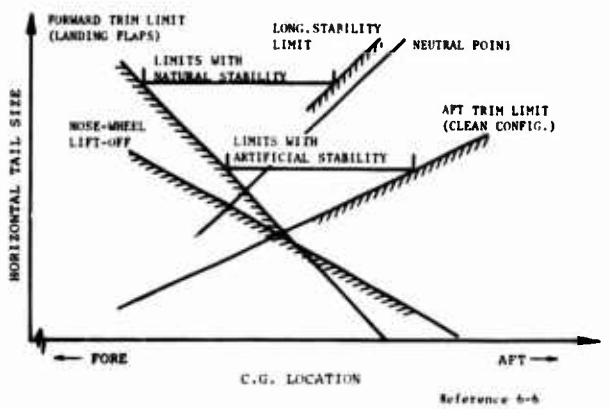

Fig.6-8 Effect of stabilization by active control on horizontal tail size requirement

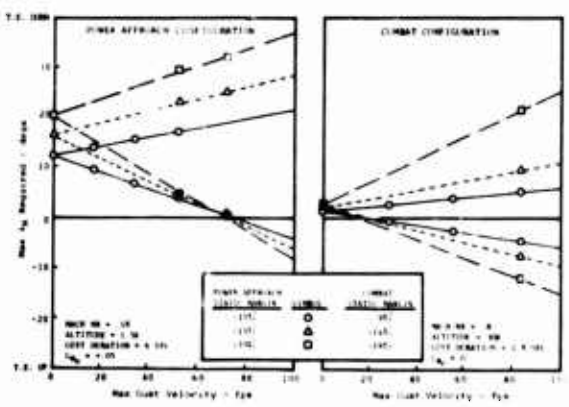

Fig.6-9 Discrete gust effect on required horizontal tail limits-preliminary small fighter design

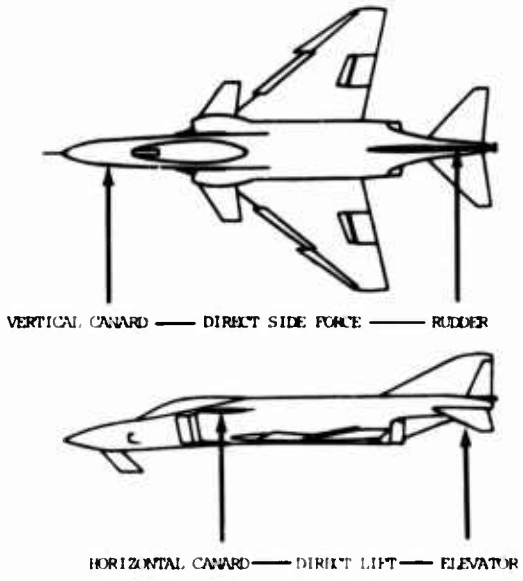

Fig.6-10 Direct lift and direct side force mechanization on a proposed modified F-4 aircraft

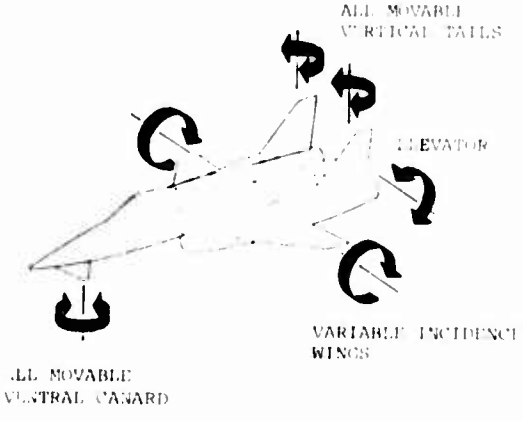

Fig.6-11 Direct lift and direct side force mechanization on the proposed McDonnel-Douglas AMDA

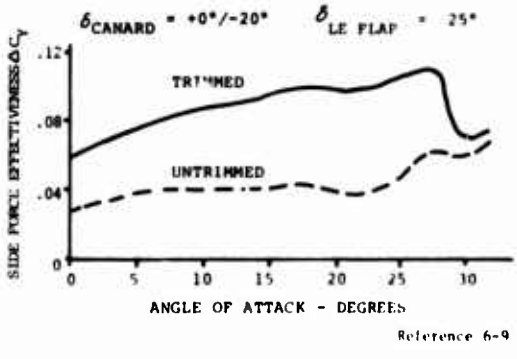

Fig.6-12 DSFC capabilities of horizontal canard on a small fighter research configuration

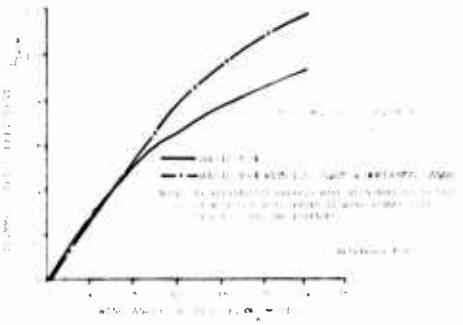

Fig.6-13 Lift comparison of the F-4 aircraft with and without canards and leading edge slats

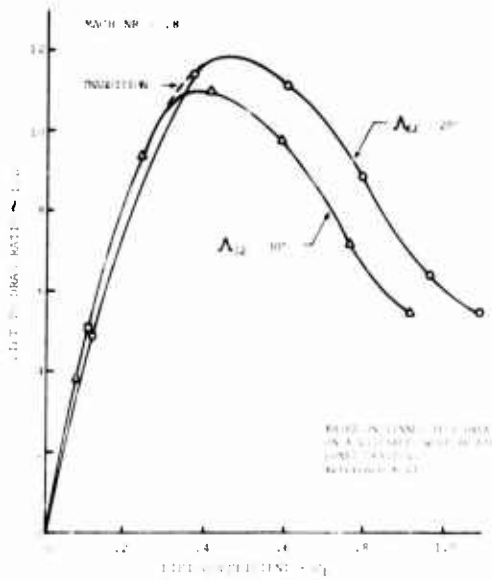

Fig.6-14 Maneuver L/D optimization by wing sweep variation

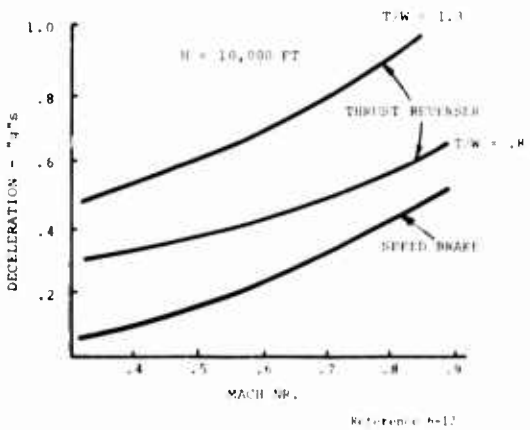

Fig.6-15 Deceleration capability comparison-speed brake and thrust reverser

Fig.6-16 Rigid sidestick assembly

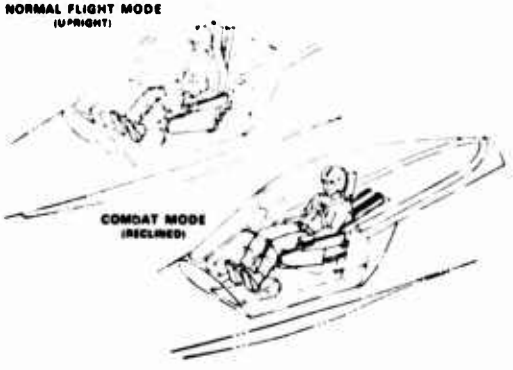

Fig.6-17 High acceleration cockpit

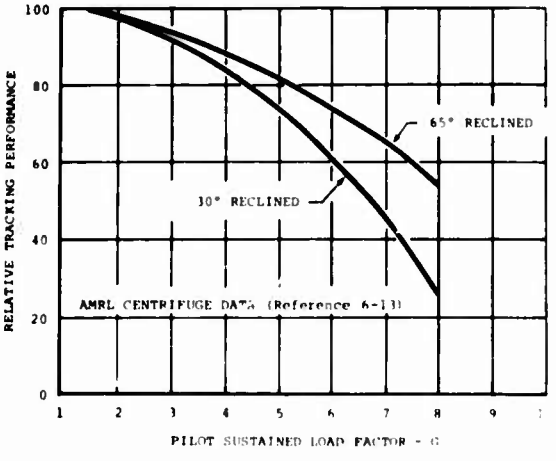

Fig.6-18 Close-in tracking improvement demonstrated for reclined seat

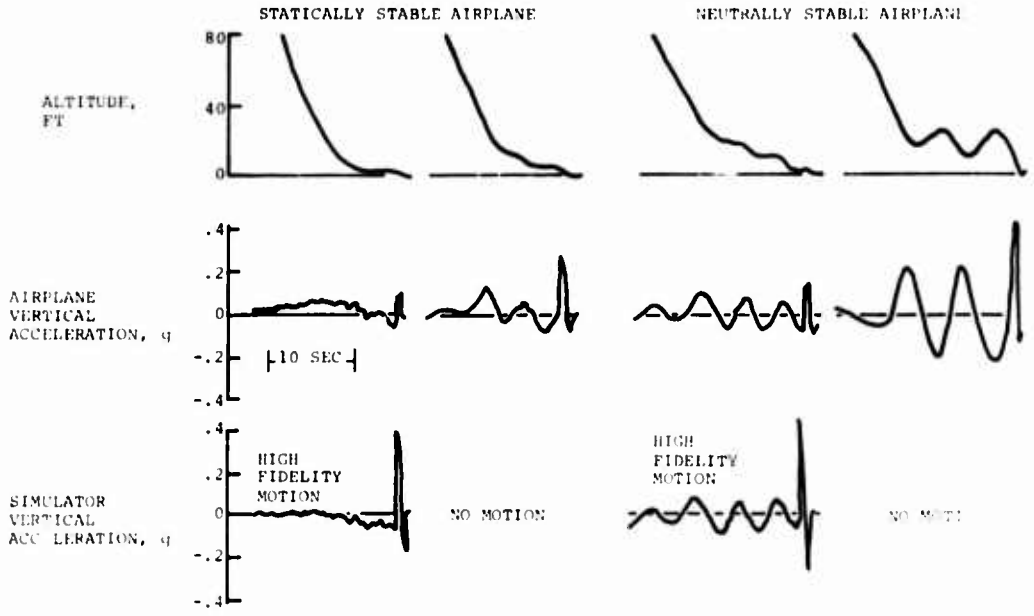

Fig.6-19 Effect of airplane stability level and motion cues on a landing simulation

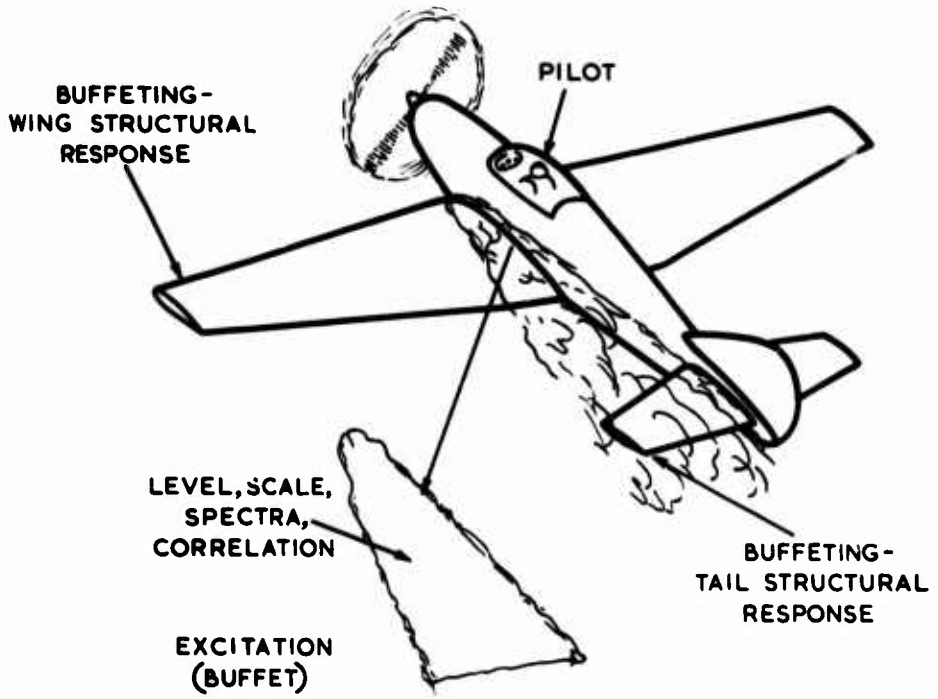

Fig.7-1 Buffeting

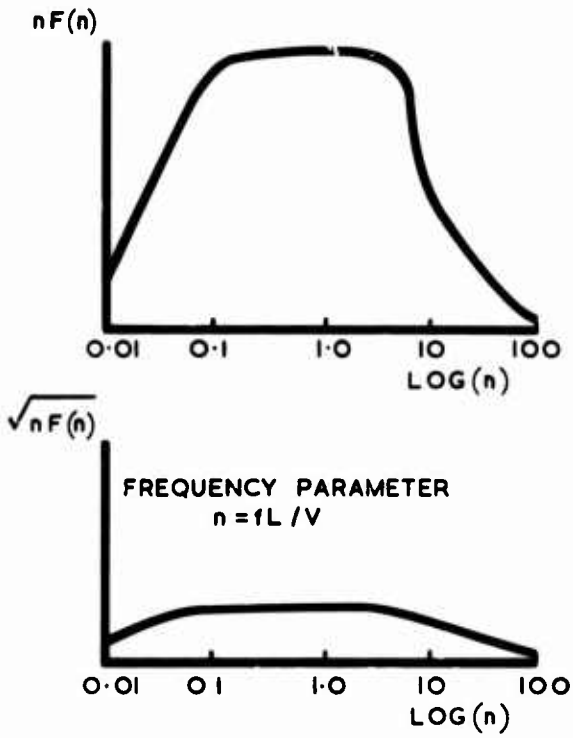

OWEN

TOTAL RMS PRESSURE
FLUCTUATION COEFFICIENT

$$\overline{p^2}/q^2 = \int_{n=0}^{n=\infty} n\,F(n)\,d\left[\text{LOG } n\right]$$

PRESSURE FLUCTUATION IN A
NARROW BANDWIDTH

$$\Delta p/q\ \sqrt{\varepsilon} = \sqrt{n\,F(n)}$$

Fig.7-2 Dimensionless representation of excitation spectra

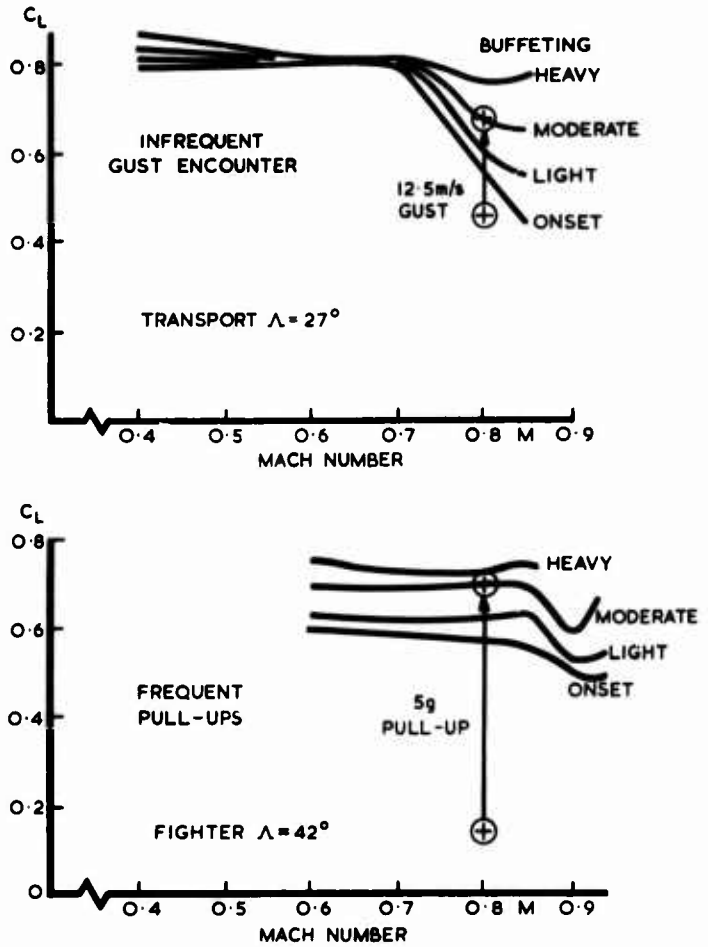

Fig.7-3 Buffeting criteria for transport and fighter aircraft

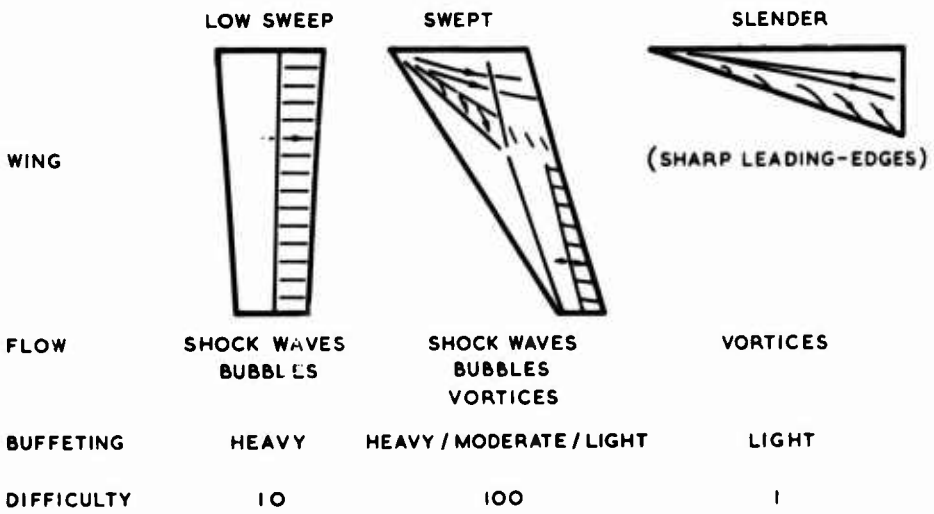

Fig.7-4 Classification of flows and associated buffeting

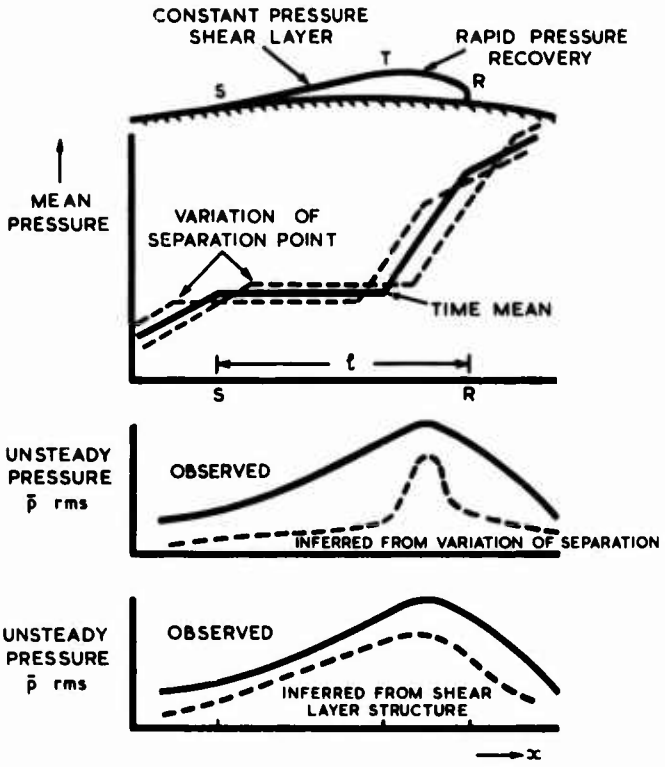

Fig.7-5 Mean flow and pressure fluctuations caused by separation bubbles

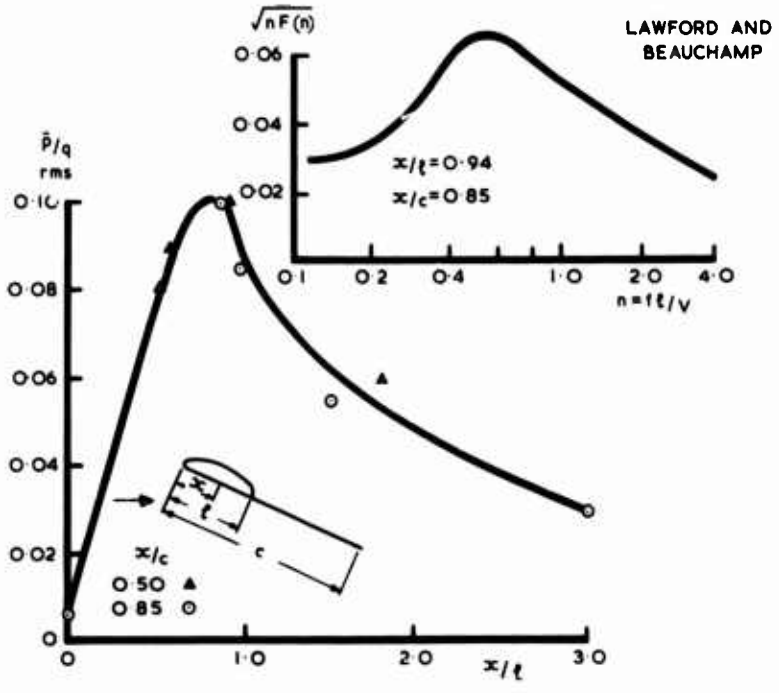

Fig.7-6a Excitation caused by leading-edge bubble, M = 0.14

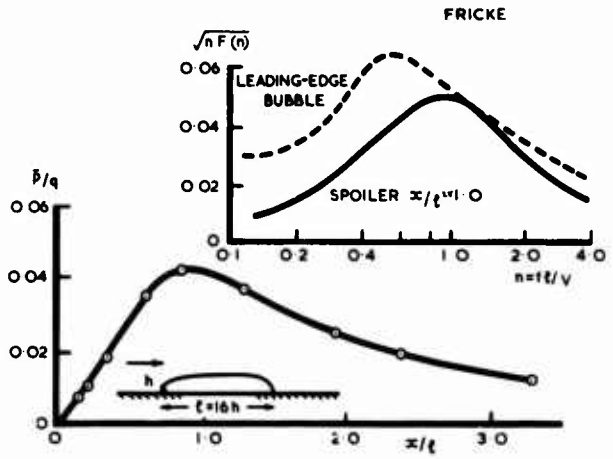

Fig.7-6b Excitation caused by a spoiler, M = 0.12

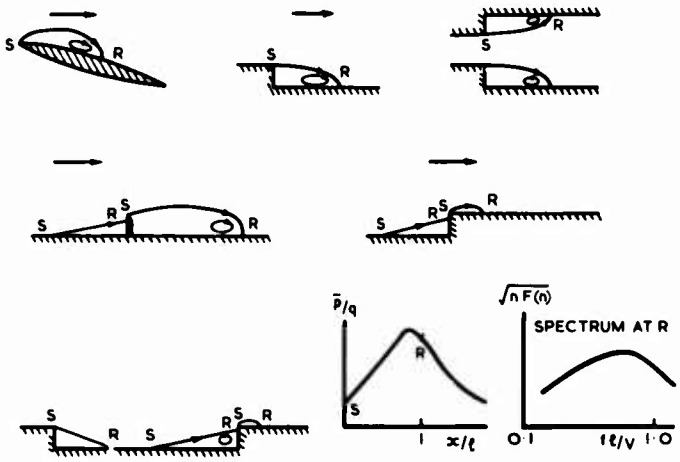

Fig.7-7 Types of bubble flow

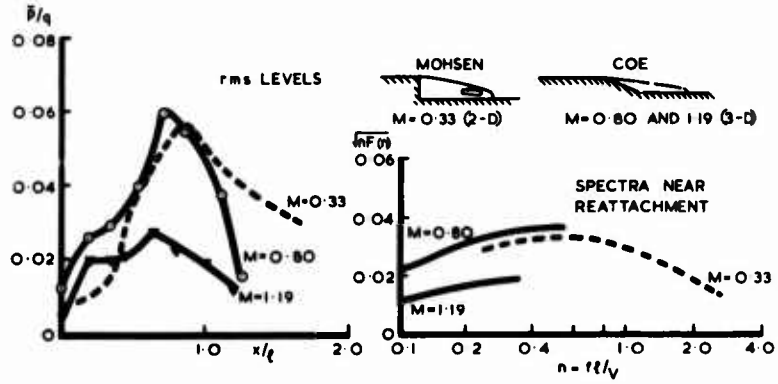

Fig.7-8 Comparison of excitation caused by the flow down a step at M = 0.33, 0.80 and 1.19

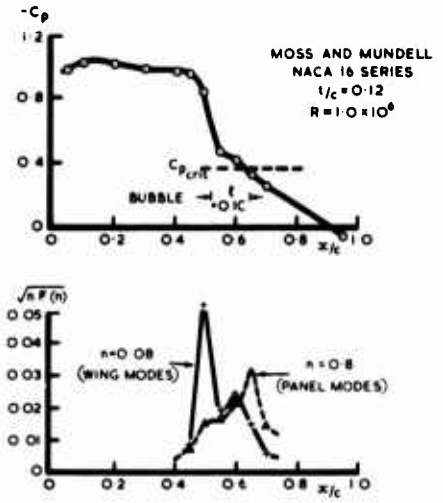

Fig.7-9 Excitation on an aerofoil near buffet onset, M = 0.82 $\alpha = 6.7°$

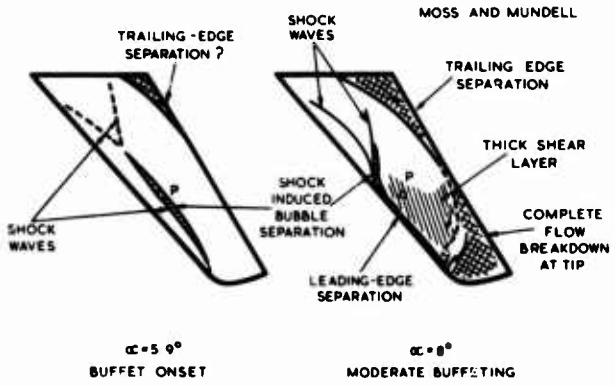

Fig.7-10 Transonic flow on a swept wing, M = 0.80

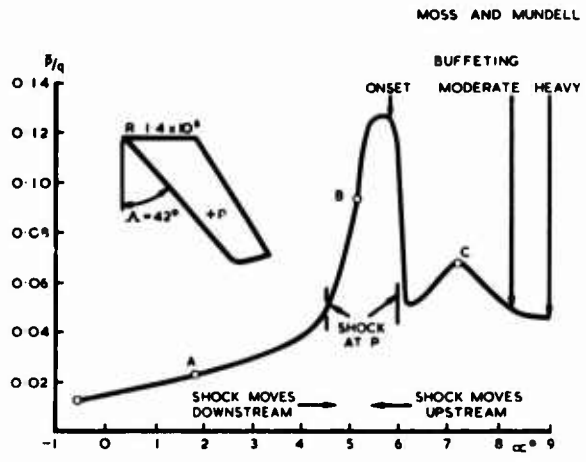

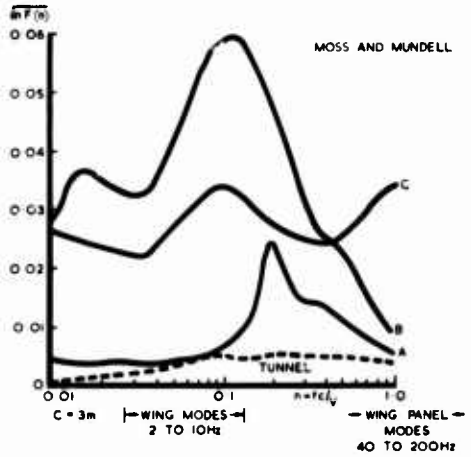

Fig.7-12 Spectra of excitation on a swept wing, M = 0.80

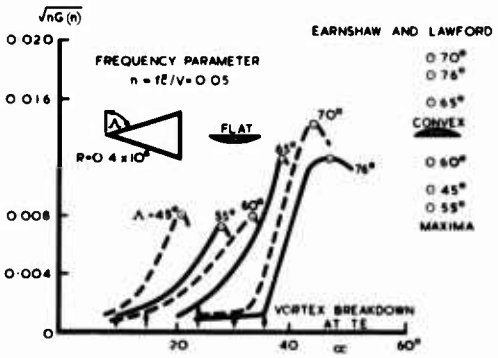

Fig.7-13 Variation of fluctuating normal force coefficient with angle of attack for delta wings, M = 0.08

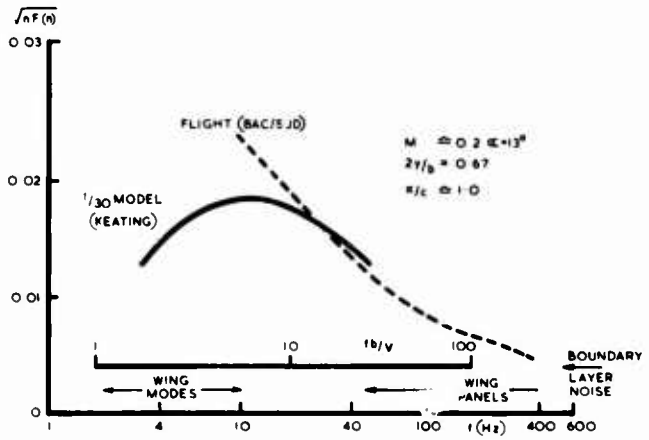

Fig.7-14 Low speed excitation on a slender wing

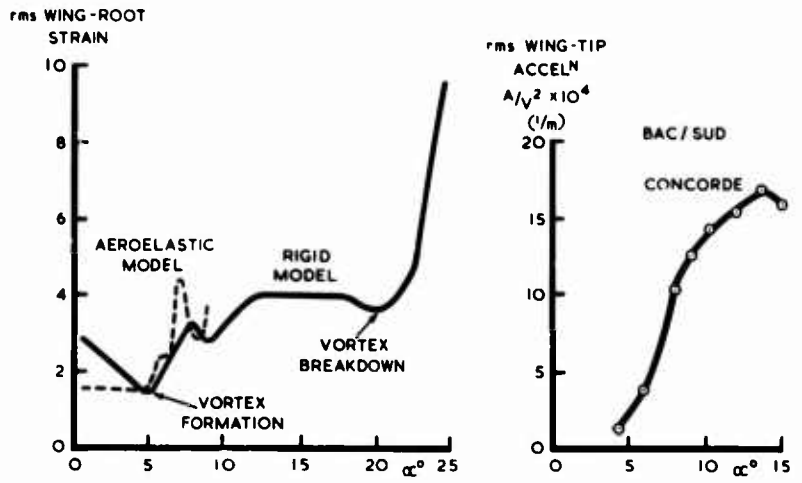

Fig.7-15 Light buffeting on slender wings, M = 0.2

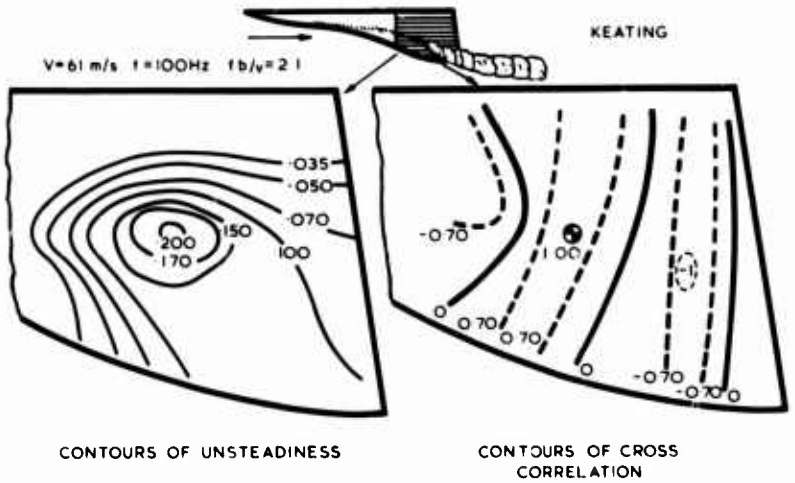

Fig.7-16 Excitating on BAC 221 at vortex breakdown, $\alpha = 21.5°$, $\beta = -3°$, M = 0.2

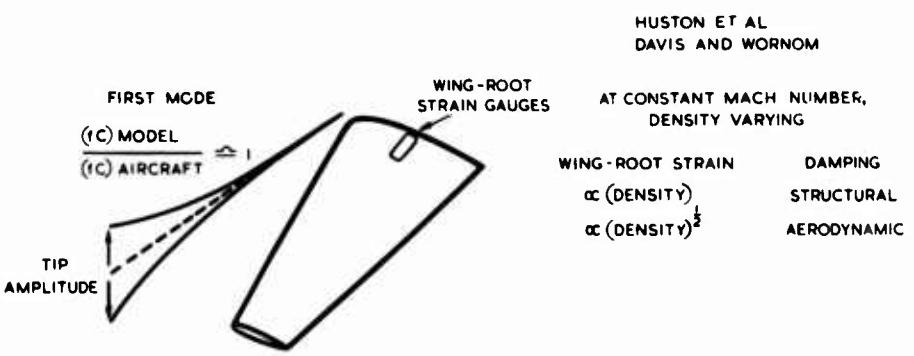

Fig.7-17 Similarity relations for buffeting

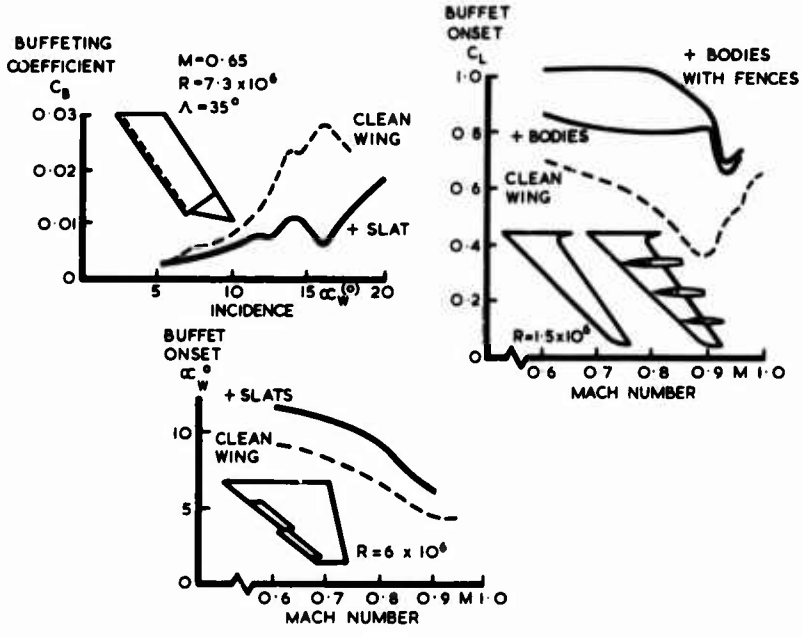

Fig.7-18 Alleviation of buffeting by wing modifications

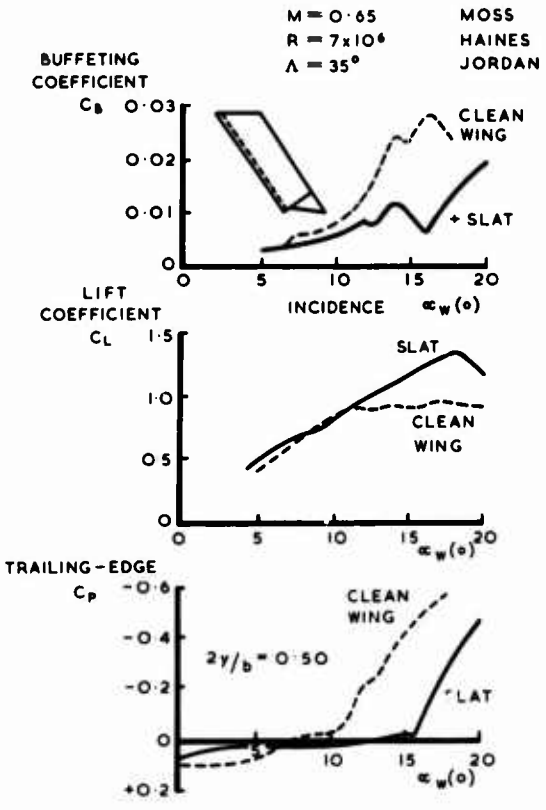

Fig.7-19 Influence of leading-edge slats on buffeting, forces and trailing-edge pressures

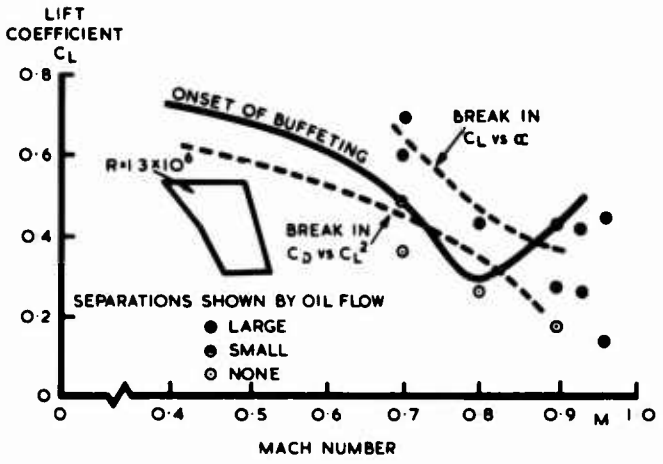

Fig.7-20 Derivation of flow separation boundaries

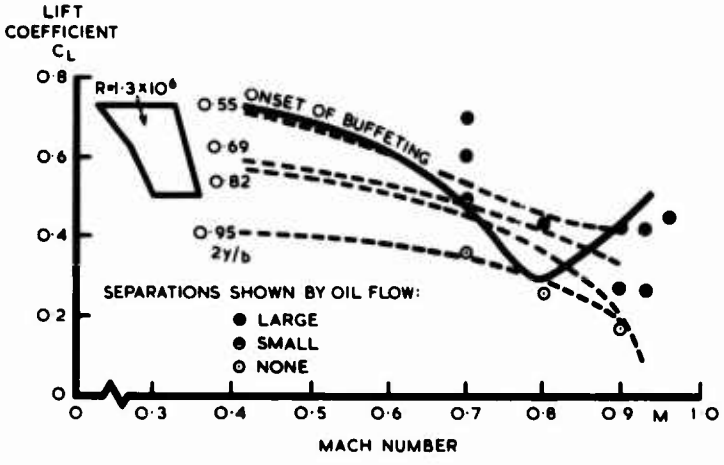

Fig.7-21 Boundaries of trailing-edge pressure divergence

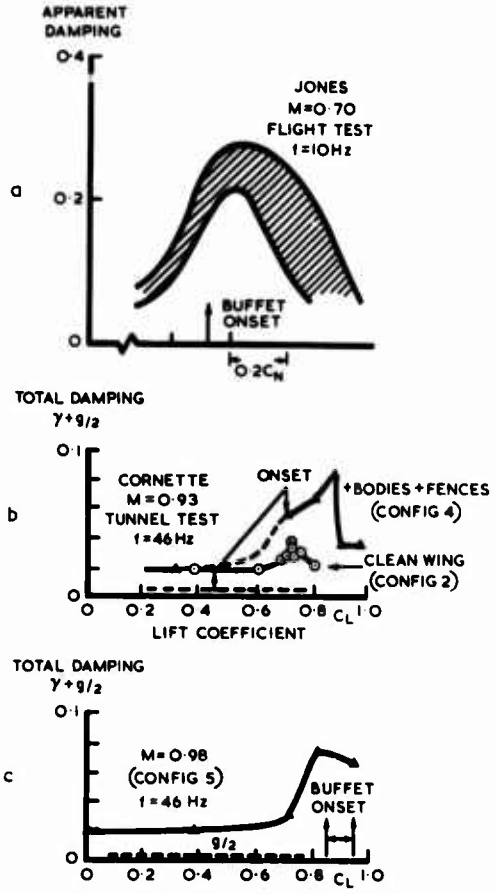

Fig.7-22 Variation of total damping with lift coefficient

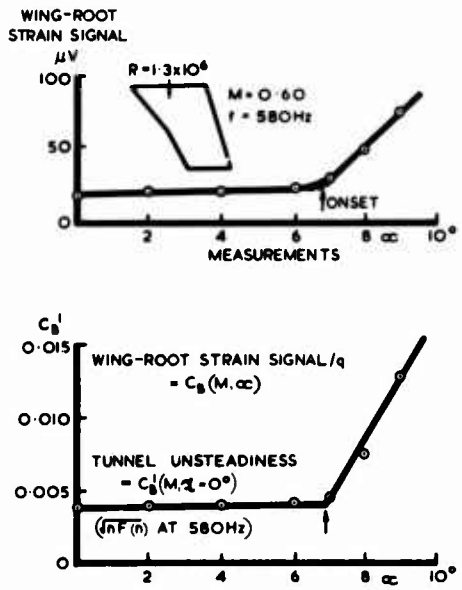

Fig.7-23 Definition of buffeting coefficients

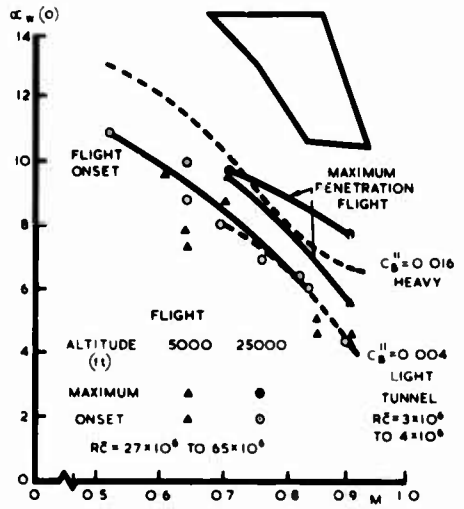

Fig.7-24 Aircraft buffeting penetration boundaries and model buffeting contours

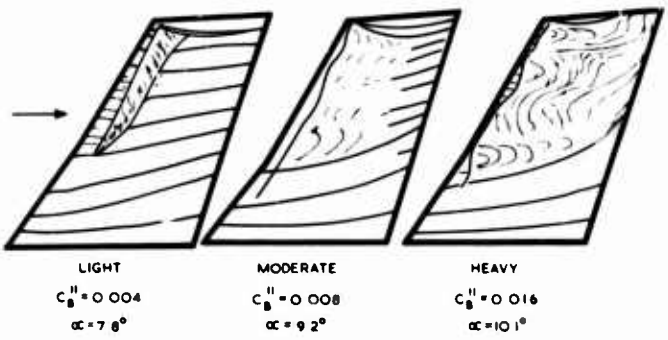

a M=0·70 R=4×10⁶

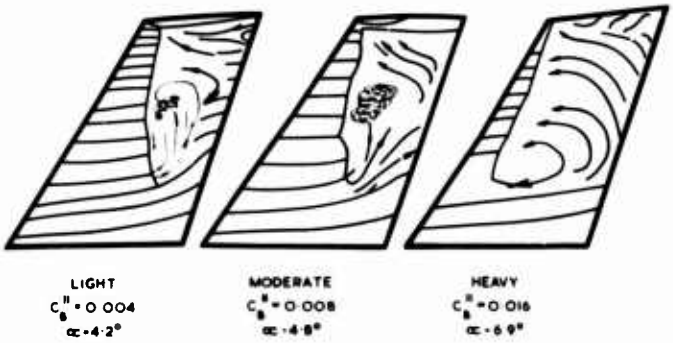

b M=0·90 R=4×10⁶

Fig.7-25a
Fig.7-25b
Surface flow patterns at different levels of buffeting

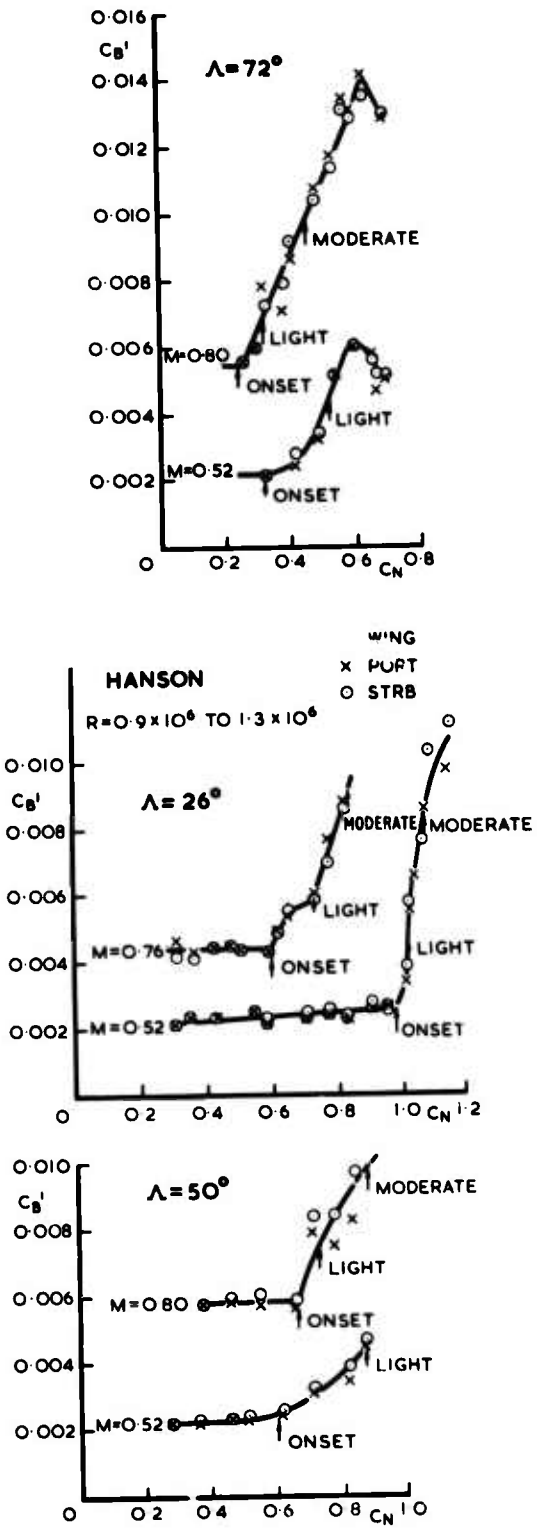

Fig.7-26 Buffeting coefficient versus normal force coefficient for a variable geometry aeroelastic model

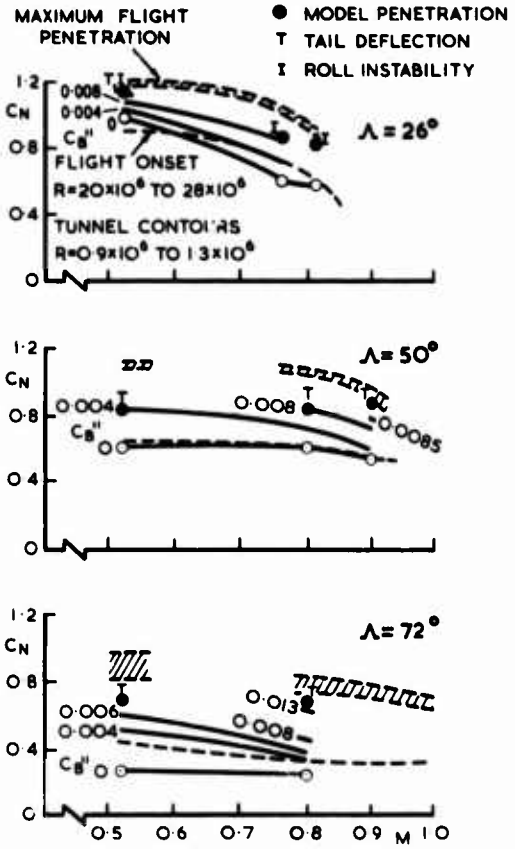

Fig.7-27 Variable geometry aircraft buffeting penetration boundaries and model buffeting contours

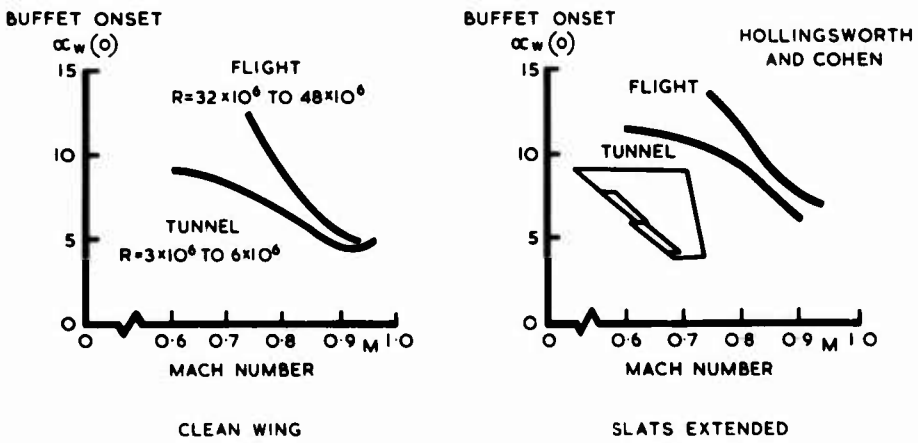

Fig.7-28 Flight/tunnel comparison for F-4 aircraft

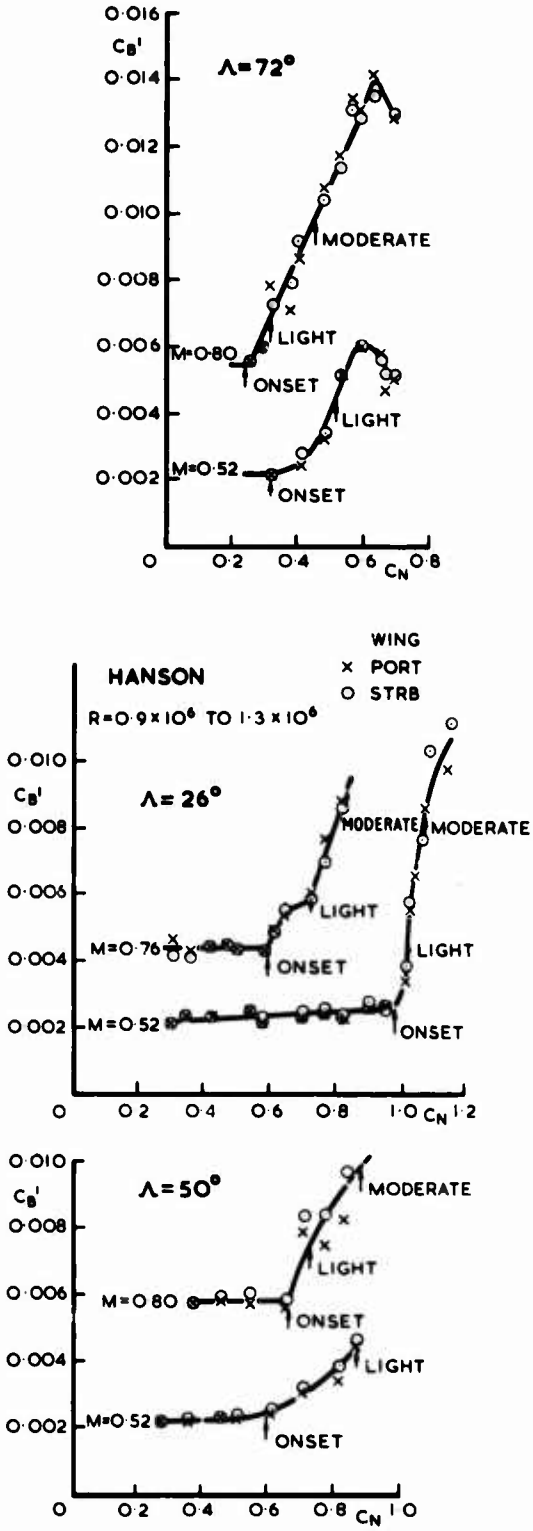

Fig.7-26 Buffeting coefficient versus normal force coefficient for a variable geometry aeroelastic model

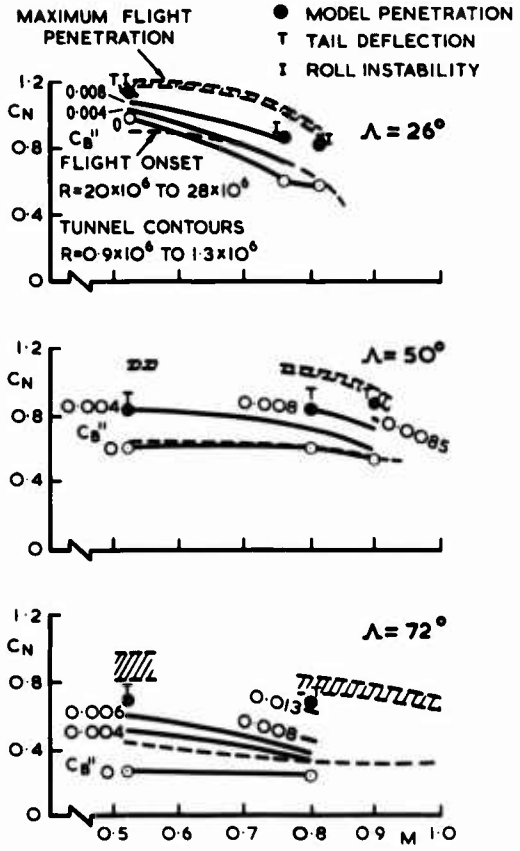

Fig.7-27 Variable geometry aircraft buffeting penetration boundaries and model buffeting contours

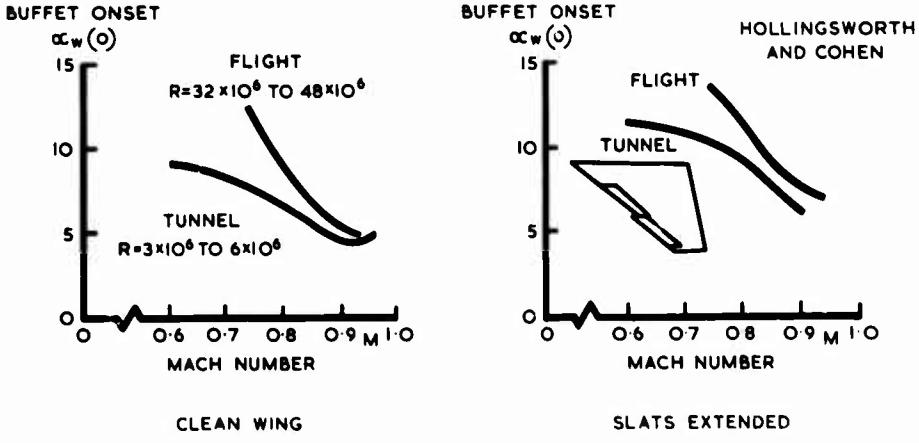

Fig.7-28 Flight/tunnel comparison for F-4 aircraft

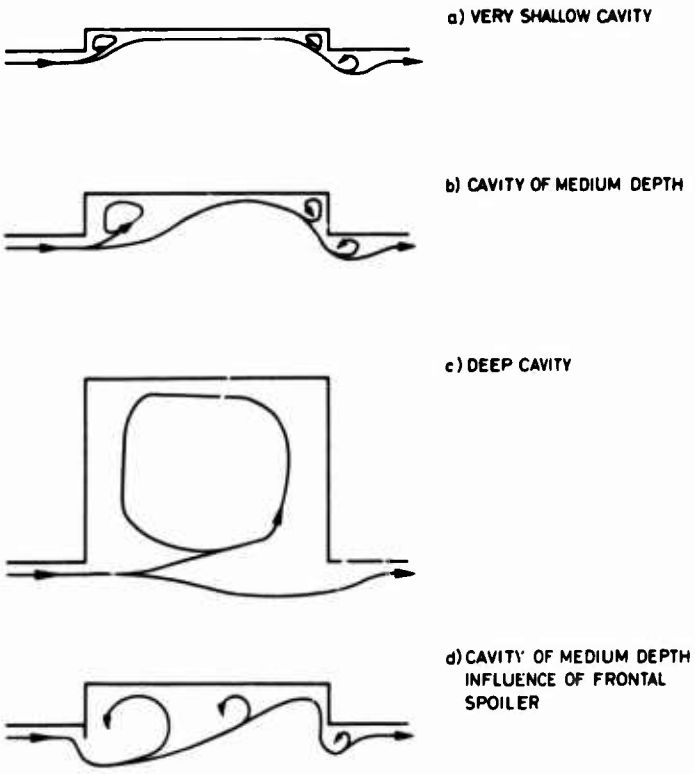

Fig.7-29 Characteristic mean flow over cavities

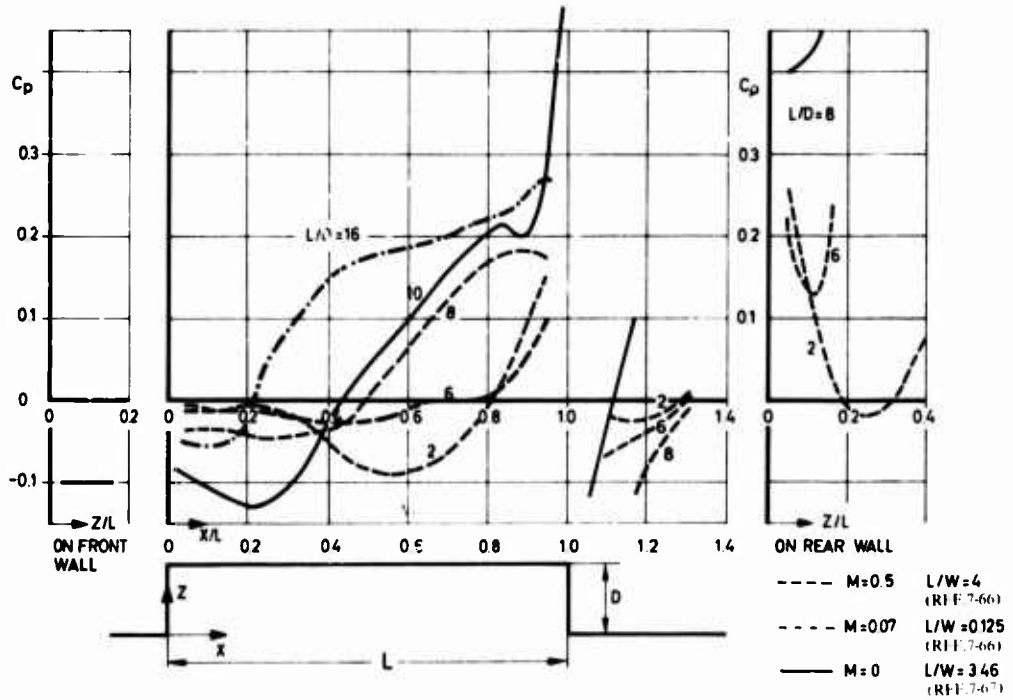

Fig.7-30 Effect of length/depth ratio on mean pressures in rectangular cavities ($\alpha = 0°$, $\beta = 0°$)

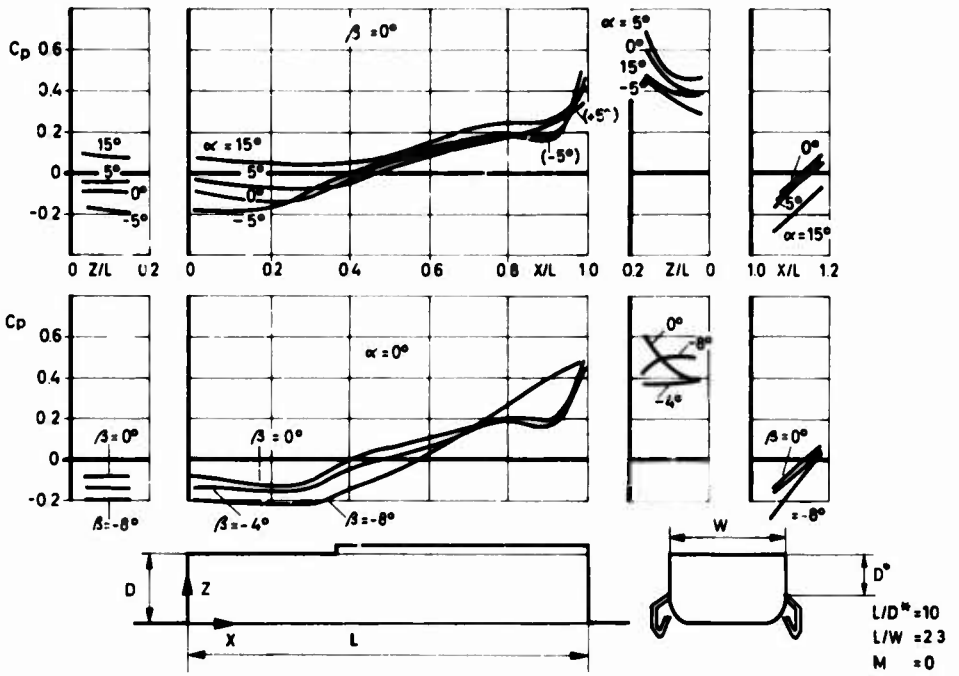

Fig.7-31 Effect of angle of attack and sideslip on mean pressures in and around a cavity (Ref.7-67)

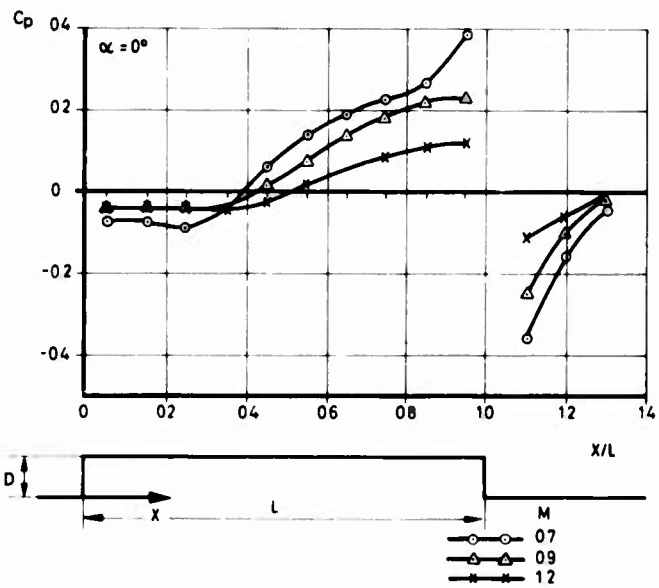

Fig.7-32 Effect of Mach number on mean pressures in and around rectangular cavity in flat plate, L/D = 10, L/W = 4 (Ref.7-66)

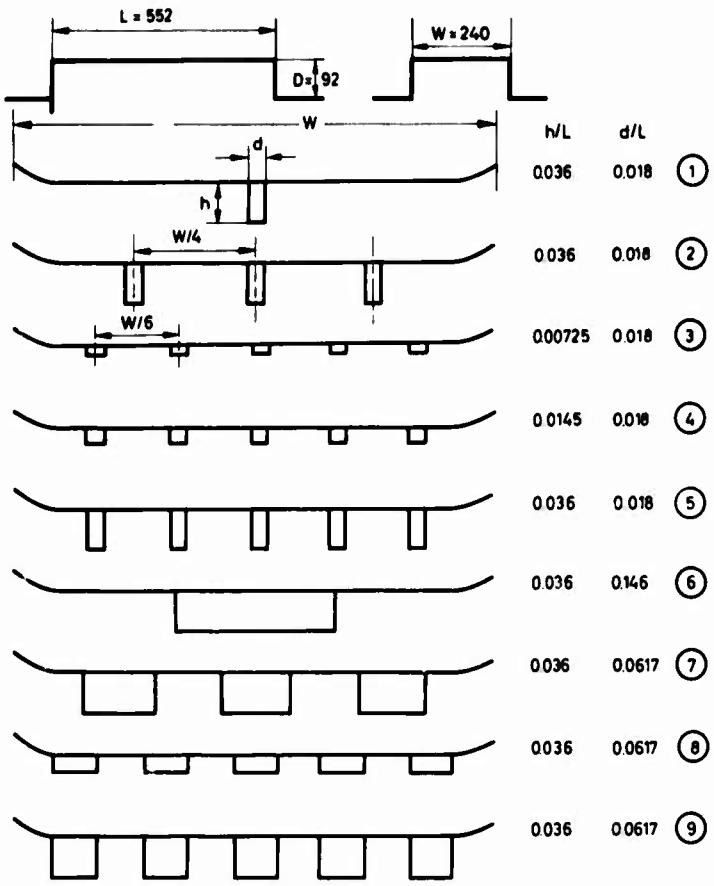

Fig.7-33 Cavity geometry and spoiler configurations

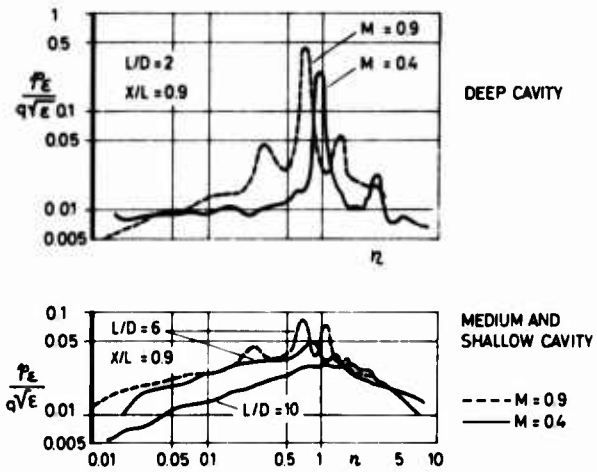

Fig.7-34 Typical frequency spectra of pressure fluctuations in cavities

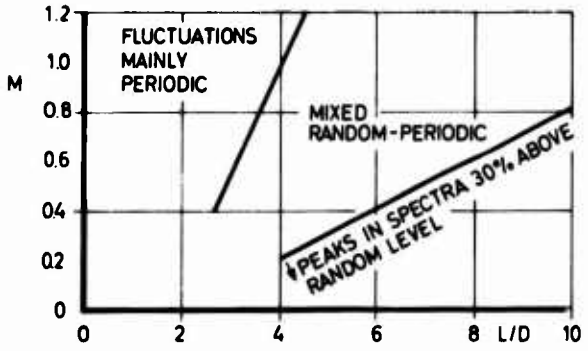

Fig. 7-35 Boundaries for the occurrence of random and periodic pressure fluctuations in cavities

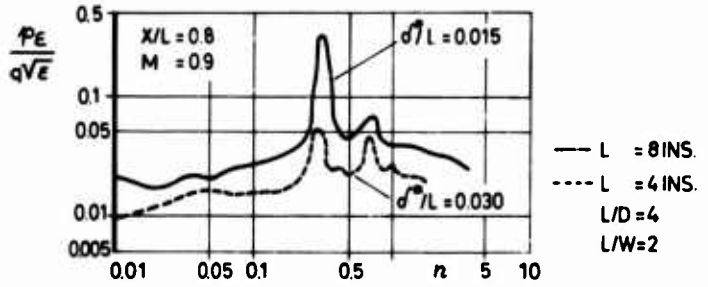

Fig. 7-36 Effects of boundary layer thickness on spectra of pressure fluctuations

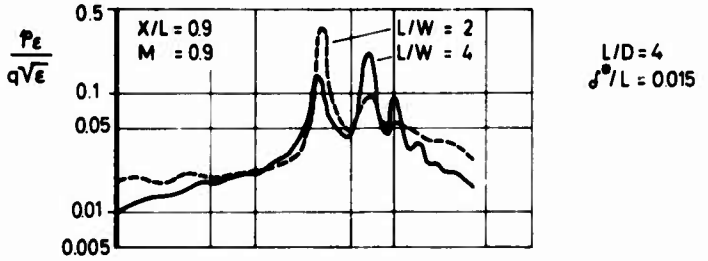

Fig. 7-37 Effect of cavity width on spectra of pressure fluctuations

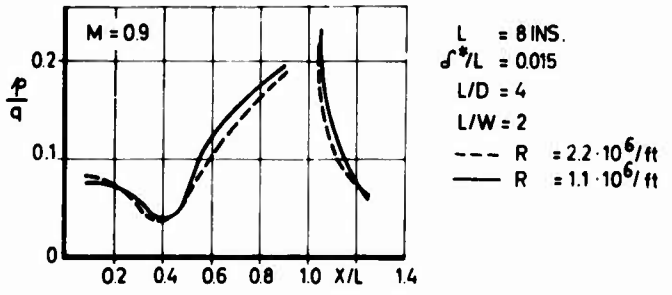

Fig. 7-38 Reynolds number effect on RMS pressure fluctuations

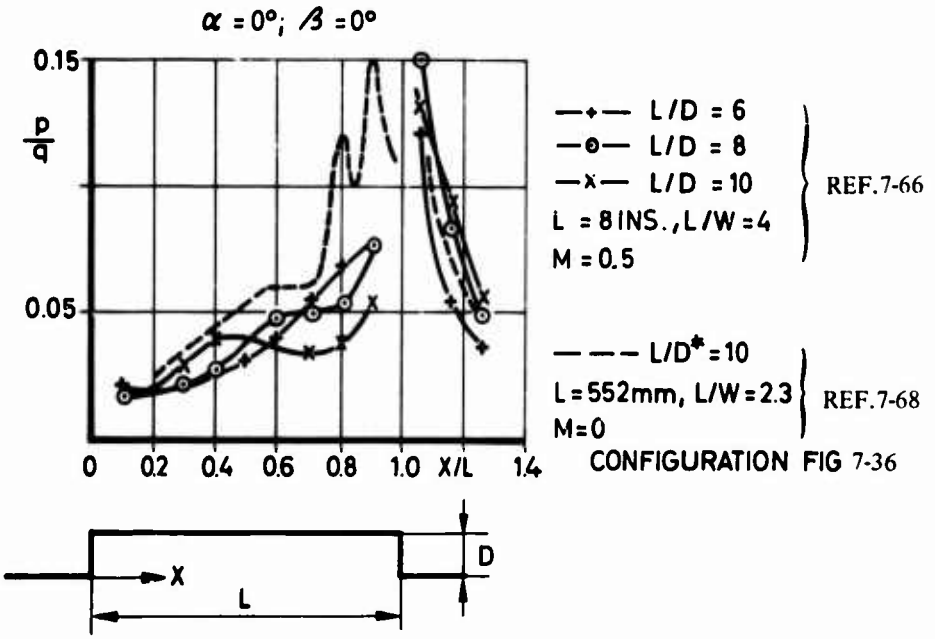

Fig.7-39 RMS pressure distribution in shallow rectangular cavities, effect of length/depth ratio

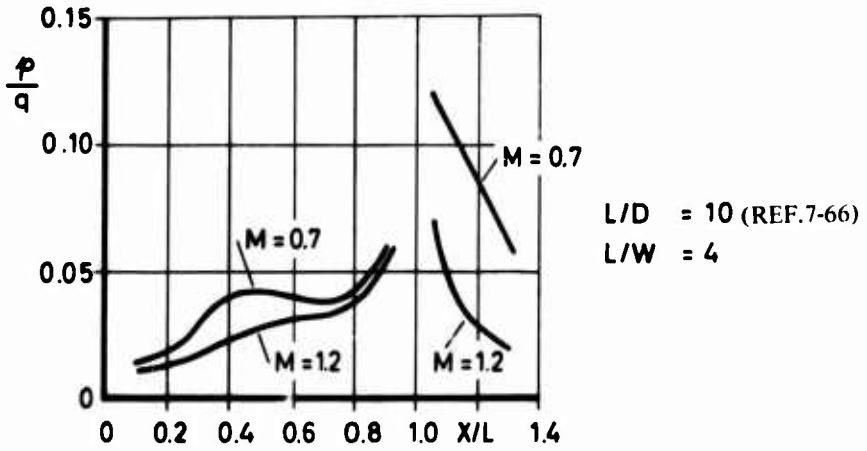

Fig.7-40 Effect of Mach number on RMS pressure fluctuations in rectangular shallow cavity

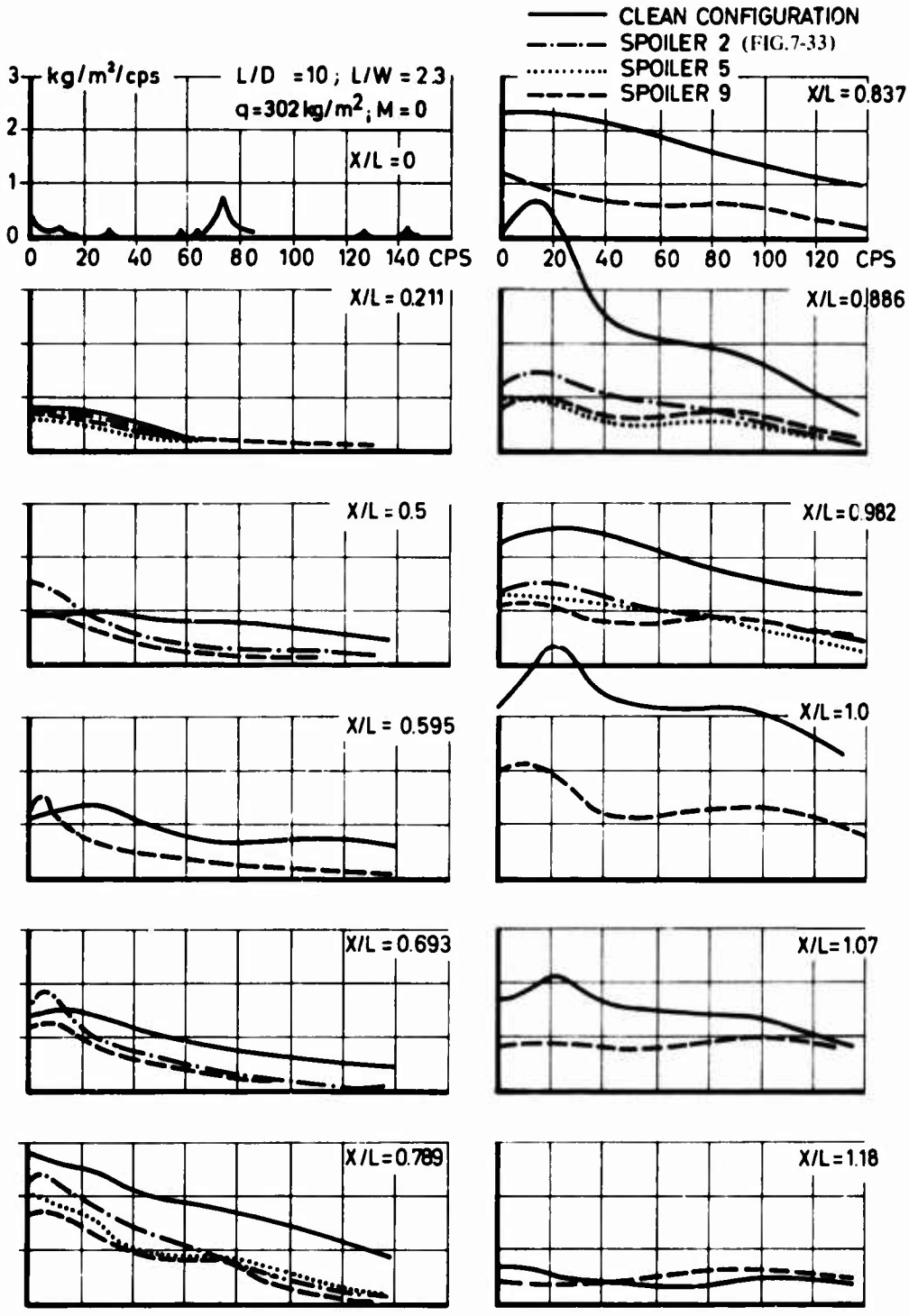

Fig.7-41 Comparison of spectra of pressure fluctuation efficiency for different spoiler configurations

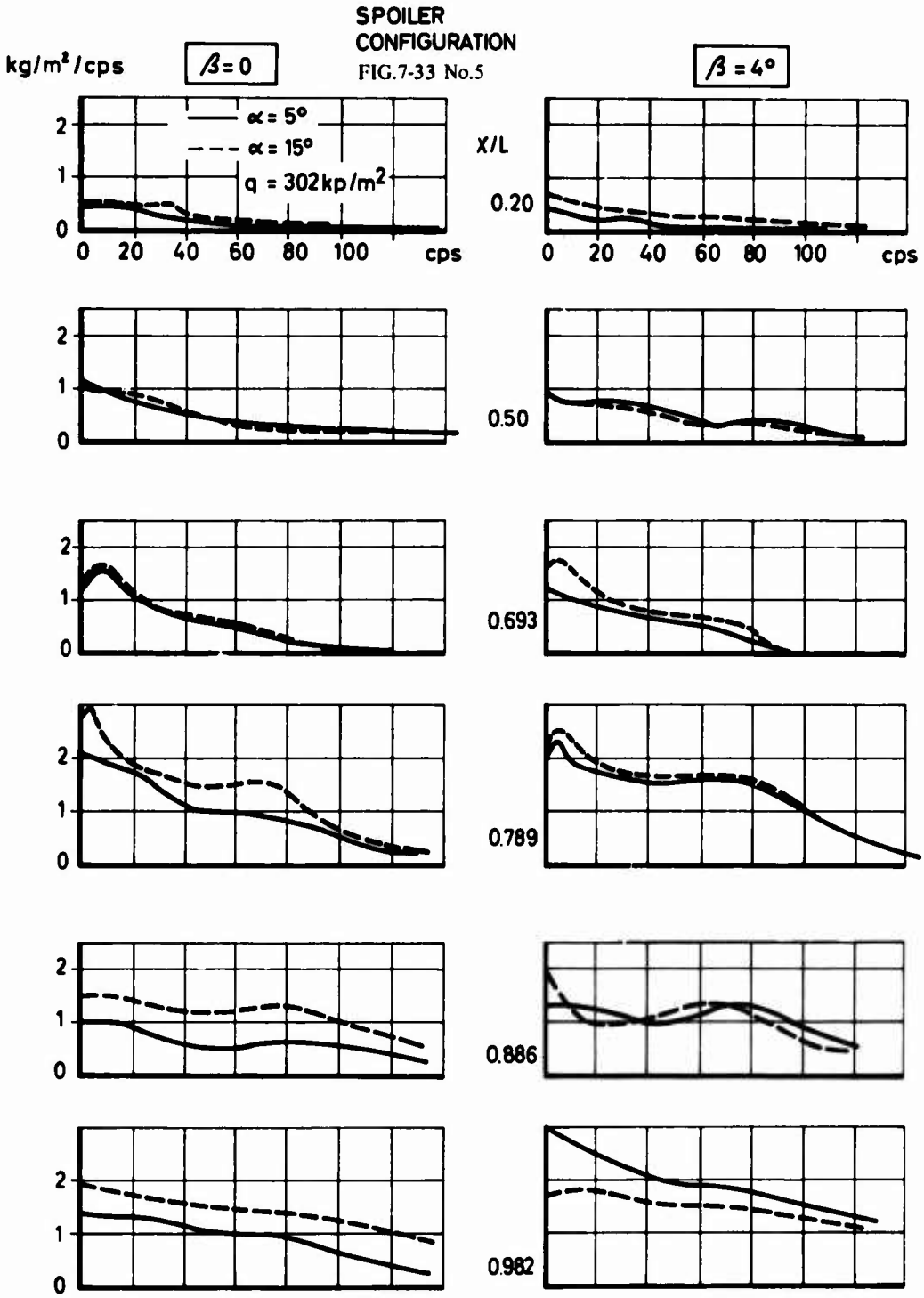

Fig.7-42 Effect of angle of attack and sideslip on spectra of pressure fluctuations

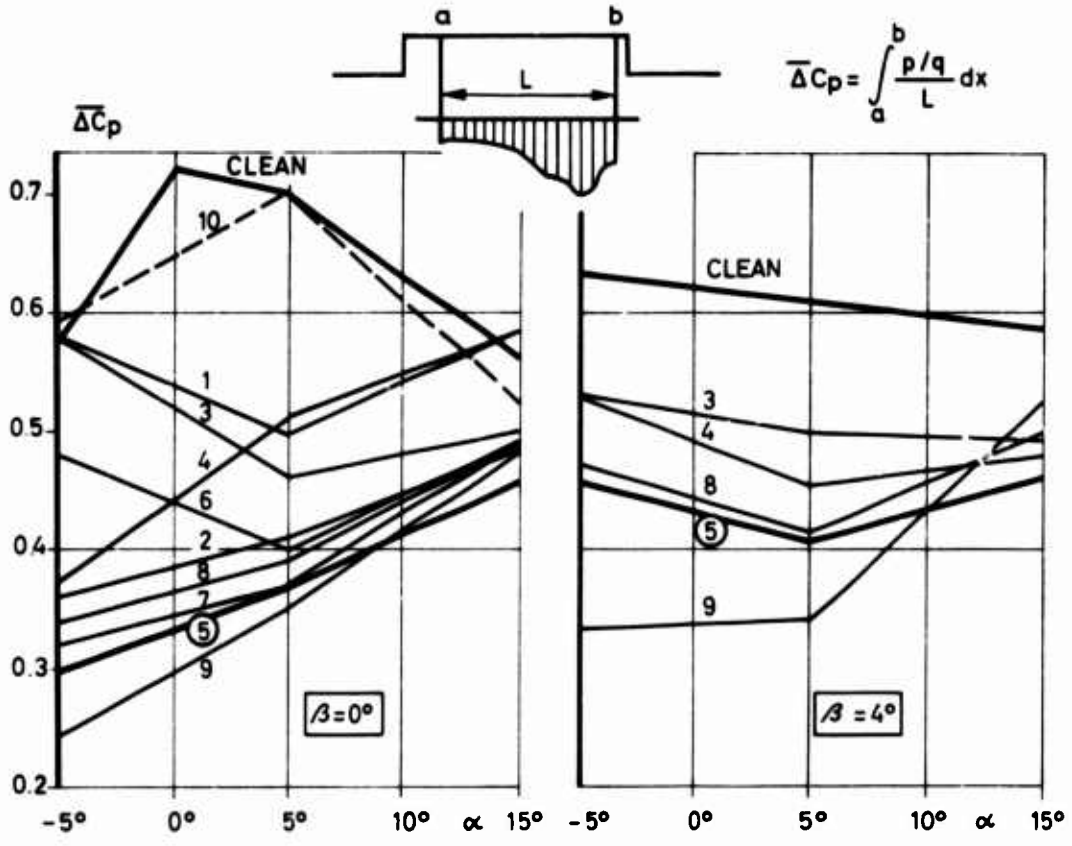

Fig.7-43 Efficiency of different spoiler geometry and number on RMS pressure fluctuations for cavity in varying attitudes (L/D = 10, L/W = 2.3, M = 0), spoiler numbers shown in Fig.7-33

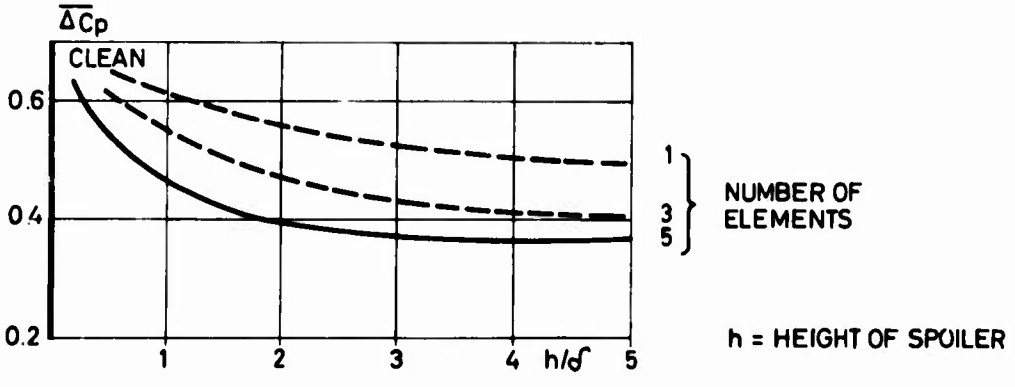

Fig.7-44 Reduction of RMS pressure fluctuations for varying spoiler length and number

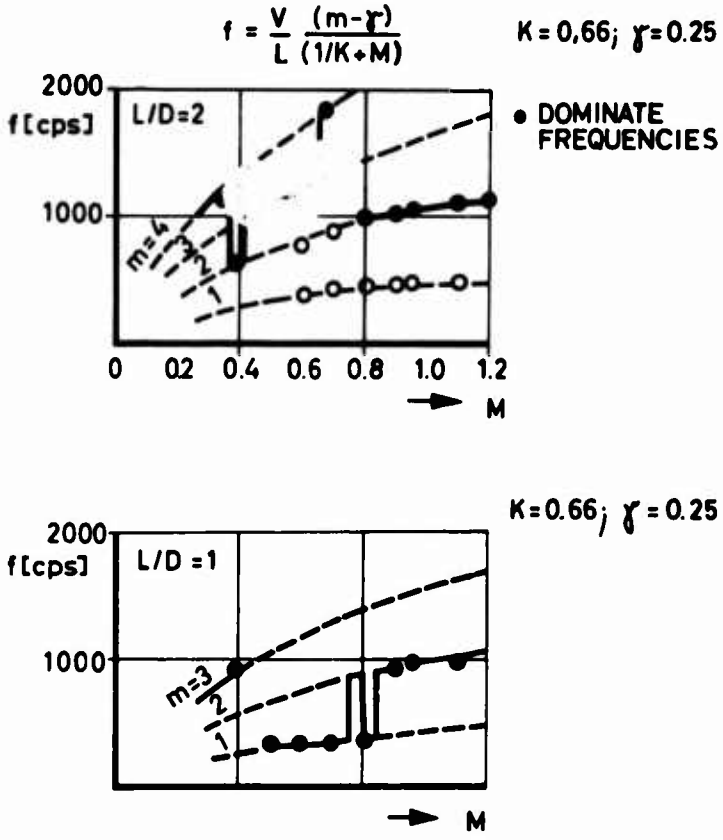

Fig.7-45 Frequency of periodic pressure fluctuations in deep cavities (L = 8ins, L/W = 4)

1 RMS DEVIATION OF BENDING MOMENT

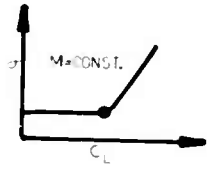

2 TRAILING EDGE PRESSURE DEVIATION

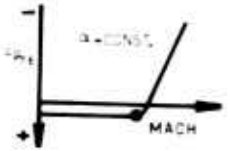

3 LOCAL LIFT CURVE SLOPE REDUCTION

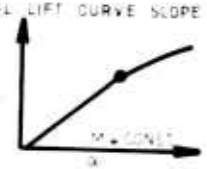

4 DESTABILIZING PITCHING MOMENT SLOPE CHANGE

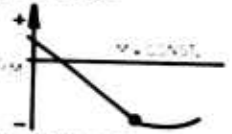

5 WING WAKE WIDTH AT T.E

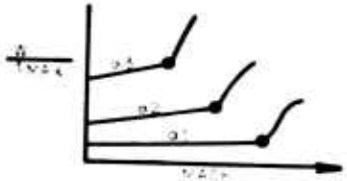

6 SHOCK WAVE POSITION

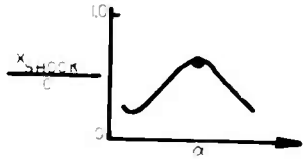

7. SHOCK DOWNSTREAM MACH NO. GREATER THAN SONIC

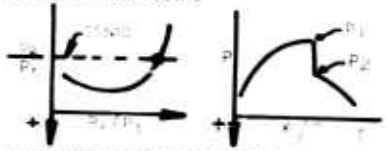

8. ACCELEROMETER RECORDINGS

9 FLOW VISUALIZATION

(a) OIL FLOW
(b) TUFTS
(c) SCHLIEREN

10. AXIAL FORCE DEVIATION

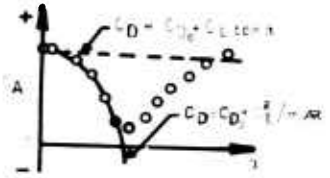

11. ROLLING MOMENT DEVIATION

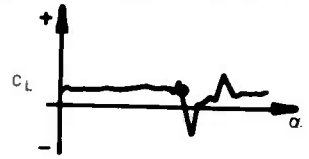

12. THIN FILM SKIN FRICTION GAUGES FOR FLOW SEPARATION DETECTION

13. HOT WIRE PROBES (FOR TURBULENCE MEASUREMENTS)

14. PRESSURE FLUCTUATION MEASUREMENTS
(a) ACOUSTIC MEANS
(b) RAPID RESPONSE PRESSURE TRANSDUCERS

15. PILOT OPINION

Fig.8-1 Methods of buffet/flow separation detection

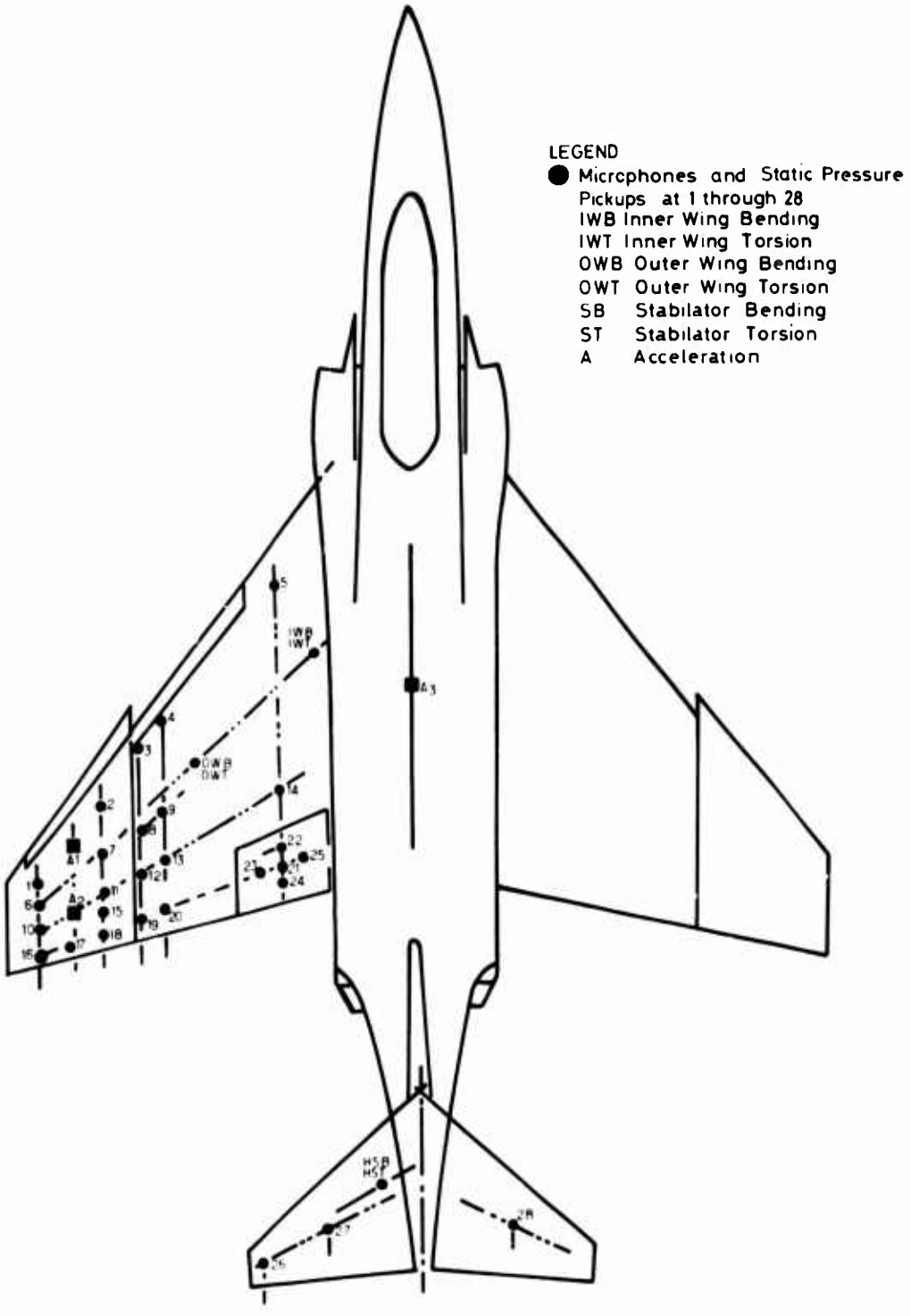

Fig.8-2 Model instrumentation

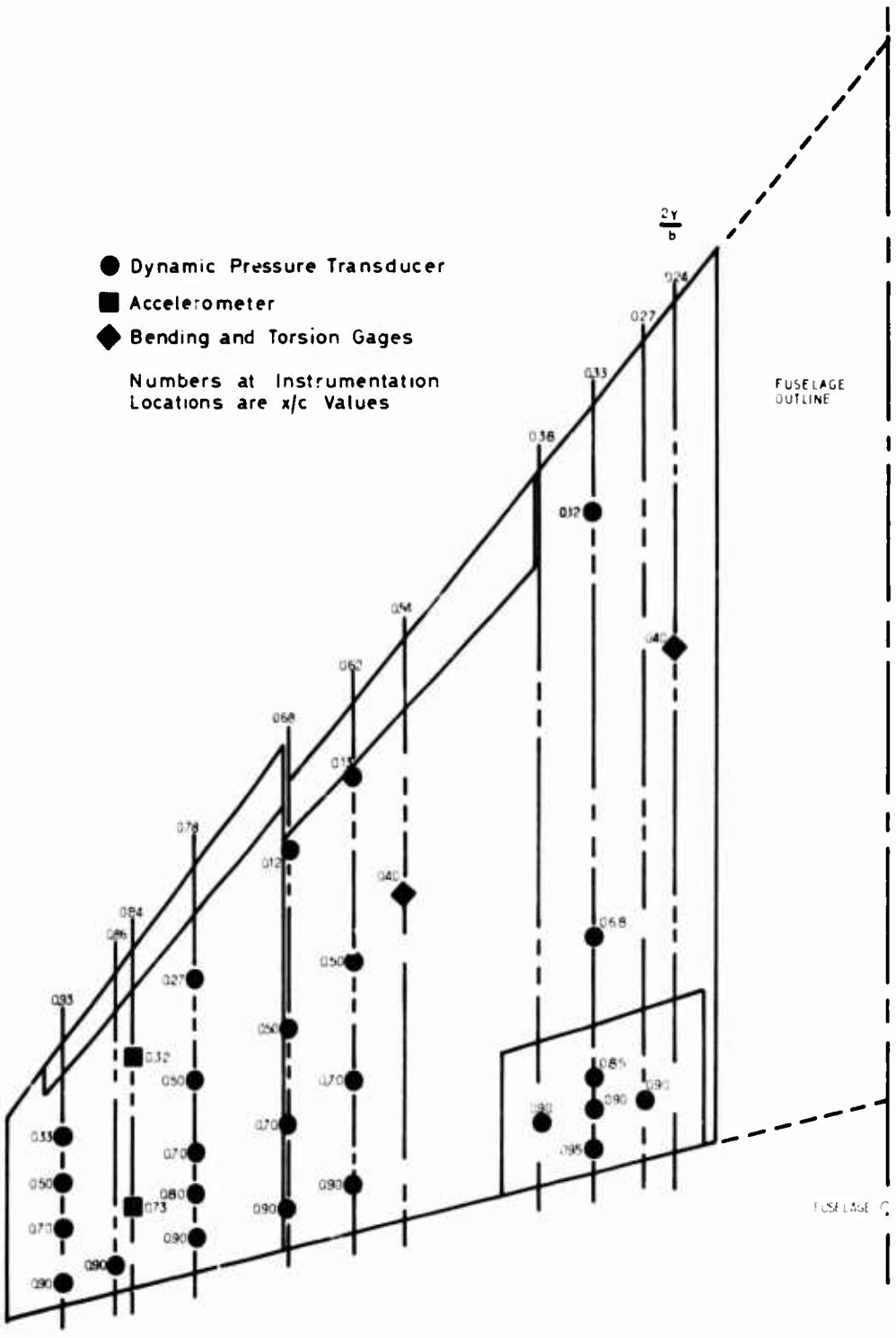

Fig.8-3 Wing instrumentation locations

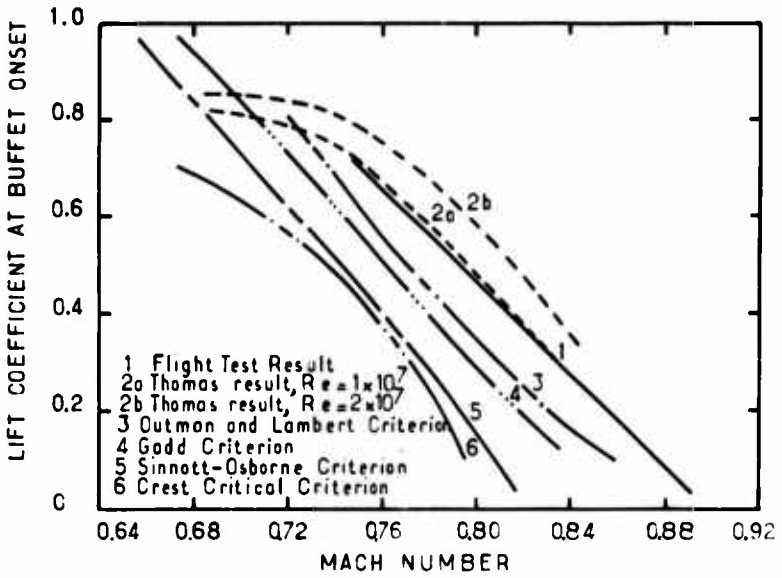

Fig.8-4 Buffet boundary for X-1 aircraft (Refs. 8-1 and 8-11)

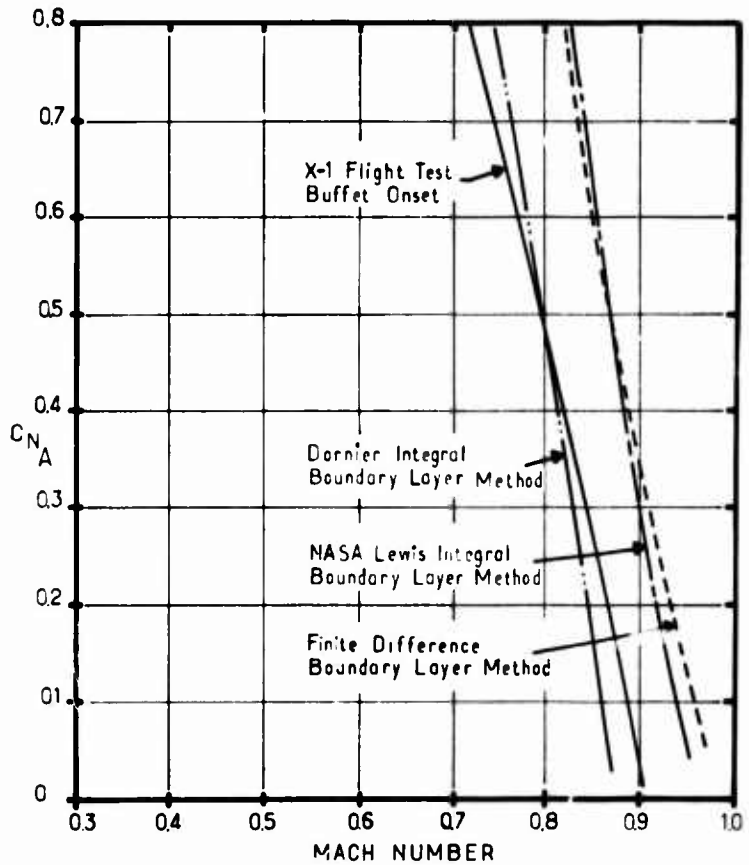

Fig.8-5 Comparison of buffet onset calculations for X-1 airfoil. Re = 1 x 10^7, buffet criteria of dS/dM = 0, $C_{N_A} = c_n$

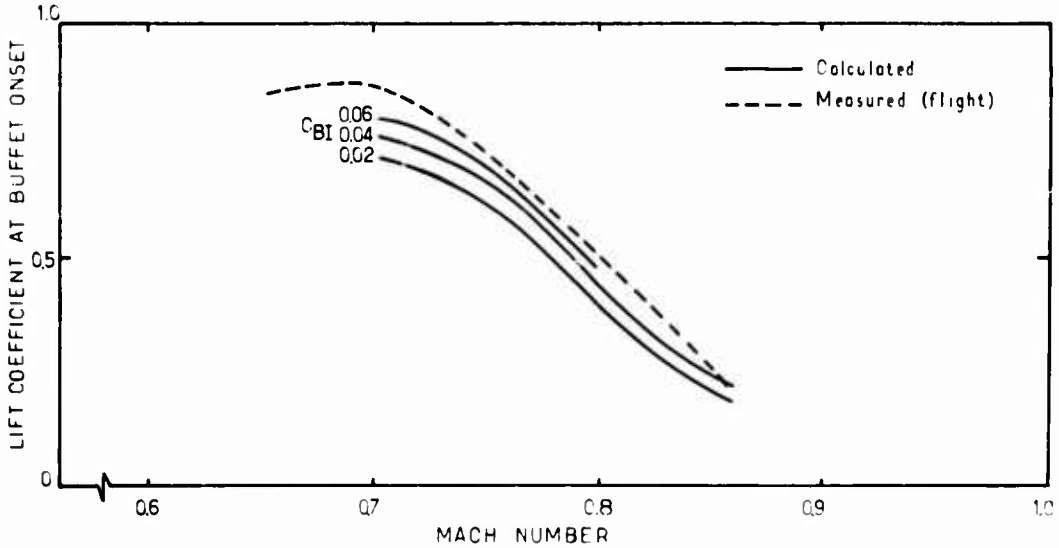

Fig. 3-6 Comparison of calculated and measured buffet data (Bell X-1 aircraft)

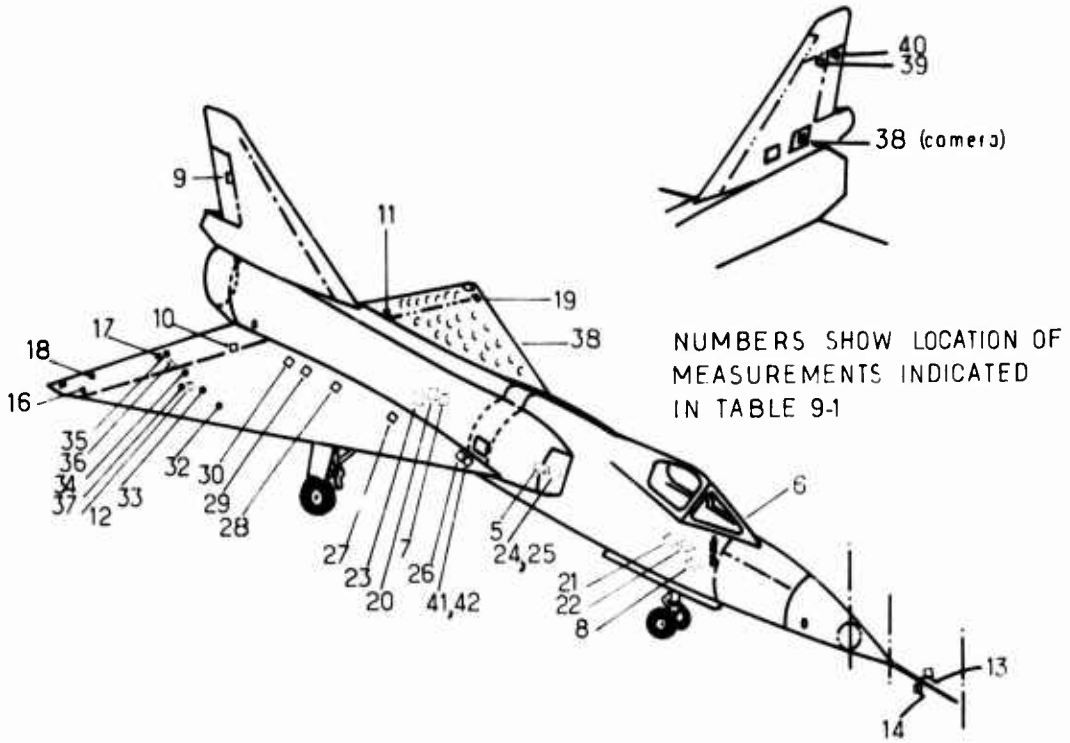

Fig.9-1 Locations of buffet instrumentation

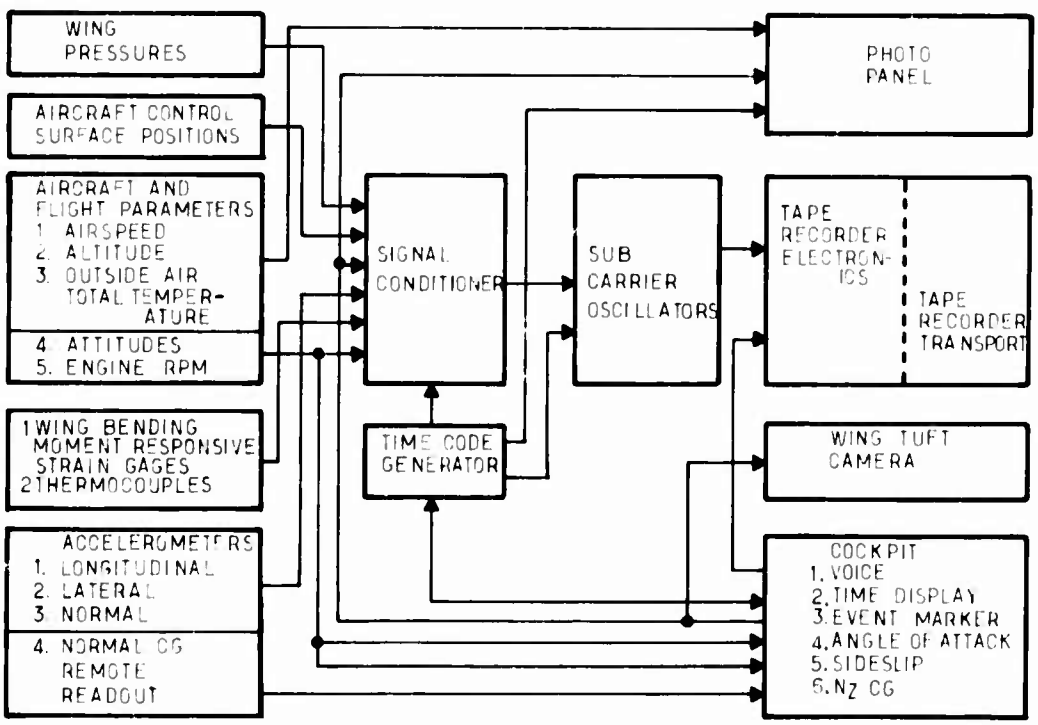

Fig.9-2 Block diagram of buffet instrumentation system

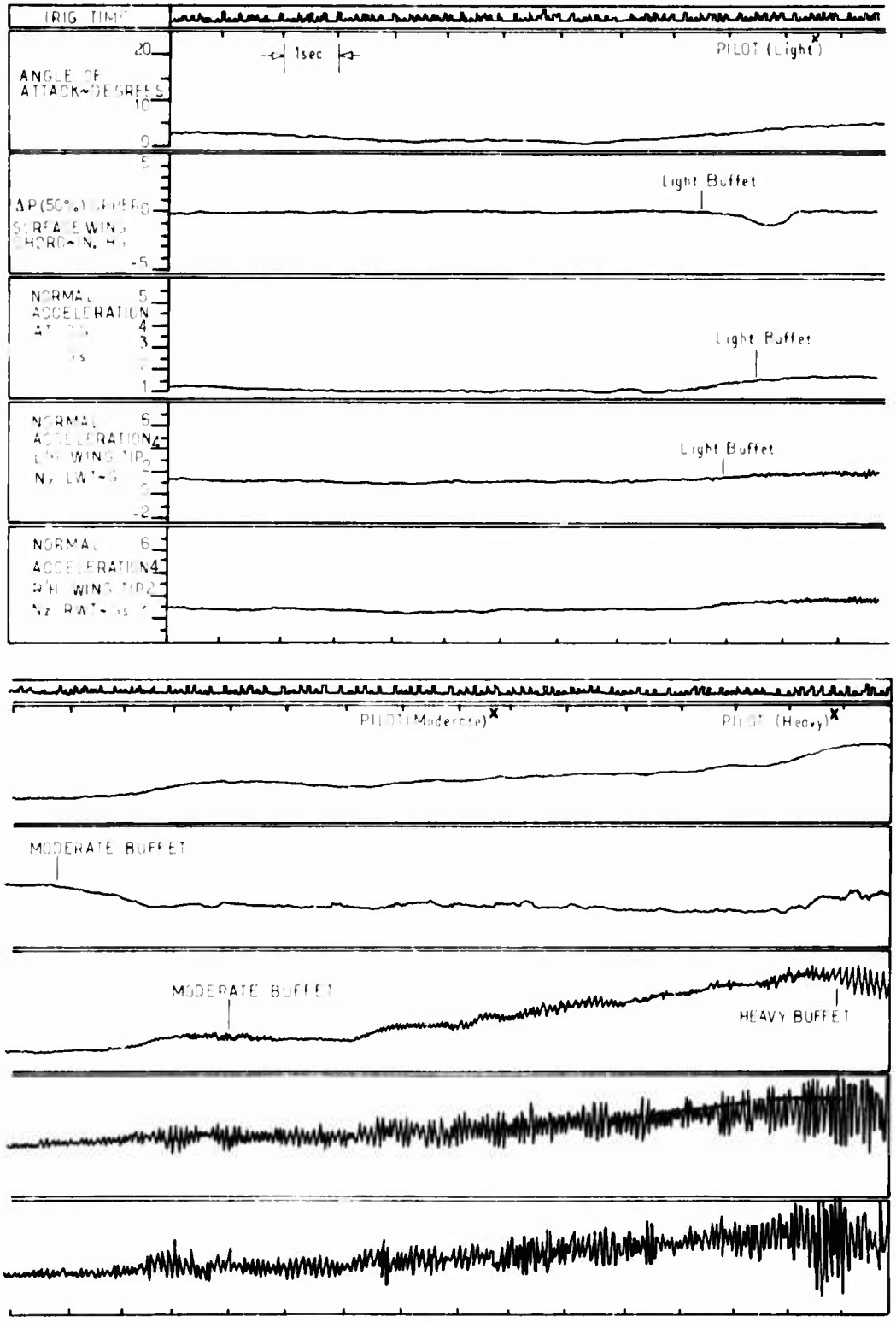

Fig.9-3 Flight buffet data

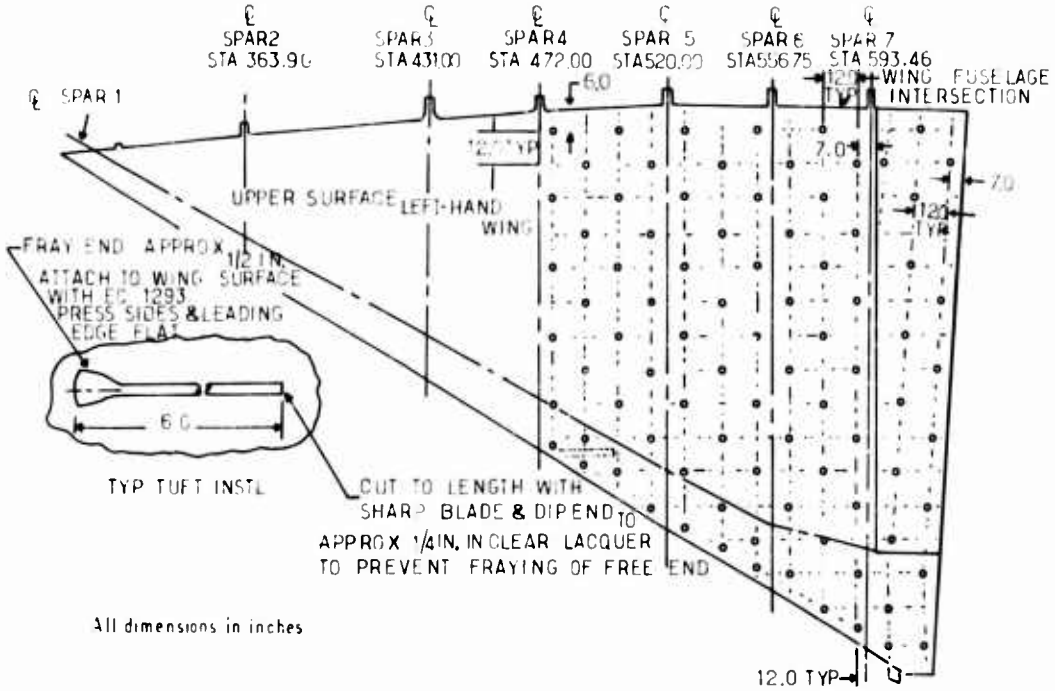

Fig.9-4 Wing tuft grid pattern

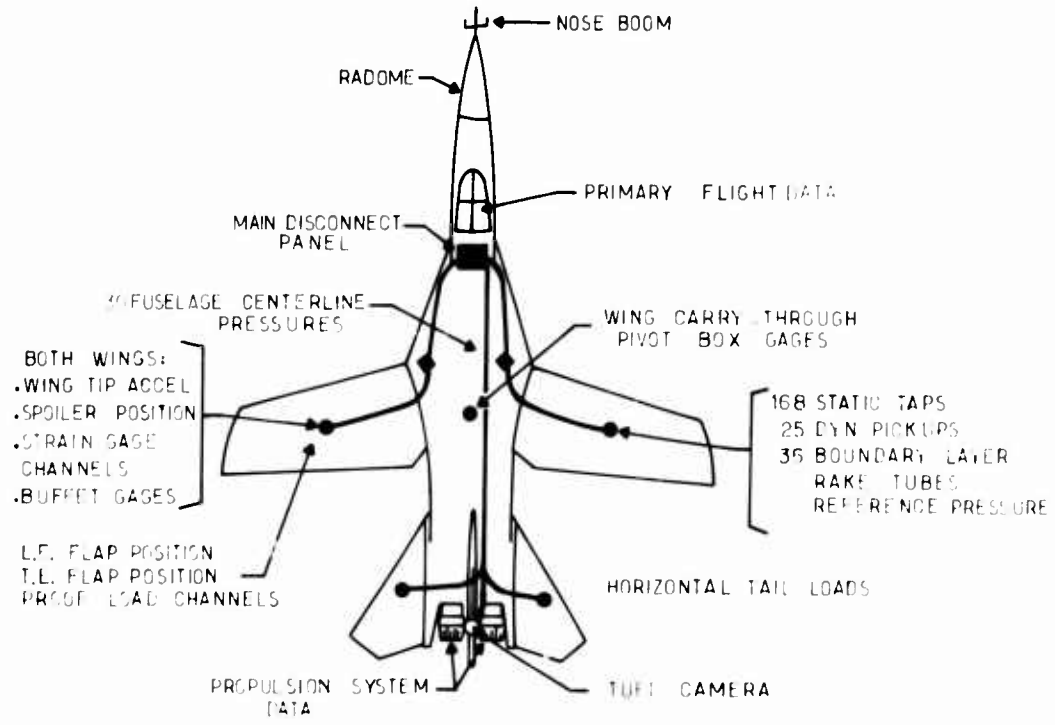

Fig.9-5 Flight test instrumentation (TACT program)

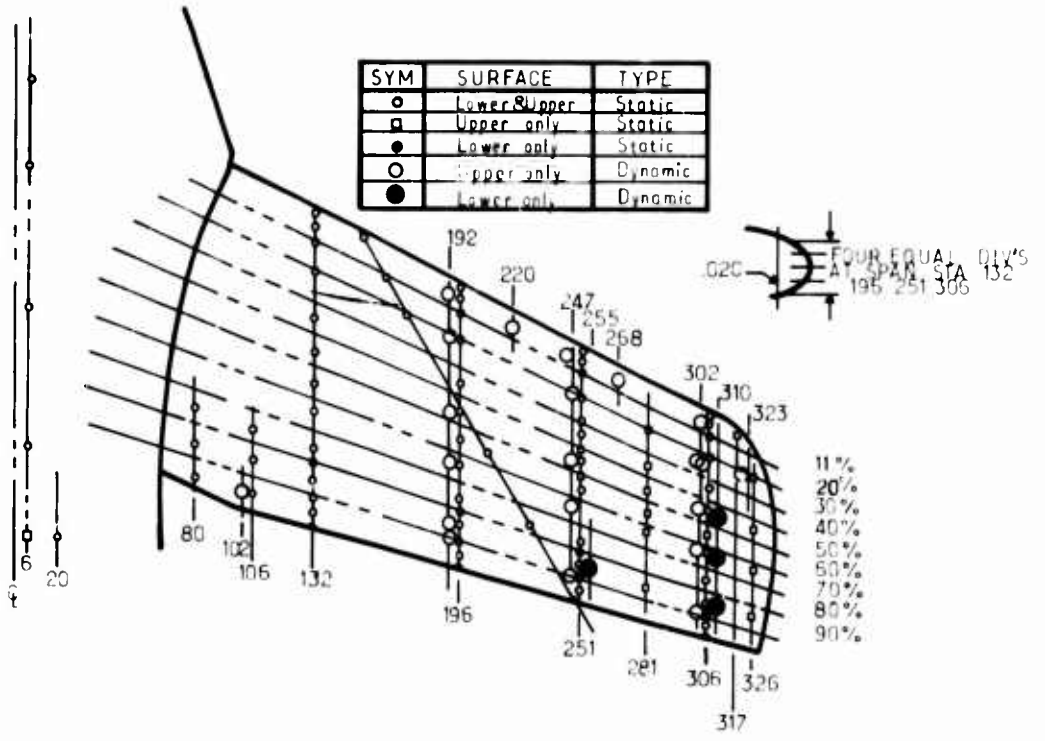

Fig.9-6 Wing pressure orifice locations (TACT program)

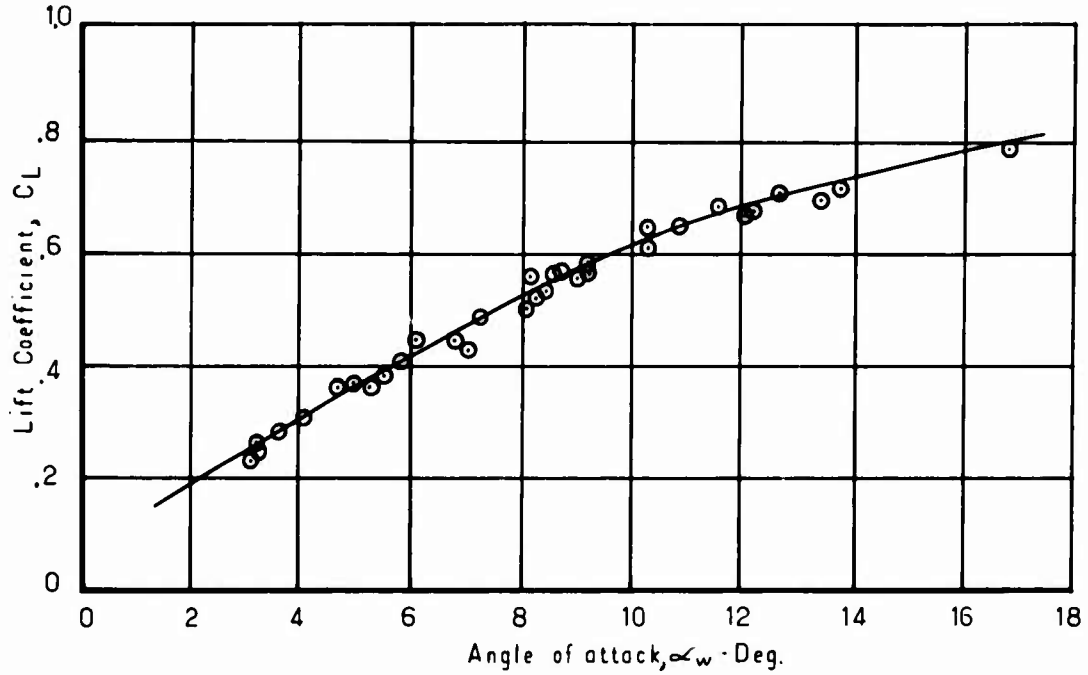

Fig.9-7 Buffet flight test lift curve

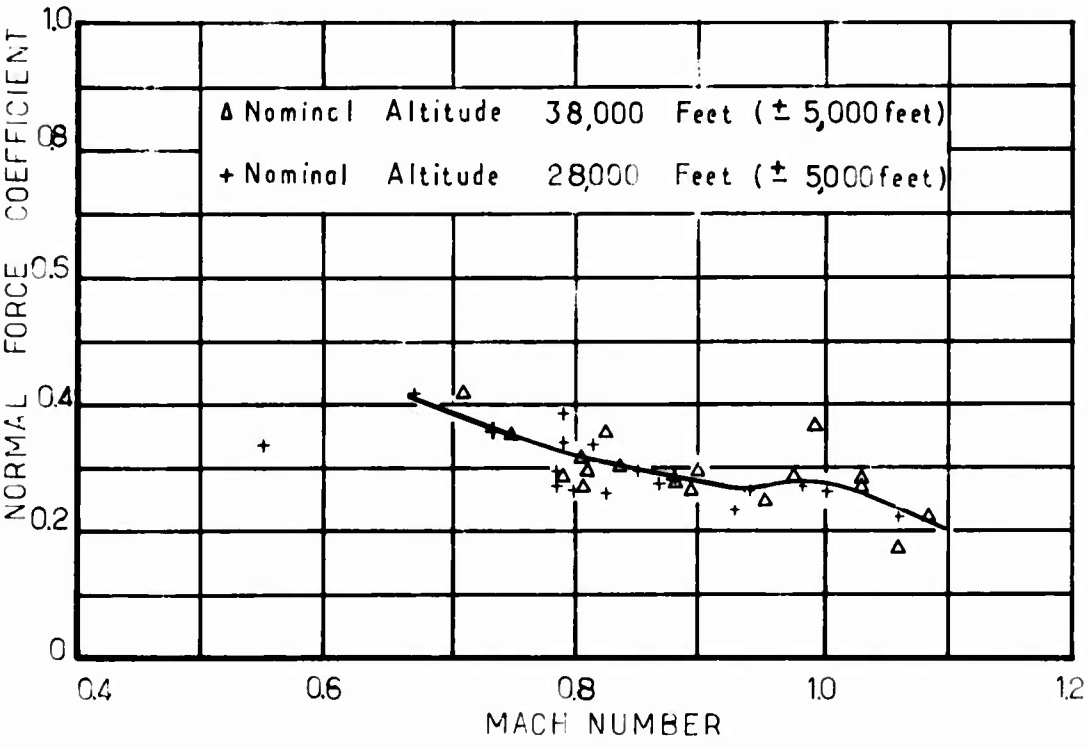

Fig.9-8 Flight test light buffet onset data

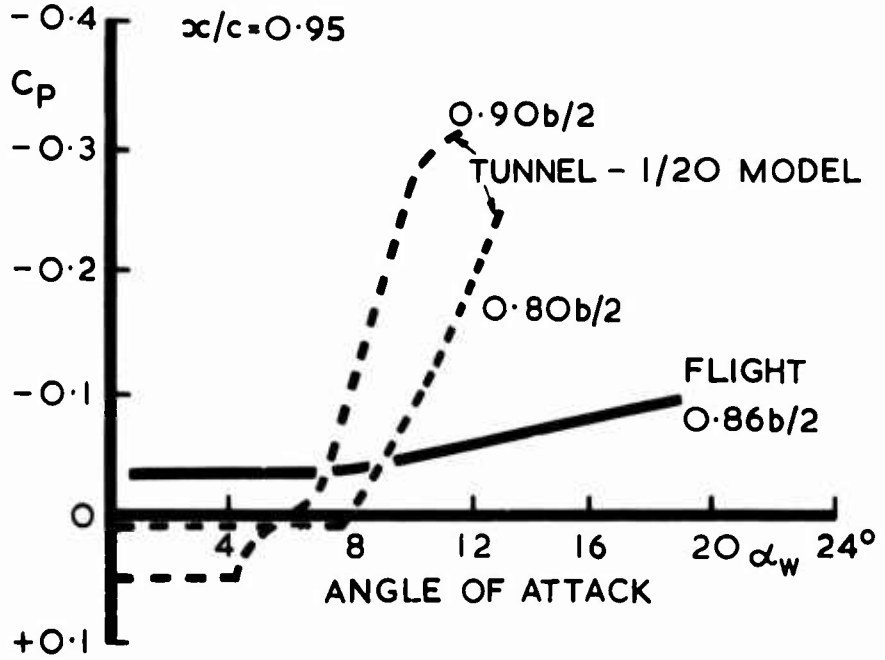

Fig.10-1 F-4E aircraft: comparison of wind tunnel and flight pressure coefficients close to the trailing-edge M = 0.8

	M	α_W	$R_C \times 10^{-6}$	C_ℓ	MODEL	BOUNDARY LAYER TRIP
—-x—	0·90	7·9°	3·9	0·56	1/10	15% c No.60 GRIT
--◇--	0·90	8·0°	7·7	0·57	1/10	15% c No.60 GRIT
—o—	0·89	7·9°	44·4	0·59	FLIGHT	NONE

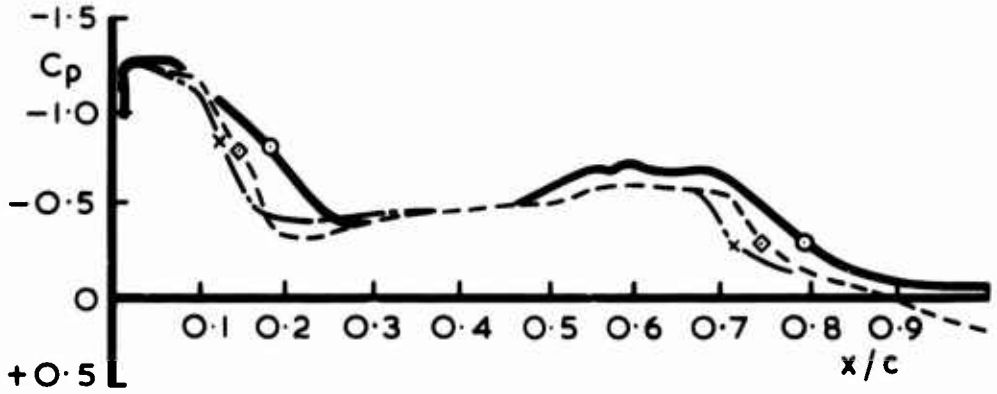

Fig.10-2 F-4 aircraft: comparison of wind tunnel and flight chordwise pressure distributions on the inner wing M = 0.90 $\alpha \sim 8°$

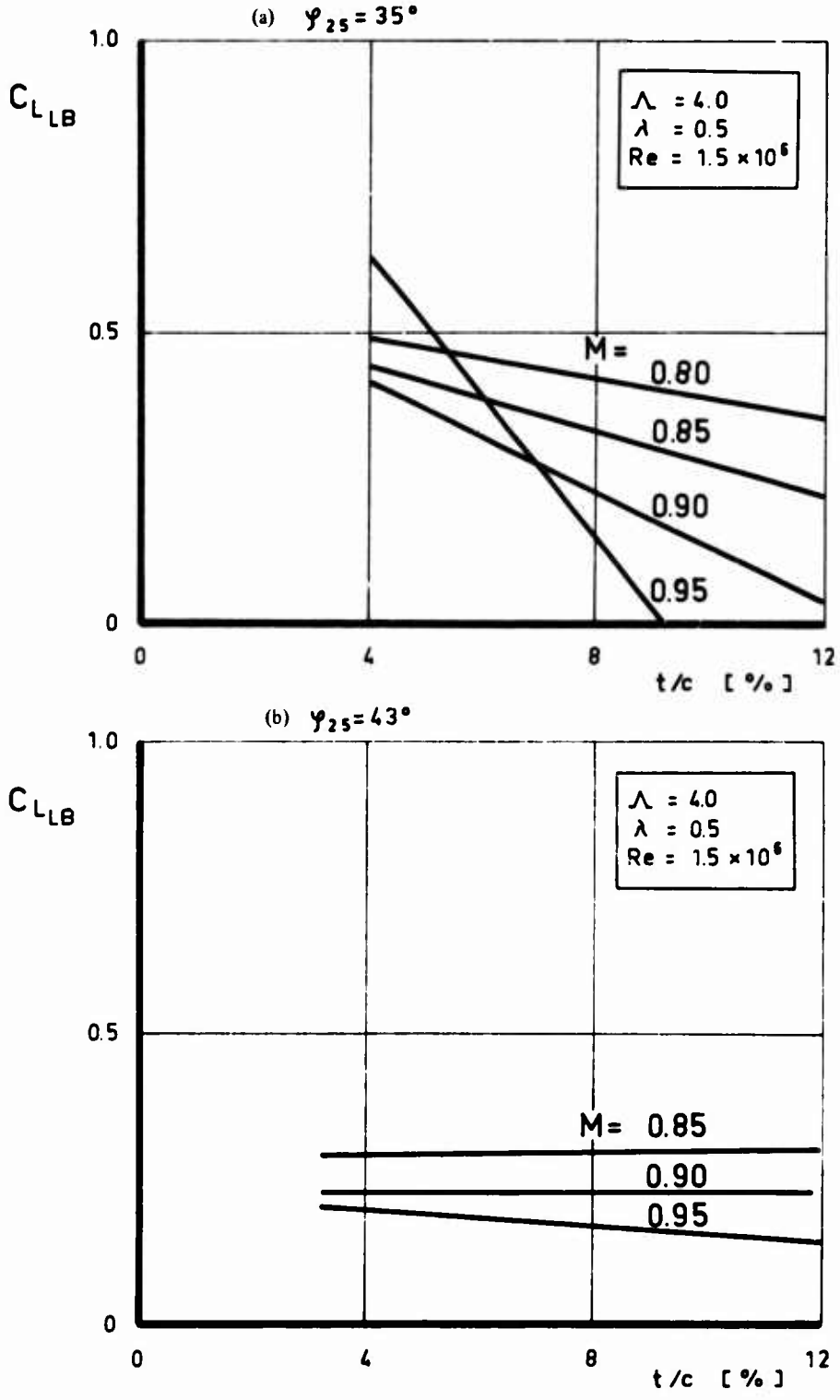

Fig.11-1 Influence of maximum thickness on buffet boundary "light buffet" (Ref.11-2)

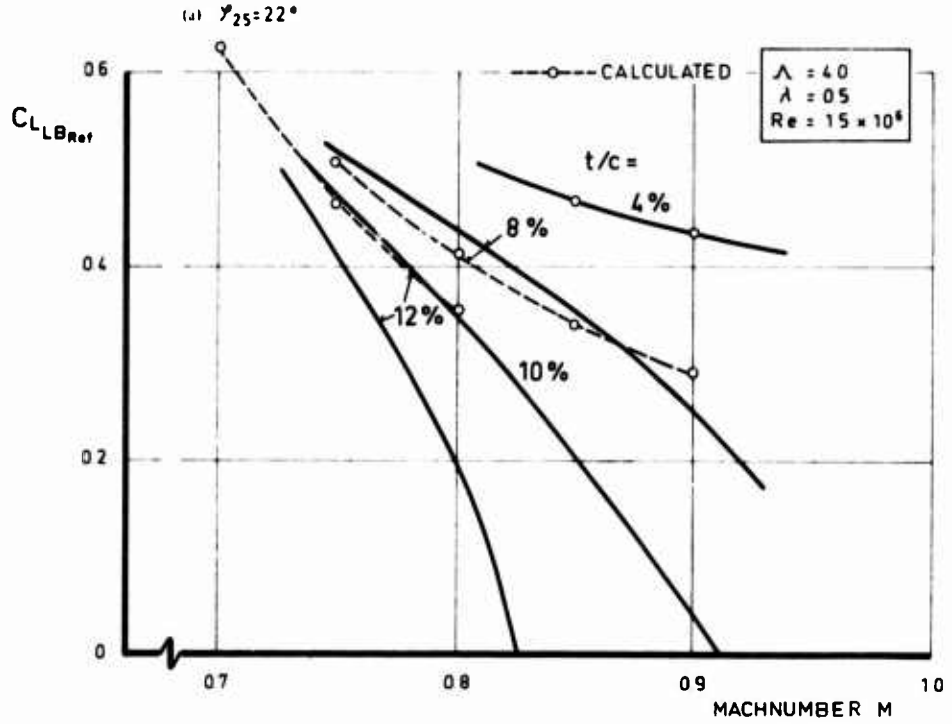

Fig.11-2 Influence of thickness, sweep angle, and Mach number on buffet boundary – "light buffet" (Ref.11-2)

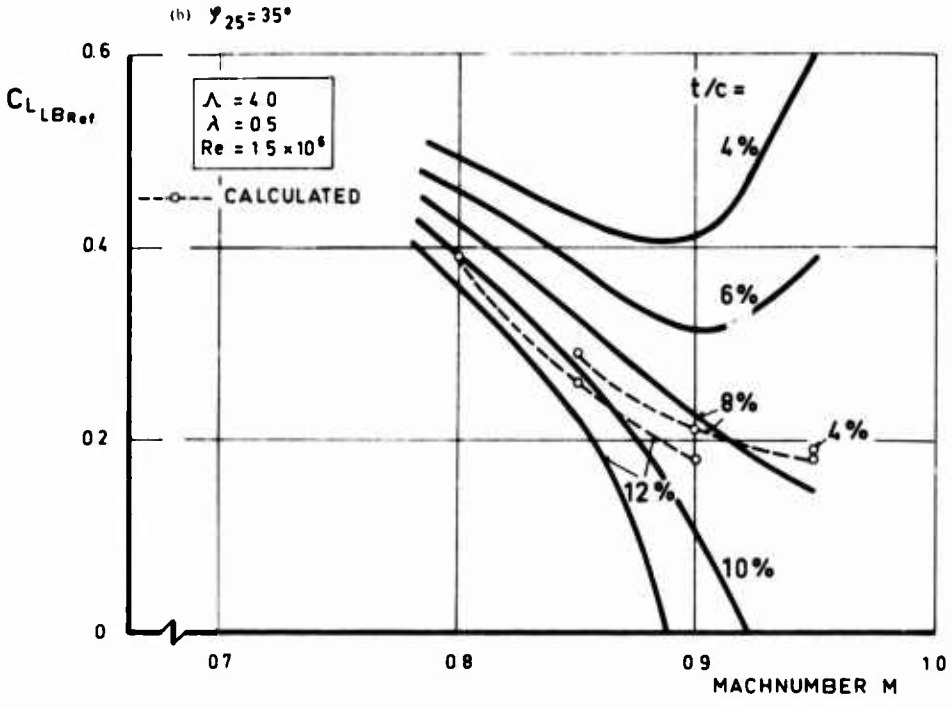

Figure 11-2 (continued)

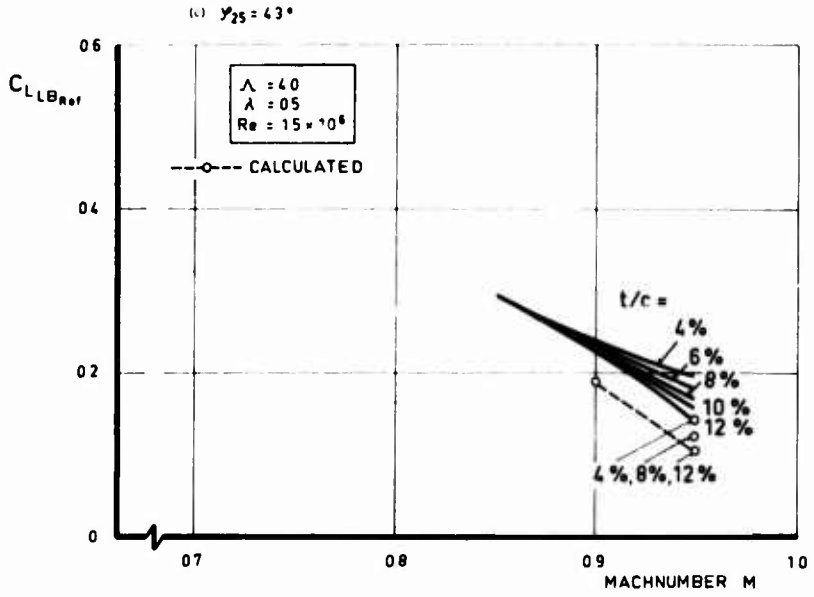

Figure 11-2 (concluded)

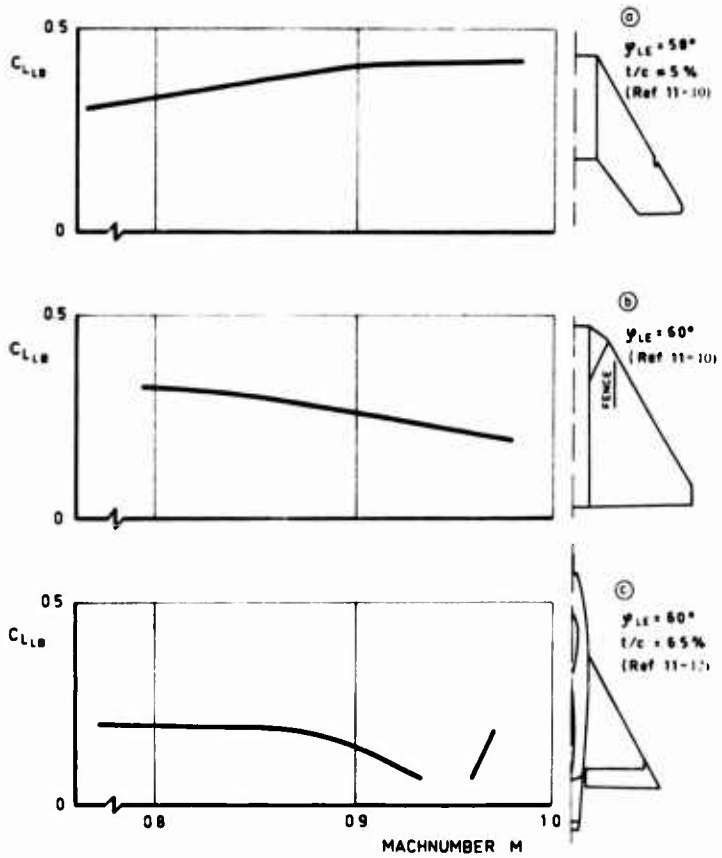

Fig.11-3 Light buffet boundaries of highly swept wings (flight tests)

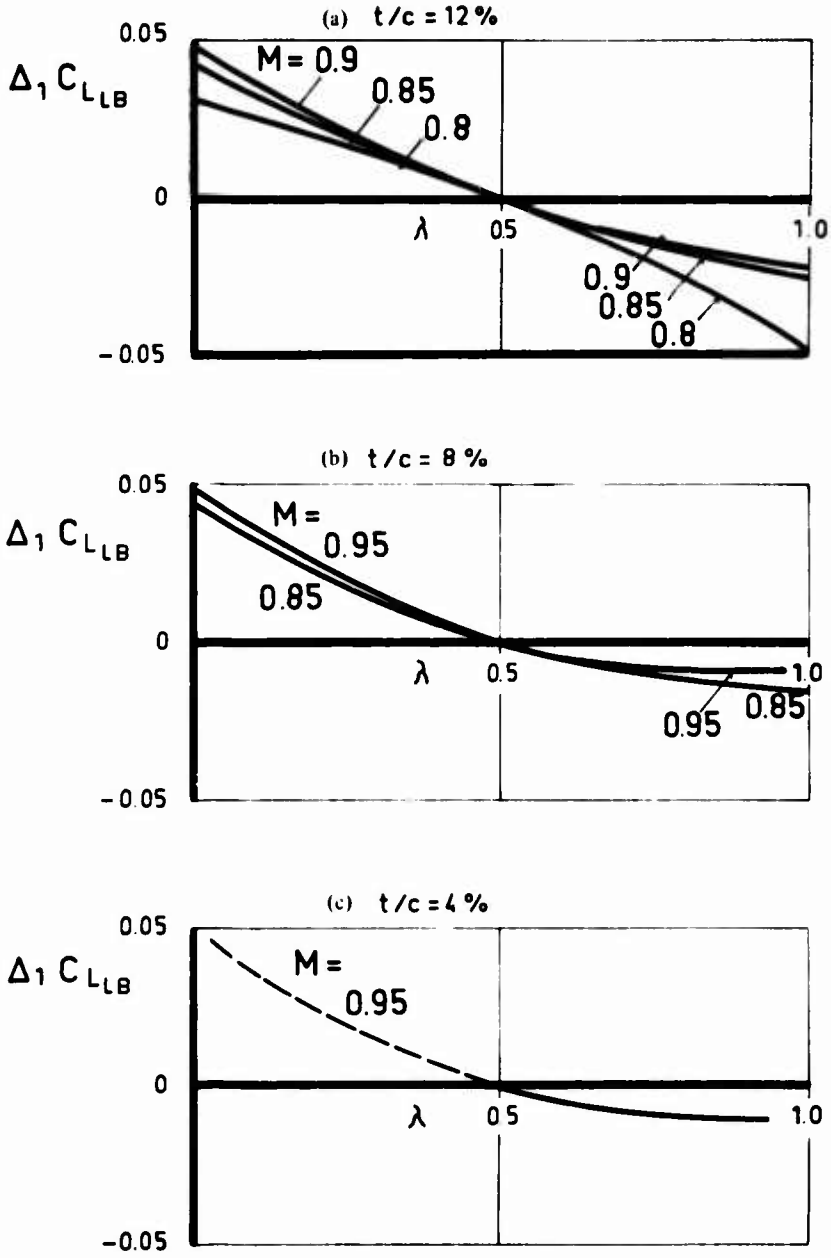

Fig.11-4 Influence of taper ratio on buffet boundary — "light buffet" (Ref.11-2)

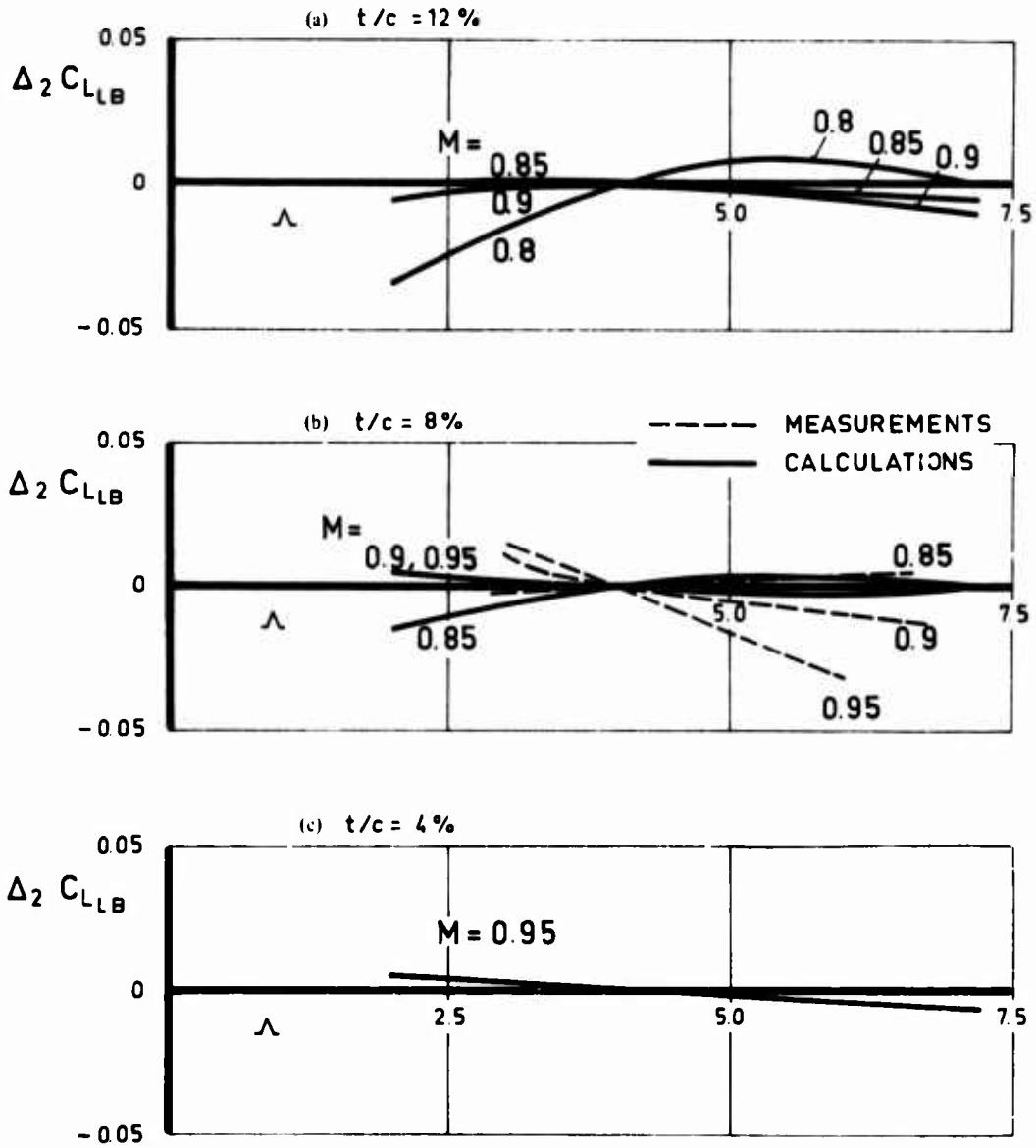

Fig.11-5 Influence of aspect ratio on buffet boundary – "light buffet" (Ref.11-2)

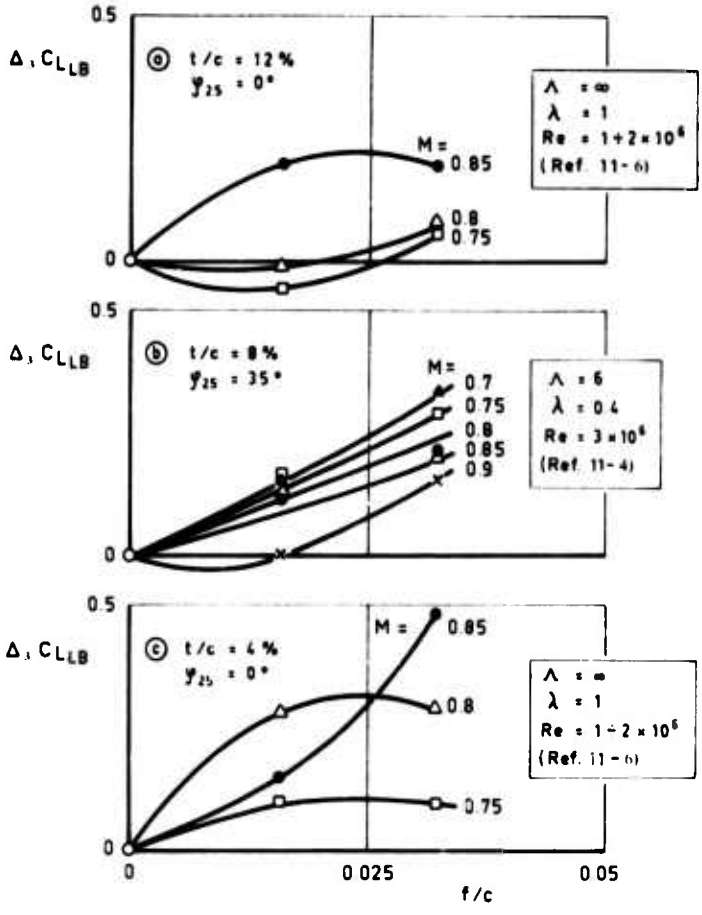

Fig.11-6 Influence of camber on buffet boundary "light buffet"

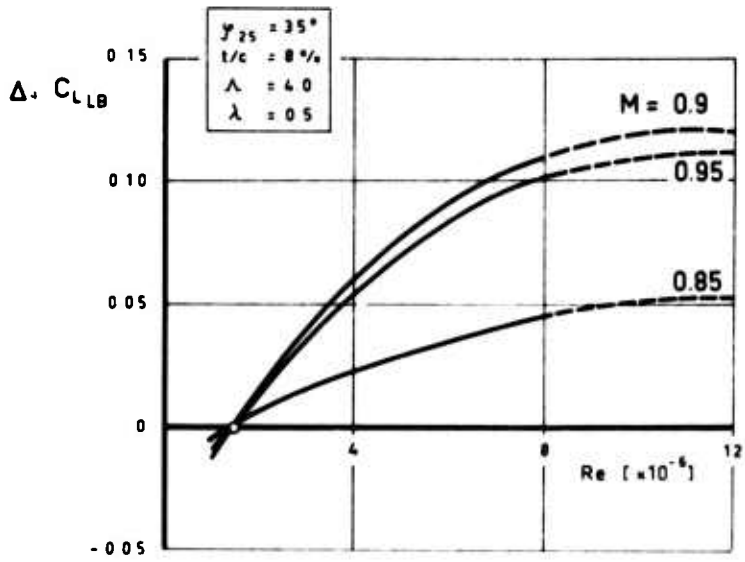

Fig.11-7 Influence of Reynolds number on buffet boundary "light buffet" (Ref.11-2)

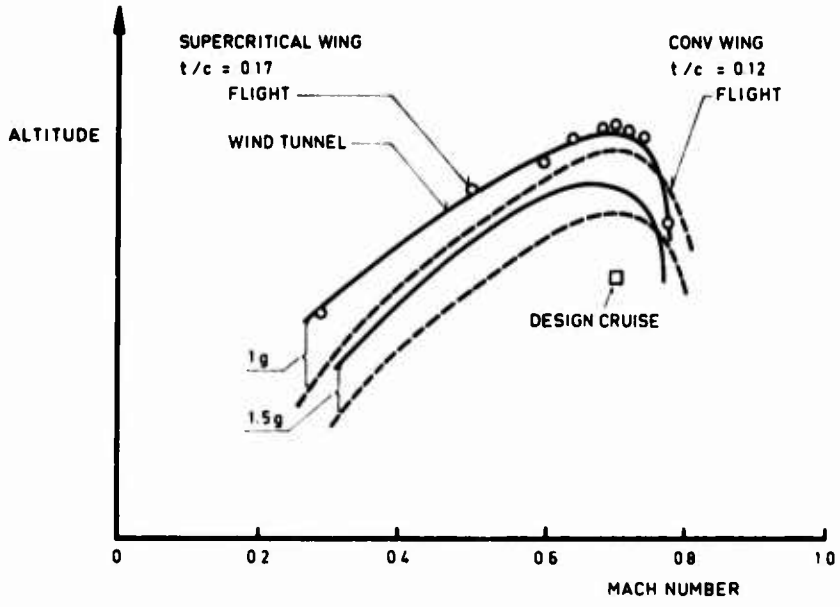

Fig.11-8 Buffet boundaries for the T-2C (Ref.11-13)

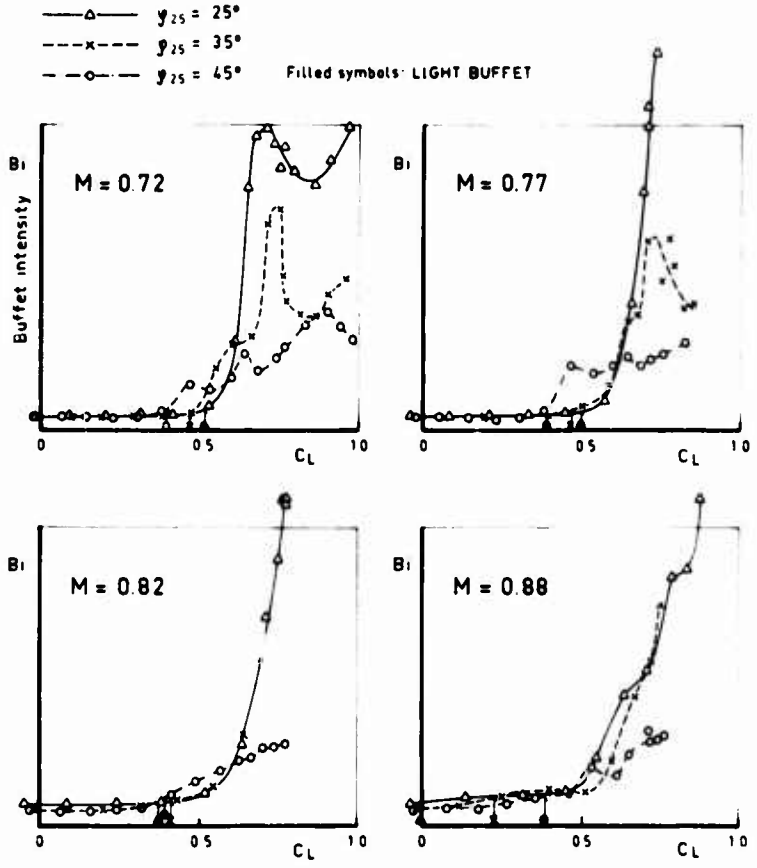

Fig.11-9 Influence of sweep on buffet intensity A = 6, NACA 63 A 008, (Ref.11-4)

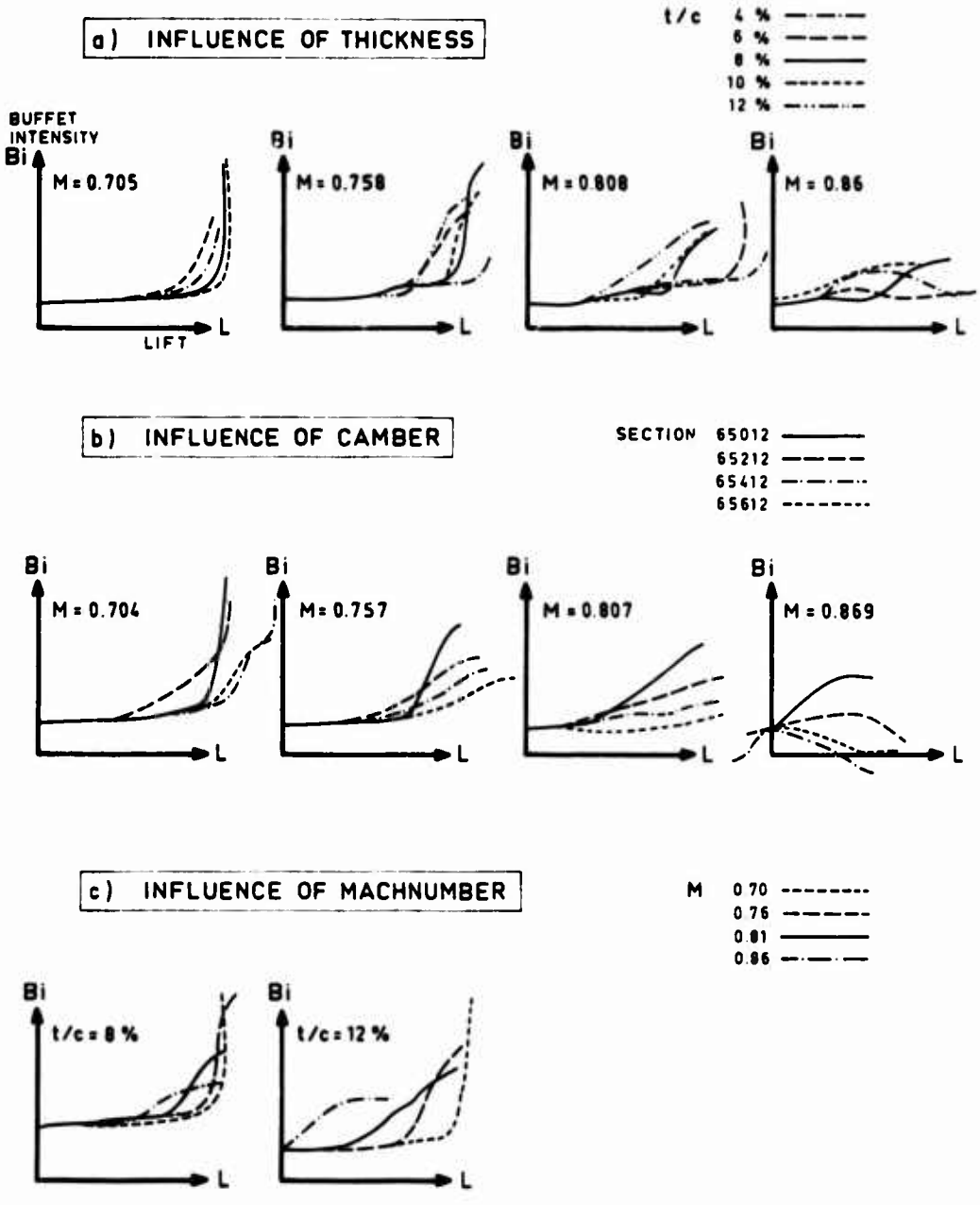

Fig.11-10 Increase in buffet intensity on airfoils (Ref.11-2)

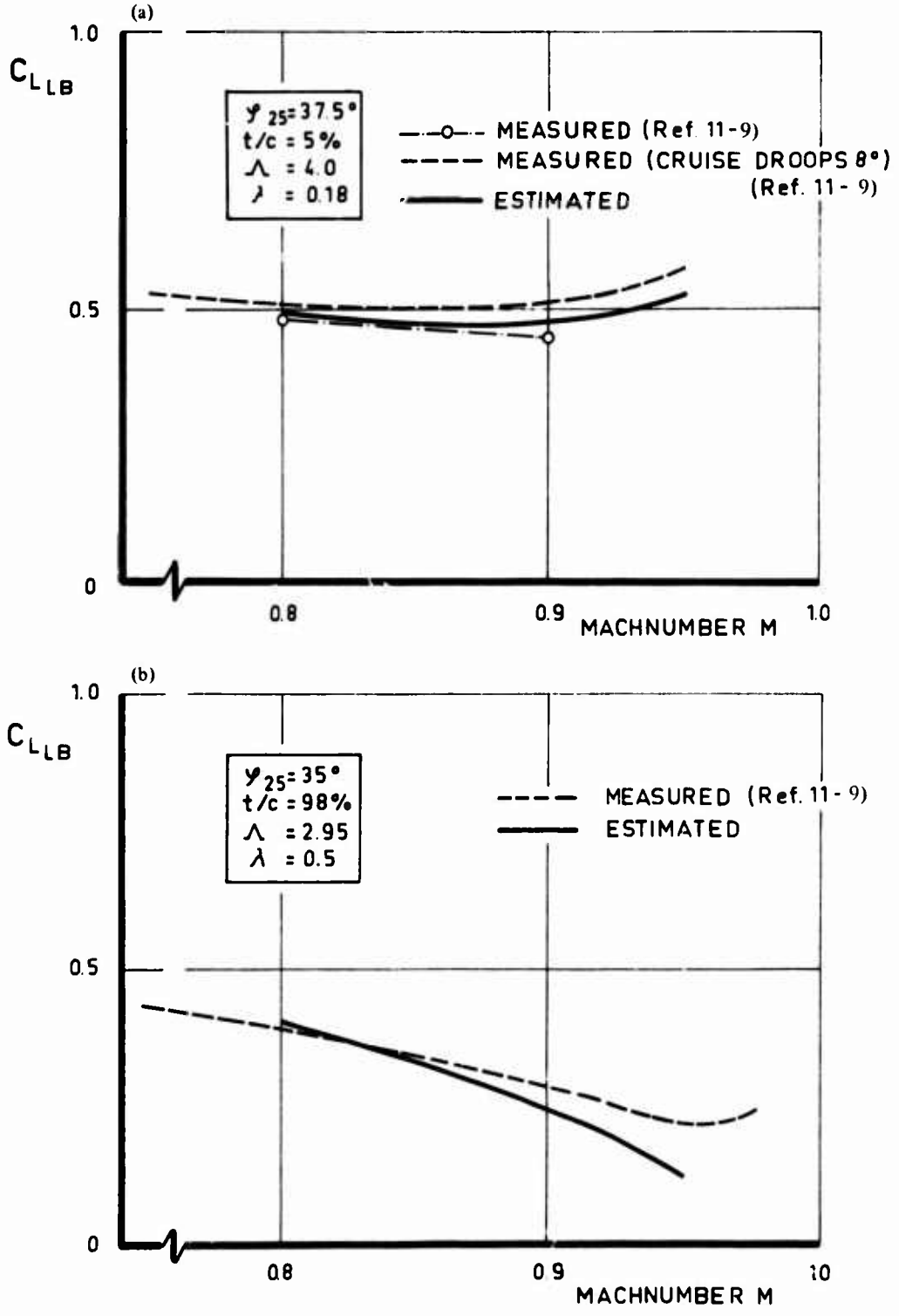

Fig.11-11 Comparison of estimated and measured buffet boundaries "light buffet"

(c)

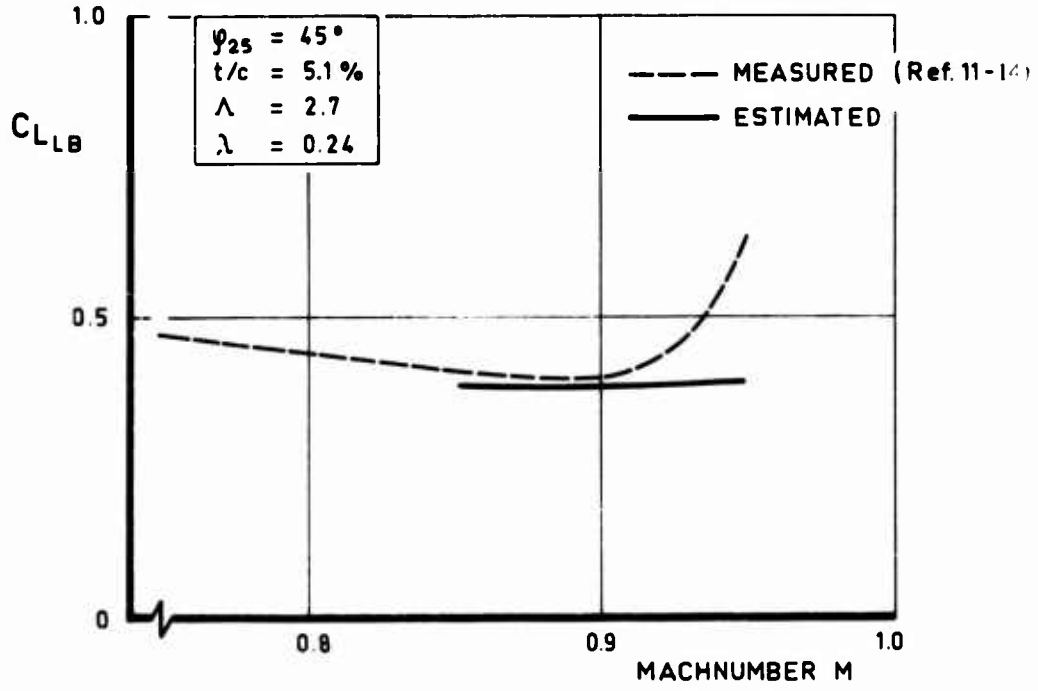

(d)

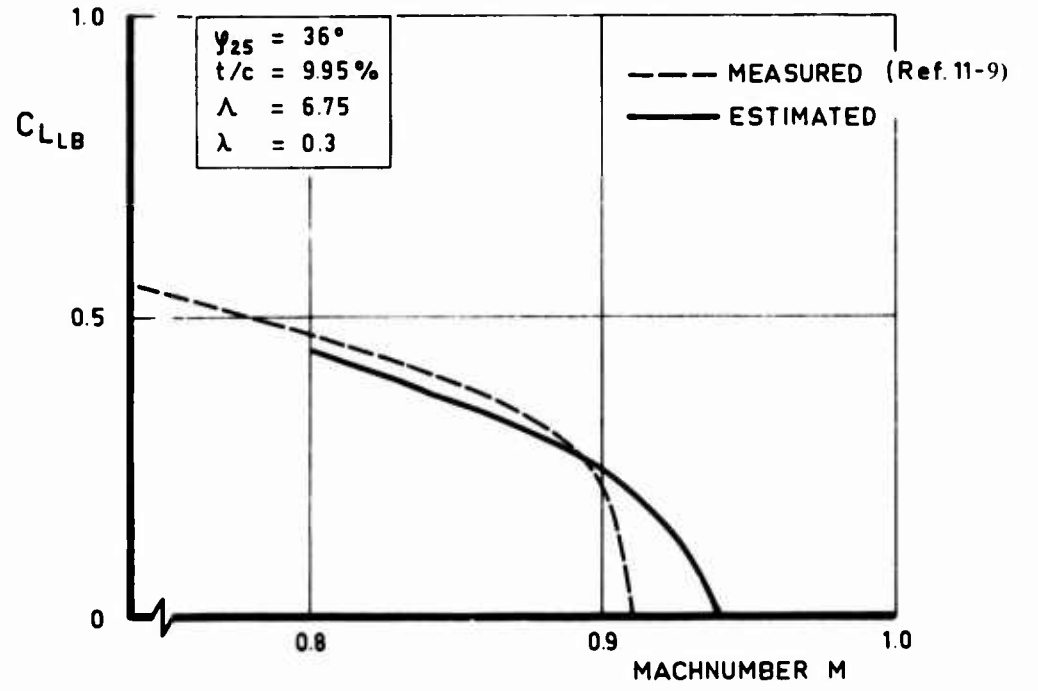

Figure 11-11 (continued)

(e)

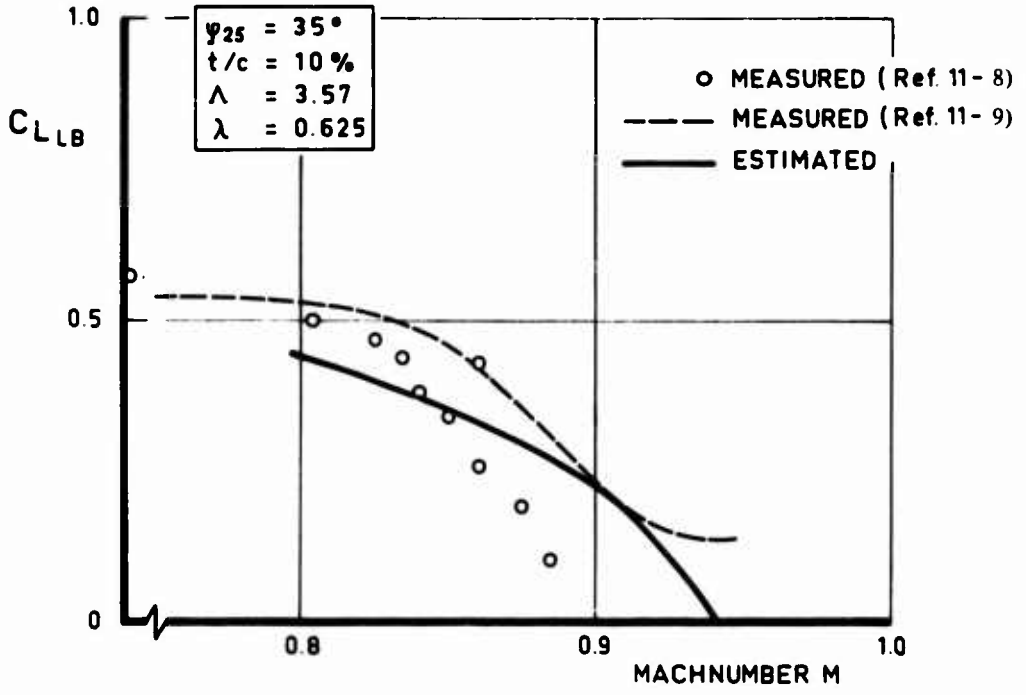

(f)

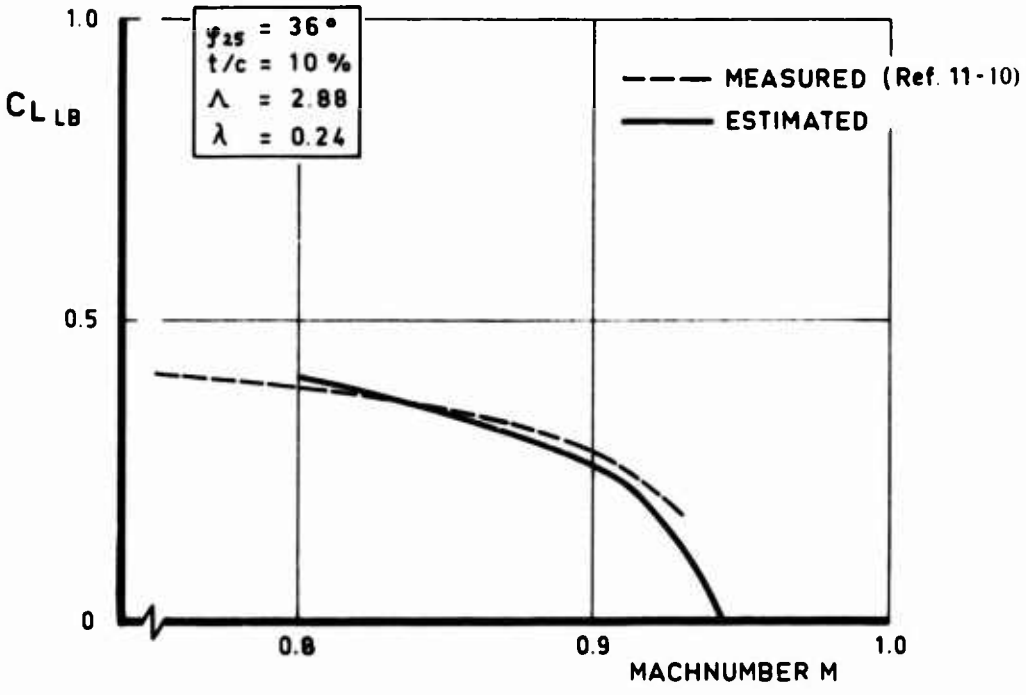

Figure 11-11 (continued)

(g)

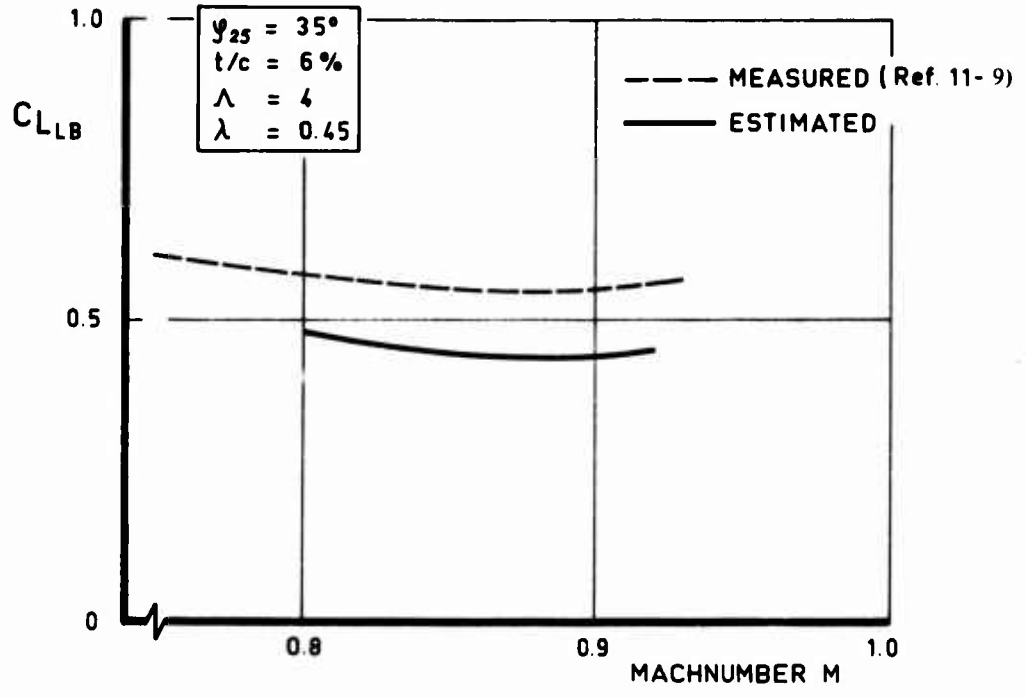

(h)

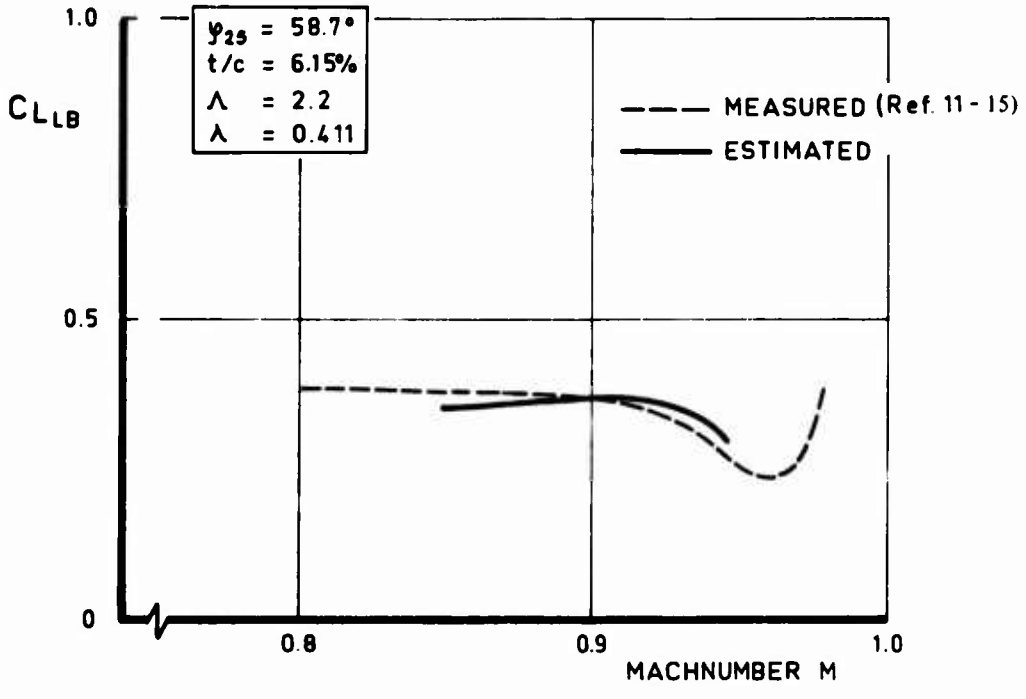

Figure 11-11 (continued)

(i)

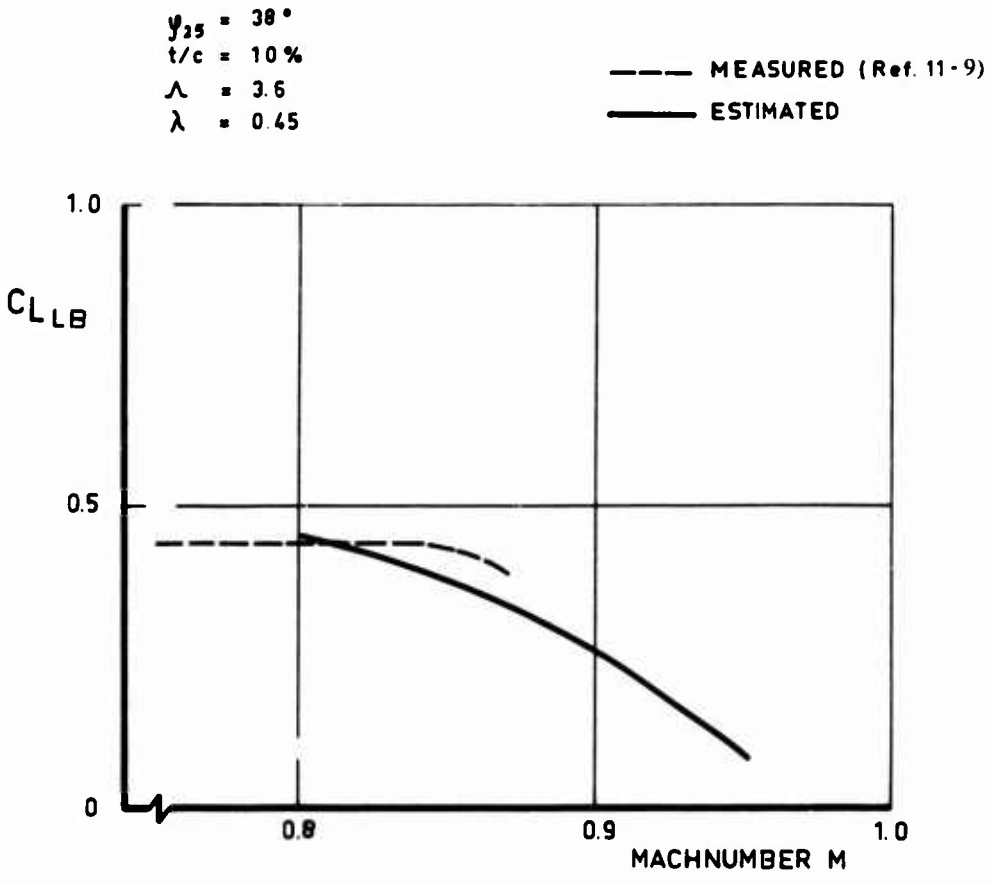

Figure 11-11 (concluded)

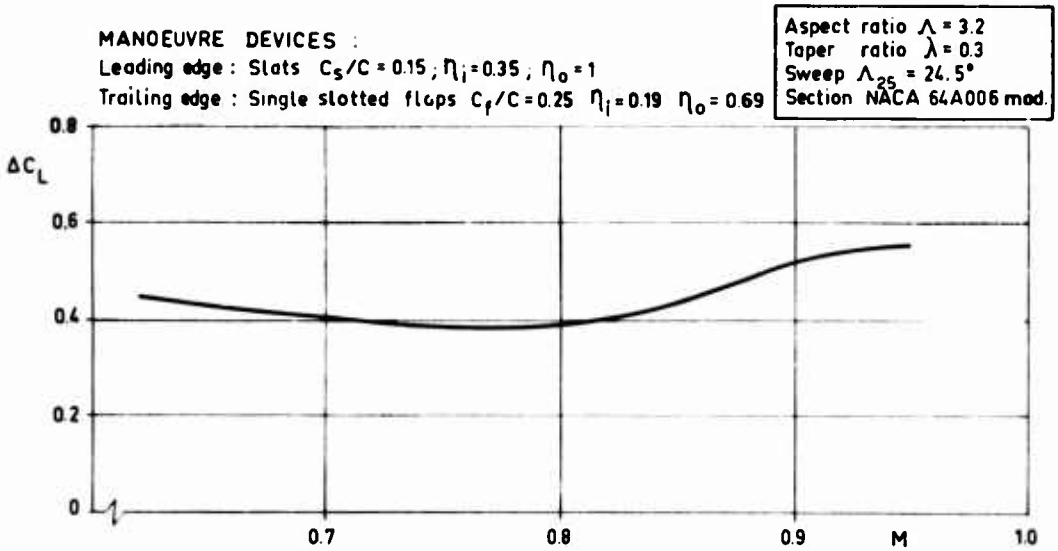

Fig.12-1 Influence of manoeuvre devices on buffet onset (Ref.12-9)

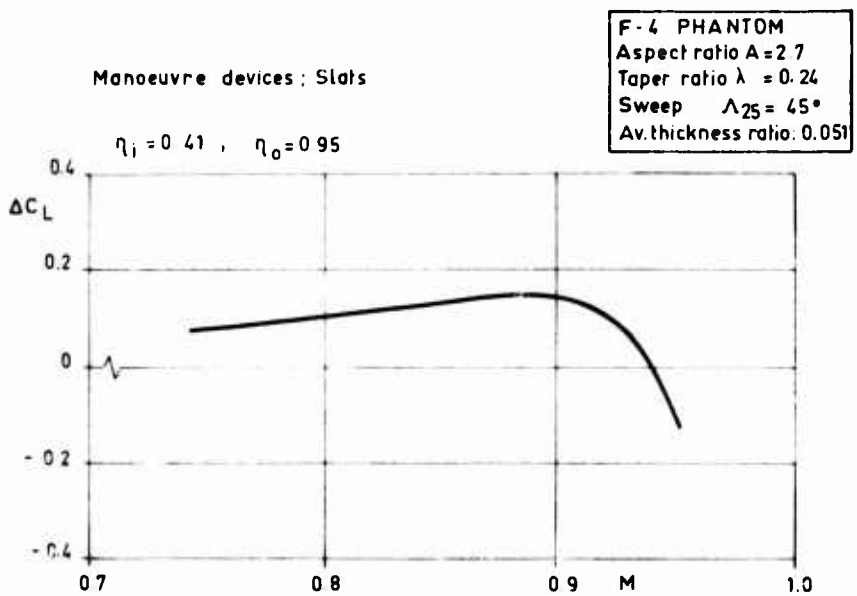

Fig.12-2 Influence of manoeuvre devices on buffet onset (Ref.12-9)

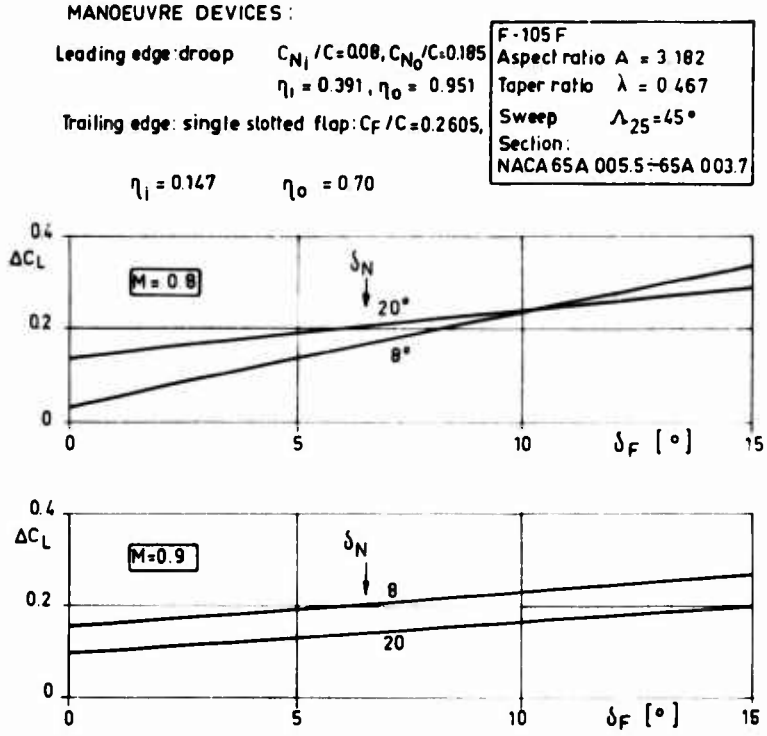

Fig.12-3 Influence of manoeuvre devices on buffet onset (Ref.12-9)

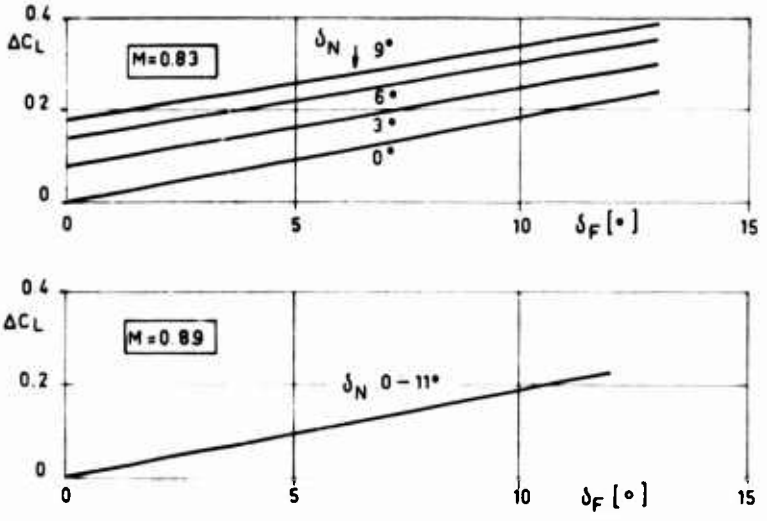

Fig.12-4 Influence of manoeuvre devices on buffet onset (Ref.12-9)

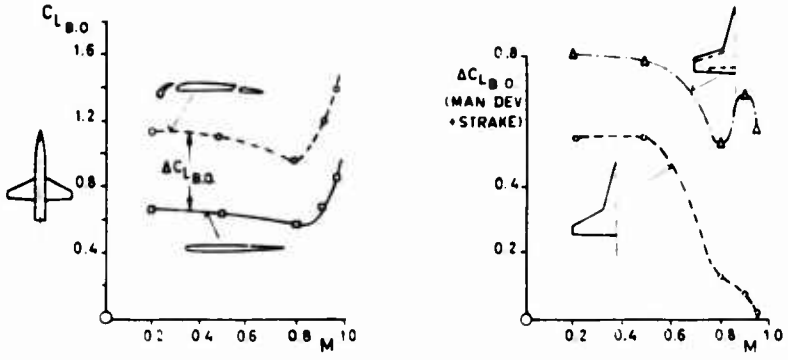

Fig.12-5 Influence of manoeuvre devices on buffet (Ref.12-10)

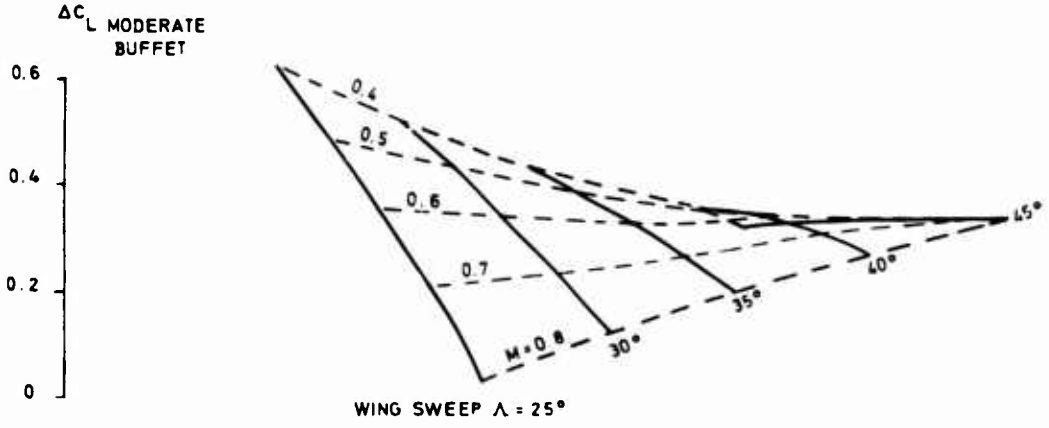

Fig.12-6 Usable lift increment due to manoeuvre slats + flaps, fighter configurations, (PANAVIA research)

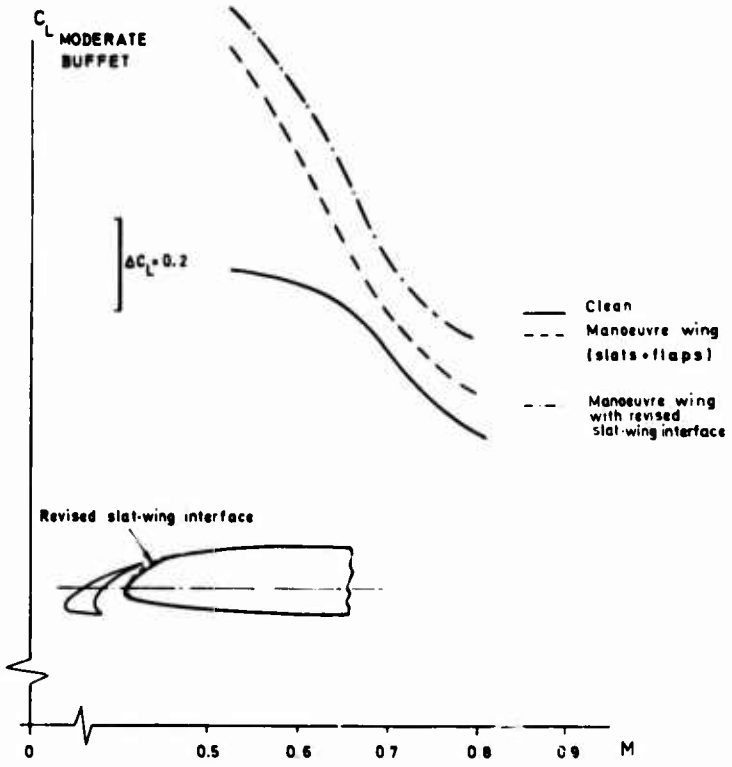

Fig.12-7 Effect of slat-wing interface optimisation on buffet limits, fighter configuration ($\Lambda = 25°$) (PANAVIA research)

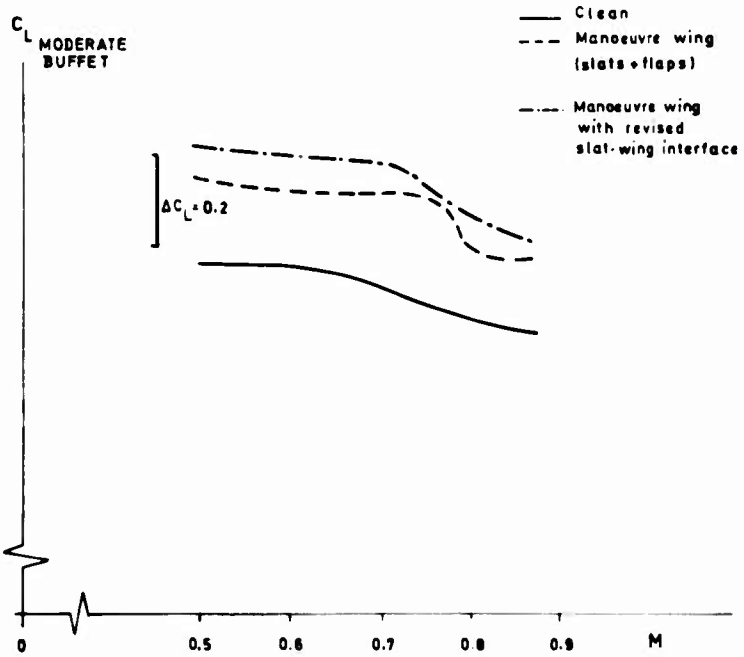

Fig.12-8 Effect of slat-wing interface optimisation on buffet limits, fighter configuration ($\Lambda = 45°$) (PANAVIA research)

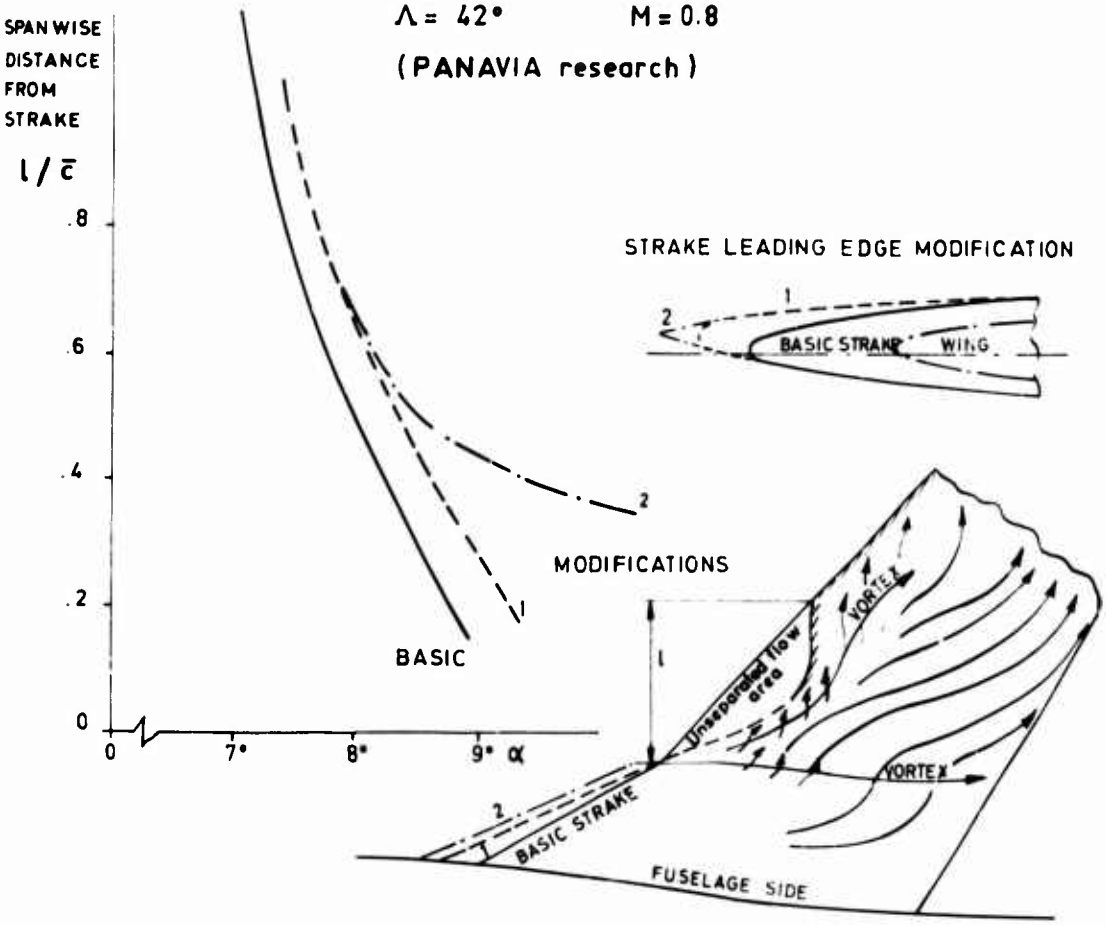

Fig. 12-9a Influence of strake leading edge on collapse of flow outboard of strake at moderate buffet C_L, $\Lambda = 42°$, $M = 0.8$, (PANAVIA research)

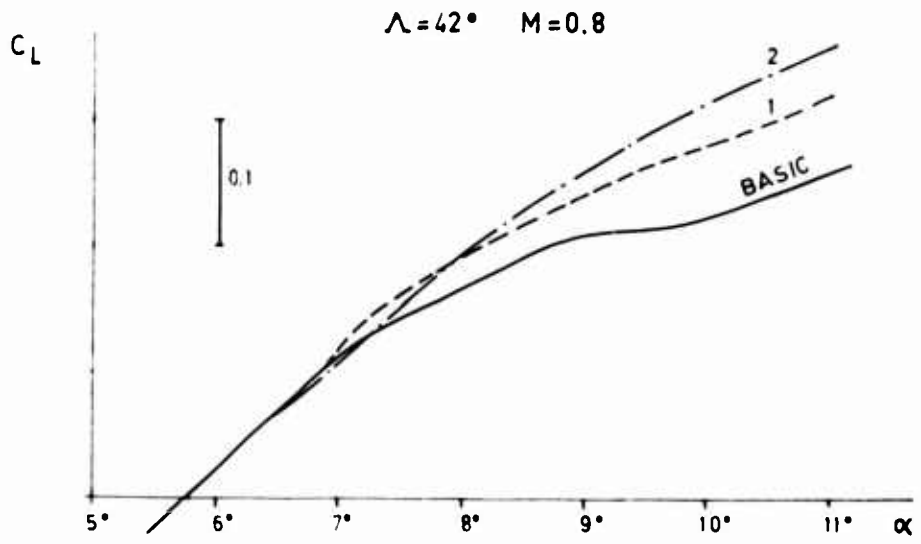

Fig. 12-9b Influence of strake leading edge on lift characteristics $\Lambda = 42°$, $M = 0.8$

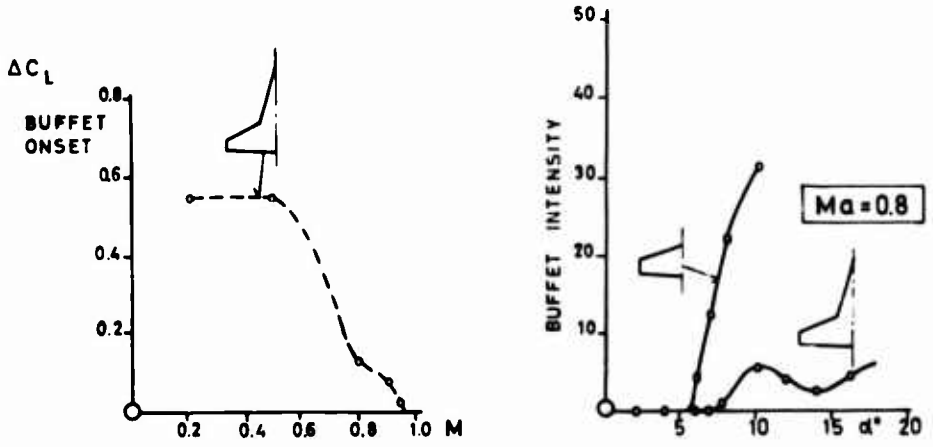

Fig.12-10 Influence of strakes on buffet (Ref.12-10)

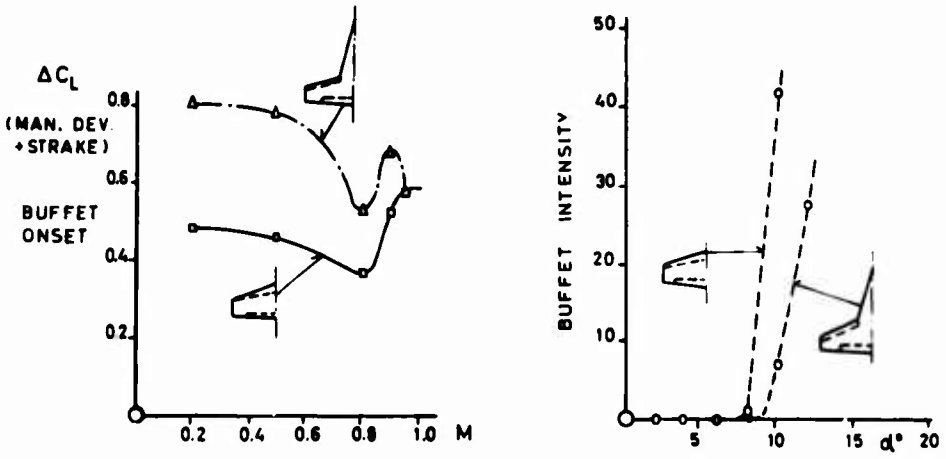

Fig.12-11 Influence of strakes on buffet (Ref.12-10)

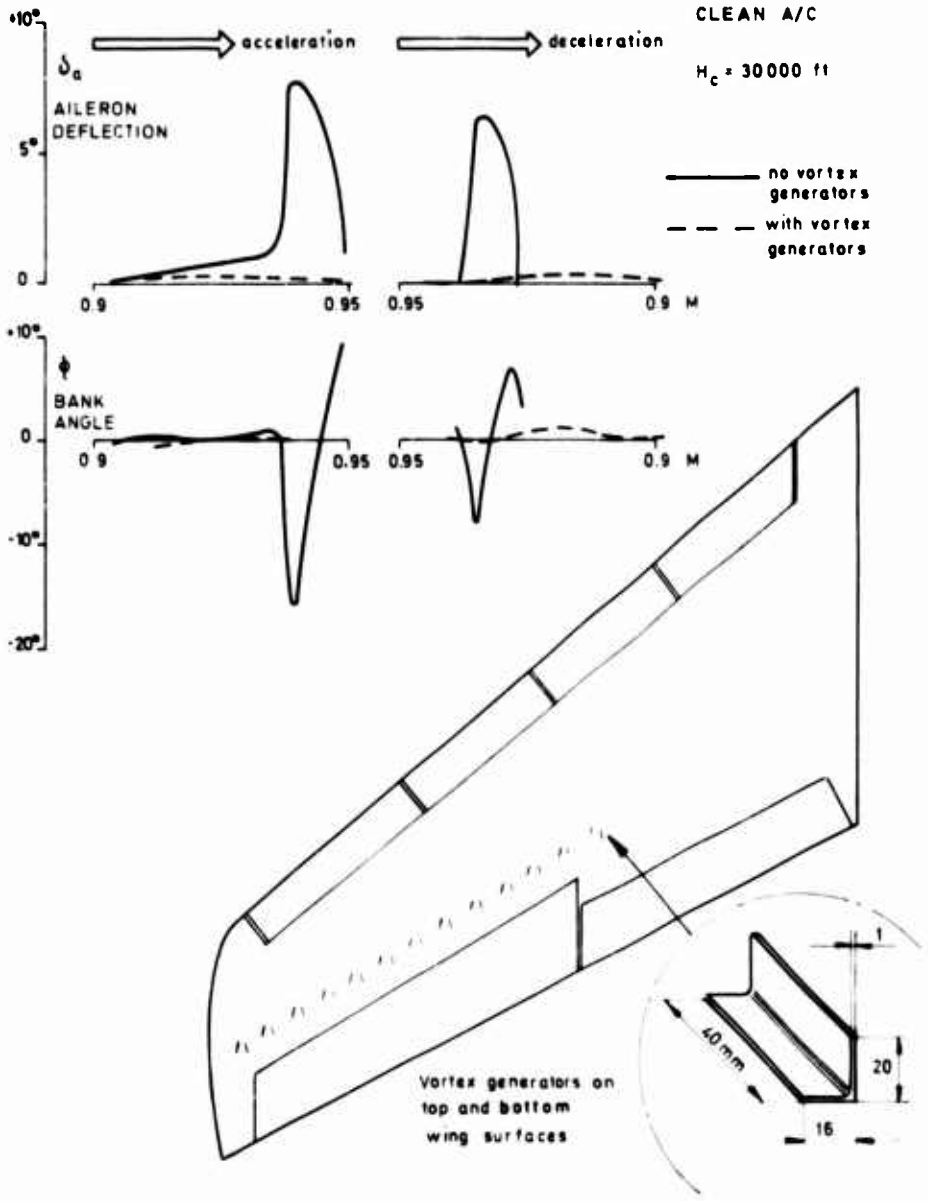

Fig.12-12 Vortex generators on the jet fighter G 91 Y wing drop investigation

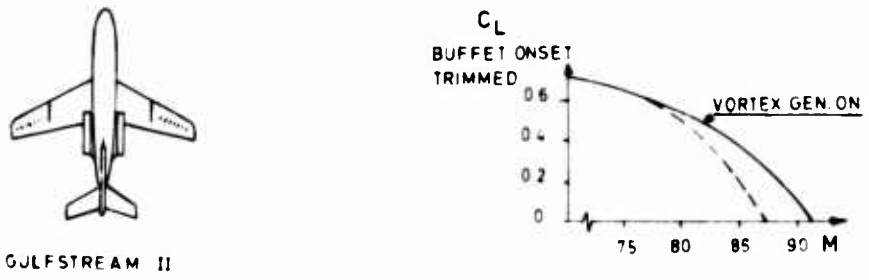

Fig.12-13 Effect of vortex generators on buffet boundary

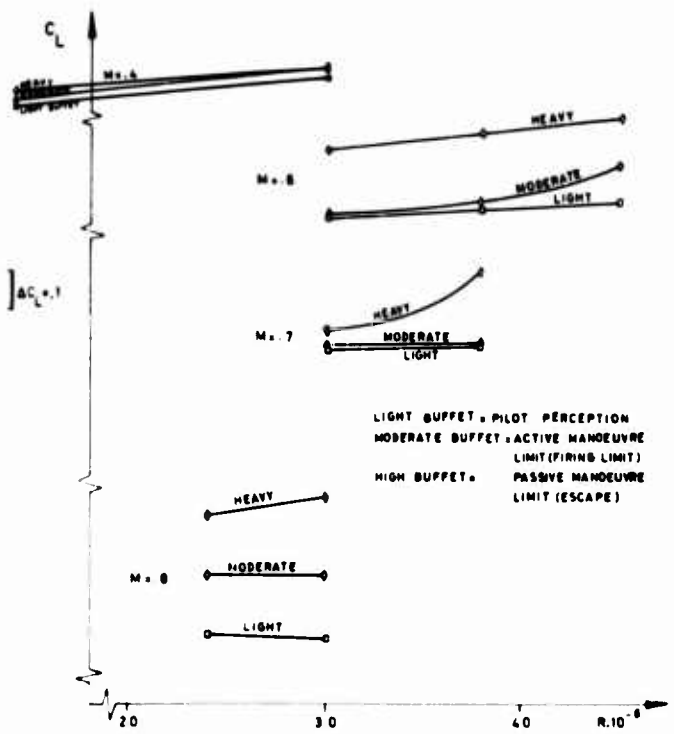

Fig.12-14 Effect of Reynolds number on buffet limits, fighter configuration ($\Lambda = 25°$) (PANAVIA research)

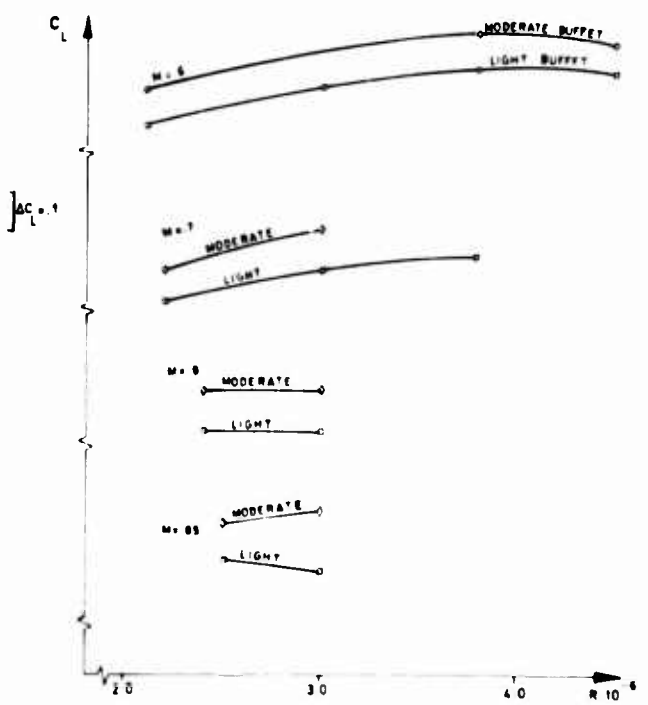

Fig.12-15 Effect of Reynolds number on buffet limits, fighter configuration ($\Lambda = 45°$) (PANAVIA research)

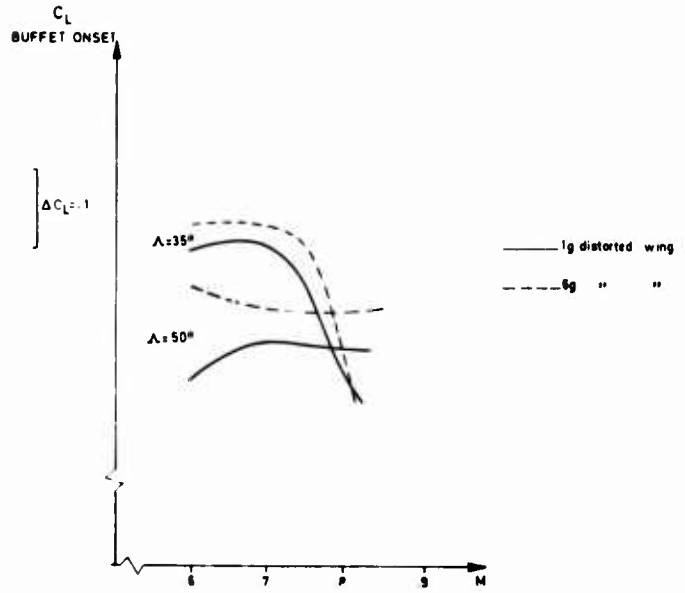

Fig.12-16 Effect of wing aeroelastic distortion on buffet onset, fighter configurations (PANAVIA research)

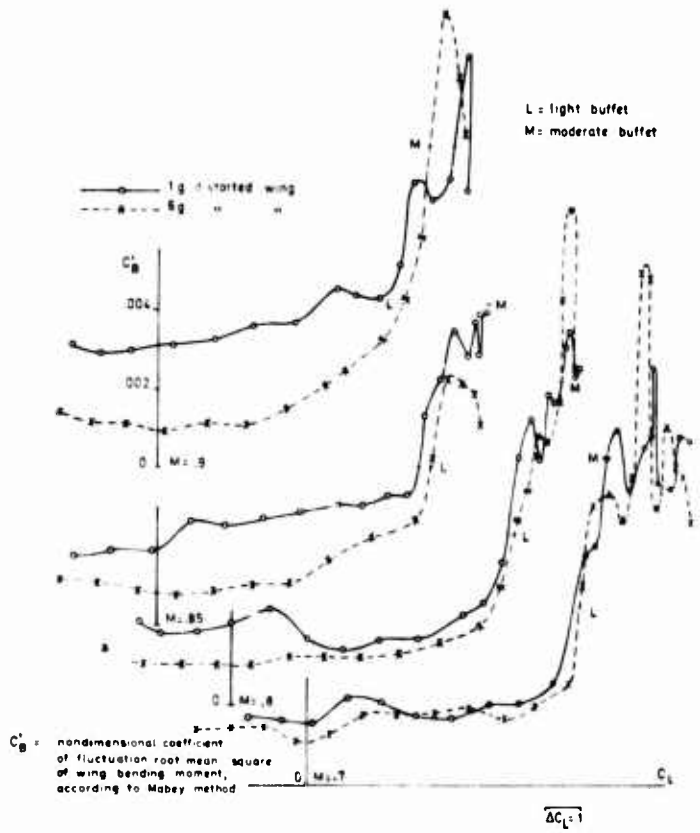

Fig.12-17 Effect of wing aeroelastic distortion on buffet penetration, fighter configuration ($\Lambda = 45°$) (PANAVIA research)

Fig.12-18 G91 fighter

Fig.12-19a G91Y fighter aircraft before afterbody modification

Fig.12-19b G91Y fighter aircraft after afterbody modification

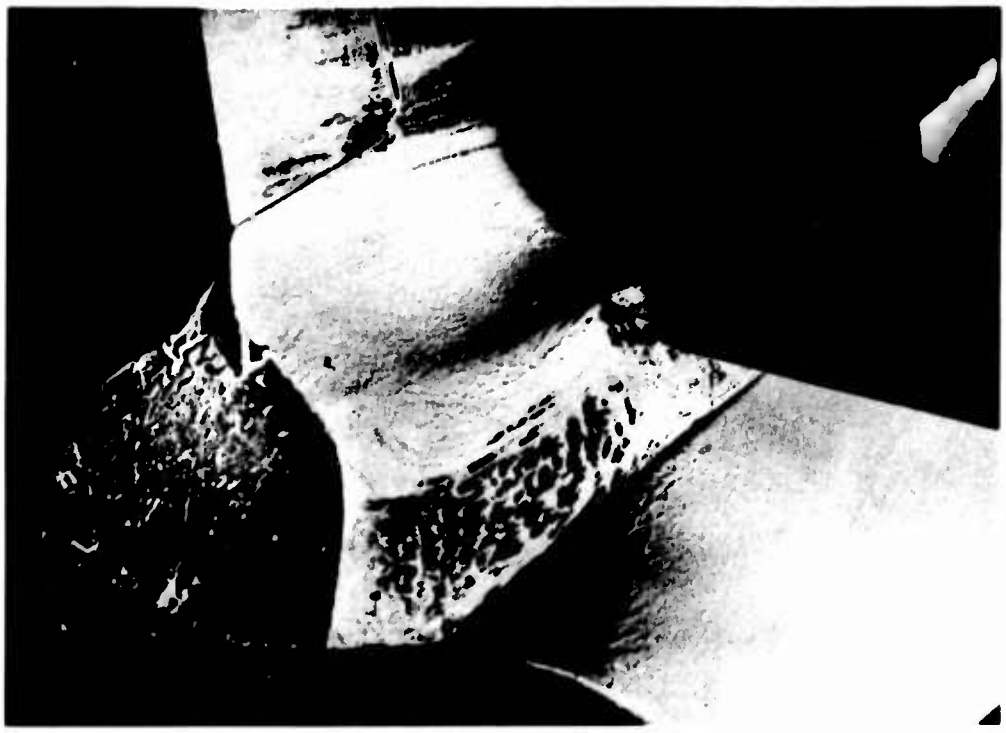

Fig.12-20 G91Y wind tunnel tests, flow field visualization on original afterbody M = 0.9, $\alpha = 0°$

Fig.12-21 G91Y wind tunnel tests, flow field visualization on modified afterbody M = 0.9, $\alpha = 0°$

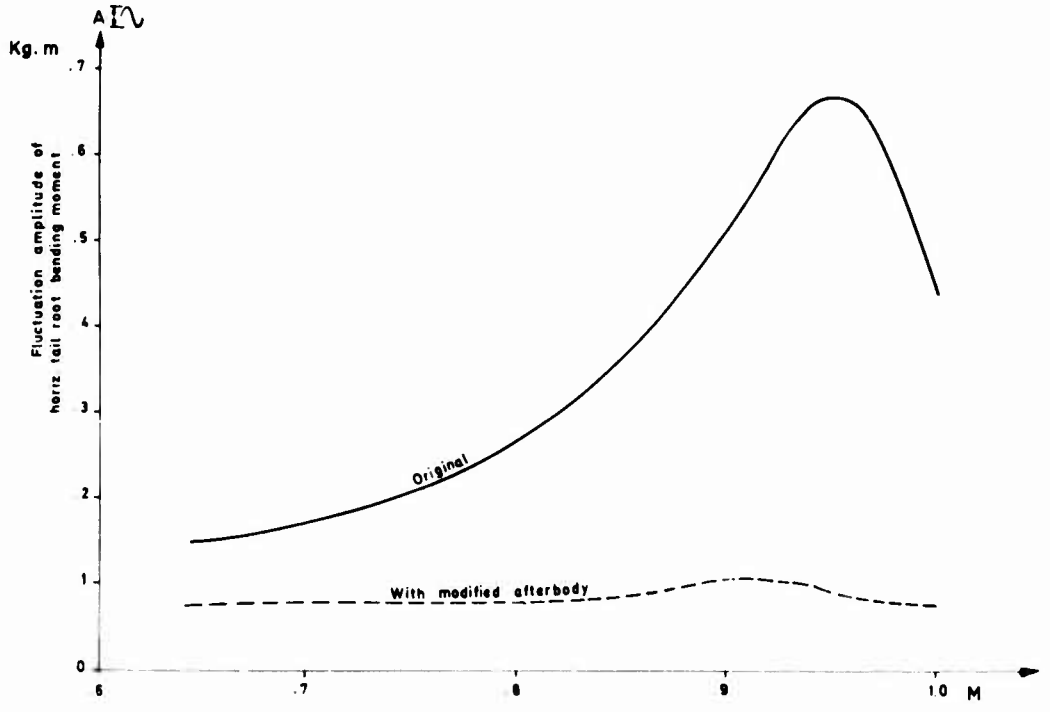

Fig.12-22 G91Y effect of afterbody modification on tail buffet, transonic wind tunnel tests

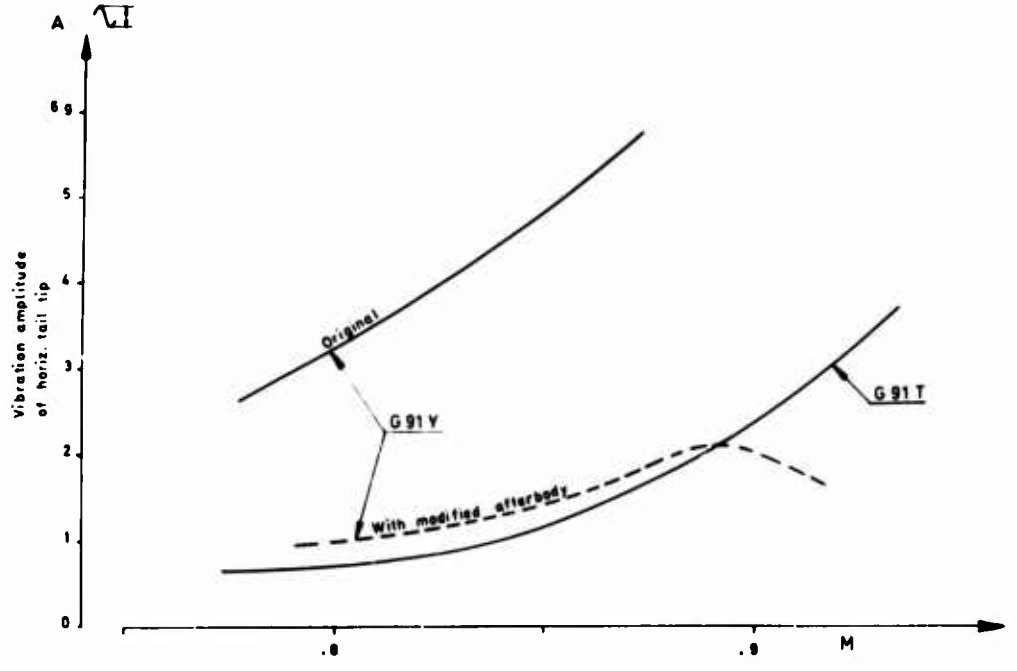

Fig.12-23 Effect of afterbody modification on tail buffet, flight tests

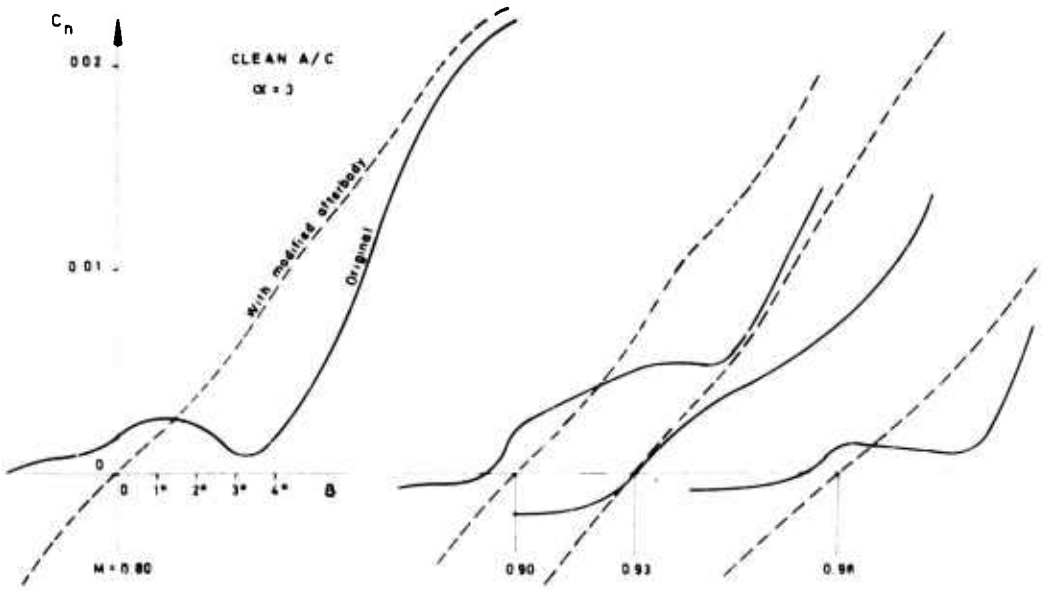

Fig.12-24 G91Y wind tunnel tests, effect of afterbody modification on directional stability

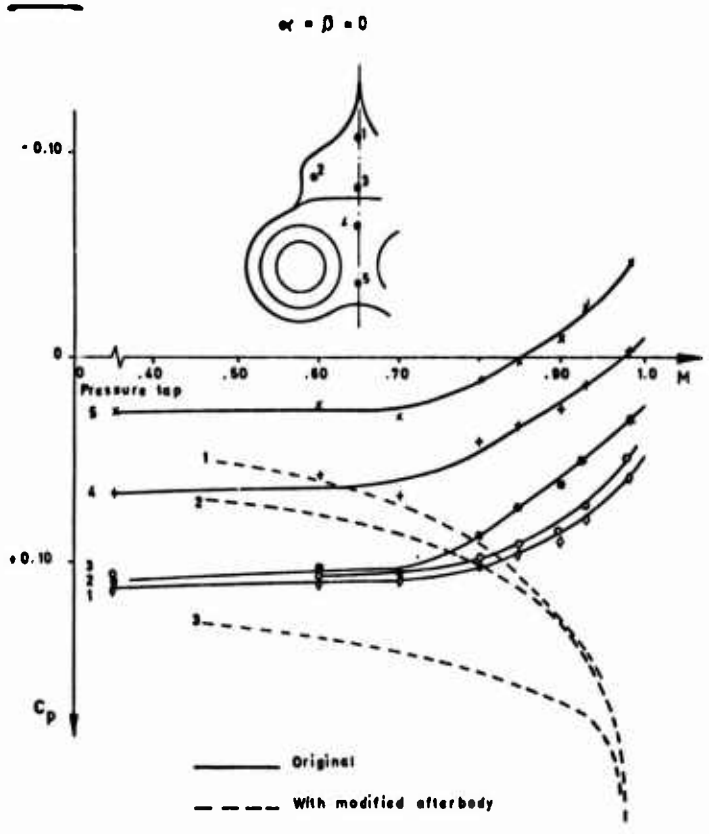

Fig.12-25 G91Y wind tunnel tests, effect of afterbody modification on base pressures

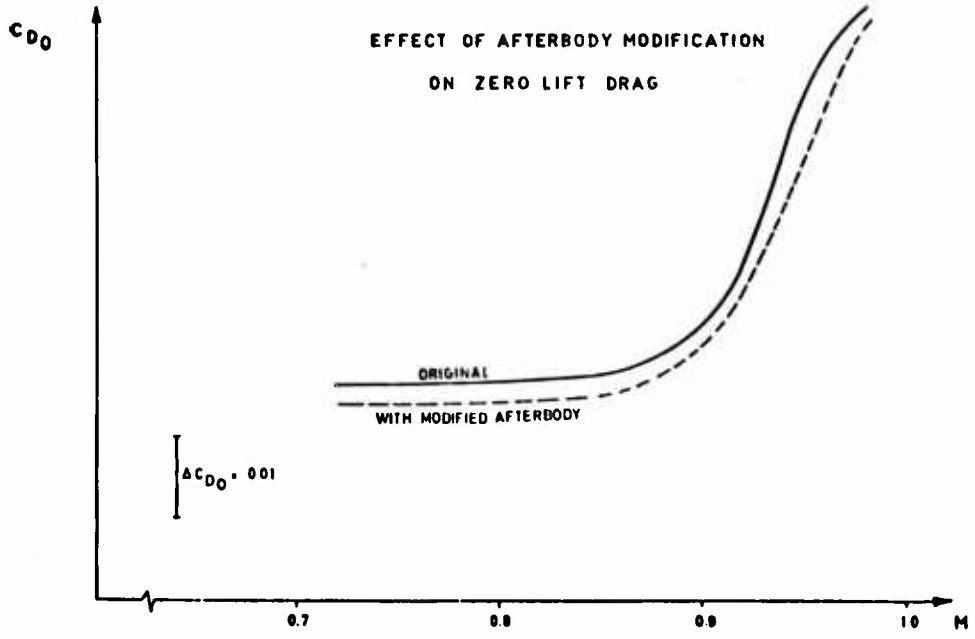

Fig.12-26 G91Y wind tunnel tests, effect of afterbody modification on zero lift drag